DOC.20050825.0007

QA: QA

MDL-NBS-HS-000007 REV 03

August 2005

Mountain-Scale Coupled Processes (TH/THC/THM) Models

Prepared for:
U.S. Department of Energy
Office of Civilian Radioactive Waste Management
Office of Repository Development
1551 Hillshire Drive
Las Vegas, Nevada 89134-6321

Prepared by:
Bechtel SAIC Company, LLC
1180 Town Center Drive
Las Vegas, Nevada 89144

Under Contract Number
DE-AC28-01RW12101

DISCLAIMER

This report was prepared as an account of work sponsored by an agency of the United States Government. Neither the United States Government nor any agency thereof, nor any of their employees, nor any of their contractors, subcontractors or their employees, makes any warranty, express or implied, or assumes any legal liability or responsibility for the accuracy, completeness, or any third party's use or the results of such use of any information, apparatus, product, or process disclosed, or represents that its use would not infringe privately owned rights. Reference herein to any specific commercial product, process, or service by trade name, trademark, manufacturer, or otherwise, does not necessarily constitute or imply its endorsement, recommendation, or favoring by the United States Government or any agency thereof or its contractors or subcontractors. The views and opinions of authors

QA: QA

Mountain-Scale Coupled Processes (TH/THC/THM) Models

MDL-NBS-HS-000007 REV 03

August 2005

2. Type of Mathematical Model

☒ Process Model ☐ Abstraction Model ☐ System Model

Describe Intended Use of Model

The purpose of this report is to develop the Mountain-Scale Thermal-Hydrologic (TH), Thermal-Hydrologic-Chemical (THC), and Thermal-Hydrologic-Mechanical (THM) Models and evaluate the effects of coupled TH/THC/THM processes on mountain-scale UZ flow at Yucca Mountain, Nevada.

3. Title

Mountain-Scale Coupled Processes (TH/THC/THM) Models

4. DI (including Rev. No.):

MDL-NBS-HS-000007 REV 03

	Printed Name	Signature	Date
5. Originator	Y.-S. Wu		8/24/05
6. Independent Technical Reviewer	R. Andrews		8/24/05
7. Checker	B. Kirstein		8/24/05
8. QER	K. Gilkerson		8/24/05
9. Responsible Manager/Lead	W. Duffy		8/24/05
10. Responsible Manager	E. Hardin		8/24/05

11. Remarks

- Sumit Mukhopadhyay and Keni Zhang (LBNL) contributed to the TH model; Eric Sonnenthal and Nic Spycher (LBNL) contributed to the THC model; and Jonny Rutqvist (LBNL) contributed to the THM model.
- Junghun Leem (BSC) was responsible for report integration.
- Kenrick Lee (LLNL) contributed to this report.

Change History

12. Revision No.	13. Description of Change
REV 00	Initial Issue
REV 01	The entire model documentation was revised. Side bars are not used because the changes were too extensive to use Step 5.8d(1) per AP-SIII.10Q, Rev. 2/ICN 0. Rev 01 Errata 01.

REV 01 Errata 01	Model report and associated DIRS corrected to reference BSC 2003 [DIRS 166512]-TBV 5666 *Drift Scale Coupled Processes (DST and TH seepage) Models* MDL-NBS–HS-00015 REV 00C, per CR-1100. Model report updated to include missing information on Pages 53, 216 and 241 per CR-1667.
REV 02	The entire model documentation was revised. Side bars are not used because the changes were too extensive to use Step 5.8d(1) per AP-SIII.10Q, Rev. 2/ICN 0. Rev 01 Errata 01. The main Revisions were: • Made edits to enhance traceability in response to Regulatory Integration Team evaluation • Address included FEPs, identifying the FEP number and specifying how it is included in the model. The disposition of each FEP conforms to the guidance provided in *The Enhanced Plan For Features, Events, and Processes (FEPs) at Yucca Mountain* (BSC 2002, Section 3 and Appendix A). • Perform numerical simulation of coupled TH/THC/THM processes at the mountain scale, using a dual continuum approach and an active fracture model. Analyze the uncertainty in models by using sensitivity cases, e.g., by comparing results of 2-D and 3-D simulations for the TH models, Address uncertainties of additional input parameters and their impact using qualitative methods • Perform additional evaluation of model validation including the use of natural analogues to provide confidence in the model predictions
REV 03	Revisions to the validation section of the document (Section 7) to address CR99 and CR4961. The revisions were made for post-development model validation comments documented in Section 7 and Appendix VIII. Additional revisions were made in: • Organizing and formatting the report to achieve transparency and readability. • Adding information, as appropriate, to more clearly establish the relationships among this report and related reports (either upstream or downstream) and the TSPA. • Incorporating regulatory comments from the Regulatory Integration Team evaluation of the previous report, as applicable. • Addressing data traceability, quality, and pedigree issues identified during the Regulatory Integration Team evaluation of the previous report. • Addressing CRs against the previous report: outstanding CRs (2049 TWP revision, 2050 model validation, and 2051 non-convergence) and TBVs (various reference citation issues, Impact Review Action Notices). • Developing and incorporating information to address the NRC *Yucca Mountain Review Plan* (NUREG-1804) (NRC 2003), and the KTIs, and agreements, as appropriate. • Deleting all discussion of the drift-collapse THC modeling (which had been part of the previous report).

	• Moving the description of the post-processing of results from the THC seepage model, to this report from *Engineered Barrier System: Physical and Chemical Environment*. • Removing all discussion of radionuclide K_d temperature sensitivity (which had been part of the previous report).

INTENTIONALLY LEFT BLANK

CONTENTS

Page

CONTENTS (Continued)

Page

CONTENTS (Continued)

Page

CONTENTS (Continued)

Page

FIGURES

Page

FIGURES (Continued)

Page

FIGURES (Continued)

Page

FIGURES (Continued)

Page

FIGURES (Continued)

Page

FIGURES (Continued)

Page

FIGURES (Continued)

Page

INTENTIONALLY LEFT BLANK

TABLES

Page

INTENTIONALLY LEFT BLANK

ACRONYMS AND ABBREVIATIONS

CFu	Crater Flat undifferentiated hydrolgeologic unit
CHn	Calico Hills nonwelded hydrogeologic unit
DST	Drift Scale Test
DTN	data tracking number
FEP	feature, event, and process
GFM	geological framework model
HM	hydrologic-mechanical
masl	meters above sea level
N-S	North-South
PTn	Paintbrush nonwelded hydrogeologic unit
STN	software tracking number
SZ	saturated zone
TDMS	Technical Data Management System
TH	thermal-hydrologic
THC	thermal-hydrologic-chemical
THM	thermal-hydrologic-mechanical
TM	thermal-mechanical
TSPA-LA	total system performance assessment for the license application
TSw	Topopah Spring welded hydrogeologic unit
TWP	technical work plan
UZ	unsaturated zone
YMP	Yucca Mountain Project
YMRP	*Yucca Mountain Review Plan, Final Report*

INTENTIONALLY LEFT BLANK

1. PURPOSE

This report documents the development and validation of the mountain-scale thermal-hydrologic (TH), thermal-hydrologic-chemical (THC), and thermal-hydrologic-mechanical (THM) models. These models provide technical support for screening of features, events, and processes (FEPs) related to the effects of coupled TH/THC/THM processes on mountain-scale unsaturated zone (UZ) and saturated zone (SZ) flow at Yucca Mountain, Nevada (BSC 2005 [DIRS 174842], Section 2.1.1.1). The purpose and validation criteria for these models are specified in *Technical Work Plan for: Near-Field Environment and Transport: Coupled Processes (Mountain-Scale TH/THC/THM, Drift-Scale THC Seepage, and Drift-Scale Abstraction) Model Report Integration* (BSC 2005 [DIRS 174842]). Model results are used to support exclusion of certain FEPs from the total system performance assessment for the license application (TSPA-LA) model on the basis of low consequence, consistent with the requirements of 10 CFR 63.342 [DIRS 173273]. Outputs from this report are not direct feeds to the TSPA-LA. All the FEPs related to the effects of coupled TH/THC/THM processes on mountain-scale UZ and SZ flow are discussed in Sections 6 and 7 of this report.

The mountain-scale coupled TH/THC/THM processes models numerically simulate the impact of nuclear waste heat release on the natural hydrogeological system, including a representation of heat-driven processes occurring in the far field. The mountain-scale TH simulations provide predictions for thermally affected liquid saturation, gas- and liquid-phase fluxes, and water and rock temperature (together called the flow fields). The main focus of the TH model is to predict the changes in water flux driven by evaporation/condensation processes, and drainage between drifts. The TH model captures mountain-scale three-dimensional flow effects, including lateral diversion and mountain-scale flow patterns. The mountain-scale THC model evaluates TH effects on water and gas chemistry, mineral dissolution/precipitation, and the resulting impact to UZ hydrologic properties, flow and transport. The mountain-scale THM model addresses changes in permeability due to mechanical and thermal disturbances in stratigraphic units above and below the repository host rock. The THM model focuses on evaluating the changes in UZ flow fields arising out of thermal stress and rock deformation during and after the thermal period (the period during which temperatures in the mountain are significantly higher than ambient temperatures).

Direct inputs to this model are listed in Table 4.1-1. The following sources provide direct input to this report:

- Net infiltration from *Simulation of Net Infiltration for Modern and Potential Future Climates*
- Geologic and hydrogeologic data from *Geologic Framework Model*
- Drift-scale calibrated properties from *Calibrated Properties Model and Analysis of Hydrologic Properties Data*
- Mountain-scale calibrated properties and boundary conditions from *UZ Flow Models and Submodels*

- Mineral volume fractions and surface areas from *Mineralogic Model (MM3.0) Analysis Model Report*
- Thermal-mechanical properties from *Drift Scale THM Model*
- Ventilation efficiency from *Ventilation Model and Analysis Report*
- Thermal load from *D&E / PA/C IED Emplacement Drift Configuration and Environment*
- Time dependent thermal load from *Repository Design, Repository/PA IED Subsurface Facilities Plan, Sheet 5 of 5*
- Drift dimensions and drift spacing from *Subsurface Facility Description Document*
- Thermal properties from *Drift-Scale Coupled Processes (DST and TH Seepage) Model*.

The following sources provide indirect input to this report:

- *Conceptual Model and Numerical Approaches for UZ Flow and Transport*
- *UZ Flow Models and Submodels*
- *Calibrated Properties Model*
- *Analysis of Hydrologic Properties Data*
- *Features, Events, and Processes in UZ Flow and Transport*
- *Development of Numerical Grids for UZ Flow and Transport Modeling*
- *Drift-Scale Coupled Processes (DST and TH Seepage) Models*
- *Drift-Scale THC Seepage Model*
- *Drift Scale THM Model*
- *Drift Degradation Analysis*
- *Future Climate Analysis*
- *In Situ Field Testing of Processes*
- *Multiscale Thermohydrologic Model*
- *Radionuclide Transport Models Under Ambient Conditions*.

The following documents use information from this report as direct input:

- *Features, Events, and Processes in UZ Flow and Transport*
- *Features, Events, and Processes in SZ Flow and Transport.*

The following documents use information from this report as indirect input:

- *Drift-Scale THC Seepage Model*
- *Drift Scale THM Model*
- *Screening Analysis for Criticality Features, Events, and Processes for License Application*

- *Drift-Scale Radionuclide Transport*
- *Multiscale Thermohydrologic Model*
- *Screening Analysis of Criticality Features, Events, and Processes for License Application*
- *Post-Processing Analysis for THC Seepage*
- *Probability of Postclosure Criticality*
- *UZ Flow Models and Submodels*
- *Parameter Sensitivity Analysis for Unsaturated Zone Flow*
- *Particle Tracking Model and Abstraction of Transport Processes*
- *Mineralogic Model (MM3.0) Analysis Model Report*.

Mountain-scale TH/THC/THM simulations are carried out using the UZ flow and transport model (UZ model) developed in *UZ Flow Models and Submodels* (BSC 2004 [DIRS 169861]). These simulations provide mountain-scale thermally perturbed flow fields that directly incorporate thermal effects on UZ flow. The flow fields are developed with a spatially varying mean infiltration rate and varying climates during the compliance period of 10,000 years. The simulations use the base case thermal load and ventilation scenario.

Predictions of thermal-loading effects in such models require developing and using mathematical models that accurately represent the physics of heat and fluid transport in the UZ. The mountain-scale predictions are performed using TOUGH2 codes (LBNL 2003 [DIRS 161491]; Pruess 1987 [DIRS 100684]; 1991 [DIRS 100413]), which incorporate continuum models, and the van Genuchten capillary pressure and relative permeability relationships. These codes adequately describe the behavior of the UZ under thermal loading conditions. This formulation is based on the traditional energy and mass conservation relationships, together with appropriate constitutive equations (Pruess 1987 [DIRS 100684]; 1991 [DIRS 100413]). In addition to the formulations for UZ flow employed in TOUGH2 (LBNL 2003 [DIRS 161491]), the THC models rely on the equations describing aqueous and gaseous species advective and diffusive transport, and gas–water–mineral reactions via kinetic and equilibrium relations, as incorporated in TOUGHREACT V3.0 (LBNL 2002 [DIRS 161256]) and described in *Drift-Scale THC Seepage Model* (BSC 2005 [DIRS 172862]). The THM modeling relies on equations describing the mechanical stresses resulting from thermal expansion of rock mass, and the changes in fracture permeability resulting from changes in mechanical stress, as incorporated in FLAC3D (LBNL 2002 [DIRS 154783]) and TOUGH2 (LBNL 2003 [DIRS 161491]).

As indicated in the technical work plan (TWP), Level I or II validation is sufficient for the mountain-scale TH/THC/THM models (BSC 2005 [DIRS 174842], Section 2.2.1.1). During model development, confidence is established by adhering to sound, generally accepted scientific principles, and by justification of the use of input parameters as well as initial and boundary conditions. All input data are taken from the Technical Data Management System or

prescribed by planned repository operating conditions. Confidence in mountain-scale TH/THC/THM models is also gained during model development by examining model results for heat, mass, and force balance, and conformity with generally accepted physical principles of energy and mass transport. In addition, confidence in the mountain-scale TH/THC/THM models is gained by reviewing the validation of the corresponding drift-scale models. The mountain-scale TH/THC/THM models use the same conceptual models as those of the drift-scale TH/THC/THM models. Thus, since conceptual models supporting the drift-scale TH/THC/THM models are validated by comparison with measured data, the conceptual models underlying the mountain-scale TH/THC/THM models can be considered valid. Further confidence in validation of the mountain-scale TH/THC/THM models is provided by publications in refereed professional journals and through the use of natural analogues.

The limitations of the mountain-scale TH/THC/THM models are defined by the limitations of the underlying conceptual models and the associated assumptions listed in Section 5. For example, the mountain-scale TH/THC/THM models are deterministic continuum models that use only the mean values of hydrologic and thermal properties for each of the constituent stratigraphic units. However, as discussed in sections 6 and 7, these limitations do not affect the ability to use this model and corresponding analyses to evaluate the potential significance of features, events, and processes to performance assessment.

2. QUALITY ASSURANCE

This report has been developed in accordance with LP-SIII.10Q-BSC, *Models*, and with the modeling activities specified in *Technical Work Plan for: Near-Field Environment and Transport: Coupled Processes (Mountain-Scale TH/THC/THM, Drift-Scale THC Seepage, and Drift-Scale Abstraction) Model Report Integration* (BSC 2005 [DIRS 174842]). Approved QA procedures identified in the TWP (BSC 2005 [DIRS 174842], Section 4) have been used to conduct and document the activities described in this model report. Electronic management of information was evaluated in accordance with LP-SV.1Q-BSC, *Control of the Electronic Management of Information*, and controlled under YMP-LBNL-QIP-SV.0, *Management of YMP-LBNL Electronic Data*.

This report provides model predictions of repository thermal effects on mountain-scale TH, THC, and THM processes in the Yucca Mountain UZ (above and below the repository), which is a natural barrier and classified in *Q-List* (BSC 2005 [DIRS 174269], Table A-2) as "Safety Category" and "Important to Waste Isolation," as defined in AP-2.22Q, *Classification Analyses and Maintenance of the Q-List*. The present report contributes to the analysis of data used to support postclosure performance assessment; the conclusions do not directly impact engineered features important to preclosure safety, as defined in AP-2.22Q.

INTENTIONALLY LEFT BLANK

3. USE OF SOFTWARE

The software and routines used in this study are listed in Table 3-1. These are appropriate for the intended application, were obtained from Software Configuration Management, and were used only within the range of validation. These codes have been qualified in accordance with LP-SI.11Q-BSC, *Software Management.*

The TH aspects of the numerical simulations in this report were performed with the computer program TOUGH2 V1.6 (LBNL 2003 [DIRS 161491]), using equation-of-state module EOS3. The THC and THM simulations were carried out with TOUGHREACT V3.0 (LBNL 2002 [DIRS 161256]) and TOUGH2 V1.6 (LBNL 2003 [DIRS 161491])/FLAC3D V2.0 (LBNL 2002 [DIRS 154783]), respectively. To process the TOUGH2 V1.6 (LBNL 2003 [DIRS 161491]) and FLAC3D V2.0 (LBNL 2002 [DIRS 154783]) output for plotting, the codes EXT V1.0 (LBNL 1999 [DIRS 147562]) and EXT V1.1 (LBNL 1999 [DIRS 160768]), postprocessors for the TOUGH2 family of codes, were used. The software infil2grid V1.7 (LBNL 2002 [DIRS 154793]) was used to map the infiltration flux from the infiltration maps onto the numerical grid. The code WINGRIDDER V2.0 (LBNL 2002 [DIRS 154785]) was used to generate numerical grids. The code GridReader V1.0 (LBNL 2003 [DIRS 167237]) was used to convert the eight-character mesh files to five-character mesh files. All these codes have been qualified under LP-SI.11Q-BSC.

The documentation for the routines listed in Table 3-1 is provided in the Software Routine Reports submitted under the software tracking numbers (STNs) in Table 3-1. These were used for pre- and post-processing of files.

Standard, commercially available spreadsheet and graphics software programs (TecPLOT V8.0, TecPLOT V9.0, Grapher V1.25, and EXCEL 97 SR-1) were also used for post-processing simulation results in Sections 6.2, 6.3, 6.4, and 6.5. Details and procedures for using the standard functions of TecPLOT and EXCEL in postprocessing and simulation extraction for plotting are documented by Wang (2003 [DIRS 165927]), as well as in Appendix IV.

Input and output files for the model simulations documented in this report have been submitted to the Technical Data Management System (TDMS) as summarized in Table 8-1 and discussed under each modeled scenario in Section 6.

Table 3-1. Software Tracked by Software Configuration Management

Software Name / Version	STN	Platform / Operating System	Brief Description of Software (Range of Use / Selection / Limitations)
TOUGH2 V1.6 [DIRS 161491]	10007-1.6-01	Alpha system OSF1 V4.0	A general-purpose numerical simulator for nonisothermal, multiphase, multicomponent fluid flow in porous and fractured media. Selected for its capability to model effects of heat on flow in fractured media. Limitations are provided by definitions in the equations of state for thermodynamic properties of pure water, the physical domain of the model and the valid ranges of model parameters.
TOUGHREACT V3.0 [DIRS 161256]	10396-3.0-00	Alpha System OSF1 V5.1	TOUGHREACT V3.0 is used to calculate coupled thermal-hydrologic and chemical processes for kinetic and/or equilibrium mineral–water reactions and equilibrium gas–water reactions. TOUGHREACT applies to porous media in a temperature range limited by its thermodynamic database (currently 0 to 300°C).
FLAC3D V2.0 [DIRS 154783]	10502-2.0-00	PC Windows 98	A commercial numerical simulator designed for rock and soil mechanics with thermal-mechanical and hydrologic-mechanical interactions. Used for mechanical analysis and for linked TOUGH2 and FLAC3D coupled THM analysis.
EXT V1.1 [DIRS 160768]	10005-1.1-00	SUN Ultra-Sparc SunOS 5.5.1	The EXT code extracts data from TOUGH2 output files for plotting. The input and output formats must be standard TOUGH2 input and output formats, with eight-character element names TOUGH2 mesh.
EXT V1.0 [DIRS 147562]	10047-1.0-00	SUN Ultra-Sparc SunOS 5.5.1	The EXT code extracts data from TOUGH2 output files for plotting. The input and output formats must be standard TOUGH2 input and output formats, five-character element names TOUGH2 mesh.
Infil2grid V1.7 [DIRS 154793]	10077-1.7-00	PC MS-DOS V4.00.1111 under Windows 95	This software is used to extract surface infiltration rates to the top of TOUGH2 model grids. This routine is limited to eight-character element names TOUGH2 mesh.
WINGRIDDER V2.0 [DIRS 154785]	10024-2.0-00	PC Windows NT V4.0	A grid generator program used to produce 1-D, 2-D, or 3-D grids for numerical modeling of flow and transport problems based on the integral difference method. Output grid files are in the format compatible with TOUGH2. Inputs are distance, area, and volume that must be non-negative.

Table 3-1. Software Tracked by Software Configuration Management (Continued)

Software Name / Version	STN	Platform / Operating System	Brief Description of Software (Range of Use / Selection / Limitations)
GridReader V1.0 [DIRS 167237]	10994-1.0-00	PC Windows NT V4.0	Gridreader V1.0 is a package of utility tools used to 1) read a grid generated by WinGridder V2.0 and write a mesh input file for TOUGH2 with high precision x-, y-, and z-coordinates; 2) convert a TOUGH2 mesh file with 8-character cell names into a TOUGH2 mesh file with 5-character cell names. This software is to be used only with the TOUGH2 family of codes.
Gpzones.dat V1.0 [DIRS 154792]	10509-1.0-00	PC Windows 98	The software is used to find out which zones are connected to each grid point and how much zone volumes are connected to each grid point, and to calculate the interpolation of temperatures from TOUGH2 nodes to FLAC3D nodes. This routine is a FISH routine that can only be used for FLAC3D V2.0 or higher.
Tin V1.1 [DIRS 162038]	10889-1.1-00	PC Windows 98	This software takes temperature output from TOUGH2 and interpolates it into FLAC3D for coupled THM simulations. Used to transfer temperatures from TOUGH2 Version1.6 to FLAC3D Version 2.0 during linked TOUGH2 and FLAC3D coupled THM analyses.
Delb.dat V1.0 [DIRS 154791]	10507-1.0-00	PC Windows 98	This code is used to calculate changes in fracture aperture for linked TOUGH2 and FLAC3D coupled THM analyses. This software is tested for normal stress ranging from +10 MPa to –100 MPa.
2KGRIDV1.F V1.0 [DIRS 147553]	10244-1.0-00	SUN Ultra-Sparc SunOS 5.5.1	This software is used to process data for TOUGH2 modeling of Yucca Mountain. The use of this software is limited to the size of primary grids and conventions used in YMP hydrogeological units/layers.
2kgridv1a.f V1.0 [DIRS 153067]	10382-1.0-00	PC DOS emulation	This code is used to generate 2K grids for the TOUGH2 family of codes. The use of this software is limited to the size of primary grids and conventions used in YMP hydrogeological units/layers.
gen_incon-v0.f V1.0 [DIRS 147023]	10220-1.0-00	DEC Alpha OSF1 V4.0	This software is used to calculate top and bottom boundary temperatures and the initial block “INCON” for starting a TOUGH2 simulation. This software only processes valid “ELEME” block input format for the TOUGH2 family of codes.
get_a_layer_v0.f V1.0 [DIRS 147025]	10221-1.0-00	DEC Alpha OSF1 V4.0	This software is used to extract data of a given list of elements from TOUGH2 outputs for plotting. This software only processes valid “ELEME” block input format for the TOUGH2 family of codes and valid EOS3 TOUGH2 V1.4 output file formats.

Table 3-1. Software Tracked by Software Configuration Management (Continued)

Software Name / Version	STN	Platform / Operating System	Brief Description of Software (Range of Use / Selection / Limitations)
get_temp_v0.f V1.0 [DIRS 147027]	10222-1.0-00	DEC Alpha OSF1 V4.0	This software is used to search for the nearest tabulated value of temperature to assign bottom boundary conditions. The coordinates x, y and temperature (T) are within real range.
toptemp_v0.f V1.0 [DIRS 147030]	10224-1.0-00	DEC Alpha OSF1 V4.0	This software is used to generate top temperature boundary conditions. All valid "ELEME" range of TOUGH2 input, real range of elevation, and average temperature on the Yucca Mountain surface.
hsource_v0.f V1.0 [DIRS 147031]	10225-1.0-00	DEC Alpha OSF1 V4.0	This software is used to generate thermal GENER terms for TOUGH2 input files. All valid "ELEME" range of TOUGH2 input, the valid range of time (>0 years), and the valid decay value (>0).
2kgrid8.for V1.0 [DIRS 154787]	10503-1.0-00	PC MS-DOS V4.00.1111 under Windows 95	This software is used to generate dual permeability meshes for the TOUGH2 family of codes. This software is limited to eight-character element names for the TOUGH2 family of codes.

4. INPUTS

4.1 DIRECT INPUT

Input data and parameters used in TH/THC/THM model development are listed in Table 4.1-1 and include the parameters discussed below. The THC and THM models require all of the same inputs as the TH model, plus the additional inputs listed for each individual model.

All Mountain-Scale TH/THC/THM Models

- Fracture properties (frequency, permeability, van Genuchten α and m parameters, porosity, and interface area) for each UZ model layer
- Matrix properties (porosity, permeability, van Genuchten α and m) for each UZ model layer
- Thermal properties (grain density, wet and dry thermal conductivity, and grain specific heat) for each model layer
- Fault properties (matrix and fracture) for each hydrogeologic unit
- Repository thermal-load and ventilation efficiency
- Infiltration maps for present and future climates
- Numerical model grids.

THC Model

- Mineralogy (volume fractions and reactive surface areas in each layer)
- Water and gas chemistry (initial and boundary)
- Thermodynamic and kinetic data for mineral–water–gas reactions
- Transport properties for aqueous and gaseous species
- Fracture aperture and spacing for calculating changes to fracture permeability.

THM Model

- Mechanical properties (bulk modulus and shear modulus)
- Thermal-mechanical (TM) properties (thermal expansion coefficient)
- Hydrologic-mechanical (HM) properties (parameters for the stress dependency of hydraulic properties).

Specific input data sets and associated data tracking numbers (DTNs) are provided in Table 4.1-1. Complete references are also presented in Section 9.3. The following discusses the direct inputs summarized in Table 4.1-1.

The data listed in Table 4.1-1 are appropriate for this study because they represent fracture, matrix, and thermal properties calibrated for the coupled process TH/THC/THM models at Yucca Mountain. The technical product outputs listed in Table 4.1-1 are also appropriate for this study because they represent the planned operating conditions (repository thermal load) and the calculated efficiency of planned ventilation. The appropriateness of the data for use in model development is also discussed in Section 6.

4.1.1 Net Infiltration

The mountain-scale coupled processes models (TH/THC/THM) require as input the net infiltration of water at the ground surface. The information contained in DTN: GS000308311221.005 [DIRS 147613] presents the results of analysis that accounts for the various components of water flow (precipitation, surface runoff, evapotranspiration, etc.) for the hydrologic cycle at Yucca Mountain. The files used are *modernm.dat*, *monsoonm.dat* and *glacialm.dat* in the System Performance Assessment database in the TDMS. The development of these inputs is described in detail in *Simulation of Net Infiltration for Modern and Potential Future Climates* (BSC 2004 [DIRS 170007], Section 6.3.2). DTN: GS000308311221.005 [DIRS 147613] contains nine files that correspond to the three climates (modern, monsoon, and glacial) and the lower, mean, and upper percolation cases. Each input file contains the coordinates of sampling points based on the Universal Transverse Mercator (UTM) projection (zone 11, NAD27) (BSC 2004 [DIRS 170007], Section 6.3.2), with the various components of flow identified. In particular, the net infiltration along each column was used to assign net infiltration at the top boundary of the mountain-scale coupled processes model and is a location-specific distribution for this model domain, as discussed in Section 6.4.2.3. As discussed in Section 6.1.4, the data are also used to develop in plan view the spatial distribution for the three mean infiltration maps superimposed onto the grid blocks for the model presented in Figures 6.1.3 through 6.1.5. These figures, and the calculation of mean values for net infiltration for the three climates, are presented in Section 6.1.4.

4.1.2 Calibrated Three-Dimensional Hydrologic Properties

The models require the calibrated three-dimensional hydrologic properties for the welded and nonwelded tuffs above and below the repository horizon. These units are modeled as dual continuum media with fracture and matrix continua. The hydrologic properties for the various repository units are presented in DTN: LB03013DSSCP3I.001 [DIRS 162379]. As discussed in *UZ Flow Model and Submodels* (BSC 2004 [DIRS 169861], Section 6.1.2), the properties include:

- Fracture properties (frequency, permeability, van Genuchten α and m parameters, porosity, and interface area per unit volume rock) for each UZ model layer
- Matrix properties (porosity, permeability, and the van Genuchten α and m parameters) for each UZ model layer.

The calibrated parameter sets also include an estimate for each model layer of the active-fracture parameter, γ, which accounts for the reduction in interaction between matrix and fracture flow resulting from flow fingering and channelization (Liu et al. 1998 [DIRS 105729]). Note that the

properties developed by inverse modeling are specific to climate and the lower, mean, and upper net infiltration cases. These properties are discussed in more detail in Section 6.1.2.

4.1.3 Thermal Properties for Model Layers

The model requires thermal properties for the model units. The thermal properties required are the matrix thermal conductivity under dry and wet (saturated) conditions, the grain density, the specific heat capacity, and the lithophysal porosity. These properties are obtained from DTN: LB0210THRMLPRP.001 [DIRS 160799].

Note that since the time of the original analysis, an updated data set that includes modifications to the thermal properties became available, i.e., DTN: LB0402THRMLPRP.001 [DIRS 168481]. However, the property values from DTN: LB0210THRMLPRP.001 [DIRS 160799] are judged as justified for their intended use in the mountain-scale models based on analyses conducted in Appendices V, VI, and VII. Additional simulation runs were conducted to determine the impact of the new data set on TH, THC, and THM results. Section 6.1.6 presents more information on the use of these properties. A more detailed description of thermal properties can be found in *Drift-Scale Coupled Process (DST and TH Seepage) Models* (BSC 2005 [DIRS 172232], Appendix F).

4.1.4 Ventilation Efficiency

The current repository design includes a preclosure period of 50 years in which ventilation in the emplacement drifts removes a significant amount of heat.

The integrated ventilation efficiency provided by current Yucca Mountain Project (YMP) reports is 88% (DTN: MO0307MWDAC8MV.000 [DIRS 165395]; BSC 2004 [DIRS 169862], Table 8-2) when the emplacement drift is 600 m in length. When the emplacement drift is 800-m long, integrated ventilation efficiency is calculated to be 86% (DTN: MO0307MWDAC8MV.000 [DIRS 165395]; BSC 2004 [DIRS 169862], Table 8-2). For further details on how these ventilation efficiencies are calculated, refer to calculations in *Ventilation Model and Analysis Report* (BSC 2004 [DIRS 169862], Section 6.3). Uncertainties in calculated integrated ventilation efficiencies have also been reported (BSC 2004 [DIRS 169862], Section 6.11, Table 6-10). The standard deviation (σ) of the calculated ventilation efficiency is 3% for both 600-m and 800-m-long drifts (BSC 2004 [DIRS 169862], Table 8-2). Thus, using $\pm 1\sigma$, the ventilation efficiency ranges from 85 to 91% for a 600-m-long drift. For 800 m long drifts, the $\pm 1\sigma$ range of ventilation efficiency is 83 to 89%.

The value 86.3% for ventilation efficiency, originally reported in *Ventilation Model* (BSC 2002 [DIRS 160975], Table 6-6), has been used to represent the percentage of the time-varying line load that is effectively removed from the repository. This ventilation efficiency value, which was the best estimate available at the time that the majority of the analysis in this report was conducted, is adequate for use in this report by corroboration with the more recent, qualified data presented in the previous paragraph, in accordance with the data qualification plan included in *Drift Scale Coupled Process (DST and TH Seepage) Models* (BSC 2005 [DIRS 172232], Appendix H). This value is almost in the middle of the current calculated ranges of ventilation

efficiency values presented above. Therefore, the use of the older value in the modeling is justified.

4.1.5 Repository Thermal Load and Decay Data

The average thermal line load is 1.45 kW/m (BSC 2004 [DIRS 168489]). This value refers to the initial thermal line load that decreases with time as a result of radioactive decay. The time-dependent thermal-line-load values used in the present report were derived from *Repository Design, Repository/PA IED Subsurface Facilities Plan Sht. 5 of 5* (BSC 2002 [DIRS 159527]).

These sources have been superseded by more current design documents. The line-averaged loading as a function of time for the current repository design is presented in *IED Waste Package Decay Heat Generation [Sheet 1 of 1]* (BSC 2005 [DIRS 173705]). The average line load of 1.45 kW/m has not changed. The two decay curves are within 1% of each other and the heat output is slightly greater in the earlier repository design drawing (BSC 2002 [DIRS 159527]) than in the later one (BSC 2005 [DIRS 173705]). Use of the older decay curve is justified because it is similar to the newer curve and yields higher thermal loads. These inputs are discussed in Sections 6.1.5 and 6.5.6 for the TH and the THM calculations, respectively.

4.1.6 Rock and Fracture Properties for Model Layers

Hydrologic properties (such as permeability, van Genuchten parameters, residual saturation for both the fractures and the matrix, and the active fracture parameter for the fractures) used in the drift-scale THM model are excerpted from the UZ drift-scale calibrated property set for the mean infiltration scenario (DTN: LB0208UZDSCPMI.002 [DIRS 161243]). The approach and method adopted in developing these properties can be found in *Calibrated Properties Model* (BSC 2004 [DIRS 169857], Section 6.3.2). Other sources used for hydrologic, thermal, and mechanical properties are consistent with current UZ analyses and analyses of coupled processes. This includes other hydrologic properties such as fracture porosity, frequency, aperture, and interface areas obtained from DTN: LB0205REVUZPRP.001 [DIRS 159525].

The mountain-scale THM model uses fracture spacing in the development of the FLAC3D (LBNL 2002 [DIRS 154783]) model presented subsequently in Section 6.5.5. This fracture spacing is obtained from DTN: LB0205REVUZPRP.001 [DIRS 159525] for the main repository horizon for units Tptpmn and Tptpll.

4.1.7 Three-Dimensional Thermal Model Grid with Repository Layout

The direct input to the mountain-scale coupled processes model includes the repository footprint as contained in DTN: LB0303THERMESH.001 [DIRS 165168]. The basis for the repository footprint is found in the drawing entitled *D&E/RIT IED Subsurface Facilities [Sheet 1 of 4]* (BSC 2004 [DIRS 172801]). This drawing contains a table of repository drift-coordinate starting and ending points (BSC 2004 [DIRS 172801], Table 2). The information in DTN: LB0303THERMESH.001 [DIRS 165168] adequately represents the current repository footprint and the repository layout by capturing the repository drift-coordinate starting and ending points in the model.

Other repository design information used in the model includes the drift spacing of 81 m and the repository emplacement drift diameter of 5.5 meters (see Table 4.1-1), which are obtained from *Subsurface Facility Description Document* (BSC 2005 [DIRS 174514], Section 4.1.1.2). This repository layout information is used in Section 6.1.1.

4.1.8 Boundary and Initial Conditions

The temperature boundary and initial temperatures are required model inputs for the TH, THC, and THM coupled-process models. The ambient TH model also provides a database for an estimate of water table temperatures. These temperatures are compiled in DTN: LB0303THERMSIM.001 [DIRS 165167]. The data are technical product output from *UZ Flow Models and Submodels* (BSC 2004 [DIRS 169861]). The three-dimensional ambient thermal model was calibrated against qualified temperature data measured from five boreholes, using the base-case present-day infiltration parameter set with a three-dimensional dual-permeability thermal grid. Simulated temperature results are in good agreement with the observed temperature profiles from the boreholes. The temperature boundary conditions are discussed in Section 6.1.3.

4.1.9 Vertical Geological Layering

The two-dimensional TH and THC cross-section models were developed using the geological framework model (GFM) (DTN: MO0012MWDGFM02.002 [DIRS 153777]), as discussed in Section 6.1.1. The report *UZ Flow Models and Submodels* (BSC 2004 [DIRS 169861]) developed a north–south cross section that provides the vertical geological layering for the models (DTN: LB030432DGRIDS.001 [DIRS 163937]). The THM model uses geological input from a column at the center of the TH north–south cross section, as described in Section 6.5.6.

4.1.10 Rock Mass Properties

The THM model requires the rock mass deformation modulus that accounts for both intact rock properties, and the properties of fractures. These geotechnical properties are obtained from DTNs: LB0306DRSCLTHM.001 [DIRS 169733] and SNL02030193001.026 [DIRS 108436]. The mechanical rock mass properties used in the THM model are discussed in Section 6.5.8. Mountain-scale properties for rock-mass stress-permeability relationship and rock-mass thermal expansion coefficient are developed in this report according to Section 6.5.9. The input sources for the maximum joint closure and drift-scale exponent α documented in *Drift-Scale THM Model* (BSC 2004 [DIRS 169864], Table 6.4.5-1) are traceable to direct inputs described in Section 4.1 of that report. The maximum joint closure and drift-scale exponent α for Equation 6.2-9 in *Drift-Scale THM Model* (BSC 2004 [DIRS 169864]) was developed by model calibration against field experiments as shown in Figure 6.4.4-2 of that report. The figure is based on input data described in Table 4.1-1b in *Drift-Scale THM Model* (BSC 2004 [DIRS 169864]).

4.1.11 Thermodynamic Data

Thermodynamic data to perform the THC calculations in this report were taken from DTN: LB0307THMDBRTM.001 [DIRS 164434]. Most of these data are originally from the

thermodynamic database *data0.ymp.R2* (DTN: MO0302SPATHDYN.000 [DIRS 161756]). Documentation of changes from the *data0.ymp.R2* database is provided in *Drift-Scale THC Seepage Model* (BSC 2005 [DIRS 172862], Section 4.1.4). The most important changes from the data taken from *data0.ymp.R2* (DTN: MO0302SPATHDYN.000 [DIRS 161756]) are:

- Aluminum aqueous species data.
- Revised aqueous silica thermodynamic properties.
- Solubility constants for albite and anorthite.
- Solubility constants for K-feldspar. Without this adjustment, calculated potassium concentrations in pore waters are too small compared to actual measurements.
- Revised clay (smectite and illite) data. Without this revision, the calculated pH of pore waters through time, under ambient conditions (no thermal load), becomes unrealistically elevated (BSC 2005 [DIRS 172862], Section 6.5.5.2.1).
- Revised zeolite (stellerite, heulandite, mordenite, and clinoptilolite) data. Without this revision, an unrealistic calcium depletion is predicted to occur in pore waters under ambient conditions (no thermal load), due to the precipitation of large amounts of calcium zeolites (BSC 2005 [DIRS 172862], Section 6.5.5.2.1).

Of these changes, the last two have the most significant effect on simulation results compared to results obtained using the project database (DTN: MO0302SPATHDYN.000 [DIRS 161756]). The stellerite thermodynamic data in *data0.ymp.R2* reflect a significantly higher stability for this mineral than the new data. The clay data in the database also reflect a greater stability than the revised data used here. The justification for use of these data is provided in the documentation accompanying the DTN and in *Drift-Scale THC Seepage Model* (BSC 2005 [DIRS 172862], Sections 6.4.8 and 6.5.5.4), which provides the basis for identical application of the data in this report

4.1.12 Kinetic Data

Kinetic data refer to the reaction rate constants (k_o), activation energies (E_a), and related data required to describe the rates of dissolution and precipitation of minerals as a function of temperatures and fluid chemistry. Reaction rate laws can take numerous forms, of which a restricted number are used for the model analyses. Model simulations were conducted using the kinetic data from DTN: LB0307KNTDBRTM.001 [DIRS 164433]. The qualification of this kinetic data DTN is documented in *Drift-Scale THC Seepage Model* (BSC 2005 [DIRS 172862], Appendix H), which provides the basis for identical application of these data in this report.

4.1.13 Geochemical Data

Geochemical data used to develop the THC model include the initial mineral abundances assigned to each hydrogeologic unit by the Yucca Mountain 3-D Mineralogic Model V3.0 (DTN: LA9908JC831321.001 [DIRS 113495]). Fracture mineralogy data are derived from

DTNs: LA9912SL831151.001 [DIRS 146447] and LA9912SL831151.002 [DIRS 146449]. These data were used to calculate initial mineral volume fractions and reactive surface areas for mineral phases (Section 6.4.2.4, Appendices I and II). Initial pore water and gas composition for the middle non-lithophysal unit of the Topopah Spring Tuff was selected for use in the model, using DTN: MO0005PORWATER.000 [DIRS 150930]. Average values calculated from DTN: MO0005PORWATER.000 [DIRS 150930] were used for initial pore-water and gas composition presented in *Drift-Scale THC Seepage Model* (BSC 2005 [DIRS 172862], Table 6.2-1). These values are based upon the average of two pore water samples, ESF-HD-PERM-2 (depths of 30.1 – 30.5 feet) and ESF-HD-PERM-2 (depths of 34.8 – 35.1 ft), from DTN: MO0005PORWATER.000 [DIRS 150930]. The source groundwater compositions are direct input to *Drift-Scale THC Seepage Model* (BSC 2005 [DIRS 172862], Table 4.1-1.) and therefore Table 6.2-1 of that report is qualified as a source in this report. The data from DTN: MO0005PORWATER.000 [DIRS 150930] and the calculated averages are used as direct input to the THC model.

4.1.14 Temperature Data

Temperatures at the top layer of the TH model are controlled mainly by atmospheric temperatures. These data were derived from measured near-surface temperatures in boreholes USW NRG-6 and USW NRG-7 (DTNs: GS960308312232.001 [DIRS 105573], GS951108312232.008 [DIRS 106756], and GS950208312232.003 [DIRS 105572]), which include several years of continuous temperature monitoring data. A dry adiabatic atmospheric lapse rate of 0.01°C/m (Driscoll 1986 [DIRS 116801], p. 50) was used to adjust the average measured temperatures to any elevation of the model. There are two lapse rates, the dry adiabatic lapse rate as noted here and the wet adiabatic lapse rate of 0.006°C/m (Driscoll 1986 [DIRS 116801], p. 50). The lapse rate is given by White (1986 [DIRS 111015], p. 60, Equation 2.26) as 0.0065°C/m. The value is said to be determined "by international agreement," and is based on the U.S. Standard Atmosphere. Driscoll (1986 [DIRS 116801], p. 50) explains why the dry adiabatic lapse rate is greater than the wet adiabatic lapse rate. Therefore, the value of 0.01°C/m for the dry adiabatic lapse rate being greater than the value of the wet adiabatic lapse rate is thus corroborated and reasonable. These data were utilized in Section 6.1.3 to set boundary conditions.

Table 4.1-1. Input Data and Design Parameter Source and Data Tracking Numbers

Input Source	Data Description	Used in	Comments
INPUT FOR ALL MOUNTAIN-SCALE TH/THC/THM MODELS			
DTN: LB0303THERMESH.001 [DIRS 165168]	Three-dimensional thermal model grid, repository layout	Section 6.1.1, Figure 6.1-1	Three-dimensional thermal model mesh as presented in files *mesh_th.v1* and *mesh_th.vf*
DTN: MO0012MWDGFM02.002 [DIRS 153777]	Geologic model used for developing the two-dimensional TH model	Section 6.1.1	Geologic framework model (GFM 2000) used for developing the TH models
DTN: LB0205REVUZPRP.001 [DIRS 159525]	Fracture properties for model layers	Sections 6.4.2.2, 6.5.5	Fracture properties (aperture, frequency parameters, van Genuchten parameters, permeability, interface area, porosity) in spreadsheet *FRACTURE_PROPERTY.xls*
DTN: LB0208UZDSCPMI.002 [DIRS 161243]	Calibrated fracture and matrix properties sets for mean infiltration	Section 6.4.2.2	Properties used include permeability porosity, residual saturation and van Genuchten's alpha and m contained in spreadsheet *Drift-scale calibrated properties for mean infiltration2.xls*.
DTN: LB03013DSSCP3I.001 [DIRS 162379]	Calibrated three-dimensional hydrologic properties	Section 6.1.6; Table 6.5.9-1	Data used are the calibrated parameters for the mean infiltration scenario as presented in file *props_3d.doc*.
DTN: LB0210THRMLPRP.001 [DIRS 160799]	Thermal properties for model layers	Sections 6.1.6, 6.4.2.2	Density, specific heat, wet and dry thermal conductivities for the UZ model layers contained in spreadsheet *Therm_Prop_Model_layers.xls*
BSC 2004 [DIRS 168489]	Average initial thermal line load	Section 6.1.5; Table 6.5.6-1	Table 1, average thermal line load of 1.45 kW/m used in TH models
BSC 2002 [DIRS 159527]	Time-dependent thermal line load	Section 6.1.5; Table 6.5.6-1	Sheet 5, thermal decay function over 10,000-year compliance period used in TH models
BSC 2005 [DIRS 174514]	Spacing of 81 m between repository drifts, and drift diameter of 5.5 m	Section 6.1.1	Section 4.1.1.2, drift spacing (81 m) and diameter (5.5 m) used to develop numerical grids
BSC 2004 [DIRS 169862], Table 8-2	Ventilation efficiency	Section 6.1.5	Overall ventilation heat removal efficiency for a location 600 m from the drift entrance for 50-year ventilation duration
DTN: GS000308311221.005 [DIRS 147613]	Net infiltration maps–mean, upper, and lower boundaries	Sections 6.1.4, 6.4.2.3; Figures 6.1-3, 6.1-4, 6.1-5; Table 6.1-2	Data used are the mean infiltration grid maps for the present day/modern, monsoon, and glacial transition climate scenarios. The files used are *modernm.dat*, *monsoonm.dat* and *glacialm.dat*.

Table 4.1-1. Input Data and Design Parameter Source and Data Tracking Numbers (Continued)

Input Source	Data Description	Used in	Comments
DTN: LB0303THERMSIM.001 [DIRS 165167]	Boundary and initial conditions, water table temperatures	Section 6.1.3	3-D UZ temperature distribution modeling calibrated with temperature measurement data contained in file *th_pqm_keni.out_2_20_03*
DTN: GS960308312232.001 [DIRS 105573]	Annual average temperatures	Section 6.1.3	Near-surface temperatures measured in boreholes at Yucca Mountain
DTN: GS951108312232.008 [DIRS 106756]	Annual average temperatures	Section 6.1.3	Near-surface temperatures measured in boreholes at Yucca Mountain
DTN: GS950208312232.003 [DIRS 105572]	Annual average temperatures	Section 6.1.3	Near-surface temperatures measured in boreholes at Yucca Mountain
Driscoll 1986 [DIRS 116801]	Lapse Rate .01°C/m	Section 6.1.3	The dry adiabatic lapse rate is approximately 0.01°C/m for atmosphere above the model domain.
INPUT FOR MOUNTAIN-SCALE THC MODELS			
DTN: LA9908JC831321.001 [DIRS 113495]	Model input and output files for Mineralogical Model "MM3.0" Version 3.0.	Section 6.4.2.4	Data from 3-D mineralogical model
DTN: LA9912SL831151.001 [DIRS 146447]	Drift Scale Test and Single Heater Test fracture description	Section 6.4.2.4	Fracture Attitude data of drill core samples from ESF-HD-TEMP-2, table S00013_001
DTN: LA9912SL831151.002 [DIRS 146449]	Drift Scale Test and Single Heater Test fracture mineralogy	Section 6.4.2.4	Mineral and oxide abundance data
DTN: MO0005PORWATER.000 [DIRS 150930]	Tptpmn pore-water analyses	Section 6.4.2.4; Table 6.4-2	Tptpmn pore-water analyses for boreholes ESF-HD-PERM-2 (30.1'-30.5') and ESF HD-PERM-3 (34.8'-35.1')
BSC 2005 [DIRS 172862], Table 6.2-1	Initial pore-water compositions for selected components	Table 6.4-2	Calculated values for HCO_3^-, Al^{3+}, Fe^{3+}, log (pCO_2)
DTN: LB0307KNTDBRTM.001 [DIRS 164433]	Kinetic data	Section 6.4.2.4	Kinetic data for reactive transport modeling contained in file *kinetic_data_table.doc*
DTN: LB0307THMDBRTM.001 [DIRS 164434]	Thermodynamic data	Section 6.4.2.4	Chemical thermodynamic data adjusted from values taken from *data0.ymp.R2* database

Table 4.1-1. Input Data and Design Parameter Source and Data Tracking Numbers (Continued)

Input Source	Data Description	Used in	Comments
INPUT FOR MOUNTAIN-SCALE THM MODELS			
DTN: LB030432DGRIDS.001 [DIRS 163937]	Vertical geological layering; temperature, pressure, saturation at top and bottom boundaries for THM model	Section 6.5.6; Table 6.5.6-1	North-South Cross Section, file *NS_TH.tar.gz*
DTN: LB0306DRSCLTHM.001 [DIRS 169733]	Mechanical rock-mass properties	Sections 6.5.6, 6.5.8	Overburden saturated bulk rock density = 2200 kg/m^3. TSw2 Young's Modulus = 14.77 GPa, TSw2 Poisson's Ratio = 0.21
DTN: SNL02030193001.026 [DIRS 108436]	Mechanical rock-mass properties	Section 6.5.8	CHn Young's Modulus = 5.63 GPa, CHn Poisson's Ratio = 0.17 (both based on mean of 3 values in SEP Table S99119_002)
BSC 2004 [DIRS 169864], Figure 6.4.3-1	Thermal expansion coefficient	Section 6.5.9; Equation 6.5.9-1	$\alpha_T = 5 + 0.0583 \cdot T$ (10^{-6}/°C)
BSC 2002 [DIRS 159527]	Thermal decay data used to construct THM model	Section 6.1.5; Table 6.5.6-1	Sheet 5 of 5
BSC 2004 [DIRS 169864], Table 6.4.5-1	Drift-scale maximum joint closure, and drift scale exponent a	Table 6.5.9-1	Hydrologic-mechanical properties

4.2 CRITERIA

Technical requirements to be satisfied by performance assessment are based on 10 CFR 63.114 [DIRS 173273], "Requirements for Performance Assessment." These technical requirements are also identified in *Project Requirements Document* (Canori and Leitner 2003 [DIRS 166275]). The acceptance criteria that will be used by the Nuclear Regulatory Commission to determine whether the technical requirements have been met are identified in *Yucca Mountain Review Plan, Final Report* (YMRP) (NRC 2003 [DIRS 163274]). The pertinent requirements and acceptance criteria for this report are summarized in Table 4.2-1.

Table 4.2-1. Project Requirements and YMRP Acceptance Criteria Applicable to This Report

Requirement Number	Requirement Title	10 CFR 63 Link	YMRP Acceptance Criteria
PRD-002/T-015	Requirements for Performance Assessment (from Canori and Leitner 2003 [DIRS 166275])	10 CFR 63.114 (a-c) [DIRS 173273]	Criteria 1 to 5 for *Flow Paths in the Unsaturated Zone* (from NRC 2003 [DIRS 163274], Section 2.2.1.3.6.3)

The acceptance criteria identified in Section 2.2.1.3.6.3 of the YMRP (NRC 2003 [DIRS 163274]) are given below. A description of their applicability to this report is found in Section 8.6.

- Acceptance Criterion 1, *System Description and Model Integration Are Adequate.*

  (1) The total system performance assessment adequately incorporates, or bounds, important design features, physical phenomena, and couplings, and uses consistent and appropriate assumptions throughout the flow paths in the unsaturated zone abstraction process. Couplings include thermal-hydrologic-mechanical-chemical effects, as appropriate;

  (2) The aspects of geology, hydrology, geochemistry, physical phenomena, and couplings that may affect flow paths in the unsaturated zone are adequately considered. Conditions and assumptions in the abstraction of flow paths in the unsaturated zone are readily identified and consistent with the body of data presented in the description;

  (3) The abstraction of flow paths in the unsaturated zone uses assumptions, technical bases, data, and models that are appropriate and consistent with other related U.S. Department of Energy abstractions. For example, the assumptions used for flow paths in the unsaturated zone are consistent with the abstractions of quantity and chemistry of water contacting waste packages and waste forms, climate and infiltration, and flow paths in the saturated zone (Sections 2.2.1.3.3, 2.2.1.3.5, and 2.2.1.3.8 of the Yucca Mountain Review Plan, respectively). The descriptions and technical bases are transparent and traceable to site and design data;

(4) The bases and justification for modeling assumptions and approximations of radionuclide transport in the unsaturated zone are consistent with those used in model abstractions for flow paths in the unsaturated zone and thermal-hydrologic-mechanical-chemical effects;

(5) Sufficient data and technical bases to assess the degree to which features, events, and processes have been included in this abstraction are provided;

(6) Adequate spatial and temporal variability of model parameters and boundary conditions are employed in process-level models to estimate flow paths in the unsaturated zone, percolation flux, and seepage flux;

(7) Average parameter estimates used in process-level models are representative of the temporal and spatial discretizations considered in the model;

(8) Reduction in unsaturated zone transport distances, after a climate-induced water table rise, is considered; and

(9) Guidance in NUREG–1297 [Altman et al. 1988 DIRS 103597] and NUREG–1298 [Altman et al. 1988 DIRS 103750], or other acceptable approaches for peer review and data qualification, is followed.

- Acceptance Criterion 2, *Data Are Sufficient for Model Justification.*

(1) Hydrologic and thermal-hydrologic-mechanical-chemical values used in the license application are adequately justified. Adequate descriptions of how the data were used, interpreted, and appropriately synthesized into the parameters are provided;

(2) The data on the geology, hydrology, and geochemistry of the unsaturated zone, are collected using acceptable techniques;

(3) Estimates of deep-percolation flux rates constitute an upper bound, or are based on a technically defensible unsaturated zone flow model that reasonably represents the physical system. The flow model is calibrated, using site-specific hydrologic, geologic, and geochemical data. Deep-percolation flux is estimated, using the appropriate spatial and temporal variability of model parameters, and boundary conditions that consider climate-induced change in soil depths and vegetation;

(4) Appropriate thermal-hydrologic tests are designed and conducted, so that critical thermal-hydrologic processes can be observed, and values for relevant parameters estimated;

(5) Sensitivity or uncertainty analyses are performed to assess data sufficiency, and verify the possible need for additional data;

(6) Accepted and well-documented procedures are used to construct and calibrate numerical models;

(7) Reasonably complete process-level conceptual and mathematical models are used in the analyses. In particular: (i) mathematical models are provided that are consistent with conceptual models and site characteristics; and (ii) the robustness of results from different mathematical models is compared; and

(8) Any expert elicitation conducted is in accordance with NUREG–1563 (Kotra et al. 1996 [DIRS 100909]), or other acceptable approaches.

- Acceptance Criterion 3, *Data Uncertainty Is Characterized and Propagated Through the Model Abstraction*.

(1) Models use parameter values, assumed ranges, probability distributions, and bounding assumptions that are technically defensible, reasonably account for uncertainties and variabilities, and do not result in an under-representation of the risk estimate;

(2) The technical bases for the parameter values used in this abstraction are provided;

(3) Possible statistical correlations are established between parameters in this abstraction. An adequate technical basis or bounding argument is provided for neglected correlations;

(4) The initial conditions, boundary conditions, and computational domain used in sensitivity analyses and/or similar analyses are consistent with available data. Parameter values are consistent with the initial and boundary conditions and the assumptions of the conceptual models for the Yucca Mountain site;

(5) Coupled processes are adequately represented; and

(6) Uncertainties in the characteristics of the natural system and engineered materials are considered.

- Acceptance Criterion 4, *Model Uncertainty Is Characterized and Propagated Through the Model Abstraction.*

(1) Alternative modeling approaches of features, events, and processes, consistent with available data and current scientific understanding, are investigated. The results and limitations are appropriately considered in the abstraction;

(2) The bounds of uncertainty created by the process-level models are considered in this abstraction; and

(3) Consideration of conceptual model uncertainty is consistent with available site characterization data, laboratory experiments, field measurements, natural analogue information and process-level modeling studies; and the treatment of conceptual model uncertainty does not result in an under-representation of the risk estimate.

- Acceptance Criterion 5, *Model Abstraction Output Is Supported by Objective Comparisons*.

  (1) The models implemented in this total system performance assessment abstraction provide results consistent with output from detailed process-level models and/or empirical observations (laboratory and field testing and/or natural analogues);

  (2) Abstractions of process-level models conservatively bound process-level predictions; and

  (3) Comparisons are provided of output of abstracted model of flow paths in the unsaturated zone with outputs of sensitivity studies, detailed process-level models, natural analogues, and empirical observations, as appropriate.

4.3 CODES, STANDARDS, AND REGULATIONS

No codes, standards, or regulations other than those identified in Section 4.2 apply to this modeling activity.

5. ASSUMPTIONS

This section presents the rationale and justification for assumptions, discusses whether further confirmation is needed, and references the sections in the report where these assumptions are used. Modeling approaches, approximations, and idealizations that form part of the models are documented in the respective model development sections: Sections 6.1 through 6.3 for the TH models, Section 6.4 for the THC model, and Section 6.5 for the THM model.

5.1 ASSUMPTIONS FOR THE MOUNTAIN-SCALE TH MODEL

TH model assumptions are listed below. Modeling approaches, approximations, and idealizations that form part of the TH model are documented in Section 6.1.

TH model assumptions:

1. In the mountain-scale TH model, perched-water effects are ignored.

   Basis: The occurrence of perched water and its effects on the UZ flow fields are discussed in *UZ Flow Models and Submodels* (BSC 2004 [DIRS 169861]). Perched-water conditions are confined mainly to the lower units of the Topopah Spring welded (TSw) hydrogeological unit and on top of the Calico Hills nonwelded unit (CHn). Over the repository domain, perched water locations are typically 100 to 150 m below the repository horizon (Wu et al. 1999 [DIRS 117167]). The dominant heat-transfer mechanism at perched locations is heat conduction because boiling conditions that could lead to large-scale mobilization of perched water are not attained. Therefore, the effect of repository thermal load on perched-water bodies is ignored. This assumption is considered adequate and requires no further justification or confirmation.

2. An equivalent heat load is evenly distributed within emplacement drifts and released from time zero after waste emplacement, according to the predicted heat load history (thermal decay curve).

   Basis: Actual thermal load at the repository is discretely distributed in both space and time. The approach of evenly distributing the thermal source over all the drifts has little effect on far-field TH processes at the mountain scale, because detailed thermal-load distributions affect only drift-scale processes and are limited to the first few years of thermal load. This assumption is considered adequate and requires no further justification or confirmation.

3. Waste emplacement drifts are assigned zero capillary pressure, and fracture properties of the hydrogeological unit in which they are located.

   Basis: Excavation of the drifts substantially affects only the near-field environment. Mountain-scale TH models are designed to evaluate the TH processes primarily on the large scale of the UZ system, as well as averaged behavior near the drifts over tens of thousands of years. Over this period, the near-drift processes have little impact on

mountain-scale TH processes. This assumption is considered adequate and requires no further justification or confirmation.

4. Ventilation removes thermal energy only. The amount of water vapor and air removed by ventilation is ignored.

   Basis: When ventilation is used to remove most of the heat generated by the emplaced waste, ventilation is treated as removing the heat only; the effects of ventilation and associated air circulation on water vapor and air at the repository are ignored. Although ventilation may remove some water vapor from the drifts and surrounding rock, the amount removed is negligible because, for most of the 50-year ventilated period, the ventilation is carried out by forced air or gas flow through completely dry drifts due to a combination of thermal vaporization and ventilation effect on rock moisture. This assumption is considered adequate and requires no further justification or confirmation.

5. Within the numerical models for gas and heat flow simulations, the bottom model boundary representing the water table has a fixed gas pressure, equal to standard atmospheric pressure at that elevation. All lateral boundaries, as shown in Figure 6.1-1, are treated as no-flow (closed), adiabatic boundaries, which allow mass and heat flow only along the vertical plane.

   Basis: This treatment is reasonable for the eastern boundary, which is along or near the Bow Ridge fault, because faults have high vertical permeability and lower capillary forces (see fault properties estimated in BSC 2004 [DIRS 169857]). The western and northern lateral boundaries have little effect on moisture flow within and near the repository areas, because these boundaries are separated from the repository by faults. The southern lateral boundary also has little influence, because it is located far from the repository (Figure 6.1-1). Use of constant gas pressure at the bottom boundary is justified by observed gas profiles in boreholes and by rapid gas equilibration within the unsaturated zone (BSC 2004 [DIRS 169861], Section 6.1.3). This assumption is considered adequate and requires no further justification or confirmation.

6. The water table is selected as the lower model boundary with temperatures that are constant in time but spatially variable.

   Basis: During the entire thermal-loading period, the changes in water table temperatures do not produce any significant impact on UZ percolation, or TH, THC, or THM behavior near the repository. However, as documented in earlier modeling studies, neglecting changes in temperature at the water table may have some impact on temperature evolution in stratigraphic units near the water table after 1,000 years or later (CRWMS M&O 2000 [DIRS 144454]). It is also to be noted that temperature rise at the water table in the previous mountain-scale TH model (CRWMS M&O 2000 [DIRS 144454]) may have been overestimated because that model did not account for convective cooling by regional groundwater flow. This cooling effect due to the influx of cooler groundwater flowing from locations upstream of the repository, combined with the large distance of the water table from the repository horizon, may indeed give rise to

nearly constant temperatures at the water table. This assumption is considered adequate and requires no further justification or confirmation.

7. The effects of THM and THC processes on TH properties as a result of thermal loading are ignored.

   Basis: THC and THM effects may have a significant impact on simulated TH processes only at or near drifts during the first few years of the thermal period (BSC 2005 [DIRS 172862], Section 6; BSC 2004 [DIRS 169864], Section 6). On the mountain-scale domain, in the long-term, the effects of THC and THM on flow and transport properties are small because of predicted small temperature rise away from drifts (Sections 6.4 and 6.5). This assumption is considered adequate and requires no further justification or confirmation.

8. Hysteresis effects are negligible.

   Basis: In addition to THM and THC effects, the thermal load creates significant dryout and rewetting phenomena near the drifts (BSC 2005 [DIRS 172232], Section 6.2). Hysteresis effects accompany these drying (drainage) and rewetting (imbibition) processes. This leads to slightly different curves of relative permeability and capillary pressure for describing drainage and imbibition processes, respectively. In this work, hysteresis effects are ignored because they are small compared to the uncertainty inherent to the development of the capillary pressure and relative permeability relationships. This assumption is considered adequate and requires no further justification or confirmation.

5.2 ASSUMPTIONS FOR THE MOUNTAIN-SCALE THC MODEL

The mountain-scale THC model is based on the model presented in *Drift-Scale THC Seepage Model* (BSC 2005 [DIRS 172862]), and therefore assumptions documented in Section 5 of that report also apply to the mountain-scale THC model. These assumptions are summarized as follows:

- THC model results are assumed to be representative of all repository host rock units because: previous model sensitivity analyses showed that lithology had little effect on predicted water chemistry; the repository host rock units are uniform with respect to elemental abundance, with minor differences in mineralogy; and the five starting waters used with the drift-scale THC model are chosen to represent the range of available data, and include compositions based on samples from three of the four host rock units.

- THC runs based on the five starting waters represent the range of possible seepage water composition. This assumption is not used directly in the mountain-scale THC model, however, because the mountain-scale THC model is based on the "W0" starting water composition (Section 4.1.13), one of the five compositions used with the drift-scale model (BSC 2005 [DIRS 172862], Table 6.2-1). The "W0" composition was used in validation of the drift-scale THC model based on comparison with data from the Drift Scale Test, and selection of this water is a reasonable simplification for the mountain-scale THC model considering its intended use. Whereas the drift-scale THC

model uses results based on all five starting water compositions to represent uncertainty in predicted water chemistry, the same uncertainty description applies to the mountain-scale THC model. This condition is not significant to application of the mountain-scale THC model for FEP screening because far-field impacts of THC coupled processes on the flow field in the unsaturated zone are small, or are considered to be insensitive to variations in far-field water chemistry (see Section 7.2.2).

- The composition of infiltrating fracture water (upper boundary condition), and of the initial fracture water, are identical to the initial matrix water. This assumption is justified in the drift-scale THC model documentation (BSC 2005 [DIRS 172862], Section 5) and is used exactly in the mountain-scale THC model.

- Aqueous species are unreactive (forming a normative distribution of selected salts) at solution ionic strength greater than 4 molal. This assumption is justified in the drift-scale THC model documentation (BSC 2005 [DIRS 172862], Section 5) and is used exactly in the mountain-scale THC model.

- Axial transport effects (gas, vapor, and heat transport parallel to the drift axis) would not significantly impact drift-scale THC model results. The mountain-scale THC model is a two-dimensional profile that perpendicularly cross-cuts multiple emplacement drifts, consistent with the drift-scale THC model.

- Seepage composition in the event of complete drift collapse is the same as seepage for uncollapsed drifts. This assumption is not directly used in the mountain-scale THC model, which does not consider any aspect of drift collapse, a drift-scale phenomenon.

The mountain-scale THC model also uses the TH modeling assumptions documented in Section 5.1 and TH modeling approaches discussed in Section 6.1.

5.3 ASSUMPTIONS FOR THE MOUNTAIN-SCALE THM MODEL

Assumptions used to develop the drift-scale THM model (BSC 2004 [DIRS 169864], Section 5) apply to the mountain-scale THM model documented in Section 6.5 of this report. These assumptions are summarized as follows:

- Differences in updated stratigraphic models are not significant to the results of the drift-scale or mountain-scale THM models. This assumption is justified in the drift-scale THM model documentation (BSC 2004 [DIRS 169864], Section 5) and is used exactly in the mountain-scale THM model.

- Best-available information on the in situ stress state is adequate for THM models, which are primarily concerned with the effects from thermal stress changes.

- Properties of the TSw3 thermomechanical unit are represented by the TSw2 unit, to include the effects of fracturing. Also, the rock mass properties of the CHn thermomechanical unit are represented by available information on matrix properties, because this unit is relatively unfractured. These assumptions are justified in the

drift-scale THM model documentation (BSC 2004 [DIRS 169864], Section 5) and are used exactly in the mountain-scale THM model.

- Axial transport effects (gas, vapor, and heat transport parallel to the drift axis) would not significantly impact drift-scale THM model results. The mountain-scale THM model is a two-dimensional profile that perpendicularly cross-cuts multiple emplacement drifts, consistent with the drift-scale THM model.

- The same values defining the THM effect on fracture permeability that were developed using observations from the Drift Scale Test (Tptpmn unit) are applicable to all rock units. This assumption is justified in the drift-scale THM model documentation (BSC 2004 [DIRS 169864], Section 5) and is used exactly in the mountain-scale THM model.

The mountain-scale THM model also uses the TH modeling assumptions documented in Section 5.1 and TH modeling approaches discussed in Section 6.1.

INTENTIONALLY LEFT BLANK

6. MODEL DISCUSSION

As discussed in Section 1, this report documents the development of and the results from using the mountain-scale coupled processes (TH/THC/THM) models. This section describes conceptual and numerical models developed, numerical grids and model parameters used, and model results for these coupled-processes models. It consists of the following sections:

- Mountain-Scale TH Model Description (Section 6.1)
- Two-Dimensional Mountain-Scale TH Model Results and Analyses (Section 6.2)
- Three-Dimensional Mountain-Scale TH Model Results and Analyses (Section 6.3)
- Mountain-Scale THC Model (Section 6.4)
- Mountain-Scale THM Model (Section 6.5).

Model development and results for mountain-scale TH/THC/THM models are documented in scientific notebooks listed in Table 6-1.

Table 6-1. Scientific Notebooks

LBNL Scientific Notebook ID	M&O Scientific Notebook ID	Page Numbers	Citation
YMP-LBNL-YSW-3	SN-LBNL-SCI-199-V1	pp. 105 to 108, 215 to 232	Wang 2003 [DIRS 165927]
YMP-LBNL-YSW-KZ-1	SN-LBNL-SCI-202-V1	pp. 134, 141 to 151	Wang 2003 [DIRS 165927]
YMP-LBNL-YSW-3.1	SN-LBNL-SCI-199-V2	pp. 7 to 140	Wang 2003 [DIRS 165927]
YMP-LBNL-ELS-GL-2	SN-LBNL-SCI-219-V2	pp. 67 to 73	Wang 2003 [DIRS 165927]
YMP-LBNL-YSW-KZ-2	SN-LBNL-SCI-202-V2	pp. 6 to 10	Wang 2003 [DIRS 165927]
YMP-LBNL-JR-2	SN-LBNL-SCI-204-V2	pp. 185 to 235, 271 to 273	Wang 2003 [DIRS 165927]
YMP-LBNL-THC-GZ-1	SN-LBNL-SCI-238-V1	pp. 7 to 92	Wang 2003 [DIRS 165927]

Results of this report are used to support exclusion of features, events, or processes (FEPs) identified in DTN: MO0407SEPFEPLA.000 [DIRS 170760] from the total system performance assessment for the license application (TSPA-LA) model on the basis of low consequence. The basis for exclusion of these large-scale thermal-related FEPs is documented in *Features, Events, and Processes in UZ Flow and Transport* (BSC 2005 [DIRS 174191]) and *Features, Events, and Processes in SZ Flow and Transport* (BSC 2005 [DIRS 174190]). Outputs from the present report are not direct feeds to the TSPA and are used only to corroborate the results of the multiscale thermohydrologic model (BSC 2005 [DIRS 173944]). Consequently, no FEPs are considered to be included through this report. This represents no deviation from the tables listed in *Technical Work Plan for: Near Field Environment and Transport: Coupled Processes (Mountain-Scale TH/THC/THM, Drift-Scale THC Seepage, and Drift-Scale Abstraction) Model Report Integration* (BSC 2005 [DIRS 174842], Table 3) except in the case of FEPs 2.2.10.08.0A and 2.2.10.13.0A, which were not used specifically in *Features, Events, and Processes in SZ Flow and Transport* (BSC 2005 [DIRS 174190]), although that list of FEPs (as reflected in the

updated DTN: MO0407SEPFEPLA.0000 [DIRS 170760]) was considered as part of the formulation of the models described in this report.

6.1 MOUNTAIN-SCALE TH MODEL DESCRIPTION

The conceptual models used for the mountain-scale TH model are documented in this report as well as in *UZ Flow Models and Submodels* (BSC 2004 [DIRS 169861], Section 6.3). The conceptual and numerical models are presented in this section so that a complete discussion of the model is provided.

6.1.1 Geological Model and Numerical Grids

The geological model used for developing the TH model is the geological framework model (GFM) (DTN: MO0012MWDGFM02.002 [DIRS 153777]). Based on this geological model, two grids, one three-dimensional and one two-dimensional, are developed and used in the mountain-scale TH model. The development of the three-dimensional TH model grid is documented in *UZ Flow Models and Submodels* (BSC 2004 [DIRS 169861]). Detailed description of the process of generating numerical grids from geological stratigraphic data is presented in *Development of Numerical Grids for UZ Flow and Transport Modeling* (BSC 2004 [DIRS 169855]). Table 6.1-1 lists the geological units/layers for different hydrogeologic units and the relationship with the TH model numerical grid-layer information. These geological formations are organized into layered hydrogeologic units, based primarily on the degree of welding (Montazer and Wilson 1984 [DIRS 100161]). These units are the Tiva Canyon welded (TCw) hydrogeologic unit, the Paintbrush nonwelded unit (PTn), the Topopah Spring welded (TSw) unit, the Calico Hills nonwelded unit (CHn), and the Crater Flat undifferentiated (CFu) units.

The three-dimensional TH model grid is shown in the plan view of Figure 6.1-1 (BSC 2004 [DIRS 169861], Section 6.3). The mesh used in three-dimensional TH simulation is obtained from DTN: LB0303THERMESH.001 [DIRS 165168] (file 2kgrid8_output: mesh_th.v1 for the dual-k grid). This model grid, which covers a smaller domain than the three-dimensional TSPA-LA grid used in the unsaturated zone ambient model, has been developed to be consistent with the engineering layout of the repository (BSC 2004 [DIRS 169861], Section 6.3), including the orientation of the emplacement drifts (for a schematic drawing of the repository layout, see BSC 2003 [DIRS 165572], Figure 5). The thermal model grid domain covers approximately 20 km^2 of the area and uses a refined mesh in the vicinity of the repository. The thermal model domain is selected to focus on geothermal conditions and thermal-loading effects at and near the repository area. The smaller TH model domain is considered to provide sufficient accuracy for these studies because of the small impact of the thermal effect in the lateral directions. The smaller grid domain also reduces the total number of gridblocks and thus the computational intensity required for TH modeling.

The thermal grid incorporates every repository drift explicitly by taking into account orientations, lengths, elevations, and spacing of the repository drifts. Specifically, a grid spacing of 81 m is used in the direction perpendicular to drifts (BSC 2005 [DIRS 174514], Section 4.1.1.2). At the repository horizon, a segment of a 5.5-m-diameter cylinder (BSC 2005 [DIRS 174514], Section 4.1.1.2) represents waste emplacement drifts for thermal-loading TH studies

(BSC 2003 [DIRS 165572]). Drift elements have the same hydrologic properties as the surrounding matrix, except for zero capillarity and slightly less than 100% porosity. Heat sources are introduced into the drift elements. In the three-dimensional TH model grid, faults are explicitly represented in the model by vertical or inclined 30 m wide zones, but properties for grid blocks within the fault zones are adjusted to represent specific fault configurations (BSC 2004 [DIRS 169855], Section 6.6.1). Calibrated base-case mountain-scale flow properties developed in *UZ Flow Models and Submodels* (BSC 2004 [DIRS 169861]) are used in the TH models.

The three-dimensional TH model grid of Figure 6.1-1 consists of 980 mesh columns of both fracture and matrix continua, 86,440 gridblocks, and 343,520 connections in a dual-permeability grid. Vertically, the thermal grid has an average of 45 computational grid layers.

Table 6.1-1. GFM 2000 Lithostratigraphy, TH Model Layer, and Hydrogeologic Unit Correlation Used in the Mountain-Scale TH Model

Major Unit	Lithostratigraphic Nomenclature	TH Model Grid Layer
Tiva Canyon welded (TCw)	Tpcr	tcw11
	Tpcp	tcw12
	TpcLD	
	Tpcpv3	tcw13
	Tpcpv2	
Paintbrush nonwelded (PTn)	Tpcpv1	ptn21
	Tpbt4	ptn22
	Tpy (Yucca)	
		ptn23
		ptn24
	Tpbt3	
	Tpp (Pah)	ptn25
	Tpbt2	ptn26
	Tptrv3	
	Tptrv2	
Topopah Spring welded (TSw)	Tptrv1	tsw31
	Tptrn	
		tsw32
	Tptrl, Tptf	tsw33
	Tptpul, RHHtop	
	Tptpmn	tsw34
	Tptpll	tsw35
	Tptpln	tsw36
		tsw37
	Tptpv3	tsw38
	Tptpv2	tsw39 (vit, zeo)

Table 6.1-1. GFM 2000 Lithostratigraphy, TH Model Layer, and Hydrogeologic Unit Correlation Used in the Mountain-Scale TH Model (Continued)

Major Unit	Lithostratigraphic Nomenclature	TH Model Grid Layer
Calico Hills nonwelded (CHn)	Tptpv1	ch1 (vit, zeo)
	Tpbt1	
	Tac (Calico)	ch2 (vit, zeo)
		ch3 (vit, zeo)
		ch4 (vit, zeo)
		ch5 (vit, zeo)
	Tacbt (Calicobt)	ch6 (vit, zeo)
Calico Hills nonwelded (CHn) (Continued)	Tcpuv (Prowuv)	pp4
	Tcpuc (Prowuc)	pp3
	Tcpmd (Prowmd)	pp2
	Tcplc (Prowlc)	
	Tcplv (Prowlv)	pp1
	Tcpbt (Prowbt)	
	Tcbuv (Bullfroguv)	
Crater Flat undifferentiated (CFu)	Tcbuc (Bullfroguc)	bf3
	Tcbmd (Bullfrogmd)	
	Tcblc (Bullfroglc)	
	Tcblv (Bullfroglv)	bf2
	Tcbbt (Bullfrogbt)	
	Tctuv (Tramuv)	
	Tctuc (Tramuc)	tr3
	Tctmd (Trammd)	
	Tctlc (Tramlc)	
	Tctlv (Tramlv)	tr2
	Tctbt (Trambt) and below	

Source: BSC 2004 [DIRS 169855], Table 6-5.

In addition to the three-dimensional model grid, the TH model also uses a north–south two-dimensional cross-sectional grid, with the plan location (N-S) shown in Figure 6.1-1. The two-dimensional TH model grid shown in Figure 6.1-2 and was developed using the same methodology and stratigraphic information used for the three-dimensional model grids (BSC 2004 [DIRS 169855]; BSC 2004 [DIRS 169861]). The two-dimensional cross-sectional grid is a refined north–south grid (Figure 6.1-1) and is specifically developed for detailed study of TH processes. The grid has a total of 306 grid columns and 64 grid layers, resulting in 39,000 gridblocks and 100,000 connections in a dual-permeability grid (see DTN: LB0310MTSCLTH2.001, file *mesh_ns.v2b*). The two-dimensional grid has a more refined spatial resolution (Figure 6.1-2) than the three-dimensional TH model grid, with a uniform horizontal grid spacing of 21.297 m (= 85.188/4; here, 85.188 m is the drift spacing along the N-S direction of Figure 6.1-1). The rock thermal and flow properties were assigned from the calibrated base case properties based on the stratigraphic units along the cross section (Section 6.1.6).

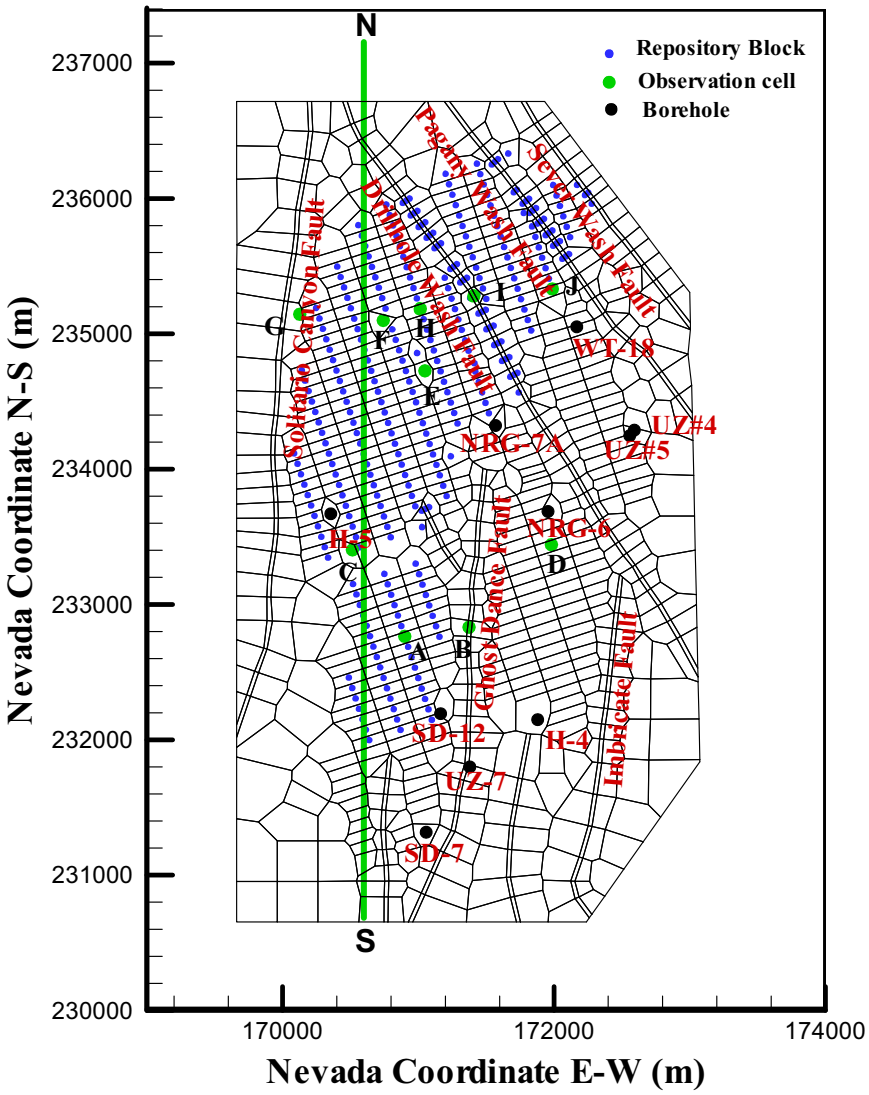

Source: DTN: LB0303THERMESH.001 [DIRS 165168].

NOTE: The north–south green line is a trace of the two-dimensional model grid shown in Figure 6.1-2. The THC model uses a subset of the green line (see Figure 6.4-2). Observation cells are locations within the grid for which model results are calculated and plotted.

Figure 6.1-1. Plan View of the Three-Dimensional TH Model Grid Showing the Model Domain, Faults Incorporated, Several Borehole Locations, and TH Model Boundaries

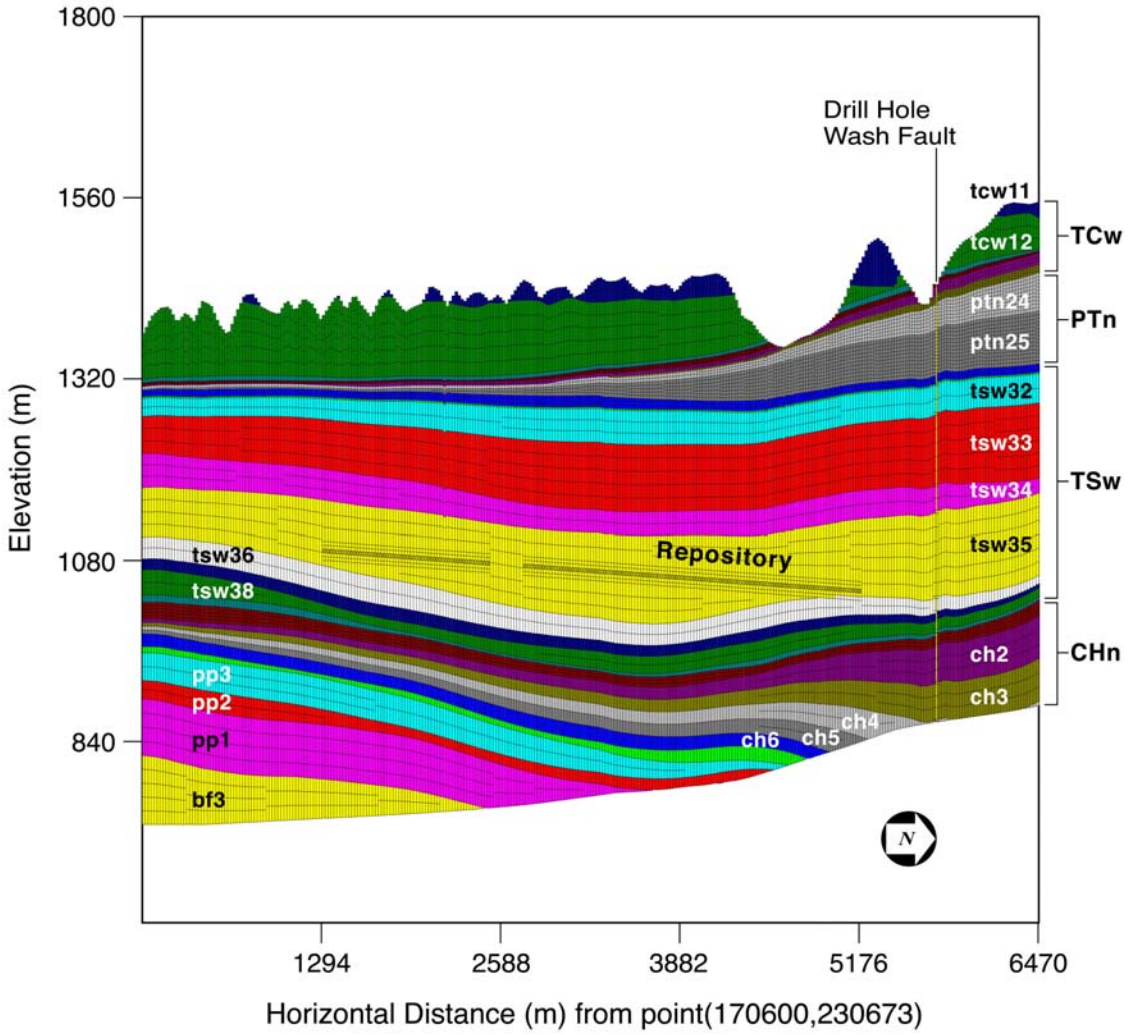

Output DTN: LB0310MTSCLTH2.001.

Figure 6.1-2. Two-Dimensional North–South Cross-Sectional Model Domain and Grid Showing Lateral and Vertical Discretization, Hydrogeological Layers, Repository Layout, and a Fault

6.1.2 Numerical Codes and TH Modeling Approach

The model simulation results presented in this report were carried out using TOUGH2 V1.6 (LBNL 2003 [DIRS 161491]) for TH simulations. To model TH processes in the UZ system at Yucca Mountain, mathematical models or governing equations are needed to describe the physical processes quantitatively. The physical processes associated with flow and transport in porous media are governed by the fundamental conservation laws (i.e., conservation of mass, momentum, and energy), which govern the behavior of fluid flow, chemical migration, and heat transfer through fractured porous media. The macroscopic continuum approach has been most commonly used in practical applications (Bear 1972 [DIRS 156269]). In this approach, the physical laws governing flow of several fluids, transport of multicomponents, and heat transfer in porous media are represented mathematically on the macroscopic level by a set of partial differential or integral equations. Fluid and heat flow and chemical-transport processes in

fracture and matrix systems in the UZ are described using a macroscopic, dual-permeability continuum approach.

In addition to the conservation or continuity equations of mass and thermal energy in fracture and matrix systems, specific relationships or *mechanisms* are needed that describe how fluid flow, solute/tracer transport, and heat transfer occur in porous and fractured media. The following specific constitutive laws act as such mechanisms by governing local fluid flow, component transport, and heat-transfer processes in porous and fractured media:

- Darcy's law is applied to describe the two-phase flow of gas and water in both fractures and matrix (Pruess et al. 1999 [DIRS 160778], pp. 144 to 161). In particular, the two-phase equation of the TOUGH2 EOS3 module is used in describing nonisothermal liquid and gas flow through the UZ at Yucca Mountain. Relative permeability and capillary functions of both fractures and matrix follow the model of van Genuchten (1980 [DIRS 100610]).

- The generalized Fourier's law (Wu and Pruess 2000 [DIRS 153972], pp. 704 to 707), including heat conduction and advection transfer in a multiphase porous and fractured system, is used to evaluate heat transfer processes. This includes transfer of latent heat by vapor.

In both research and application, the multiphase extension of Darcy's law (Pruess et al. 1999 [DIRS 160778], pp. 144 to 161), and the generalized Fourier's law (Wu and Pruess 2000 [DIRS 153972], pp. 704 to 707), have been used as fundamental laws that govern multiphase fluid and heat flow processes within porous-medium and fractured rocks. These fundamental laws or correlations, based on theory, experiment, and field studies, reflect the current understanding of porous-medium physics.

In the mountain-scale TH model, perched-water effects are ignored**.** The occurrence of perched water and its effects on the UZ flow fields are discussed in *UZ Flow Models and Submodels* (BSC 2004 [DIRS 169861]). Perched-water conditions are confined mainly to the lower units of the Topopah Spring welded (TSw) hydrogeological unit and on top of the Calico Hills nonwelded unit (CHn). Over the repository domain, perched water locations are typically 100 to 150 m below the repository horizon (Wu et al. 1999 [DIRS 117167]). Because the dominant heat-transfer mechanism at these locations is heat conduction and boiling conditions are not attained, the effect of repository thermal load on perched-water bodies is ignored.

Another key issue for simulating fluid and heat flow in the fractured-porous rock of Yucca Mountain is how to handle fracture and matrix interaction under multiphase and nonisothermal conditions. The available methods for treating fluid flow in fractures and the rock matrix using a numerical approach include: (1) an explicit discrete-fracture and matrix representation; (2) the dual-continuum method, including double- and multiporosity, dual-permeability, or the more general "multiple interacting continua" method (Pruess and Narasimhan 1985 [DIRS 101707]); and (3) the generalized effective continuum method. For the work documented in this report, the dual-permeability conceptual model is applied to evaluate fluid and heat flow in the fracture-matrix system of the Yucca Mountain UZ.

The dual-continuum conceptualization provides an appropriate representation of the UZ processes within the UZ at Yucca Mountain (Doughty 1999 [DIRS 135997]) and is much less demanding in computational effort or in data requirements than the discrete-fracture-modeling approach. Therefore, the dual-continuum method has become the main approach used in the modeling studies of the Yucca Mountain Project (Wu et al. 1999 [DIRS 117161]; 2002 [DIRS 160195]). In this report, the dual-permeability formulation is considered to be appropriate for simulating flow and transport through fractured tuffs of the Yucca Mountain UZ. As applied in this report the traditional dual-permeability concept is first modified using an active fracture model (Liu et al. 1998 [DIRS 105729]) to represent fingering effects of liquid flow through fractures. The active fracture model is validated in *Conceptual and Numerical Approaches for UZ Flow and Transport* (BSC 2004 [DIRS 170035]). In addition, the dual-permeability model is further modified by adding additional global fracture-matrix connections at the interfaces of TCw-PTn, PTn-TSw, and vitric-nonvitric units to better simulate fracture-matrix flow at these transitions.

Use of the discrete fracture or weeps-type model as an alternative is limited by (1) large uncertainties in the distribution of fractures within the mountain and (2) an extensive computational burden owing to the large amount of data required to describe the fracture system. On the other hand, the effective continuum model approach, although computationally the most efficient, may not capture important nonequilibrium fracture-matrix TH processes under thermal loading conditions (BSC 2004 [DIRS 170035], Section 6.4).

6.1.3 TH Model Boundary and Initial Conditions

In TOUGH2 (LBNL 2003 [DIRS 161491]), boundary conditions are generally specified by means of appropriately chosen volume elements and flow connections. Boundary conditions can be of two basic types. Dirichlet conditions prescribe thermodynamic conditions, such as pressure or temperature on the boundary, while Neumann conditions prescribe fluxes of mass or heat crossing boundary surfaces (Pruess 1991 [DIRS 100413], pp. 33 to 37). A special case of the Neumann boundary conditions is the no-flux boundary. In the Integral Finite Difference Method used in TOUGH2 (LBNL 2003 [DIRS 161491]), this case is handled by not specifying any flow conditions across the boundary. Dirichlet-type boundary conditions, such as constant pressures or temperatures, can be specified by introducing appropriate boundary elements and connections. This approach has been implemented as follows:

- Thermal conditions at the top and bottom boundaries are represented using temperatures that are fixed in time, but variable in space. In addition, top and bottom model boundaries are also subject to constant pressure and saturation conditions.

  The use of constant temperature, pressure, and saturation boundaries has been discussed extensively (e.g., Wu et al. 1999 [DIRS 117161]). The fixed temperature condition at the top and bottom boundaries is a simplified representation of the heat exchange on the boundary "surfaces" between the model domain and the atmosphere or the water table. The top boundary of the model, made up of the land surface or tuff-alluvial contact, is controlled mainly by the atmosphere, whereas temperatures at the water table are determined by the ambient geothermal gradients and infiltration flux. The two boundaries are both far away from the repository horizon; therefore, the effects of

specified temperatures on thermal behavior at or near the repository are small. As a result, constant temperatures, estimated from field-measured values along these boundaries, provide a good approximation of the TH system that was simulated.

The models also use the following approach to assign drift boundary conditions as justified in Section 5:

- An equivalent heat load is evenly distributed within emplacement drifts and released from time zero after waste emplacement, according to the predicted heat load history (thermal decay curve).

- Waste emplacement drifts are assigned matrix permeabilities, zero capillary pressures, and other properties of the hydrogeological unit in which they are located.

- Ventilation removes thermal energy only. The amount of water vapor and air removed by ventilation is ignored.

The TH model boundary and initial conditions are specified in the same way as in the ambient TH model (BSC 2004 [DIRS 169861], Section 6.1.3). In general, the ground surface of the mountain (or the tuff-alluvium contact in areas of significant alluvial cover) is taken as the top model boundary; the water table is treated as the bottom model boundary. Both the top and bottom boundaries of the model are treated as Dirichlet-type conditions with specified constant but spatially varying temperature and gas pressure. A constant liquid saturation value of approximately 1.0, corresponding to saturated water table conditions, was set for the bottom boundary. Surface infiltration, as discussed below in Section 6.1.4, is applied using a source term in the fracture gridblocks within the second grid layer from the top. This method was adopted because the first layer is treated as a Dirichlet-type boundary, with constant pressure, saturation, and temperature, to represent average atmospheric conditions at the mountain.

The water table is used as the bottom model boundary, a surface where the water pressure is a fixed, single value. Within the numerical models for gas and heat flow simulations, the bottom model boundary representing the water table has a fixed gas pressure, equal to the atmospheric pressure at the elevation. All lateral boundaries, as shown in Figure 6.1-1, are treated as no-flow (closed) boundaries, which allow flow only along the vertical plane. This treatment is reasonable for the eastern boundary, which is along or near the Bow Ridge fault, because faults have high vertical permeability and lower capillary forces (see fault properties estimated in BSC 2004 [DIRS 169857]). The western and northern lateral boundaries have little effect on moisture flow within and near the repository areas, because these boundaries are separated from the repository by faults. The southern lateral boundary also has little influence, because it is located far from the repository (Figure 6.1-1).

The spatially distributed values of temperatures along the top and bottom boundaries of the UZ flow model are based on field observation. This treatment is corroborated by data reported by Sass et al. (1988 [DIRS 100644]) and the calibrated temperature distribution along the water table (BSC 2004 [DIRS 169861]).

Pressure conditions at both top and bottom boundaries of the model are similar to those used in the UZ flow model (BSC 2004 [DIRS 169861], Section 6.1.3). The water table, which is the bottom boundary of the mountain-scale TH model, is shown to be a relatively flat, stable surface in most of the model domain, increasing its elevation only in the north (BSC 2004 [DIRS 169855], Figure 6-9). For most areas in the middle and southern part of the model domain, the flat portion of the water table is about 730 meters above sea level (masl). The water table rises to about 810 masl in the northern part of the repository (BSC 2004 [DIRS 169855], Figure 6-9). The rise in the water table elevation near the northern end of the model domain is explicitly included by raising the bottom boundary accordingly at that location. The gas pressures are estimated as 92 kPa at an elevation of 730 m. This pressure was estimated using a pressure profile for air under standard conditions with a pressure of 101 kPa at mean sea level. Surface gas pressures are determined by running the TOUGH2 code (LBNL 2003 [DIRS 161491]), EOS3 module to steady-state under given temperature, bottom pressure, and surface infiltration conditions. This is necessary to generate a steady-state, equilibrated gas-pressure boundary to avoid artificial airflow or circulation, which may occur if nonequilibrated pressures are imposed on the ground-surface boundaries.

To account for variations in atmospheric temperature with surface elevations in the mountain, measured mean surface temperatures and a linear equation that correlates surface temperature with elevation are used. The annual-average temperature was measured for near-surface sensors in boreholes USW NRG-6 and USW NRG-7a (DTNs: GS960308312232.001 [DIRS 105573], GS951108312232.008 [DIRS 106756], and GS950208312232.003 [DIRS 105572]), with several years of continuous temperature monitoring data. The surface temperatures T_s at any elevation Z are then computed using the software routine toptemp_v0.f V1.0 (LBNL 2000 [DIRS 147030]) and are treated as constants according to the following equation (Wu et al. 1999 [DIRS 117161], Equation 4):

$$T_s = T_{ref} - \lambda[Z - Z_{ref}] \qquad \text{(Eq. 6.1.3-1)}$$

where T_{ref} is mean surface temperature at reference elevation Z_{ref} and λ is the dry adiabatic atmospheric lapse rate in °C/m. This lapse is 0.01°C/m (Driscoll 1986 [DIRS 116801], p. 50), as discussed in Section 4.1.14. In this formulation, the surface reference temperatures used are based on the field measurements in *UZ Flow Models and Submodels* (BSC 2004 [DIRS 169861]). The reference temperature (T_{ref}) used is 18.23°C, averaged using measured data from borehole NRG-6, at a reference elevation (Z_{ref}) of 1,231.0 m. The averaged temperature measurement of NRG-7a at an elevation of 1,282.2 m is 17.78°C. The calculated mean lapse rate, based on these two field measurements, is 0.009°C/m, which is in close agreement with the adiabatic rate of 0.01°C/m used in this model (BSC 2004 [DIRS 169861], Section 6.3.2). The top boundary temperature conditions influence estimates of heat exchange with the unsaturated zone.

The temperature distributions at the bottom boundary of the three-dimensional TH model were taken from the ambient TH model (BSC 2004 [DIRS 169861], Section 6.1.3). Note that the ambient TH model also provides a database for estimate of water table temperatures with DTN: LB0303THERMSIM.001 [DIRS 165167]. This database is used to obtain bottom-temperature boundary conditions for the two-dimensional TH model. The software

routine GET_TEMP_V0.F V1.0 (LBNL 2000 [DIRS 147027]) was first used to estimate temperatures for a flat surface at an elevation of 730 m. Because the water table is no longer flat with the current UZ and TH models, the actual estimates of the water table or bottom model-boundary temperatures were interpolated between the values at 730 m elevation and the model surface boundary. Note that the bottom temperature boundaries of both two-dimensional and three-dimensional TH models are not extended 1,000 m below the water table, as done for the previous mountain-scale TH models (CRWMS M&O 2000 [DIRS 144454]). Selection of the water table as the lower model boundary is justified as follows: during the entire thermal-loading period, the changes in water table temperatures do not produce any significant impact on UZ percolation, or TH, THC, or THM behavior near the repository. However, neglecting changes in temperature at the water table may have some impact on temperature evolution in stratigraphic units near the water table after 1,000 years or later (CRWMS M&O 2000 [DIRS 144454]). It is also noted that temperature rise at the water table in the previous mountain-scale TH model (CRWMS M&O 2000 [DIRS 144454]) may have been overestimated because that model did not account for convective cooling by regional groundwater flow. This cooling effect due to the influx of cooler groundwater flowing from locations upstream of the repository, combined with the large distance of the water table from the repository horizon, justifies the use of constant temperatures at the water table.

6.1.4 Infiltration Scenarios

Water entering the UZ as net infiltration from precipitation at the land surface is the major control on overall hydrologic and thermal-hydrologic conditions within the UZ at Yucca Mountain. This is because net infiltration is the ultimate source of percolation through the UZ. Water percolating downward through the UZ is the principal means by which radionuclides may be transported from the repository to the water table. Such percolation could also have a direct impact on the evolution of TH processes near the waste emplacement drifts.

The mountain-scale TH model uses net infiltration rates as surface-water-recharge boundary conditions. The net infiltration rates consist of present-day and future scenarios, determined by studies of modern and future climates. Three mean net infiltration maps during each climate (DTN: GS000308311221.005 [DIRS 147613]) implemented with the TH model are documented in *Simulation of Net Infiltration for Modern and Potential Future Climates* (BSC 2004 [DIRS 170007]). They include present-day (modern), monsoon, and glacial transition mean infiltration rates. The actual schedule and the averages of the three infiltration rates in the TH models are shown in Table 6.1-2, indicating average values over the model domain for three time periods. Table 6.1-2 shows that the mountain-scale TH model implements three infiltration rates over three time periods for the thermal-loading investigation. The future climates are considered to act sequentially over the modeled period: present (0 to 600 years), monsoon (600 to 2,000 years), and then glacial transition (2,000 years and beyond).

Table 6.1-2. Averaged Infiltration Rates and Time Period over the Mountain-Scale TH UZ Model Domain

Scenario	Time Period	Mean Infiltration (mm/yr)
Present-Day/Modern	0 to 600 Years	3.6
Monsoon	600 to 2,000 Years	10.4
Glacial Transition	2,000 and beyond	16.1

NOTE: Values averaged from DTN: GS000308311221.005 [DIRS 147613].

As shown in Table 6.1-2, with the UZ model grid the average rate over the model domain for present-day mean infiltration is 3.6 mm/yr, which is considered a base-case infiltration scenario. The two future climate scenarios, the monsoon and glacial transition periods, are used to account for projected climate-induced changes in precipitation and net infiltration. The average values in Table 6.1-2 are estimated using the three-dimensional TH model grid, shown in Figure 6.1-1 for infiltration maps (DTN: GS000308311221.005 [DIRS 147613]), and the software routine infil2grid V1.7 (LBNL 2002 [DIRS 154793]). The routine calculates an area of influence for each infiltration coordinate and assigns the net infiltration rate to the model gridblock into which the area falls. The mean infiltration rates shown in Table 6.1-2 are area-weighted using gridblock areas. Net infiltration is handled in a consistent manner in this report, i.e., mapping the infiltration maps to model grids.

A plan view of the spatial distribution for the three mean infiltration maps, as interpolated into the three-dimensional UZ TH model grid, is shown in Figures 6.1-3, 6.1-4, and 6.1-5, respectively, for the present-day, monsoon, and glacial transition mean infiltration scenarios. The figures show similar patterns of flux distributions for the three infiltration rates, with higher infiltration rates in the northern part of the model domain and along the mountain ridge east of the Solitario Canyon fault. For the two-dimensional TH model, infiltration at the top boundary was extracted from the infiltration map discussed above. The average (over the two-dimensional TH model grid) infiltration during present-day, monsoon, and glacial transition climatic periods are 5.8 mm/yr, 17.0 mm/yr, and 28.8 mm/yr, respectively. Note that these are averages only for the upper surface of the two-dimensional TH model, and not for the entire three-dimensional domain.

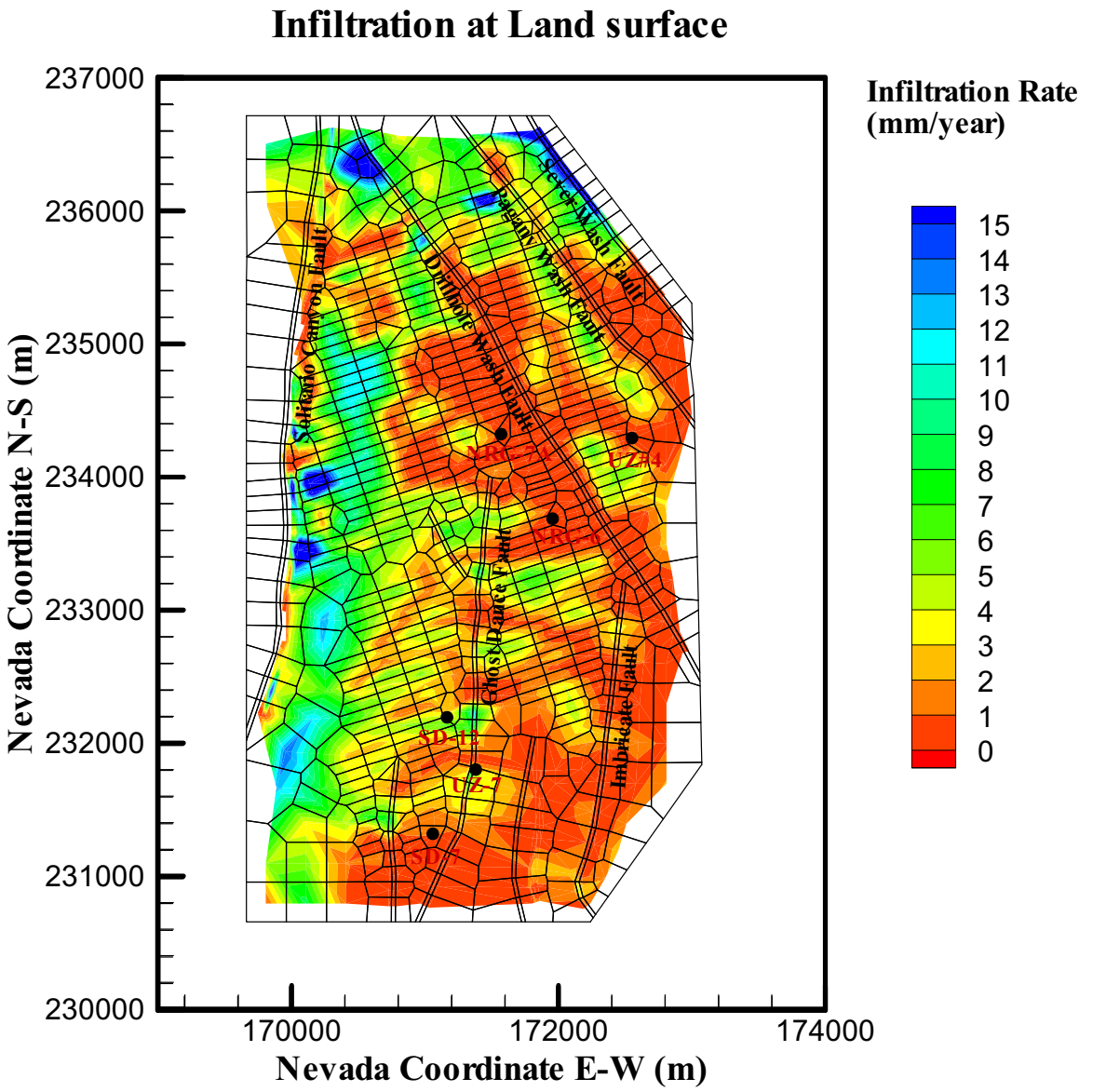

Source: DTN: GS000308311221.005 [DIRS 147613].

Figure 6.1-3. Plan View of Net Infiltration Distributed over the Three-Dimensional TH Model Grid for the Present-Day Mean Infiltration Scenario for the First 600 Years of Thermal Load

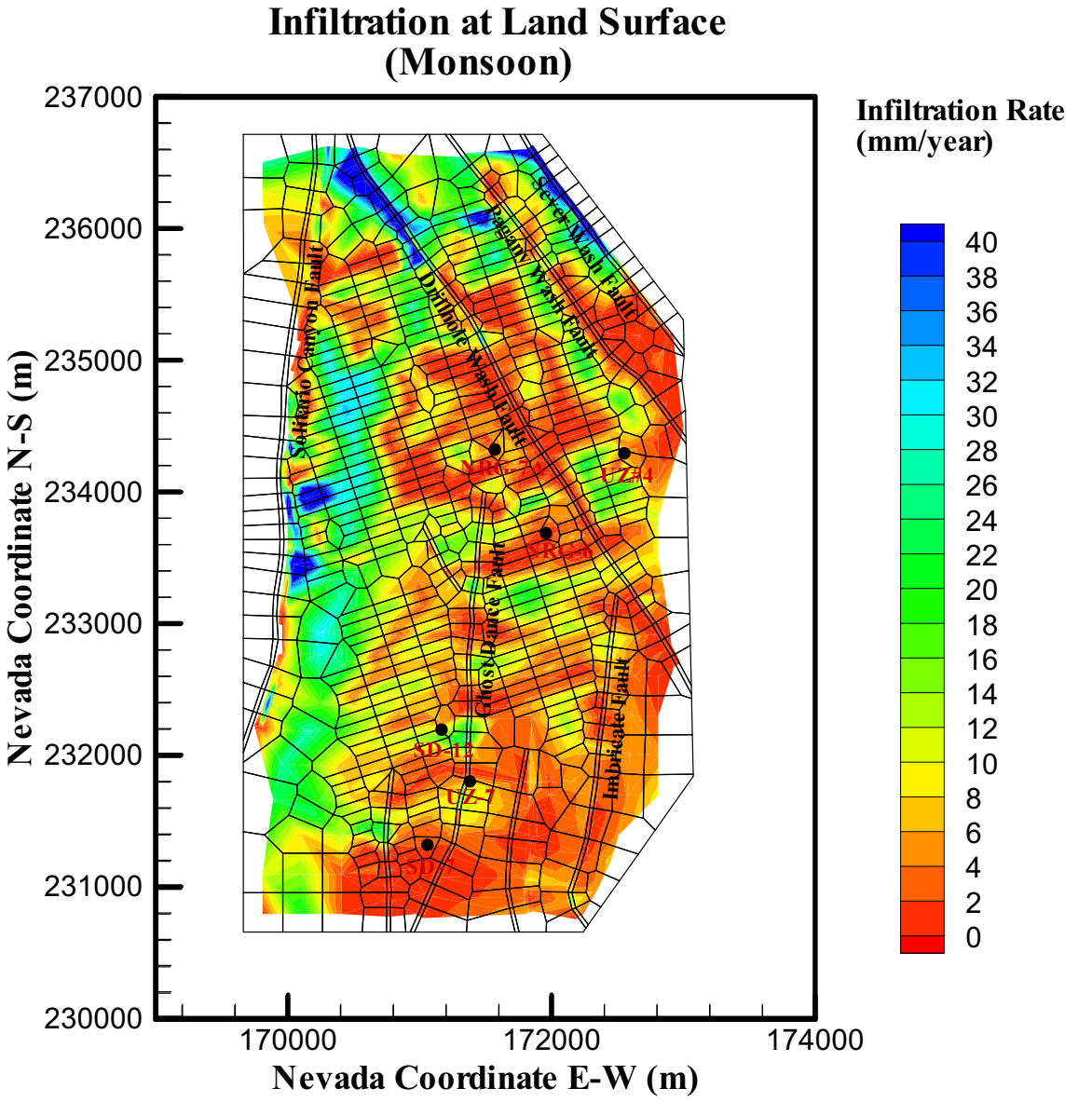

Source: DTN: GS000308311221.005 [DIRS 147613].

Figure 6.1-4. Plan View of Net Infiltration Distributed over the Three-Dimensional TH Model Grid for the Monsoon Mean Infiltration Scenario for 600 to 2,000 Years of Thermal Load

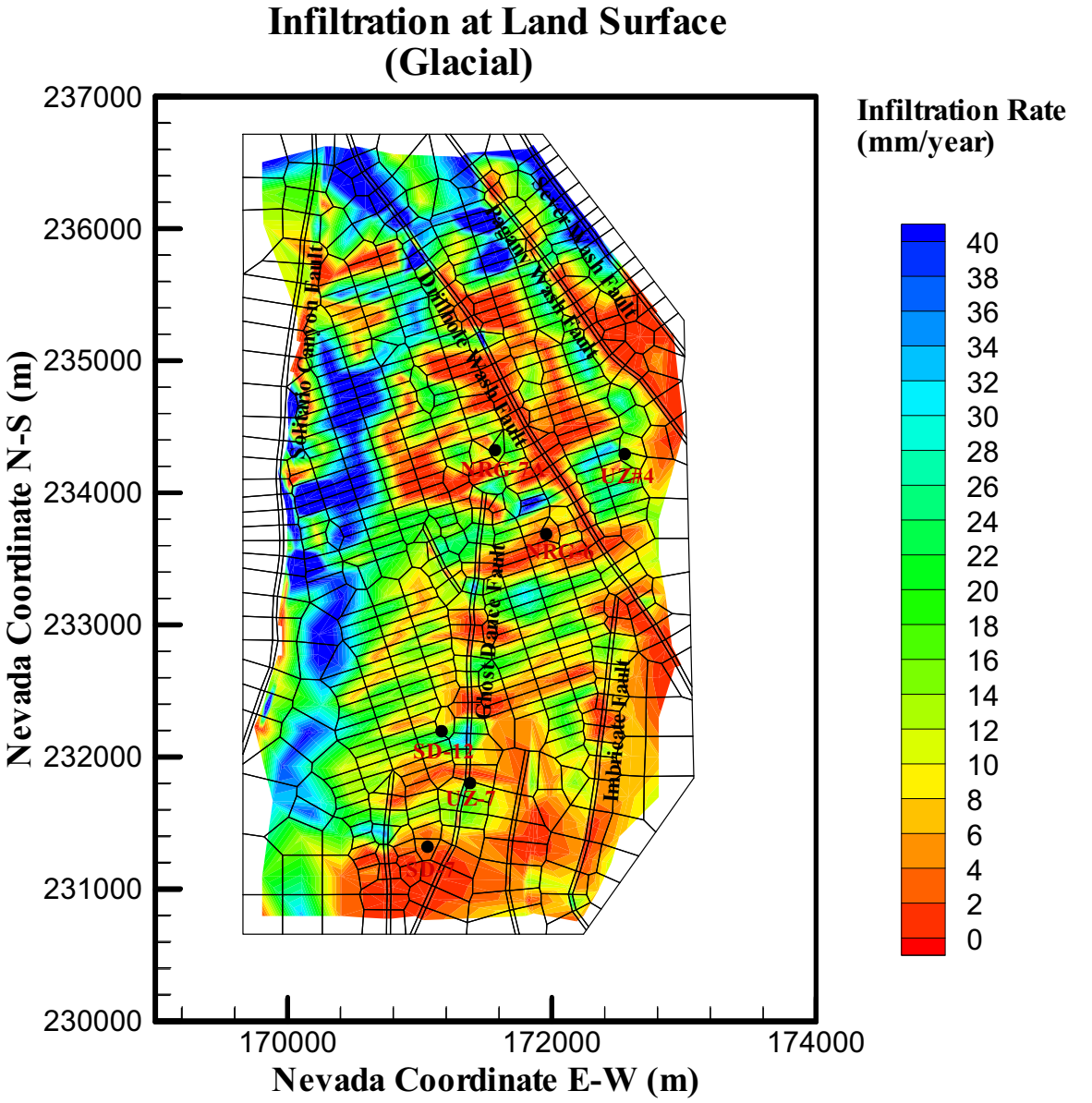

Source: DTN: GS000308311221.005 [DIRS 147613].

Figure 6.1-5. Plan View of Net Infiltration Distributed over the Three-Dimensional TH Model Grid for the Glacial Transition Mean Infiltration Scenario for 2,000 Years and Beyond of Thermal Load

6.1.5 Repository Thermal Load

The average thermal line load of 1.45 kW/m (BSC 2004 [DIRS 168489], Table 1) and the time dependent thermal load decay (BSC 2004 [DIRS 159527]) used in the mountain-scale TH models are obtained from *Repository Design, Repository/PA IED Subsurface Facilities Plan Sht. 5 of 5* (BSC 2002 [DIRS 159527]), as discussed in Section 4.1.5. The value of 1.45 kW/m refers to the initial thermal line load that decreases with time as a result of radioactive decay. As explained in Section 4.1.5, these values are similar to current design values in *IED Waste Package Decay Heat Generation [Sheet 1 of 1]* (BSC 2005 [DIRS 173705], Table 1). During the 50-year preclosure period, ventilation in the drifts is used to remove 86.3% of the heat (BSC 2002 [DIRS 160975], Table 6-6), which was enclosed by the range of ventilation efficiency (BSC 2004 [DIRS 169862], Table 8-2), as documented in Section 4.1.4. After 50 years, the full line load is implemented. This is referred to as the base-case thermal loading scenario.

The thermal load and the resulting temperature field influence many TH-related processes. These processes can directly impact the performance of the repository. For example, emplacement of heat-generating high-level waste elevates the temperature and causes the redistribution of in situ moisture at the repository, and in the unsaturated zone. As heat is released from the waste unit and transferred to the surrounding host rock, the temperature near the waste packages approaches or exceeds the boiling point of water (approximately 96°C at ambient pressure). Boiling of formation water then takes place, with the associated increase in vapor pressure and overall gas-phase pressure. This results in forced convection of the gas phase, with a redistribution of water accompanied by large latent heat effects. Under favorable conditions, this may result in a "heat-pipe," the steady counter-current flow of liquid towards the repository and vapor-phase away from the repository. This liquid-phase and gas-phase flow perturbs the in situ fluid saturation in both fractures and matrix, and may result in a large two-phase zone above the repository, as well as an increase in the potential for changes in the flow properties within the condensation zones. The local impact of heat on TH processes depends on the thermal load and its distribution within repository drifts.

The repository drifts are modeled with the properties of the UZ model layers in which they are located. In the model, the heat source is applied to drift elements at intervals controlled by the discrete representation of the drifts at the repository horizon and the grid spacing. For example, in the three-dimensional model, because the grid spacing within the repository is equal to the drift spacing, a laterally continuous (smeared) heat source is modeled across the repository. This approach does not provide detailed resolution of TH processes in terms of temperature, saturation, and flux for the intervening space between the drifts (drift pillars). Rather, this coarse-grid model allows for an adequate, simple, and fast estimation of the long-term, average response to thermal load over the entire model domain. Except for the early time, heat distribution is sufficiently diffused at the repository such that a smeared heat source model presents a good approximation of the heat-source distribution during the compliance period. The major advantage of this modeling approach is that it allows for direct comparison of fluid, temperature, and flux distribution between the three-dimensional ambient flow field models (BSC 2004 [DIRS 169861]) and the TH model over the repository domain. The impact of TH on flow and transport can then be directly estimated using flow fields extracted from the TH model.

Although the repository thermal load is computed based on the total acreage of the repository, the heat-generating radioactive waste is stored in the drifts within the repository at a discrete spacing. The current repository design has emplacement drifts of 5.5-m diameter, spaced 81 m apart (BSC 2003 [DIRS 165572], Table 8; BSC 2005 [DIRS 174514], Section 4.1.1.2). Because of the large spacing between the drifts and the disparity in infiltration across the model, a potential for large differences or gradients in temperature, saturation, and flux exists between the heated drifts.

To address some of these issues, a two-dimensional grid was designed with the repository nodes subdivided to explicitly include an element that approximates the dimensions of the drift. This discrete (drift-by-drift) model provides a refined grid that allows for investigation of thermal effects at the drifts and between the drifts, as well as in the far field. In this grid, a 5.0-m-square drift element is inserted along the N-S cross-sectional grid for every four repository grid blocks spaced 85.2/4 = 21.3 m. This is equivalent to an 81-m lateral spacing along the direction perpendicular to repository drifts (Figure 6.1-1) (for details on the grid generation processes, see BSC 2004 [DIRS 169855]). This is because the repository drifts are not exactly in the east-west direction, i.e., they are not perpendicular to the N-S cross section. The thermal load for the three-dimensional TH model is computed based on the initial thermal line-load value of 1.45 kW/m, and the length of the inserted drift cylinders, and applied to the discrete drift elements.

A 5.0 × 5.0 m drift element is used (about same area as the 5.5-m drift diameter used to represent a drift tunnel) in the two-dimensional grid, because 5.0-m layers are used in the numerical grid. In the two-dimensional grid, every fourth repository grid block is subdivided laterally into the drift element plus one element on each side of the drift element (two equal elements each (21.3 − 5)/2 = 8.15 m wide). Therefore, in this refined grid, each drift element is laterally separated by five elements between the drifts. This locally refined grid of the two-dimensional TH model allows for flow between drifts. However, since the refinement is limited to the repository level, the applied surface infiltration is based on the original grid with spacing of 21.3 m. The N-S two-dimensional model is 1 m wide, but because the drifts are not E-W, each element represents more than 1 meter of drift length. Therefore, the thermal load applied is computed based on the initial thermal line load value of 1.45 kW/m, divided by the cosine of the angle between the drift orientation and true E-W, and applied to the discrete drift elements. This thermal load is used in the TH, THC, and THM simulations using the two-dimensional cross-section models.

6.1.6 Rock and Thermal Properties

The key input rock and fluid-flow parameters and thermal properties in this report are summarized in Section 4. These rock and fluid-flow parameters were provided in *UZ Flow Models and Submodels* (BSC 2004 [DIRS 169861]) (DTN: LB03013DSSCP3I.001 [DIRS 162379]). Thermal properties include grain density, wet and dry thermal conductivity, and grain-specific heat for each model grid layer (DTN: LB0210THRMLPRP.001 [DIRS 160799]) and have been updated in DTN: LB0402THRMPRPT.001 [DIRS 168481], which is qualified in *Drift-Scale Coupled Process (DST and TH Seepage) Models* (BSC 2005 [DIRS 172232], Appendix F). Note that updated properties in DTN: LB0402THRMPRPT.001

[DIRS 168481] are only used in sensitivity simulations (Appendices V, VI and VII) and are not direct input to the mountain-scale TH/THC/THM models. Temperature-dependent fluid properties, such as fluid density, viscosity, and specific enthalpy, are incorporated in the formulation of the TOUGH2 V1.6 (LBNL 2003 [DIRS 161491]) code using properties of pure water.

The rock and thermal parameter specification in the TH model is, in general, layer-wise uniform as described in *UZ flow Models and Submodels* (BSC 2004 [DIRS 169861]). However, certain portions of the CHn stratigraphic unit are partly altered from vitric to zeolitic. In these altered layers, different rock properties are specified for vitric or zeolitic zones. All the geological units, including those representing fault zones, are treated as fracture-matrix systems using a dual-permeability approach, except the CHn vitric zones, which are treated as a single-continuum matrix because flow within these units is matrix dominated and units exhibit sparse fracturing. To model transition from single continuum to fracture-matrix dual continuum, global fracture-matrix connections are added across interfaces between TCw-PTn, PTn-TSw, and vitric-nonvitric CHn units. The van Genuchten relative permeability and capillary pressure functions (van Genuchten 1980 [DIRS 100610]) are used here to describe flow in both fractures and matrix. The van Genuchten functions have been traditionally used for analyzing unsaturated flow through Yucca Mountain tuffs, using data from core-sample analysis to estimate the model parameters. Note that the van Genuchten relations were developed for porous soils rather than fracture networks. However, a recent study (Liu and Bodvarsson 2001 [DIRS 160110]) found that the van Genuchten model is a valid approximation under the lower fracture saturation conditions that occur in the UZ of Yucca Mountain.

Flow and transport properties can be affected by changes in temperature through THM effects. Similarly, dissolution, precipitation, adsorption, and other geochemical reactions resulting from THC coupling can alter flow and transport properties. Fully coupled TH/THC/THM models are not developed. In this report, THC and THM effects are investigated separately to assess impacts on TH processes as described in Section 6.4 (mountain-scale THC model) and Section 6.5 (mountain-scale THM model).

6.2 TWO-DIMENSIONAL MOUNTAIN-SCALE TH MODEL RESULTS AND ANALYSES

TH processes occur at different spatial and temporal scales. During the early part of the heating period, important TH processes occur near the emplacement drifts. These are the drift-scale processes documented in *Drift-Scale Coupled Process (DST and TH Seepage) Models* (BSC 2005 [DIRS 172232]). At the drift-scale, variability in heat output from individual waste packages and different times of waste emplacement may give rise to variability in the extent of dryout, rewetting, and water flux along the drifts. Also at this scale, the availability of additional water in the condensation zone may lead to an augmented fracture liquid flux much greater than the ambient fracture flux. This increased fracture liquid flux may result in seepage of water into the emplacement drifts during the thermal period with elevated temperatures (BSC 2005 [DIRS 172232]). The present report does not address this issue of thermal seepage when water is able to overcome the capillary barrier of the open drift. However, it analyzes the magnitude of percolation flux augmentation caused by long-term heating at the repository. Changes in

percolation flux at the mountain-scale affect the potential for seepage into drifts during the thermal period.

At later times following waste emplacement, TH coupled processes at the mountain scale (i.e., the perturbation in temperature, liquid saturation, and percolation flux) take place over a much larger space domain compared to drift-scale effects (Haukwa et al. 2003 [DIRS 165165]). These mountain-scale TH processes include repository edge effects, large-scale enhanced water and gas flow, and temperature elevation in the far field. This section presents model results and analyses of the mountain-scale TH effects from the two-dimensional TH model. The use of two-dimensional modeling to predict long-term mountain-scale processes is acceptable because any effects related to the two-dimensional nature of the model have been found to be of short-term duration only. For example, any two-dimensional restriction on the axial flow of water vapor is of a short duration because any pressure build-up is quickly dissipated from the open drift through the high permeability fracture system.

As shown in Figure 6.1-1, the two-dimensional model vertical cross section is nearly perpendicular to the direction of the repository drifts. Therefore, it cannot simulate fluid and heat flow that occurs into or from the eastern and western directions (i.e., parallel to the drift axis). In particular, water-vapor transport and associated heat transfer along drift tunnels, and their effect on TH conditions near the repository, cannot be described by the two-dimensional model. Water-vapor migrating into the cooler regions (such as the access tunnel) and then condensing, occurring while the boiling front is expanding, is considered to be unimportant with respect to long-term prediction(s) of mountain-scale thermohydrology. This is because the maximum extent of boiling occurs in a few tens of years after 50 years of ventilation, whereas the mountain-scale TH prediction time frame is hundreds to thousands of years. Therefore, water-vapor migration predicted by the two-dimensional TH model for short time frames does not have a significant effect on long-term and mountain-scale TH behavior. Furthermore, in drift scale models the boiling front returns to near the drift wall in about 1,000 years so that any early, tens-of-years phenomena have no lasting effect on long-term TH responses (BSC 2005 [DIRS 172232], Section 6.2).

6.2.1 Base-Case Model Results and Analyses

As discussed in Section 6.1.5 and above, the base-case TH model (i.e., Base Case Thermal Loading) uses only 13.7% (BSC 2002 [DIRS 160975], Table 6-6; see Section 6.1.5 for more details) of the total thermal load in the first 50 years after waste emplacement (ventilation efficiency 86.3%). After 50 years, 100% of the available thermal load is applied to the repository drifts. As discussed at the beginning of this section, the important mountain-scale TH changes are perturbations in temperature, fracture and matrix liquid saturation, and fracture fluxes. In this report, contours showing evolution of temperature and fracture liquid saturation at different times are discussed first. These contour plots provide an overall picture of the TH perturbation in the entire two-dimensional mountain-scale TH model domain. Second, line plots (profiles) of temperature, fracture and matrix liquid saturation, and fracture fluxes at various locations and times are analyzed to develop a more specific understanding of the TH processes. The locations of interest in the two-dimensional TH model domain are the north–south axis just above and below the repository, the bottom of the PTn stratigraphic unit (about 125 to 150 m above the emplacement drifts), and the bottom of the TSw stratigraphic unit (about 75 to 100 m

below the emplacement drifts). Analyzing the TH responses at these locations provides quantitative and qualitative evaluation of the extent of TH perturbation both near and far away from the emplacement drifts.

6.2.1.1 Contours of Temperature and Fracture Saturation

Evolution of temperature and liquid saturation near the drifts and within the unsaturated zone provides for an assessment of the distribution of liquid water that potentially contributes to seepage into drifts. Temperature at or above boiling conditions precludes seepage because of vaporization. Likewise, extensive dry or reduced liquid saturation conditions preclude seepage because local liquid build-up to saturation conditions is required to initiate seepage.

Figures 6.2-1 through 6.2-5 show the evolution of temperature and liquid saturation at selected times from 100 to 8,000 years. These figures show the spatial and temporal extent of heating and drying, which sets the stage for the modeling of THC and THM processes later.

The predicted TH conditions in the rock 100 years after the emplacement of waste are shown in Figures 6.2-1a and 6.2-1b. These figures, generated from the base-case simulations (data extraction and plotting procedures are summarized in Appendix IV, Section IV.1), show the contours of temperature and fracture liquid saturation, respectively, in the two-dimensional N-S refined grid of the UZ model grid. Note that the thick, blue zone, indicating higher (~80%) saturation in the lower, southern portion of Figure 6.2-1b shows matrix saturation, not fracture saturation, because this layer is vitric and simulated as a non-fractured zone (i.e., without a fracture continuum). At this early time, the model results also show that there is little change in both fracture and matrix liquid saturation along the cross section except in the immediate vicinity of the drifts (Figure 6.2-1b). The contours of fracture liquid saturation show drying (reduction from ambient saturation condition) around the drifts. The impact of heat 100 years after emplacement is significant only within a few meters for liquid saturation (Figure 6.2-1b) and a few tens of meters for temperature (Figure 6.2-1a). While the temperatures in regions immediately surrounding the drifts rise to boiling conditions (~96°C) at 100 years, the space between two adjacent drifts (i.e., the pillar region) is still at a temperature of about 60°C.

Later, TH changes occur over a larger space domain. After 500 years (Figures 6.2-2a and 6.2-2b), contours of temperature and fracture saturation show that perturbations in temperature extend more than 150 m above and below the repository. Temperatures at the pillar region at this time remain well below boiling conditions. At 500 years, perturbations in liquid saturation (in the form of drying) are still restricted to within a few meters of the drift. At this time, matrix liquid saturation in the pillar region is predicted to be ambient, i.e., no drying is evident in the pillar region. Drying around the emplacement drifts is also evident in the fracture liquid saturation (Figure 6.2-2b). Laterally, the extent of drying in the fractures is not observed beyond a few meters from the emplacement drifts. Fractures in the pillar region remain at ambient conditions after 500 years of heating. These same trends in temperature, matrix, and fracture liquid saturation are observable even at 1,000 years of heating (see Figures 6.2-3a and 6.2-3b).

At 5,000 years of heating, however, temperatures have cooled down considerably (see Figure 6.2-4a), even close to the emplacement drifts. Though temperature perturbation exists

over a large area, nowhere in the mountain is it predicted to be more than 70°C to 80°C. The liquid saturation in both the rock matrix and the fractures (Figure 6.2-4b) has returned to mostly ambient conditions at 5,000 years. Figures 6.2-5a and 6.2-5b show the temperature and fracture liquid saturation, respectively, at 8,000 years. With continuous radioactive decay, temperatures have declined further and are below 55°C everywhere in the mountain. Matrix and fracture liquid saturation have also returned to their preheating conditions. The thermal period in the mountain does not last much longer than 8,000 years. Beyond this time, conditions are essentially ambient in the mountain.

6.2.1.2 Temperature along the North–South Axis

In Figure 6.2-6a, temperatures at different times are shown along the north–south cross section through the emplacement drifts for the base-case thermal-loading scenario. At 100 years, the temperatures reach 96°C (boiling conditions) at the drifts as shown by peaks in temperature, while temperature within the pillar regions is around 60°C. After 500 years, the drifts are still at around 96°C but the mid-pillar regions have reached a temperature of about 84°C. The maximum mid-pillar temperature is predicted to be around 88°C at 1,000 years (8 degrees below boiling conditions at the drifts). After 1,000 years, temperatures start to decline, and the large difference in temperature between the drifts and the mid-pillar regions begins to decrease. For example, at 3,000 years, temperatures at both the locations directly above the drift and the mid-pillar regions have declined below 80°C, and the difference between the peaks (directly above drifts) and the troughs (mid-pillar regions) is no more than 3 to 4°C. After 8,000 years, temperatures at the crown of the drift across the north–south axis of the repository are predicted to decline below 55°C.

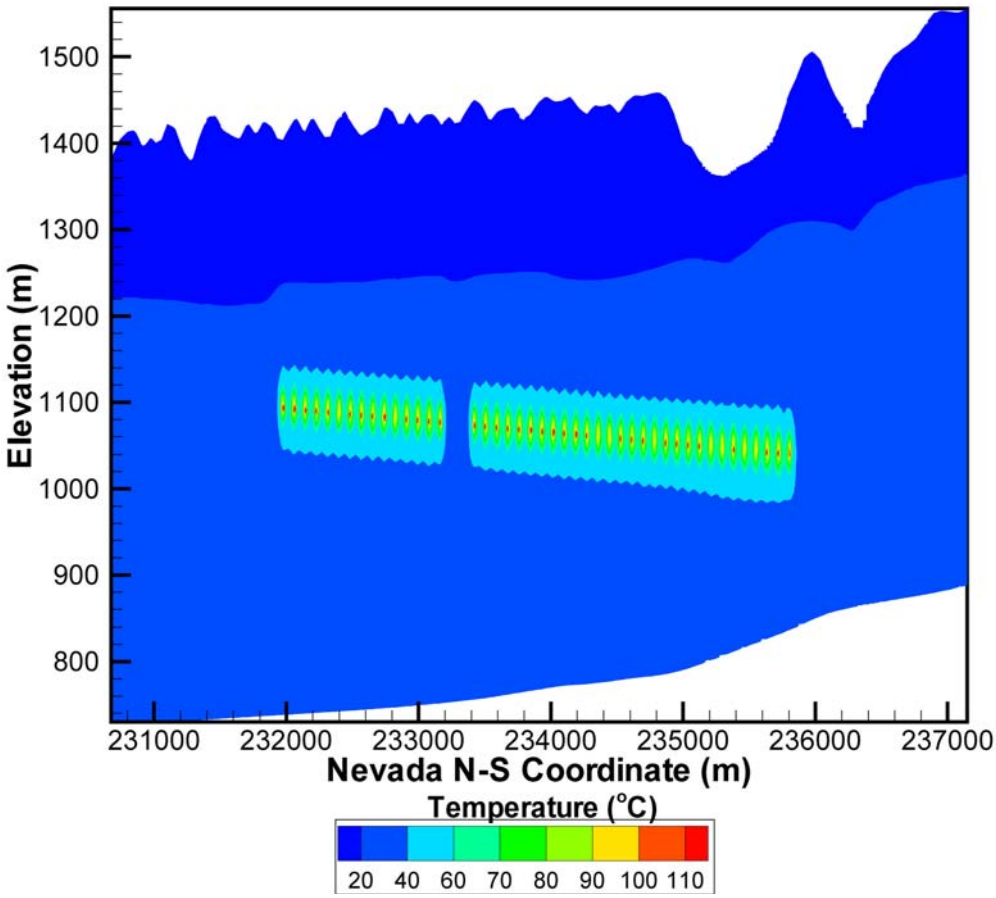

Output DTN: LB0310MTSCLTH2.001.

Figure 6.2-1a. Contours of Temperature in the Two-Dimensional North–South Cross Section of the UZ Model Grid at 100 Years: Base-Case Thermal Loading

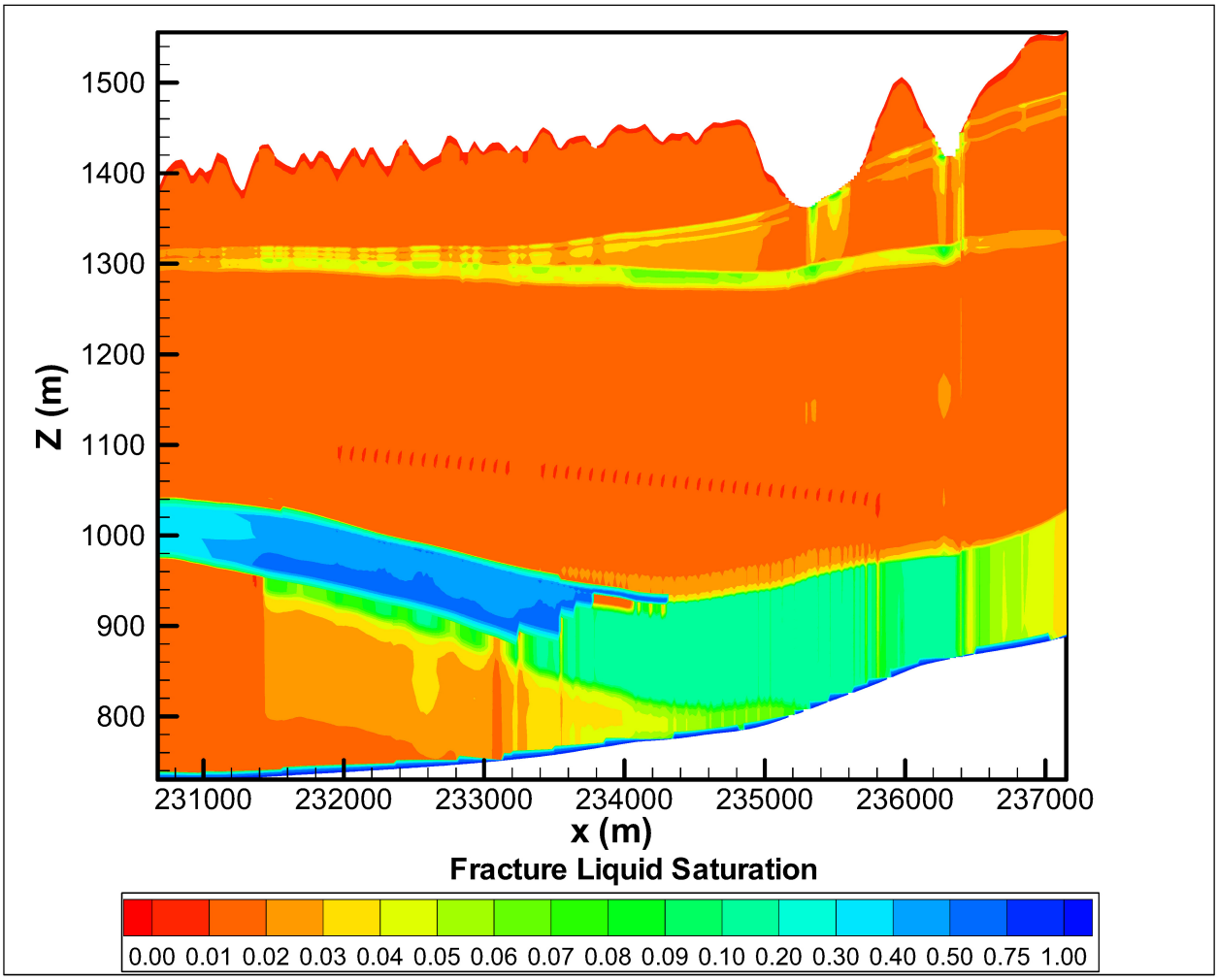

Output DTN: LB0310MTSCLTH2.001.

NOTE: The thick, blue layer at the lower left side of the figure represents matrix saturation, as the vitric layer in that region is simulated as nonfractured (i.e., the fracture continuum is absent in that region).

Figure 6.2-1b. Contours of Fracture Liquid Saturation in the Two-Dimensional North–South Cross Section of the UZ Model Grid at 100 Years: Base-Case Thermal Loading

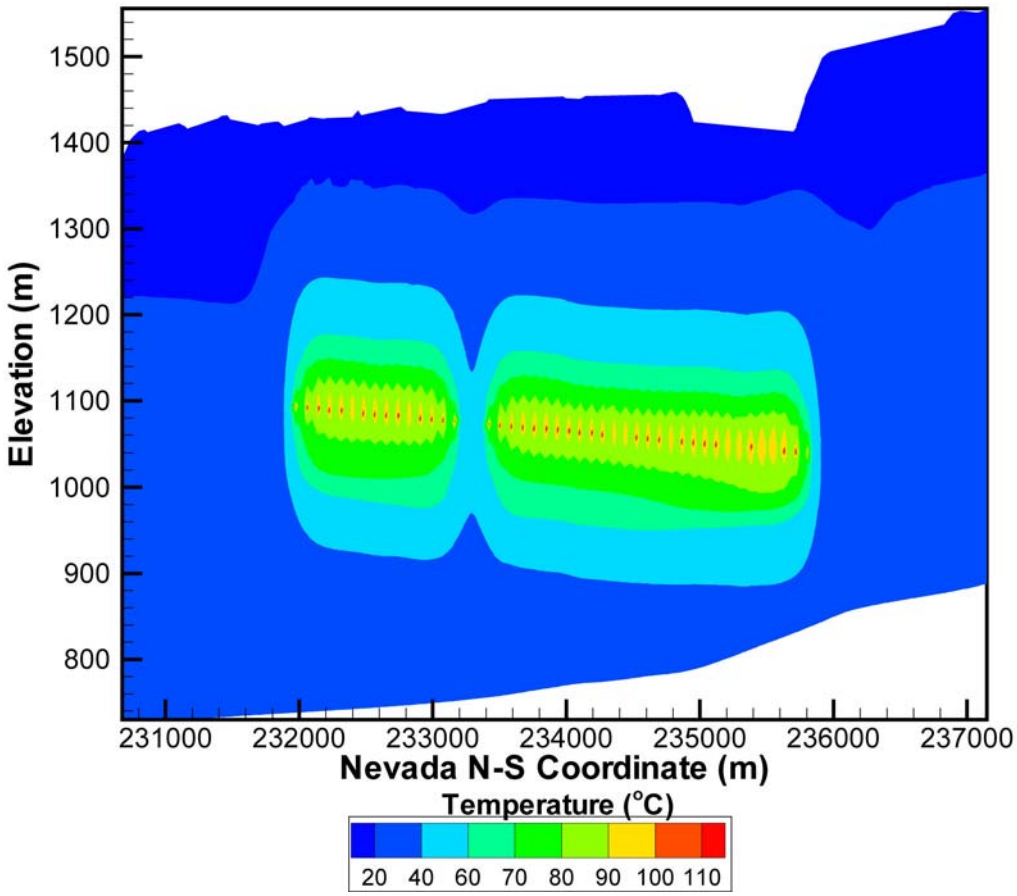

Output DTN: LB0310MTSCLTH2.001.

Figure 6.2-2a. Contours of Temperature in the Two-Dimensional North–South Cross Section of the UZ Model Grid at 500 Years: Base-Case Thermal Loading

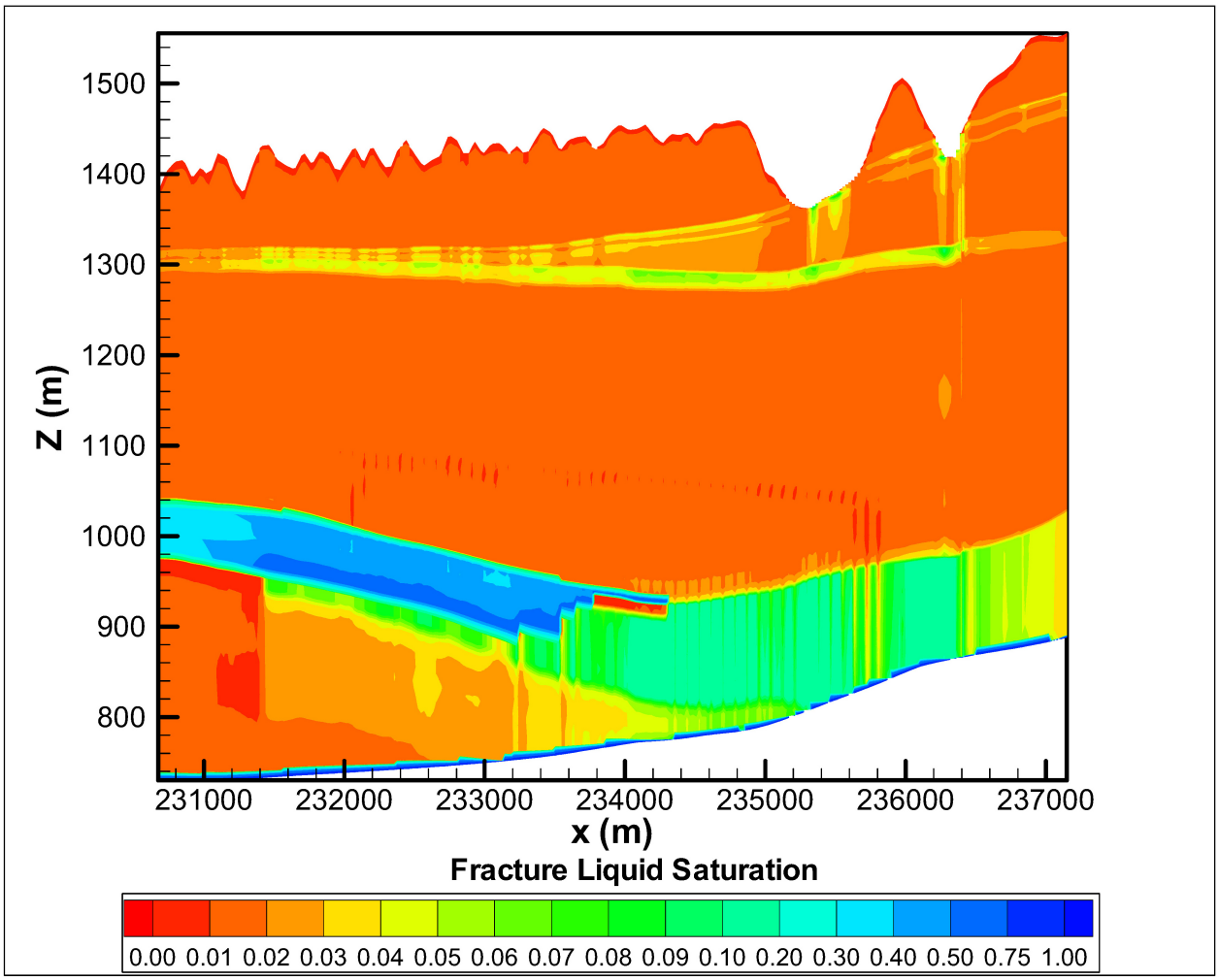

Output DTN: LB0310MTSCLTH2.001.

NOTE: The thick, blue layer at the lower left side of the figure represents matrix saturation, as the vitric layer in that region is simulated as nonfractured (i.e., the fracture continuum is absent in that region).

Figure 6.2-2b. Contours of Fracture Liquid Saturation in the Two-Dimensional North–South Cross Section of the UZ Model Grid at 500 Years: Base-Case Thermal Loading

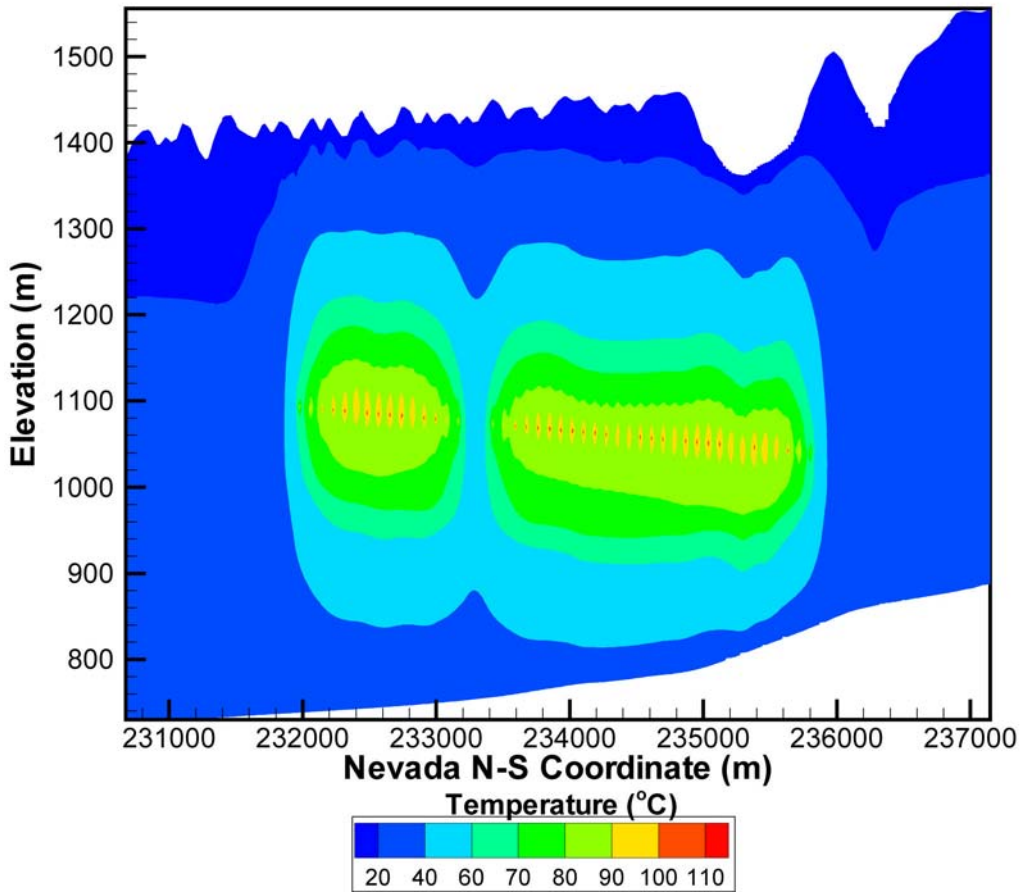

Output DTN: LB0310MTSCLTH2.001.

Figure 6.2-3a. Contours of Temperature in the Two-Dimensional North–South Cross Section of the UZ Model Grid at 1,000 Years: Base-Case Thermal Loading

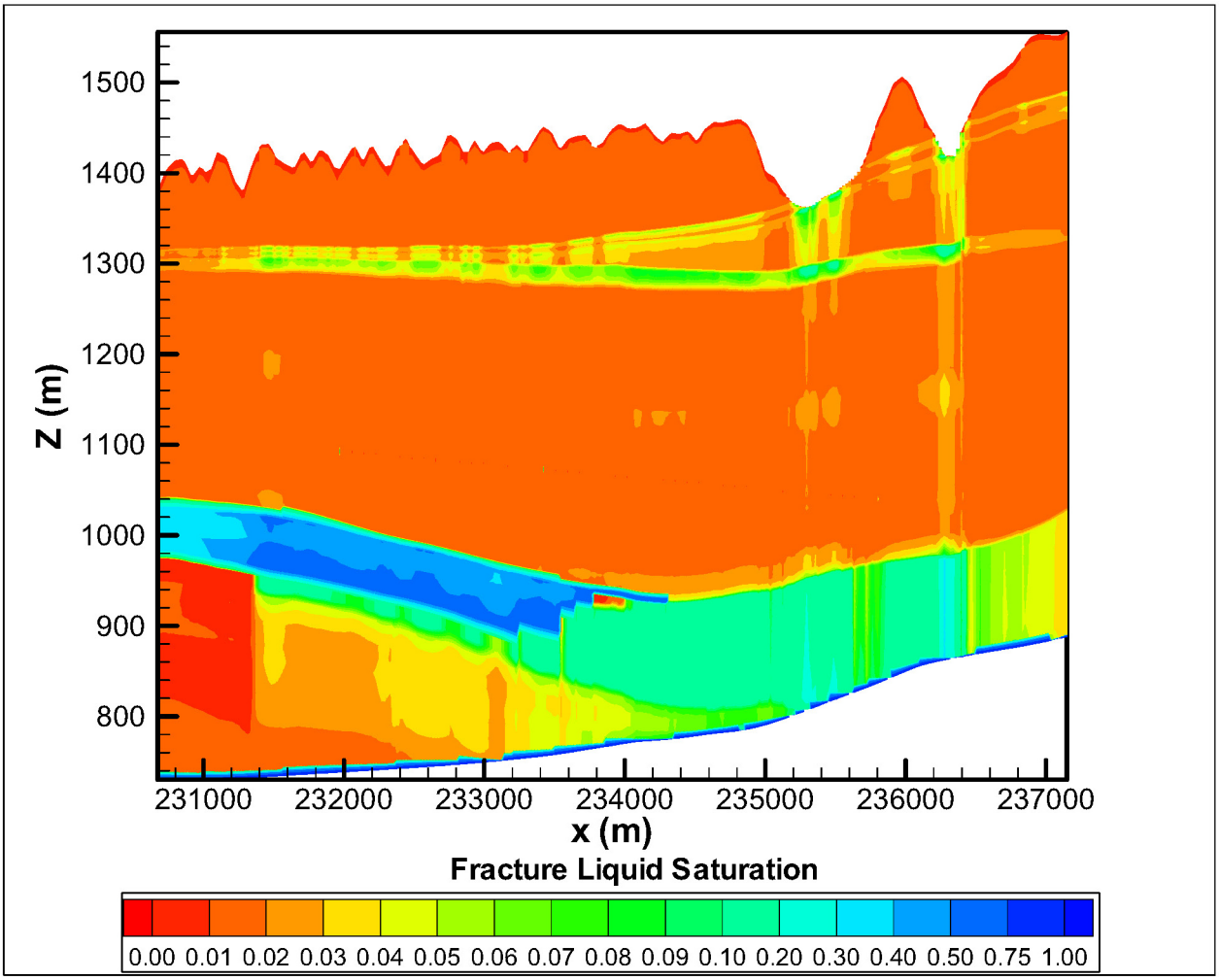

Output DTN: LB0310MTSCLTH2.001.

NOTE: The thick, blue layer at the lower left side of the figure represents matrix saturation, as the vitric layer in that region is simulated as nonfractured (i.e., the fracture continuum is absent in that region).

Figure 6.2-3b. Contours of Fracture Liquid Saturation in the Two-Dimensional North–South Cross Section of the UZ Model Grid at 1,000 Years: Base-Case Thermal Loading

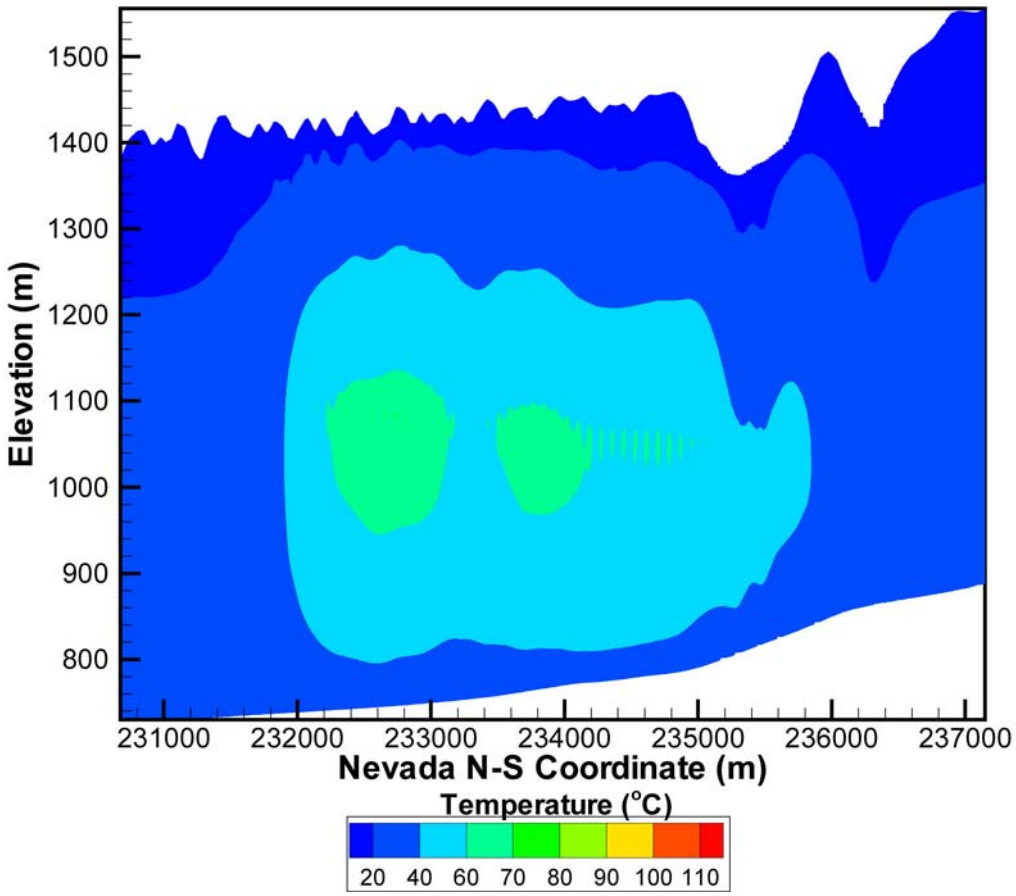

Output DTN: LB0310MTSCLTH2.001.

Figure 6.2-4a. Contours of Temperature in the Two-Dimensional North–South Cross Section of the UZ Model Grid at 5,000 Years: Base-Case Thermal Loading

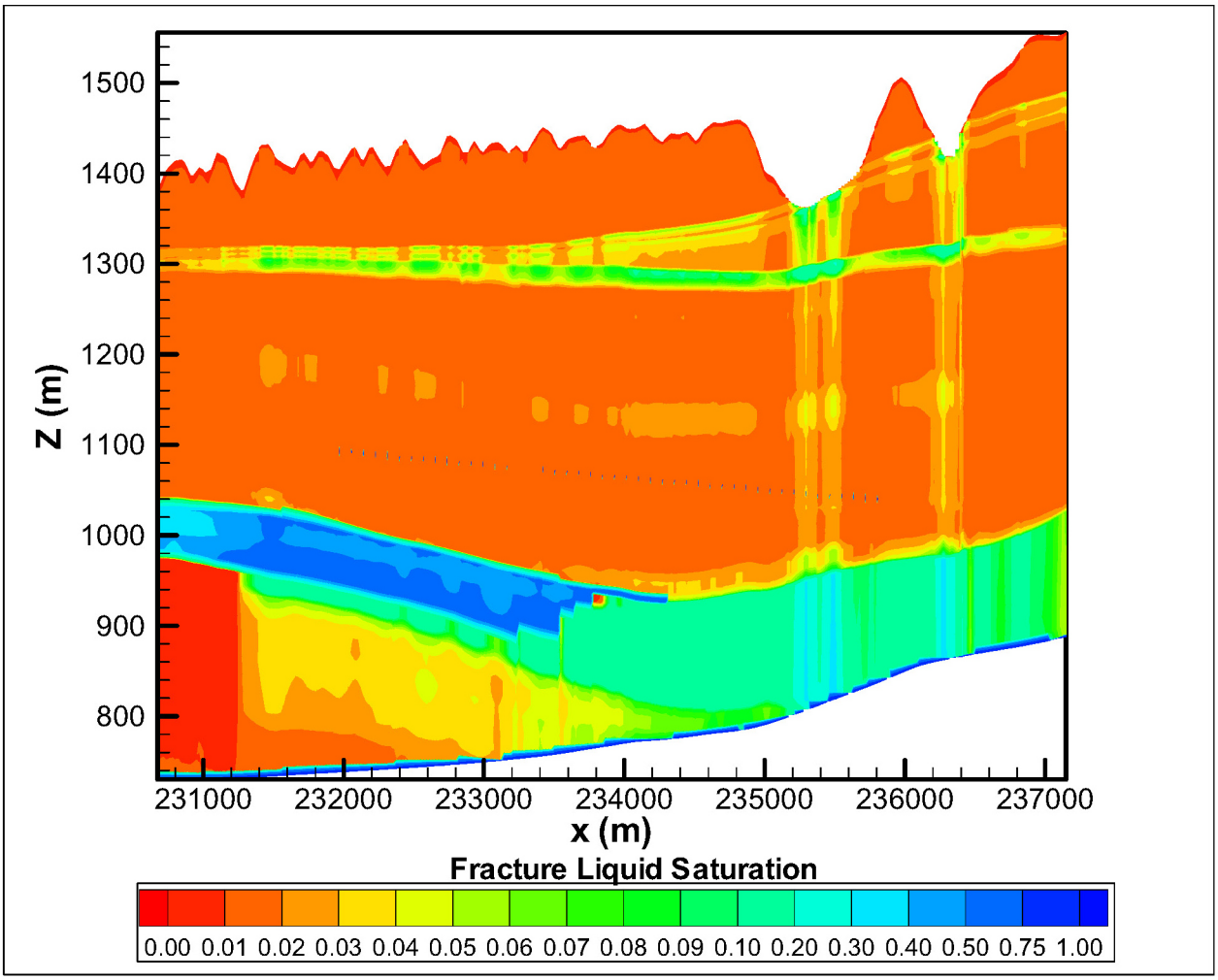

Output DTN: LB0310MTSCLTH2.001.

NOTE: The thick, blue layer at the lower left side of the figure represents matrix saturation, as the vitric layer in that region is simulated as nonfractured (i.e., the fracture continuum is absent in that region).

Figure 6.2-4b. Contours of Fracture Liquid Saturation in the Two-Dimensional North–South Cross Section of the UZ Model Grid at 5,000 Years: Base-Case Thermal Loading

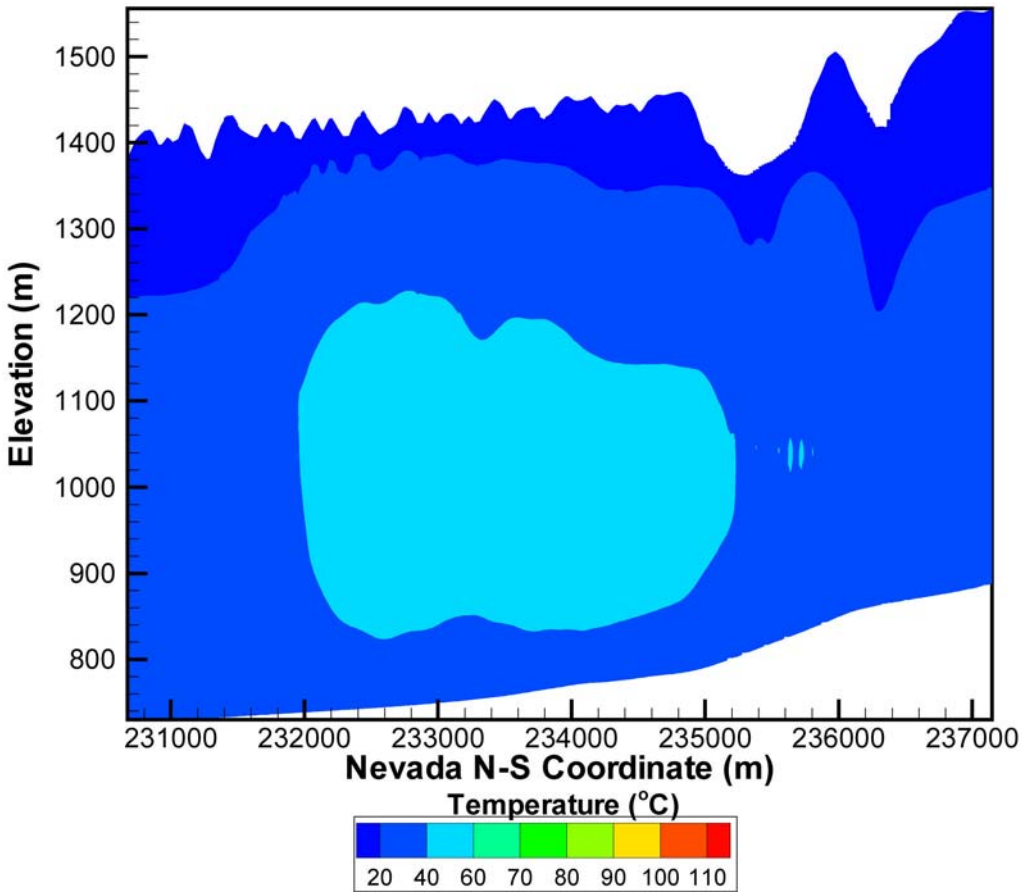

Output DTN: LB0310MTSCLTH2.001.

Figure 6.2-5a. Contours of Temperature in the Two-Dimensional North–South Cross Section of the UZ Model Grid at 8,000 Years: Base-Case Thermal Loading

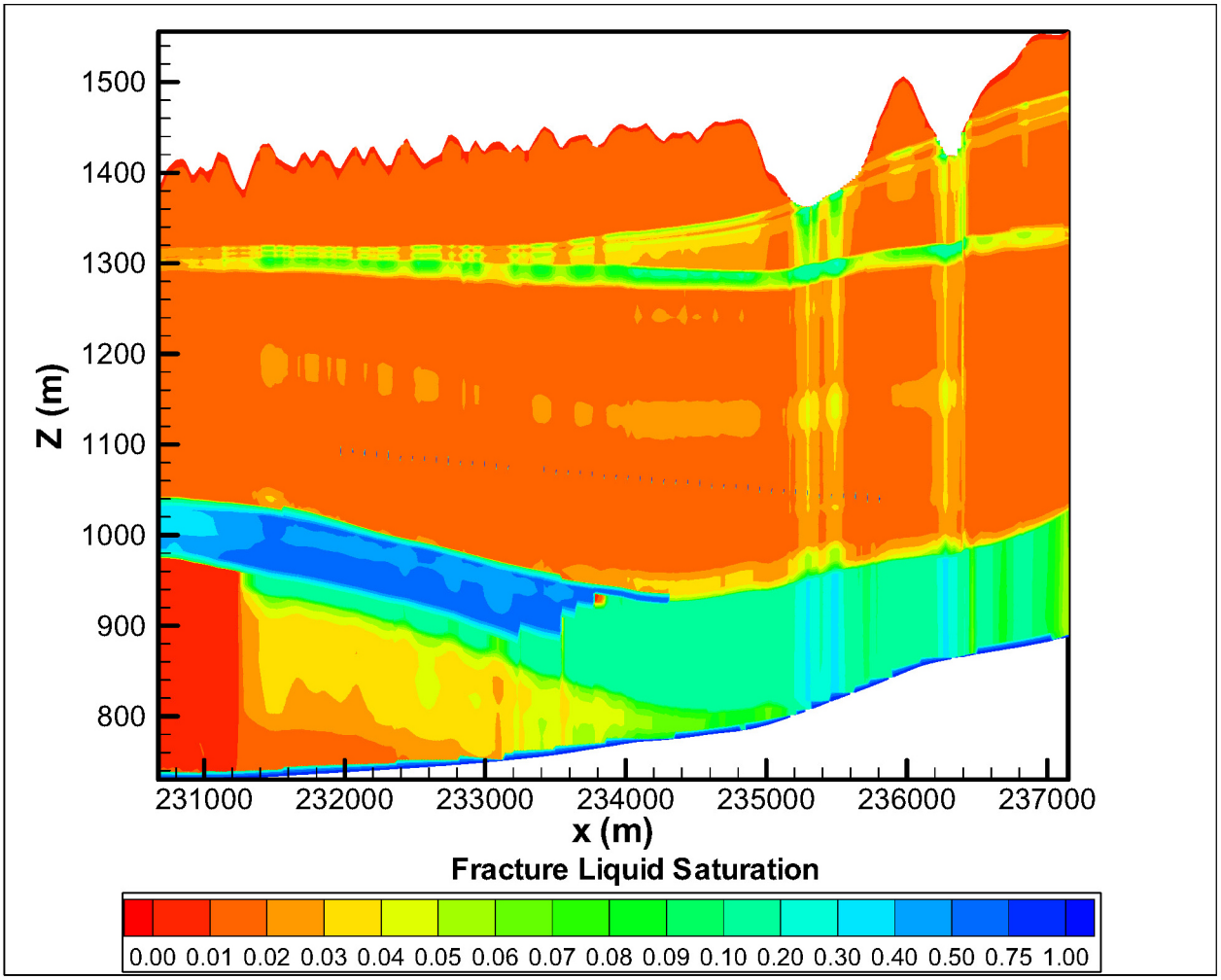

Output DTN: LB0310MTSCLTH2.001.

NOTE: The thick, blue layer at the lower left side of the figure represents matrix saturation, as the vitric layer in that region is simulated as nonfractured (i.e., the fracture continuum is absent in that region).

Figure 6.2-5b. Contours of Fracture Liquid Saturation in the Two-Dimensional North–South Cross Section of the UZ Model Grid at 8,000 Years: Base-Case Thermal Loading

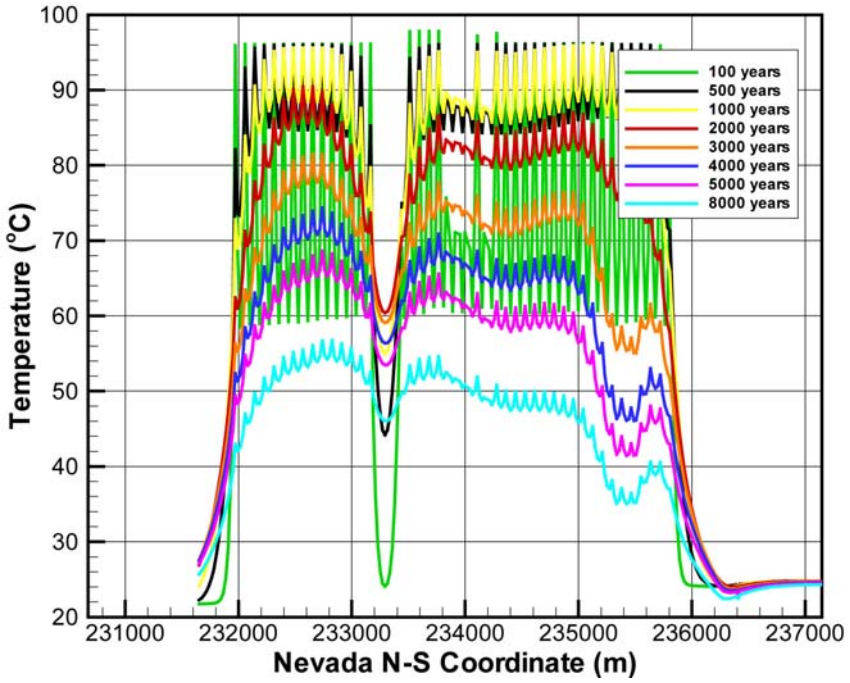

Output DTN: LB0310MTSCLTH2.001.

Figure 6.2-6a. Temperature along the North–South Cross Section across the Emplacement Drifts: Base-Case Thermal Loading

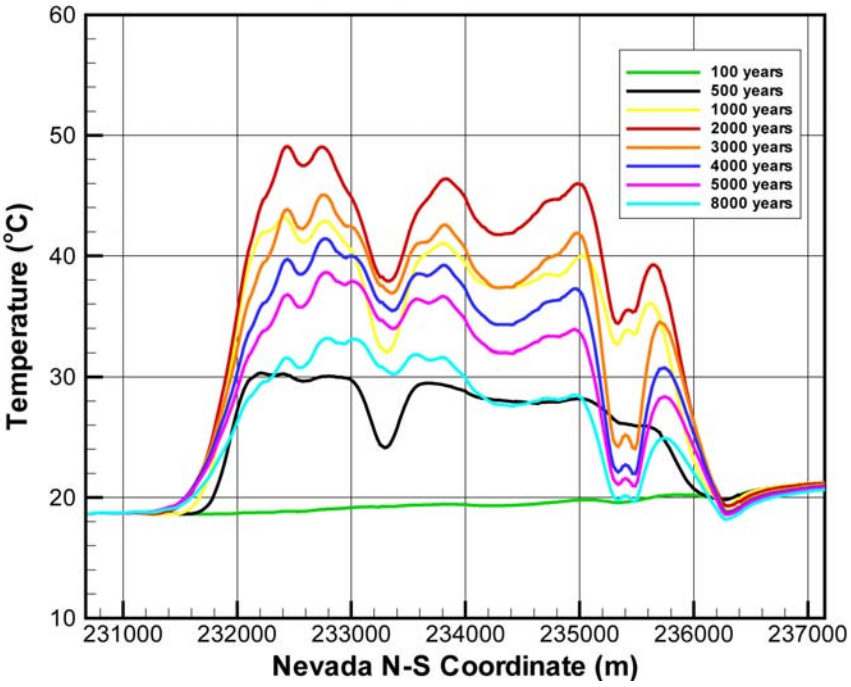

Output DTN: LB0310MTSCLTH2.001.

Figure 6.2-6b. Temperature along the North–South Cross Section at the Bottom of PTn: Base-Case Thermal Loading

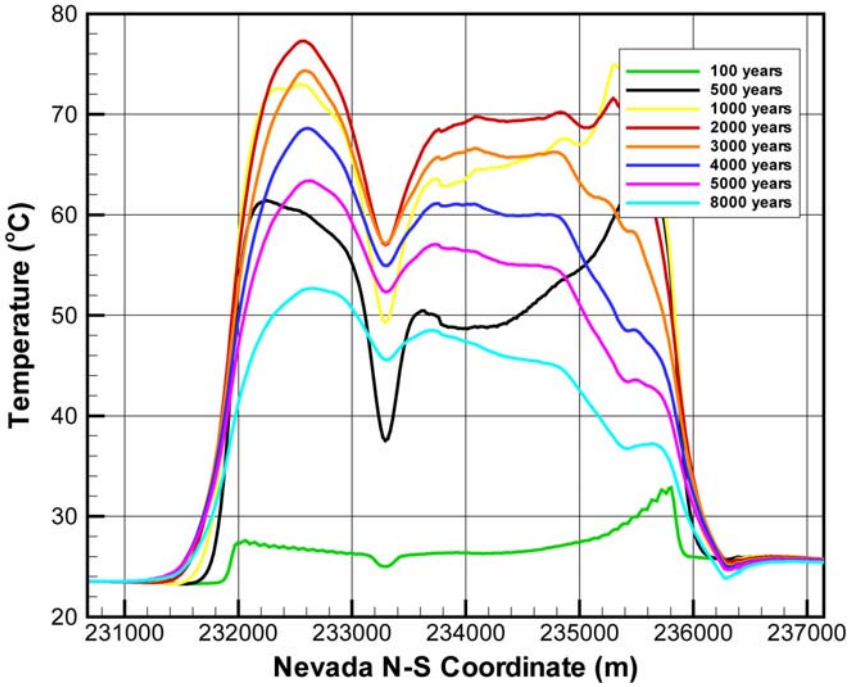

Output DTN: LB0310MTSCLTH2.001.

Figure 6.2-6c. Temperature along the North–South Cross Section at the Bottom of TSw: Base-Case Thermal Loading

Figure 6.2-6b is similar to Figure 6.2-6a except that it shows temperature at the bottom of the PTn. At 100 years, temperatures at the bottom of the PTn are still below 20°C. In other words, temperatures are still ambient, and the impact of heat has not extended up to the bottom of the PTn. At 500 years, however, temperatures at the bottom of the PTn have started to increase due to heat from the emplaced waste. Temperatures at the bottom of the PTn are predicted to reach a maximum of about 50°C at 2,000 years. After this period, temperatures start to decline, and by 8,000 years temperatures at the PTn bottom have steadily cooled to just above 30°C and are predicted to return to ambient conditions soon after. Therefore, the bottom of the PTn experiences a thermal perturbation not more than 30°C above ambient conditions during the 10,000-year compliance period.

The extent and duration of the thermal perturbation below the repository can be seen in Figure 6.2-6c, which shows temperatures at the bottom of the TSw along the north–south axis of the repository. The pattern of temperature rise and decline in this figure is similar to that in Figure 6.2-6b. Here, however, the maximum predicted temperature is about 75°C at 2,000 years (Figure 6.2-6c). After that, temperatures gradually decline to about a maximum of 50°C at 8,000 years. The higher peak temperature at the bottom of TSw compared to the bottom of PTn can be attributed to its location close to the repository horizon. Also, since the water table in the present TH model is maintained at a constant temperature, the predicted increase in temperature at the bottom of the TSw is somewhat underestimated (less than 5°C). The smaller peak temperatures at the northern end of the repository are attributed to higher infiltration rates in the north

compared to the southern areas of the unsaturated zone domain (BSC 2004 [DIRS 169861], Section 6.1).

6.2.1.3 Matrix Liquid Saturation along the North–South Axis

Figures 6.2-7a to 6.2-7c show the matrix liquid saturation at different times for three different locations. Figure 6.2-7a shows the matrix liquid saturation along the north–south axis at the repository horizon directly above the repository drift. Drying associated with a heated drift is predicted, reducing the saturation to a minimum between 100 to 1,000 years after emplacement of waste. After 1,000 years, resaturation commences, and the matrix saturation at the crown of the drift returns to ambient condition at or around 5,000 years. The slight increase in matrix saturation above the present-day saturation during later times results from increased infiltration after climate change (around 2,000 years). Matrix liquid saturation at the bottom of the PTn is shown in Figure 6.2-7b. Since the peak temperature at the bottom of the PTn was never higher than 50°C and never approached boiling, the changes in matrix saturation at the PTn bottom caused by heating are negligible. The step-wise increase in matrix saturation at 1,000 years and 3,000 years in Figure 6.2-7b results from climate changes at 600 years and 2,000 years, respectively. Figure 6.2-7c similarly shows the matrix liquid saturation at the bottom of the TSw. Because of the below-boiling conditions prevailing at this location, changes in matrix liquid saturation from ambient saturation values are minimal at any time. The significantly different matrix saturations for the northern and southern ends of the repository at the bottom of TSw result from vitric-zeolitic transition.

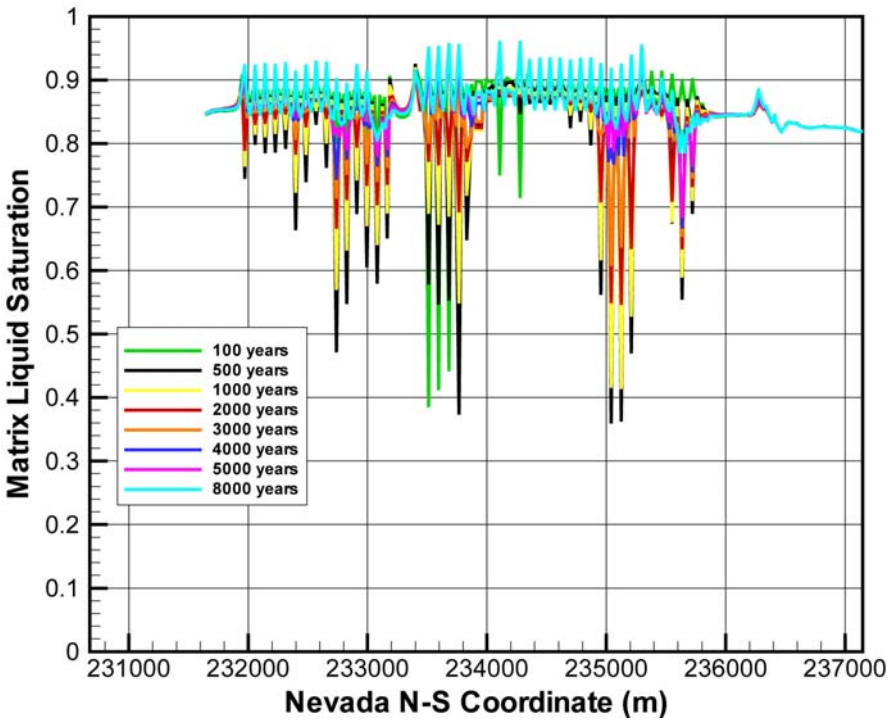

Output DTN: LB0310MTSCLTH2.001.

Figure 6.2-7a. Matrix Liquid Saturation at the Repository Horizon along the North–South Cross Section: Base-Case Thermal Loading

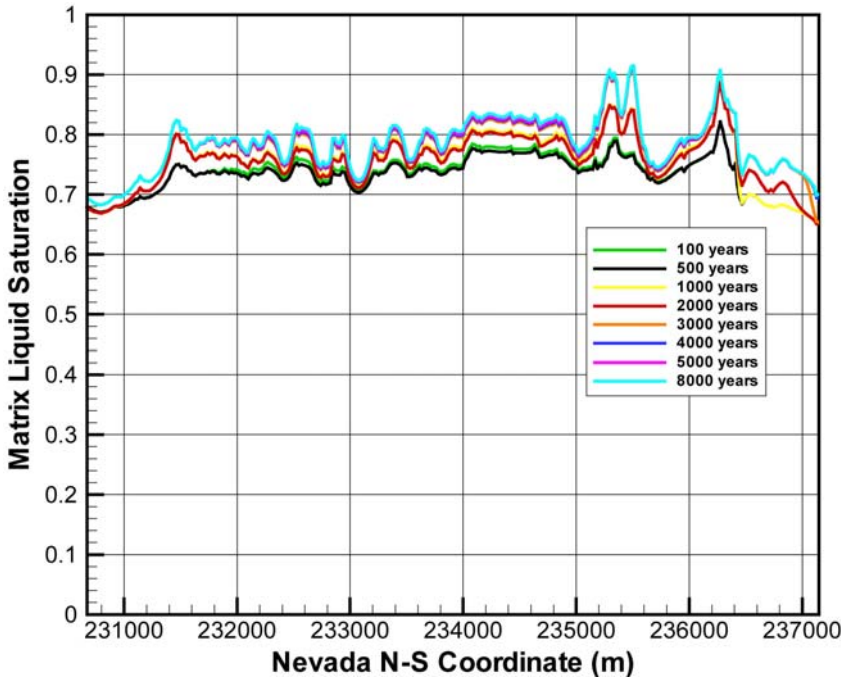

Output DTN: LB0310MTSCLTH2.001.

Figure 6.2-7b. Matrix Liquid Saturation at the Bottom of PTn: Base-Case Thermal Loading

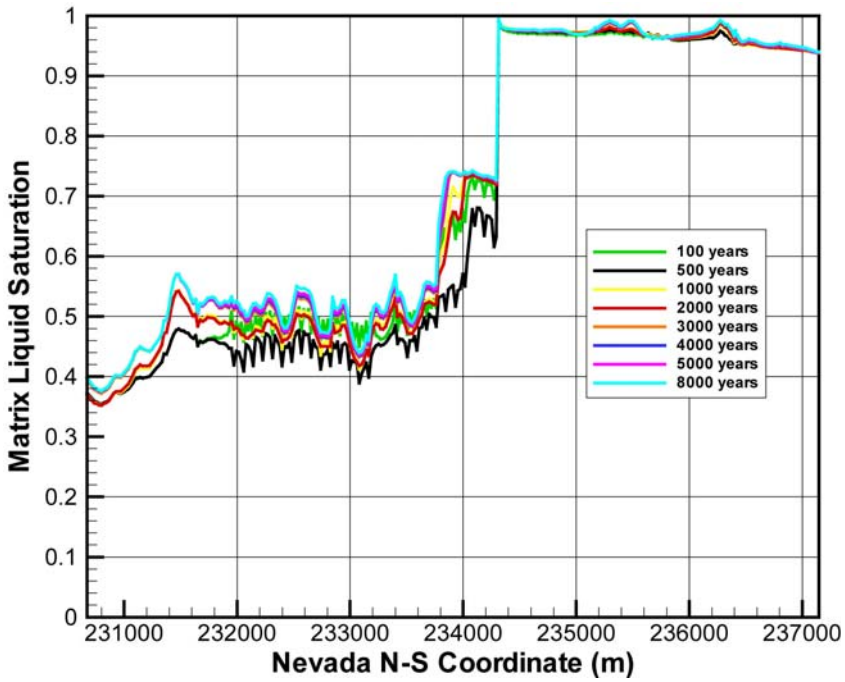

Output DTN: LB0310MTSCLTH2.001.

Figure 6.2-7c. Matrix Liquid Saturation at the Bottom of TSw: Base-Case Thermal Loading

6.2.1.4 Fracture Liquid Saturation along the North–South Axis

Figures 6.2-8a to 6.2-8d illustrate fracture liquid saturation during the thermal period. Figure 6.2-8a shows fracture liquid saturation along the north–south axis (directly above drift and within drift pillars) at the repository horizon. Under ambient conditions, fractures in Yucca Mountain are dry compared to the matrix because of the large fracture apertures and relatively smaller capillary suction in the fractures compared to the rock matrix. Heating during the thermal period mobilizes some of the matrix pore water through the fractures after condensation of the boiled water. However, since no large-scale boiling is evident with the base-case thermal loading, fractures remain essentially dry and retain their ambient conditions at most locations. Fractures above the emplacement drifts show limited drying. Fractures in the pillar region show almost no sign of drying. Also, because of climate changes, fractures are more saturated in the future than at present. Figure 6.2-8b similarly shows the fracture liquid saturation along the north–south axis just below the repository. The patterns are similar to those in Figure 6.2-8a, except that drying is more extensive below the drifts than above, mostly because of the capillary barrier effects of the emplacement drifts. The increase in fracture saturation at future times is attributed to climate changes. Figures 6.2-8c and 6.2-8d similarly illustrate that thermal perturbations in fracture liquid saturation at the bottom of the PTn and the bottom of the TSw, respectively, are minimal at any time during the thermal period. The predicted changes are primarily due to climate induced changes in net infiltration.

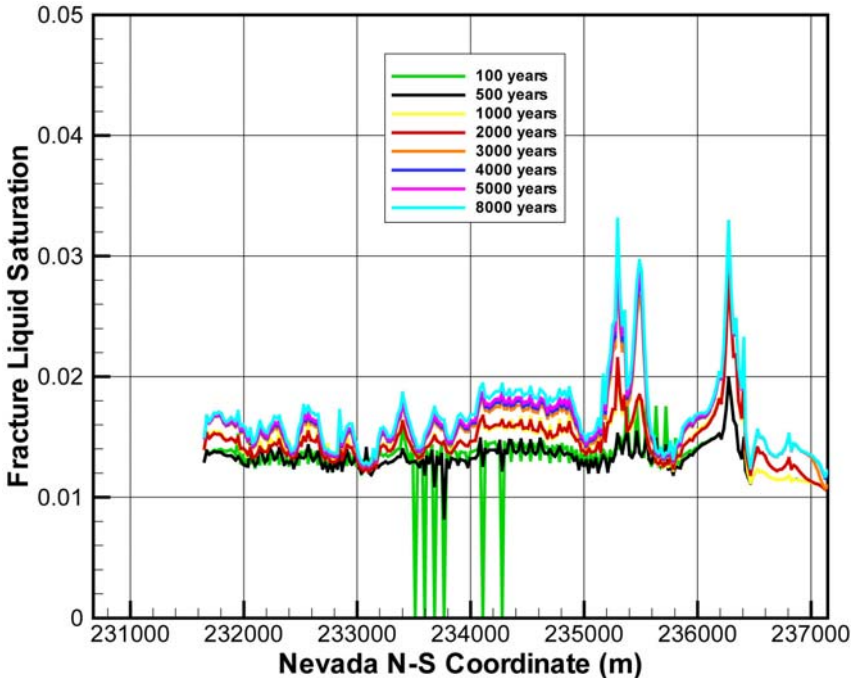

Output DTN: LB0310MTSCLTH2.001.

Figure 6.2-8a. Fracture Liquid Saturation at the Repository Horizon, above the Emplacement Drifts and between Drift Pillars: Base-Case Thermal Loading

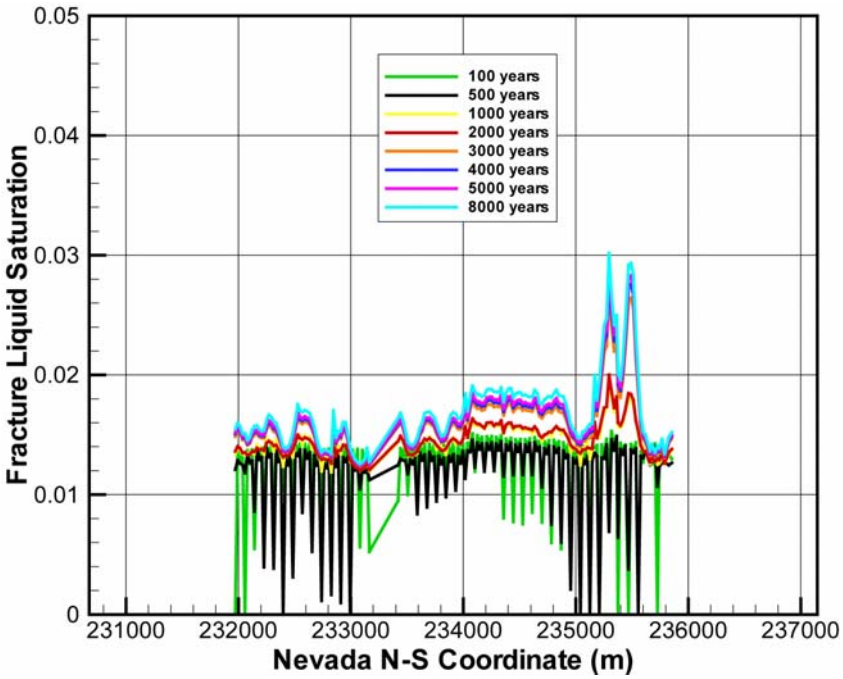

Output DTN: LB0310MTSCLTH2.001.

Figure 6.2-8b. Fracture Liquid Saturation at the Repository Horizon below the Emplacement Drifts and between Drift Pillars: Base-Case Thermal Loading

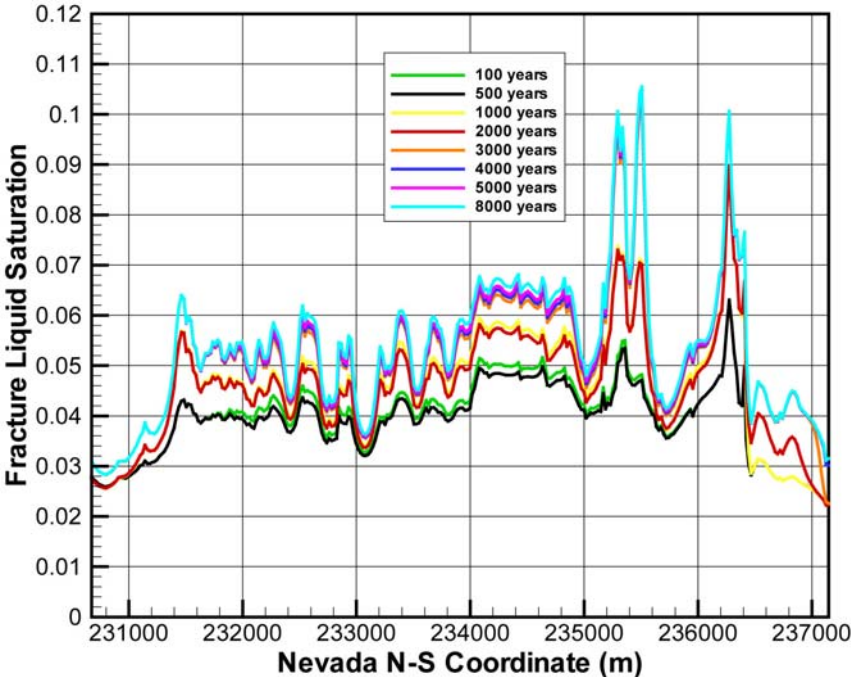

Output DTN: LB0310MTSCLTH2.001.

Figure 6.2-8c. Fracture Liquid Saturation at the Bottom of PTn: Base-Case Thermal Loading

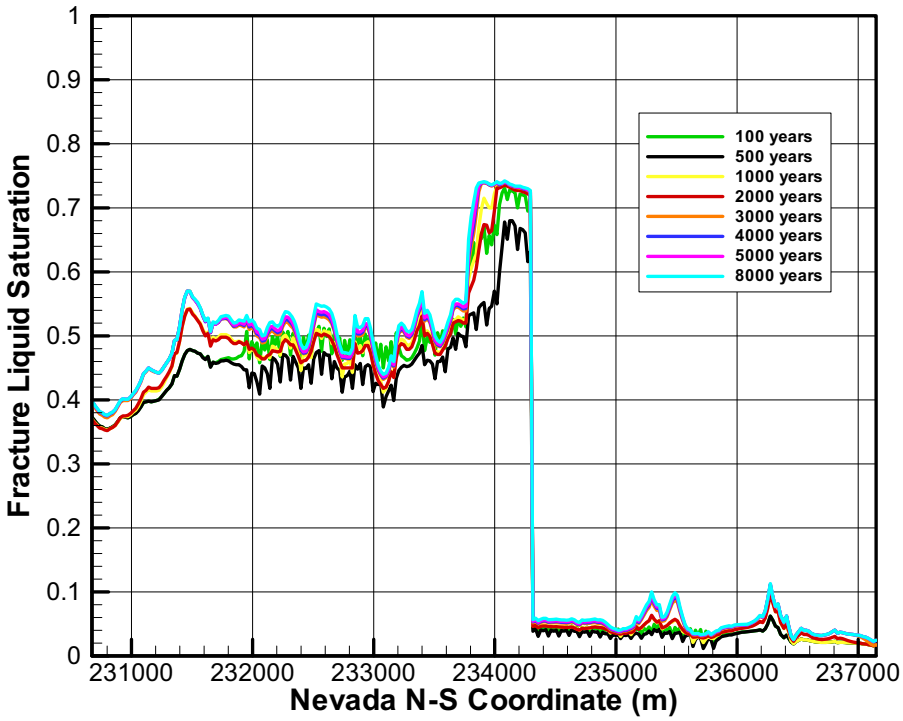

Output DTN: LB0310MTSCLTH2.001.

Figure 6.2-8d. Fracture Liquid Saturation at the Bottom of TSw: Base-Case Thermal Loading

6.2.1.5 Vertical Profiles of Temperature, Liquid Saturation, and Fracture Flux

A further estimate of the extent of perturbation in temperature and saturation can be obtained by analyzing the vertical profiles of these variables at selected locations along the cross section. Figures 6.2-9a to 6.2-9d show the temperature, matrix liquid saturation, and fracture liquid saturation along column "b62" of the two-dimensional N-S cross-sectional grid. Column "b62" is situated approximately at N-S coordinate 234100 m and runs from the surface to the water table; in this column, the repository is at an elevation of 1063.5 m. Figure 6.2-9a shows that the temperature reaches a maximum of about 96°C at the repository horizon at 100 years. Temperatures are lower above and below the repository horizon, although they increase with time, reaching maximum values between 1,000 to 2,000 years after waste emplacement. After 2,000 years temperatures decline everywhere. At 8,000 years, maximum temperature in this column has declined to about 50°C. Matrix liquid saturation (Figure 6.2-9b) along the vertical column shows little variation from its ambient condition, except for limited drying at the repository horizon during the peak thermal period. Figure 6.2-9c shows fracture liquid saturation along column "b62." At almost every location, particularly above the repository horizon, there is little change in fracture liquid saturation from ambient conditions through the thermal period. However, just above the repository, considerable build-up of saturation occurs. This is partly a result of the capillary barrier effect, which prevents water from entering the emplacement drift, resulting in some build-up in saturation just above the repository. Another source of this build-up is the increased surface infiltration rates during the monsoon and glacial transition climates. Gravity-induced drainage through the pillar regions, that is, the region

between the adjacent drifts, is evident in the fracture saturation profile of Figure 6.2-9c. The increase in saturation below about 925 m in elevation (and no build-up at all above the repository horizon) is a result of fast gravity drainage through the highly conductive fractures and between the drifts through the pillar regions during the wetter monsoon and glacial transition climates.

Figure 6.2-9d shows the vertical fluxes (per unit cross section) in fractures as a function of elevation along column "b62." In this figure, vertical fluxes in fractures, expressed as millimeters per year, are shown at various times. In column b62, the vertical fracture flux at the ground surface (elevation ~1,450 masl) is about 9 mm/yr. At 100 years, there is a significant (~100 mm/yr) build-up of flux between the first node above drift and the emplacement drift (at ~1,063 masl). Because of the capillary barrier effects of the emplacement drifts, vertical fluxes immediately below the drift are nonexistent. This results in a spike in vertical fracture fluxes just above and below the drift. On the other hand, the spike in vertical fracture fluxes at approximately 940 masl is an artifact of the modeling approach adopted in this study. Recall that the vitric layer present at that location has been modeled as a nonfractured matrix continuum. Since there are no fractures present at that location, vertical fractures are represented as zero. The jump in vertical fracture fluxes at 1,000 years and 3,000 years in Figure 6.2-9d results from the modeling assumption of step changes in infiltration flux due to changes in climatic conditions at 600 years (transition from present-day to monsoon climate) and 2,000 years (transition from monsoon to glacial transition climate), respectively.

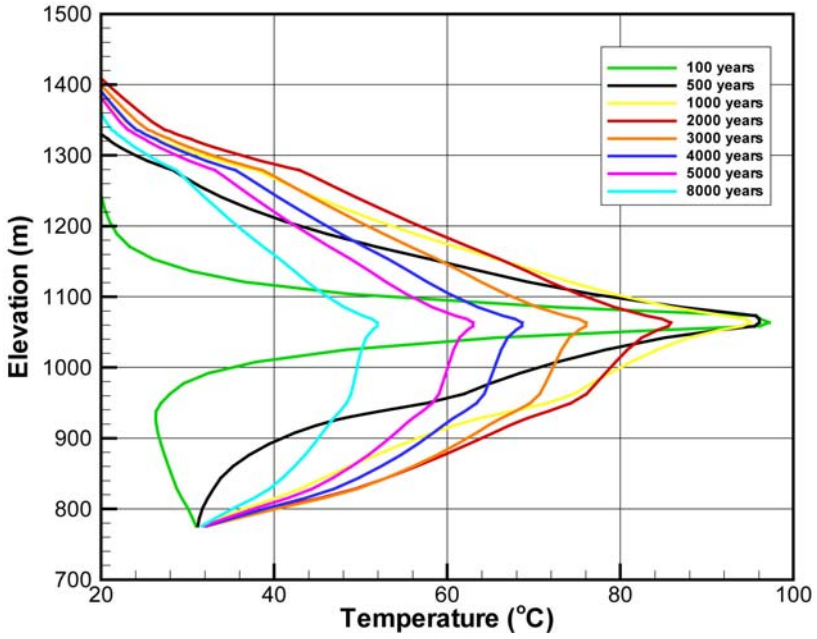

Output DTN: LB0310MTSCLTH2.001.

NOTE: Column "b62" is a model location near the center of the north–south cross section, at 234100 m in Figure 6.1-1.

Figure 6.2-9a. Temperature along a Vertical Column ("b62") from Ground Surface to Water Table: Base-Case Thermal Loading

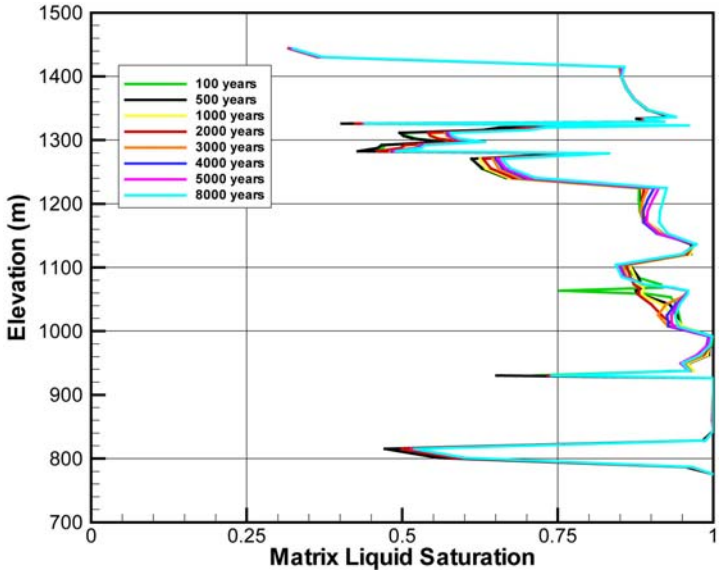

Output DTN: LB0310MTSCLTH2.001.

NOTE: Column "b62" is a model location near the center of the north–south cross section, at 234100 m in Figure 6.1-1.

Figure 6.2-9b. Matrix Liquid Saturation along a Vertical Column ("b62") from Ground Surface to Water Table: Base Thermal Loading

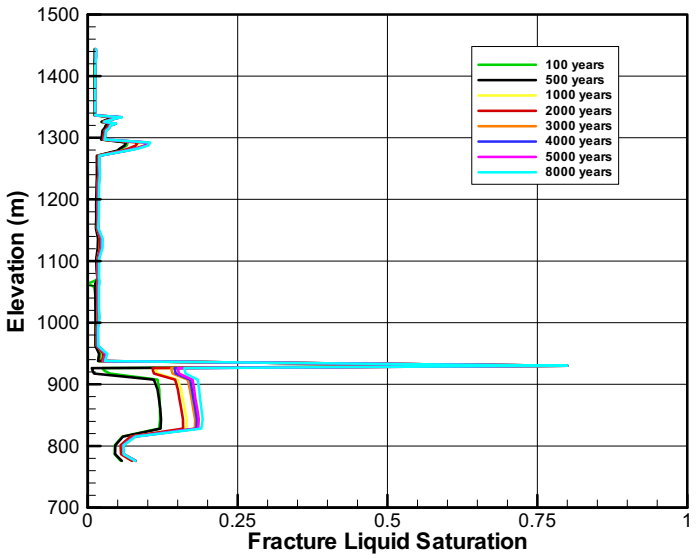

Output DTN: LB0310MTSCLTH2.001.

NOTE: Column "b62" is a model location near the center of the N–S cross section, at 234100 m in Figure 6.1-1. The spike in the fracture liquid saturation at 940 m is due to the presence of the vitric layer, which was simulated as a nonfractured matrix continuum (i.e., no fracture continuum present for that layer).

Figure 6.2-9c. Fracture Liquid Saturation along a Vertical Column ("b62") from Ground Surface to Water Table: Base-Case Thermal Loading

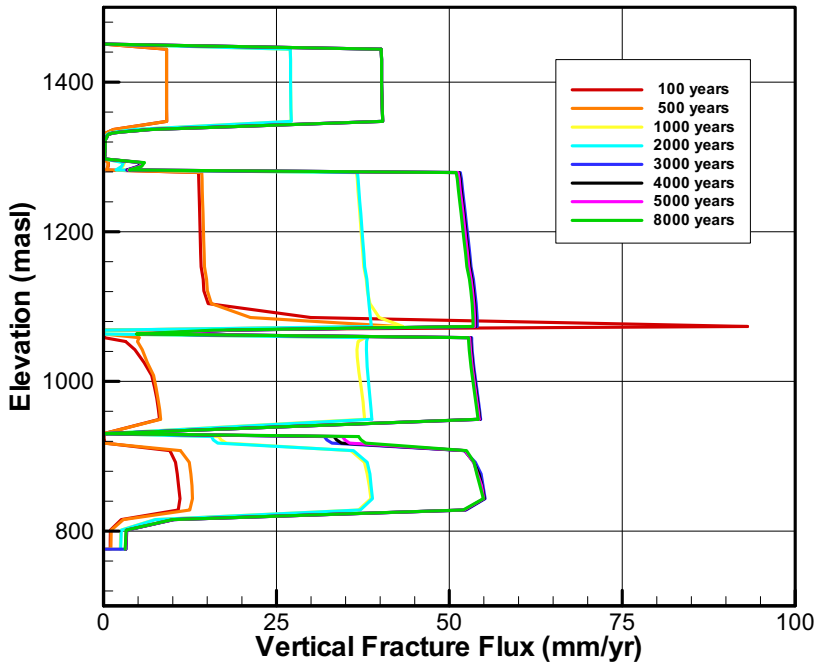

Output DTN: LB0310MTSCLTH2.001.

NOTE: Column "b62" is a model location near the center of the N–S cross section, at 234100 m in Figure 6.1-1). The '"zero" fracture flux at ~940 masl results from the vitric layer in that location being modeled as a nonfractured matrix continuum (i.e., the fracture continuum is absent there, resulting in a zero fracture flux).

Figure 6.2-9d. Vertical Fluxes in Fractures along Column "b62" at Various Times

6.2.1.6 Fracture Flux

Drainage through fractures is illustrated in Figure 6.2-10a. This figure shows the magnitude of vertical liquid flux in fractures along the north–south axis just above the repository. The vertical fracture fluxes are shown by solid lines at 100, 500, 1,000, 3,000, and 5,000 years after emplacement of wastes. Figure 6.2-10a also shows the surface infiltration (dotted lines) along the north–south axis for present day (black), monsoon (purple), and glacial transition (blue) periods. Fracture fluxes appear to be elevated in the pillar regions. This is further clarified in Figure 6.2-10b, where a close-up of the vertical fracture fluxes in the pillar regions is shown. Though a more refined numerical grid would have provided a clearer picture of drainage through pillars, Figure 6.2-10b is sufficiently informative. First, no fracture liquid flow is predicted directly above the emplacement drifts. Because of vaporization and capillarity effects, water is diverted away from the crown of the emplacement drifts, resulting in elevated fluxes in the pillar regions adjacent to drifts. This diversion of water flux downward through the pillars, away from the drift, is consistent with drift-scale models that predict no seepage during the thermal period (BSC 2005 DIRS 172232], Section 6.2). The elevation in fracture fluxes in the middle pillar region is not significant in the base case because only limited displacement of water by boiling takes place in this thermal-loading scenario.

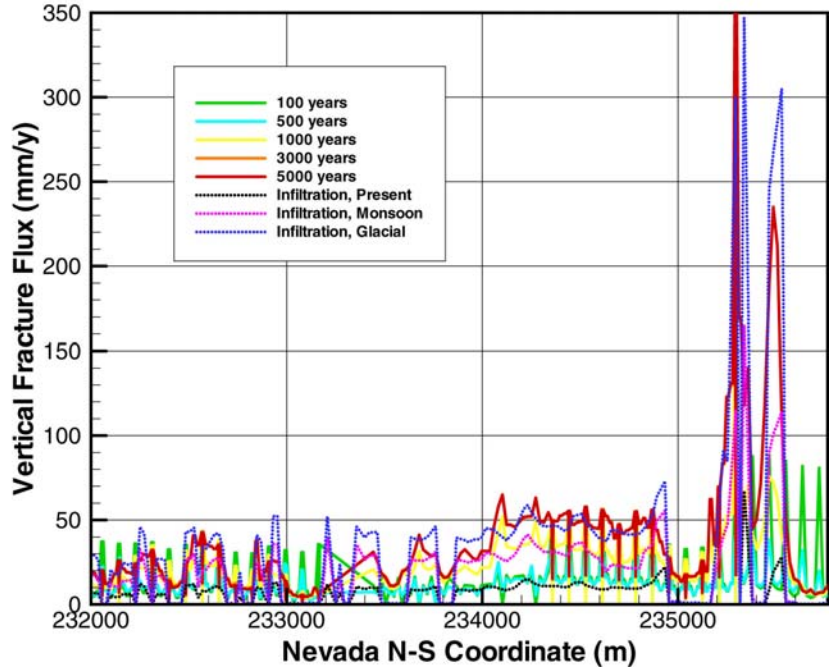

Output DTN: LB0310MTSCLTH2.001.

Figure 6.2-10a. Vertical Downward Fluxes in the Fractures above the Emplacement Drifts and within Drift Pillars: Base-Case Thermal Loading

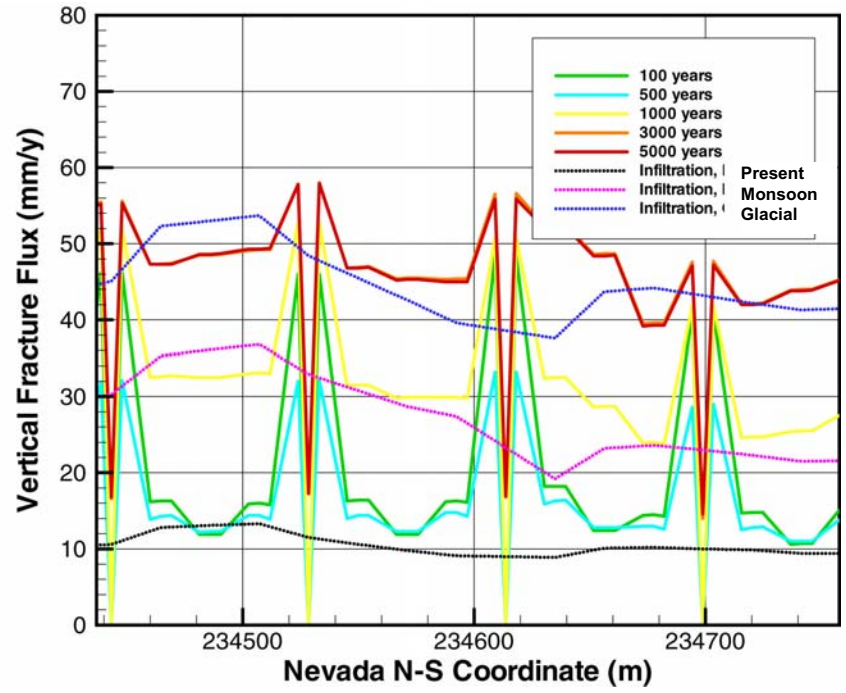

Output DTN: LB0310MTSCLTH2.001.

Figure 6.2-10b. Detail View of the Vertical Downward Fluxes in Fractures above Emplacement Drifts and within Drift Pillars: Base-Case Thermal Loading

6.3 THREE-DIMENSIONAL MOUNTAIN-SCALE TH MODEL RESULTS AND ANALYSES

Mountain-scale TH effects caused by thermal load at the repository are three-dimensional phenomena lasting hundreds to thousands of years after waste emplacement. Thus, three-dimensional models provide the most accurate approach to predicting TH effects. In this section, three-dimensional TH simulations are used to analyze the evolution of temperature, saturation, and percolation flux under thermal-loading conditions. As discussed in Section 6.1.5, the three-dimensional TH model uses the same thermal-loading scenario over the entire repository as the two-dimensional TH model (Section 6.2), in which 86.3% of the heat load is removed by ventilation in the first 50 years after initial waste emplacement. Similarly, the net infiltration rates over the three-dimensional model domain consist of three time periods for future climates, as given in Table 6.1-2. The future climates in both thermal-loading scenarios are represented by the same three sequential modeled periods: present-day (0 to 600 years), monsoon (600 to 2,000 years), and then glacial transition (2,000 years and beyond). These climates result in a step increase in net surface infiltration rates (at 600 years and at 2,000 years) applied over the model top boundary.

The results of three-dimensional TH model simulations are presented and discussed using two-dimensional contour plots of temperature, saturation, and flux at the bottom of PTn, the top of CHn, the repository horizon, and a north–south (N-S) vertical cross section. In addition, plots of the evolution of temperature, saturation, and vertical flux are provided for several one-dimensional columns, selected from the three-dimensional model grid. Coordinates and corresponding columns for these selected observation cells along the one-dimensional grid columns are listed in Table 6.3-1, and the locations of these observation cells are also shown in Figure 6.1-1 in plan view. For the mountain-scale TH model, this report is primarily concerned with the extent of the thermally disturbed zone and the predicted mountain-scale changes in temperature, saturation, and percolation flux under the influence of repository thermal load. Appendix IV (Section IV.2) documents the procedures of data extraction and plotting of three-dimensional TH model simulation results.

6.3.1 Base-Case Model Results and Analyses

As discussed in Section 6.1.5 and above, the base-case TH model uses only 13.7% of the total thermal load in the first 50 years after waste emplacement. After 50 years, 100% thermal load is introduced into repository drifts. The base-case TH model results are displayed using several (two-dimensional) plots along selected horizontal layers, the N-S vertical cross section, and one-dimensional vertical columns of Table 6.3-1 (Figure 6.1-1) to show the changes in temperature, saturation, and flux near the repository and the UZ system under the effect of repository thermal load.

Table 6.3-1. Cells, Grid Columns, and Coordinates of the Three-Dimensional TH Model Used to Show Model Predictions

Cell	Column	X (m)	Y(m)
A	d 3	170901.9	232754.1
B	B58[a]	171376.6	232822.1
C	h57	170516.1	233394.2
D	e42	171983.8	233432.5
E	h50	171051.3	234717.3
F	h47	170743.5	235090.3
G	a71	170127.5	235135.7
H	b60	171016.5	235176.1
I	A41[a]	171411.7	235271.2
J	b72	171991	235322.4

Source: DTN: LB0310MTSCLTH3.001.

[a] Fault columns.

6.3.1.1 Temperature

Figures 6.3.1-1 through 6.3.1-5 show the simulated temperatures at the repository horizon, bottom of the PTn, and top of the CHn at 100, 500, 1,000, 2,000, and 5,000 years after emplacement. Note that in the three-dimensional model, the grid layers, such as the selected repository horizon, PTn bottom, and CHn top layers, are not exactly horizontal (see Figure 6.1-2 for the stratigraphic layers and their spatial distributions along the N-S cross section), and they have varying thickness and elevations over the model domain, in accordance with the geological model. These temperature distribution contours indicate how TH conditions along these layers are impacted by the repository thermal load at different times. The simulated temperatures at the repository horizon, as shown in Figures 6.3.1-1a, 6.3.1-2a, 6.3.1-3a, 6.3.1-4a, and 6.3.1-5a, indicate that after 100 years a boiling condition at the ambient atmospheric pressure is reached in many drift elements located at or near the center of the northern repository layout block. Note that temperatures shown in these figures are for the rock surrounding the drift and not for the drift itself, where temperatures reach boiling conditions. The boiling conditions last up to 1,000 years along the central portion of drifts away from the boundaries of the repository. These temperature contours also show that, at the repository horizon, the highest-temperature period is from 500 to 1,000 years. After 1,000 years, the temperatures at the repository start to decrease. After 2,000 years, the temperatures at and near the repository are significantly cooled down. At 5,000 years, the majority of the system returns almost to ambient conditions, and temperatures at the hottest spots within the repository area are no more than 60°C, as illustrated in Figures 6.3.1-5a and 6.3.1-5b.

At earlier times (up to 100 years), the simulation results (Figures 6.3.1-1a and 6.3.1-1b) show limited spatial thermal disturbance from repository heating. During this period, repository thermal load has little impact on the TH conditions at the bottom of PTn and the top of CHn. As repository heating continues, the thermal impact extends into the far field. Figures 6.3.1-2b, 6.3.1-3b, and 6.3.1-4b show that the temperature along the bottom of the PTn unit rises from the

ambient 20°C to above 40°C at 500 years, to more than 50°C in certain areas between 1,000 years and 2,000 years. Similarly, the temperatures below the repository (Figures 6.3.1-2c, 6.3.1-3c, and 6.3.1-4c), along the top of the CHn, also increase from ambient 27°C to more than 50°C at 500 years, to 65°C at 1,000 years, and to 75°C at 2,000 years. These changes in far-field temperature, predicted by the three-dimensional TH model, reach their peak values about 2,000 years after waste emplacement, which is consistent with those temperatures simulated by the two-dimensional model discussed in Section 6.2. In general, the TH model results indicate that a larger increase in temperature (or stronger TH impact) occurs at the top of CHn than at the bottom of PTn, since the top of CHn is much closer to the repository horizon than the PTn bottom (See Figure 6.1-2).

The vertical spatial variations in temperature along the N-S cross section of the three-dimensional model (Figure 6.1-1) at 1,000 years are shown in Figure 6.3.1-3d. At this time, the heated zones around the repository start cooling down, and the predicted maximum temperature is 95°C at repository rock, slightly less than boiling conditions at this elevation. As Figures 6.3.1-5a and 6.3.1-5b indicate, at 5,000 years after waste replacement, the highest temperatures within the repository horizon are only at 60°C.

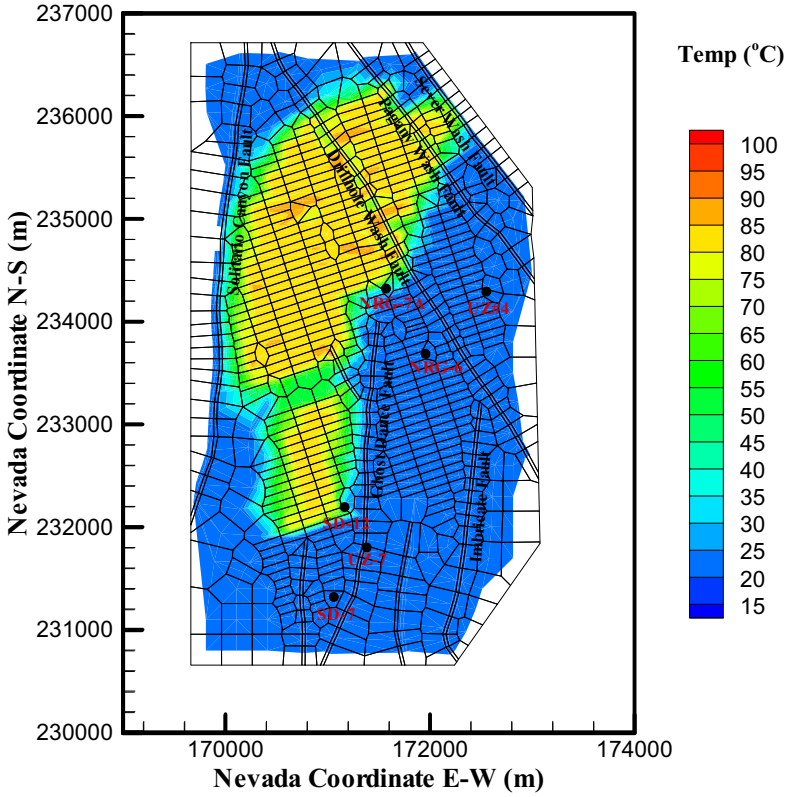

Output DTN: LB0310MTSCLTH3.001.

Figure 6.3.1-1a. Model-Predicted Rock Temperature Distribution at Repository Horizon 100 Years after Waste Emplacement: Base-Case Model with Ventilation

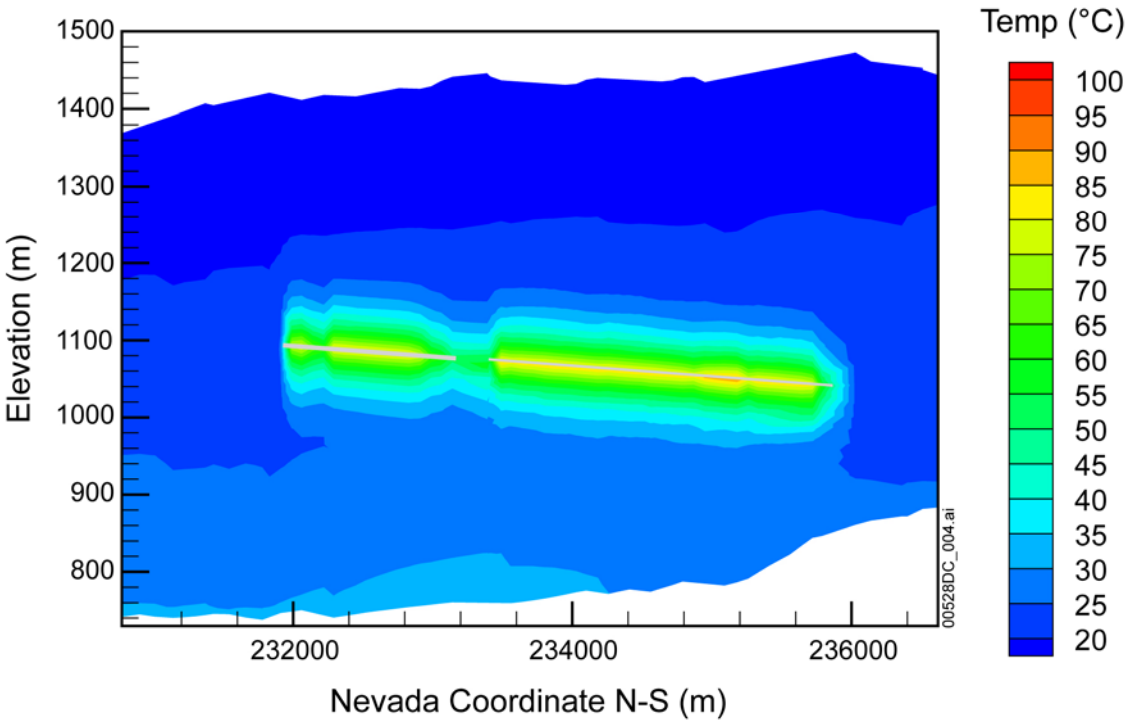

Output DTN: LB0310MTSCLTH3.001.

Figure 6.3.1-1b. Model-Predicted Temperature Distribution at North–South Cross Section 100 Years after Waste Emplacement: Base-Case Model with Ventilation

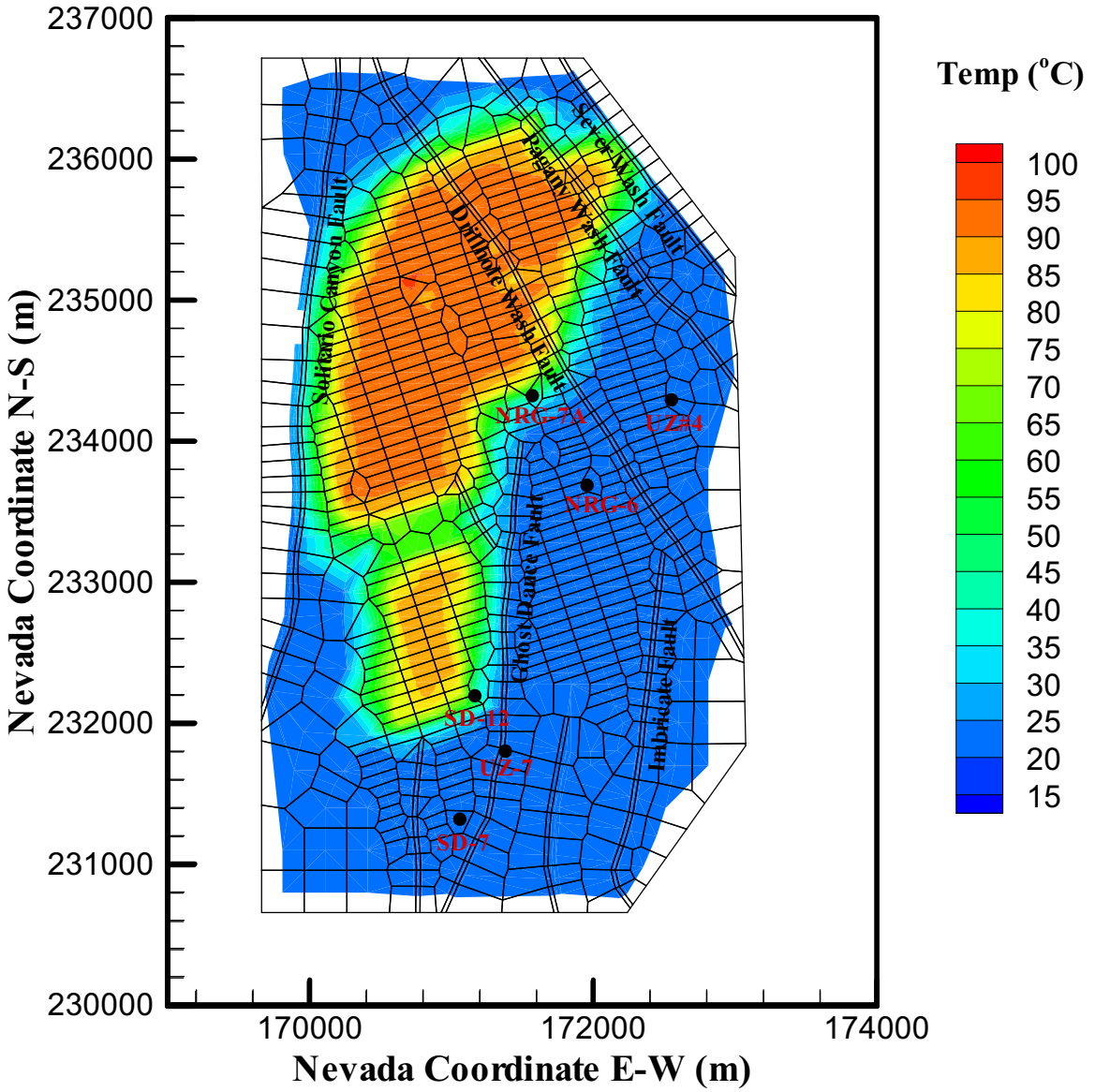

Output DTN: LB0310MTSCLTH3.001.

Figure 6.3.1-2a. Model-Predicted Rock Temperature Distribution at Repository Horizon 500 Years after Waste Emplacement: Base-Case Model with Ventilation

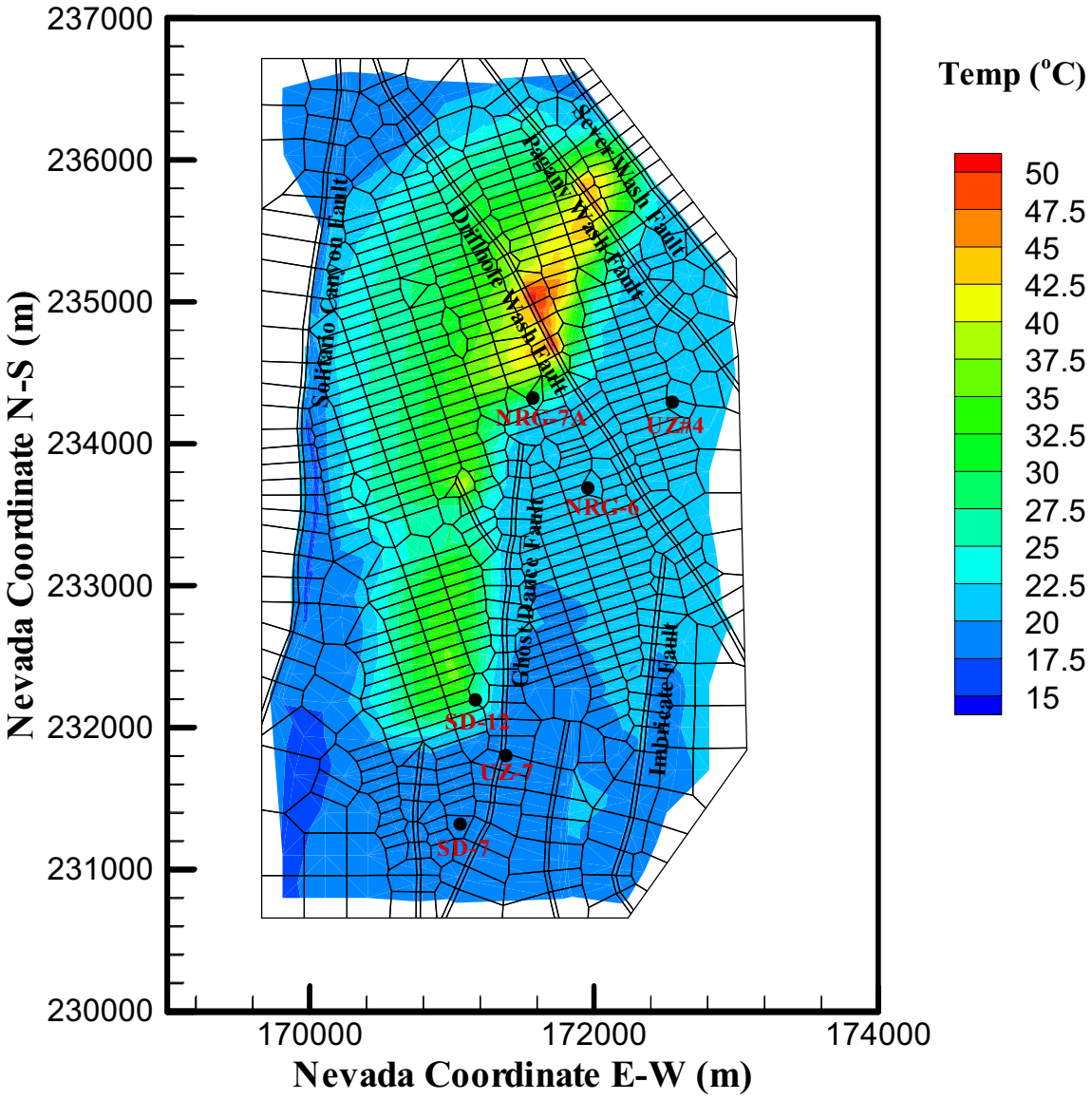

Output DTN: LB0310MTSCLTH3.001.

Figure 6.3.1-2b. Model-Predicted Rock Temperature Distribution at Bottom of PTn Unit 500 Years after Waste Emplacement: Base-Case Model with Ventilation

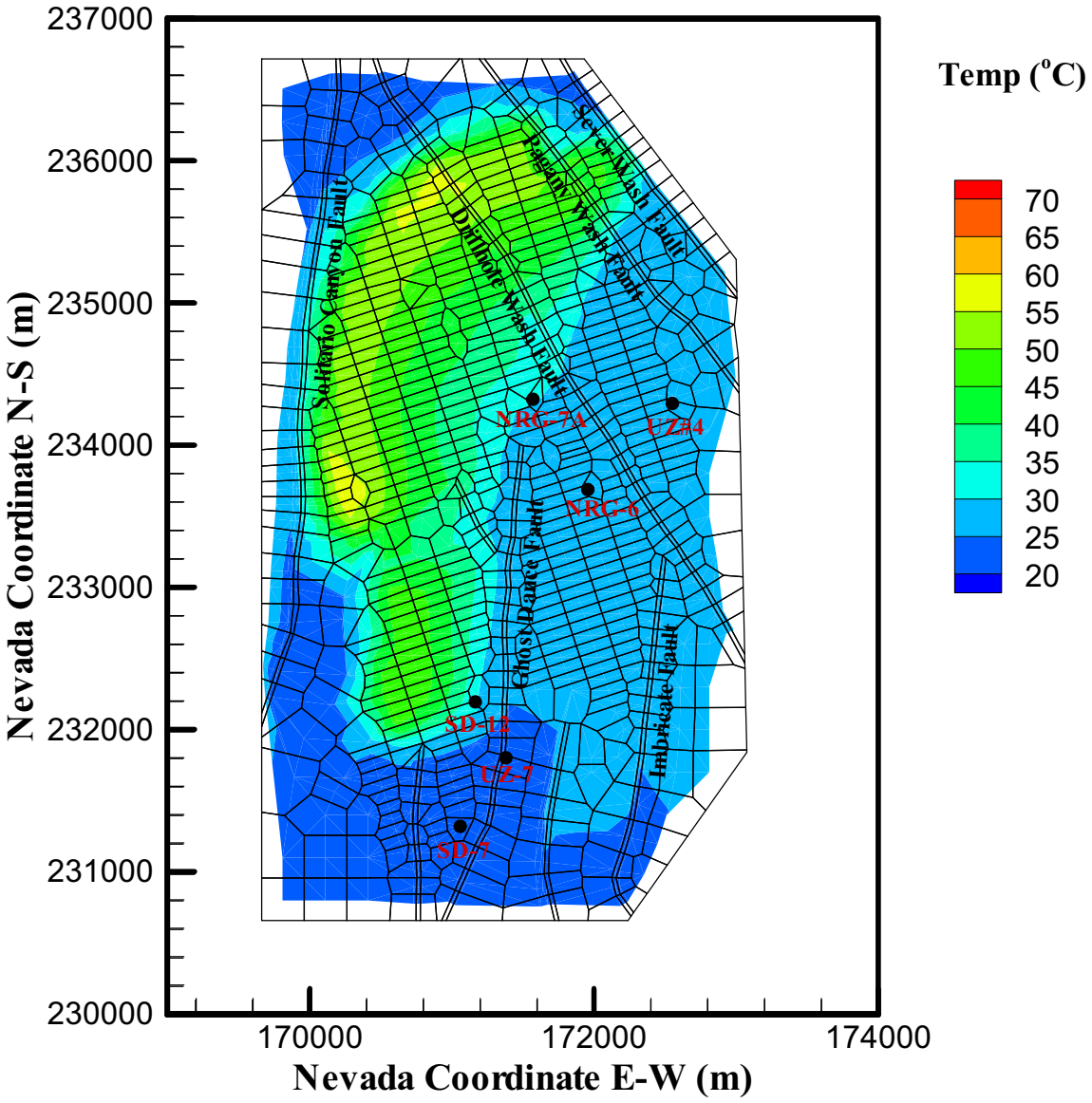

Output DTN: LB0310MTSCLTH3.001.

Figure 6.3.1-2c. Model-Predicted Rock Temperature Distribution at Top of CHn Unit 500 Years after Waste Emplacement: Base-Case Model with Ventilation

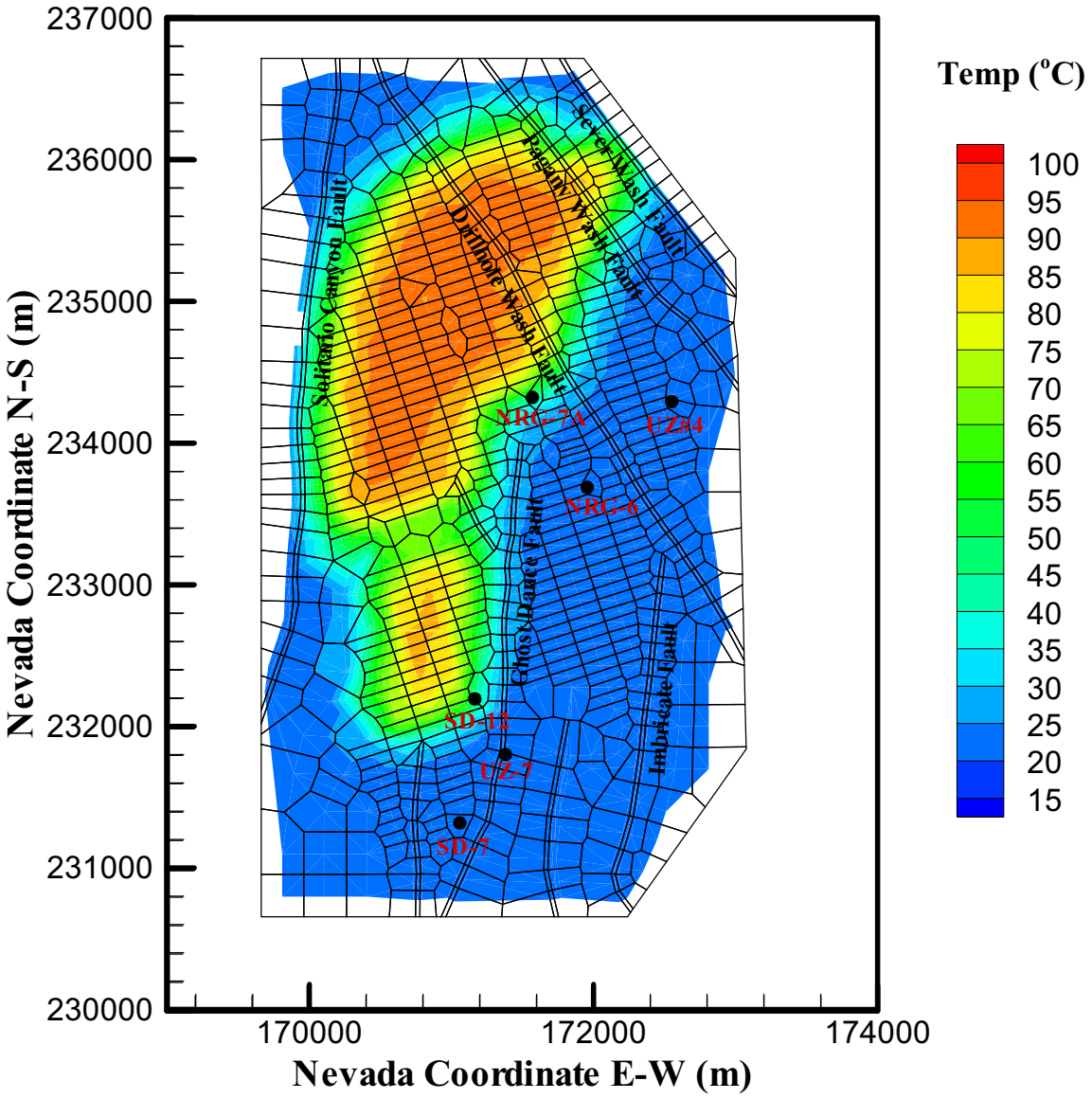

Output DTN: LB0310MTSCLTH3.001.

Figure 6.3.1-3a. Model-Predicted Rock Temperature Distribution at Repository Horizon 1,000 Years after Waste Emplacement: Base-Case Model with Ventilation

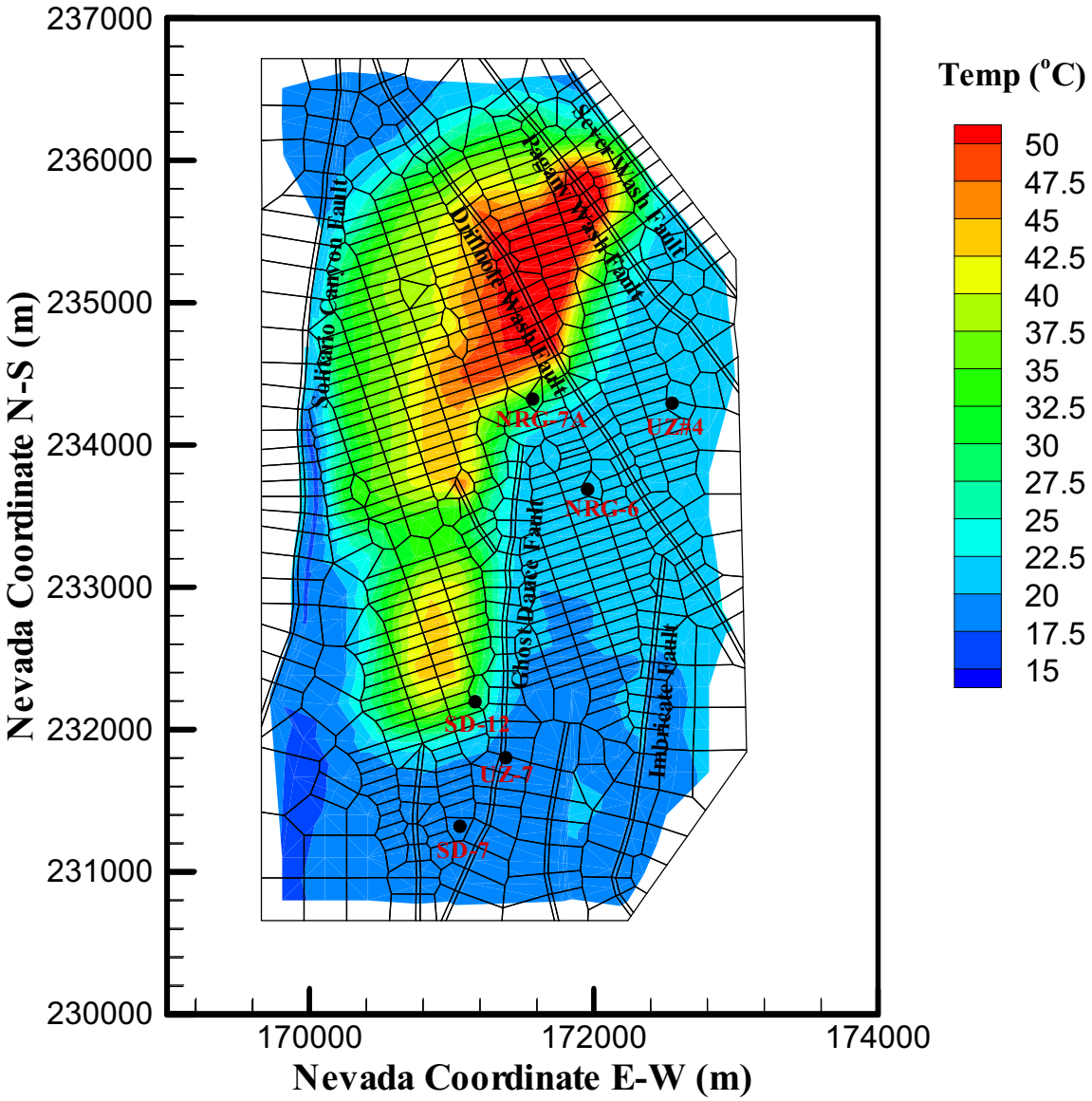

Output DTN: LB0310MTSCLTH3.001.

Figure 6.3.1-3b. Model-Predicted Rock Temperature Distribution at Bottom of PTn Unit 1,000 Years after Waste Emplacement: Base-Case Model with Ventilation

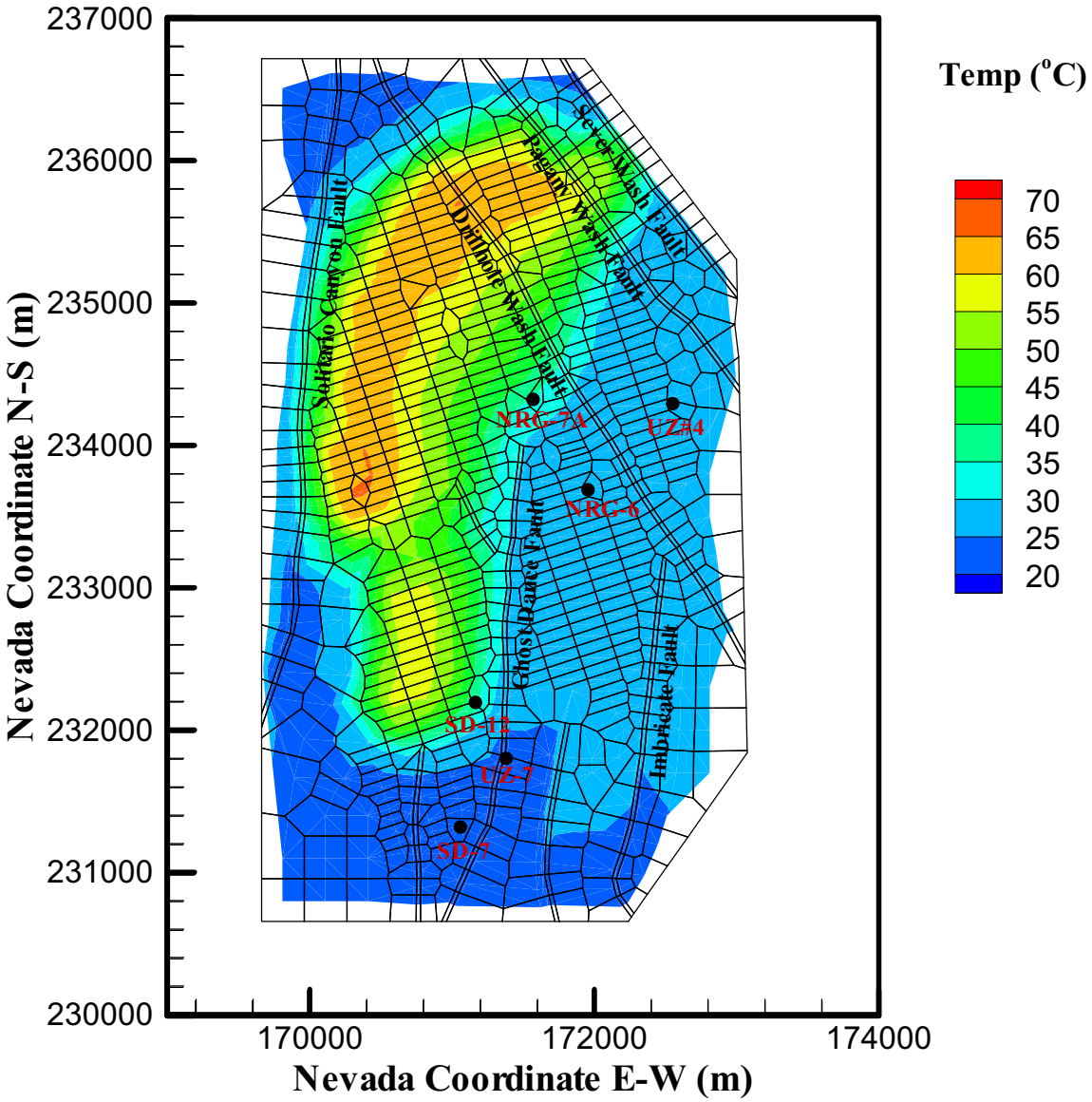

Output DTN: LB0310MTSCLTH3.001.

Figure 6.3.1-3c. Model-Predicted Rock Temperature Distribution at Top of CHn Unit 1,000 Years after Waste Emplacement: Base-Case Model with Ventilation

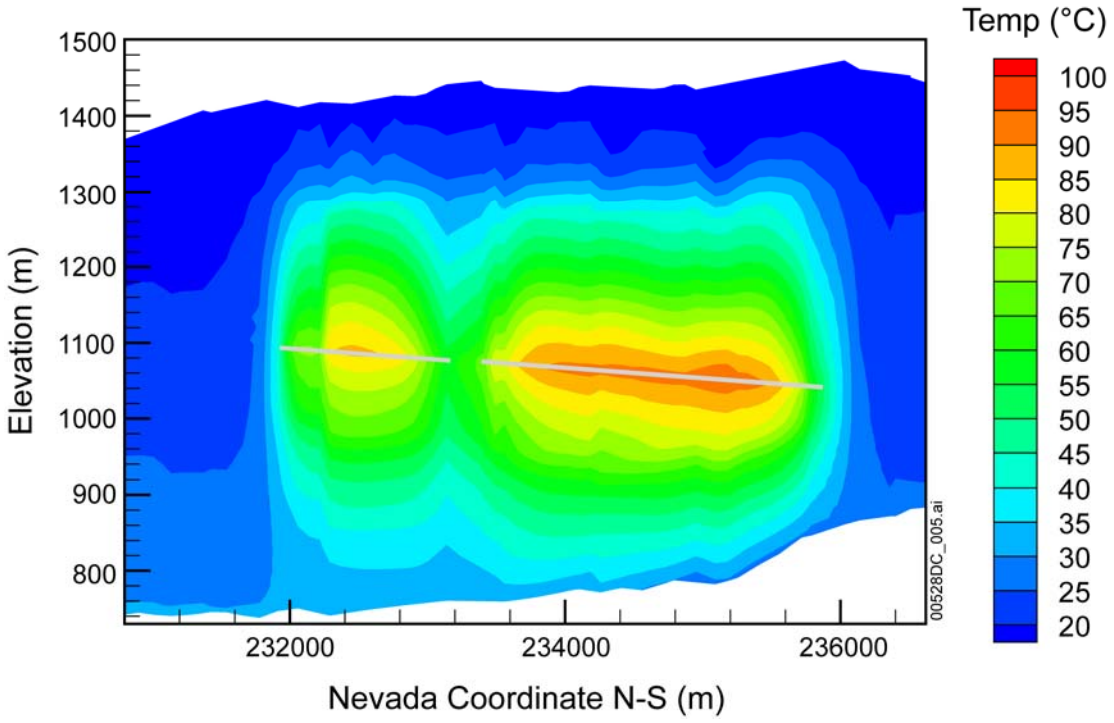

Output DTN: LB0310MTSCLTH3.001.

Figure 6.3.1-3d. Model-Predicted Temperature Distribution at North–South Cross Section 1,000 Years after Waste Emplacement: Base-Case Model with Ventilation

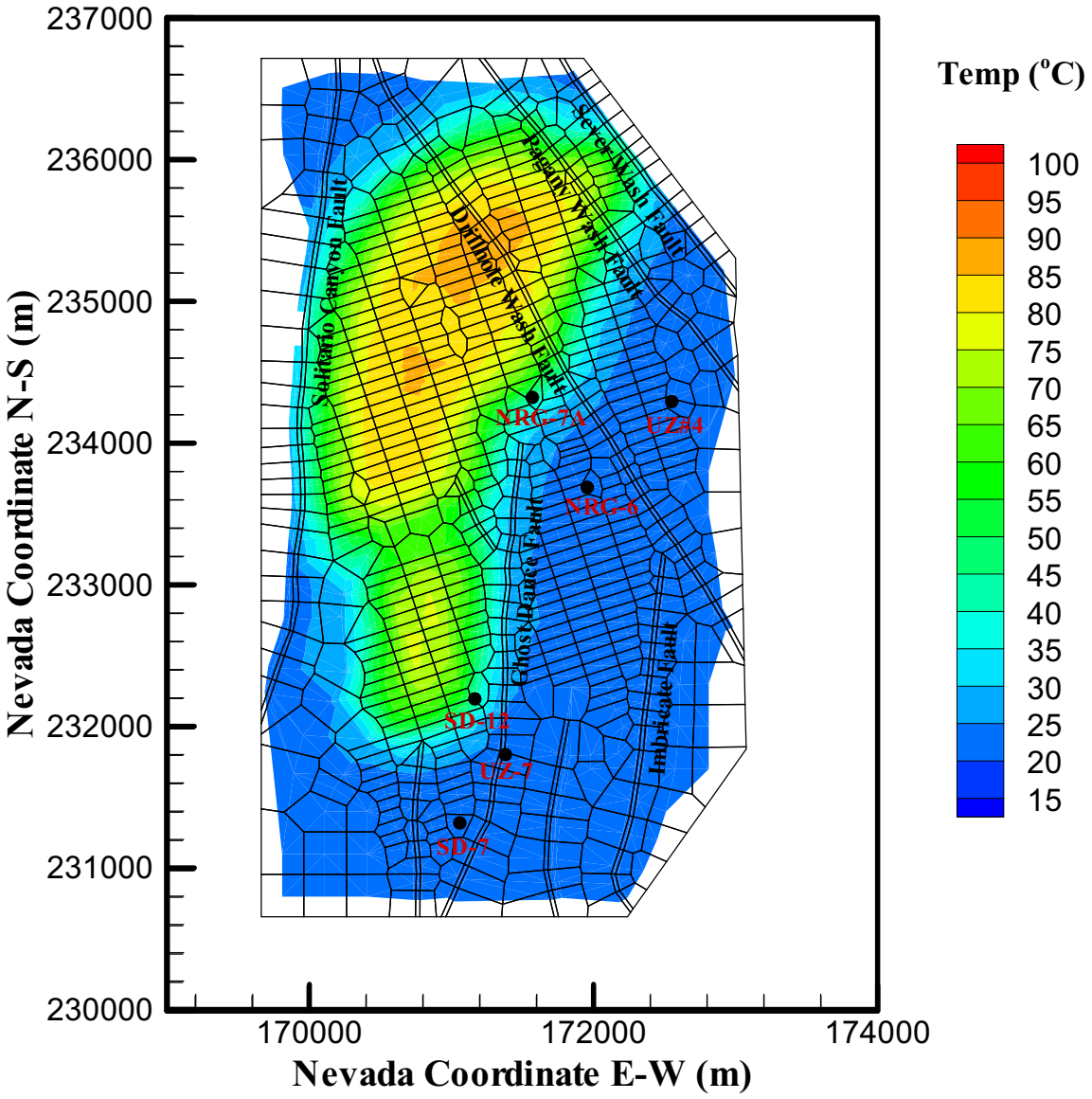

Output DTN: LB0310MTSCLTH3.001.

Figure 6.3.1-4a. Model-Predicted Rock Temperature Distribution at Repository Horizon 2,000 Years after Waste Emplacement: Base-Case Model with Ventilation

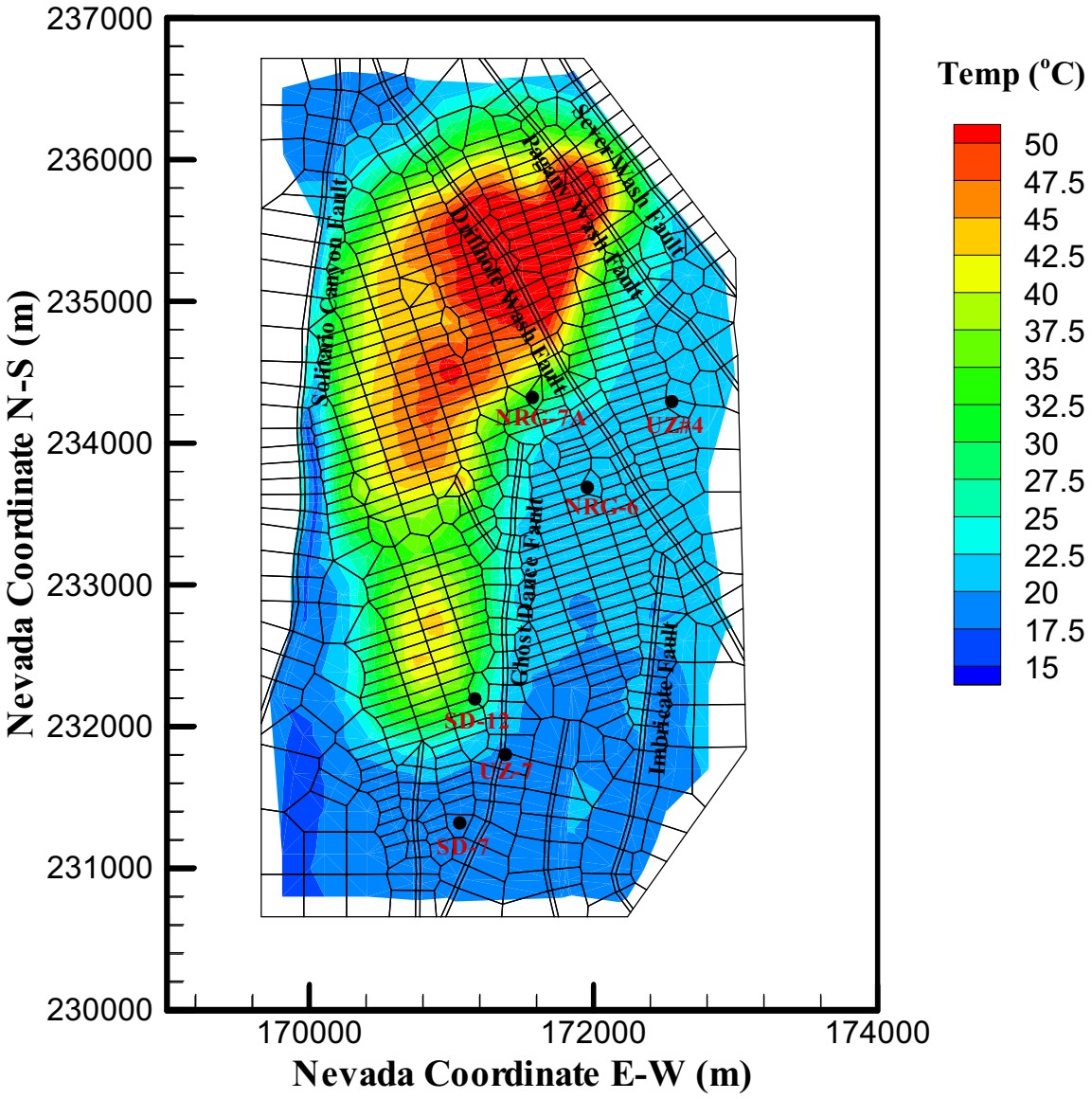

Output DTN: LB0310MTSCLTH3.001.

Figure 6.3.1-4b. Model-Predicted Rock Temperature Distribution at Bottom of PTn Unit 2,000 Years after Waste Emplacement: Base-Case Model with Ventilation

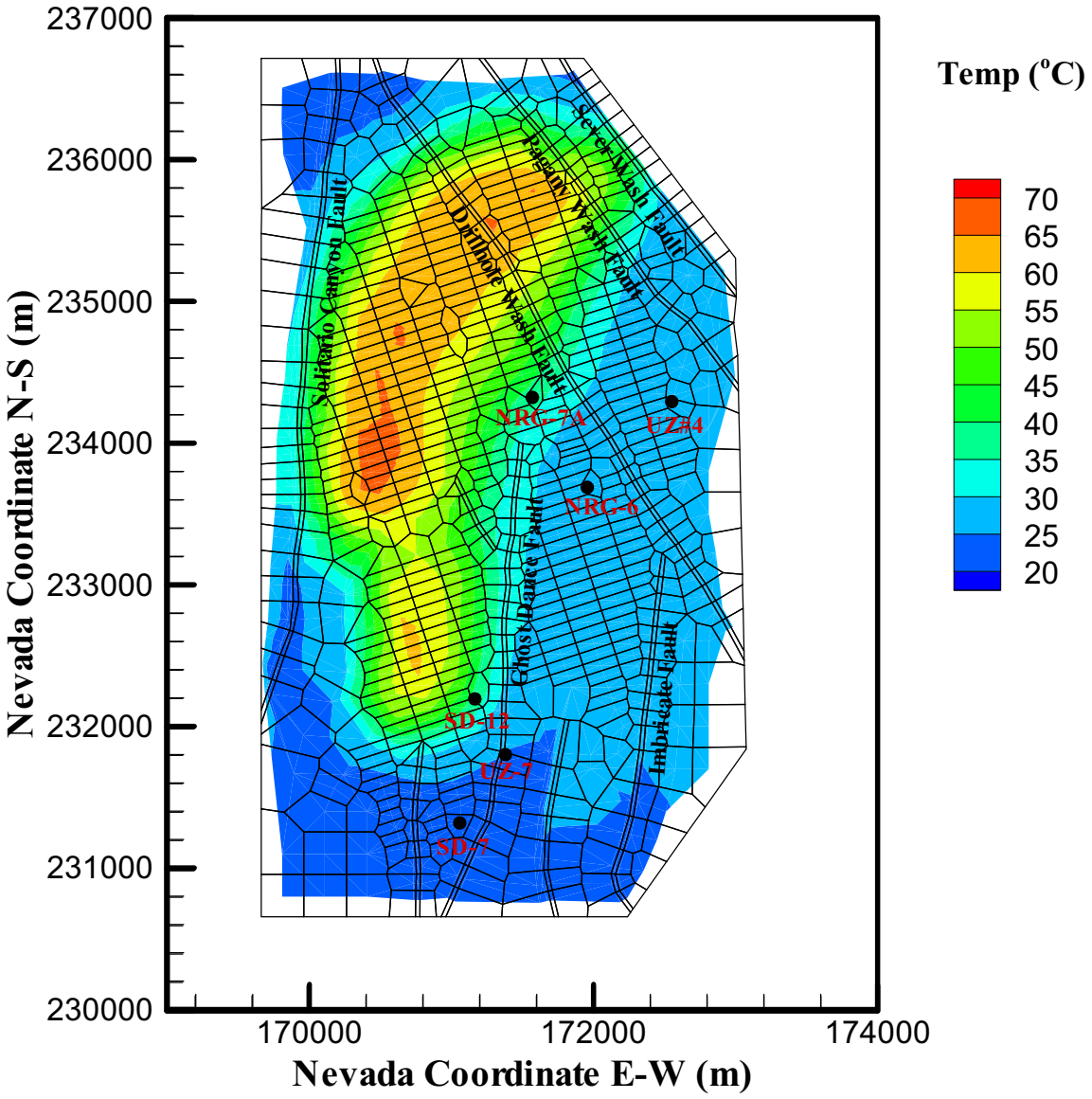

Output DTN: LB0310MTSCLTH3.001.

Figure 6.3.1-4c. Model-Predicted Rock Temperature Distribution at Top of CHn Unit 2,000 Years after Waste Emplacement: Base-Case Model with Ventilation

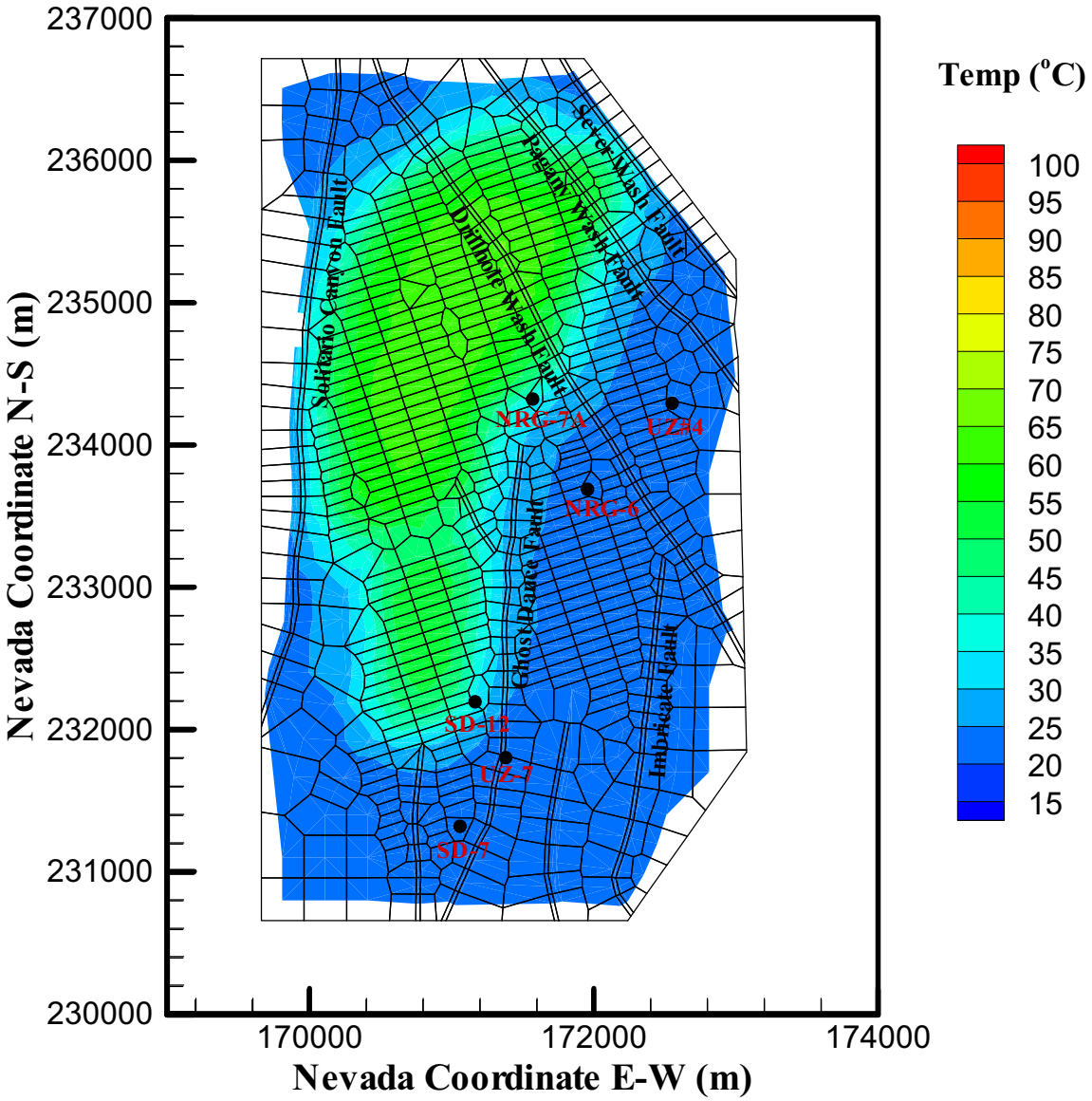

Output DTN: LB0310MTSCLTH3.001.

Figure 6.3.1-5a. Model-Predicted Rock Temperature Distribution at Repository Horizon 5,000 Years after Waste Emplacement: Base-Case Model with Ventilation

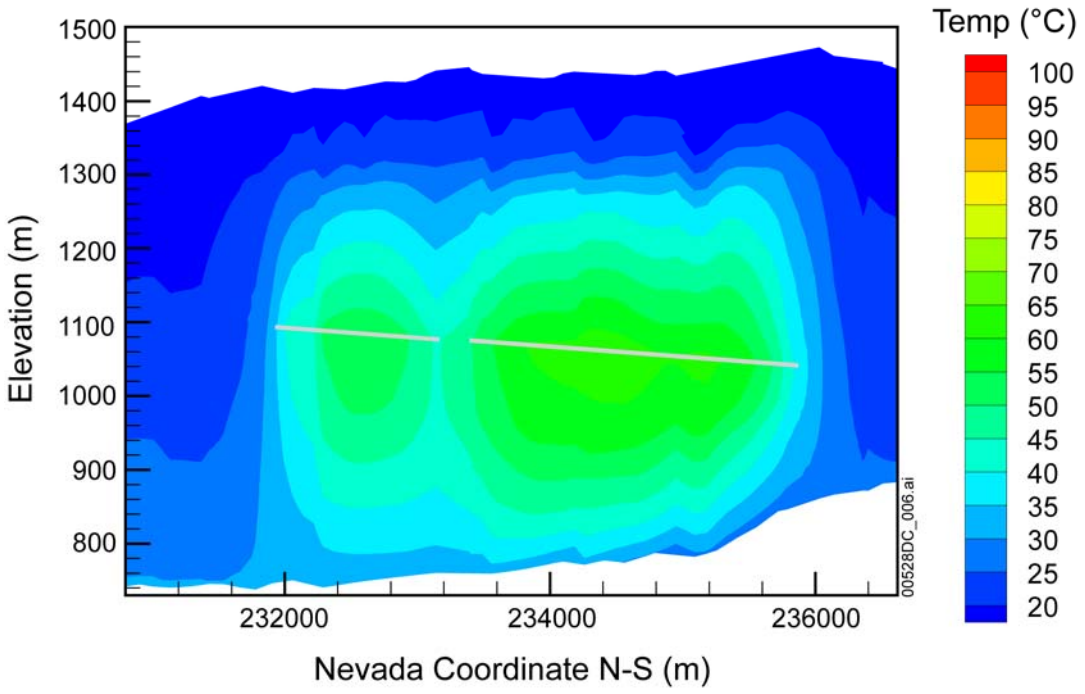

Output DTN: LB0310MTSCLTH3.001.

Figure 6.3.1-5b. Model-Predicted Temperature Distribution at North–South Cross Section 5,000 Years after Waste Emplacement: Base-Case Model with Ventilation

Figure 6.3.1-6 displays two one-dimensional vertical profiles of simulated temperatures in Observation Columns A (the center of the southern or small repository block, Figure 6.1-1) and F (the center of the northern, main repository block, Figure 6.1-1) at different times (10, 100, 500, 800, 2,000, 3,000, 5,000, and 8,000 years). The coordinates of Columns A through F are also given in Table 6.3-1. The repository elevation is at 1,083 m and 1,050 m, for Columns A and F, respectively. Both horizontal and vertical cross-sectional temperature contours above show that the boiling zones are limited for the most part to inside the northern, main repository boundary. The vertical temperature distributions at Observation Columns A and F in Figure 6.3.1-6 indicate a sharp temperature rise to boiling conditions, which develop at the repository horizon at Column F (i.e., the center of the northern or main repository block) during a period of 100 to 500 years in this particular location. In the southern part of the repository, the temperatures do not rise to boiling point during the entire thermal-loading period. The temperature profiles along the two columns (Figure 6.3.1-6) also indicate that the highest temperatures at the base of the PTn and top of the CHn units occur at about 2,000 years.

Figure 6.3.1-7 shows variations of simulated temperatures with time at three elevations along Column F, the repository level, the lower portion of the PTn, and the upper CHn. The results show that the maximum temperature at the repository horizon for this location is about 100°C after 130 years. At this location, temperatures at the repository drift rise to boiling conditions shortly before 100 years. The figure shows near-constant temperature at the repository drift between 100 to 600 years, indicating boiling conditions. The cooldown phase almost coincides with the change of climate at 600 years, and temperature drops below boiling after 1,000 years.

Figure 6.3.1-7 also shows that temperatures near the PTn bottom and upper CHn portion reach their highest values at about 2,000 years after waste emplacement.

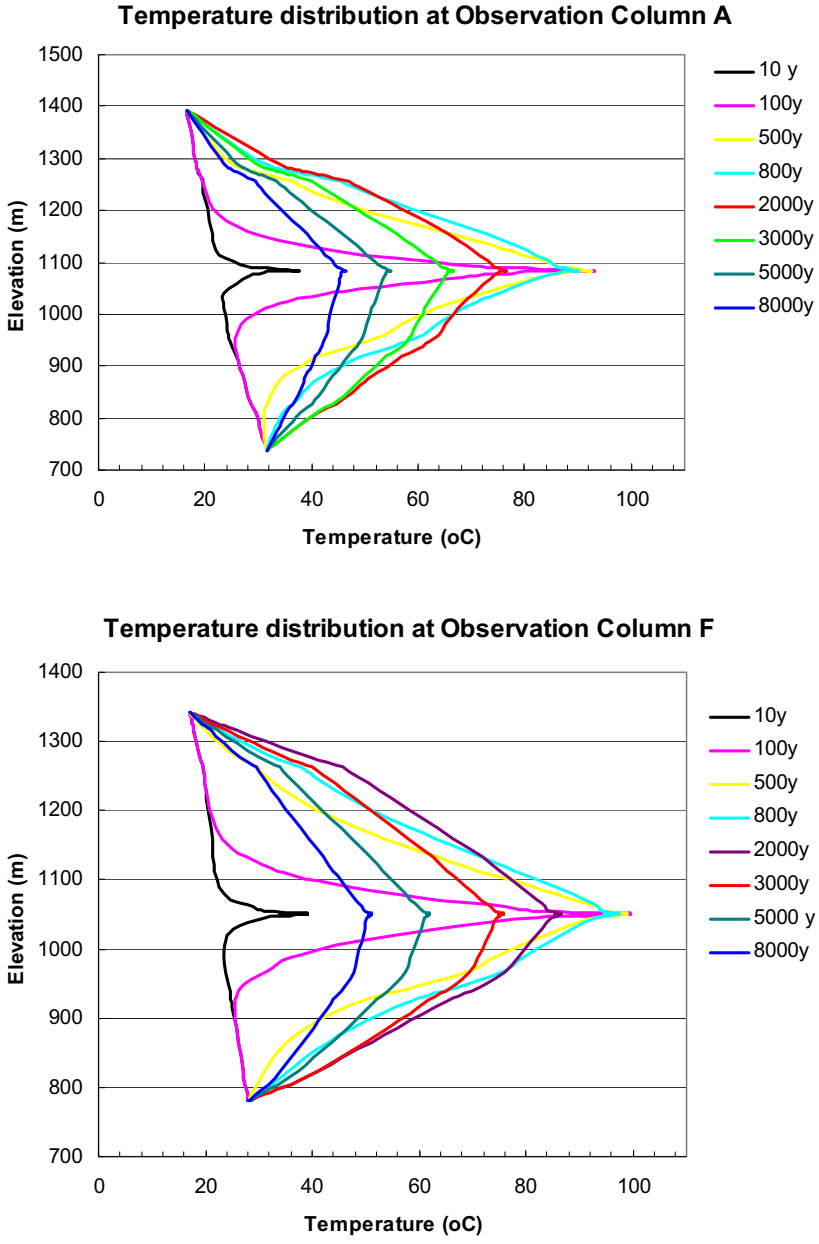

Output DTN: LB0310MTSCLTH3.001.

NOTE: Observation column A is situated in the southern repository block center; observation column F is situated in the northern, main repository block center.

Figure 6.3.1-6. Model-Predicted Temperature Profiles at Different Times along Observation Columns A and F: Base-Case Model with Ventilation

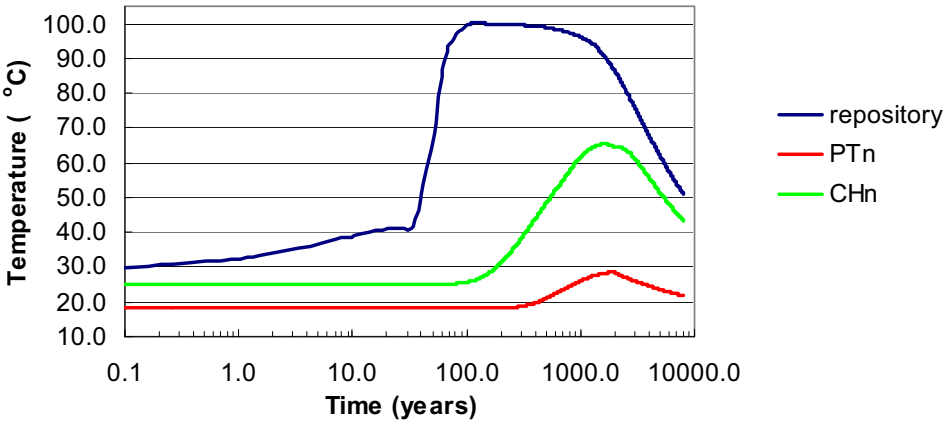

Output DTN: LB0310MTSCLTH3.001.

NOTE: Observation column F is situated in the northern, main repository block center. The bottom of PTn is at an elevation of 1,307.5 m; the top of CHn is at an elevation of 961 m.

Figure 6.3.1-7. Model-Predicted Temperature Changes with Time at Repository Horizon, Bottom PTn, and Top CHn along Observation Column F: Base-Case Model with Ventilation

6.3.1.2 Liquid Saturation

Changes in liquid saturation in the host rock at and near repository drifts are important for several reasons. They determine the period during which the repository remains dry. They are also used to assess the potential desaturation-induced changes in porosity and hydraulic conductivity (for example, in the zeolitic units). Liquid saturation also quantifies the thermally induced flow mobilization and focusing that may affect UZ flow and the potential for seepage into drifts. Finally, they also help identify the onset of rewetting processes and the subsequent potential for possible waste package corrosion at the repository horizon.

Figures 6.3.1-8 through 6.3.1-10 show the plots of matrix liquid saturation at the repository horizon at times of 500, 1,000, and 2,000 years, respectively. The contour plots of the matrix liquid saturation at 500 and 1,000 years after initial thermal load along the N-S cross section are shown in Figures 6.3.1-11 and 6.3.1-12. In addition, Figure 6.3.1-13 presents the matrix liquid saturation in Observation Column H (near the center of the northern repository block) at different times.

Comparing the simulated matrix liquid saturations at the same locations for different times and with their initial values, the three-dimensional model in general predicts small changes in matrix liquid saturation on the mountain scale, under the base-case thermal-load scenario. Therefore, no large spatial-scale mobilization of liquid by vaporization is created by the designed repository heating. Figures 6.3.1-8 through 6.3.1-10 indicate that the predicted matrix liquid saturations at the repository horizon are scarcely different for the three different times. They are also almost identical to the ambient saturation distribution at the repository horizon. The distribution of liquid saturation at the N-S cross section at 500 years and 1,000 years of thermal load (Figures

6.3.1-11 and 6.3.1-12) are also similar at the two times. Note that Figure 6.3.1-11a presents vertical saturation distributions at 500 years after waste emplacement along the N-S cross section of the three-dimensional model, showing little difference from the ambient or initial condition of Figure 6.3.1-11b for the same cross section.

Figure 6.3.1-13 shows a slight change of matrix saturation along the vertical column. However, these changes result mainly from changes in climates, i.e., from the increase in net infiltration rates. Note that the repository elevation is about 1,050 m at this location. The three-dimensional numerical model does not predict extensive dryout zones or zero saturation in matrix blocks anywhere within the repository domain in the three-dimensional model. This is primarily because of (1) the relatively low thermal load for the base-case with ventilation; (2) the coarse gridding around the drifts results in large volume averaging; and (3) the increase in infiltration rates at 600 and 2,000 years. Note that drifts are simulated as an equivalent porous material with zero capillary pressure and zero initial liquid saturation, i.e., completely dry, and are not included in these plots.

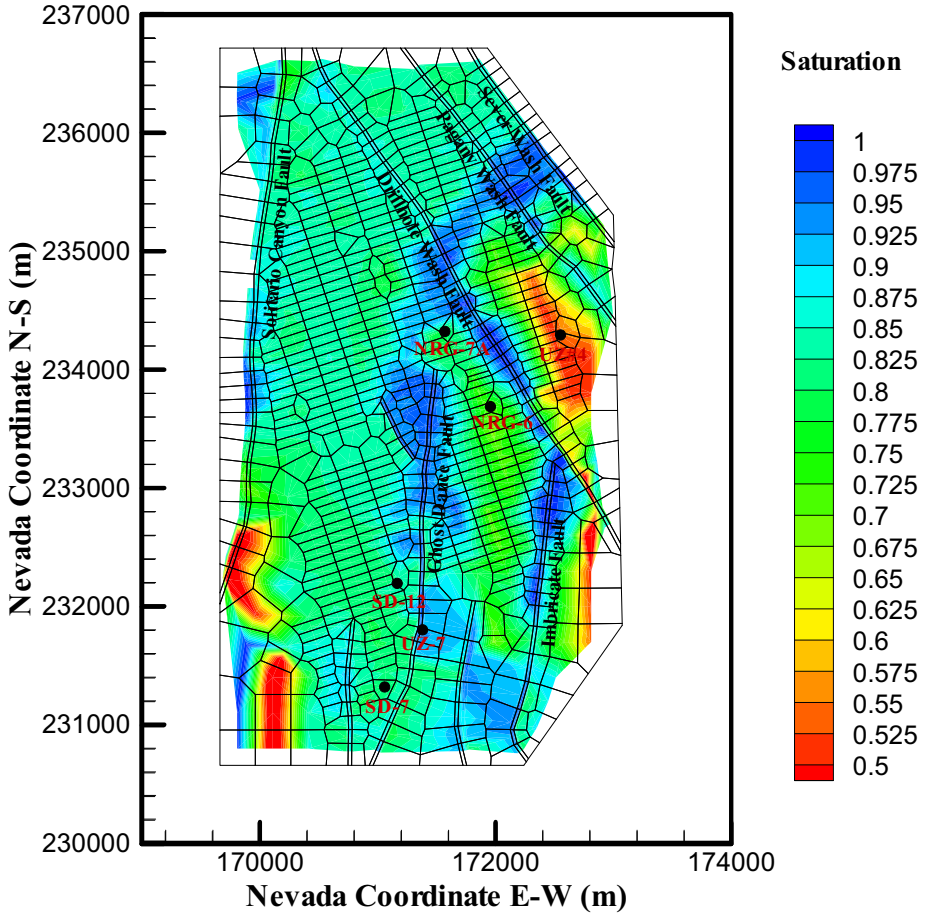

Output DTN: LB0310MTSCLTH3.001.

Figure 6.3.1-8. Model-Predicted Matrix Liquid Saturation Distribution at Repository Horizon 500 Years after Waste Emplacement: Base-Case Model with Ventilation

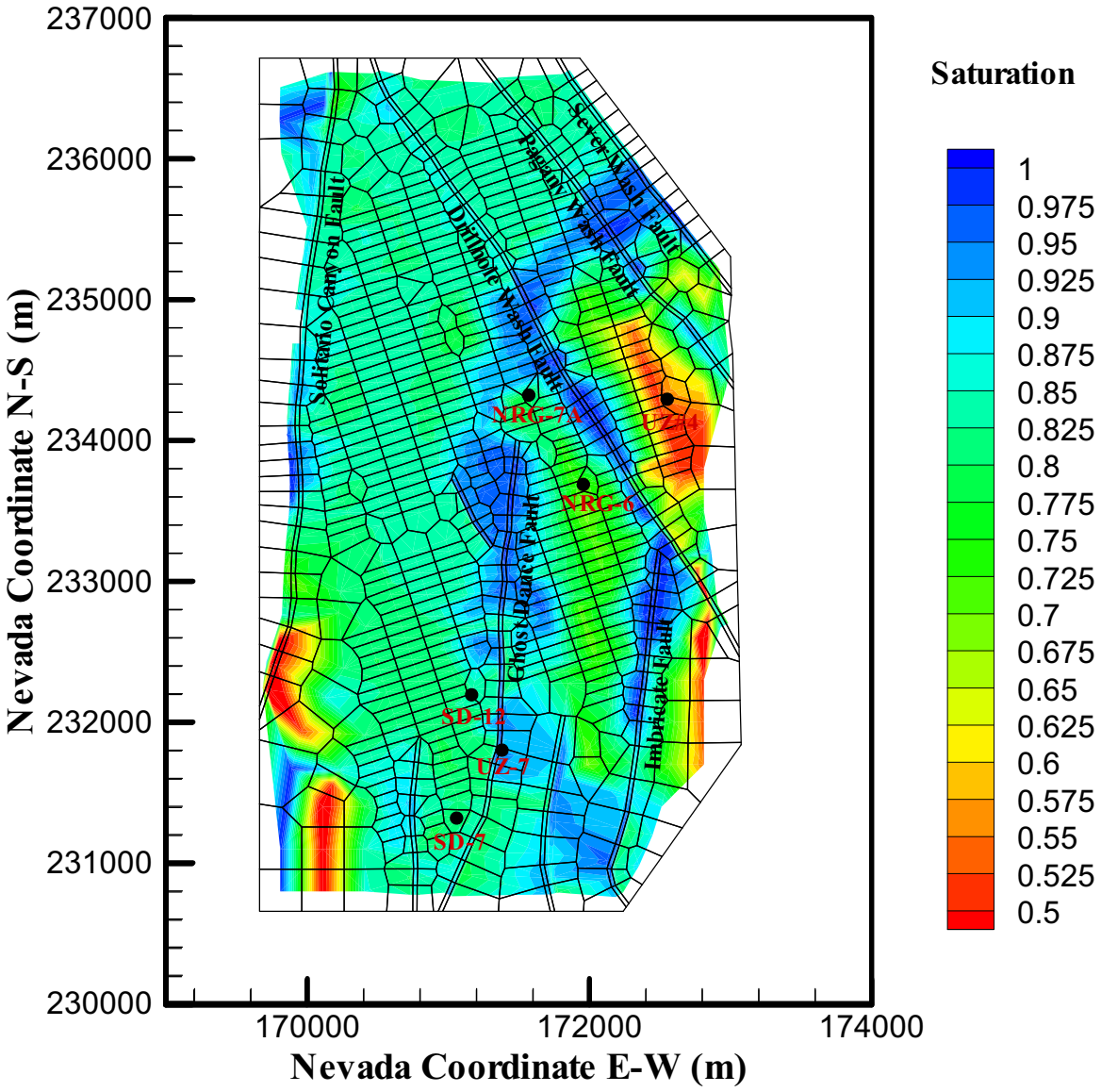

Output DTN: LB0310MTSCLTH3.001.

Figure 6.3.1-9. Model-Predicted Matrix Liquid Saturation Distribution at Repository Horizon 1,000 Years after Waste Emplacement: Base-Case Model with Ventilation

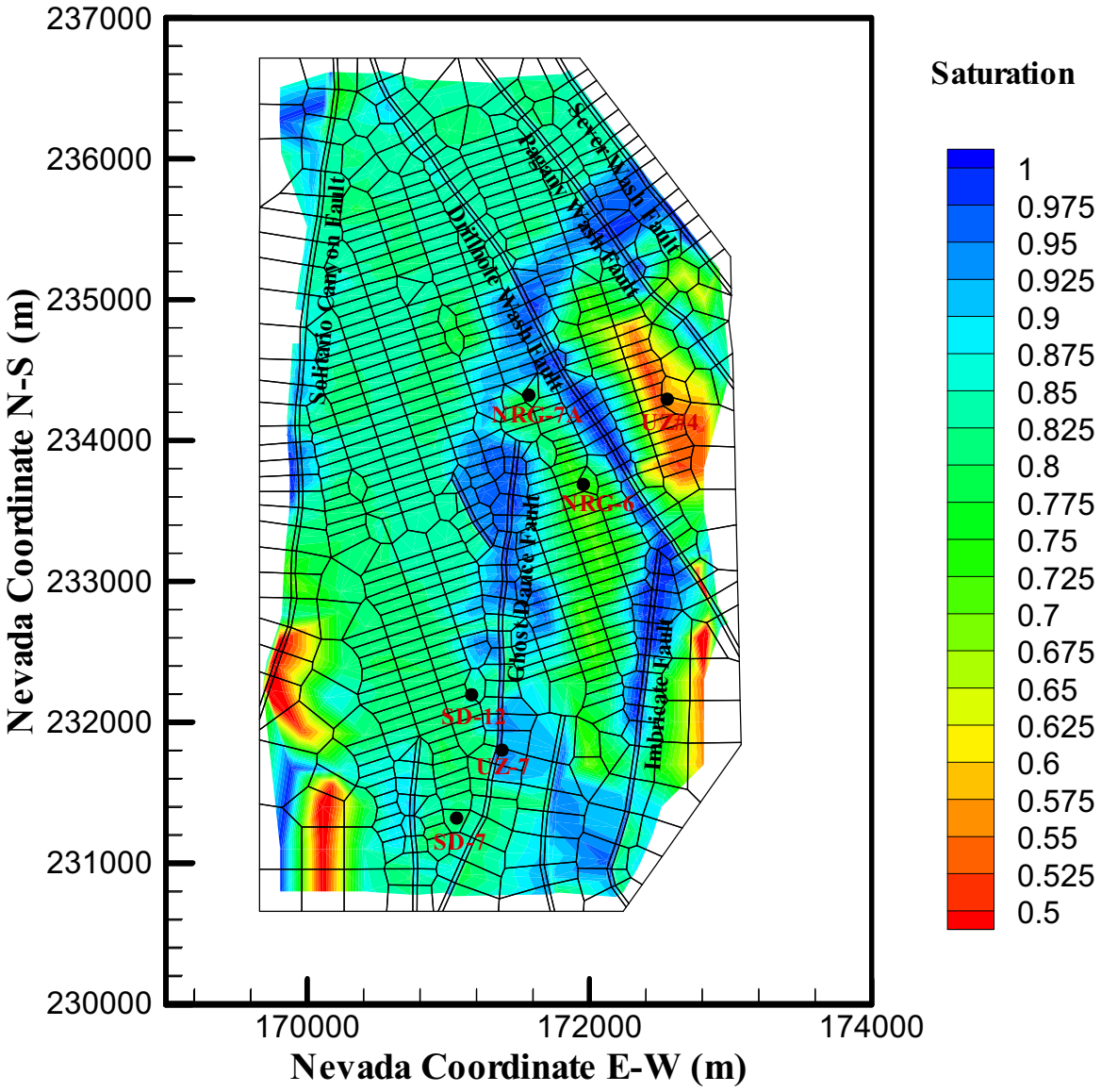

Output DTN: LB0310MTSCLTH3.001.

Figure 6.3.1-10. Model-Predicted Matrix Liquid Saturation Distribution at Repository Horizon at 2,000 Years after Waste Emplacement: Base-Case Model with Ventilation

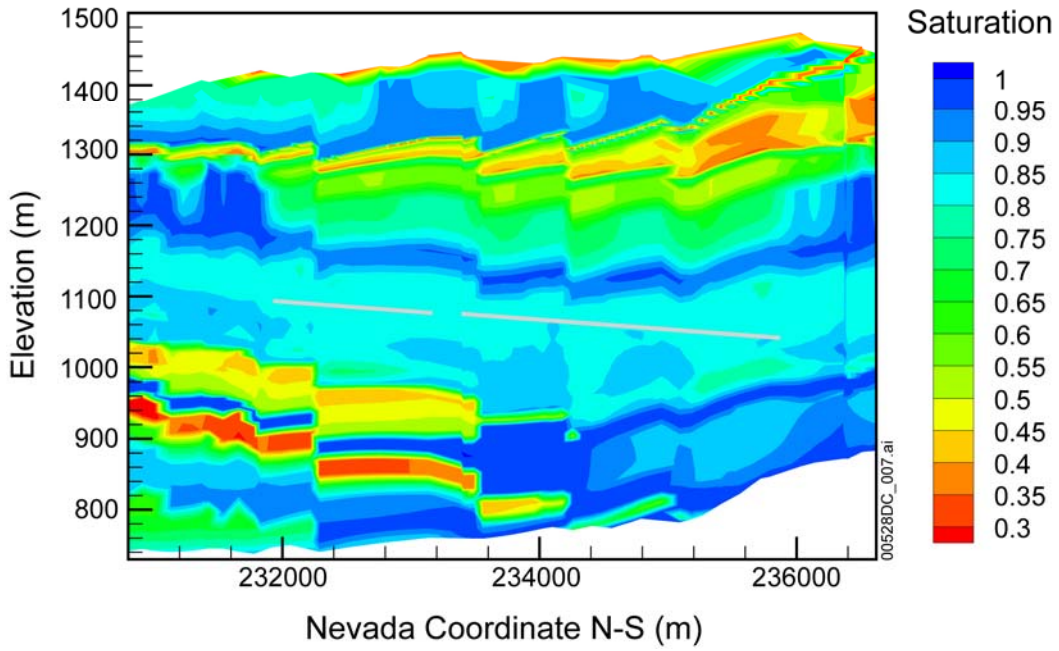

Output DTN: LB0310MTSCLTH3.001.

Figure 6.3.1-11a. Model-Predicted Matrix Liquid Saturation Distribution at North–South Cross Section 500 Years after Waste Emplacement: Base-Case Model with Ventilation

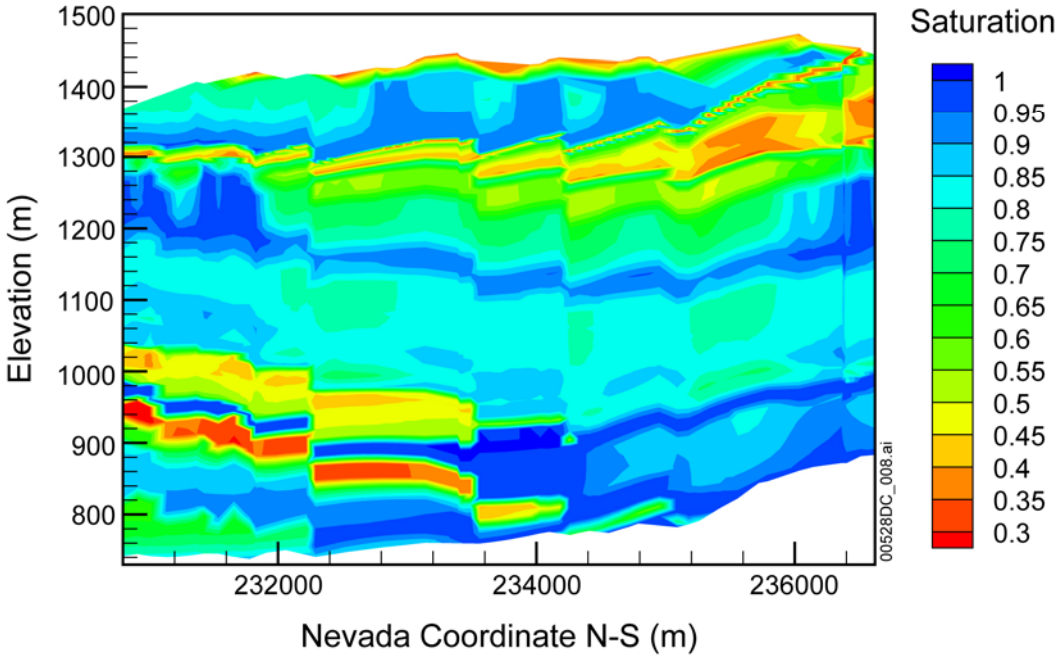

Output DTN: LB0310MTSCLTH3.001.

Figure 6.3.1-11b. Model-Predicted Matrix Liquid Saturation Distribution at North–South Cross Section at the Ambient Condition with the Present-Day, Mean Infiltration Rates

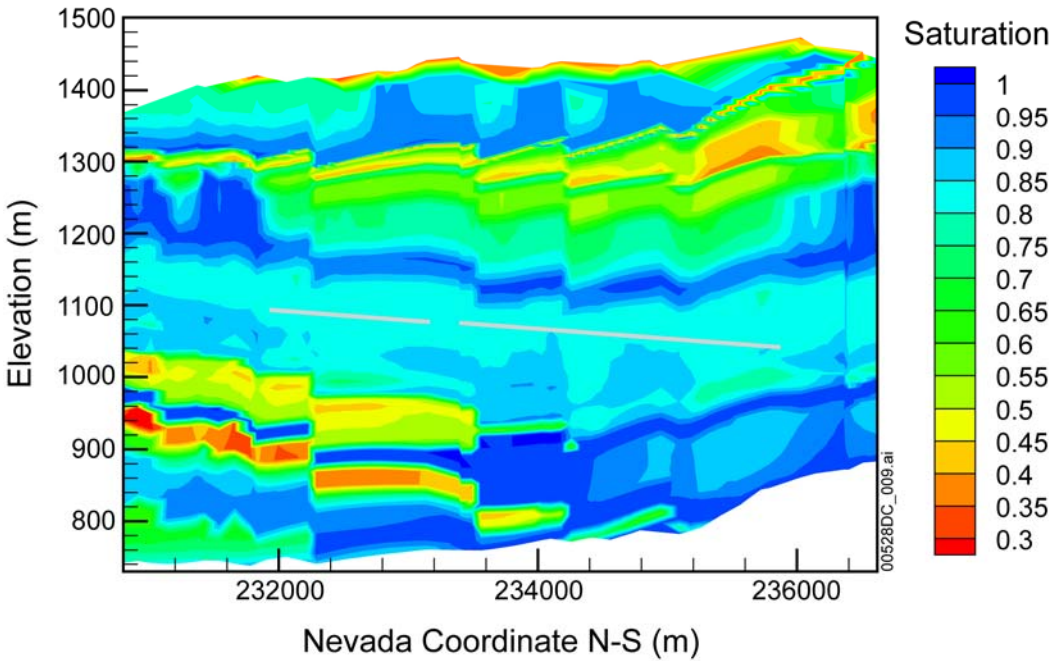

Output DTN: LB0310MTSCLTH3.001.

Figure 6.3.1-12. Model-Predicted Matrix Liquid Saturation Distribution at North–South Cross Section 1,000 Years after Waste Emplacement: Base-Case Model with Ventilation

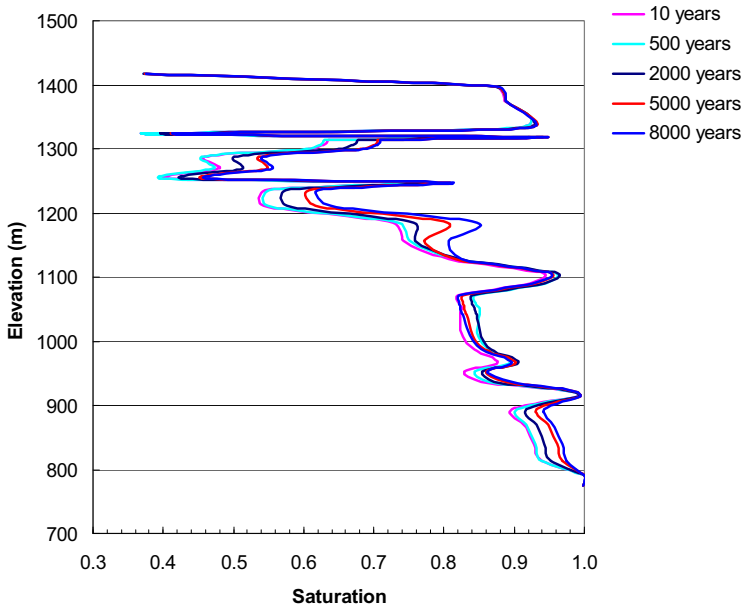

Output DTN: LB0310MTSCLTH3.001.

NOTE: Infiltration rates at the top of column H are: Present day 6.558mm/yr; Monsoon 20.451 mm/yr; and Glacial transition 29.920 mm/yr.

Figure 6.3.1-13. Model-Predicted Matrix Liquid Saturation Distribution along Observation Column H at Different Times: Base-Case Model with Ventilation

6.3.1.3 Percolation Flux

Thermally induced flux evolution can also be analyzed using the three-dimensional TH model results. Figures 6.3.1-14 through 6.3.1-16 show the vertical liquid fluxes in the fracture continuum initially and 500 years after emplacement at the PTn bottom, repository horizon, and top of CHn. Figures 6.3.1-14b, 6.3.1-15b, and 6.3.1-16b show the effect of the thermal load, after 500 years, on the percolation fluxes above the repository, at the repository horizon, and below the repository. Figures 6.3.1-14a, 6.3.1-15a, and 6.3.1-16a show their corresponding ambient fluxes. In general, percolation flux increases within the repository gridblocks, or at the PTn bottom and at the CHn top, only in areas directly above or below the repository. The maximum increase is observed at the repository horizon (Figure 6.3.1-15b versus Figure 6.3.1-15a), because of the strongest thermal impact from repository heating. The flux increase at the bottom of the PTn (Figures 6.3.1-14b and 6.3.1-14a) is small and caused mainly by vapor condensation. Therefore, the models do not predict large-scale changes in liquid flux at or above the repository that could contribute to increased seepage into drifts. Below the repository horizon, the increase in flux at the top of the CHn (Figures 6.3.1-16b and 6.3.1-16a) is also relatively small and caused by drainage of condensed liquid as well as climate-induced increase in net infiltration.

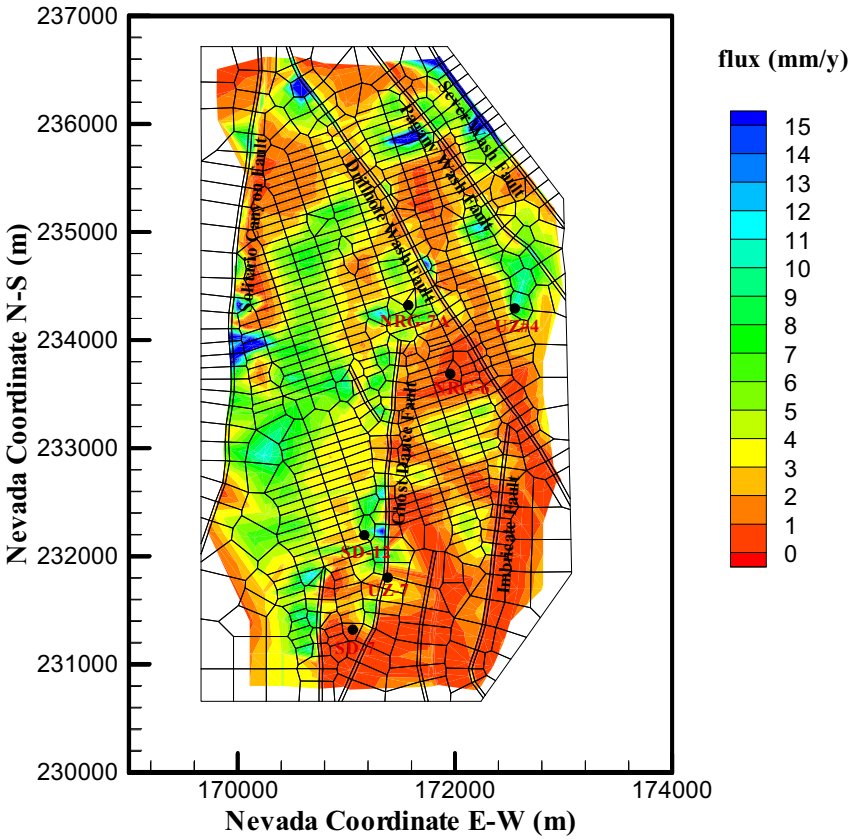

Output DTN: LB0310MTSCLTH3.001.

Figure 6.3.1-14a. Model-Predicted Total Vertical Flux Distribution at Bottom of PTn Unit at the Ambient Condition with the Present-Day, Mean Infiltration Rates

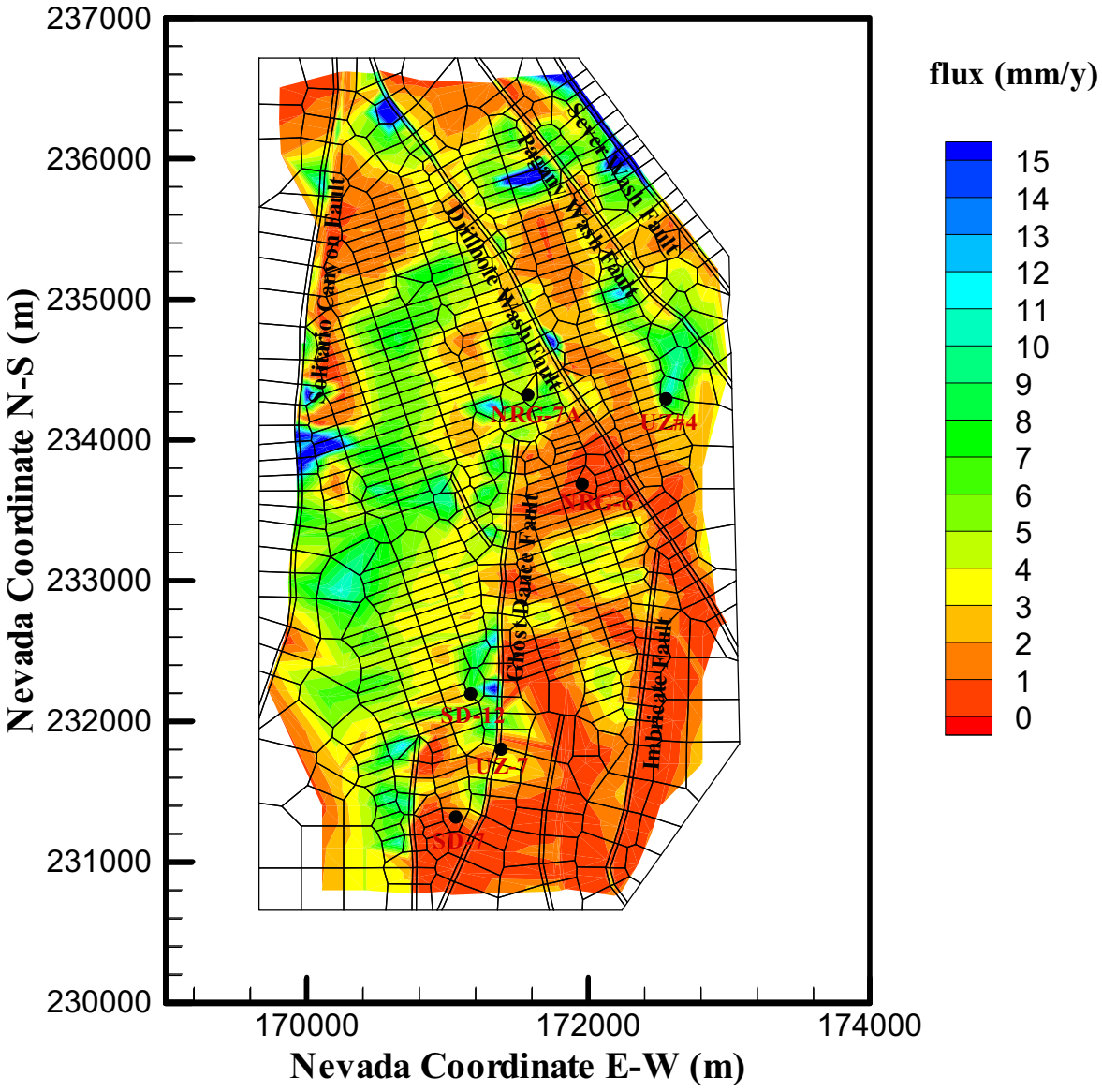

Output DTN: LB0310MTSCLTH3.001.

Figure 6.3.1-14b. Model-Predicted Total Vertical Flux Distribution at Bottom of PTn Unit 500 Years after Waste Emplacement: Base-Case Model with Ventilation

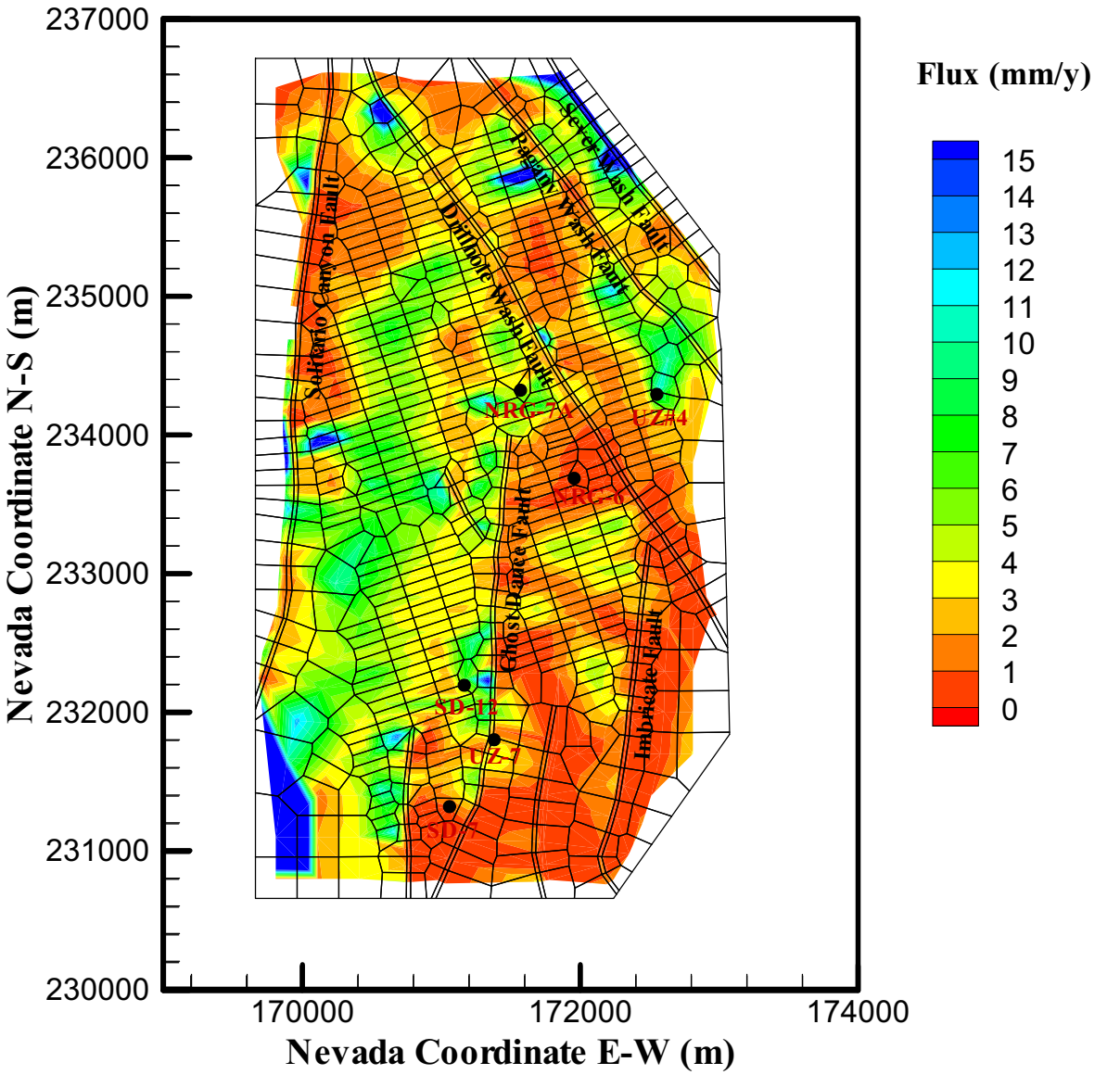

Output DTN: LB0310MTSCLTH3.001.

Figure 6.3.1-15a. Model-Predicted Total Vertical Flux Distribution at Repository Horizon at the Ambient Condition with the Present-Day, Mean Infiltration Rates

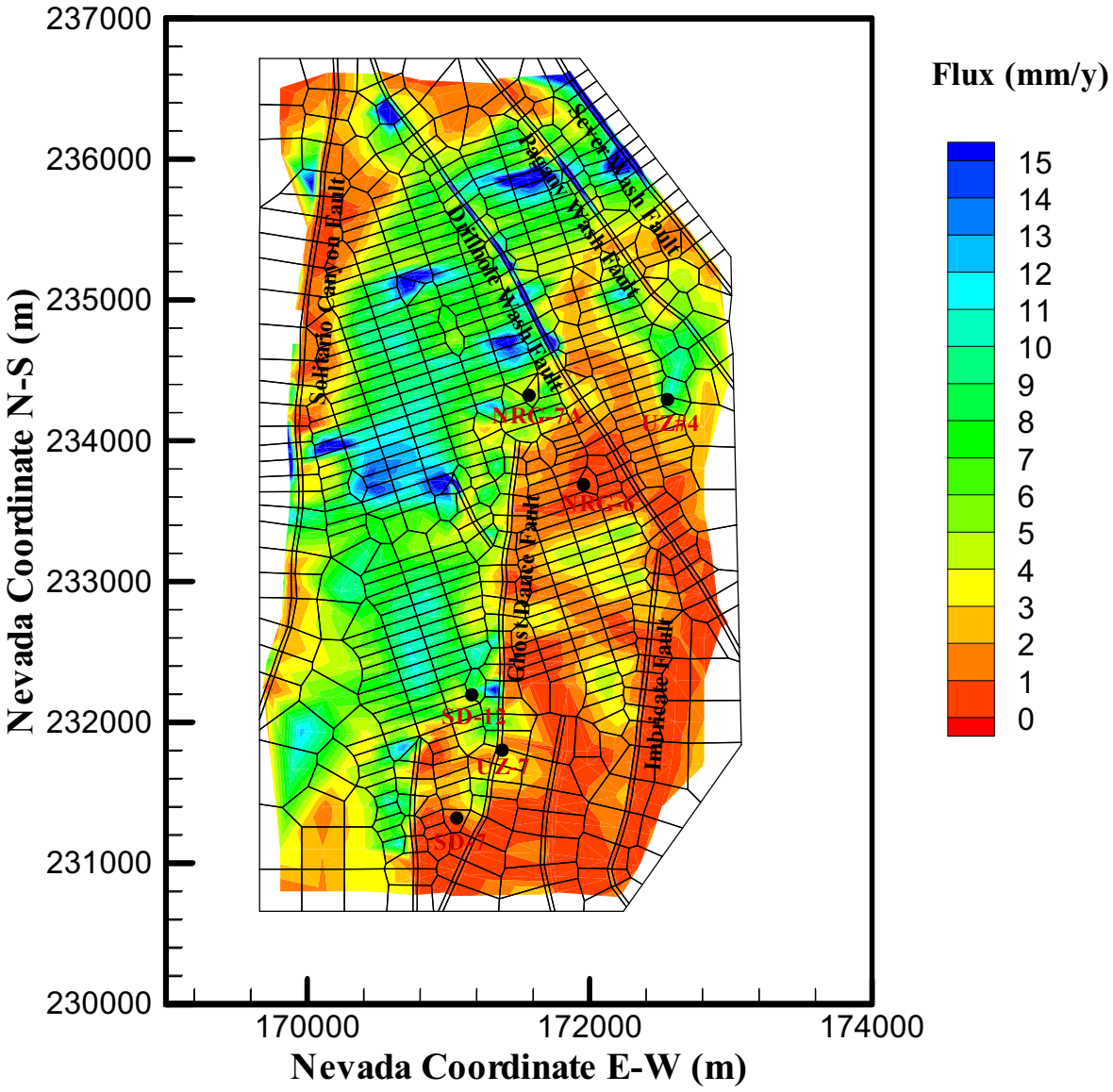

Output DTN: LB0310MTSCLTH3.001.

Figure 6.3.1-15b. Model-Predicted Total Vertical Flux Distribution at Repository Horizon 500 Years after Waste Emplacement: Base-Case Model with Ventilation

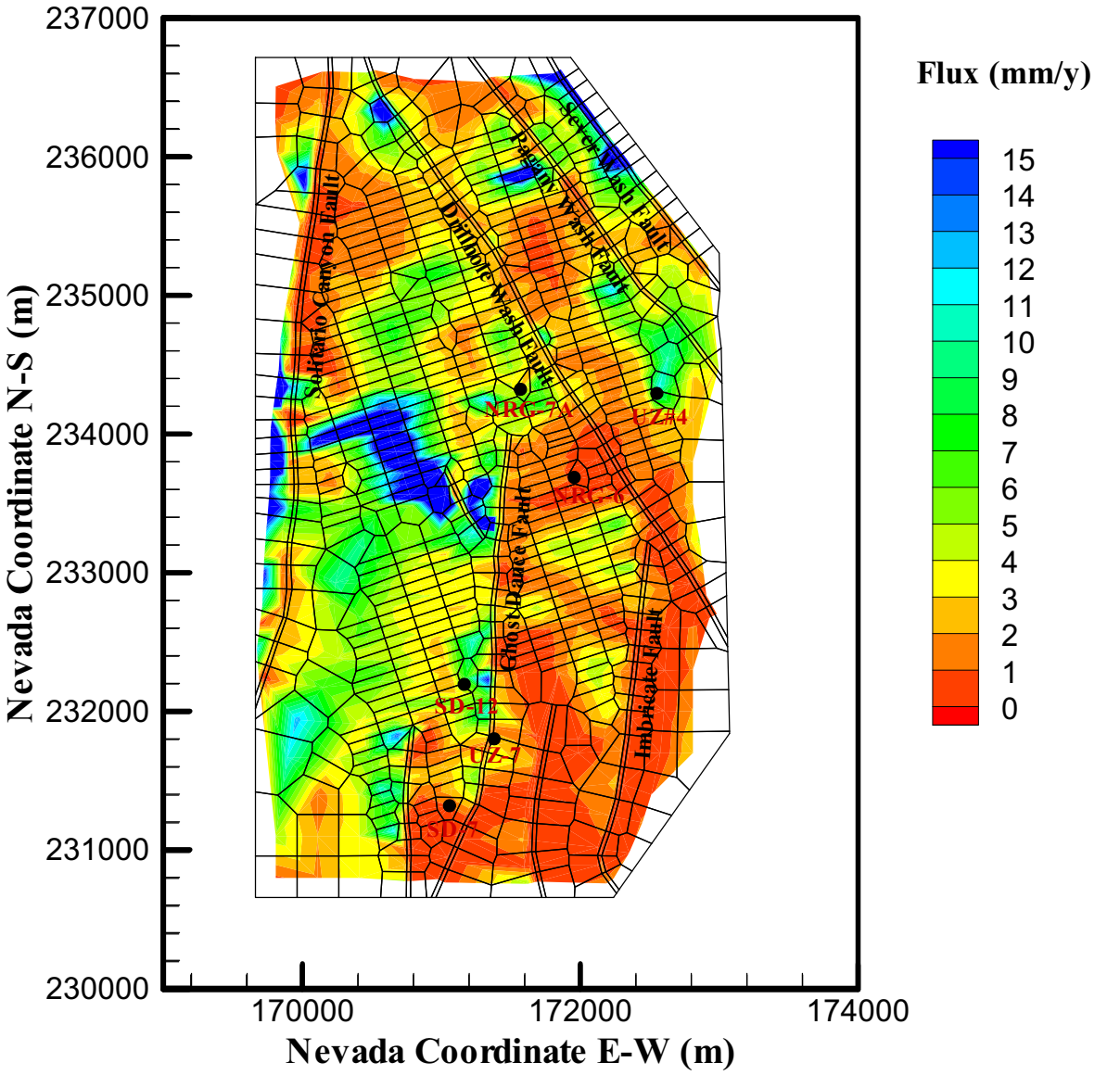

Output DTN: LB0310MTSCLTH3.001.

Figure 6.3.1-16a. Model-Predicted Total Vertical Flux Distribution at Top of CHn Unit at the Ambient Condition with the Present-Day, Mean Infiltration Rates

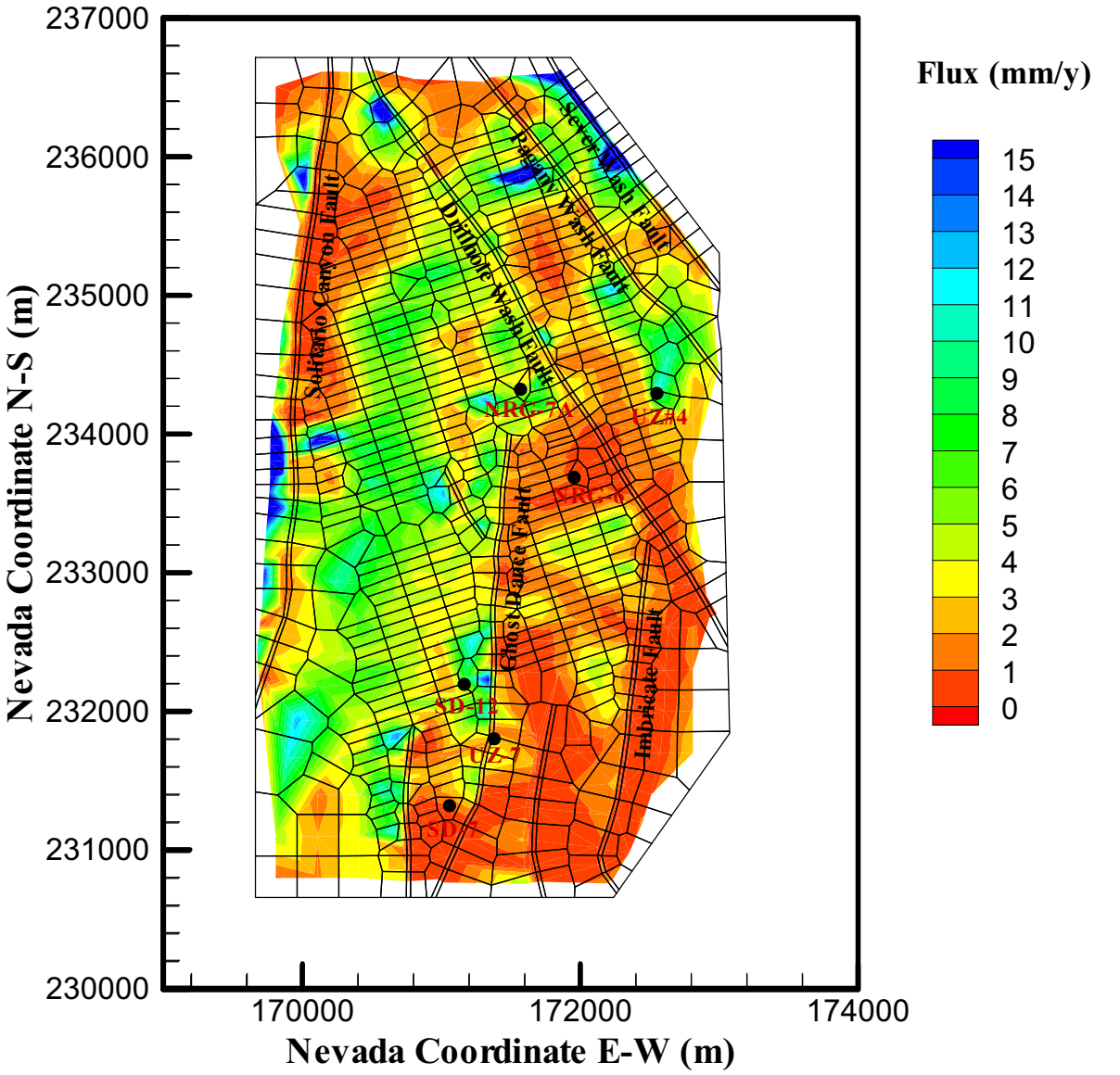

Output DTN: LB0310MTSCLTH3.001.

Figure 6.3.1-16b. Model-Predicted Total Vertical Flux Distribution at Top of CHn Unit 500 Years after Waste Emplacement: Base-Case Model with Ventilation

Figures 6.3.1-17 and 6.3.1-18 show vertical liquid fluxes and their thermally induced variation along Observation Columns F and C (Figure 6.1-1) at different times from 10 to 8,000 years. The coordinates of Observation Columns F and C are also given in Table 6.3-1. As shown in Figure 6.1-1, Column F crosses the center of the northern, main repository block, and Column C is located just outside of the southern edge of the northern repository block. The surface infiltration rate at Column F is approximately 4.5 mm/yr. As shown in Figure 6.3.1-17, along Column F there are three distinctly different vertical percolation fluxes, which correspond to changes in infiltration rate from present day (less than 600 years), monsoon (600 to 2,000 years), and glacial transition (greater than 2,000 years) climates. The figure indicates that significant impact of repository heating on percolation fluxes occurs only during the first 1,000 years. The maximum increase (factor of 3) in repository percolation fluxes is at 500 years of waste emplacement. Above and below the repository horizon, percolation fluxes are only elevated slightly by the repository thermal loading at early times (less than 1,000 years), as indicated in Figure 6.3.1-17. After 2,000 years, however, as repository heat decreases, the thermal effect on percolation fluxes diminishes.

Vertical percolation fluxes and their variations with time at Location C are shown in Figure 6.3.1-18. Note that Column C is located just outside and close to the repository boundary. The ambient infiltration rates at Column C are about 8 mm/yr, which is almost twice as high as that in Column F. Yet Figure 6.3.1-18 shows only a slight effect of repository heating on vertical fluxes, i.e., the vertical flux distribution in Column C remains similar to ambient distribution through the entire thermal-loading period. This is because Column C is located outside the repository area. The boiling front never reaches this location; hence, no thermal effects on flux are predicted in Column C.

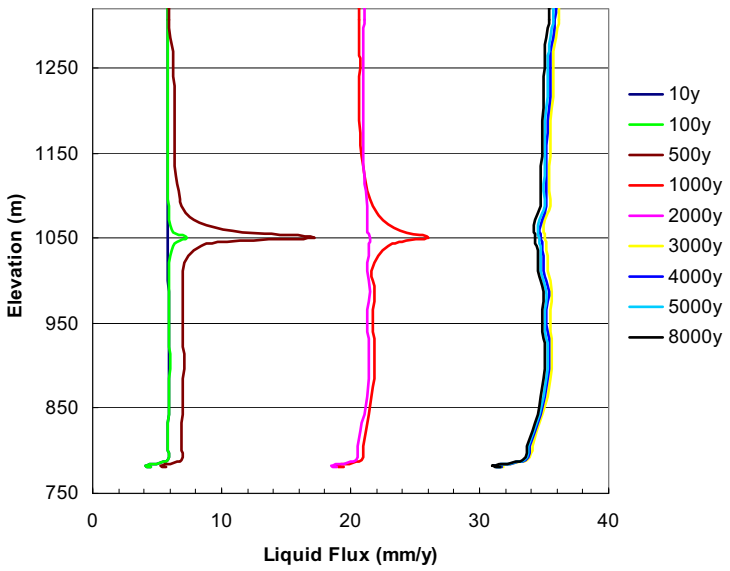

Output DTN: LB0310MTSCLTH3.001.

NOTE: Observation column F is situated at the center of the northern repository block.

Figure 6.3.1-17. Model-Predicted Total Vertical Flux Distribution along Observation Column F at Different Times: Base-Case Model with Ventilation

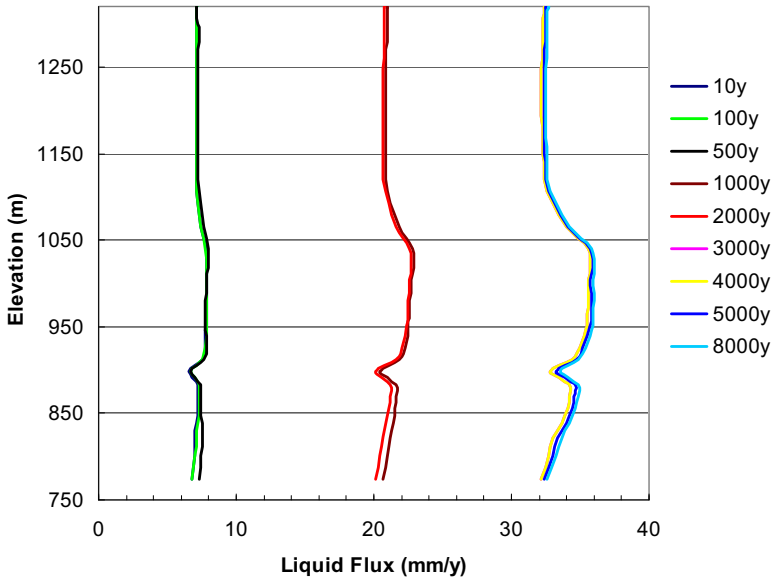

Output DTN: LB0310MTSCLTH3.001.

NOTE: Observation column C is situated outside the northern repository block.

Figure 6.3.1-18. Model Predicted Total Vertical Flux Distribution along Observation Column C at Different Times: Base-Case Model with Ventilation

6.4 MOUNTAIN-SCALE THC MODEL

The purpose of the mountain-scale THC model is to evaluate the coupled thermal-hydrologic-chemical (THC) processes caused by variations in geology (structure and lithology), infiltration rate, and temperature at a mountain or repository scale. This section summarizes the modeling and uncertainty studies performed for the evaluation of THC effects on flow and chemistry in the UZ at the mountain scale. This section addresses the following issues: (1) mountain-scale effects of THC processes on flow and transport, and (2) mountain-scale THC effects on the variability of water chemistry entering drifts under thermal-loading conditions. The mountain-scale THC model is a two-dimensional model based on the mountain-scale TH model documented in Section 6.2 (the two-dimensional grid used for the mountain-scale THC model is a subset of the two-dimensional TH model grid shown in Figures 6.1-1 and 6.1-2), and the conceptual models and data for THC processes documented in *Drift-Scale THC Seepage Model* (BSC 2005 [DIRS 172862]). Many of the uncertainties in the conceptual models, and data used for input and model validation, are identical to those discussed in the latter report. However, the drift-scale THC models are focused primarily on processes that affect seepage (and the chemistry of potential seepage) into drifts. On the other hand, the mountain-scale THC model provides predictions of the effect of THC processes on flow in the Paintbrush hydrogeologic unit (PTn), the basal vitrophyre of the Topopah Spring Tuff, and in the vitric and zeolitic zones in the Calico Hills unit below the repository. These far-field changes are not of particular concern for the drift-scale THC models.

The THC processes are processes that affect the percolation flux to the repository horizon (relevant to seepage), and flow below the repository (relevant to radionuclide transport in the UZ). Small-scale and localized processes, such as mineral precipitation in the boiling zone, can only be captured in finely gridded drift-scale models. Thus, the mountain-scale THC model is focused on larger-scale changes in chemistry and flow that are not localized to small regions adjacent to the drift. Large-scale gas-phase convection and lateral flow are not represented in the drift-scale THC models, and therefore the mountain-scale THC model can also address uncertainties in phenomena that may not arise in the drift-scale “chimney” models.

6.4.1 Conceptual Model for Mountain-Scale THC Processes

The conceptual model for THC processes provides a comprehensive basis for modeling the pertinent mineral–water–gas reactions in the host rock, under thermal loading conditions, as they influence the chemistry of water and gas in the mountain and associated changes in mineralogy. The data incorporated in the model include hydrologic and thermal properties from the calibrated property sets, geological layering from the UZ three-dimensional flow and transport model, geochemical data (fracture and matrix mineralogy, aqueous geochemistry, and gas chemistry) derived from various sources, thermodynamic data (minerals, gases, and aqueous species), data for mineral–water reaction kinetics, and transport data. Simulations of THC processes include coupling among heat, water, and vapor flow, aqueous and gaseous species transport, kinetic and equilibrium mineral–water reactions, and feedback of mineral precipitation/dissolution on porosity, permeability, and capillary pressure for a dual permeability (fracture-matrix) system.

The potentially important mountain-scale coupled THC processes are illustrated schematically in Figure 6.4-1. Some UZ processes, such as the distribution of net infiltration, may affect THC

processes. The effect of THC processes on UZ flow may include modification of the percolation flux in the nonwelded tuffs above the repository in the Paintbrush hydrogeologic unit (PTn) and alteration of flow paths (lateral flow) below the repository in the Calico Hills unit vitric and zeolitic layers (CHn), and on the basal vitrophyre of the Topopah Spring Tuff. Diversion of water around drifts and percolation fluxes through the pillars may also be influenced by porosity and permeability changes owing to mineral precipitation and dissolution. In addition, small-scale processes, such as fracture-matrix interaction, have a strong effect on the chemical evolution of the system and the distribution of mineral precipitation in fractures and the matrix. These issues are addressed in Section 6.4.3, where comparisons of conceptual processes to simulation results are made.

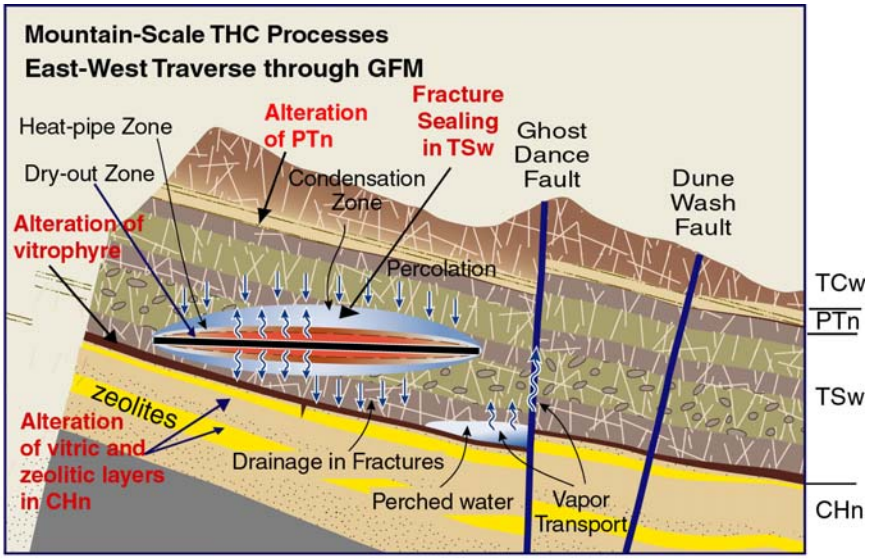

NOTE: The mountain-scale THC model represents a vertical cross section through the repository oriented approximately perpendicular to the cross section shown above.

Figure 6.4-1. Schematic East-West Cross Section through the Geological Framework Model Showing Potential Mountain-Scale THC Processes

6.4.2 Model Setup

6.4.2.1 Numerical Mesh

A 1 km long North–South vertical cross section (Figure 6.4-2) was selected for the two-dimensional THC model based on the following rationale: (1) the North–South two-dimensional vertical cross section is approximately perpendicular to the repository drifts (Figure 6.4-2) and thus better represents the spatial variance of the THC evolution than any other direction; and (2) to minimize the number of gridblocks, due to computational intensity required for a TOUGHREACT V3.0 simulation (LBNL 2002 [DIRS 161256]). For these reasons, a partial north–south vertical cross section contains 7,410 gridblocks (fracture and matrix) and 8 repository drifts (Figure 6.4-2; DTN: LB0310MTSCLTHC.001, file: Mesh). The length

between two lateral borders of the two-dimensional cross section is 1,193 m and was derived from the two-dimensional cross section discussed in Section 6.2 and therefore uses the same stratigraphic information and rock properties. A part of the cross section is outside the repository footprint, so that edge effects can be evaluated. The model results show that the range in temperatures is consistent with the TH model (see Section 6.4.3.1.1).

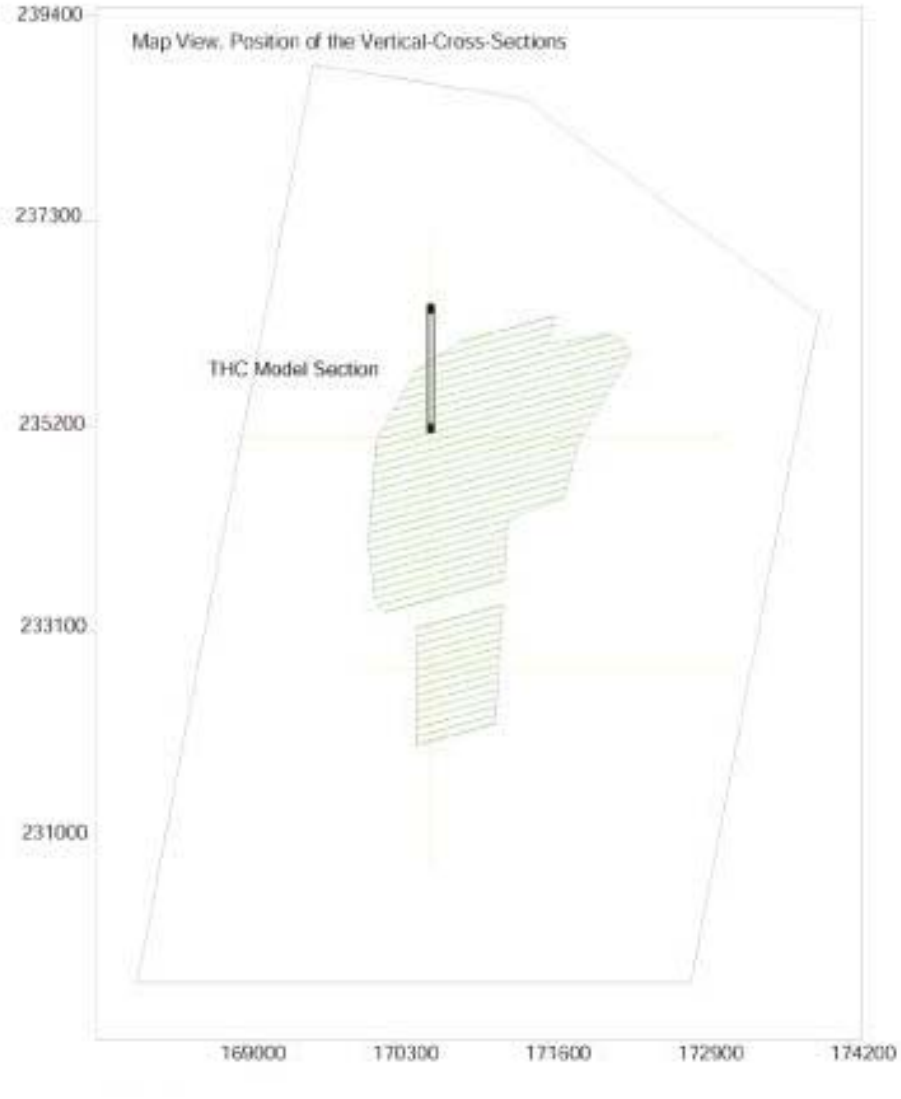

Output DTN: LB0310MTSCLTHC.001.

NOTE: The THC model grid is created by cutting the South–North cross-sectional mesh and is shown in the thin black window in the figure. This two-dimensional mesh is a subset of the two-dimensional mesh shown in Figure 6.1-2 extending only from Northing 235200 to 236392.7.

Figure 6.4-2. Map View of the Two-Dimensional Cross Section of the THC Model Grid Mesh

The upper boundary of the domain is the ground surface; the lower boundary is the groundwater table. The lateral boundaries are set exactly vertical. The northern boundary is the Drill Hole

Wash fault and the southern boundary does not correspond to any geological interface. The gridblocks are mostly tetragonal, with an average length of 21.3 m in the horizontal dimension. Vertically, the thickness of the gridblocks is restricted by the thickness of the stratigraphic layers, which vary from 1.6 m to 20 m. Gridblocks representing the repository drifts are set to be 5 m × 5 m each.

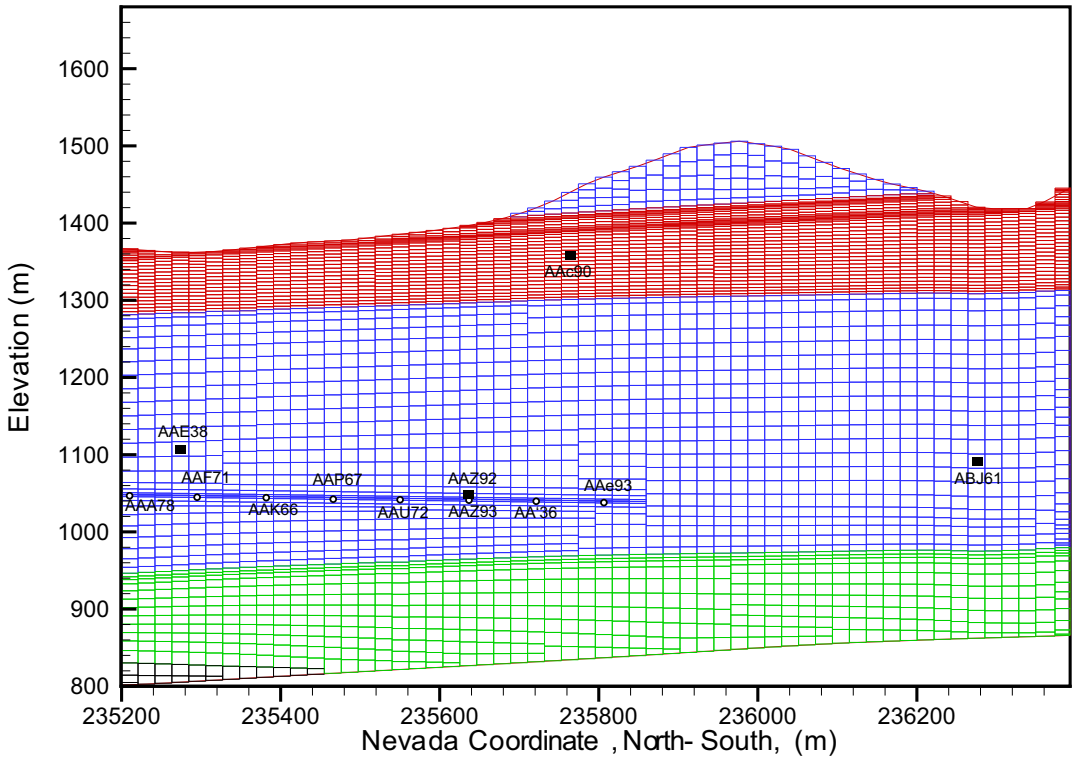

Output DTN: LB0310MTSCLTHC.001.

NOTE: Small black circles represent the repository drifts and black squares represent observation points. The labels are names of the corresponding representative gridblocks of the drifts and observation points. The actual repository blocks are not plotted, because they could hardly be seen on such a small scale.

Figure 6.4-3. Mountain-Scale THC Model Grid

6.4.2.2 Rock Properties

As discussed in Section 4.1.3, rock hydrologic properties are obtained from DTNs: LB0208UZDSCPMI.002 [DIRS 161243] and LB0205REVUZPRP.001 [DIRS 159525], and thermal properties from DTNs: LB0210THRMLPRP.001 [DIRS 160799] for the mountain-scale TH/THC/THM models and LB0402THRMLPRP.001 [DIRS 168481] for sensitivity simulations (Appendices V, VI and VII).

6.4.2.3 Hydrologic and Thermal Boundary and Initial Conditions

The infiltration is applied to the top ground surface gridblocks. Infiltration rates were derived from the infiltration map (DTN: GS000308311221.005 [DIRS 147613]) and is a location-specific distribution for this model domain extracted from the two-dimensional

infiltration distribution. Therefore, the infiltration rates used on this section are specific to this location, but are within the range population and range of infiltration used over the entire unsaturated model domain. The effect of climate change on this infiltration is consistent with that documented in Sections 4.1.1 and 6.1.4. Over the THC model grid used in this report, the average infiltration rates for the present-day, monsoon, and glacial transition climatic conditions are 8.7 mm/yr, 32.3 mm/yr, and 101.6 mm/yr, respectively. The lower boundary is the groundwater table, for which pressure is assumed to be constant. Both lateral boundaries are modeled as no-flux for mass because vertical flow is dominant in the UZ.

The temperature at the ground surface is assumed to be constant (in time), because both the infiltration rate and the enthalpy of the infiltrating water are treated as constant. Temperature of the groundwater table is constant (Section 6.1.3). The two lateral boundaries are considered as no-flux for heat as well as mass.

A steady-state flow and thermal field are required for THC simulations as initial conditions. A TH simulation under ambient conditions was performed to produce the steady-state flow and thermal field with the present-day mean infiltration rate (DTN: LB0310MTSCLTHC.001). The steady-state TH field is used as the initial condition for the TH simulations (with thermal loading) and THC simulations (with thermal loading and geochemistry).

6.4.2.4 Initial and Boundary Geochemical Conditions

The model of the geochemical system includes the major aqueous species, minerals, and gaseous components in the unsaturated zone. Additionally, minor species, such as F^-, are included for their relevance to waste package corrosion. The minerals and aqueous and gaseous species in the model geochemical system are listed in Table 6.4-1, and are the same as those in the "extended-case" geochemical system described in *Drift-Scale THC Seepage Model* (BSC 2005 [DIRS 172862]).

The geochemical model consists of the following primary aqueous species: H^+, Na^+, K^+, Ca^{2+}, Mg^{2+}, AlO_2^-, NO_3^-, SO_4^{2-}, F^-, Cl^-, HCO_3^-, SiO_2(aq), and $HFeO_2$(aq). Gaseous components include air, H_2O, and CO_2. The initial mineralogy of the tuff matrix and fracture coatings is represented by the following assemblage (some as end members of an ideal solid-solution phase): α-cristobalite, opal, tridymite, quartz, K-feldspar, albite, anorthite, Ca-smectite, Na-smectite, Mg-smectite, illite, calcite, fluorite, gypsum, rhyolitic glass, hematite, stellerite, clinoptilolite, mordenite, and heulandite. Several other secondary phases are also considered (e.g., amorphous silica, kaolinite, and sepiolite), as well as a set of potential salt phases that can precipitate during the complete dryout of a gridblock.

In cases when water flows into grid blocks that dry out in the flow calculation (by boiling or evaporation), the following solid phases are formed, stoichiometrically and in the following order: amorphous silica, calcite, gypsum, hematite, fluorite, $NaNO_3$, K_2SO_4, Na_2SO_4, $MgSO_4$, halite, and sylvite. The order is predetermined (i.e., nitrates are formed before chlorides) to ensure nitrate mass is not lost in cases where insufficient sodium remains to form $NaNO_3$ (in the absence of other nitrate salts that could have formed). The goal here is not to model evaporation accurately but to save as much mass of the dissolved constituents as possible for grid blocks that completely dry out.

Table 6.4-1. Minerals, Aqueous Species, and Gaseous Species in the Mountain-Scale THC Model

Aqueous Species (primary):	Minerals
H_2O	Calcite
H^+	Tridymite
Na^+	α–Cristobalite
K^+	Quartz
Ca^{+2}	Amorphous Silica
Mg^{+2}	Hematite
SiO_2	Fluorite
AlO_2^-	Gypsum
$HFeO_2^{-2}$	Sepiolite
HCO_3^-	Albite
Cl^-	K-Feldspar
SO_4^{-2}	Anorthite
F^-	Ca-Smectite
NO_3^-	Mg-Smectite
Gaseous Species:	Na-Smectite
CO_2	Opal
H_2O	Illite
Air	Kaolinite
	Rhyolitic Glass
	Stellerite
	Heulandite
	Mordenite
	Clinoptilolite

Source: Modified from BSC 2005 [DIRS 172862], Table 6.2-2.

Upon rewetting, the salt minerals (i.e., $NaNO_3$, K_2SO_4, Na_2SO_4, $MgSO_4$, halite, sylvite) are assumed to dissolve kinetically with a relatively fast rate constant (set here at 10^{-6} mol/m^2/s) and a dissolution rate limited by their solubility. The salt solubilities were taken from the data0.ymp.R2 database (DTN: MO0302SPATHDYN.000 [DIRS 161756]), except that $NaNO_3$ (not in that database) was given the solubility of KNO_3 in that database. Therefore, this model captures the general behavior of salt dissolution as the boiling front recedes. However, the predicted major ion concentrations during the short time when these salts dissolve are approximate, because the identity of the salt phases is not based on a thermodynamic speciation/precipitation model, and their dissolution rates are only approximate.

As discussed in Section 4.1.11 of the present report, the thermodynamic database (DTN: LB0307THMDBRTM.001 [DIRS 164434]) that was developed based on the project database (DTN: MO0302SPATHDYN.000 [DIRS 161756]) is used in the mountain-scale THC model. Similarly, the kinetic database documented in DTN: LB0307KNTDBRTM.001 [DIRS 164433] is used in the mountain-scale THC model as discussed in Section 4.1.12.

Simulations conducted in *Drift-Scale THC Seepage Model* (BSC 2005 [DIRS 172862], Section 7.1) have shown a strong effect on the pH and CO_2 concentrations of waters reacting with anorthite at low temperatures, and some effect at elevated temperatures. To allow for an

approximately steady-state initial water and gas chemistry, using the thermodynamic and kinetic data as derived, the surface area of anorthite was reduced by three orders of magnitude for the THC seepage model initial conditions. Although this reduction seems large, experimental studies comparing the dissolution rates of plagioclase feldspars have shown that the dissolution rate of anorthite is at least three to four orders of magnitude faster than all other composition plagioclase feldspars (Blum and Stillings 1995 [DIRS 126590], p. 307, Figure 7). In this model report, the effective dissolution rate for anorthite was reduced by three orders of magnitude, by reducing the initial surface area of this mineral by the same amount. This essentially resulted in the suppression of the mineral, which is consistent with the fact that one would expect calcic plagioclase to have already weathered completely during the natural thermal alteration of the mountain, which lasted millions of years.

Table 6.4-2 shows the initial pore-water and gas compositions obtained from the Drift Scale Test (DST) (BSC 2004 [DIRS 169900], Section 6.3.4; BSC 2005 [DIRS 172862], Table 6.2-1). The initial and infiltrating water chemistry was set to match that from the matrix pore water collected from the Topopah Spring middle nonlithophysal unit (Tptpmn) in Alcove 5, near the DST ("HD-PERM" water; BSC 2005 [DIRS 172862], Table 6.2-1). Although this water may not be characteristic of all pore waters in the UZ, it has been used successfully in validation studies with the DST, as shown in *Drift-Scale THC Seepage Model* (BSC 2005 [DIRS 172862], Section 7) and also as summarized in Section 7 of this report. Analyses of Al were below detection in the three samples (<0.06). The Al concentration was calculated based on equilibrium between K-feldspar and illite, because pore waters at Yucca Mountain have been observed to plot near this equilibrium boundary (BSC 2005 [DIRS 172862]).

Initial mineral abundances were assigned to each hydrogeologic unit based on data from the three-dimensional mineralogical model V3.0 (DTN: LA9908JC831321.001 [DIRS 113495]) from a single column taken near the center of the repository footprint. Therefore, each model layer is characterized by uniform mineralogical abundances, although some layers may change from zeolitic to vitric along strike. There is no other lateral geologic variability in this model, except for changes in the thickness of the layers. Mineral abundances were converted from weight percent to volume fraction and normalized to 100%. Solid solution phases were recalculated to end-member compositions. Some minerals were given small amounts (such as fluorite) because of their observed occurrence. Illite abundances were estimated to be 10% of the smectite abundances for both the fractures and matrix. Fracture mineralogy data for the TSw welded units are derived from DTNs: LA9912SL831151.001 [DIRS 146447] and LA9912SL831151.002 [DIRS 146449]. Initial mineral volume fractions for each rock layer are presented in Appendix I. The procedures to calculate the initial mineral volume fractions (starting from the mineral abundance data in DTNs: LA9908JC831321.001 [DIRS 113495], LA9912SL831151.001 [DIRS 146447], and LA9912SL831151.002 [DIRS 146449]) are also described in Appendix I.

Table 6.4-2. Initial Pore-Water and Gas Compositions

Sample ID: / Water Input Type:	Units	HD-PERM (Alcove 5)
Temperature	°C	25
pH (measured)	pH	8.31
Na^+	mg/L	61.5
K^+	mg/L	8
Ca^{2+}	mg/L	101
Mg^{2+}	mg/L	17
$SiO_{2(aq)}$	mg/L	70.5
Cl^-	mg/L	117
SO_4^{2-}	mg/L	116
HCO_3^- (calc)[a]	mg/L	200
NO_3^-	mg/L	6.5
F^-	mg/L	0.86
Al^{3+} (calc)[a]	molal	6.173E-10
Fe^{3+} (calc)[a]	molal	1.155E-12
$\log(pCO_2)$[a]	bar	–3.1
CO_2 (approx)[b]	ppmv	~900

Sources: BSC 2005 [DIRS 172862], Table 6.2-1,
DTN: MO0005PORWATER.000 [DIRS 150930].

[a] Calculated (see BSC 2005 [DIRS 172862], Table 6.2-1).
[b] Approximately converted to ppmv assuming total pressure equal to one bar. Detailed discussion is presented in BSC 2005 [DIRS 172862], Section 6.2.2.1.

NOTE: HD-PERM values represent average of Tptpmn pore-water analyses ESF-HD-PERM-2 (30.1'-30.5'), ESF HD-PERM-3 (34.8'-35.1') in DTN: MO0005PORWATER.000 [DIRS 150930].

Reactive surface areas for mineral phases were calculated based on the geometric properties of the fracture and matrix media, and the consideration of the extent of pre-existing alteration of the rock. The methodology for the calculation of reactive surface areas is given in *Drift-Scale THC Seepage Model* (BSC 2005 [DIRS 172862], Section 6.4.3.2). Fracture and matrix mineral reactive surface areas for each rock layer are given in Appendix II. The procedures to calculate the matrix and fracture reactive surface areas are further elaborated in Appendix II. Permeability coupling parameters (BSC 2005 [DIRS 172862]) are given in Appendix III. The source of the permeability coupling parameters is DTN: LB0205REVUZPRP.001 [DIRS 159525], and the procedures to calculate the permeability coupling parameters are explained in Appendix III.

6.4.2.5 Numerical Code and Simulation Methods

Using TOUGHREACT V3.0 (LBNL 2002 [DIRS 161256]), simulations were performed that coupled multiphase fluid flow (water and air), heat flow, aqueous and gaseous species transport,

and kinetic and equilibrium mineral–water–gas reactions. The simulations used the equation of state module EOS3, considering water and gas flow under nonisothermal conditions with vapor-air diffusion. Effects of vapor-pressure lowering were not considered in these simulations because comparison simulations in *Drift-Scale THC Seepage Model* (BSC 2005 [DIRS 172862]) showed only minor differences in the chemical compositions of waters around drifts, although computational times were significantly greater.

6.4.3 Mountain-Scale THC Model Results

This section discusses a stepwise approach to evaluation of coupled THC processes under thermal-loading conditions at the mountain scale. This stepwise approach introduces increasing levels of transport and reaction, as well as thermal loading conditions, to better distinguish the roles of the various coupled-processes occurring simultaneously. The series of simulation steps was performed as follows:

- Steady-state flow of water and heat under ambient conditions
- Thermal-hydrologic (TH) simulation under thermal loading conditions (with 86.3% heat removal by ventilation for the first 50 years) and the climate change scenario (Section 6.4.3.1), with and without vapor diffusion
- Steady-state aqueous and gaseous species transport, CO_2-water equilibration under ambient temperatures (Section 6.4.3.2)
- Aqueous and gaseous species transport, CO_2-water equilibration under thermal loading and climate change scenario (Section 6.4.3.3.1)
- Aqueous and gaseous species transport, CO_2-water equilibration, mineral–water reactions under thermal loading and climate change scenario (Sections 6.4.3.3.2-6.4.3.3.4).

In this report, results from all the simulations except the initial steady-state flow field (used for initial conditions only) are presented. Table 6.4-3 summarizes the specific aspects of the simulations.

Table 6.4-3. Summary of the TH/THC Simulations

Model	Case Name	Infiltration	Thermal Load	Heat-Removal by Ventilation	Aqueous Chemistry	Minerals	Section
1	Steady state	Present-day mean	None	N/A	No	No	
2	Chemical steady state	Present-day mean	None	N/A	Yes	No	6.4.3.2
3	TH–v86 (harmonic weighting on absolute permeability, no vapor diffusion)	Present-day mean (0 to 600 years), Monsoon mean (600 to 2,000 years), Glacial transition mean (2,000 to 10,000 years)	Yes	86.3%	No	No	6.4.3.1
4	TH-v86 (upstream weighting on absolute permeability, vapor diffusion)		Yes	86.3%	No	No	
5	THC–v86a		Yes	86.3%	Yes	No	6.4.3.3.1
6	THC_86_5		Yes	86.3%	Yes	Yes	6.4.3.3.2 to 6.4.3.3.4

NOTE: Sources listed in Section 6.1.5.

As given in Table 6.4-3, three infiltration scenarios were combined to produce a transient infiltration scenario for the TH (with thermal loading) and THC simulations. The simulation period from 0 to 600 years was modeled with the present-day mean infiltration rate, 600 to 2,000 years with the monsoon mean infiltration rate, and 2,000 to 10,000 years with the glacial transition mean infiltration rate. Two alternative TH simulations were considered. The first one omitted vapor diffusion and used harmonic weighting for the absolute permeability. The second simulation used upstream weighting for the absolute permeability (as well as for the relative permeability) and considered vapor-air diffusion. The THC runs with all aqueous species, gaseous species, and minerals used the latter TH setup.

TH results are presented in the next section in order that the THC processes that are directly affected by TH processes can be directly compared. There are no systematic differences between the TH model discussed in this section compared to those described in the previous sections; however, because the cross section is much more limited, there are boundary condition effects that lead to different local behavior in flow and temperature.

6.4.3.1 Results of TH–v86

Results from the TH simulations with two different model setups (3 and 4 in Table 6.4-3) show similar temperature and saturation but different percolation flux through the repository horizon. Simulation with upstream weighting on absolute permeability and consideration of vapor diffusion gives larger percolation fluxes through the repository horizon. Here the plotting is for temperatures and saturations calculated with the model setup of harmonic weighting of permeability and without consideration of vapor diffusion (the temperature and saturation obtained with another model setup are similar). This setup is consistent with the

two-dimensional TH model in Section 6.2. The calculated percolation fluxes through the repository horizon are compared for different model setups.

6.4.3.1.1 Temperature

Results from the TH simulation (86.3% heat removal by ventilation) show that the temperature at representative gridblocks of the drift wall increased immediately after the thermal power loading imposition (see Section IV.3 of Appendix IV for procedures of postprocessing and plotting of the THC model results). During the ventilation period, the temperature at the drift wall reaches a peak value, 47.6°C, at year 22. After the peak temperature is reached, the drift-wall temperature drops to around 45°C (Figure 6.4-4). Once the ventilation ends, the drift-wall temperature increases sharply and reaches its peak, 100.6°C, at year 73, then drops to 96.3°C and tends thereafter to slowly decrease. The drop in the drift-wall temperature becomes more rapid due to an increase in the infiltration rate at year 600. At locations above the drift, the temperature is strongly affected by the increase of the infiltration rate (see curve AAE38 in Figure 6.4-5). The drift-wall temperatures at different drifts are slightly different from each other. These differences are smaller than 3°C and correspond to the spatial variation of the infiltration rate. The temperature approaches close to the ambient value in 100,000 years (Figure 6.4-5). Figure 6.4-6 shows the temperature spatial distribution at different times. The simulated temperature is consistent with the two-dimensional TH model results shown in Figures 6.2-1a, 6.2-2a, 6.2-3a, 6.2-4a, and 6.2-5a.

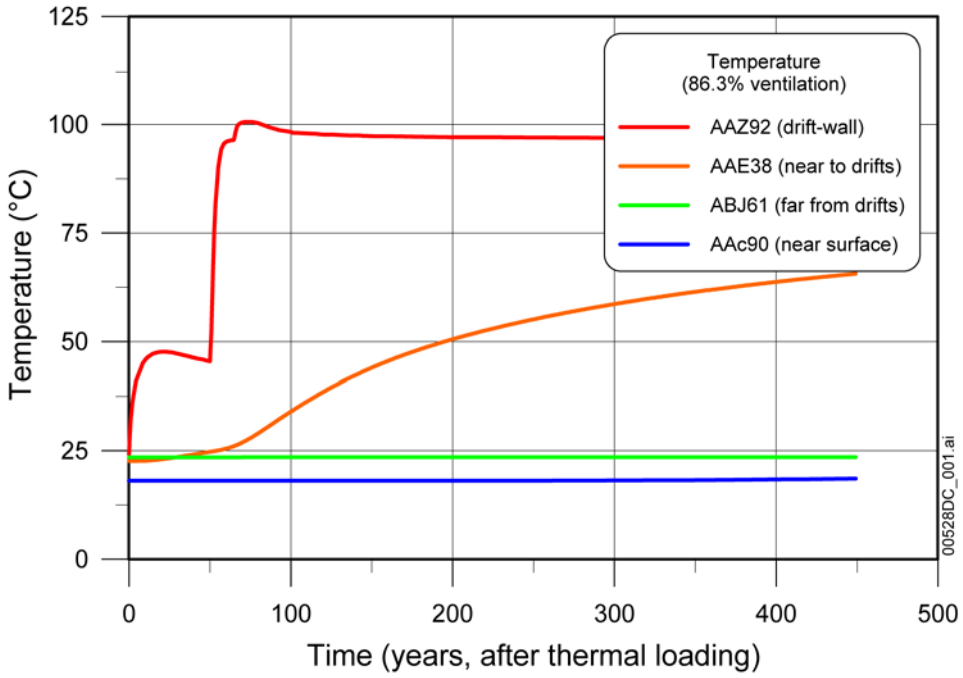

Output DTN: LB0310MTSCLTHC.002.

NOTE: Locations are shown in Figure 6.4-3. Distance from the nearest drift: AAE38, 64.25 m; ABJ61, 492.54 m; AAc90, 323.94 m.

Figure 6.4-4. Short-Term Temperature Evolution Curves at Different Locations

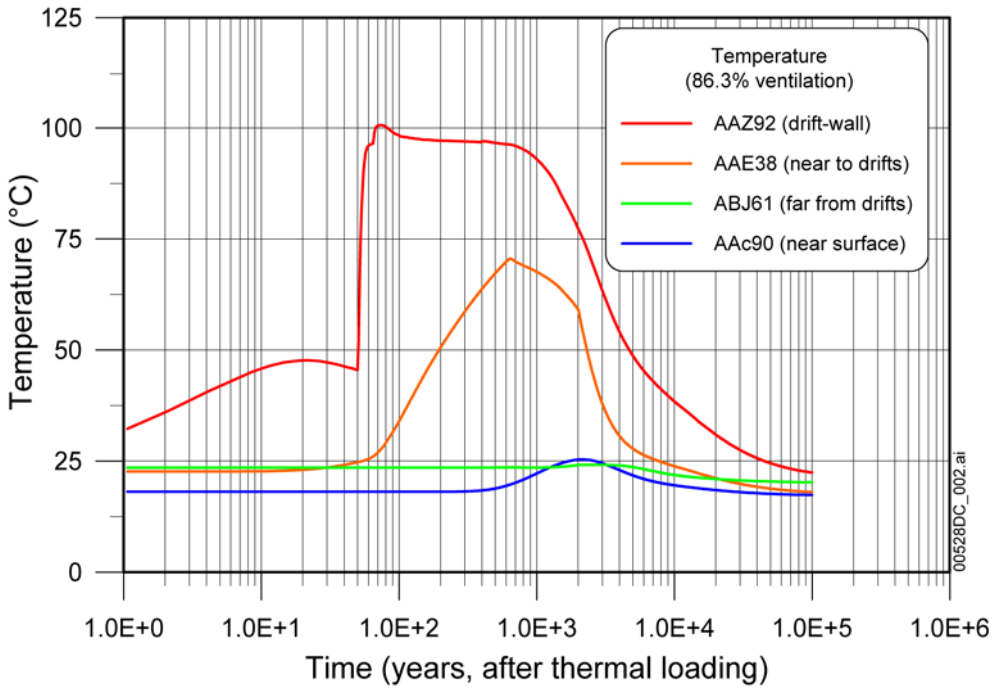

Output DTN: LB0310MTSCLTHC.002.

NOTE: Locations are shown in Figure 6.4-3. Distance from the nearest drift: AAE38, 64.25 m; ABJ61, 492.54 m; AAc90, 323.94 m.

Figure 6.4-5. Long-Term Temperature Evolution Curves at Different Locations

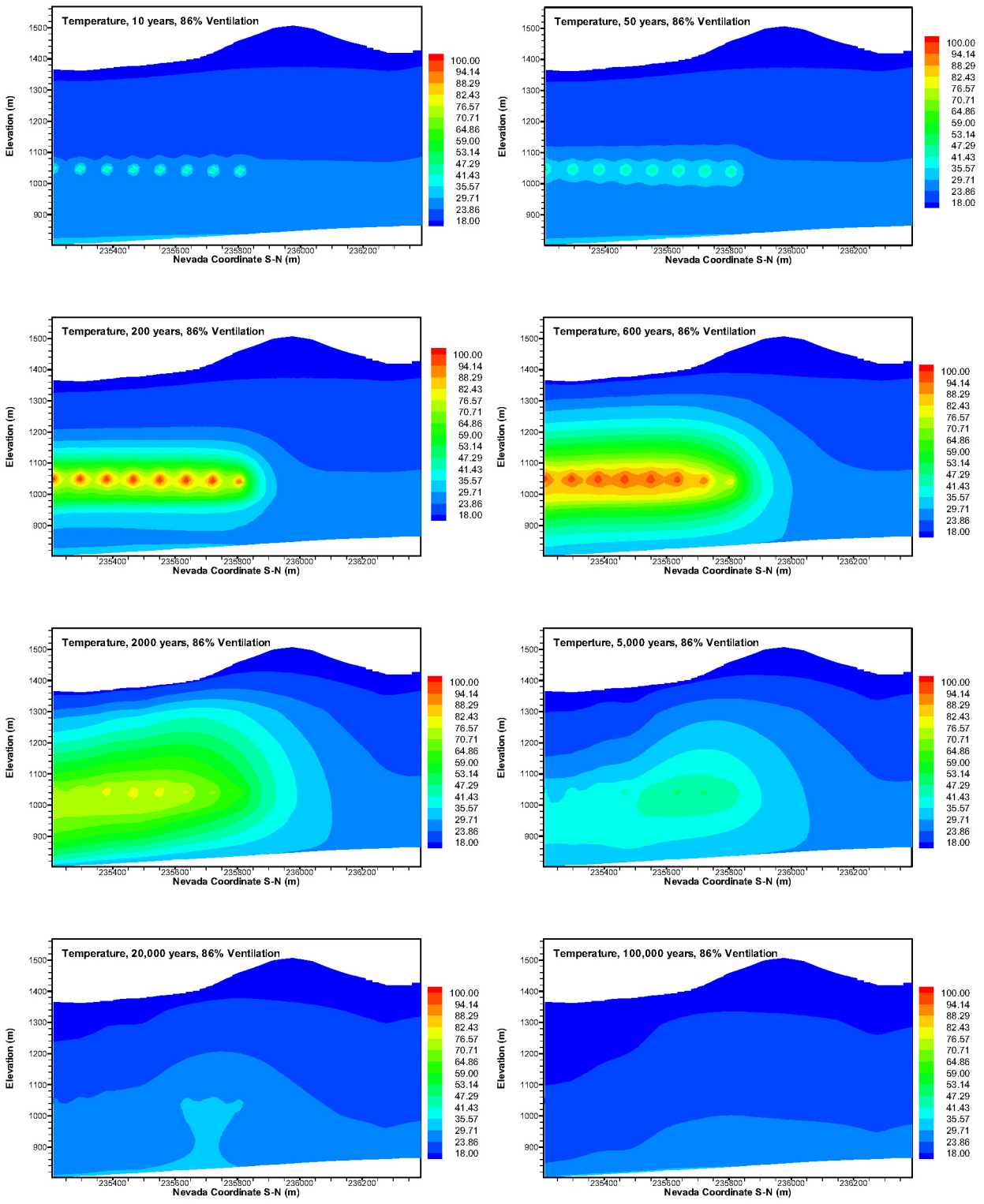

Output DTN: LB0310MTSCLTHC.002.

Figure 6.4-6. Temperature Spatial Distribution at Different Times

6.4.3.1.2 Liquid Saturation

During the ventilation period, the water saturation in the matrix is almost unchanged (Figure 6.4-7). A slight increase (4 years to 20 years) followed by a gentle decrease (20 years to 50 years) can be seen at the drift-wall (curve AAZ92 in Figure 6.4-7). After the ventilation period, the matrix water saturation at the drift wall first increases slightly (50 years to 60 years) and then decreases sharply. From 400 years to 500 years, the rock matrix at the drift wall is completely dry. Afterwards, the liquid saturation increases until 100,000 years, reaching nearly the ambient condition. In the near-drift area, the matrix saturation increases from 100 years to 3,000 years, due to vapor condensation from the evaporation of the drifts (curve AAE38 in Figure 6.4-7). Saturation in areas far from the drifts is not affected by heating. However, the effects of infiltration-rate increases can be easily recognized in these areas (curve AAc90 and ABJ61). The final saturation profile (at 100,000 years) is controlled by the larger (glacial transition mean) infiltration (Figure 6.4-8).

The fracture saturation trend is similar to that of the matrix, but with some differences: (1) the fracture saturation is more sensitive to heating, and (2) the affected areas are larger than those in the matrix. Figure 6.4-9 shows the fracture saturation distribution maps at different times. As the figure illustrates, the overall saturation profile is still controlled by the infiltration spatial distribution. The disturbance in the overall fracture saturation profile is recognizable from 50 years to 1,000 years at the drifts and near drift areas (less than 100 m from the drifts).

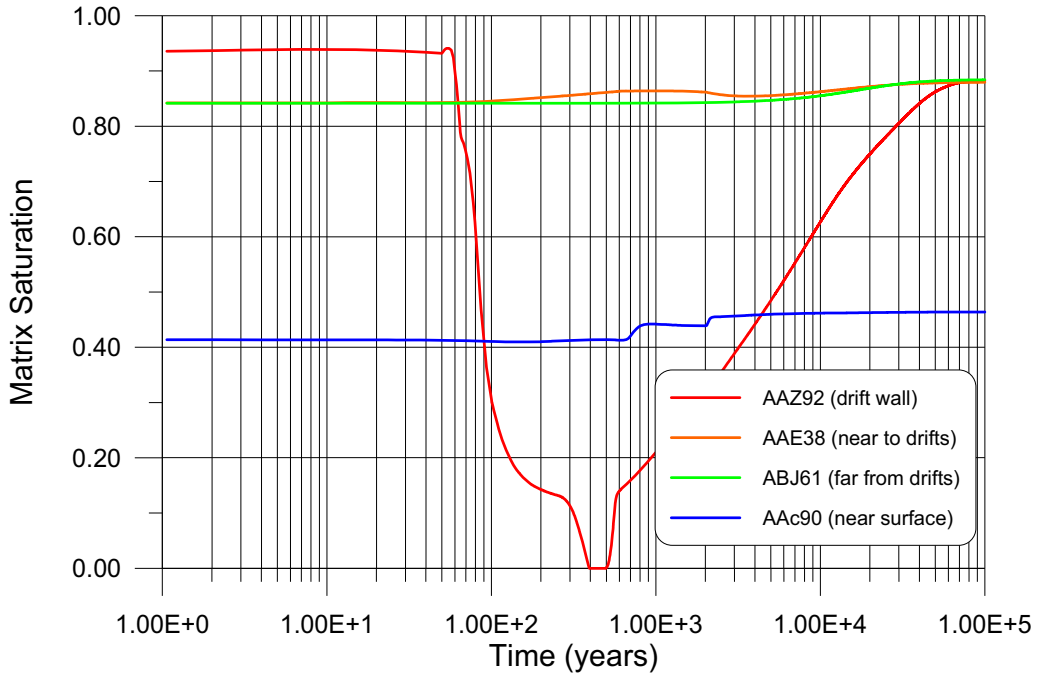

Output DTN: LB0310MTSCLTHC.002.

NOTE: Locations are shown in Figure 6.4-3. Distance from the nearest drift: AAE38, 64.25 m; ABJ61, 492.54 m; AAc90, 323.94 m.

Figure 6.4-7. Matrix Saturation Evolution Curves at Different Locations

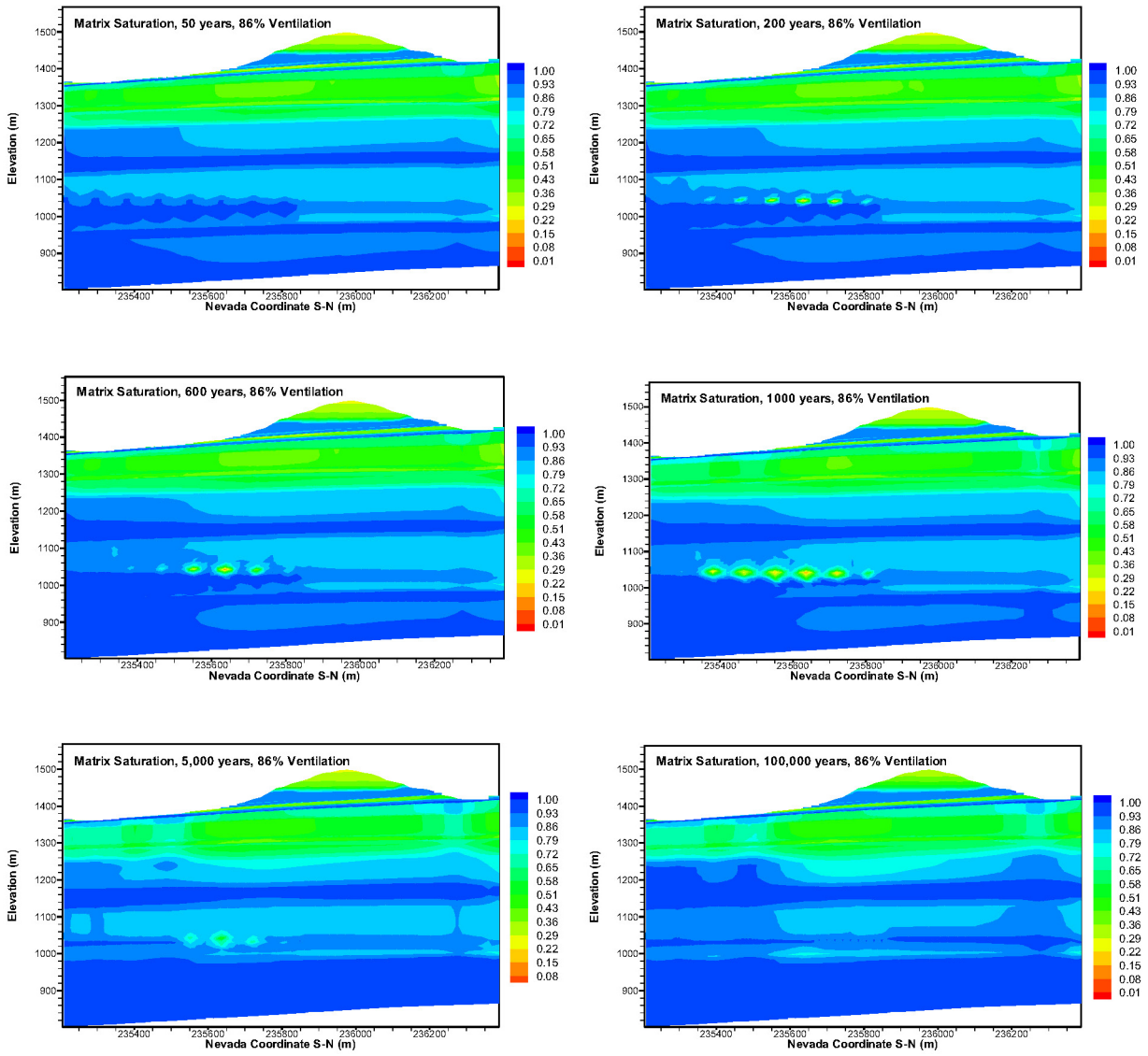

Output DTN: LB0310MTSCLTHC.002.

Figure 6.4-8. Matrix Saturation Distribution Maps at Different Times

The shadow zone (drier region below drifts formed by vaporization and capillary diversion of percolating water around drifts) can be seen from fracture saturation distribution maps more easily than from matrix distribution maps. The shadow zone extends to CHn units in the fractures (Figure 6.4-9) and its presence affects transport of released radionuclides from the drift (BSC 2004 [DIRS 164500]). The drier zones are different in size because of the large spatial variation in infiltration rates.

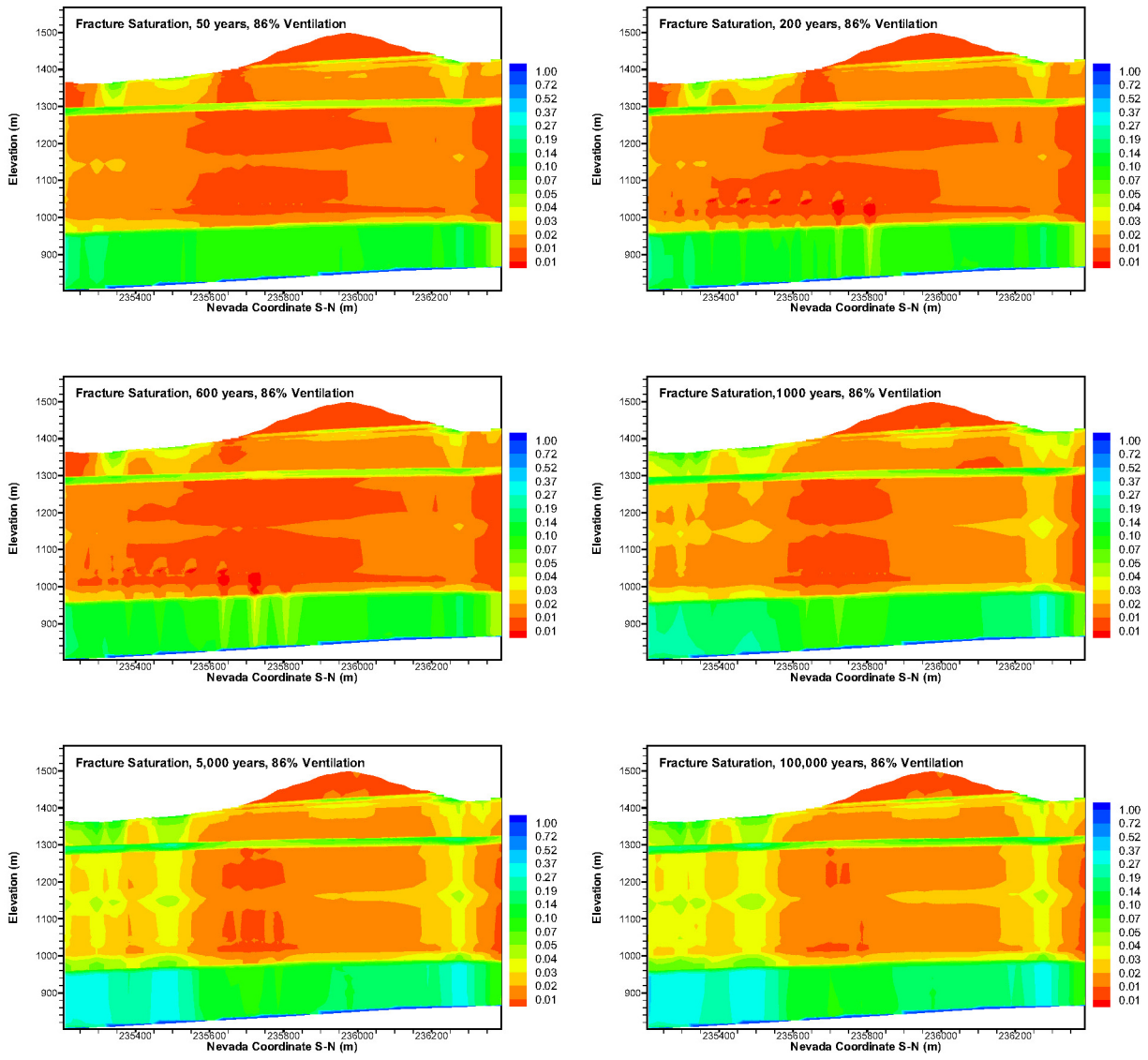

Output DTN: LB0310MTSCLTHC.002.

NOTE: Duplicate values in contour intervals are due to rounding errors.

Figure 6.4-9. Fracture Saturation Distribution Maps at Different Times

6.4.3.1.3 Percolation Fluxes

The rise in drift temperature drives moisture in the surrounding rock out into cooler regions, primarily through permeable fractures. Moisture in the drifts and the surrounding rock boils, and the fracture moisture around the drifts reaches a maximum, several meters to around 10 m from the drift center, from 200 years to 600 years, and almost no liquid water penetrates into the drifts (Figure 6.4-10). After 600 years, the percolation flux increases, mostly due to the infiltration rate increase (the infiltration rate is elevated to monsoon mean). Water from the condensation zone also contributes to the increase in percolation flux. Simulation results show that from 1,000 to 2,000 years, the percolation flux is almost stable. After 2,000 years, the percolation flux increases, again in response to the infiltration increase (transition to glacial transition mean infiltration rate), and reaches a maximum. From 5,000 years to 100,000 years the percolation flux shows almost no change. The spatial variation of the percolation flux at the drift horizon is mainly caused by the infiltration distribution. Percolation flux in the near-drift rock is readjusted not only by the heating, but also by the drifts themselves, which act as capillary barriers diverting water into the surrounding rock and into the pillar regions between the drifts. This diversion of flow is permanent.

6.4.3.2 Chemical Steady State for Aqueous and Gaseous Species

A simulation (Model 2, Table 6.4-3) was performed to obtain a chemical steady state under present-day ambient condition for aqueous and gaseous species transport and gas-water equilibration (for CO_2). The simulations were conducted using initial pore-water and infiltration water composition HD-PERM (Table 6.4.2) determined from pore-water composition at 25°C. This simulation serves two purposes. First, it allows for a better understanding of the role of spatial differences in infiltration, lateral flow, and the geothermal gradient in the transport of aqueous and gaseous species at the mountain-scale. Second, it serves as a potentially better set of initial conditions for simulations under repository thermal-loading conditions and for those simulations that include mineral–water reactions.

No mineral–water reactions were considered, so that the only active processes were aqueous and gaseous species transport by advection and diffusion, along with equilibration of CO_2 in the gas with bicarbonate in the aqueous phase. For this ambient steady-state simulation, the gridblocks are treated strictly as fractures at the locations of repository drifts. The system was then simulated, under the ambient temperature distribution, with the infiltrating water equilibrating with the CO_2 gas in the atmosphere for about 10 million years. The infiltration rates were kept constant at the present-day mean values.

The steady-state pH distribution is shown in Figure 6.4-11. The range in the pH (8.26 to 8.38) is rather small, and is related to the temperature gradient, the infiltration rate, and changing partial pressures of CO_2. Differences in other aqueous species are negligible because the concentrations in infiltrating water were set to be spatially uniform.

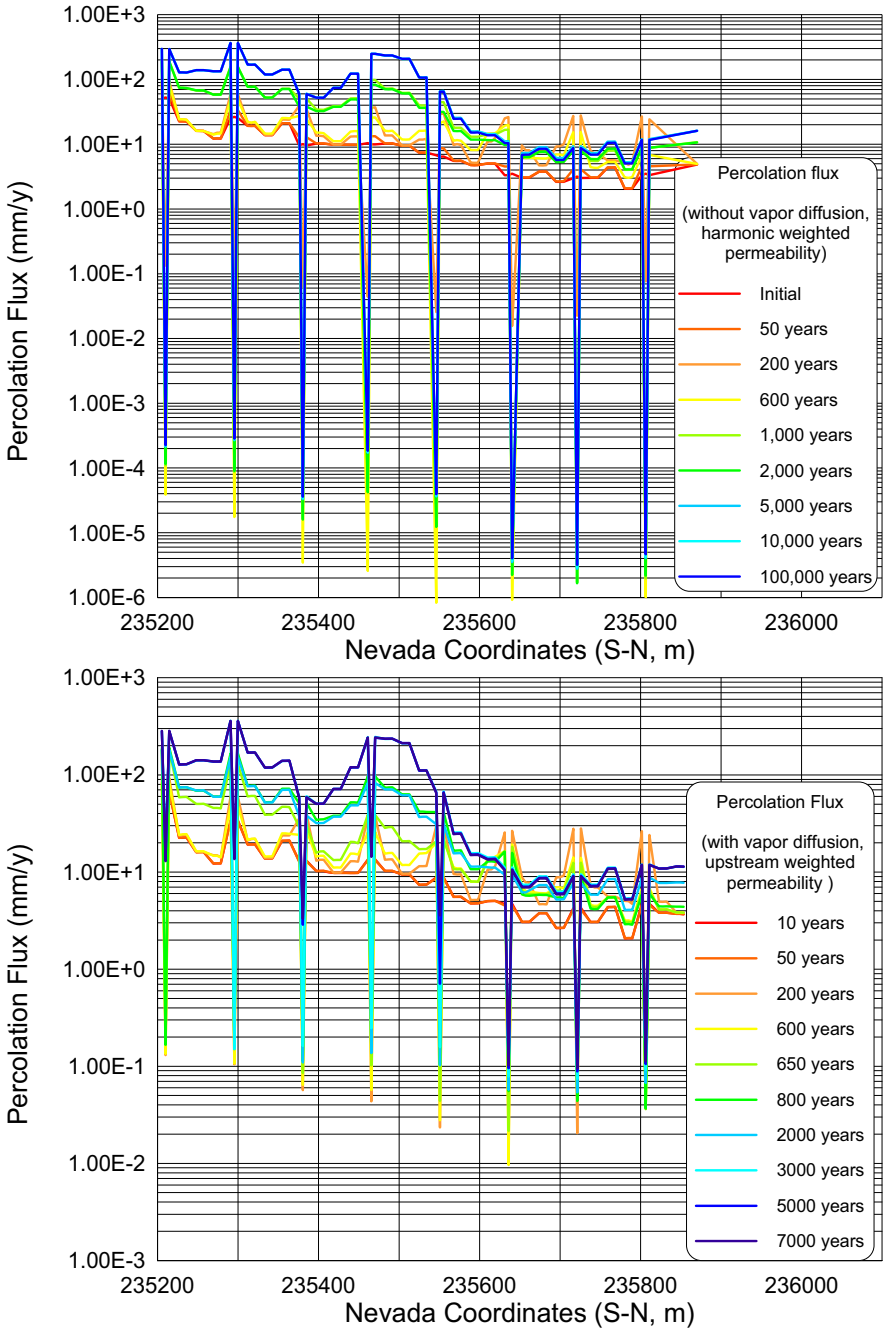

Output DTN: LB0310MTSCLTHC.002.

NOTE: Locations are shown in Figure 6.4-3. The top plot shows percolation fluxes simulated with harmonic weighted permeability; vapor diffusion is not considered. The percolation flux shown in this figure is consistent with the two-dimensional TH model results (Figure 6.2-10a). The bottom plot shows the percolation fluxes simulated with upstream weighted permeability and consideration of vapor diffusion.

Figure 6.4-10. Percolation Fluxes at the Drift Horizon at Different Times, Simulated by Different Model Setups

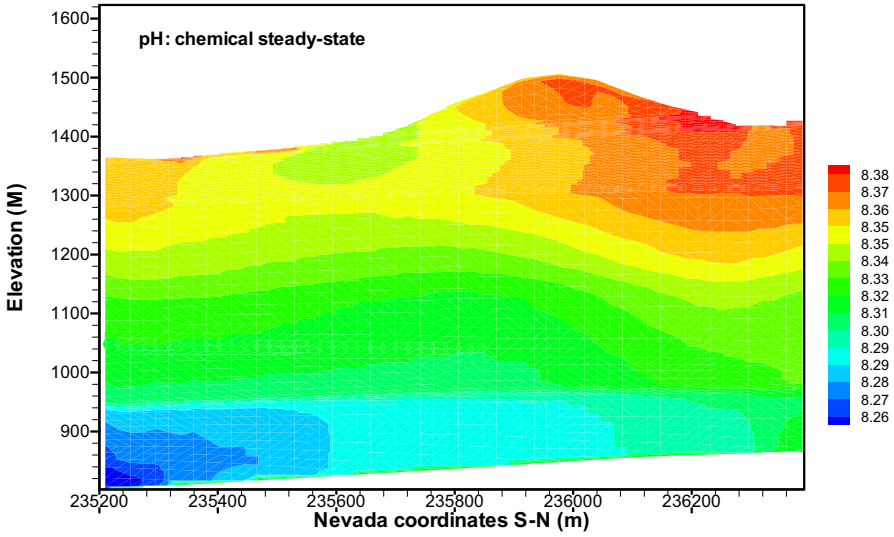

Output DTN: LB0310MTSCLTHC.002.

NOTE: Duplicate values in contour intervals are due to rounding errors.

Figure 6.4-11. Distribution of pH under Chemical Steady State (No Mineral–Water Reactions)

6.4.3.3 Effects of Thermal Loading on Aqueous and Gaseous Chemistry

The main purpose of the analysis of mountain-scale changes in water and gas chemistry is to document potential spatial variations in chemistry resulting from large-scale spatial variations in infiltration rates, gas convection, and repository edge effects not considered in the drift-scale THC seepage model. Therefore, the purpose of this section is to analyze differences in major chemical indicators, rather than to provide detailed predictions of numerous chemical components in seepage waters.

The processes leading to changes in water chemistry are most pronounced during the peak thermal period, when condensation in fractures results in dilution of percolating waters, and boiling zones lead to evaporative concentration. Elevated temperatures also result in greatly enhanced reaction rates and in shifts in the thermodynamic stabilities of minerals. Heating of pore water causes the exsolution of CO_2 out of the water and subsequent transport of gas via diffusion and advection. Exsolution and dissolution of CO_2 can have a significant impact on pH, with pH changes modifying mineral–water reactions and reaction rates.

6.4.3.3.1 Simulation of Aqueous and Gaseous Chemistry: No Mineral–Water Reactions

This simulation uses the steady-state flow and chemical concentrations obtained in the simulation described in Section 6.4.3.2. Thermal loading affects aqueous chemistry by reducing the solubility of CO_2 gas. Simulation of thermal loading with no mineral–water reactions allows for quantification of temperature effects on aqueous chemistry so that effects of coupled temperature and mineral–water reactions on aqueous chemistry are easily identified.

A thermal load of 1.45 kW/m, in which 86.3% of the heat is removed by ventilation, was applied to the repository gridblocks (see Sections 4.1.4, 4.1.5 and 6.1.5). A stepwise climate scenario for infiltration rates was imposed (Sections 4.1.1 and 6.1.4), so that increasing rates were applied at 600 years and at 2,000 years. The simulation was run for 100,000 years

The evolution of CO_2 concentration in the gas phase (in ppmv) is shown in Figure 6.4-12. For the first few hundred years, the higher CO_2 concentration regions are generally formed directly through degassing of matrix pore water. By 600 years, the zone of high CO_2 concentration has migrated to near the left boundary, where the percolation fluxes are highest as a result of lateral flow in the PTn. There, CO_2 is generated primarily through heating of percolating water flowing down through fractures towards the repository. As those regions cool after the increase in infiltration rate at 2,000 years, the high CO_2 concentration zone shifts back over to the drifts that are still hot.

The CO_2 exsolved from the hotter rock, resulting in a pH increase in the remaining pore water, is transported along with water vapor to cooler regions, where it dissolves in local pore waters or in water formed by vapor condensation, causing a reduction in pH. Figure 6.4-13 shows the matrix pore water pH evolution under thermal loading (86.3% heat removal by ventilation) and without any mineral–water reactions.

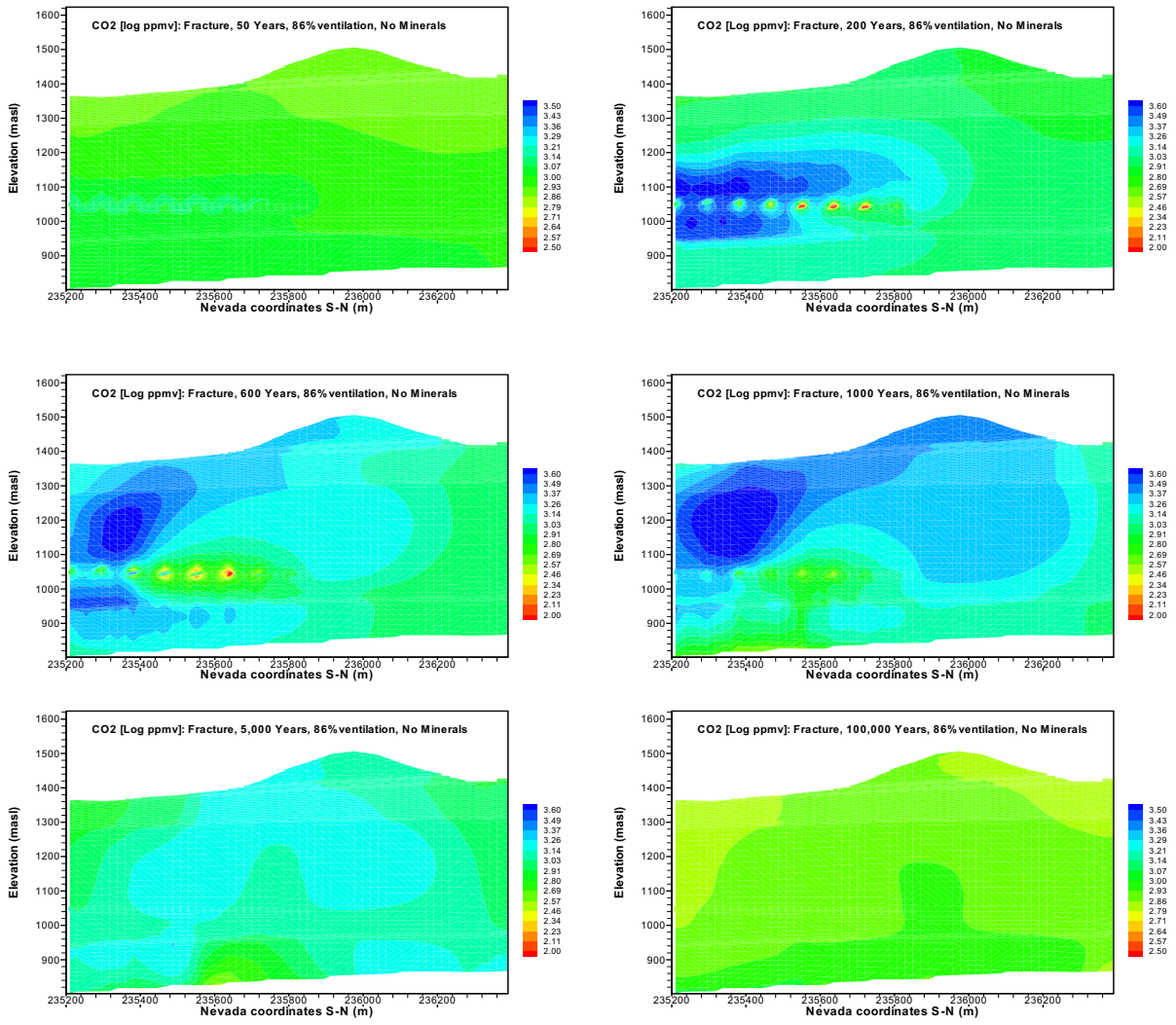

Output DTN: LB0310MTSCLTHC.002.

NOTE: Contour intervals change at different times. Aqueous and gaseous species transport; no mineral–water reactions.

Figure 6.4-12. Gas Phase CO_2 Concentrations in Fractures over 100,000 Years

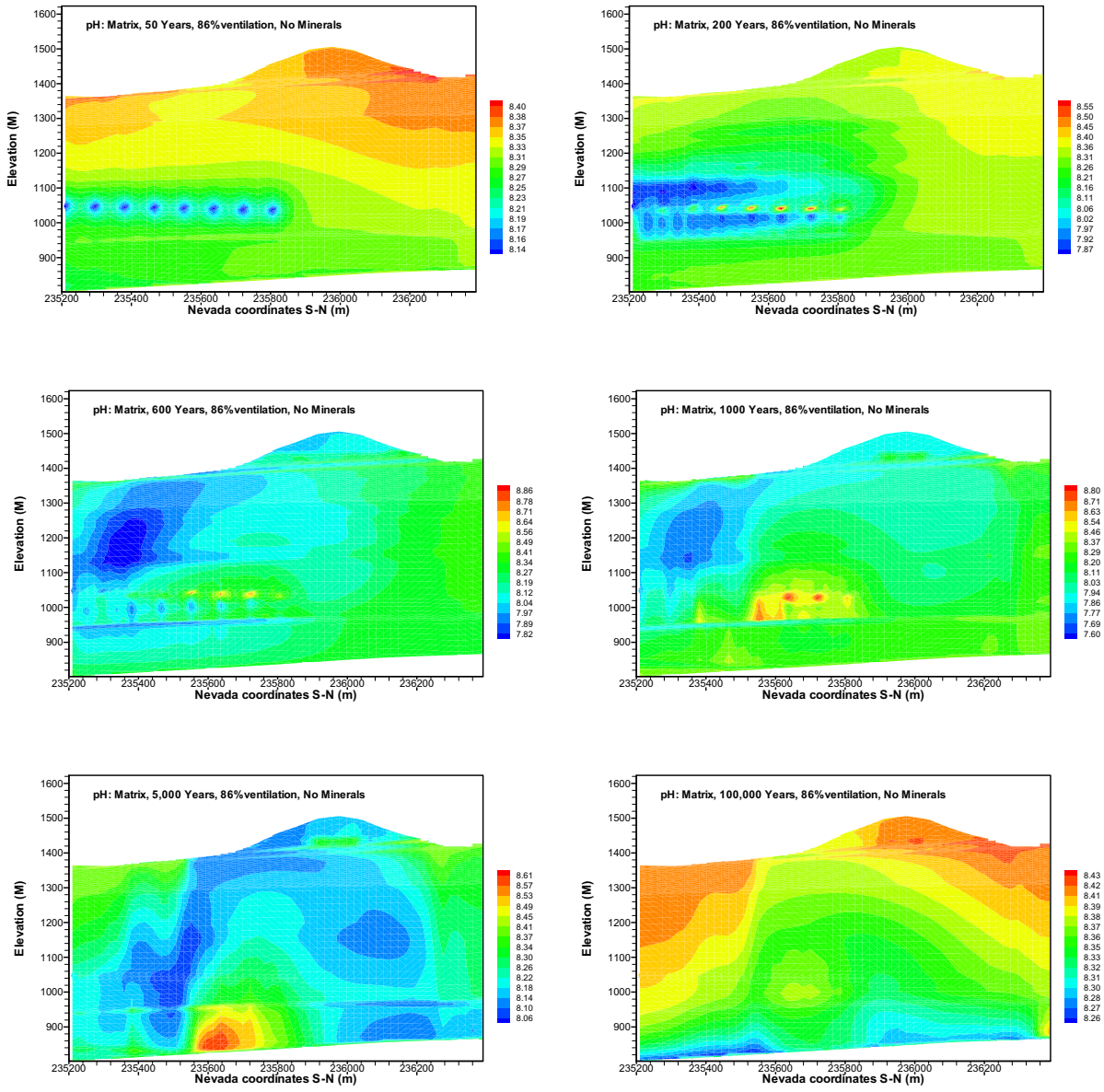

Output DTN: LB0310MTSCLTHC.002.

NOTE: Contour intervals change at different times.

Figure 6.4-13. Matrix Pore Water pH Evolution under Thermal Impact without Mineral–Water Reactions

Because matrix diffusion is slower than the changes imposed by heating, the matrix pore water pH response is slower and smoother than that in fracture. However, the distributions are similar, especially after long time periods (comparing Figures 6.4-13 and 6.4-14).

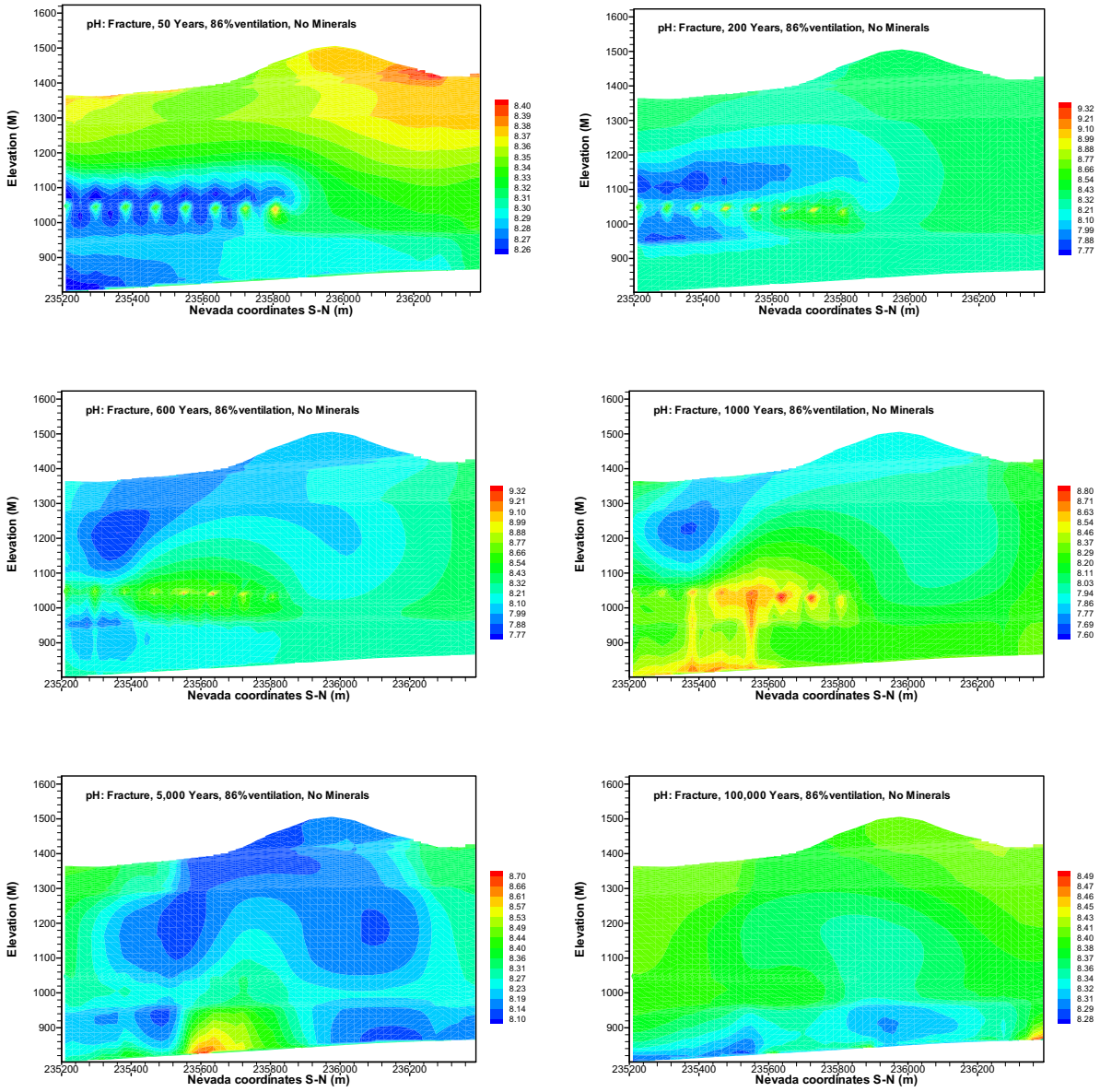

Output DTN: LB0310MTSCLTHC.002.

NOTE: Contour intervals change at different times.

Figure 6.4-14. Fracture pH Evolution under Thermal Loading without Mineral–Water Reactions

6.4.3.3.2 Effects of THC Processes, Including Mineral–Water Reactions on Water and Gas Chemistry

This section discusses the changes to water and gas chemistry for the case of full coupling between mineral–water–gas reactions, aqueous and gaseous species transport, and changes to flow owing to mineral precipitation and dissolution. The simulation discussed in this section utilized the full geochemical system of minerals, aqueous species, and gaseous species presented in Table 6.4-1, plus various salt phases. The heat load, ventilation efficiency, and climate scenarios employed are identical to those used in Section 6.4.3.2.

First, the important effect of boiling and condensation-induced concentration changes are examined. The processes of condensation driving dilution, and evaporation resulting in higher concentrations, can be followed through the evolution of conservative species, such as chloride (Cl^-). Chloride concentrations in fracture water are shown at several times from 200 to 7,000 years in Figure 6.4-15. After only 200 years, a small dryout zone and high concentrations can be seen at a few drifts. Surrounding the dryout zones are small regions of dilute fracture water where condensation is taking place. The region below the drifts is slightly drier, owing to the capillary barrier effect of the overlying drifts and vaporization of the fracture water. By 600 years, the condensation zones have grown, and drainage of the dilute water in the pillar regions has extended over 100 m below the drifts. The increased infiltration rate after 600 years enhances the elongation of the condensate drainage plumes, which are close to the water table, by 1,000 years. In addition, the drier shadow zone regions are most prominent below the hottest drifts away from the boundaries. By 2,000 years, the highest chloride concentrations are only a factor of three greater than in the initial pore water, and by 3,000 years the differences are much less. A large, slightly elevated concentration region is present around the repository edge, formed as a result of large-scale evaporation and vapor transport. After 7,000 years, the entire system is nearly back to ambient chloride concentrations.

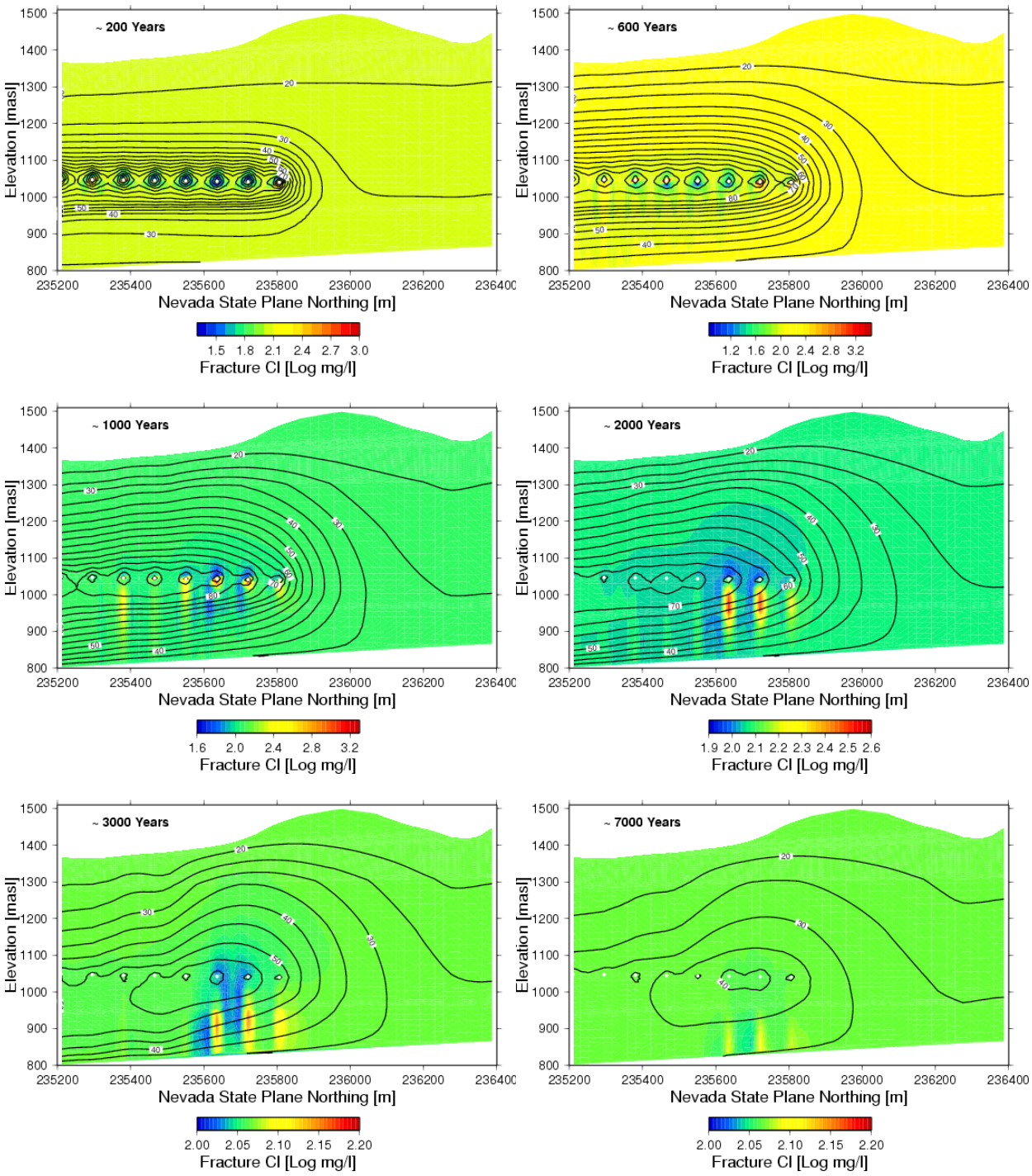

Output DTN: LB0310MTSCLTHC.001.

NOTE: Concentration scale changes over time. Temperature contours are overlain.

Figure 6.4-15. Chloride Concentrations in Fracture Water at 200, 600, 1,000, 2,000, 3,000, and 7,000 Years

The cooler drifts at the left edge of the model domain result from an increased infiltration rate in this area and a downward diversion of lateral flowing water above the repository (at the PTn–TSw contact). Although the forced diversion of lateral flow at the left boundary is clearly enhanced as a result of the boundary, it is a realistic scenario for any location in the repository where there is focused flow owing to a fault, or as a result of run-on and channelized flow in the central part of a stream channel. These differences in percolation fluxes and heat losses for repository drifts in different locations lead to spatial variations in the compositions of water potentially seeping into drifts at any particular time. Up to approximately 1,000 years, the differences in the chloride concentrations above the drifts are approximately one order of magnitude. As the drifts cool, and after percolating water rewets the dryout zones, the differences in the concentrations above the drifts become much less.

The evolution of CO_2 concentrations over time is shown in Figure 6.4-16. After 200 years, there is an increase in CO_2 concentrations that is confined to a zone extending up to about 200 meters above and 100 meters below the repository drifts. By 600 years, a plume-like zone of increased concentrations forms, with the plume center (maximum CO_2 concentration) beginning close to the third drift from the left boundary after 600 years and migrating to the fourth drift after 2,000 years. This spatial shift is caused by the increase in the infiltration rate at 600 years, resulting in enhanced lateral flow and greater cooling of the drifts near the left boundary. Large-scale patterns of gas transport above and to the right of the repository are also clearly evident in the distribution of CO_2 concentrations. Because the CO_2 solubility is a strong function of the temperature, gas-phase CO_2 concentrations remain perturbed as long as temperatures are elevated around the repository. Differences across the zone above the repository drifts are about two orders of magnitude in the first few hundred years and about one order of magnitude thereafter.

Compared to the CO_2 distributions shown in Figure 6.4-12, the range in concentrations is much larger for the case with mineral reactions. This is particularly evident in the CHn unit below the repository, where calcite dissolution has taken place (see Figure 6.4-18). Compared to water-gas equilibriation by itself, mineral–water–gas reactions change both the range and distribution of CO_2 spatially and over time.

As shown in Section 6.4.3.3.1, the evolution of pH in the waters surrounding repository drifts is strongly coupled to the exsolution of CO_2 from pore waters during heating, followed by dissolution of the transported CO_2 back into condensate water and cooler matrix pore water. The pH in fracture waters (Figure 6.4-17) shows a drop in pH from the initial value of about 8.3 to around 7 in the heated regions around the repository drifts.

The pH distribution above the repository also changes from a broad area of lower pH waters to a more plume-like region extending above the hottest drifts after about 600 years. The plume-like distribution in pH seen in Figure 6.4-17 after 600 years can be directly attributed to the transport of exsolved CO_2 above the repository drifts (Figure 6.4-16). A region of lower pH also extends through the PTn and to the surface after only about 600 years (Figure 6.4-17).

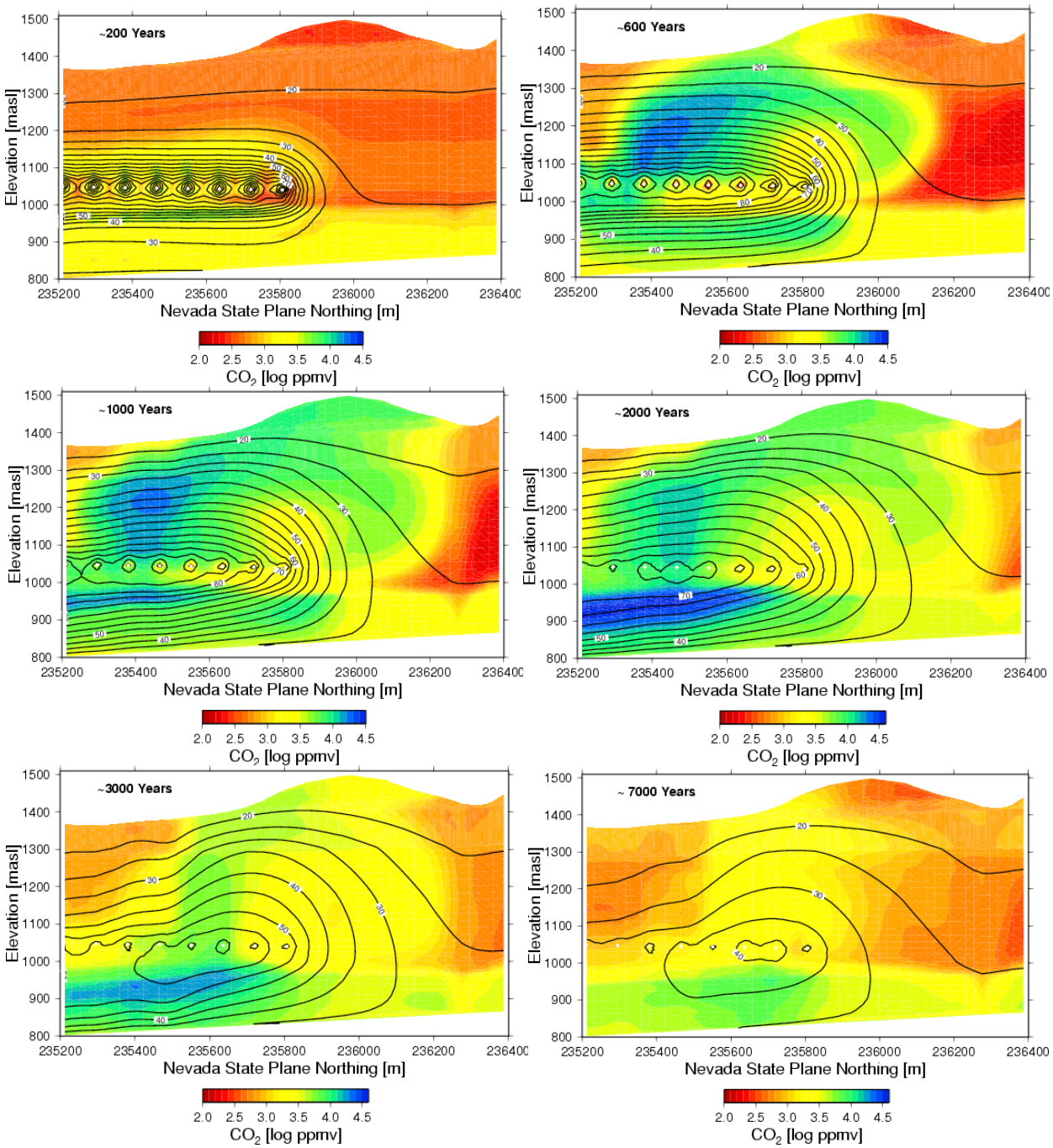

Output DTN: LB0310MTSCLTHC.001.

Figure 6.4-16. Fracture Gas CO_2 Concentrations and Temperatures at 200, 600, 1,000, 2,000, 3,000, and 7,000 Years

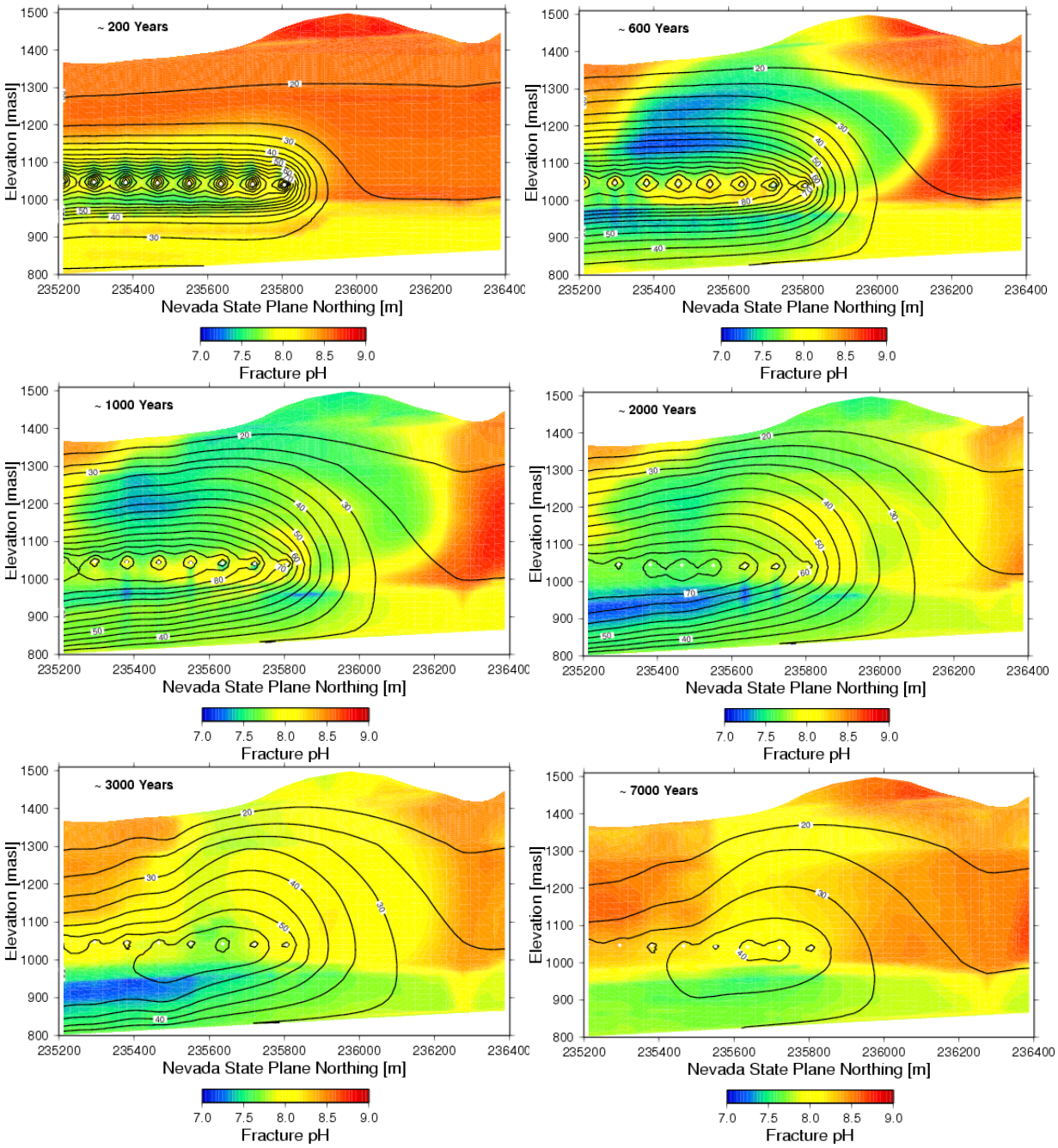

Output DTN: LB0310MTSCLTHC.001.

Figure 6.4-17. Fracture Water pH and Temperature at 200, 600, 1,000, 2,000, 3,000, and 7,000 Years

Differences across the zone above the repository drifts are about one pH unit at a given time, similar to the range in chloride concentrations. Higher pH waters tend to be in the area near the repository edge, where evaporation and vapor transport also resulted in slightly increased chloride concentrations. Below the repository, heating of the relatively confined CHn and Prow Pass units leads to a reduction in the pH to about 7. Areas still near ambient temperatures away from the repository show the pH remaining relatively stable in the range of 8 to 8.75, indicating

that the the geochemical system is roughly at steady-state, regardless of the climate change and increased infiltration rate.

6.4.3.3.3 Effects of THC Processes on Mineralogy

Mineral–water reactions may result from different major processes during repository heating. These include, but are not limited to: (1) boiling/evaporation-induced mineral precipitation as a direct result of increased concentration; (2) temperature effects on percolating waters, e.g., a decreased calcite solubility at higher temperatures; (3) changes in the thermodynamic stability of primary mineral phases (i.e., those minerals present prior to the onset of thermal loading) during heating or cooling; (4) fluid mixing resulting in a shift in mineral stability; and (5) exsolution/dissolution of CO_2 and subsequent open-system advective or diffusive transport. Close to the repository drifts, boiling-induced precipitation in fractures is the most important process that could affect near-field percolation fluxes and seepage into drifts. Above the repository, in the PTn, alteration could affect any lateral flow or modify fast-path transport through fractures or faults. Below the repository, alteration of zeolitic or vitric layers could influence radionuclide transport velocities, as well as the extent of retardation by ion exchange or sorption.

Mineral precipitation and dissolution in the boiling and condensation zones around the drifts have the highest potential for changing percolation fluxes to the drift walls and modifying flow in the pillars between drifts. In simulations of drift-scale coupled THC processes (BSC 2005 [DIRS 172862]), the most abundant phases precipitating in fractures, resulting in near-permanent changes to permeability, were amorphous silica and calcite. Other phases, such as gypsum and halite (only in dried-out gridblocks) also formed in proportions similar to calcite, but re-dissolved rapidly during rewetting. Similar mineral precipitation processes were observed in mountain-scale simulations, with some differences in the extent of alteration owing to the spatial variation of infiltration rates and flow diversion/focusing as a result of lateral flow in the PTn. Note that all mineral volume percentages are changes relative to the fracture or matrix volume.

Calcite is present as an initial fracture-lining mineral and within the matrix in some rock units. The evolution of calcite precipitation from 1,000 to 7,000 years is shown in Figure 6.4-18 (note that all mineral volume percents are changes relative to the matrix or fracture volume). After 1,000 years, there is some calcite precipitation directly around the drifts, with dissolution most prominent in the adjacent condensation and drainage zones, where lower pH waters formed (see Figure 6.4-17). Regions of dissolution are more localized above the hottest drifts after 3,000 years, and precipitation of calcite has taken place in areas where at earlier times dissolution was evident. Dissolution of calcite progresses from 1,000 to 2,000 years in the zeolitic rocks below the repository, where there are increasing CO_2 concentrations and decreasing pH. Some calcite has formed above the repository in areas of high percolation fluxes, where infiltrating waters have undergone CO_2 degassing and subsequent calcite precipitation in fractures. However, even after 5,000 years, the maximum amount of calcite formed in fractures is less than 0.2% of the fracture volume, and little change in the calcite abundances can be seen between 5,000 and 7,000 years.

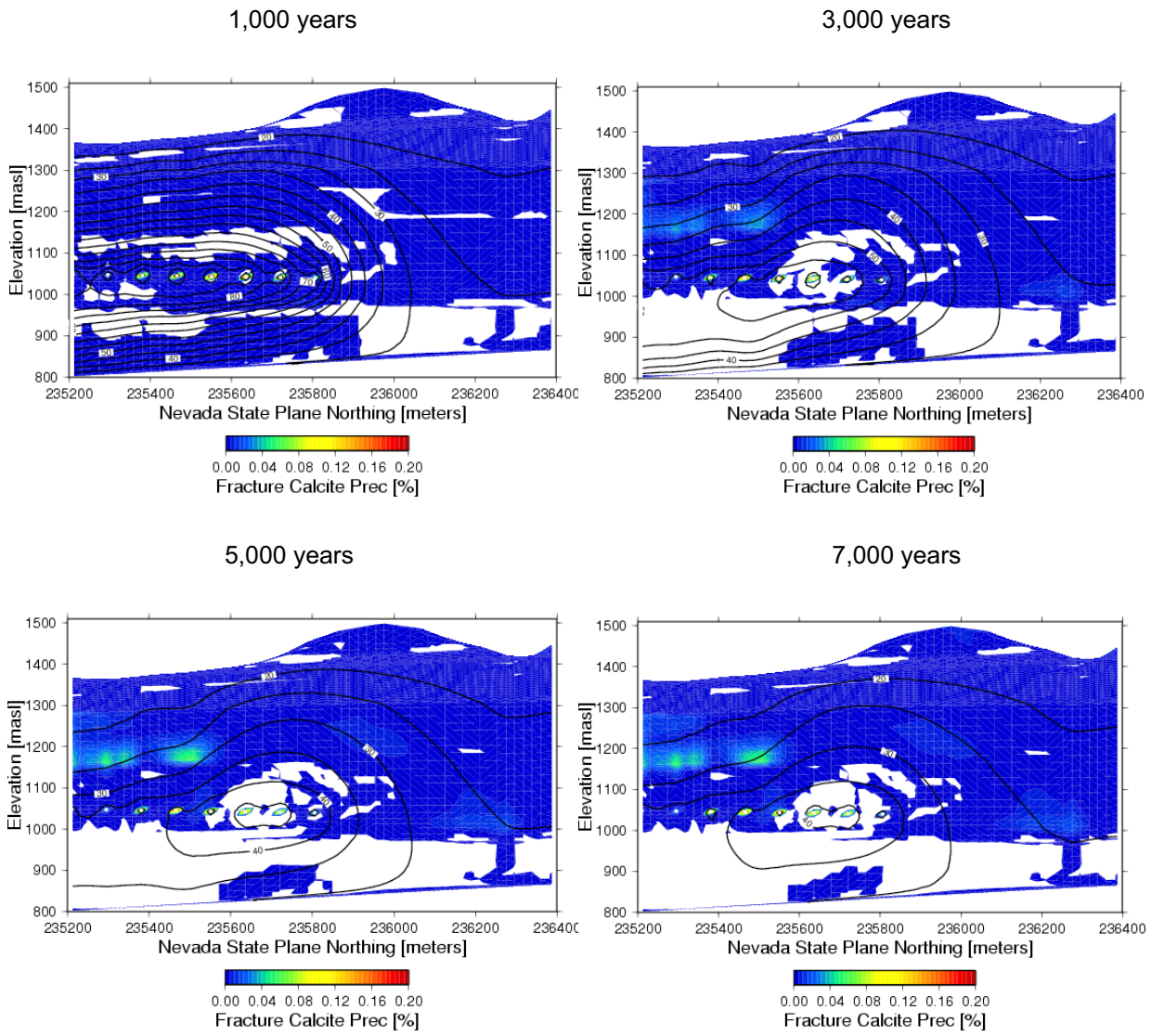

Output DTN: LB0310MTSCLTHC.001.

NOTE: White areas represent regions where some dissolution has taken place.

Figure 6.4-18. Calcite Precipitation (Volume %) in Fractures at 1,000, 3,000, 5,000, and 7,000 Years

Amorphous silica is the dominant phase that precipitates in fractures in the boiling zones. However, because above-boiling conditions are encountered only in the regions directly adjacent to the hottest drifts, amorphous silica precipitation is limited to these areas (Figure 6.4-19). After 1,000 years, nearly all of the amorphous silica has precipitated, and at 2,000 years the distribution has remained the same. After much longer time periods, percolating waters later dissolve this mineral slowly; however, the rate of amorphous silica dissolution is so slow at lower temperatures that it persists for tens of thousands of years or longer, even though it is undersaturated in the percolating waters. Therefore, the precipitation of amorphous silica can be considered a permanent change with respect to the time scale of repository performance.

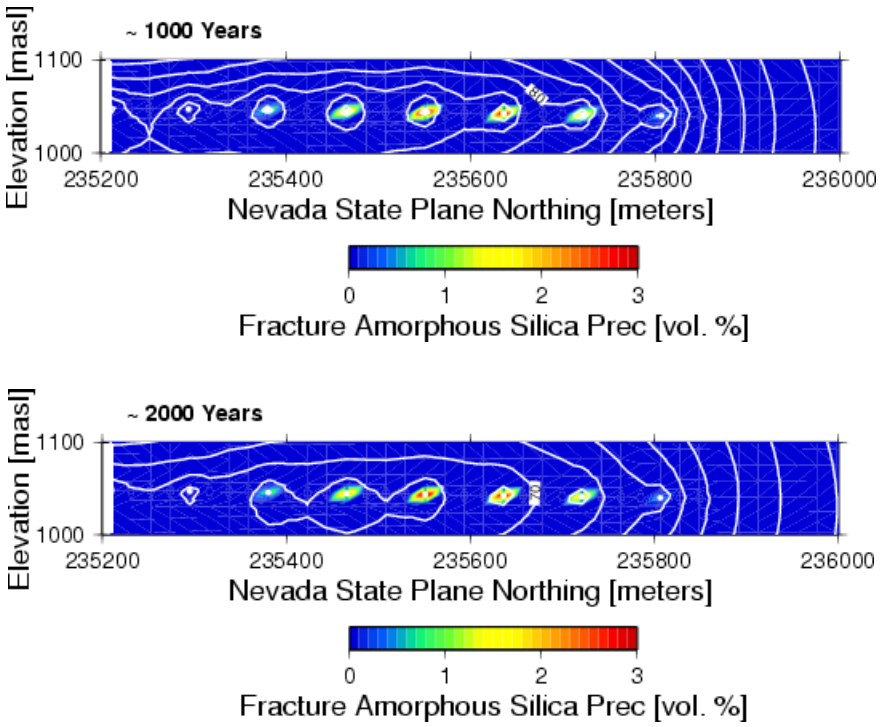

Output DTN: LB0310MTSCLTHC.001.

NOTE: Temperature contours are overlain.

Figure 6.4-19. Amorphous Silica Precipitated (Volume %) in Fractures around Drifts after 1,000 and 2,000 Years

Away from the repository, the rocks that may undergo alteration at higher temperatures are those containing abundant volcanic glass and/or zeolites. These particular layers are the basal vitrophyre of the TSw, the vitric tuffs in the Calico Hills and the PTn, and the zeolitized tuffs (also often glass-rich) in the Calico Hills, Prow Pass, and Bullfrog units. Mineral–water reactions involving volcanic glass and complex silicate phases, such as zeolites, are difficult to represent in geochemical models because of their complex chemical compositions and also because of uncertainties in their thermodynamic and kinetic properties. Zeolites, such as clinoptilolite, typically involve several end members in a solid solution series, are affected by simultaneously acting processes such as ion exchanges and dissolution/precipitation reactions, and preferentially incorporate many trace components such as Sr, all of which influence their composition and stability. Therefore, modeling results of the alteration of the vitric and zeolitic units can be considered uncertain and the model results represent the general trend in geochemical processes for these far-field locations. Yet significant alteration of the glassy rocks at Yucca Mountain is evident, whereas the crystalline devitrified rocks are little altered. Hence, the geologic record supports the tendency of the glassy units to alter preferentially. Furthermore, glass-rich bedded tuffs in the PTn show much less alteration to zeolites, indicating that the volcanic glass has not been significantly affected by ambient temperature reactions over millions of years. Therefore, the mountain-scale THC model results show some mineralogical alteration of the volcanic glass for elevated temperatures, and less change at lower near-ambient temperatures.

Model results show that in the rock matrix after 1,000 years over 5% of the volcanic glass in the basal vitrophyre of the TSw has reacted and by 7,000 years it has dissolved up to nearly 20% by volume (Figure 6.4-20; see Figures 6.4-1 and 6.4-3 for general locations of lithostratigraphic units). The zone of alteration progressed down into the CHn as temperatures increased, with significant glass alteration taking place at temperatures above approximately 50°C. Much of the reaction has taken place by 3,000 years, with the alteration rate decreasing strongly as temperatures decline in the rocks below the repository. The extent of glass alteration is limited to the strongly heated regions directly below the repository drifts, with little effects elsewhere.

The dominant phases formed by volcanic glass reactions with aqueous fluids are zeolites (i.e., stellerite; Figure 6.4-21), potassium feldspar (Figure 6.4-22; microcline in the thermodynamic data set), and albite (Figure 6.4-23). As is discussed in the following paragraphs, studies of the earlier alteration of the volcanic glass at Yucca Mountain suggest that clinoptilolite and other zeolites are likely to be alteration products of the glass rather than feldspars.

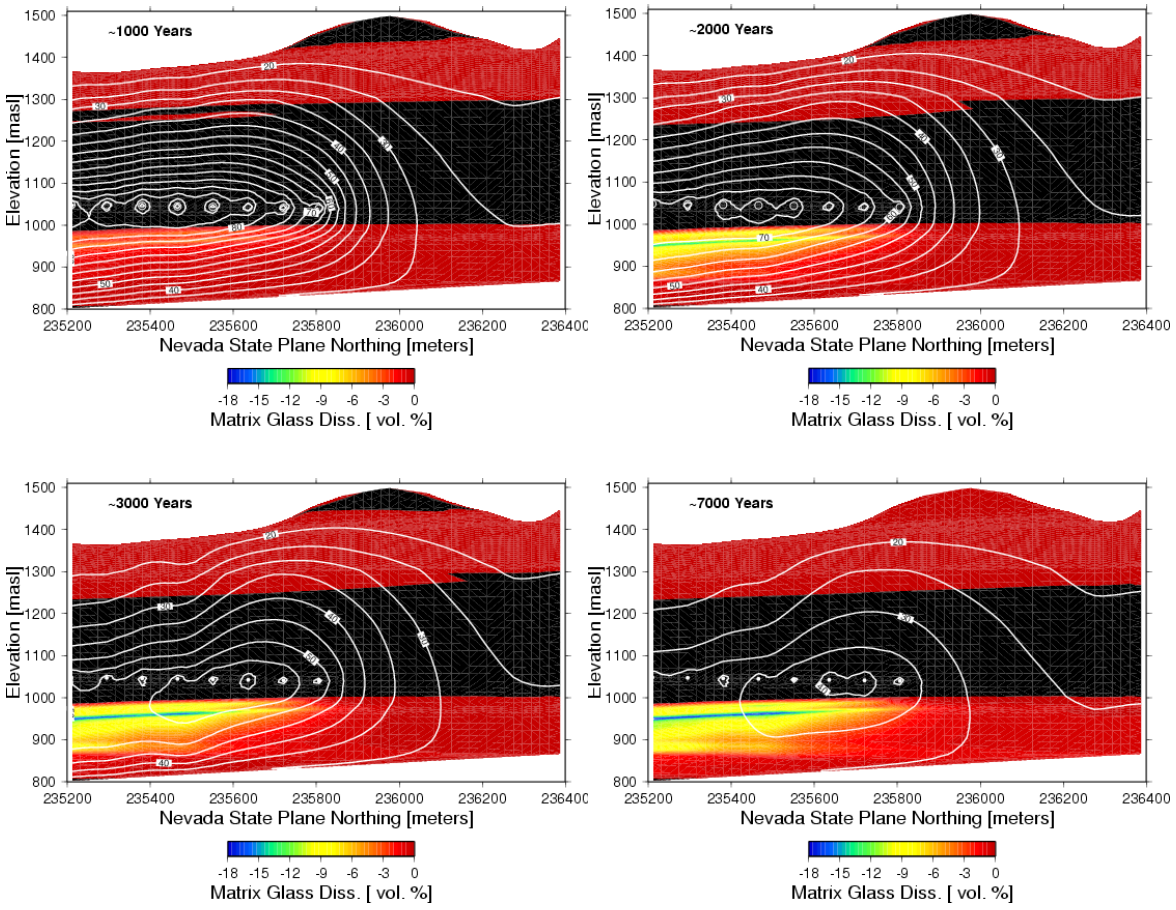

Output DTN: LB0310MTSCLTHC.001.

NOTE: Black regions are areas where glass was absent from the rock or where no dissolution has taken place. Temperature contours are overlain. Percentage is relative to volume of matrix.

Figure 6.4-20. Volcanic Glass Dissolved (Volume %) in the Rock Matrix after 1,000, 2,000, 3,000, and 7,000 Years

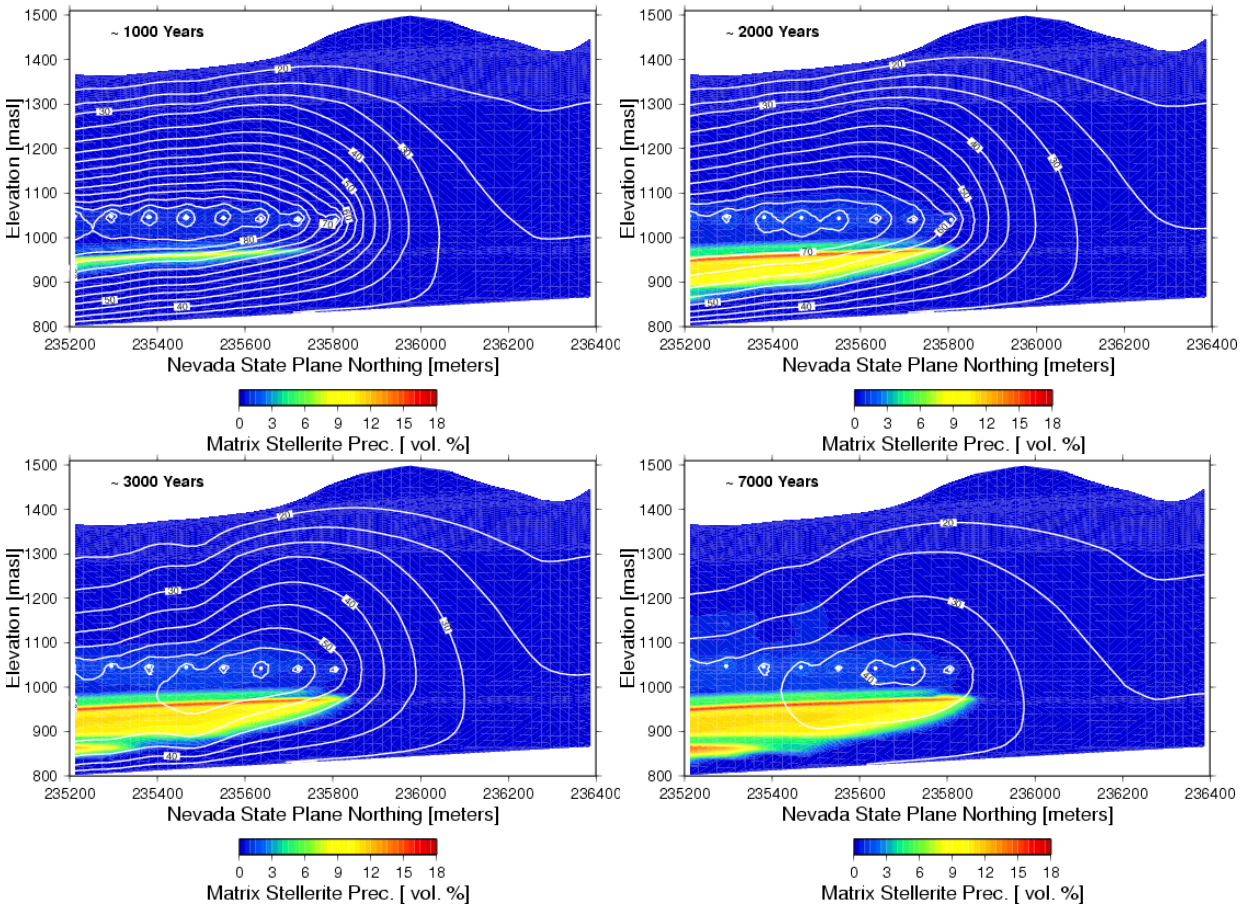

Output DTN: LB0310MTSCLTHC.001.

NOTE: Temperature contours are overlain.

Figure 6.4-21. Stellerite Precipitation (Volume %) in the Rock Matrix after 1,000, 2,000, 3,000, and 7,000 Years

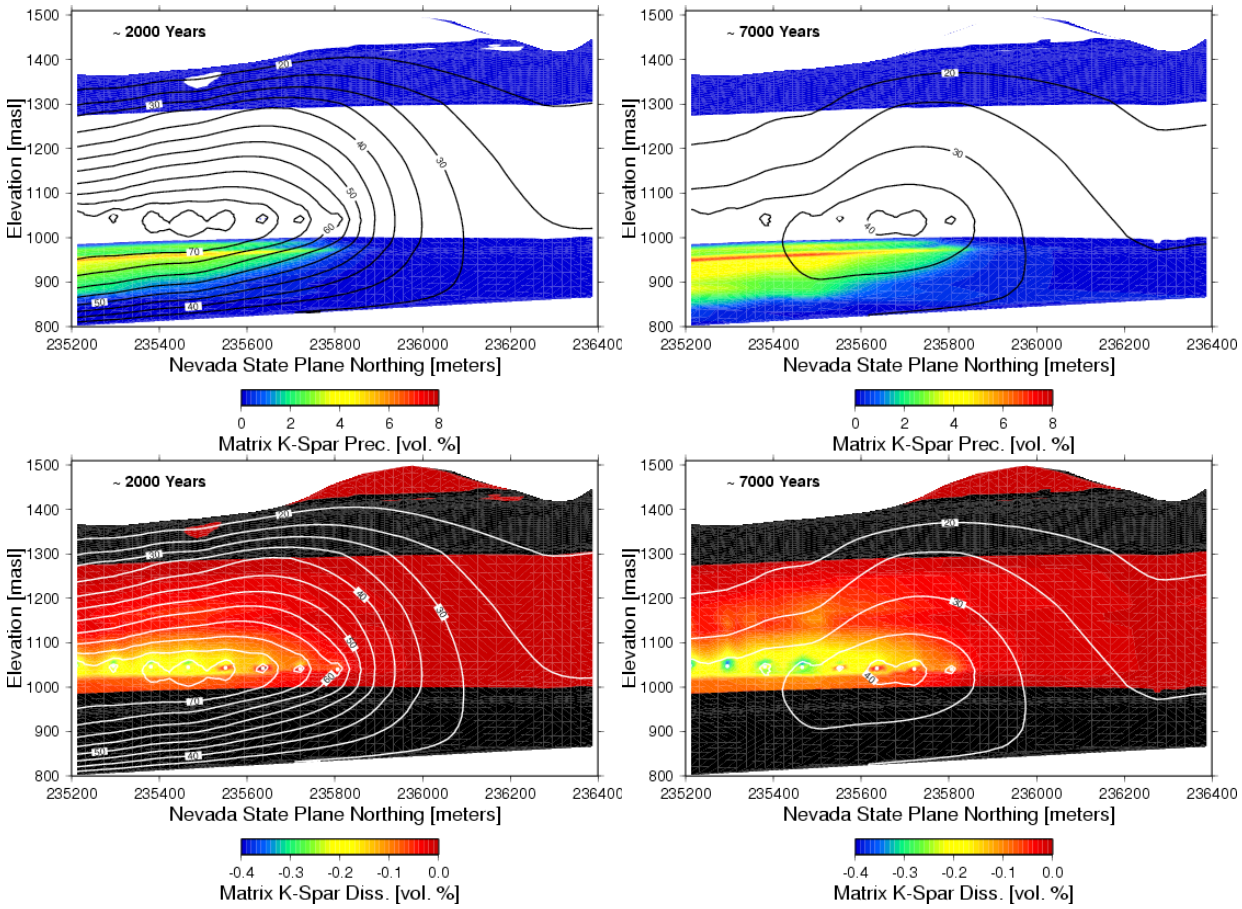

Output DTN: LB0310MTSCLTHC.001.

NOTE: Temperature contours are overlain, with precipitation plotted in the upper two figures and dissolution plotted in the lower two figures. White areas indicate dissolution and black areas indicate precipitation.

Figure 6.4-22. Potassium Feldspar (Microcline) Precipitation and Dissolution (Volume %) in the Rock Matrix after 2,000 and 7,000 Years

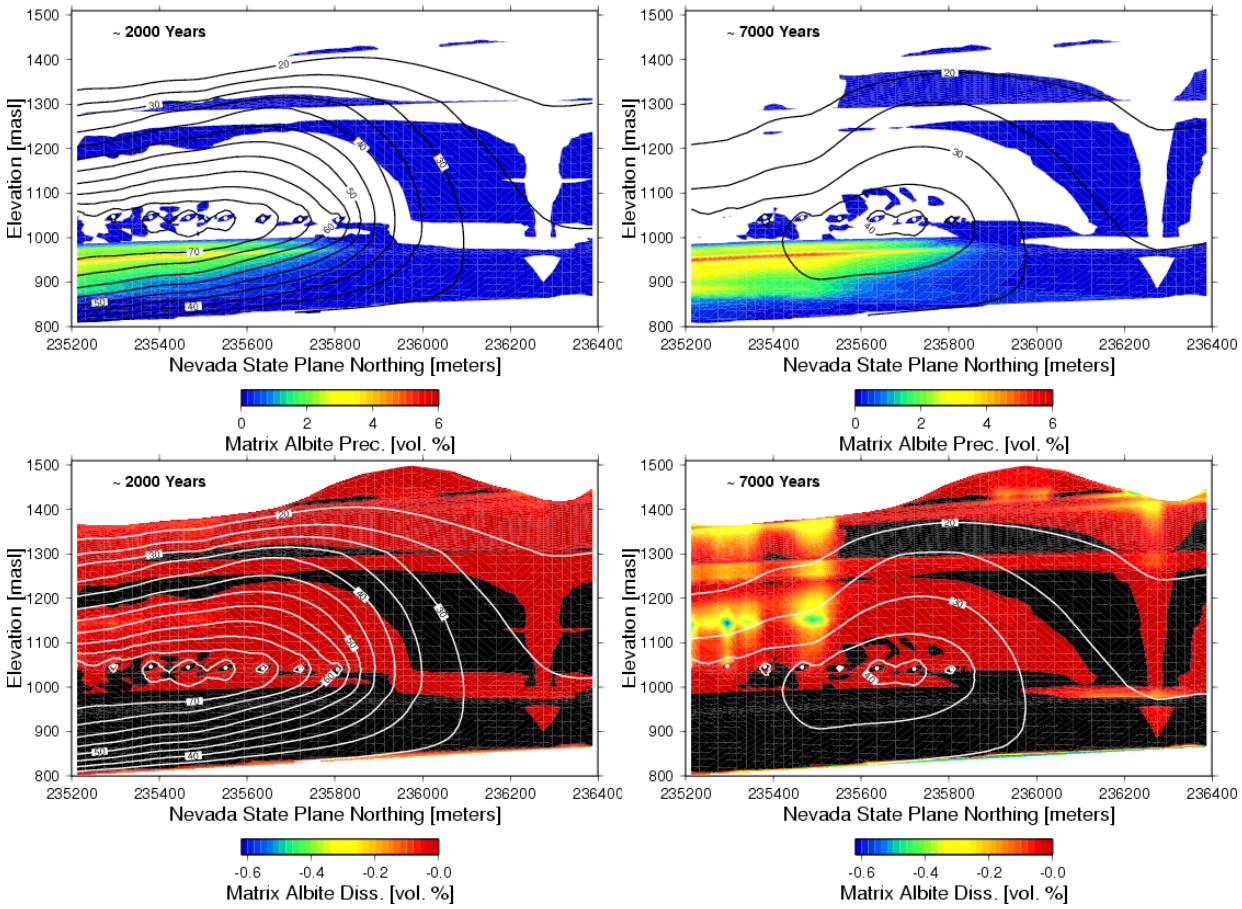

Output DTN: LB0310MTSCLTHC.001.

NOTE: Temperature contours are overlain, with precipitation plotted in the upper two figures and dissolution plotted in the lower two figures. White areas indicate dissolution and black areas indicate precipitation.

Figure 6.4-23. Albite Precipitation and Dissolution (Volume %) in the Rock Matrix after 2,000 and 7,000 Years

The basal vitrophyre of the TSw and the underlying vitric units and glass-rich zeolitic units all contain abundant clinoptilolite, which (in the model simulations) breaks down at elevated temperatures (Figure 6.4-24) to form predominantly stellerite (Figure 6.4-21). Although stellerite is common in fractures in the devitrified tuffs in the TSw, it is not typical as an alteration product of glass in the vitric units (Bish et al. 2003 [DIRS 169638]). It is likely that the fixed composition of clinoptilolite used in the thermodynamic database reduces its stability (compared to stellerite, potassium feldspar, and albite) at elevated temperatures under conditions of changing water chemistry. At near-ambient temperatures, clinoptilolite is stable in the simulation and actually precipitates preferentially in the glass-rich layers (Figure 6.4-24). This trend is consistent with the observed mineral assemblage, although the 1% reacted in 7,000 years is probably greater than that actually formed in this short period of time.

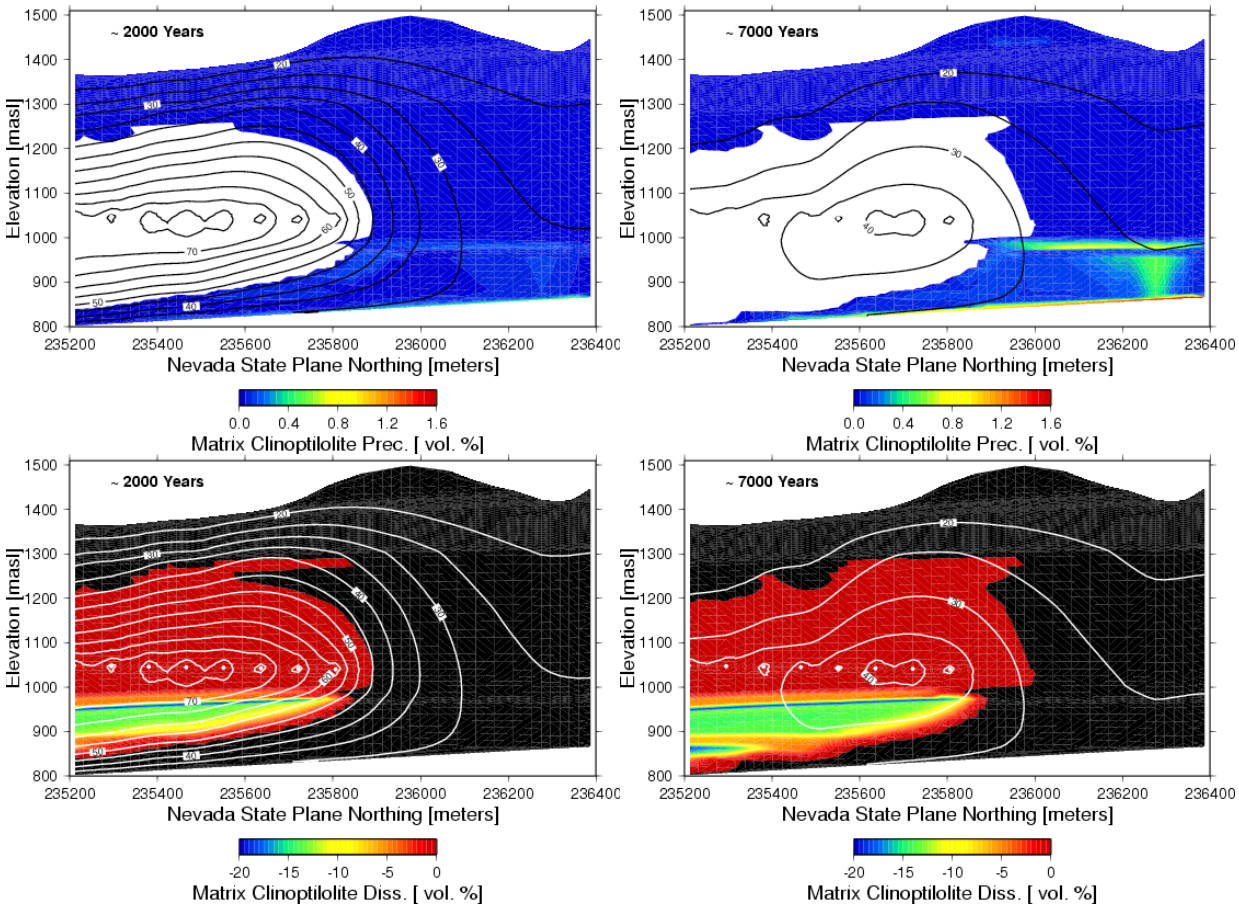

Output DTN: LB0310MTSCLTHC.001.

NOTE: Temperature contours are overlain, with precipitation plotted in the upper two figures and dissolution plotted in the lower two figures. White areas indicate dissolution and black areas indicate precipitation.

Figure 6.4-24. Clinoptilolite Precipitation and Dissolution (Volume %) in the Rock Matrix after 2,000 and 7,000 Years

Based on studies of the fossil hydrothermal system at Yucca Mountain (Bish et al. 2003 [DIRS 169638]; Bish and Aronson 1993 [DIRS 100006]), conceptual models for future mineral evolution at Yucca Mountain (Carey et al. 1997 [DIRS 101323]) suggest that the most likely mineralogical reactions caused by repository heating would include dissolution of volcanic glass and precipitation of clinoptilolite, clay and opal-CT (i.e., opal with cristobalite- and tridymite-type stacking); dissolution and precipitation of silica polymorphs (cristobalite, opal-CT, tridymite, and quartz); alteration of feldspars to clays; and, finally, reactions involving calcite and zeolites. Detailed mineralogical examination of Yucca Mountain tuffs showed that most zeolitic alteration occurred from 13 to 11.5 Ma, shortly after tuff emplacement. After formation of the major zeolitic horizons, deep-seated hydrothermal activity persisted until about 10 Ma. The preservation of low-temperature zeolites, clinoptilolite and mordenite, suggest that this activity was limited to temperatures of up to 90 to 100°C.

Nevertheless, the general trend of glass reacting to form zeolites is captured, although the modeled zeolite assemblage may not be representative of that occurring at higher temperatures,

and the modeled precipitation of stellerite and feldspars from glass and/or clinoptilolite dissolution would not be expected in the actual system. This is because the alteration of glass during the thermal evolution of Yucca Mountain, which lasted millions of years at temperatures similar to those that would result in vitric and zeolitic units from waste emplacement, was shown to be predominantly clinoptilolite. Therefore, the modeled reactions forming feldspars and stellerite from glass and clinoptilolite dissolution are likely to be thermodynamically or kinetically unfavorable in vitric and zeolitic units such as in the Calico Hills formation (CHn). In this respect, it is likely that the modeled mineral transformations in these units reflect overestimated reaction rates, and unrealistic end-products yielding greater volume changes than reasonably expected from observations of the natural thermal alteration at Yucca Mountain. This could be caused by an underestimated thermodynamic stability of clinoptilolite, as suggested by simulations results presented by Dobson et al. (2003 [DIRS 168273]). Also, model improvements including zeolite solid solutions and cation exchange reactions would likely result in better agreement between the model results and observed thermal alteration mineralogy. Given the observed alteration of glass to predominantly clinoptilolite during earlier thermal events at Yucca Mountain, the reactions forming feldspars may be thermodynamically or kinetically unfavorable.

6.4.3.3.4 Effects of THC Processes on Hydrologic Properties and Percolation Fluxes

Changes in porosity and hence permeability are related to the net effects of volume changes taking place via mineral dissolution/precipitation, as discussed in the previous section. Mineral precipitation takes place through several different mechanisms, and therefore the distribution in the changes in hydrologic properties is related to the spatial distributions of the various processes. Near the repository drifts, changes in fracture porosity (Figure 6.4-25) and permeability (Figure 6.4-26) are related primarily to boiling-induced mineral precipitation, which is dominated by amorphous silica (Figure 6.4-19). Only minor changes in fracture porosity (about 6%) are observed near the drifts. Such small fracture porosity changes do not significantly reduce the fracture permeability around the drifts (Figure 6.4-26). However, the spatial resolution of the mesh in these zones is not adequate to evaluate changes in a narrow boiling zone. Hence, the drift-scale THC seepage model predicts about twice this amount of porosity change (based on doubling the mineral amounts given in BSC 2005 [DIRS 172862], Figure 6.5-43, for a fracture medium initially having 50% rock). In the rock matrix, a small reduction in porosity of less than 1% is apparent in the repository horizon around the drifts (Figure 6.4-25), whereas in the CHn there is a modest increase in porosity of about 1%, owing primarily to the reaction of clinoptilolite and glass to feldspars and stellerite. Permeability changes in the matrix of the CHn vitric and zeolitic units are minor because of the initially high porosity of these rocks (Figures 6.4-25 and 6.4-26). Therefore, the porosity and permeability values in the matrix are essentially the same as the initial values. As noted above, volume and permeability change in the CHn vitric and zeolitic units are likely to be overestimated, and one would not expect these units to alter to much more extent than currently observed after millions of years at temperatures similar to those resulting from the proposed waste emplacement.

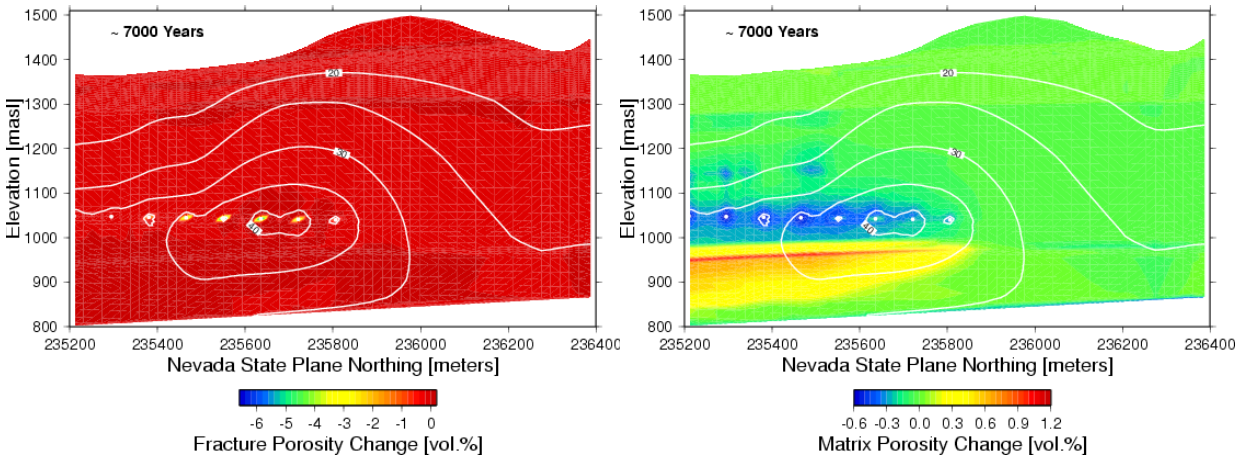

Output DTN: LB0310MTSCLTHC.001.

Figure 6.4-25. Fracture and Matrix Porosity Changes after 7,000 Years

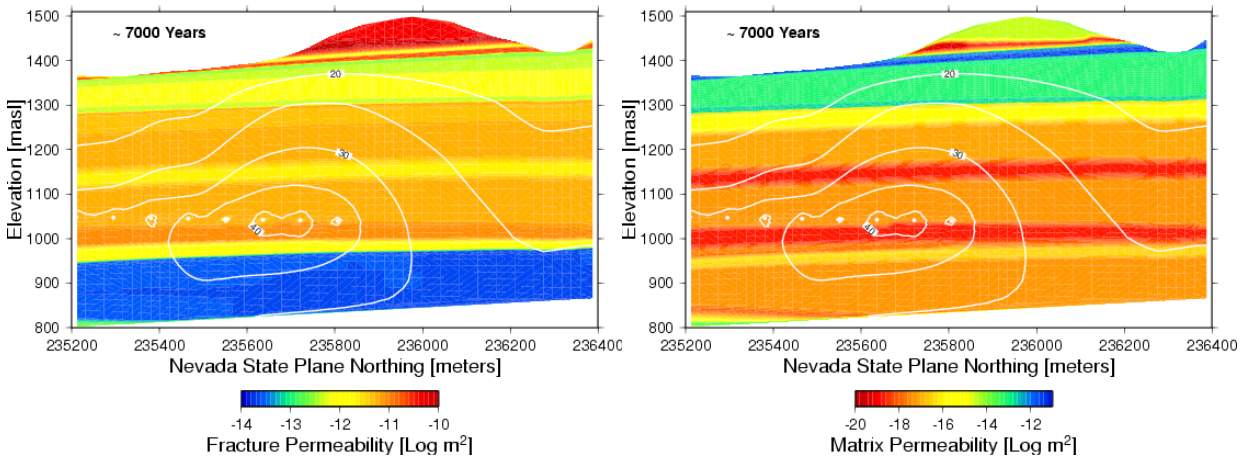

Output DTN: LB0310MTSCLTHC.001.

Figure 6.4-26. Fracture and Matrix Permeability after 7,000 Years

As a result of the relatively minor changes to hydrologic properties, the models predict corresponding small THC induced changes to percolation fluxes at the repository horizon compared to the fluxes predicted using the TH model (Figure 6.4-27). These results indicate that reactions taking place in the far-field above the repository (e.g., in the PTn) are not sufficient to affect percolation fluxes.

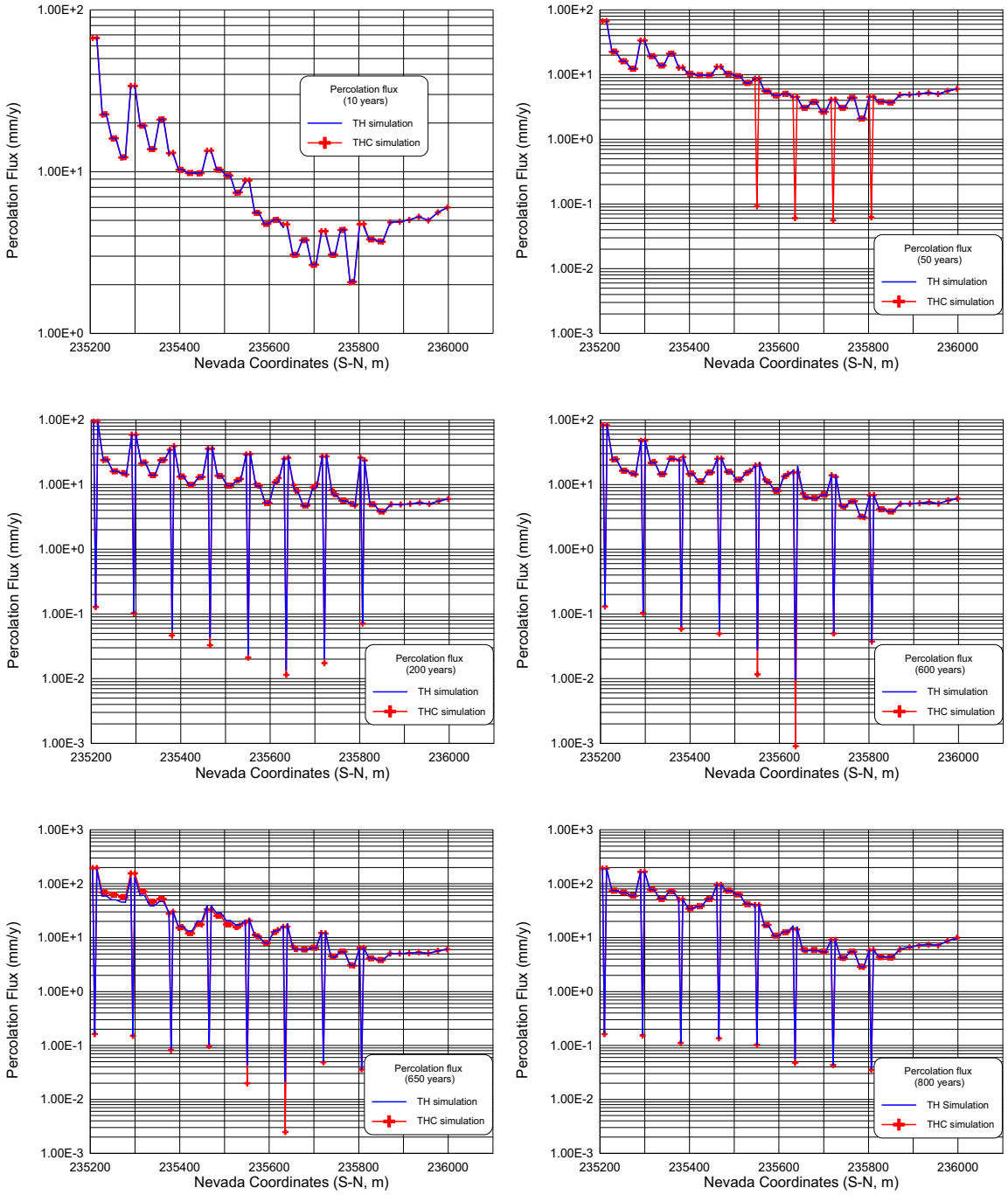

Output DTN: LB0310MTSCLTHC.001.

Figure 6.4-27. Percolation Fluxes at the Repository Horizon from the TH and THC Models

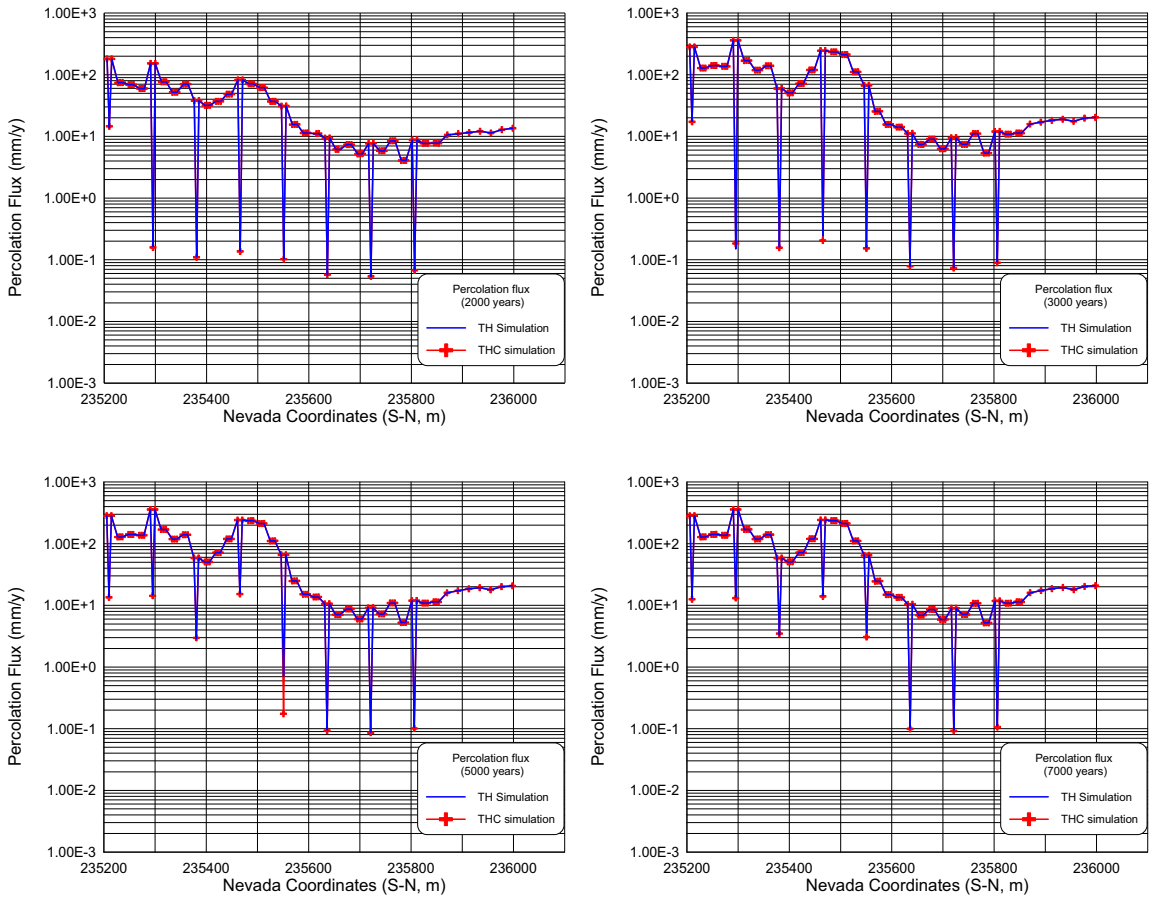

Output DTN: LB0310MTSCLTHC.001.

Figure 6.4-27. Percolation Fluxes at the Repository Horizon from the TH and THC Models (Continued)

6.5 MOUNTAIN-SCALE THM MODEL

The heat generated by the decay of radioactive waste results in elevated rock temperatures for thousands of years after waste emplacement. These temperatures cause thermal expansion of the rock, with the potential of opening or closing fractures and thus changing fracture permeability close to the repository. Changes in permeability may impact the percolation flux around the repository and thereby impact the performance of the repository. To estimate the impact of THM processes on repository performance, coupled THM analysis was conducted.

This section documents the development, implementation and results of mountain-scale modeling of coupled THM processes around the repository. Specifically, the impact of coupled THM processes on hydrologic properties and mountain-scale fluid flow are examined over a time frame of 10,000 years. This mountain-scale THM model is based on the coupled THM simulator TOUGH2-FLAC3D (Rutqvist et al. 2002 [DIRS 162048]). A similar analysis has been conducted in *Drift Scale THM Model* (BSC 2004 [DIRS 169864]) using the same conceptual model and same numerical simulator. Detailed descriptions of the technical basis for the model are given in Sections 6.1 to 6.4 of that report (BSC 2004 [DIRS 169864]) and are not

repeated here. In this section only details specifically applicable to the mountain-scale modeling are developed.

6.5.1 Introduction to Coupled THM Analysis

In this section, the impact of coupled THM processes on the mountain-scale hydrology of the repository at Yucca Mountain is assessed by comparing the result of a TH analysis to that of a THM analysis. In the partially coupled TH analysis, the coupling via mechanical processes is neglected, which means that changes in hydrologic properties induced by mechanical processes are neglected in the fluid flow calculation. To assess the impact of the THM processes on the flow field, it is sufficient to calculate changes in the mean permeability value for the bounding case of relatively large THM-induced changes in permeability. This is consistent with mean values used in UZ flow models (BSC 2004 [DIRS 169861]) and TH models discussed in Sections 6.2 and 6.3, which use mean values of permeability for each stratigraphic unit. The bounding case for the THM model is realized by adopting appropriate estimates of the coupled THM material properties, including the thermal expansion coefficient (which emphasizes thermal stress) and the stress-versus-permeability function (which emphasizes TM-induced permeability change). Using a homogeneous mean permeability to predict effects of coupled THM processes allows for easy comparison between THM and TH models, which is the basis for conclusions drawn in this model report.

6.5.2 Description of the Coupled THM Simulator

The two computer codes, TOUGH2 V1.6 (LBNL 2003 [DIRS 161491]) and FLAC3D V2.0 (LBNL 2001 [DIRS 154783]), have been coupled for the analysis of coupled multiphase flow, heat transport, and rock deformations in fractured porous media (Rutqvist et al. 2002 [DIRS 162048]). In the coupled THM simulation the TOUGH2 code (Pruess et al. 1999 [DIRS 160778]) computes thermal hydrologic processes involving multiphase, multicomponent fluid and heat transport, while FLAC3D (Itasca Consulting Group 1997 [DIRS 156788]) computes thermal mechanical changes in stress and displacement. The FLAC3D (LBNL 2002 [DIRS 154783]) and TOUGH2 (LBNL 2003 [DIRS 161491]) codes are coupled through external modules: one that calculates changes in effective stress as a function of multiphase pore pressure and thermal stress, and one that corrects porosity, permeability, and capillary pressure as a function of stress (Figure 6.5.2-1).

In the case of Yucca Mountain, coupling from hydrological to mechanical processes through pressure-induced changes in effective stress can be neglected because fractures are generally dry with an inherent capillary pressure of less than 0.01 MPa (DTN: LB03013DSSCP3I.001 [DIRS 162379], Table II-1). The minimum α_F value, where F denotes fractures, of the repository layers in the DTN is approximately 10^{-4} 1/Pa, which is equal to the inherent capillary pressure of 0.01 MPa. This implies that any change in saturation in the fractured system may give rise to fluid-pressure changes on the order of 0.01 MPa. This is a very small change in pressure for a system exposed to in situ stresses and thermal compressive stresses on the order of 10 MPa. Thus, the fluid-pressure-induced changes could be 1% or less compared to the in situ stresses and thermally induced stresses. Consequently, the coupling from hydrological processes to mechanical processes is neglected in this analysis. On the other hand, the coupling from

mechanical processes to hydrological processes is not neglected, but is rather one of the main issues investigated in this report. This coupling is important for estimating thermo-mechanically induced changes in hydrological properties and their impact on the flow field and drift seepage.

Because the coupling parameters are material-specific, specially designed coupling modules that incorporate material specific parameters have been constructed and qualified for Yucca Mountain. The coupling modules are contained in qualified software routines Tin V1.1 (LBNL 2002 [DIRS 162038]), Delb.dat V1.0 (LBNL 2001 [DIRS 154791]) and GPZones.dat V1.0 (LBNL 2001 [DIRS 154792]). The links between these coupling routines and the TOUGH2 (LBNL 2003 [DIRS 161491]) and FLAC3D (LBNL 2002 [DIRS 154783]) codes are illustrated in Figure 6.5.2-1 and described in Sections 6.5.4 and 6.5.5.

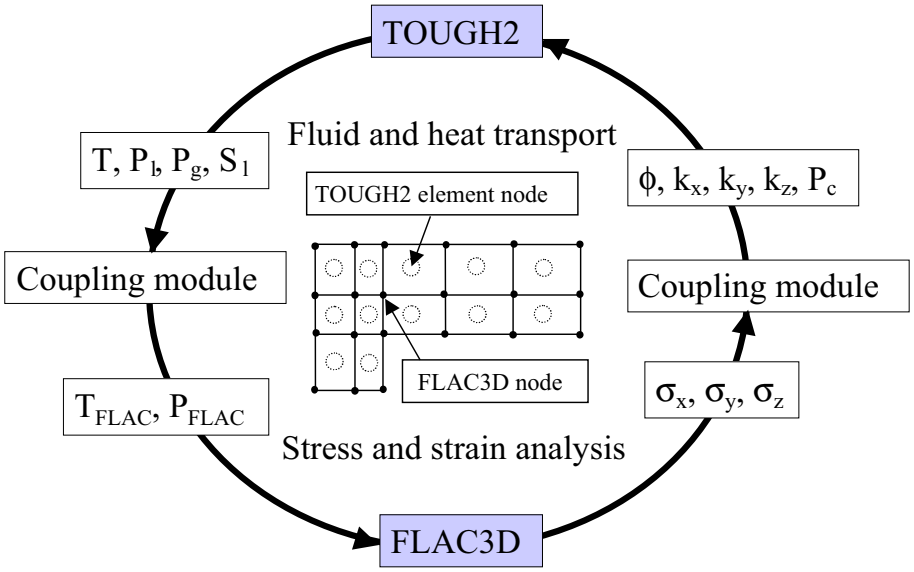

NOTE: T = Temperature; P_l = liquid fluid pressure; P_g = gas pressure; S_l = liquid saturation; T_{FLAC} = temperature at FLAC3D node; P_{FLAC} = pressure at FLAC3D node; ϕ = porosity; k_x, k_y, and k_z are permeabilities in x, y, and z-directions, respectively; P_c is capillary pressure; and σ_x, σ_y, and σ_x are stresses in x, y, and z-directions, respectively. For the unsaturated fractured hard rock zone at Yucca Mountain, the illustrated transfer of P_l, P_g and S_l from TOUGH2 to FLAC3D is not significant and therefore neglected. The fluid pressure in fractures of the unsaturated rock is very small and does not induce any significant mechanical changes. Therefore, only temperature has to be transferred from TOUGH2 to FLAC3D.

Figure 6.5.2-1. Schematic of Coupling between TOUGH2 and FLAC3D

6.5.3 Dual-Permeability Continuum Model for Analysis of THM Processes

The two main stratigraphic units in which the emplacement drifts are located (middle nonlithophysal [Tptpmn] and the lower lithophysal [Tptpll] units of the Topopah Spring Tuff) are both highly fractured, and the fractures are well connected (BSC 2004 [DIRS 167652], Section 6.3). In these rock units, three dominant sets of fractures are oriented almost orthogonal to each other (CRWMS M&O 1998 [DIRS 102679], Section 7.4.5), two subvertical and one subhorizontal, and the minimum mean fracture spacing is less than 0.4 m for the TSw2 TM unit (CRWMS M&O 1998 [DIRS 102679], Section 7.4.6). Because of the high density and connectivity of the fracture network, the conceptual model used is a dual-permeability

continuum model with interacting fractured and matrix continua consistent with the UZ flow model and other coupled analyses. The dual-permeability continuum model appropriately accounts for the difference in water retention between the fractures and matrix necessary to capture important fracture-matrix interaction processes such as matrix imbibition. Previous analyses of TM-induced displacements at two major heater tests at Yucca Mountain (the Single Heater Test and Drift Scale Test; see BSC 2004 [DIRS 169900], Sections 6.2 and 6.3) have shown that mechanical deformations in the Tptpmn unit are captured reasonably well with a linear-elastic or nonlinear-elastic mechanical model (Sobolik et al. 1998 [DIRS 162049]; BSC 2001 [DIRS 155957]; pp. 115 to 125; Sobolik et al. 1999 [DIRS 163202], p. 735). Furthermore, previous comparisons of the discrete-fracture approach and continuum approach for the modeling of mechanical displacements in the DST show only minor differences, indicating that the continuum approach is sufficiently accurate to represent in situ TM behavior at Yucca Mountain (BSC 2001 [DIRS 155957], p. 125). This implies that the bulk-rock mass behavior is essentially elastic, although locally a small slip may occur on fracture planes. Because the fractured porous medium is always in a static equilibrium, the three-dimensional stress is equivalent in the fracture and matrix continua. Therefore, the mechanical dual-continuum model reduces to a lumped fracture-matrix continuum model (equivalent continuum model). With all the above factors considered, the dual-permeability continuum model was selected as an appropriate conceptual model for this analysis.

6.5.4 TOUGH2 to FLAC3D Link for Mountain-Scale THM model

For modeling of the Yucca Mountain UZ, the linkage function from TOUGH2 (LBNL 2003 [DIRS 161491]) to FLAC3D (LBNL 2002 [DIRS 154783]) considers only thermally induced strain and stresses. In this model, changes in effective stress caused by the multiphase fluid pressure and saturation changes are neglected, because the resulting stress changes are much smaller than changes induced by thermal-mechanical effects (Section 6.5.2; BSC 2004 [DIRS 169864], Section 6.2.2). Thus, the coupling module for the link from TOUGH2 to FLAC3D transfers only the temperature field from TOUGH2 nodes to FLAC3D nodes. This coupling is provided by routine Tin V1.1 (LBNL 2002 [DIRS 162038]) and the volume interpolation factors are calculated by routine GPZones.dat V1.0 (LBNL 2001 [DIRS 154792]). These are qualified routines developed with FLAC3D (LBNL 2002 [DIRS 154783]).

6.5.5 FLAC3D to TOUGH2 Link for Mountain-Scale THM model

For Yucca Mountain, the linkage function between FLAC3D (LBNL 2002 [DIRS 154783]) and TOUGH2 (LBNL 2003 [DIRS 161491]) corrects hydrologic properties for changes in the three-dimensional stress field, using a conceptual model of highly fractured rock shown in Figure 6.5.5-1. This conceptual model is adequate for estimating the impact of mechanical processes on hydrologic properties at Yucca Mountain. This is because it captures all relevant THM processes observed at several in situ experiments conducted at Yucca Mountain (BSC 2004 [DIRS 169864], Section 7). This simplified conceptual model is consistent with the intense fracturing and a well-connected fracture network observed at Yucca Mountain. For the main repository units, Tptpmn and Tptpll, a mean fracture spacing of less than 0.4 m has been derived, using mappings of fractures with a trace length larger than a meter (DTN: LB0205REVUZPRP.001 [DIRS 159525]). However, as pointed out in *Drift*

Degradation Analysis (BSC 2004 [DIRS 166107], Section 6.3.3), 80% of the fractures have a trace length of less than one meter, and therefore, counting all fractures, the fracture spacing should be less than 0.4 m. The concept of a well-connected fracture network for fluid flow is confirmed by air-permeability measurements conducted at Yucca Mountain boreholes with short (1 ft.) packer intervals at several excavated niches (BSC 2004 [DIRS 170004], Section 6.1). In these tests, the permeability at each 0.3-m interval of the boreholes is several orders larger than the matrix permeability, indicating that at least one hydraulic conductive fracture intersects every 0.3 m and is connected to a network of conducting fractures. For such intensely fractured rock, the detailed fracture geometry does not impact the coupled THM behavior significantly, and hence, the adopted conceptual model is appropriate.

Using the conceptual model in Figure 6.5.5-1, the porosity, ϕ, permeability, k, and capillary pressure, P_c in the fractured continuum are corrected for any change in the stress field using the following relationships (BSC 2004 [DIRS 169864], Section 6.2.2):

$$\phi = F_{\phi} \times \phi_i \qquad \text{(Eq. 6.5.5-1)}$$

$$k_x = F_{kx} \times k_{ix}, \; k_y = F_{ky} \times k_{iy}, \; k_z = F_{kz} \times k_{iz} \qquad \text{(Eq. 6.5.5-2)}$$

$$P_c = F_{Pc} \times P_{ci} \qquad \text{(Eq. 6.5.5-3)}$$

where F denotes various correction factors and subscript i denotes initial conditions. Porosity and permeability correction factors are calculated from the initial and current apertures, b, in Fracture Sets 1, 2, and 3, according to:

$$F_{\phi} = \frac{b_1 + b_2 + b_3}{b_{1i} + b_{2i} + b_{3i}} \qquad \text{(Eq. 6.5.5-4)}$$

$$F_{kx} = \frac{b_2^3 + b_3^3}{b_{2i}^3 + b_{3i}^3}, \; F_{ky} = \frac{b_1^3 + b_3^3}{b_{1i}^3 + b_{3i}^3}, \; F_{kz} = \frac{b_1^3 + b_2^3}{b_{1i}^3 + b_{2i}^3} \qquad \text{(Eq. 6.5.5-5)}$$

where fractures in Fracture Sets 1, 2, and 3 are equally spaced and oriented normal to x, y, and z directions, respectively, and a parallel-plate fracture flow model (Witherspoon et al. 1980 [DIRS 123506]) is adopted. The capillary pressure is corrected with porosity and permeability changes according to the following function (Leverett 1941 [DIRS 100588]):

$$F_{Pc} = \sqrt{\frac{F_{\phi}}{F_k}} \qquad \text{(Eq. 6.5.5-6)}$$

where

$$F_k = \sqrt[3]{F_{kx} \times F_{ky} \times F_{kz}} \qquad \text{(Eq. 6.5.5-7)}$$

In this study, the current fracture aperture b depends on the current effective normal stress σ'_n, according to the following exponential function (Rutqvist and Tsang 2003 [DIRS 162584]):

$$b = b_r + b_m = b_r + b_{\max}\left[\exp\left(\alpha\sigma'_n\right)\right] \quad \text{(Eq. 6.5.5-8)}$$

where b_r is a residual aperture, b_m is mechanical aperture, b_{max} is the maximum mechanical aperture (frequently denoted as maximum closure in rock mechanics literature), and α is a parameter related to the curvature of the function (Figure 6.5.5-2). This relationship is expressed in terms of an initial aperture, b_i, and changes in aperture, Δb, as:

$$b = b_i + \Delta b = b_i + b_{\max}\left[\exp\left(\alpha\sigma_n\right) - \exp\left(\alpha\sigma_{ni}\right)\right] \quad \text{(Eq. 6.5.5-9)}$$

where σ'_{ni} is the initial effective stress normal to the fractures. This expression is inserted into Equation (6.5.5-5) to derive expressions for rock-mass permeability-correction factors in x, y, and z directions. In this formulation, the permeability changes as a function of normal stress across each fracture set, while no shear-induced permeability changes are considered. This formulation is sufficient because closure of vertical fractures caused by thermally induced horizontal stresses has a dominating impact on the permeability changes. Furthermore, the potential for shear-induced permeability changes is evaluated indirectly from the results of the stress analysis. The calculation of fracture aperture changes is conducted in the qualified software routine Delb.dat V1.0 (LBNL 2001 [DIRS 154791]), which is then transferred into the TOUGH2 (LBNL 2003 [DIRS 161491]) code for the correction of hydrologic properties.

The most important parameter for estimating stress-induced changes in hydraulic properties is the relationship between fracture aperture and stress, defined in Equation 6.5.5-8. For a well-connected fracture network, fracture spacing and fracture orientation have little importance in the relationship between stress and permeability in comparison with that between fracture-aperture and stress. The relationship between fracture hydraulic aperture and stress has been determined both in laboratory samples and in the field for various types of rock (Rutqvist and Stephansson 2003 [DIRS 162583]). This relationship depends on fracture characteristics such as roughness and degree of mineral filling. Aperture-versus-normal stress relationships derived from small-scale laboratory samples are generally not applicable in the field. The effect of size on the permeability and normal stiffness of fractures has been confirmed in both theoretical and experimental studies (Rutqvist and Stephansson 2003 [DIRS 162583], p.15). Because of potential effects of size and nonrepresentative sampling, it is important to determine the stress-versus-aperture relationship in situ (Rutqvist and Stephansson 2003 [DIRS 162583], p. 7). Such in situ determination seeks to determine the basic parameters b_{max} and α for fractures in the underlying conceptual model. The determination of the stress-versus-aperture relationship for mountain scale is further discussed in Section 6.5.9.

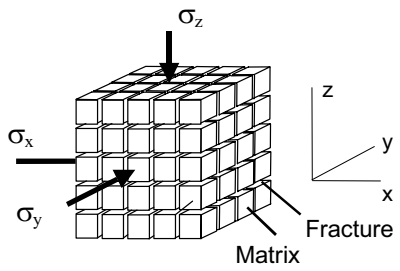

$$k_x = k_x(\sigma_y, \sigma_z)$$

$$k_y = k_y(\sigma_x, \sigma_z)$$

$$k_z = k_z(\sigma_x, \sigma_y)$$

NOTE: σ_x, σ_y, σ_x and k_x, k_y, k_z are stresses and permeabilities in x, y and z-directions, respectively.

Figure 6.5.5-1. Conceptual Model Used for Calculation of Stress-Induced Changes in Hydraulic Properties

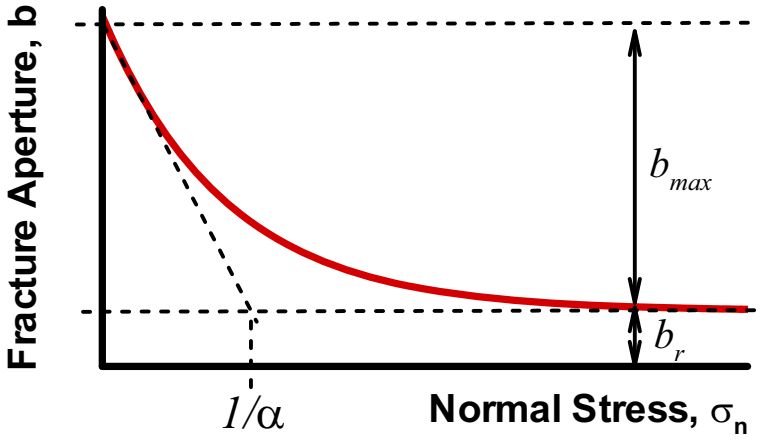

NOTE: b_{max} and α are parameters that determine the shape of the exponential function and b_r is the residual aperture when the fracture is completely compressed from a mechanical point of view at a high normal stress.

Figure 6.5.5-2. Schematic for Normal Stress versus Aperture Relation

6.5.6 Coupled THM Model Domain

The mountain-scale THM model is a vertical two-dimensional cross section extending from the ground surface down to the groundwater table (see Figure 6.5.6-1). The model domain is designed by first taking a multiple-layered column extending vertically from the ground surface down to the water table. The vertical layering for the model is chosen to correspond to the vertical contacts at the Nevada State Plane Coordinates 170600 m (Easting) and 234017 m (Northing), near the center of the repository (see Figure 6.1-1 for location in the 3-D grid). The geological data are derived from the "b58" column of the two-dimensional Yucca Mountain UZ

model grid (DTN: LB030432DGRIDS.001 [DIRS 163937], file *mesh-ns.vf*). The layers are extended horizontally to form a two-dimensional section that runs north–south along the UZ two-dimensional TH model (See Figure 6.1-1 for location of the two-dimensional section). The model is half-symmetric, containing 21.5 waste emplacement drifts located at a depth of about 384 m (1065 m elevation) in the in the Tptpll unit (see Section 6.1.1). The emplacement drifts are located in 5-by-5-m elements, which each contains thermal line loads. The 5-by-5-m drift elements are not removed from the model, which implies that mechanical stress changes caused by excavation are not considered in this analysis. Excavation induced mechanical changes may be significant within a few meters distance from the drift wall and are considered in *Drift Scale THM Model* (BSC 2004 [DIRS 169864], Section 6.5.1 and 6.6.1).

The boundary conditions applied to the mountain-scale THM model and numerical values of domain are given in Figure 6.5.6-1b. The left boundary is closed to heat and fluid flow by symmetry and is allowed zero normal displacement mechanically (i.e., "on rollers"). The right boundary is set at a distance of 5 km from the right edge of the repository. At this boundary, a constant stress is maintained with a gradient according to Section 5.3, and no heat or fluid flow across it. The ground surface boundary was set at a constant temperature and atmospheric pressure, mechanically free, and the water-table boundary was set at constant temperature and zero normal displacement (Figure 6.5.6-1a and Table 6.5.6-1). The specific values of temperature, pressure, and saturation at the top and bottom boundary were extracted from column "b58" located 234017 m along the two-dimensional TH model cross section (Section 6.2). The pre-emplacement ambient thermal and hydrologic conditions are derived by running a TH model to steady state, using the prescribed boundary conditions at the ground surface and the present-day infiltration rate of about 6 mm/yr (5.8 mm/yr according to Table 6.5.6-1). The infiltration rates for present-day, monsoon, and glacial transition climates in the mountain-scale THM model are the mean infiltration rates over the north–south two-dimensional TH model sections used in Section 6.2 (Table 6.5.6-1). Thus the mean infiltration rates used in the mountain-scale THM model simulation are consistent with mean infiltration rates of the mountain-scale TH model simulation in Section 6.2

The initial stress field represents the best estimate of the stress field at the repository horizon (see Section 5.3). The initial vertical stress is estimated based on the weight of the overburden rock mass, with an average saturated bulk rock density of 2,200 kg/m^3. This is the average value of the bulk rock density calculated for the rock mass overlying the repository drifts, using saturated rock densities (DTN: LB0306DRSCLTHM.001 [DIRS 169733]). The magnitude of maximum and minimum principal compressive horizontal stresses are estimated to be a factor of about 0.6 (ranging from 0.3 to 1.0) and 0.5 (ranging from 0.3 to 0.8) of the vertical stress, with the maximum stress oriented N32E (CRWMS M&O 1997 [DIRS 103564], p. 3-23, Table 3-2,). The adopted initial stress field in this model simulation is shown in Figure 6.5.6-1. This estimate of the initial stress is considered sufficiently accurate because the present report concerns itself with thermally induced stresses, which are largely independent of the initial stress field.

During the 10,000-year postclosure regulatory period, a varying infiltration rate was applied at the ground surface according to the mean infiltration scenario described in Section 4.1.1. For the location of the mountain-scale THM model, the average infiltration rate applied uniformly over the two-dimensional section is given in Table 6.5.6-1.

Table 6.5.6-1. THM Model Boundary Conditions

Boundary	Boundary Condition	Reference
Top of model domain, which represents the conditions at the ground surface	T = 16.05 °C S_g = 0.997 P = 84,309 Pa Infiltration rate: 5.8 mm/yr 0 to 600 years 17.0 mm/yr 600 to 2,000 years 28.8 mm/yr >2,000 years	T, S_g and P from DTN: LB0310MTSCLTH2.001, file incon_th_2d_1.dat element "TP TPb58"; infiltration rates from DTN: LB0310MTSCLTH2.001; files GENER_PRESENT_VENT_0.863.2D GENER_MONS_VENT_0.863.2D GENER_GLACIAL_VENT_0.863.2D.
Bottom of model domain, which represents the conditions at the groundwater table	T = 31.13 °C S_g = 0.00001 P = 91,604 Pa	T, S_g and P from DTN: LB0310MTSCLTH2.001, file incon_th_2d_1.dat element "BT BTb58"
Waste package thermal load	Initial heat of 1.45 kW/m, decreasing with time (due to radioactive decay), and reduced by 86.3% during the first 50 years (due to removal by ventilation; see Section 6.1.5)	Heat load: BSC 2004 [DIRS 168489] Thermal decay function: BSC 2002 [DIRS 159527] Ventilation efficiency: BSC 2002 [DIRS 160975], Table 6-6

NOTE: T = Temperature, S_g = gas saturation, P = pressure.

In the THM model, the thermal load is imposed on the 21.5 drift elements located in the lower lithophysal unit of the Topopah Spring welded tuff (Figure 6.5.6-1a). The half drift is located at the mid symmetry line on the left side of the model. The initial thermal line load used is 1.45 kW/m, with a 50-year ventilation period in which 86.3% of the thermal load is removed as described in Section 6.1.5.

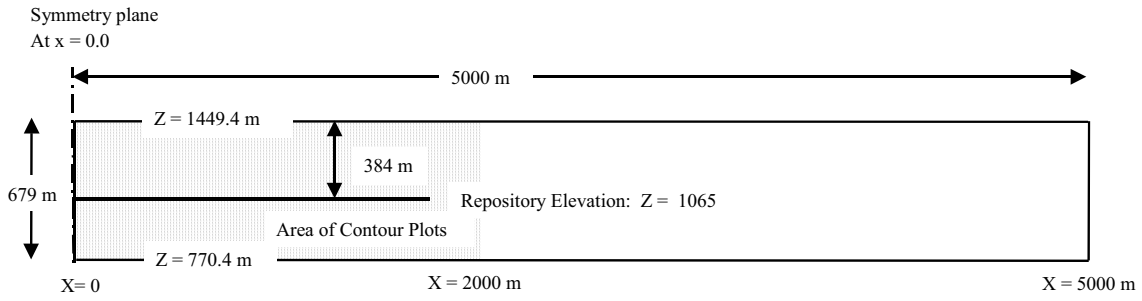

(a) Model Domain

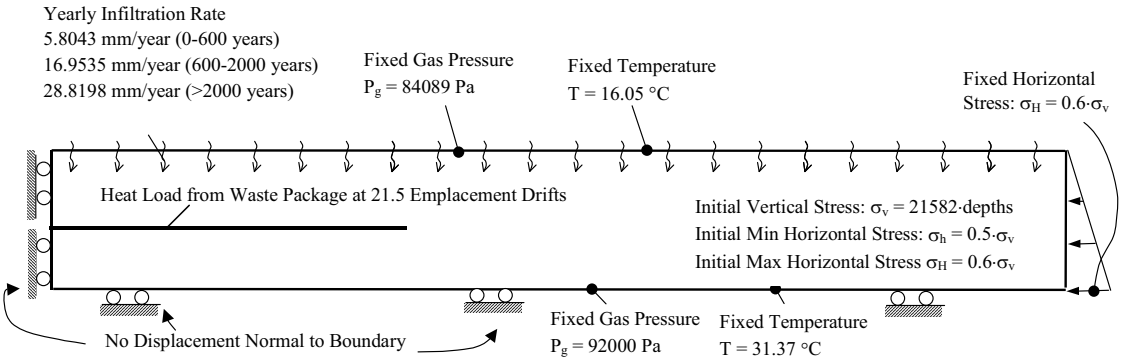

(b) Boundary and Initial Conditions

Figure 6.5.6-1. Domain and Boundary Conditions for the Mountain-Scale THM Model

6.5.7 TH Rock Properties

The thermal and hydrological properties used in the mountain-scale THM model, along with their sources, are the same as properties used for the mountain-scale TH analysis in Section 6.1.

6.5.8 Mechanical Rock Mass Properties

The definition of thermal mechanical (TM) units for the THM model is provided in *Drift Scale THM model* (BSC 2004 [DIRS 169864], Figure 6.4-1). The basic mechanical properties of the rock mass (Young's modulus and Poisson's ratio) are developed for TCw, PTn, TSw1 and TSw2 TM units in the spreadsheet "THM rock mass modulus v1.xls," which has been submitted to the TDMS under DTN: LB0306DRSCLTHM.001 [DIRS 169733].

The values of rock mass deformation modulus derived in this study are consistent with values used in related geotechnical studies at Yucca Mountain. For example, Young's Modulus and Poisson's Ratio are based on data for the TSw2 TM unit (Tptpmn and Tptpll lithostratigrahic

units, combines tsw34, tsw35, and tsw36 in Table 6.1-1) at 40% cumulative frequency. Figure 8-55 of *Subsurface Geotechnical Parameters Report* (BSC 2003 [DIRS 166660]) provides the cumulative probability for Young's Modulus for the Tptpmn lithostratigraphic unit. Linearly interpolating the data (25% probability equals 12.986 and 50% probability equals 16.743) yields a value of 15.24 GPa at 40% cumulative probability. This compares favorably with the value of 14.77 GPa from DTN: LB0306DRSCLTHM.001 [DIRS 169733] as used in this report for the TSw2 TM unit. The relatively small change in the updated value justifies the use of 14.77 GPa to assess bulk deformation effects. A Young's Modulus of 14.77 GPa for the Tptpll unit closely represents a Young's Modulus of Category 4 rock type in *Drift Degradation Analysis* (BSC 2004 [DIRS 166107], Table 6-41). A Poisson's Ratio of 0.21 (DTN: LB0306DRSCLTHM.001 [DIRS 169733]) is identical to the value given in Section 8.5.2.3 of *Subsurface Geotechnical Parameters Report* (BSC 2003 [DIRS 166660]). These elastic parameters represent the bulk rock mass (including the effects of fractures). A Young's Modulus of 14.77 GPa for the Tptpmn and Tptpll repository layers is about 50% lower than the Young's Modulus of intact rock determined on core samples from the site. As described in *Drift Scale THM Model* (BSC 2004 [DIRS 169864], Section 6.4.2), a reduction of the deformation modulus to about 50% of the intact rock value is reasonable and is consistent with in situ measurements of rock-mass deformation modulus, both at Yucca Mountain and elsewhere.

Assumptions documented in *Drift Scale THM Model* (BSC 2004 [DIRS 169864], Section 5, Assumptions 3 and 4) justify the choice of mechanical properties for TSw3 and CHn TM units located below the repository drift. The elastic properties of the CHn are taken from measurements on intact core samples (DTN: SNL02030193001.026 [DIRS 108436]). The three values of Young's Modulus and Poisson's Ratio for CHn (DTN: SNL02030193001.026 [DIRS 108436], SEP Table S99119_002) yield mean values of 5.63 GPa and 0.17, respectively. It should be noted that bulk modulus and shear modulus instead of Young's modulus and Poisson's ratio are used as input for the FLAC3D (LBNL 2002 [DIRS 154783]) simulations. The values of bulk modulus and shear modulus are calculated based on values of Young's modulus and Poisson's ratio by using Equations 14 and 13, respectively, from Jaeger and Cook (1979 [DIRS 106219], p. 111).

6.5.9 Coupled TM and HM Rock Properties

TM and HM properties of the rock mass were developed in *Drift Scale THM Model* (BSC 2004 [DIRS 169864], Section 6.4) and were validated in Section 7 of that report specifically through comparison of simulated and measured THM responses at the Yucca Mountain DST. As described in Section 6.5.1 of this report, to assess the impact of the THM processes on the flow field, it is sufficient to calculate changes in the mean value of the permeability for an upper-bound case of relatively large THM-induced changes in permeability. This upper-bound case is realized by adopting estimates of the coupled TM and HM material that emphasize thermal stress, and a stress-versus-permeability function that emphasizes TM-induced permeability change. However, because the TM and HM properties were developed for the drift scale, a scale dependency is considered when applying these properties for the mountain scale.

The temperature-dependent thermal expansion coefficient adopted for the mountain-scale THM model was derived from laboratory measurements on intact rock samples, as presented in *Drift Scale THM Model* (BSC 2004 [DIRS 169864], Figure 6.4.3-1):

$$\alpha_T = 5 + 0.0583 \cdot T \ (10^{-6}/^{\circ}\mathrm{C}) \qquad \text{(Eq. 6.5.9-1)}$$

The correlation is based upon the laboratory test values of thermal expansion coefficients. The source thermal expansion coefficients are direct input to *Drift Scale THM Model* (BSC 2004 [DIRS 169864], Table 4.1-1b) and are qualified as a source in this report. As noted in *Drift Scale THM Model* (BSC 2004 [DIRS 169864], Section 6.4), the thermal expansion coefficient in the field could theoretically be equal to or lower than the intact value because of the presence of fractures. However, analyses of the MPBX displacements at the DST (Sobolik et al. 1999 [DIRS 163202], p. 741; BSC 2001 [DIRS 155957], pp. 21 and 115 to 125; BSC 2004 [DIRS 169864], Section 7.4.2) have shown that the displacements are well predicted if an intact-rock thermal expansion coefficient is used. Adopting a thermal expansion coefficient that represents the intact rock values is considered an upper-bound estimate, because it leads to the highest possible thermally induced stress. This is because the intact rock value is the upper bound of the possible in situ thermal expansion coefficient. Figure 6.4.3-1 in *Drift Scale THM Model* (BSC (2004 [DIRS 169864]) shows that the adopted function closely represents intact-rock thermal expansion coefficients for various rock units at Yucca Mountain. Therefore, the linear function defined in Equation 6.5.9-1 is adopted for all rock units in the mountain-scale THM model.

In this report, the stress-permeability relationship derived for the drift-scale THM model is applied to the mountain-scale THM model, with corrections for possible scale effects. The parameters in the stress-aperture function (Equation 6.5.5-9) were estimated in *Drift Scale THM Model* (BSC 2004 [DIRS 169864], Section 6.4) through model calibration against air-permeability measurements conducted at several field experiments at Yucca Mountain. As noted in that report (BSC 2004 [DIRS 169864], Section 6.4), it is essential that b_{max} and α be determined in situ, at a relevant scale, because of the potential size dependency of the coupled HM properties of rock fractures (Rutqvist and Stephansson 2003 [DIRS 162583], p. 15). Also, as noted in Section 7.10 of *Drift Scale THM Model* (BSC 2004 [DIRS 169864]), the thermal and mechanical properties at Yucca Mountain show little or no size dependency at meter size and larger. Hydrologic properties, for example fracture permeability, have been shown to be dependent on the measurement scale (BSC 2004 [DIRS 170038], Section 6.1.1.1). At Yucca Mountain, mountain scale calibrated fracture permeability is generally one to two orders of magnitude higher than drift-scale calibrated fracture permeability (BSC 2004 [DIRS 169857], Sections 6.3.2 and 6.3.3). Specific values of drift-scale and mountain-scale fracture permeability values are given in Table 6.5.9-1. The associated aperture, *b*, is calculated from the mean fracture frequency, *f*, and the isotropic initial permeability, for an ideal cubic block model, leading to the formula (BSC 2004 [DIRS 169864], Equation 6.4-4):

$$b = \sqrt[3]{6 \times k / f} \qquad \text{(Eq. 6.5.9-2)}$$

In this report, two methods are investigated for up-scaling of drift-scale stress versus permeability function to that of the mountain scale. The two methods were developed as part of

an ongoing effort in the international cooperative project DECOVALEX (acronym for DEvelopment of COupled models and their VALidation against EXperiments in nuclear waste isolation). In the DECOVALEX project, the TOUGH2-FLAC3D simulator is applied in a benchmark test to the up-scaling of THM properties at Sellafield, UK. The rock at Sellafield consists of welded tuff, a similar type of rock to the repository units at Yucca Mountain. The up-scaling strategy adopted in this report is the one used for the DECOVALEX project as described by Liu et al. (2003 [DIRS 166017]).

In the first method of up-scaling, Method 1, the parameters b_{max} and α are kept the same as at the drift scale, whereas the initial aperture b_i (and hence the residual aperture b_r) is increased as a result of the higher initial permeability at mountain scale. The initial aperture for all rock units is calculated from Equation 6.5.9-2. In the second method, Method 2, the parameters b_{max}, b_i, and b_r are increased proportionally. The mountain-scale parameters are calculated based on Equation 6.5.9-2, leading to the following relationships:

$$\frac{b_{\max}}{b_{\max}^{d}} = \frac{b_r}{b_r^{d}} = \frac{b_i}{b_i^{d}} = \left(\frac{k}{k^{d}}\right)^{1/3} \qquad \text{(Eq. 6.5.9-3)}$$

where superscript d denotes drift-scale parameters (note that no superscript indicates mountain-scale parameters). Because all aperture parameters b_{max}, b_r, and b_i are increased proportionally, the parameter α becomes independent of scale and hence $\alpha = \alpha^d$. Given the mountain-scale and drift-scale fracture permeability, the ratio $(k/k^d)^{1/3}$ is found to be 1.9 for both the Tptpmn and Tptpll units (Table 6.5.9-1). Therefore, the parameter b_{max} is up-scaled by a factor of 1.9. The resulting parameters for Tptpmn and Tptpll units are given in Table 6.5.9-1.

Arguments can be made for both Method 1 and 2. Method 1 is more realistic and agrees with the general observations at the niche excavation tests that for larger initial permeability, the permeability changes less upon excavation (BSC 2004 [DIRS 169864], Figure 7.5-1). This essentially signifies that the hydraulic permeability (as represented by the initial aperture b_i) increases with scale while mechanical "stiffness" of the fractures (as represented by the parameters b_{max} and α) does not change from drift scale to mountain scale. This is in agreement with observations from other fractured rock sites, which indicate that permeable, highly conductive fracture zones are generally less sensitive to stress than zones of more competent rock (Rutqvist and Stephansson 2003 [DIRS 162583], page 7). The logic behind Method 2 is that large-scale fracture flow may be dominated by the largest and most open fractures, which are also the roughest. As such, the residual aperture, b_r, and the maximum closure parameter, b_{max} (both of which may be a function of roughness), should increase proportionally to the increase in the initial aperture b_i.

While method 1 is more realistic and reflects observations noted above, Method 2 is extreme, giving the most sensitive stress-versus-permeability relationship at the mountain scale. For this reason Method 2 is considered a reasonably conservative choice for investigation of coupled THM processes on the mountain scale. Parameters developed using Method 2 are adopted for further analysis and modeling in the mountain-scale THM model.

Note that the ideal cubic-block model is only used for estimating anisotropic stress-induced permeability changes in one vertical and two horizontal directions. Theoretically, for a model that consists of three orthogonal fracture sets, the elastic properties would be anisotropic, and would vary with stress as fractures open or close. In this study, isotropic rock-mass mechanical properties derived by the empirical rock-engineering methods within the YMP are used rather than by elasticity theory. As described in Section 6.5.8, the rock mass deformation modulus derived by these empirical methods is supported by several field measurements, such as plate loading tests. However, as shown in *Drift Scale THM Model* (BSC 2004 [DIRS 169864], Section 6.4.4), a theoretical cubic block model and the exponential normal-stress-versus-aperture function in Equation 6.5.5-8 can be used to derive a rock-mass modulus that is consistent with values used in this report. That is, the parameter values used for the stress-versus-permeability relationship are consistent with the parameter values used for the rock-mass mechanical properties.

Table 6.5.9-1. Summary of HM Parameters Developed in This Report

Geologic Unit		Tptpmn (TSw34)	Tptpll (TSw35)	Source
Drift-scale fracture permeability	k^d (m^2)	$0.33 \cdot 10^{-12}$	$0.91 \cdot 10^{-12}$	LB0205REVUZPRP.001 [DIRS 159525]
Drift-scale maximum joint closure	b^d_{max} (μm)	200	200	BSC 2004 [DIRS 169864], Table 6.4.5-1.
Drift-scale exponent α	α^d (1/Pa)	5.2×10^{-7}	5.2×10^{-7}	BSC 2004 [DIRS 169864], Table 6.4.5-1.
Mountain-scale permeability	k (m^2)	0.221×10^{-11}	0.608×10^{-11}	LB03013DSSCP3I.001 [DIRS 162379]
Ratio of $(k/k^d)^{1/3}$		1.9	1.9	Calculated based on values of k and k^d given in this table
Maximum joint closure for up-scaling Method 1	b_{max} (μm)	200	200	Equal to b^d_{max}
Maximum joint closure for up-scaling Method 2	b_{max} (μm)	380	380	Calculated using Equation (6.5.9-3)
Mountain-scale exponent for α for both up-scaling Methods 1 and 2	α (1/Pa)	5.2×10^{-7}	5.2×10^{-7}	Equal to α^d

NOTE: Superscript *d* refers to drift-scale properties.

6.5.10 Evolution of Temperature at Yucca Mountain

Figures 6.5.10-1 and 6.5.10-2 present calculated temperature evolution (see Section IV.4 of Appendix IV for details on postprocessing and plotting of the THM model results). Figure 6.5.10-1 shows that after emplacement of the waste in the excavated drift, the temperature in the drift wall rises rapidly and peaks at about 70 years, a few tens of years after the end of the forced ventilation period. The simulated temperature in the rock mass away from the drift continues to rise, and the mid-pillar temperature peaks at about 89°C (Figure 6.5.10-1b) after 900 years (Mid-pillar refers to a point located at mid-horizontal distance between two adjacent drifts, in this case between the first and second drift near the left vertical side boundary

of the model, near the center of the repository). The temperature evolution shown in Figure 6.5.10-1 is consistent with the calculated temperature evolution in the drift-scale THM model (BSC 2004 [DIRS 169864], Figure 6.5.2-1). Figure 6.5.10-2 shows that, although the temperature near emplacement drifts peaks at about 100 years after emplacement, the maximum average temperature at the repository level occurs at about 1,000 years. This is the time when the maximum impact of THM-induced changes in hydraulic properties and the flow field occurs. After about 1,000 years, a general decline in temperature at the repository level takes place. At the same time, the thermal gradient around the repository becomes smaller with the declining temperature difference between the drift wall and the mid-pillar. However, at 10,000 years, the temperature is above 50°C at the repository level, which is still significantly higher than the initial temperature of 24°C.

Figure 6.5.10-3 presents a comparison of temperature profiles at the repository level for TH and THM models. The figure shows that the temperature evolution and peak temperature is almost identical for TH and THM models. Thus, the THM coupling does not impact the evolution of temperature.

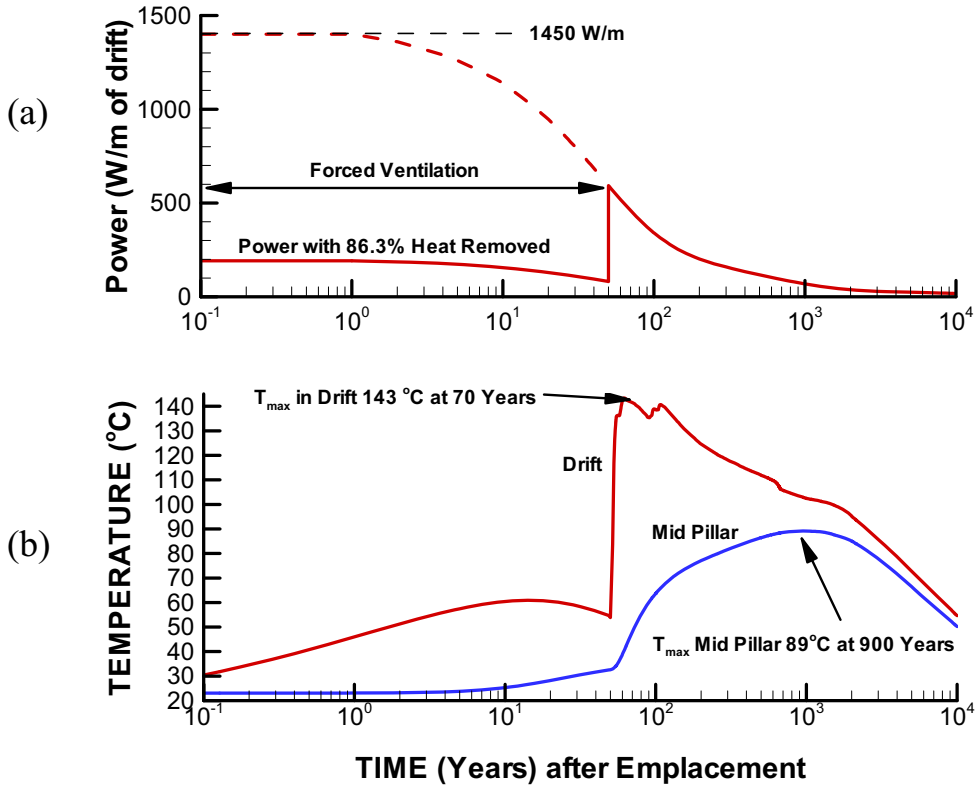

Output DTN: LB0310MTSCLTHM.002.

NOTE: Mid-pillar is a point located at the mid-distance between neighboring repository drifts. Waste packages are emplaced at the same time for the entire repository.

Figure 6.5.10-1. Calculated Evolution of (a) Thermal Power from Waste Package and (b) Temperature at Two Points on the Level of the Emplacement Drifts

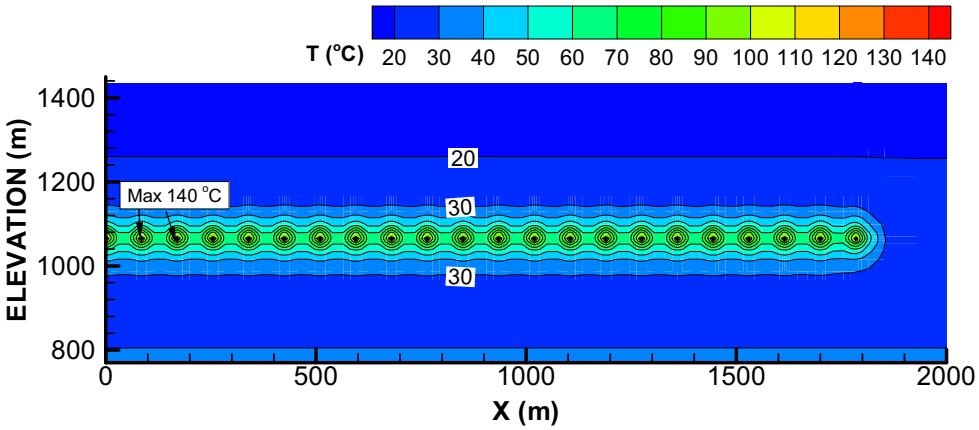

(a) 100 Years

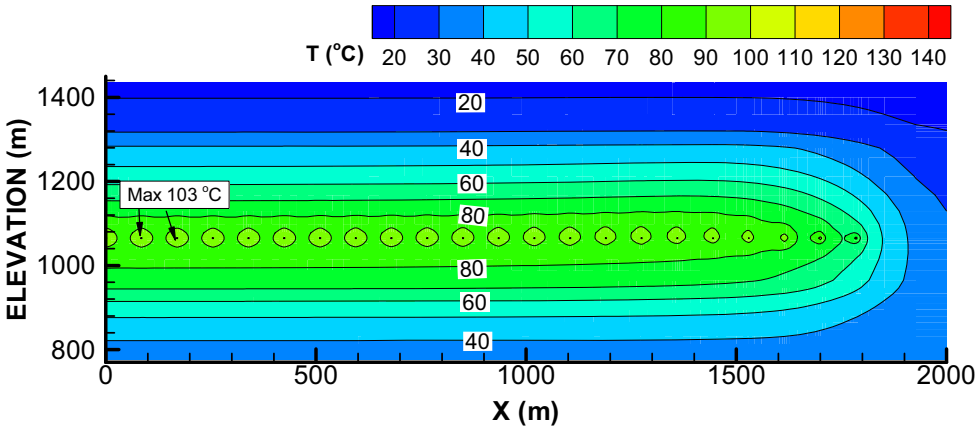

(b) 1,000 Years

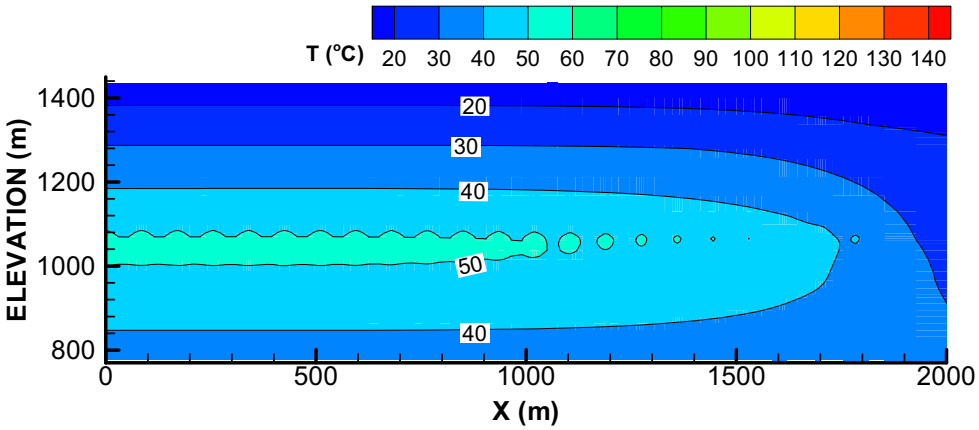

(c) 10,000 Years

Output DTN: LB0310MTSCLTHM.002.

Figure 6.5.10-2. Calculated Temperature Distribution in the Mountain

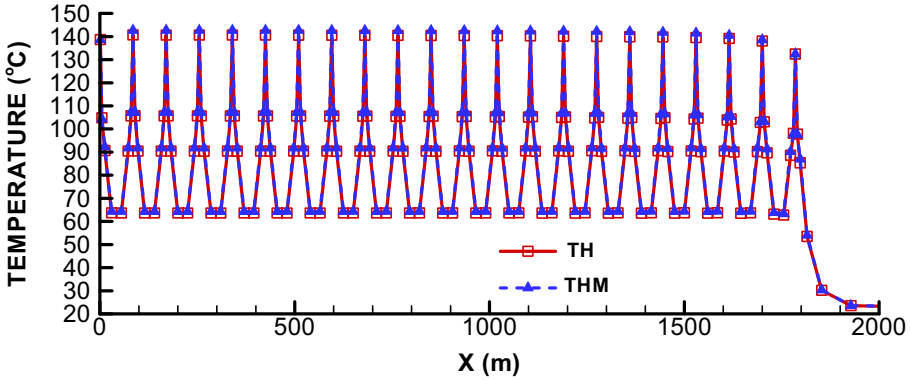

(a) 100 Years

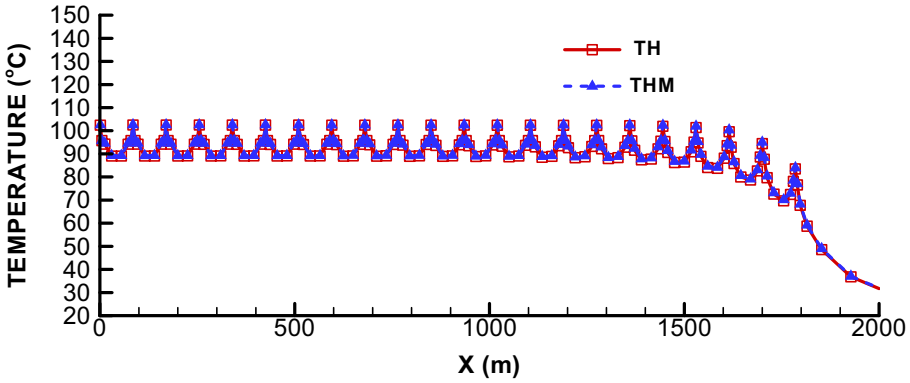

(b) 1,000 Years

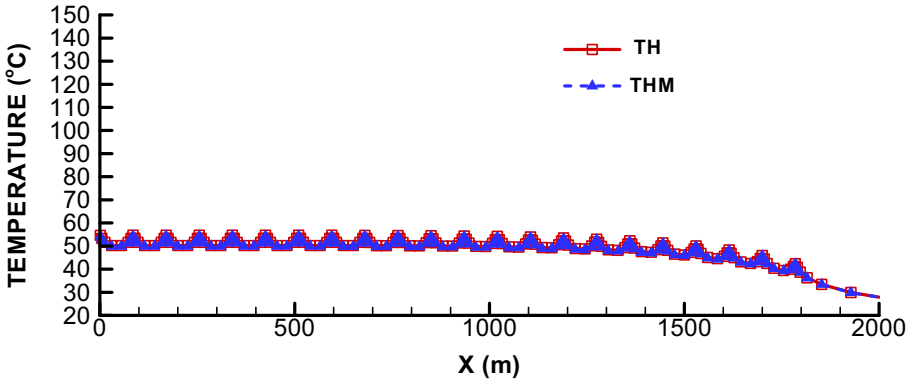

(c) 10,000 Years

Output DTN: LB0310MTSCLTHM.002.

Figure 6.5.10-3. Temperature Profiles through the Repository for TH and THM Analyses

6.5.11 Evolution of Thermal Stress

Figure 6.5.11-1 shows the distribution of mountain-scale horizontal stresses. Increased compressive stresses near the repository level are caused by thermal expansion of the rock mass. The magnitude of thermally induced stresses generally depends on the temperature and the distribution of the heat source, the rock-mass thermal expansion coefficient, and the rock-mass modulus of elasticity. The highest thermal stresses are created in the horizontal direction because of a larger extension of the heat source along the repository plane. At 100 years, the maximum compressive stress is about 18 MPa near the emplacement drifts. At 1,000 years, a zone of increased horizontal stress extends more than a hundred meters below and above the repository, with a maximum stress of about 12 MPa at the repository level. At 10,000 years, the compressive stresses at the repository level have generally declined as a result of decreasing temperature and decreasing thermal gradient. Smaller thermal stresses develop in the vertical direction (not shown). This is a result of the free-moving ground surface parallel to the extension of the heat source, and hence, a lack of mechanical confinement in the vertical direction.

Figure 6.5.11-1b shows that, near the ground surface, a zone of tensile stresses exists. This zone of tension is caused by the redistribution of horizontal compressive stresses from the relatively cool regions near the ground surface towards hot regions near the repository level. This redistribution of stresses preserves the balance of horizontal force over the entire vertical extent of the model. The evolution of thermal stresses calculated for the mountain-scale THM model is consistent with that of the drift-scale THM model (BSC 2004 [DIRS 169864], Section 6.5.2). The exception is for areas adjacent to the drift wall and for areas near the ground surface. The drift-scale model contains more refined discretization gridblocks near the drift wall and is therefore more accurate for calculation of stresses within a zone of about one drift diameter. Far away from the drift, the mountain-scale model is more accurate, since it captures the redistribution of stresses from the cooler regions near the ground surfaces toward hotter regions near the heat source. The impact of near-surface tensile stress is discussed in Section 6.5.14.

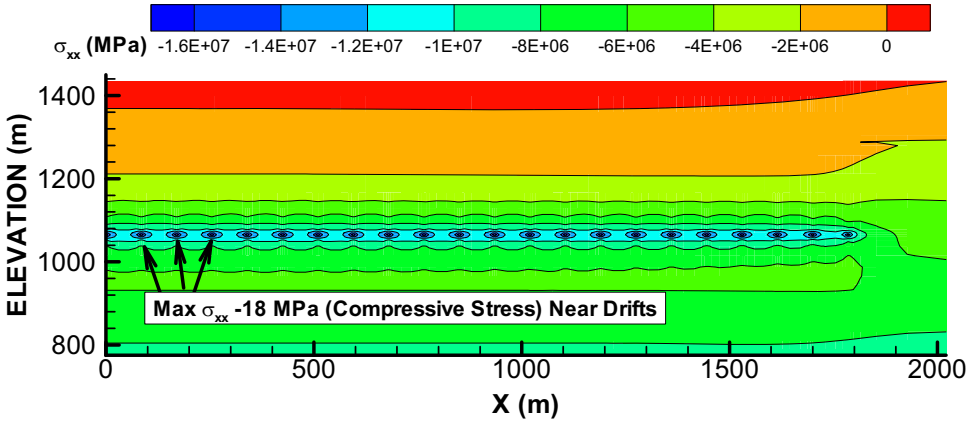

(a) 100 Years

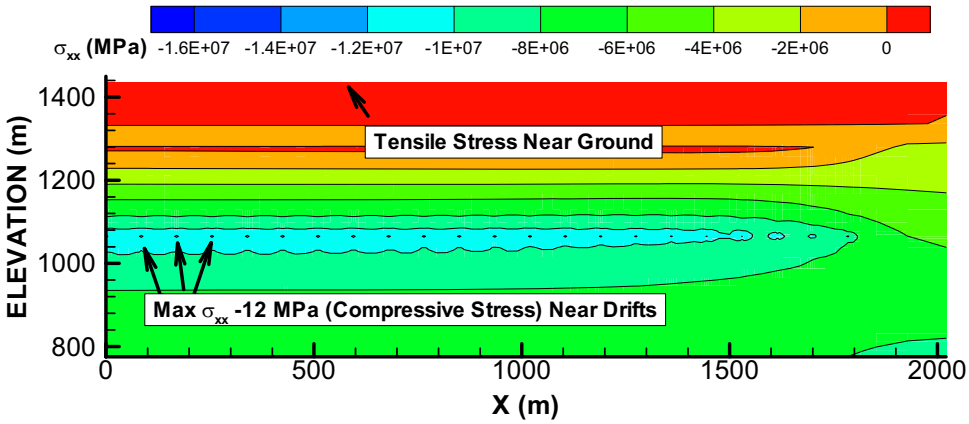

(b) 1,000 Years

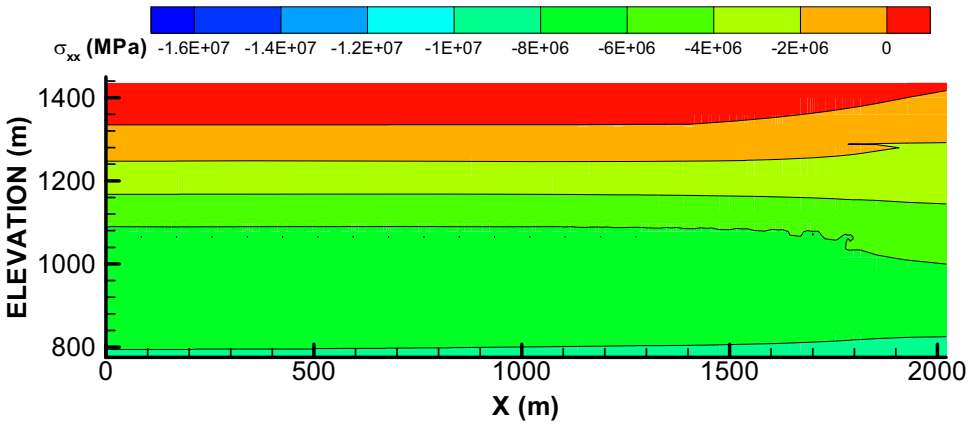

(c) 10,000 Years

Output DTN: LB0310MTSCLTHM.002.

Figure 6.5.11-1. Evolution of Horizontal Stress (σ_{xx}) in the Mountain

6.5.12 Evolution of Hydraulic Properties

Figures 6.5.12-1 through 6.5.12-2 present vertical and horizontal permeability change factors at 100, 1,000, and 10,000 years for the case of b_{max} = 380 μm. The general results of the coupled THM analysis presented in Figures 6.5.12-1 and 6.5.12-2 show that TM-induced compressive stresses around the repository level act across fractures, closing them to a smaller aperture, with an associated decrease in permeability. The decreased aperture and permeability is also accompanied by an increase in capillary pressure (not illustrated) according to the Leverett scaling defined in Equation 6.5.5-6. Outside the heated region, near the ground surface, reduction in horizontal stresses tends to open vertical fractures, with the result of increase in the vertical permeability and reduction in capillary pressure. Such an increase in permeability immediately outside a heated region is consistent with observations at the Yucca Mountain DST (BSC 2004 [DIRS 169864], Figure 7.4.3-2). The calculation shows that the vertical permeability (Figure 6.5.12-1) changes much more than the horizontal (Figure 6.5.12-2), corresponding to the result that horizontal fractures stay open during the entire heating cycle, whereas vertical fractures tighten to their residual aperture. The horizontal fractures remain open because no significant thermal stress develops in the vertical direction, on account of the free-moving ground surface. Vertical fractures, on the other hand, close because thermal stresses develop in the horizontal direction. Throughout the entire 10,000-year simulation time, the calculated changes in permeability are within a factor of 0.3 to 5, whereas calculated changes in capillary pressure range between a factor of 0.7 to 1.2. At the repository unit, the vertical permeability decreases by a factor of about 0.6. These results are for the case of b_{max} = 380 μm, whereas smaller changes are obtained for the case of b_{max} = 200 μm (BSC 2004 [DIRS 169864], Appendix A).

Figure 6.5.12-3 presents vertical permeability change factors and permeability at 1,000 years along a vertical column at the left boundary of the model (representing the interior of the repository). The figure illustrates that a change factor ranging from 0.3 to 5 is relatively small compared to the general variability in permeability between different layers at the mountain.

The evolution of hydraulic properties calculated for the mountain-scale THM model is consistent with that of the drift-scale THM model (BSC 2004 [DIRS 169864], Section 6.6.1), but with slightly smaller changes obtained for the former. Furthermore, the increase in permeability at the ground surface was not captured in the drift-scale THM model (BSC 2004 [DIRS 169864], Section 6.6.1) because no zone of tensile stress developed in that analysis. The modeling of permeability changes near the ground surface (Figures 6.5.12-1 and 6.5.12-2) is likely to be more realistic in the mountain-scale model, because it captures the redistribution of stresses from the cooler regions near the ground surfaces toward hotter regions near the heat source (see Section 6.5.11).

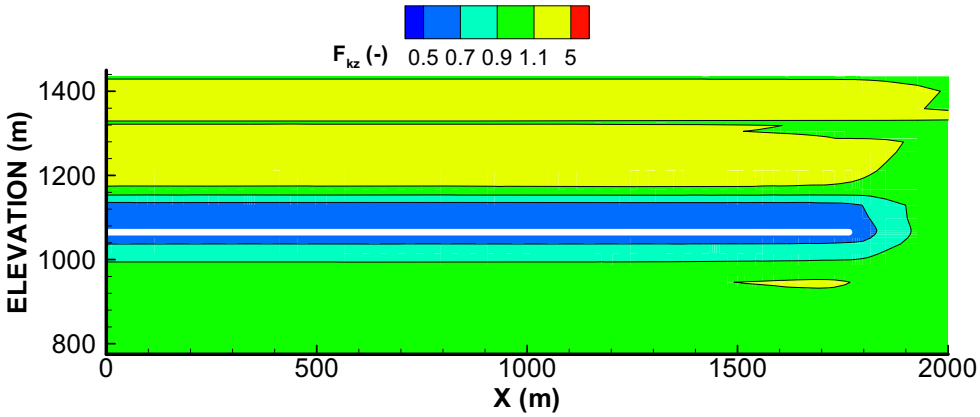

(a) 100 Years

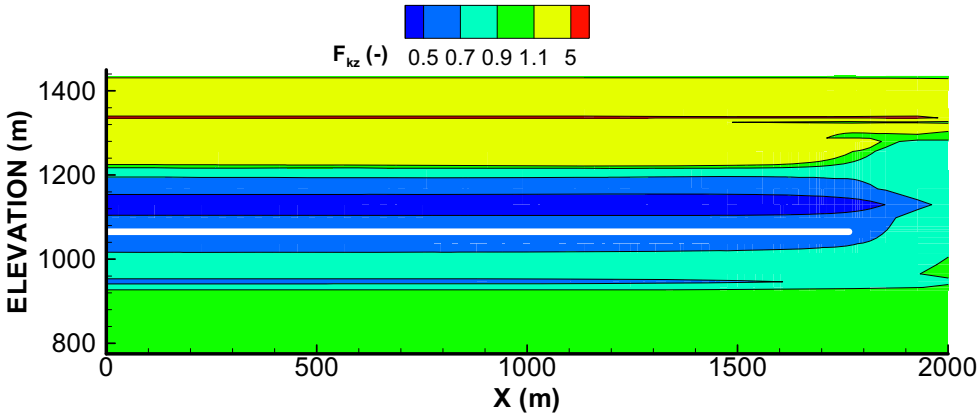

(b) 1,000 Years

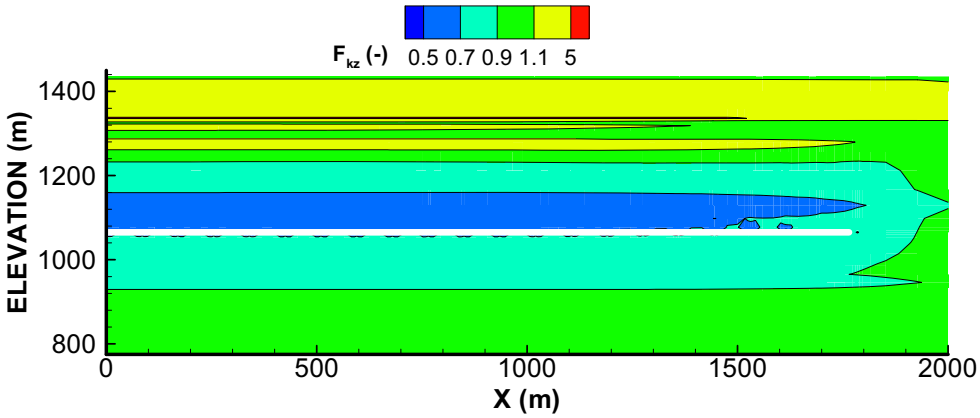

(c) 10,000 Years

Output DTN: LB0310MTSCLTHM.002.

Figure 6.5.12-1. Evolution of Vertical Permeability Correction Factor (F_{kz} = k_z/ki) Relative to Preemplacement Permeability

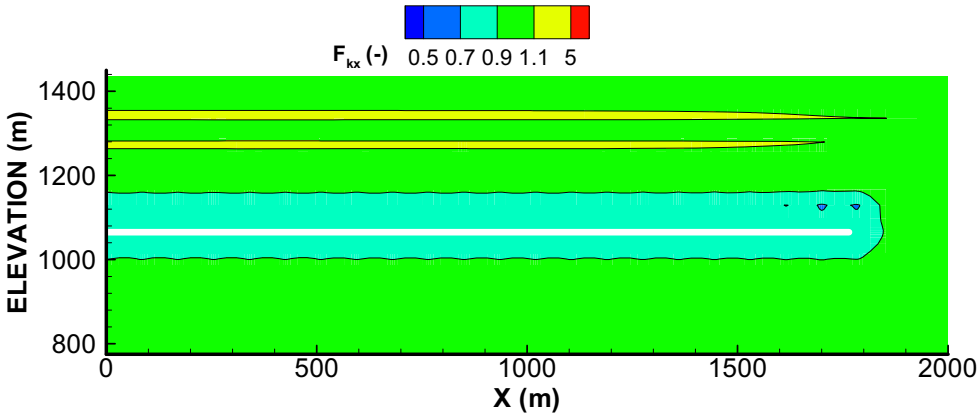

(a) 100 Years

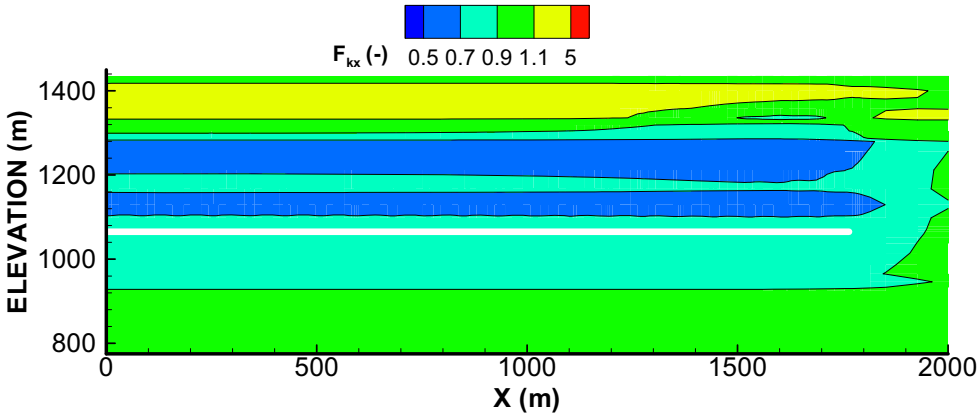

(b) 1,000 Years

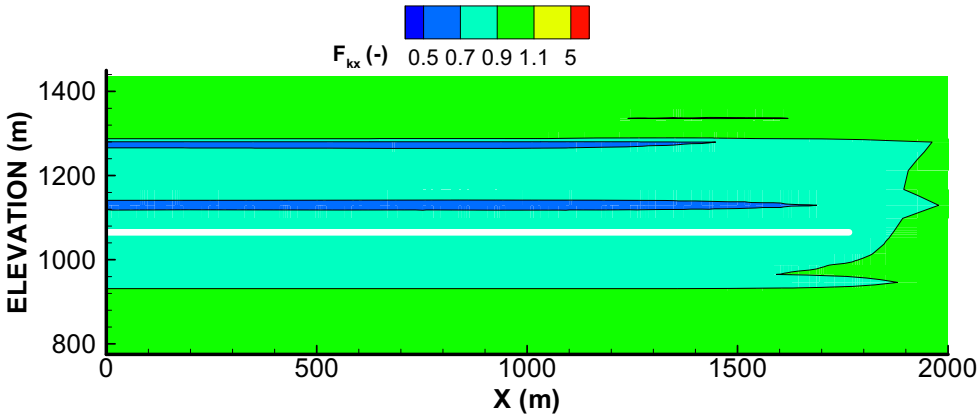

(c) 10,000 Years

Output DTN: LB0310MTSCLTHM.002.

Figure 6.5.12-2. Evolution of Horizontal Permeability Correction Factor ($F_{kx} = k_x/k_I$) Relative to Preemplacement Permeability.

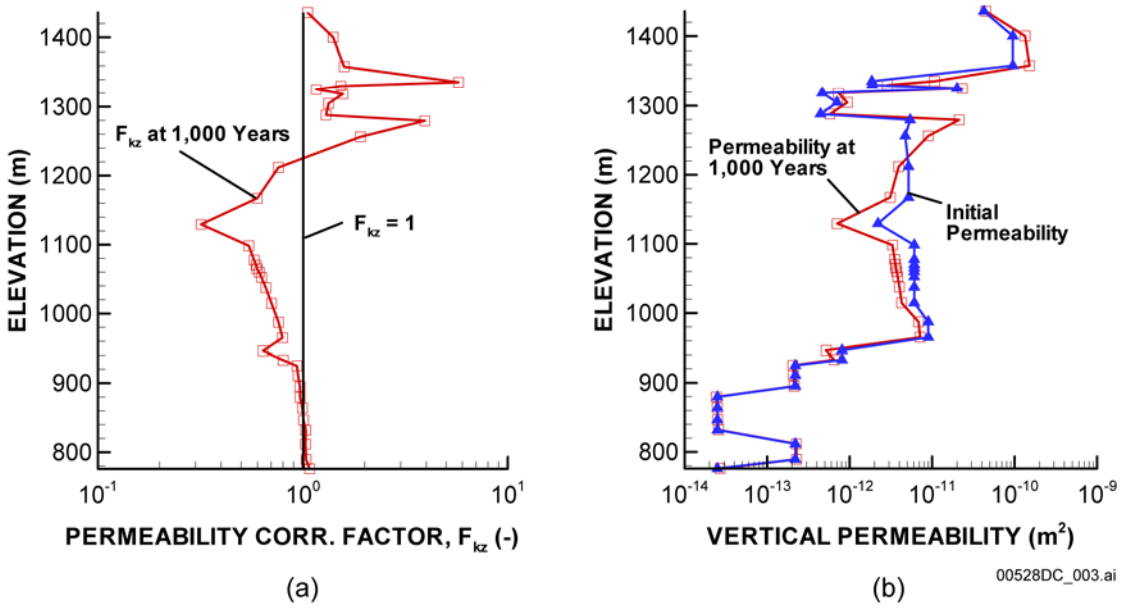

Output DTN: LB0310MTSCLTHM.002.

NOTE: (a) represents the vertical permeability correction factor ($F_{kz} = k_z/k_i$) at 1,000 years relative to preemplacement; (b) represents the vertical permeability at 1,000 years compared to preemplacement (initial) permeability.

Figure 6.5.12-3. Vertical Permeability at 1,000 Years along a Vertical Column at the Left Boundary of the Mountain-Scale THM Model Representing the Interior of the Repository

6.5.13 Fluid Flow Field

Figures 6.5.13-1 through 6.5.13-6 present the evolution of vertical-percolation-flux distribution in the mountain for both the TH and THM models. In both cases, above-boiling temperatures near the emplacement drift cause drying of the rock around the emplacement drifts. A dryout zone is formed around each drift, and diversion of the vertical flux around the dryout zone is predicted between 100 and 1,000 years. At 10,000 years, the results of TH and THM models are identical, because rewetting has taken place and temperatures are close to ambient. The simulated results of vertical flux distribution from the ground surface to the groundwater table, and the flow diversion around the drifts, are consistent with simulation results obtained in the drift-scale THM model (BSC 2004 [DIRS 169864], Section 6.6.2).

Figure 6.5.13-7 presents a profile of vertical flux through the repository level, for a detailed comparison of the TH solution with the THM solution. As explained in Section 6.5.2, in the TH simulation, the hydrologic properties of the rock mass are constant in time, which means that THM coupling is neglected in that case. Figure 6.5.13-7 shows that the vertical liquid flow is almost identical for TH and THM. This indicates that that there is no significant impact from THM coupling on the mountain-scale fluid flow field. One reason for the similarity in the flow field for TH and THM simulation cases is that the reduced vertical permeability in the THM case is accompanied by a higher relative permeability from increased liquid saturation. Thus, a THM-induced reduction in vertical permeability is compensated for by a higher relative permeability, leading to an unchanged flow mobility. The results show that THM coupling has

little impact on the mountain-scale fluid flow field, which is consistent with results of the drift-scale THM model (BSC 2004 [DIRS 169864], Sections 6.5 and 6.6).

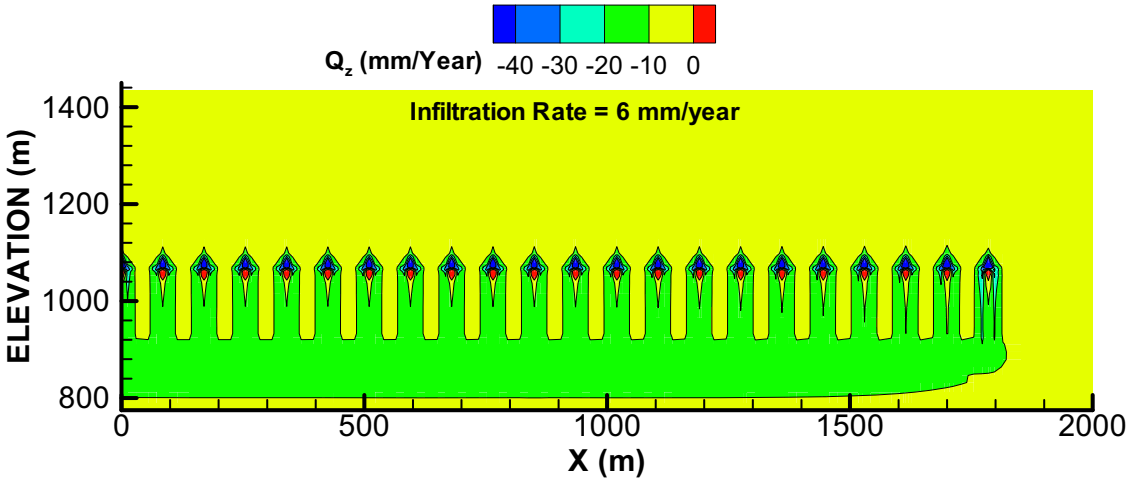

(a) TH Solution

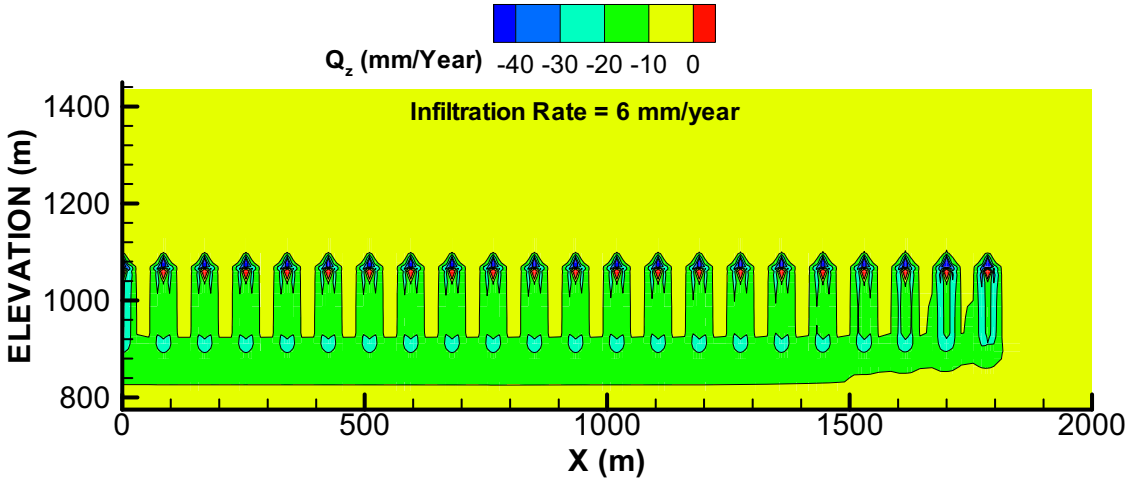

(b) THM Solution

Output DTN: LB0310MTSCLTHM.002.

NOTE: See also Figure 6.5.13-4.

Figure 6.5.13-1. Distribution of Vertical Percolation Flux (Q_z) at 100 Years after Emplacement for (a) TH and (b) THM Solutions

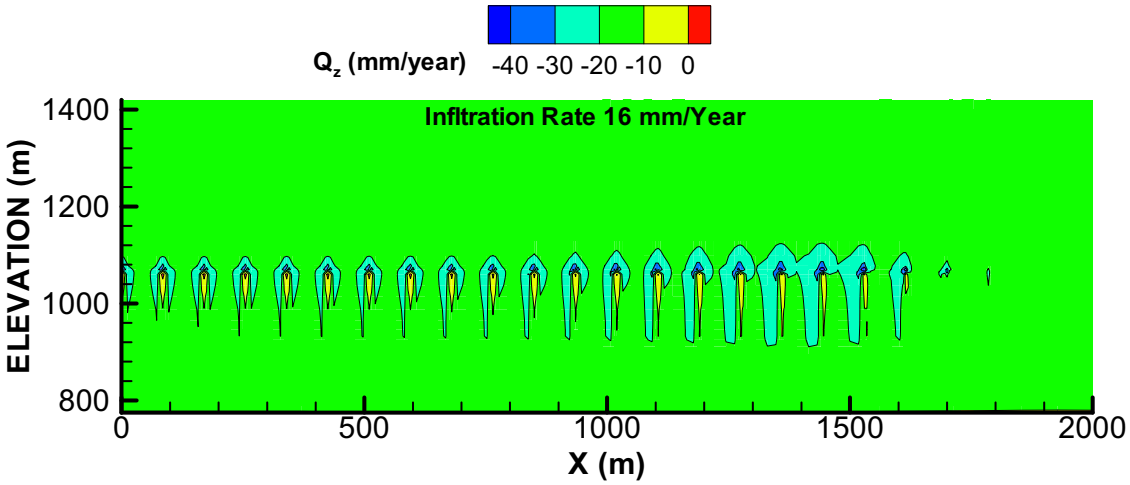

(a) TH Solution

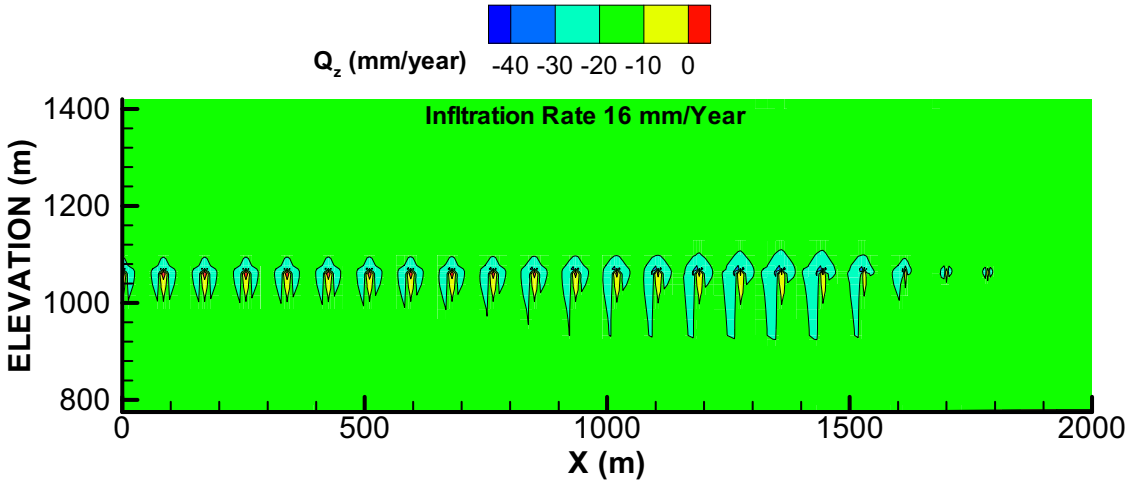

(b) THM Solution

Output DTN: LB0310MTSCLTHM.002.

NOTE: See also Figure 6.5.13-5.

Figure 6.5.13-2. Distribution of Vertical Percolation Flux (Q_z) at 1,000 Years after Emplacement for (a) TH and (b) THM Solutions

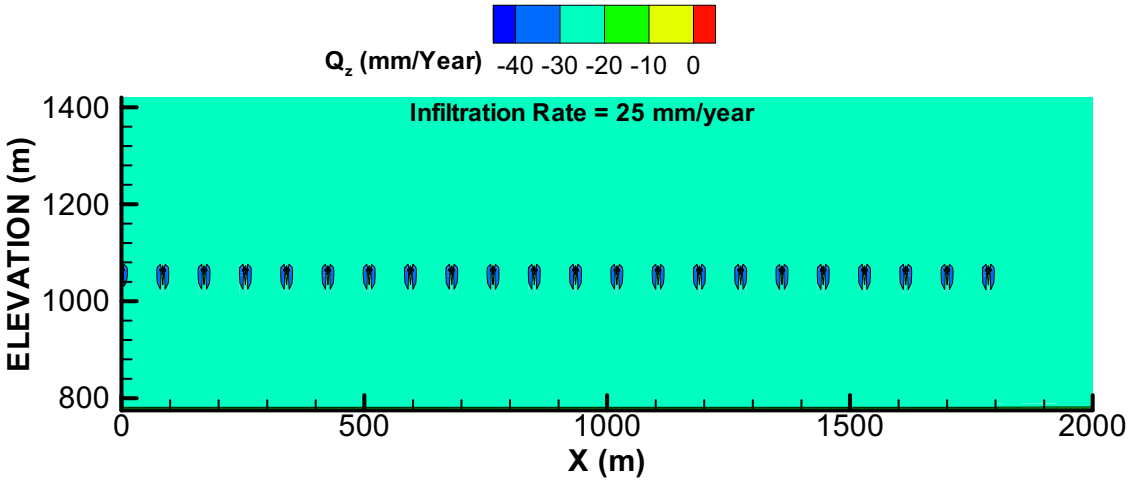

(a) TH Solution

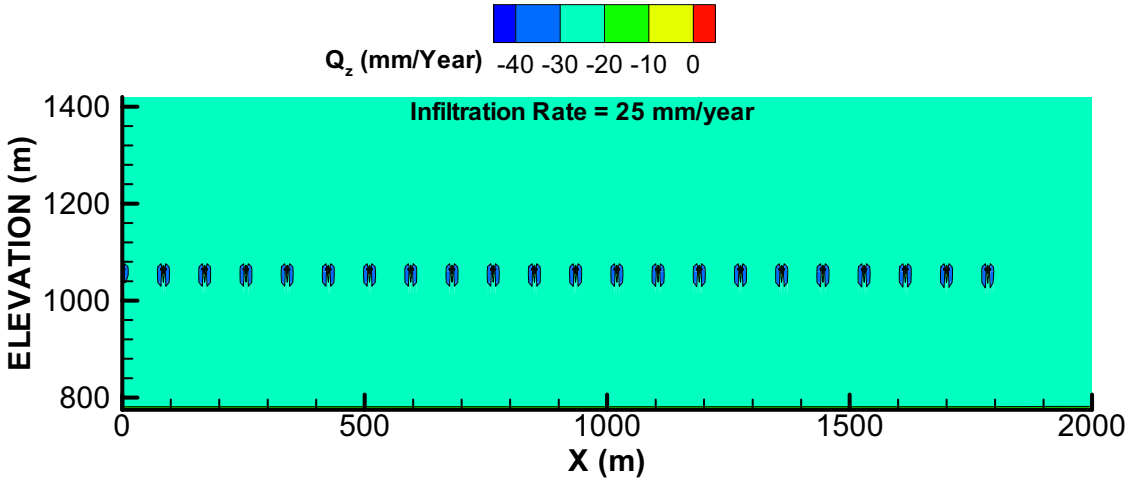

(b) THM Solution

Output DTN: LB0310MTSCLTHM.002.

Figure 6.5.13-3. Distribution of Vertical Percolation Flux (Q_z) at 10,000 Years after Emplacement for (a) TH and (b) THM Solutions

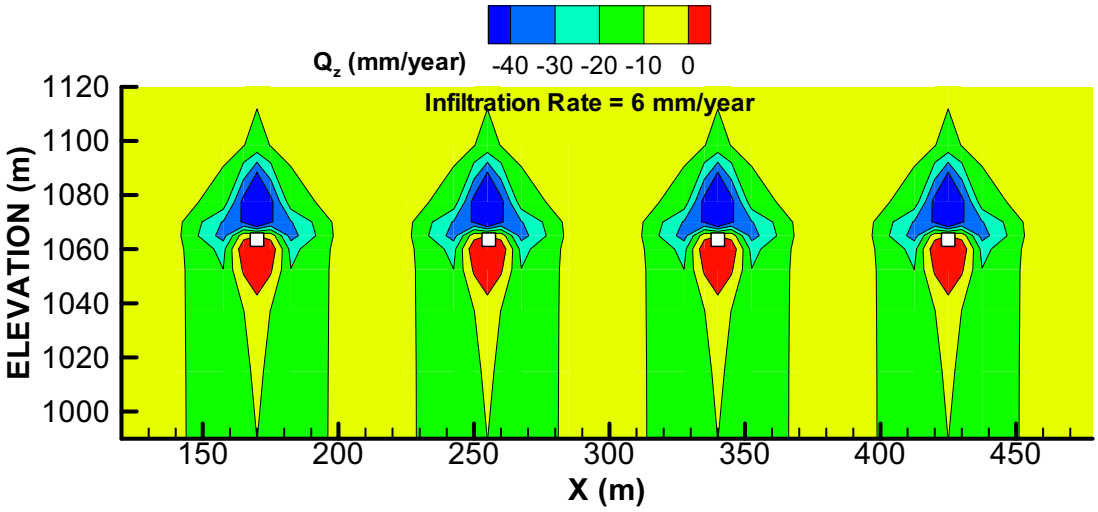

(a) TH Solution

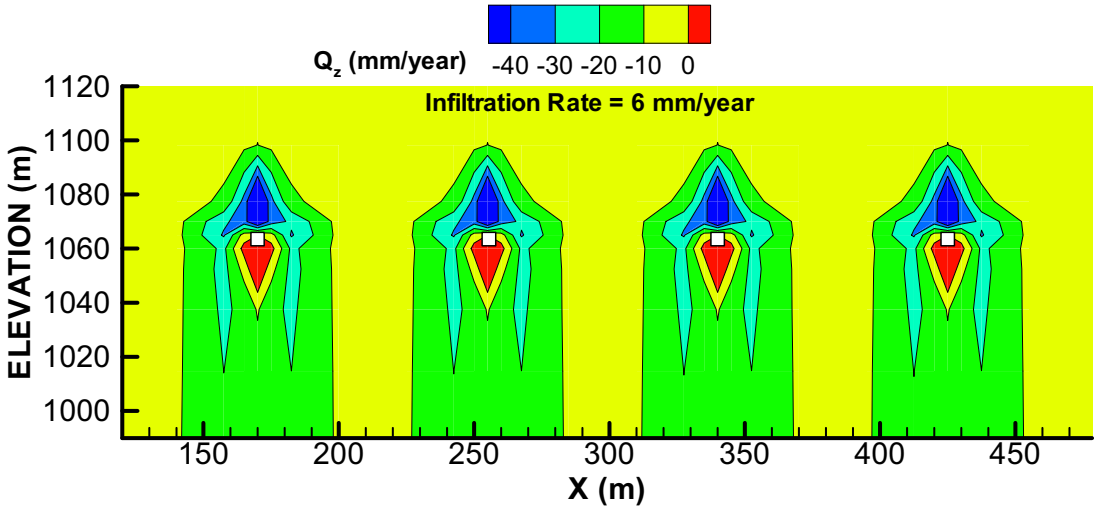

(b) THM Solution

Output DTN: LB0310MTSCLTHM.002.

Figure 6.5.13-4. Distribution of Vertical Percolation Flux near Four Emplacement Drifts in the Interior of the Repository (Q_z) at 100 Years after Emplacement for (a) TH and (b) THM Solutions

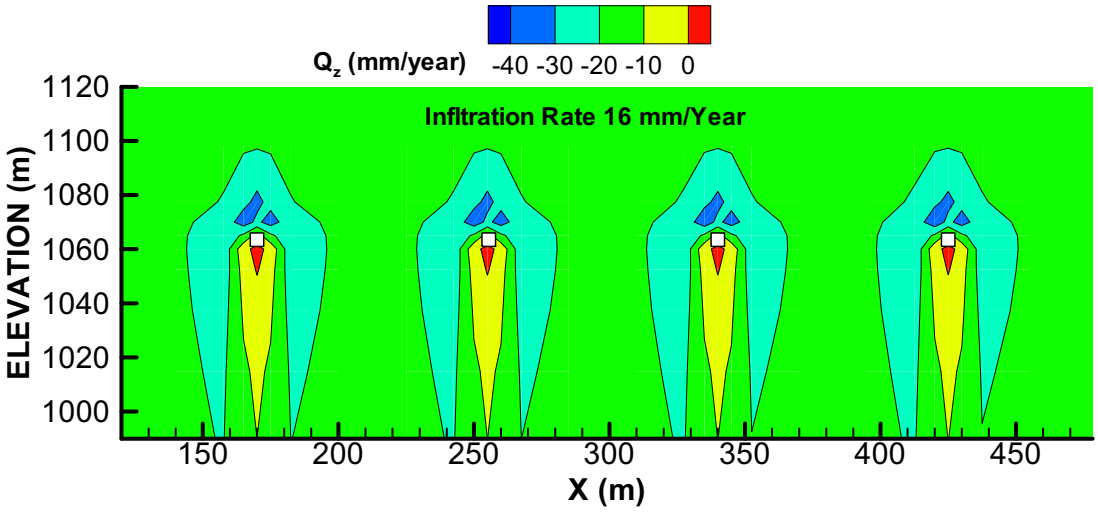

(a) TH Solution

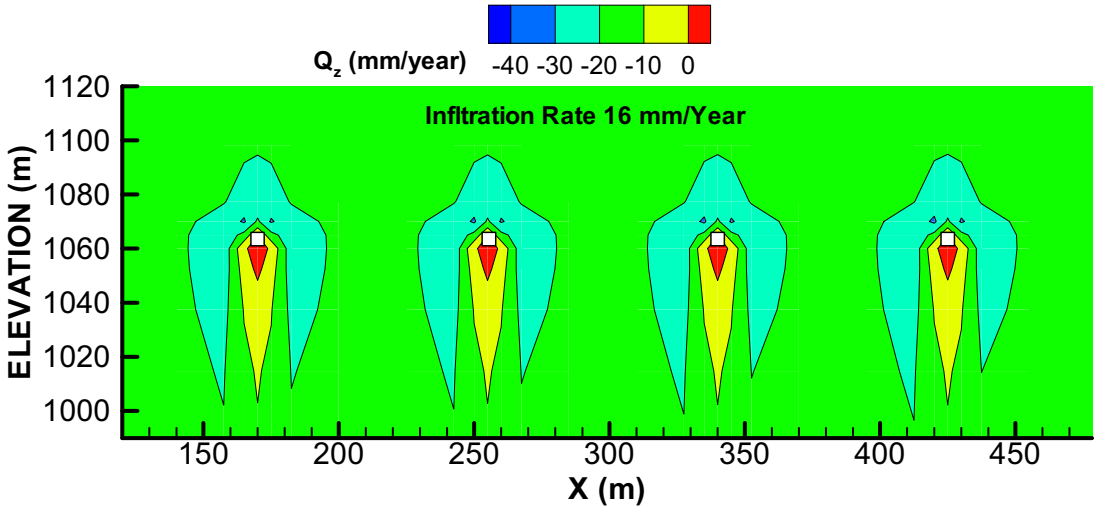

(b) THM Solution

Output DTN: LB0310MTSCLTHM.002.

Figure 6.5.13-5. Distribution of Vertical Percolation Flux near Four Emplacement Drifts in the Interior of the Repository (Q_z) at 1,000 Years after Emplacement for (a) TH and (b) THM Solutions

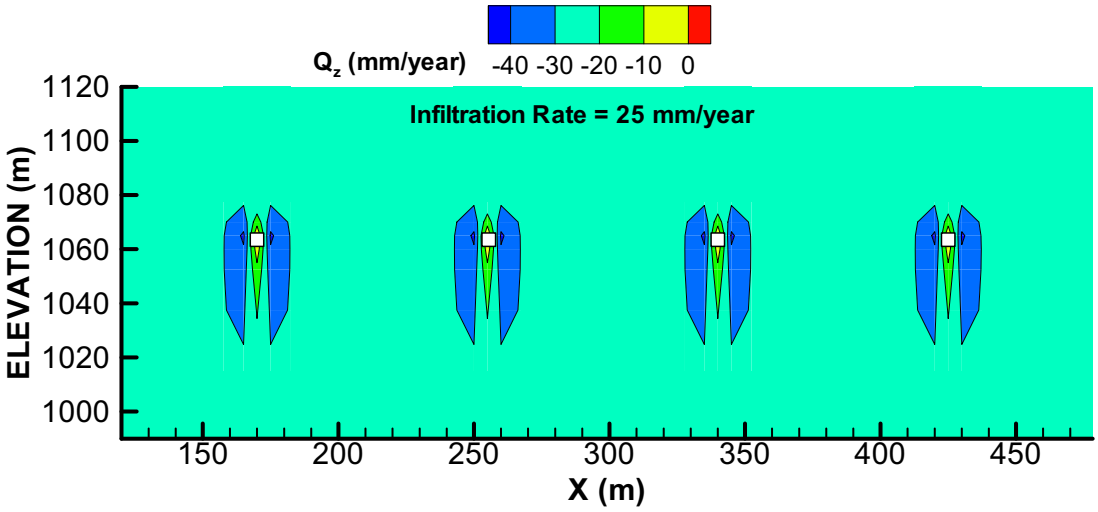

(a) TH Solution

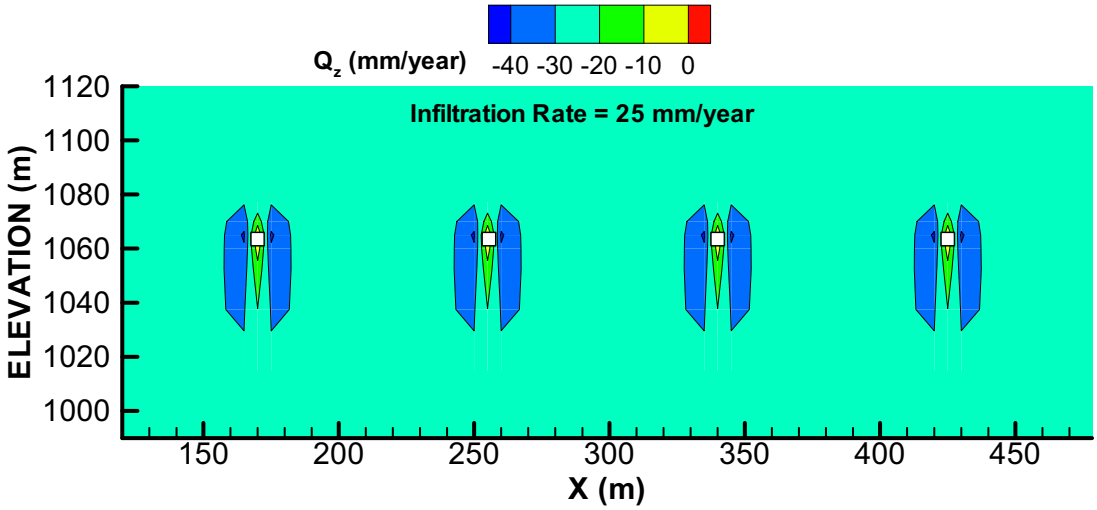

(b) THM Solution

Output DTN: LB0310MTSCLTHM.002.

Figure 6.5.13-6. Distribution of Vertical Percolation Flux near Four Emplacement Drifts in the Interior of the Repository (Q_z) at 10,000 Years after Emplacement for (a) TH and (b) THM Solutions

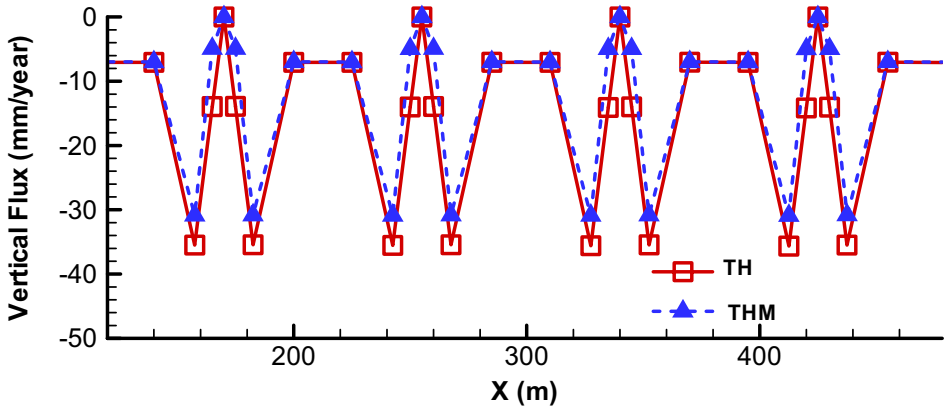

(a) 100 Years

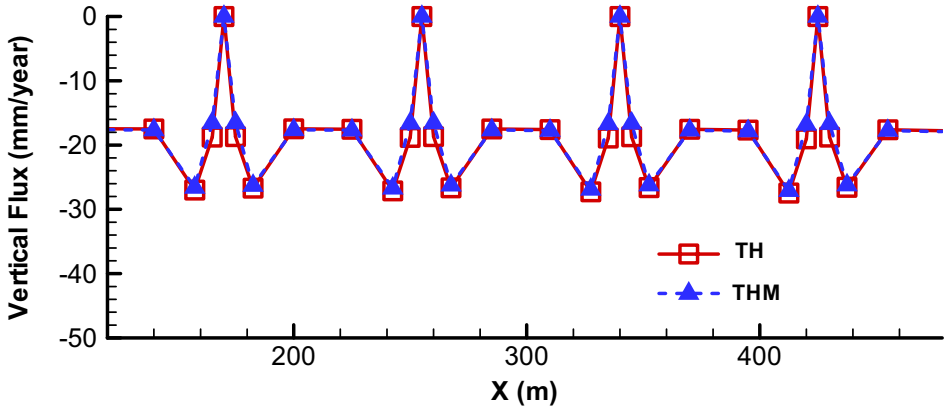

(b) 1,000 Years

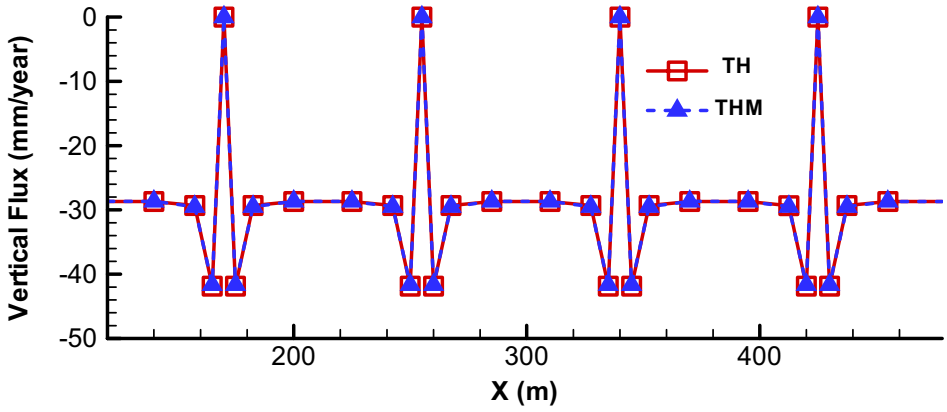

(c) 10,000 Years

Output DTN: LB0310MTSCLTHM.002.

Figure 6.5.13-7. Vertical Percolation Flux (Q_z) across the Repository Horizon near Four Emplacement Drifts for a TH Simulation and a THM Simulation

6.5.14 Impact of Possible Fracturing and Shear Slip near Ground Surface

The stress analysis presented in Section 6.5.11 showed that a zone of horizontal tensile stresses develops near the ground surface (Figure 6.5.11-1). In reality, tensile stresses would lead to fracturing and/or complete opening of preexisting fractures. Furthermore, in this zone of complete unloading of compressive stresses (compressive stress relief), the shear strength along fractures is reduced, and as a result shear slip can occur. Fracturing and shear slip along preexisting fractures leads to additional fracture opening and permanent (irreversible) changes in hydraulic properties. The possible permeability changes caused by such fracturing and shear slip near the ground surface were not fully accounted for in the coupled THM analysis of Sections 6.5.10 to 6.5.13. Therefore, the possible effects of such changes are evaluated in this section.

The potential for shear slip is evaluated from the ratio of shear stress to normal stress (σ_s/σ_n). A high ratio (when the shear stress is large compared to the normal stress) means that the potential for shear slip is greater. Figure 6.5.14-1 presents the evolution of xz-shear stress. At 100 years, the highest shear stress develops near repository drifts and at the edge of the repository. The shear stresses are high near the repository drifts at 100 years because it is a few tens of years after the end of the ventilation period, when the temperature at the repository drift peaks and the thermal gradient is the highest. At 1,000 years, the shear stresses near the drifts have decreased, while the zone of high shear stress near the edge of the repository has expanded and propagated towards the ground. At 10,000 years, the shear stresses have decreased further, with some remaining at the edge of the repository.

The potential for shear slip was evaluated by contouring the σ_s/σ_n ratio from stresses acting on vertical and horizontal fractures for 100, 1,000, and 10,000 years. The potential for shear slip along vertical fractures was evaluated by plotting the ratio σ_x/σ_{xz}, where σ_x is the stress in the x-direction (i.e., normal to vertical fractures) and σ_{xz} is the shear stress along vertical fractures. Similarly, the potential for shear slip along horizontal fractures is evaluated by plotting the ratio σ_z/σ_{xz}. Figure 6.5.14-2 shows the results at 1,000 years, which is the time when the highest potential for shear slip occurs. In recent studies of crystalline rock, it has been found that high-permeability fractures are frequently oriented such that the ratio $\sigma_s/\sigma_n \approx 0.6$ (Barton et al. 1995 [DIRS 153826]). Using a conventional Coulomb criterion for shear failure along a fracture (Jaeger and Cook 1979 [DIRS 106219], Section 4.6), a shear-slip ratio of $\sigma_s/\sigma_n = 0.6$ corresponds to zero cohesion and a friction angle of about 31°. Based on the above-mentioned field observations by Barton et al. (1995 [DIRS 153826]), an σ_s/σ_n ratio above 0.6 is likely to induce shear slip with accompanying permeability enhancement. Figure 6.5.14-2 indicates that the highest potential for shear slip is along vertical fractures in regions near the ground surface. For horizontal fractures, on the other hand, σ_s/σ_n is less than 0.6, and therefore shear slip is not likely along horizontal fractures. Note that the red contours in Figure 6.5.14-2a generally coincide with areas of complete unloading of tensile stresses, which means that the shear strength goes to zero.

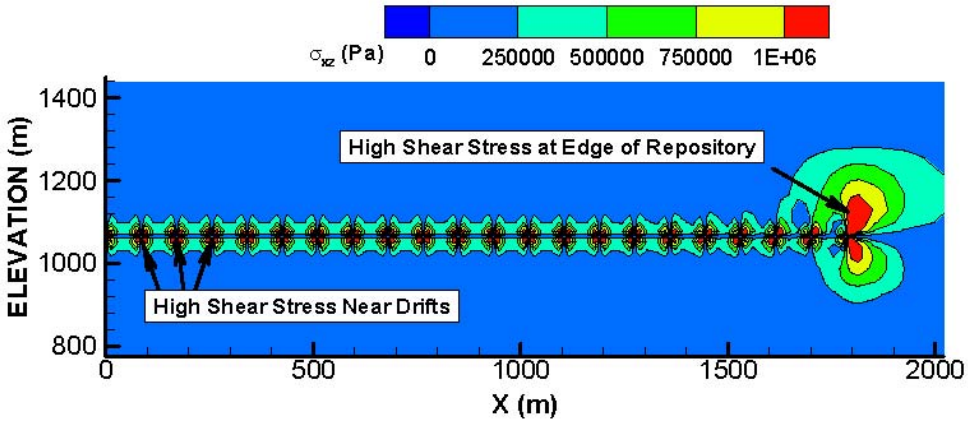

(a) 100 Years

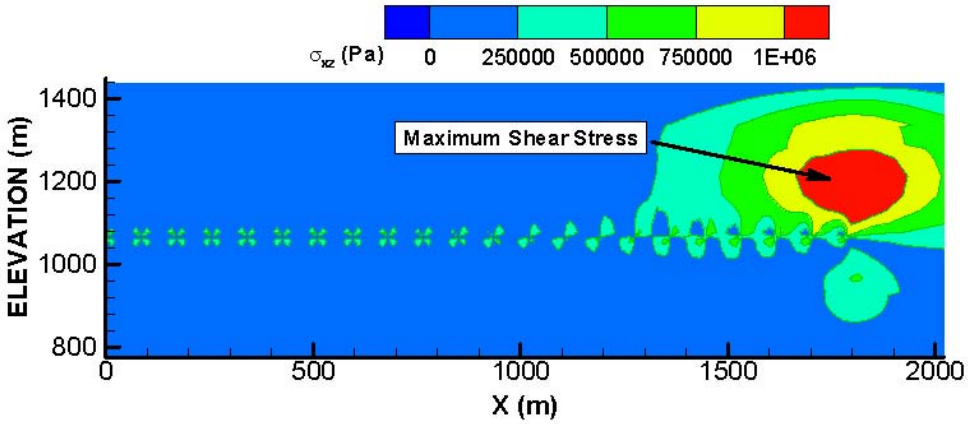

(b) 1,000 Years

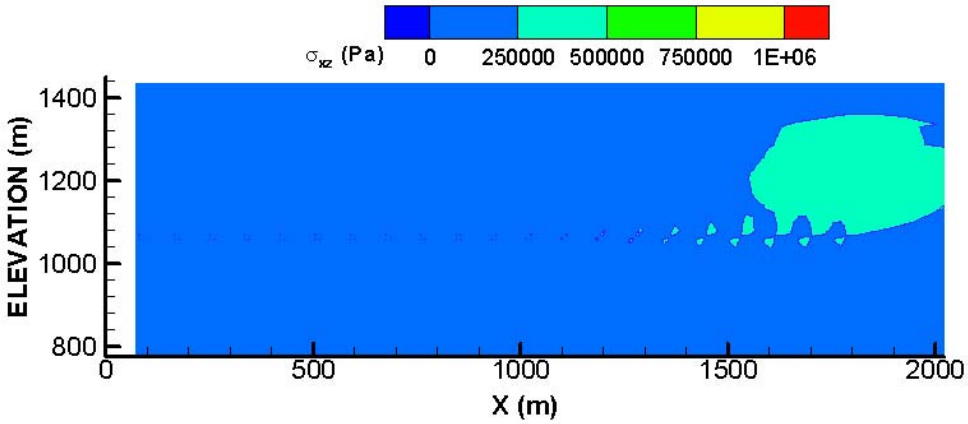

(c) 10,000 Years

Output DTN: LB0310MTSCLTHM.002.

Figure 6.5.14-1. Evolution of xz Shear Stress (σ_{xz}) in the Mountain

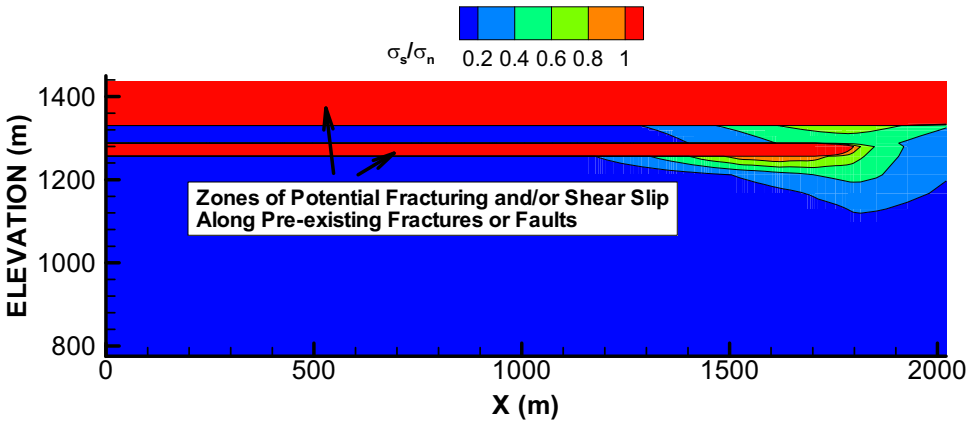

(a) Vertical Fractures

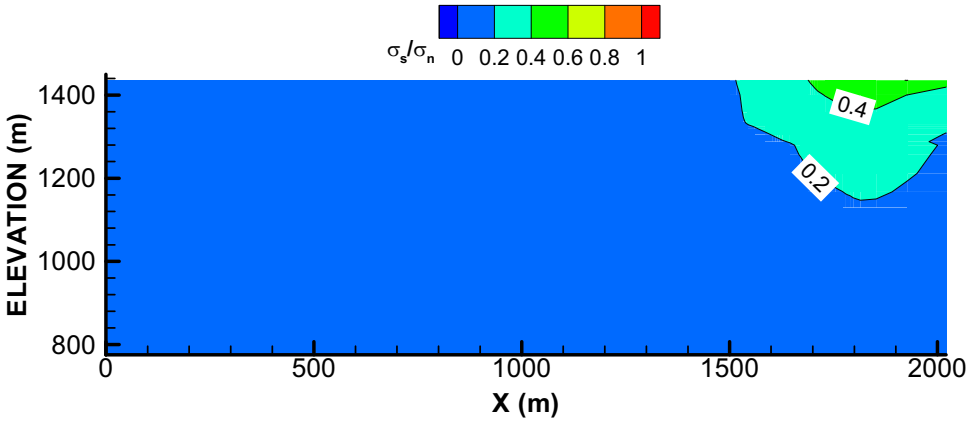

(b) Horizontal Fractures

Output DTN: LB0310MTSCLTHM.002.

Figure 6.5.14-2. Ratio of σ_s/σ_n from Stresses Acting on Vertical and Horizontal Fractures in the Mountain at 1,000 years

Fracturing and shear slip at the ground surface could create permanent (irreversible) permeability changes that would last well over 10,000 years. The magnitude of permanent permeability increases is difficult to estimate because of lack of field evidence at a mountain scale. Laboratory tests of shear versus permeability generally show that permeability increases by 1 to 2 orders of magnitude during shearing (Rutqvist and Stephansson [DIRS 162583], p. 17). This would represent a fully dilated fracture during shear. A further estimate of the possible permeability increase may be derived from detailed air-permeability tests in niches conducted at Yucca Mountain (BSC 2004 [DIRS 170004], Section 6.1). These tests show that the small-scale fracture permeability ranges roughly over three orders of magnitude. The largest measured fracture permeability values are likely to represent fully dilated shear fractures that have unmated fracture surfaces. The variability of in situ fracture permeability would also be affected by fracture properties such as roughness and degree of mineral filling. However, an upper-bound estimate of possible increase during shear is obtained by assuming that a three-order-of-magnitude variability in fracture permeability is caused by shear dilation of initial mated

fractures. Thus, an upper-bound estimate of possible permeability increase in the completely unloaded zone at the ground surface is three orders of magnitude.

An evaluation of the impact of a three-order-of-magnitude increase in permeability in the upper zones of Yucca Mountain is conducted through a steady-state flow simulation under 10,000 year conditions. The 10,000-year conditions are selected for this simulation because they represent the long-term conditions after the temperature has declined but permanent (irreversible) permeability changes in the upper part of the mountain would remain. The resulting vertical permeability distribution is depicted in Figure 6.5.14-3. In the zones of three-orders-of-magnitude permeability increase, the capillary pressure was reduced by one order of magnitude, which is a rough estimate based on Equation 6.5.5-6. Figure 6.5.14-4 shows a comparison of the vertical flow at the repository level, comparing this extreme case to the results of the partially coupled TH simulation presented in Figure 6.5.13-7c. It is indicated that the imposed extreme changes in permeability at the ground surface have no impact on the vertical flow field at the repository level. This shows that the infiltration rate and the hydraulic properties in the repository unit govern the flow field at the repository level. Note that the three-order-of-magnitude increase in permeability is overly conservative, since it was the upper-bound estimate of possible permeability increase in the completely unloaded zone at the ground surface (as discussed previously). Therefore, it is not suitable for any consideration on modification of the infiltration rate.

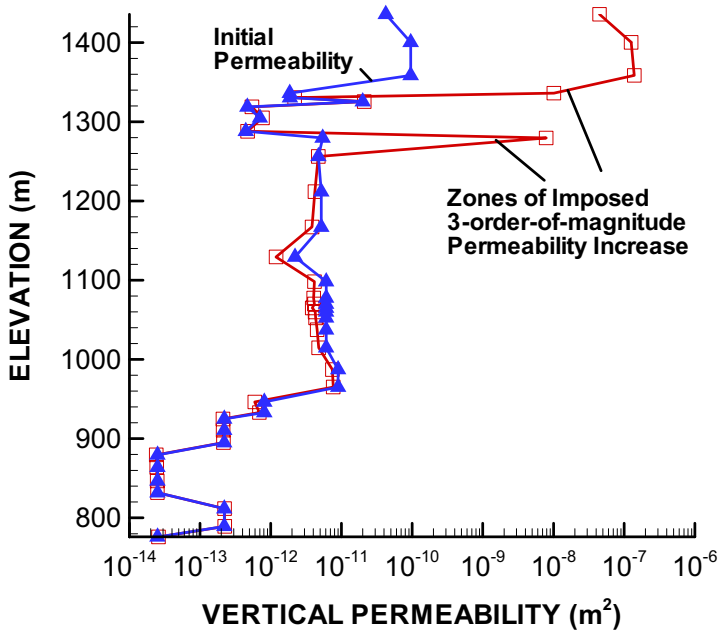

Output DTN: LB0310MTSCLTHM.002.

NOTE: Units of the permeability increase are tcw11, tcw12, and tsw31 (see Table 6.1-1).

Figure 6.5.14-3. Vertical Permeability at 10,000 Years along a Vertical Column at the Left Boundary of the Mountain-Scale THM Model, with an Imposed Three-Order-of-Magnitude Permeability Increase in Zone of Possible Fracturing near Ground Surface

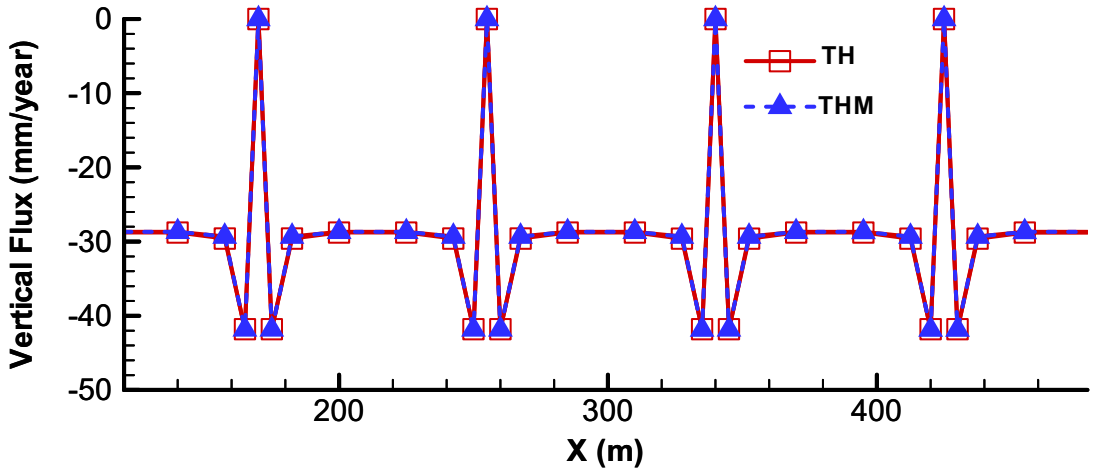

Output DTN: LB0310MTSCLTHM.002.

Figure 6.5.14-4. Comparison of the Vertical Percolation Flux (Q_z) at 10,000 Years across the Repository Horizon near Four Emplacement Drifts for a TH Simulation and a Coupled THM Simulation, with Imposed Three-Order-of-Magnitude Permeability Change in Zone of Stress Relief Near Ground Surface

6.5.15 Discussion of Uncertainties in the Mountain-Scale THM Results

The model predictions in this analysis depend on a sufficiently accurate representation of TM-induced changes in hydraulic properties, and in particular changes in fracture permeability. In this context, potential sources for uncertainties were discussed in *Drift Scale THM Model* (BSC 2004 [DIRS 169864], Section 6.10): (1) simplified conceptualization of the fracture network geometry, (2) drift-wall inelastic behavior, (3) possible fracture-shear-induced permeability enhancement, (4) fracture stress-versus-permeability relationships, (5) effects of heterogeneous rock properties, and (6) mechanical properties of the Tptpll unit. Uncertainties related to hydrologic and thermal properties, and to hydrologic conditions such as infiltration rate, are most relevant for prediction of TH responses, whereas they are of secondary importance for estimating TM-induced changes in hydraulic properties. For example, uncertainties in the thermal conductivity and thermal boundary conditions impact the temperature evolution and thereby the magnitude of the TM-induced stresses. However, in *Drift Scale THM Model* (BSC 2004 [DIRS 169864], Section 6.10), it was concluded that the fracture normal stress-versus-permeability relationship is the most important for assessing the impact of coupled THM processes.

This relationship (discussed in BSC 2004 [DIRS 169864], Section 6.10.4) is the basis for quantitative assessment of stress-induced changes in hydraulic properties around the repository. It provides for an estimate of the relative change in permeability caused by changes in stresses. In *Drift Scale THM Model* (BSC 2004 [DIRS 169864]), the upper and lower limits of the normal stress-versus-permeability relationship were determined and validated against field experiments at Yucca Mountain. The stress-permeability relationship adopted for the predictive analysis with the drift-scale THM model (BSC 2004 [DIRS 169864], Section 6.4) tends to result in larger

permeability changes, and hence to have a larger impact on the percolation flux. It was concluded that model results in *Drift Scale THM Model* (BSC 2004 [DIRS 169864], Sections 6.5 and 6.6) were upper-bound estimates of the impact of repository heating on stress and permeability changes, based on the estimates of input THM properties (thermal expansion coefficient and stress-versus-permeability function). This was deemed sufficient for bounding the possible impact of the THM processes on permeability and percolation flux at the drift-scale. An additional uncertainty for the mountain-scale THM model is the up-scaling of THM properties from drift scale to that of mountain scale. The up-scaling of THM properties was discussed in Section 6.5.9. The adopted THM properties (thermal expansion coefficient and stress-versus-permeability relationship) for the mountain scale are based on up-scaling from the estimated drift-scale properties in a fashion that maximizes the effect of stress and permeability changes. Moreover, the flow simulation investigating the potential impact of fracturing and shear slip in areas of stress relief near the ground surface was conducted by imposing a three-order-of-magnitude increase in permeability. Hence, the model results obtained in Sections 6.5.10 through 6.5.14 of this report are obtained for estimates of the input THM properties which are sufficient for bounding the possible impact of THM processes on permeability and percolation flux at the mountain scale. If thermal conductivity were lower, then the repository would be hotter and thermal stress would be greater. However, the fractures are already near residual aperture, so the effect on hydrology would be no greater. If thermal conductivity were higher, the repository would be cooler, and the effect would be less than predicted. Similarly, the fixed temperature boundary at the bottom of the model may lead to a slightly lower temperature and, hence, lower thermal stress in the bottom part (below the repository) of the model. Again, because fractures near the bottom of the model are highly compressed by the initial stresses they are close to their residual aperture and therefore a slight change in thermal stress would not impact the hydrology significant. Figure 6.5.12-3 illustrates very well the fact that changes in the lower part of the model is small, because the fractures are compressed near their residual aperture already at pre-heating conditions.

INTENTIONALLY LEFT BLANK

7. VALIDATION

Results from this mountain-scale coupled processes model report are used in *Features, Events, and Processes in UZ Flow and Transport* (BSC 2005 [DIRS 174191]), and in *Features, Events, and Processes in SZ Flow and Transport* (BSC 2005 [DIRS 174190]), to provide the technical basis for the screening of several THC and THM processes from the TSPA model, and to support other FEPs screening arguments. The mountain-scale models are primarily used to assess the significance of THC and THM processes on the overall flow regime. Outputs from this report are also used to corroborate and build confidence in the results of the multiscale thermohydrologic model (BSC 2005 [DIRS 173944]), which provides direct input to the TSPA model. However, output from this report is not a direct feed to TSPA.

Based on the uses of the mountain-scale coupled processes models, Level I validation (mountain-scale TH and THM models) or Level II validation (mountain-scale THC model) has been determined to provide an appropriate level of confidence, as detailed in *Technical Work Plan for: Near-Field Environment and Transport: Coupled Processes (Mountain-Scale TH/THC/THM, Drift-Scale THC Seepage, and Drift-Scale Abstraction) Model Report Integration* (BSC 2005 [DIRS 174842], Section 2.2.1.1).

Confidence Building During Model Development

For Level I and II validation, the relevant procedures specify:

1. *Selection of input parameters and/or input data, and a discussion of how the selection process builds confidence in the model [LP-SIII.10Q-BSC, Section 5.3.2(b)(1)].*

   The inputs to the mountain-scale coupled processes models have been obtained from appropriate sources (see Table 4.1-1, Section 4.1). Qualified, site-specific data have been used as direct input: for example, net infiltration rates were obtained from site-specific studies and used to develop percolation flux estimates. Where appropriate for the mountain scale, input data and conceptual details were selected during development to be consistent with the corresponding drift-scale models, which in turn were developed using results from in situ field testing of TH, THC, and THM processes. Detailed descriptions of model concepts are found in Sections 6.1, 6.4.1 and 6.5.1. Further discussion of confidence building during model development, and of scale dependence, is provided in Sections 7.2 through 7.4. Based on these measures this requirement is considered satisfied.

2. *Description of calibration activities, and/or initial boundary condition runs, and/or run convergences, and a discussion of how the activity or activities build confidence in the model. Include a discussion of impacts of any run non-convergences [LP-SIII.10Q-BSC, Section 5.3.2(b)(2)].*

   Detailed discussion of initial and boundary conditions for the mountain-scale coupled processes models is found in Sections 4.1, 6.1.3, 6.4.2.3, 6.4.2.4, and 6.5.6. Sections 6.2 and 6.3 describe the results of the two-dimensional and three-dimensional TH models, Section 6.4.3 describes the mountain-scale THC model results, and Sections 6.5.10

through 6.5.14 describe the results of the mountain-scale THM model. No calibration was performed for the mountain-scale models. Discussion of nonconvergence runs is not relevant for this report because all simulations satisfied convergence criteria for the numerical codes used. Thus, this requirement is considered satisfied.

3. *Discussion of the impacts of uncertainties [LP-SIII.10Q-BSC, Section 5.3.2(b)(3)].*

   Because the results from mountain-scale coupled processes models are not used as direct input to the TSPA, quantitative characterization of uncertainties in model output is not performed. However, uncertainty that potentially affects FEP screening (BSC 2005 [DIRS 174191]) is qualitatively addressed in this report, in Sections 7.2 through 7.4. Uncertainty evaluation also includes dimensional sensitivity (2-D or 3-D) of TH models (Section 8.1), and uncertainty in the THM model results (Section 6.5.15). Given the intended use of the mountain-scale models, this approach provides an adequate understanding of the impacts of uncertainties.

Validation and Confidence Building After Model Development

In addition to the steps described above, Section 2.2.1.2 of the TWP (BSC 2005 [DIRS 174842]) also specifies the use of methods for validation of the mountain scale coupled process models after development:

1. *Corroboration of model results with data acquired from the laboratory, field experiments, analog studies, or other relevant observations, not previously used to develop or calibrate the model [LP-SIII.10Q-BSC, Section 5.3.2(c), Method 1].*

   Comparison of model results with field-testing data (for example the Single Heater Test and the Drift Scale Test; see BSC 2004 [DIRS 169900], Sections 6.2 and 6.3) is the major method of validation for coupled-process models. The drift-scale models were previously validated using comparison with field-testing data, documented in separate reports (BSC 2005 [DIRS 172232], Section 7; BSC 2005 [DIRS 172862] Section 7; BSC 2004 [DIRS 169864] Section 7). Although the field-testing data were collected at scales smaller than the mountain-scale models, the approaches used to model coupled processes in the mountain-scale and the drift-scale models are similar, and in many respects identical. Therefore, successful validation of the drift-scale models using field-testing data provides confidence that mountain-scale models are valid, with appropriate consideration of scale-dependence and other differences between the models as discussed below. Sections 7.1.2, 7.2.2, and 7.3.2 describe this corroboration, and discuss explicitly how the criteria for this validation method, as defined in Section 2.2.1.4 of the TWP (BSC 2005 [DIRS 174842]), are met.

2. *Corroboration with information published in refereed journals or technical literature [LP-SIII.10Q-BSC, Section 5.3.2(c) Method 3].*

   This report also describes modeling efforts that are similar in scale (temporal or spatial) and technical approach, and are documented in peer-reviewed technical literature. Corroboration of the mountain-scale models by this means is evaluated with respect to

explicit criteria identified in Section 2.2.1.4 of the TWP (BSC 2005 [DIRS 174842]). Sections 7.1.4, 7.2.3, and 7.3.3 summarize this corroborating information.

3. *Technical review by reviewers independent of the development, checking, and review of the model documentation [LP-SIII.10Q-BSC, Section 5.3.2(c), Method 5].*

   The independent technical review for post-development validation addresses the use of the mountain-scale coupled processes models. The reviewers follow the review criteria for Method 5 of LP-SIII.10Q-BSC, Section 5.3.2(c) as discussed in Section 2.2.1.4 of the TWP (BSC 2005 [DIRS 174842]). The review criteria address these specific uses of the models. Sections 7.1.5, 7.2.4, and 7.3.4 describe this corroboration, and discuss explicitly how the criteria for this validation method, as defined in Section 2.2.1.4 of the TWP (BSC 2005 [DIRS 174842]), are met.

4. *Additional confidence-building through publication in a refereed professional journal [LP-SIII.10Q-BSC, Section 5.3.2(d)].*

   Modeling of mountain-scale TH behavior at Yucca Mountain has been presented in the open scientific literature (Haukwa et al. 2003 [DIRS 165165]) and provides additional confidence in the mountain-scale TH model. As discussed in Section 7.1.6, the modeling approach described in the article is the same as the current mountain-scale TH model with the exception of the value for ventilation efficiency (the published version uses 70% versus the current value of 86.3%). The importance of this difference is addressed.

5. *Corroboration of model results with analogue studies or other relevant observations [LP-SIII.10Q-BSC, Section 5.3.2(c), Method 2].*

   The conceptual and numerical models used in this report have been used in other applications to represent similar hydrologic, thermal, geochemical and mechanical processes. Although not required by the TWP (BSC 2005 [DIRS 174842], Section 2.2.1.2), this type of corroboration is provided as supplementary validation for the mountain-scale THM model in Section 7.3.5. Successful application in similar studies provides additional confidence that the mountain-scale coupled processes models are appropriate for their intended use.

The mountain-scale coupled processes models are used to assess the effects that repository induced changes to the natural system (thermal, hydrologic, geochemical and mechanical changes), have on flow (and related radionuclide transport) in the unsaturated zone at Yucca Mountain. The effects of heating on sorption properties used in the unsaturated zone transport model are addressed in *Radionuclide Transport Models Under Ambient Conditions* (BSC 2004 [DIRS 164500] Appendix I). For ambient conditions, tests and observations indicate that flow past the repository horizon in the Topopah Spring welded tuff (TSw) is primarily in a well-connected fracture network dominated by vertical or nearly vertical fractures. Flow is gravity driven, and the flux rates are constrained by surface infiltration and percolation from the surface to the repository horizon. Coupled TH/THC/THM processes could affect flow paths and seepage rates by altering the hydrologic properties of the rocks near the repository; however, as shown in Sections 6.4 and 6.5, the predicted changes are small and do not affect the

TH flow regime for both the near-field (BSC 2005 [DIRS 172232]) and the far-field (Sections 6.2 and 6.3).

Each of the following sections describes Level I or II validation of the specific mountain-scale model, following the directions stated in the TWP (BSC 2005 [DIRS 174842], Section 2.2.1 and its subsections).

7.1 VALIDATION OF THE MOUNTAIN-SCALE TH MODEL

The intended use of the mountain-scale TH model is to support evaluation of FEPs related to effects of coupled TH processes on mountain-scale UZ flow. The mountain-scale TH model supports the treatment of FEPs related to the TSPA component model "UZ Flow" (see BSC 2005 [DIRS 174191], Sections 6.9.9 and 6.9.16). In addition, the mountain-scale TH model provides a basis for the mountain-scale THC and THM models by establishing how TH processes are represented. Validation of the mountain-scale TH model provides the necessary validation for TH processes as they are represented in the THC and THM models. For such a model, the applicable planning procedure (LP-2.29Q-BSC, Attachment 3, Table 1) requires Level I validation. Implementation of Level I validation for the mountain-scale TH model is specified in Section 2.2.1.1 of the TWP (BSC 2005 [DIRS 174842]).

Validation of the mountain-scale TH model is achieved through confidence-building activities during model development (Section 7.1.1), by corroboration with the validation of the drift-scale TH model, as presented in *Drift-Scale Coupled Process (DST and TH Seepage) Models* (BSC 2005 [DIRS 172232]; see Section 7.1.2 below), by corroboration with relevant information from refereed technical publications (Section 7.1.4), and by technical review by reviewers independent of the development, checking, and review of the model documentation (Section 7.1.5). Additional confidence is provided by publication of the mountain-scale TH model (with minor differences, as discussed in Section 7.1.6). These measures provide confidence that the mountain-scale TH model is adequate for its intended use in FEP screening and to support the mountain-scale THC and THM models.

7.1.1 Summary of Confidence Building during Model Development

The requirements for validation of this TH model are presented in Section 2.2.1.2 of the TWP (BSC 2005 [DIRS 174842]). The mountain-scale TH model has been developed in accordance with the requirements of Section 5.3.2(b) of LP-SIII.10Q-BSC. Confidence building during model development in Sections 6.1, 6.2 and 6.3 of this TH model report involves the following items:

1. *Selection of input parameters and/or input data, and a discussion of how the selection process builds confidence in the model [LP-SIII.10Q-BSC, Section 5.3.2(b)(1)].*

   The inputs to the mountain-scale TH model have been obtained from controlled sources (see Section 4.1, Table 4.1-1), including discussion about selection of input parameters. Model assumptions have been described in Section 5. Detailed discussion about model concepts and input parameters can be found in Sections 6.1, 6.2, and 6.3. The input data to the model have been developed from the best available sources for this modeling

effort, based on site-specific information where appropriate. Calibrated, mountain-scale fracture permeability data are used. Model parameters developed from the input data are applied in a modeling framework consistent with the scale of test observations, and the scale of use in the mountain-scale model. Thus, this requirement is satisfied.

2. *Description of calibration activities, and/or initial boundary condition runs, and/or run convergences, simulation conditions set up to span the range of intended use and avoid inconsistent outputs, and a discussion of how the activity or activities build confidence in the model. Inclusion of a discussion of impacts of any non-convergence runs [(LP-SIII.10Q-BSC, Section 5.3.2(b)(2)].*

   Detailed discussion of initial and boundary conditions for the mountain-scale TH model is presented in Sections 6.1.3, 6.1.4, and 6.1.5. Sections 6.2 and 6.3 provide detailed discussion of various 2-D and 3-D model results, addressing the range of conditions studied and how this range is appropriate considering the intended use of the model. Discussion of nonconvergence is not relevant because convergence was achieved in all model runs. The use of qualified input data and design parameters, and appropriate boundary and initial conditions, helps to enhance confidence in the model during model development. The model inputs shown in Table 4.1-1 are generally site-specific and come from qualified sources, or are technically justified for use in this report. The boundary and initial conditions described in Section 6.1.3 are based on field-measured data and reasonable assumptions listed in Section 5.1 and, in particular, these boundary and initial conditions have been validated in *UZ Flow Models and Submodels* (BSC 2004 [DIRS 169861], Sections 6.3 and 7.7). These are the boundary conditions that remain essentially unchanged over the heating period because the model boundary is far away from the waste emplacement drifts. Other boundary conditions such as the heat source imposed in the drifts or drift spacing and geometry have been used as design inputs. Thus, this requirement is also satisfied.

3. *Discussion of the impacts of uncertainties to the model results including how the model results represent the range of possible outcomes consistent with important uncertainties [LP-SIII.10Q-BSC, Section 5.3.2(b)(3) and LP-2.29Q-BSC, Attachment 3, Level 1 (d) and (f)].*

   Discussions of model uncertainties, sensitivity analyses, and limitations are provided in Section 6.2, 6.3 and 8.5. Thus, this requirement is also satisfied.

7.1.2 Corroboration Using Results from Validation of the Drift-Scale TH Model

The mountain-scale TH model is similar to that presented in *Drift-Scale Coupled Process (DST and TH Seepage) Models* (BSC 2005 [DIRS 172232]), which has been validated using experimental data including those from the Drift Scale Test. As described in Section 2.2.1.4.1 of the TWP (BSC 2005 [DIRS 174842]) the underlying conceptual model, including modeling approaches, numerical codes and model results, in the mountain-scale TH model is very similar to that presented in *Drift-Scale Coupled Process (DST and TH Seepage) Models* (BSC 2005 [DIRS 172232]). In particular, the physical processes described by the mountain-scale TH model are the same as those described by the drift-scale TH model. The drift-scale model has

been validated against experimental TH data from the Drift Scale Test (BSC 2004 [DIRS 169900], Section 6.3; BSC 2005 [DIRS 172232], Section 7). Because of the similarity stated above, the results from validation of the drift-scale model support validation of the mountain-scale model, according to Method 1 (LP-SIII.10Q-BSC, Section 5.3.2(c)(1), corroboration with other relevant observations).

According to the TWP (BSC 2005 [DIRS 174842]), Section 2.2.1.4.1), validation of the mountain-scale TH model by corroboration with the validated drift-scale TH model requires evaluation of the comparison according to the following explicit criteria:

a. *Does the mountain-scale model represent the same physical and chemical processes as were validated in the drift-scale model?*

   The same TH processes have been modeled at a smaller (space and time) scale in *Drift-Scale Coupled Process (DST and TH Seepage) Models* (BSC 2005 [DIRS 172232]). The drift-scale model report uses the same conceptual and mathematical models for representing the same physical processes as those with the mountain-scale TH models. Also, the same numerical simulator is used. The drift-scale model results in that report are compared with measured temperature and saturation data from the DST. The DST is the largest of the three thermal field tests performed at Yucca Mountain (BSC 2005 [DIRS 172232], Section 7.3). The heating phase in the DST lasted slightly more than four years, and a large volume of rock was heated to temperatures close to and above boiling. Considerable high-quality TH data were collected from the DST. These data gave an adequate representation of the TH processes likely to be encountered in the near-field of the emplacement drifts. Through a detailed comparison of measured and simulated TH data, it was concluded that the TH processes were adequately represented by the model (BSC 2005 [DIRS 172232]). This corroborates the mountain-scale TH model because the underlying thermal and hydrologic transport processes are identical. Accordingly, this criterion is satisfied.

b. *Are the scale-dependent processes, properties, and initial/boundary conditions identified and treated appropriately in the corroboration?*

   The processes represented by the drift-scale and mountain-scale TH models consist of thermal conduction and convection, gas- and liquid-phase mass transport, phase change processes (vaporization and condensation), and capillarity. These are either not scale dependent (thermal conduction, phase change) or their scale dependence is described by scale-dependent property values (convective transport). The thermal and hydrological properties used in the mountain-scale TH models are identical to those used in the drift-scale TH model, except for fracture (bulk) permeability, which is the only mass transport parameter that exhibits important scale dependence. The use of mountain-scale fracture permeability is discussed in more detail in Sections 4.1 and 6.1.6.

   The boundary and initial conditions for the mountain-scale TH model were developed for the UZ flow model, and are the result of calibration against borehole temperature

measurements for ambient conditions (BSC 2004 [DIRS 169861], Sections 6.3 and 7.7). Boundary and initial conditions for the drift-scale TH model are also consistent with the UZ flow model. Note that the drift-scale model represents a point location, whereas the mountain-scale model represents a region of the repository block, and the boundary conditions are selected appropriately from the UZ flow model domain. Both the drift-scale and mountain-scale models are initialized consistent with imposed boundary conditions, using scale-dependent properties as discussed above. For both the drift-scale and mountain-scale models the boundary conditions represent steady-state conditions and are therefore independent of temporal scale.

Spatial scale dependence of TH processes is also addressed in the comparison of results from 2-D and 3-D simulations (Sections 6.2 and 6.3), in which the 2-D model uses a more refined grid. The comparisons show that the spatial scaling and grid sensitivity are not important with respect to the intended use of the mountain-scale TH model, to evaluate the potential far-field effects of heating on flow fields in the unsaturated zone. On the basis of the foregoing discussion, this criterion is satisfied.

c. *Are the similarities and differences between the mountain-scale and drift-scale model results identified?*

The only differences between the drift-scale and the mountain-scale TH models lie in the potential scaling effects associated with gridding and scale-dependent fracture (bulk) permeability. The mountain-scale TH model is based on a coarser grid, particularly at the repository horizon, and therefore generates different results for the near-field than the drift-scale models. However, the intended use of the mountain-scale model is limited to far-field effects, which are better represented by the expanded domain of the mountain-scale model. Although the drift-scale and the mountain-scale TH models used different spatial discretization, simulated temperature and liquid saturation distributions in the far-field behave similarly in response to repository heating. The differences between the mountain-scale and drift-scale model results have been identified and shown to be adequate for the intended use of the mountain-scale model. Therefore, this criterion is satisfied.

The similarity between the mountain-scale and drift-scale models and their results is further shown in Figures 7.1.2-1, 7.1.2-2, and 7.1.2-3. In these figures, temperature and saturation profiles, simulated using the mountain-scale and drift-scale models, are compared to each other at the selected location or elevation. The mountain-scale model results are extracted from the simulation with the 2-D cross sectional model of Section 6.2 (DTN: LB0310MTSCLTH2.001). Figure 7.1.2-1 displays the comparison between the two model results at a vertical location of Nevada coordinates W-E: 170,600 m and N-S: 234,103 m from the 2-D model (see Figure 6.1-1 for the repository footprint and coordinates). As shown in Figure 7.1.2-1, the two model results for simulated temperatures are almost identical at this location, except at the long time of 2,000 years. Actually, even at the long time of 2,000 years, the difference in the two model results is mainly caused by the

difference in boundary conditions specified for the two models. At this location, the bottom boundary for the mountain-scale model is at a higher elevation (due to the high water table in the north), as shown in Figure 7.1.2-1, and at long times, constant temperatures specified at top and bottom boundary conditions have impact on the temperature profiles.

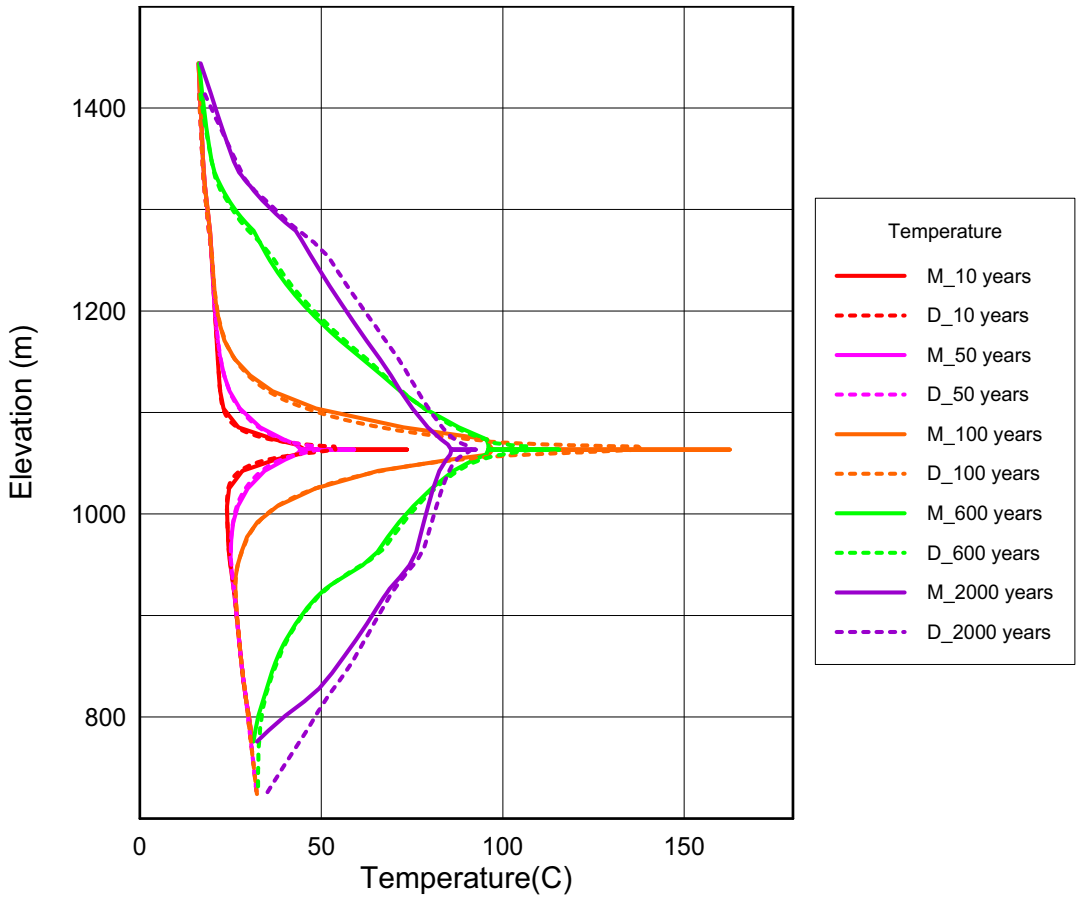

Source: DTN: LB0310MTSCLTH2.001 (for the mountain-scale THC results) and DTN: LB0303DSCPTHSM.001 [DIRS 163688] (for the drift-scale THC results).

NOTE: M_50 years stands for mountain-scale model results at 50 years, while D_50 stands for drift-scale model results at 50 years. See Appendix IV (Section IV.1.3) for details of the post-processing of the mountain-scale model results.

Figure 7.1.2-1 Comparison Between Temperature Profiles Simulated by the Mountain-Scale and Drift-Scale TH Models at Five Times of 10, 50, 100, 600 and 2,000 Years

The matrix liquid saturations simulated using the mountain-scale and drift-scale models at the same location as in Figure 7.1.2-1 are shown in Figure 7.1.2-2. As shown in Figure 7.1.2-1, the two models also produce very similar matrix liquid saturation results in general. However, there appear to be some differences, as shown in Figure 7.1.2-2, and a close examination of the two model results indicates that the differences are not caused by the model grid scales. Rather, they are caused by the difference in geological layers/units between the two models, i.e., the geological

formations represented by the two models are not the same. Secondly, there is a difference in infiltration rates between the two models, and for the 2-D mountain-scale model, the infiltration rate is spatially varying, based on the infiltration maps. In a long time of 2,000 years at the end of the monsoon climate period (600 to 2,000 years), the perched water occurs at an elevation of 900 m in the two model results, which is not predicted by the drift-scale model.

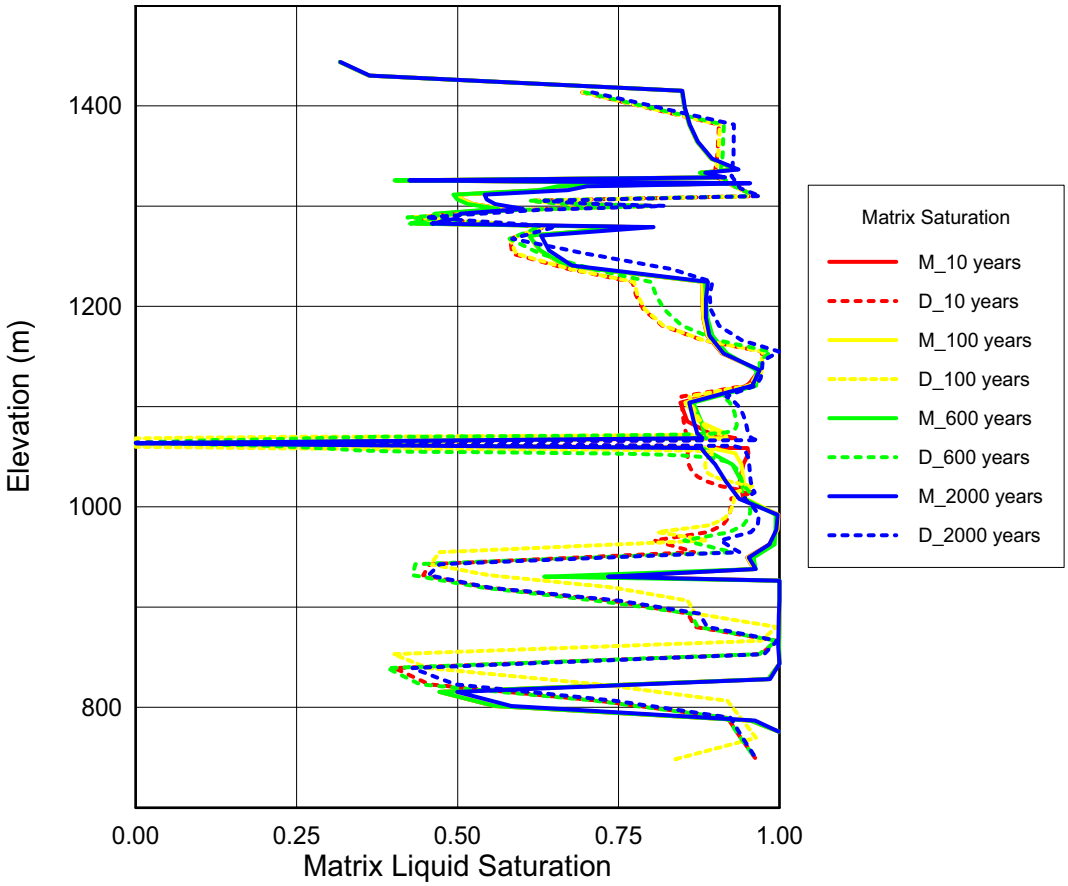

Source: DTN: LB0310MTSCLTH2.001 (for the mountain-scale THC results) and DTN: LB0303DSCPTHSM.001 [DIRS 163688] (for the drift-scale THC results).

NOTE: M_50 years stands for mountain-scale model results at 50 years, while D_50 stands for drift-scale model results at 50 years. See Appendix IV (Section IV.1.3) for details of the post-processing of the mountain-scale model results.

Figure 7.1.2-2 Comparison Between Matrix Liquid Saturation Profiles Simulated by the Mountain-Scale and Drift-Scale TH Models at Five Times of 10, 50, 100, 600 and 2,000 Years

Figure 7.1.2-3 presents a comparison of temperature variations with time at the bottom of the PTn unit, simulated using the mountain-scale and drift-scale models. Figure 7.1.2-3 shows that the two models predict very similar temperature variations at this location. Note that Figure 7.1.2-3 indicates that the mountain-scale model estimates a little higher temperature at this location, as it should be, because the gridblock of the mountain-scale model is 4+ m closer to the drift center.

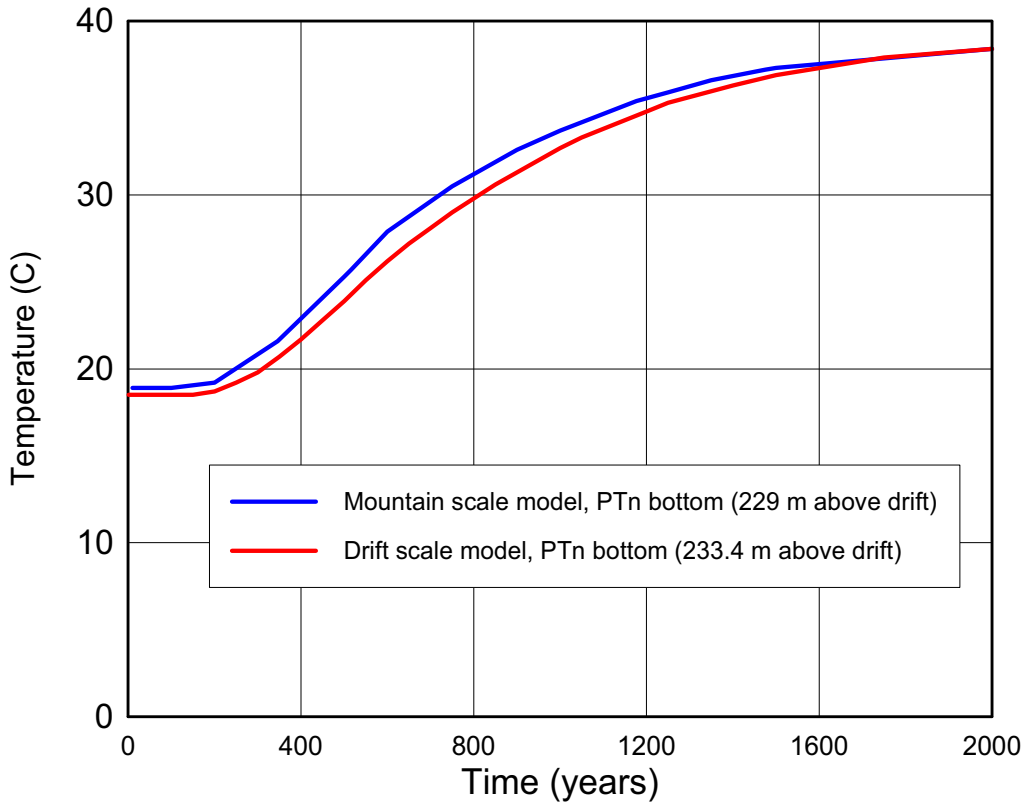

Source: DTN: LB0310MTSCLTH2.001 (for the mountain-scale THC results) and DTN: LB0303DSCPTHSM.001 [DIRS 163688] (for the drift-scale THC results).

NOTE: See Appendix IV (Section IV.1.2) for details of the post-processing of the mountain-scale model results.

Figure 7.1.2-3 Comparison Between Temperature Variations at the Bottom of the PTn Unit, Simulated by the Mountain-Scale and Drift-Scale TH Models

The comparisons shown in Figures 7.1.2-1, 7.1.2-2, and 7.1.2-3 demonstrate that the mountain-scale model produces very similar model results as compared with those of the drift-scale model at the far-fields of Yucca Mountain. Therefore, the validation efforts for the drift-scale model can be used as further evidence for validating the mountain-scale TH model.

d. *Are the scale-dependent numerical issues identified and evaluated with respect to the corroboration?*

There are no specific numerical issues that prevent corroboration of the mountain-scale TH model with the drift-scale TH model. This is because both drift-scale and mountain-scale models use the same dual-permeability concept for handling fracture-matrix interaction. In this approach, the driving forces for fracture-matrix mass and heat exchange, i.e., gradients in pressure, concentration or temperature between fractures and the matrix, are calculated as a function of fracture spacing, independent of the size of gridblocks used in the two models, and the same fracture spacing data are used for the two models. In addition, the input parameters for both models have been estimated using the same-scale spatial discretized grids,

respectively. In particular, the 1-D grid used in the inversion model for estimating drift-scale model parameters was extracted directly from the drift-scale model grid (BSC 2004 [DIRS 169857]), while the parameters for the mountain-scale model were also estimated using 1-D and 3-D mountain-scale model grids directly. Therefore, grid scale dependence or scaling effects in the two models has been implicitly considered with the model input parameters. Furthermore, the numerical approach implemented in the TOUGH2 (LBNL 2003 [DIRS 161491]) code is a control-volume, mass- and energy-conserving scheme. This scheme guarantee mass and energy conservation regardless the size of time steps or gridblocks as long as a converged solution is obtained.

7.1.3 Discussion of Relevant Information from the Technical Literature

This section presents discussion of technical information, much of it from peer-reviewed publications, that supplements validation of the mountain-scale TH model. The discussion includes the development and uses of the TOUGH2 simulation code, the multiscale model, and simulation of geothermal analogues. The section that follows (Section 7.1.4) evaluates the explicit criteria for validation by corroboration with such information, as identified in the TWP (BSC 2005 [DIRS 174842], Section 2.2.1.4.1). The evaluation against explicit criteria is limited to a few of the most important sources identified in this section.

Conceptual and mathematical models similar to the mountain-scale TH model have been widely used and validated in the field of geothermal and petroleum engineering. Two-phase fluid flow and heat transfer in fractured geologic media are the main focus of this model, and include the following physical processes: heat conduction, convective heat transfer, flow of liquid water and vapor, flow of non-condensing gas-phase components (air), vaporization and condensation, drainage through fractures and imbibition into the rock matrix, and capillarity. These processes have been routinely modeled and numerically simulated in geothermal and petroleum reservoir engineering studies. Such models have been validated against a wealth of field-scale tests and production data, on spatial and temporal scales similar to the mountain-scale TH model.

Modeling for the Yucca Mountain repository has benefited from the robust simulation techniques developed for the geothermal industry. Wu et al. (1999 ([DIRS 117161], pp. 186–188) reviewed many of the earlier TH modeling efforts. These coupled, multiphase, multicomponent models simulate the flow and distribution of moisture, gas and heat at Yucca Mountain for use in predicting current and future conditions in the UZ. For example, Tsang and Birkholzer (1999 [DIRS 137577]) used a three-dimensional coupled TH numerical model to predict the results of the Single Heater Test at Yucca Mountain. They obtained good agreement between measured temperatures and model results, and the simulated dryout and condensation zones were consistent with radar tomography and air-permeability data.

Numerical modeling of mountain-scale TH processes can play an important role in understanding the impact of heat on the unsaturated zone. The mathematical and numerical approaches used for modeling unsaturated zone isothermal (ambient) and nonisothermal processes have been demonstrated as valid, by comparing model results to small-scale field data and natural-analogue processes (BSC 2004 [DIRS 169861], Section 7). These models adequately handle heat transfer; nonlinear two-phase flow under nonisothermal conditions in

one, two, and three dimensions, including coupled fluid and heat flow; and adequately incorporate boundary conditions.

Simulation Using TOUGH2 – State-of-the-art modeling in fluid-flow and heat-transfer processes is incorporated in the mountain-scale TH modeling approach, using the simulation code TOUGH2 V1.6 (LBNL 2003 [DIRS 161491]) (Section 3). The following paragraphs describe successful applications of TOUGH2 in modeling two-phase flow and heat transfer in unsaturated fractured geologic media.

Versions of the TOUGH2 code (Pruess et al. 1999 [DIRS 160778]) have been used in a number of numerical models for evaluating thermal hydrology of a repository at Yucca Mountain (Pruess and Tsang 1994 [DIRS 117451]; Buscheck et al. 1994 [DIRS 105157]). Model conceptualizations have focused mainly on large-scale average behavior or on local simplified domains of two-dimensional representations. Both the effective continuum model and dual-permeability methods have been used in previous applications of TOUGH2 in modeling two-phase flow and heat transfer through fractured rock. The present report considers only the dual-permeability approach for handling fracture-matrix interaction.

Versions of the TOUGH2 code have also been used in sensitivity studies on thermal-hydrologic conditions near an infinite linear string of waste packages, as reported by Pruess and Wang (1984 [DIRS 140912]). They simulated fluid and heat flow (including phase-change effects) in a one-dimensional cylindrical geometry, and reported that two-phase vapor-liquid counterflow (heat pipe activity) occurred in some cases. Tsang and Pruess (1987 [DIRS 100688]) conducted repository-scale simulations with an emphasis on thermally driven natural convection. Nitao (1988 [DIRS 109911]) simulated the detailed evolution of temperature, saturation, and gas-phase composition in the hydrothermally disturbed zone. Pruess et al. (1990 [DIRS 100818]; 1990 [DIRS 100819]) used a previous version of TOUGH2 to perform a comprehensive study of the simultaneous transport of heat, liquid water, vapor, and air in partially saturated, fractured, porous rock. They used a two-dimensional simulation and included fracture effects explicitly, including most of the physical effects that could be important for multiphase fluid and heat flow in unsaturated, fractured rock containing a geologic repository.

The TOUGH2 family of codes has also been used in simulating the natural state of geothermal systems (Bodvarsson et al. 1984 [DIRS 137136]; 1986 [DIRS 136386]; 1988 [DIRS 138603]; Hanano 1992 [DIRS 137307]; Ingebritsen et al. 1988 [DIRS 137537]; O'Sullivan et al. 1990 [DIRS 137409]) and in predicting their performance under exploitation (Bodvarsson et al. 1984 [DIRS 137139]; 1987 [DIRS 136391]; 1987 [DIRS 136393]; 1990 [DIRS 136384]; 1993 [DIRS 138618]; Garg and Pritchett 1990 [DIRS 137148]; Hunt et al. 1990 [DIRS 137322]; Lam et al. 1988 [DIRS 137338]; Menzies et al. 1991 [DIRS 137923]). These geothermal systems represent coupled fluid and heat flow processes on scales comparable to the mountain-scale TH model of Yucca Mountain. Mathematical models of the two-phase flow in such systems are similar to numerical modeling of the TH response to repository thermal loading described in this report. Differences exist in the equations correlating flow and saturation and representing the existence of preferential flow paths (e.g., fingering and flow channeling). In other respects, however, the same processes are used for setting up the conceptual model,

numerical gridding, specifying boundary conditions, simulating natural conditions, and simulating transient responses.

Simulation of Geothermal Analogues – Geothermal analogues in general provide the most appropriate spatial and temporal scales for corroboration of the mountain-scale TH model (BSC 2004 [DIRS 169218], Section 11). In particular, steam-dominated geothermal systems like the Geysers in California and Larderello in Italy provide suitable analogues because two-phase fluid and heat flow occurs under partially saturated conditions, similar to conditions that prevail when boiling conditions occur in a repository in the unsaturated zone. Much of the following text has been extracted directly from Section 11.2 of *Natural Analogue Synthesis Report* (BSC 2004 [DIRS 169218]).

Extensive geothermal field data, and published model-data comparisons, are available for corroboration of the mountain-scale TH model. Agreement between field data and models of the natural states of geothermal systems, and use of the models as prediction tools for response to exploitation, provide confidence that the mountain-scale TH model, which is based on similar approaches, can be used to predict far-field TH conditions associated with the repository (BSC 2004 [DIRS 170035]). Much of the published work on simulation of geothermal analogues has involved use of the TOUGH2 family of codes described previously.

Heat and Fluid Flow Simulations for Geothermal Systems – There are many similarities between processes in geothermal systems and those that would occur in a repository. A (man-made) hydrothermal system will be created by the emplacement of heat-generating waste (Figure 7.1.3-1). For most geothermal systems, intrusion of magma at shallow crustal depths results in high heat flow (large temperature gradient) and the formation of a convective hydrothermal system. In the repository system, heat-generating waste will induce similar changes in the ambient system. Both types of systems are subjected to TH processes discussed previously (thermal conduction and convection, gas- and liquid-phase mass transport, vaporization, condensation, and capillarity). Similarities between geothermal processes and TH processes in repository simulation are summarized in Table 7-1.

While geothermal systems are found in a variety of geologic and tectonic environments and have different site-specific characteristics, they all share a number of common traits. These include: 1) heat source, 2) fluids, 3) permeable flow paths, and 4) impermeable boundaries (BSC 2004 [DIRS 169218], Section 11.2.4). Another important feature that is common in vapor-dominated geothermal systems is a heat pipe—a counterflow of liquid and heat that occurs between zones of boiling and condensation. In the repository host rock, heat-pipes may occur in a near-isothermal zone between dry rock around the drift, and the cooler region of condensation farther from the drift opening (BSC 2004 [DIRS 169218], Sections 11.2.4.5, 11.2.10, 11.2.11, and 11.2.12).
In much of the repository the maximum host rock temperature will exceed the boiling point of water for 1,000 years or longer (Sections 6.2.1.1, 6.2.1.2, 6.2.1.5, and 6.3.1.1). Host-rock thermal-hydrologic conditions will therefore be similar to conditions in a boiling geothermal system.

Applicability of Geothermal Analogues – Several important differences between geothermal analogues and the repository at Yucca Mountain are as follows (BSC 2004 [DIRS 169218], Section 11.2.7):

- The Yucca Mountain repository is located within unsaturated rocks, while most geothermal systems have saturated conditions.

- Thermal loading of the repository will be areally restricted and relatively short-lived (boiling period of approximately 1,000 to 2,000 years). Because the host rock is unsaturated, fluid pressures will typically not exceed atmospheric pressure, and boiling will occur at a temperature at or near 96°C throughout the system.

For lower thermal loading, or in regions with high ambient infiltration, or at the edges of the repository layout, host-rock temperature may not reach boiling, or the boiling duration may be decreased, such that boiling geothermal analogues may not apply.

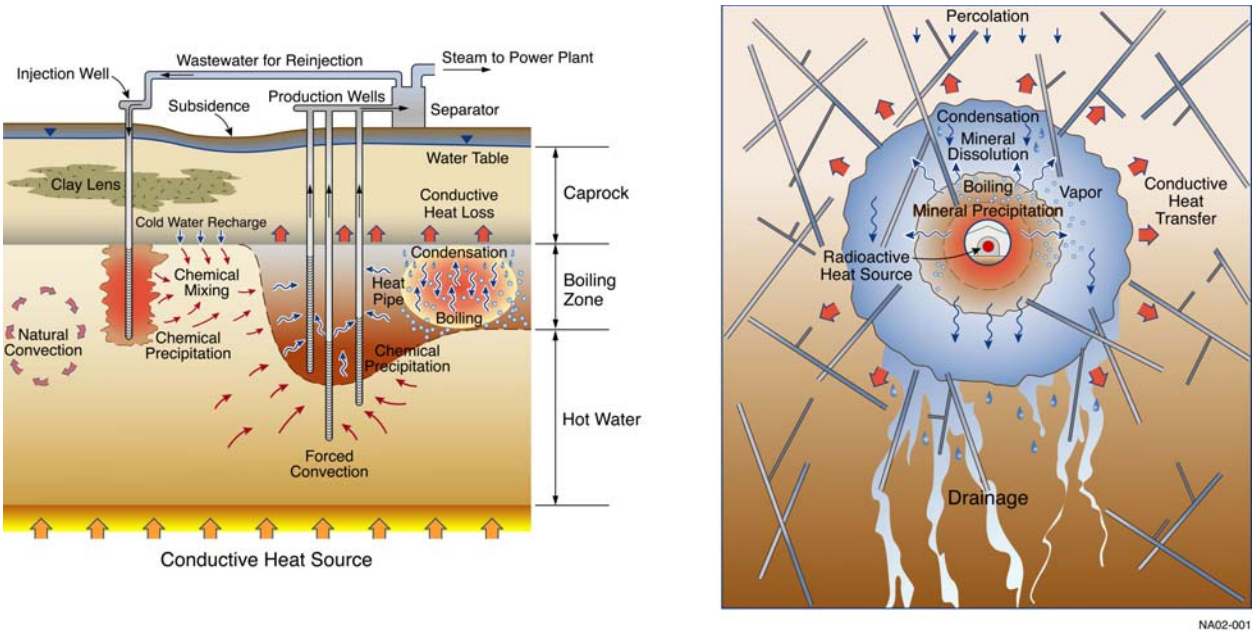

Source: Left figure adapted from Bodvarsson and Witherspoon 1989 [DIRS 156337], right adapted from CRWMS M&O 2000 [DIRS 151940].

NOTE: Similar processes include boiling and condensation, advective liquid flow, mixing, recharge (percolation), and heat conduction. A heat pipe is depicted on the right side of the geothermal system, showing countercurrent liquid and vapor flow resulting from boiling and condensation. Even though the figure on the right side is two-dimensional, refer to the discussion in Section 6.2 regarding the use of two-dimensional boundary conditions.

Figure 7.1.3-1. Comparison of Processes in a Geothermal System (left) and an Anthropogenic Thermal System (right) Created by Emplacing Heat-Generating Nuclear Waste in an Unsaturated Fractured Rock Mass

Table 7-1. Coupled Processes in Geothermal Systems and Their Applicability to Yucca Mountain

TH Process	Geothermal System Component	Geothermal Examples	Applicability to Yucca Mountain	Potential Impact to Repository Host-Rock Performance
Conductive heating	Heat transfer within low-permeability and unsaturated portions of geothermal systems	Nearly ubiquitous: examples include hot dry rock resources, upper portions of San Vicente (El Salvador), Amatitlan (Guatemala)	Principal mode of heat transfer in unsaturated host rock at Yucca Mountain.	Heating can accelerate chemical reactions (Section 7.2). Thermal expansion could alter fracture permeability (Section 7.3).
Advective heating	Heat transfer within convecting geothermal reservoir; develops near-isothermal vertical thermal profiles	Nearly ubiquitous: examples include Yellowstone (Wyoming), Salton Sea (California), Wairakei (New Zealand)	Combined with latent heat transfer; advective heating will primarily affect mass transfer (not heat transfer) in the host rock when dryout develops.	Will enhance water-rock interaction (in the condensation zone), and chemical transport (Section 7.2).
Fracture-dominated fluid flow	Fluid flow in fractured reservoir rocks with low matrix permeability	Silangkitang (Indonesia), Dixie Valley (Nevada), Los Azufres (Mexico)	Principal mode of flow and transport in welded ash flow tuffs at Yucca Mountain.	Can produce more rapid movement of fluids along fast flow paths.
Boiling	Development of two-phase and steam zones in geothermal systems due to depressurization and heating	Occurs in most high-temperature, liquid-dominated, producing geothermal systems, e.g., Awibengkok (Indonesia), Coso (California), and occurs naturally in steam-dominated systems, e.g., The Geysers (California), Karaha-Telaga-Bodas (Indonesia).	Will occur at or near drift walls for limited time.	Can cause dryout of host rock around the drift opening, and could lead to development of heat pipes. Fracture permeability could be modified by chemical precipitation associated with boiling (Section 7.2).
Dryout	Occurs during transformation from liquid-dominated to steam-dominated geothermal system	Documented for The Geysers (California), Karaha-Telaga-Bodas (Indonesia)	Will occur at or near drift walls for limited time.	Dryout zone will inhibit seepage into drift. Rewetting may lead to remobilization of soluble precipitates formed during dryout (Section 7.2).
Condensation	Occurs during transformation from liquid-dominated to steam-dominated geothermal system, and in upper levels of geothermal systems where rising vapor contacts cooler meteoric waters.	Observed in many geothermal systems where rising gas and steam is cooled and mixes with near-surface meteoric fluids, resulting in development of bicarbonate and acid-sulfate springs. Documented for Yellowstone (Wyoming), Wairakei (New Zealand), Waiotapu (New Zealand).	Will occur above drift openings where dryout develops, for limited time before cooldown.	Condensate reflux will locally increase liquid flux in the near-field host rock. Greater liquid saturation increases water-rock chemical interaction.

Source: BSC 2004 [DIRS 169218], Table 11.2-1.

Numerical simulation of geothermal fields has been performed successfully for more than three decades (BSC 2004 [DIRS 169218], Section 11.2.8.2). The Geothermal Reservoir Engineering Code Comparison Study (Molloy 1981 [DIRS 156407]) evaluated several geothermal simulators with six test problems. The codes tested all performed reasonably well, indicating that the physics of the test problems were correctly represented. Numerical simulation of geothermal fields has proven to be of economic importance in optimizing steam production capacity (Simmons and Bodvarsson 1997 [DIRS 126511]). A recent examination of geothermal simulations shows that more than 100 field simulations have been carried out worldwide since 1990 using a variety of simulators (O'Sullivan et al. 2001 [DIRS 156353]).

Over the decades of geothermal reservoir simulation, a robust modeling process has been developed. The process includes data collection and evaluation, conceptual model development, numerical model development, natural-state modeling, history matching, prediction, and post-study evaluation. Each step depends on the preceding steps, and thus changes in any preceding step require modifications in all subsequent steps, allowing for continued calibration and validation of the modeling approach.

In the first step, available data are evaluated. The data may come from flow tests, well logs (temperature, lithology, electrical resistivity, self-potential), fluid chemistry, measurements on core samples, topography, location and flow rates from hot springs and fumaroles, seismic data, precision gravity surveys, and other techniques. The numerical model is constructed to account for conceptual-model processes supported by field data. The modeling domain, gridding parameters, boundary conditions, and equations of state are selected.

Model calibration begins with natural-state modeling, in which the numerical model is tested by placing a heat source into the system at an appropriate time in the past and running the model forward to produce present-day conditions that are consistent with field measurements. If an adequate match is not obtained, parameters are altered within the bounds of the conceptual model and the field data, and the process is repeated. Several iterations may be required, and this procedure may be partially automated (White et al. 1997 [DIRS 156340]; Bullivant and O'Sullivan 1998 [DIRS 144410]; Finsterle 1999 [DIRS 104367]). The relative importance of specific field features may be identified in this step (e.g., the effects of faults).

The next step in model calibration is history matching, which can be performed when fluids have been produced from the geothermal system. In history matching, the field perturbation (caused by fluid extraction) is modeled, with the results compared to field measurements (temperature, pressure, enthalpy, brine composition). Again, parameters are adjusted until a reasonable match is obtained. Since natural-state modeling is performed for long time frames (e.g., thousands of years) and history matching over shorter time frames (years to decades), different types of parameters can be inferred. In natural-state modeling, parameters such as permeability are inferred. In history matching, storage-type parameters like porosity are inferred. Changes in parameters at any stage require verification in earlier stages. Calibration of a model using both natural-state modeling and history matching is a significant milestone in the creation of a viable subsurface system model and becomes increasingly refined as the available data increase.

Upon completion of successful natural-state modeling and history matching, the model is used for predictive purposes. Geothermal fields are modeled for a variety of reasons, but generally to

devise a strategy for energy extraction. These models are generally evaluated and updated when development is planned. Post-extractive model testing provides additional confidence that model predictions are reliable indicators of future performance. Although few such evaluations of geothermal field models have been published, model performance is generally monitored as part of field management. For example, the post-extractive study of Olkaria East Geothermal Field, Kenya (Bodvarsson et al. 1990 [DIRS 136384], pp. 399 to 414), showed that the field-wide decline in steam rate was in good agreement with model predictions. A well-by-well comparison showed adequate simulation of flow rate and evolution of enthalpy for 75% of the wells. Many of the wells for which prediction was inadequate had limited production when the initial model was constructed, and thus had insufficient history on which to base the predictions. In a post-extractive evaluation of the Nesjavellir Field, Iceland (Bodvarsson et al. 1993 [DIRS 138618]), acceptable agreement was reported between modeled and measured data, particularly considering that the prediction time (6 years) was longer than the calibration period (1 to 3 years). A second evaluation was performed of the Nesjavellir geothermal system (Steingrimsson et al. 2000 [DIRS 156686]) because the model underestimated enthalpy decline in some wells. Recalibration led to slight changes in the conceptual model for the producing region of the reservoir. The new model matched well data better, but the larger-scale reservoir performance predictions remained unchanged.

The geothermal industry relies heavily on the use of models, and at many fields several generations of models have been used. Beginning in the early 1980s, three-dimensional models of U.S., Philippine, and Indonesian geothermal fields were developed and maintained (Williamson 1992 [DIRS 156613]; Strobel 1993 [DIRS 156614]; Murray et al. 1995 [DIRS 156612]). The Wairakei geothermal field (New Zealand) has been modeled several times at varying levels of complexity since the late 1960s (O'Sullivan et al. 1998 [DIRS 154567]). The Kawerau geothermal field (New Zealand) has also been extensively modeled for more than a decade (White et al. 1997 [DIRS 156340]). These models have been upgraded over time as new information, codes, and techniques have become available. The long-term use of reservoir simulation models in several fields indicates confidence in geothermal modeling as a field management tool and provides confidence in application of similar techniques for mountain-scale TH modeling of a Yucca Mountain repository.

Paiute Ridge Analogue – Another useful natural analogue for corroborating the effects of heat and fluid flow and resulting water-rock interaction is the Paiute Ridge intrusive complex, located about 40 km northeast of Yucca Mountain along the northern boundary of the Nevada Test Site. At Paiute Ridge, basaltic intrusions were emplaced at an estimated paleodepth of about 200 m, similar to the depth planned for the Yucca Mountain repository. The tuffaceous host rock surrounding the intrusions was hydrothermally altered to varying extent, depending on the distance from the intrusions (Matyskiela 1997 [DIRS 100058], pp. 1117 to 1118; Lichtner et al. 1999 [DIRS 121006], p. 8). Three main alteration zones were identified in the tuff near the basaltic intrusion: (1) a vitrophyre zone immediately adjacent to the sill contact, (2) a baked zone, and (3) an altered zone characterized by opal veining. Although there was voluminous mobilization of silica along fractures created during the basaltic intrusion, subsequent fluid flow was probably significantly reduced because of the impermeable opal veins. Localized chemical variations are noted in the host tuffs adjacent to the basaltic sills, and are more pronounced in samples collected near the contact. Zones of hydrothermal alteration

generally occurred within 10 to 15 m of some of the larger basaltic intrusions, especially sills. The pervasive anastomosing opal veins and associated secondary minerals (e.g., clinoptilolite, calcite, cristobalite) appear to have reduced matrix or fracture permeability in the immediate vicinity of the basaltic intrusion.

The Paiute Ridge analogue indicates that changes in permeability resulting from alteration effects related to the heating event are localized to a 10 to 15 m zone around the heat source. These observations suggest that the coupled changes in flow properties related to the heating and resultant water-rock interaction caused by emplacement of waste packages at Yucca Mountain would be similarly restricted to the near-field environment, and that the mountain-scale system would be minimally affected by the localized hydrothermal perturbation.

Comparison with the Multiscale Model – The multiscale thermohydrologic model (BSC 2005 [DIRS 173944]) provides additional confidence in the mountain-scale TH model, although the most recent version of the multiscale model is not published in peer-reviewed literature. The multiscale thermohydrologic model uses an approach that accounts for processes occurring at spatial scales from a few centimeters up to the mountain scale. The multiscale model documentation (BSC 2005 [DIRS 173944], Section 6.4) presents a comparative study of model results with a simulation using an earlier version of the mountain-scale TH model. The comparison shows similar results for simulated near-field temperatures, for similar thermal loading and boundary conditions. Note that the mountain-scale TH model used in that comparison was based on: 1) coarser grid discretization at the repository horizon than the multiscale TH model, 2) line-averaged representation of waste package heat output versus discrete heat sources, and 3) heating of the entire cross section of each emplacement drift versus heating only the waste packages within the drift.

7.1.4 Corroboration with Information from Refereed Technical Literature

As stated in the TWP (BSC 2005 [DIRS 174842]), Section 2.2.1.4.1) validation of the mountain-scale TH model is also provided by corroboration with information published in refereed journals or literature (LP-SIII.10Q-BSC, Section 5.3.2(c), Method 3). The refereed publications evaluated for this purpose include two that describe supporting drift-scale TH modeling (Birkholzer and Tsang 2000 [DIRS 154608]; Mukhopadhyay and Tsang 2003 [DIRS 160790]), and two that describe analogous geothermal modeling of The Geysers geothermal field (Williamson 1992 [DIRS 156613]; Antunez et al. 1994 [DIRS 172954]). Description of The Geysers field is supplemented by two ancillary sources which are not the central focus of the validation discussion (Moore and Gunderson 1995 [DIRS 172947]; Moore et al. 2000 [DIRS 156318]). The following discussion presents the evaluation of these publications using explicit criteria from the TWP:

1. *Does the corroboration information represent the same physical and chemical processes as the mountain-scale model?*

   The physical processes underlying the mountain-scale TH model are identical to those described for published drift-scale TH models (Birkholzer and Tsang 2000 [DIRS 154608]; Mukhopadhyay and Tsang 2003 [DIRS 160790]). These papers describe modeling of the Drift Scale Test, which, as discussed above, represents the important

physical processes of thermal conduction and convection, gas- and liquid-phase mass transport, vaporization, condensation, and capillarity.

Steam-dominated geothermal systems such as The Geysers in California (Williamson 1992 [DIRS 156613]; Antunez et al. 1994 [DIRS 172954]; Moore and Gunderson 1995 [DIRS 172947]; Moore et al. 2000 [DIRS 156318]) are appropriate analogues for the same set of physical properties because two-phase fluid and heat flow occurs under partially saturated conditions, similar to conditions that will prevail in the repository. The Geysers geothermal system, the world's largest developed geothermal field, is located in northern California near the Clear Lake volcanic field (Antunez et al. 1994 [DIRS 172954]; Moore and Gunderson 1995 [DIRS 172947]). The geothermal field consists of two hydraulically connected steam reservoirs: a primary reservoir with vapor-dominated, near-isothermal (~240°C) conditions and an underlying high-temperature zone located in the northwest portion of the field. Young, shallow granitic plutons serve as the heat source for The Geysers hydrothermal system, which has evolved from a liquid-dominated system to one with vapor-dominated conditions (Moore and Gunderson 1995 [DIRS 172947]; Moore et al. 2000 [DIRS 156318]). The key feature of this geothermal system (and certain others throughout the world) for corroboration of the mountain-scale TH model is the vapor-dominated zone.

Williamson (1992 [DIRS 156613]) developed a reservoir model for the entire Geysers geothermal field. This model is used to predict changes in reservoir pressure resulting from extraction of steam from the primary reservoir for power generation purposes. The model was constructed through the use of field observations to obtain appropriate estimates of fracture and matrix permeability and porosity, pressure and temperature gradients, liquid saturation conditions, and the thickness and lateral limits of the geothermal reservoir. The model was calibrated using history matching with production data from 1957 to 1987, and then tested against observed field behavior for the period of 1987 to 1989. The predicted steam production for this period compared well with observed results.

Antunez et al. (1994 [DIRS 172954]) conducted numerical simulations of the Coldwater Creek steam-field, located in the northwest portion of The Geysers geothermal field. The objectives of this study were to evaluate the connectivity of the deep high-temperature reservoir with the primary reservoir and to predict the production capacity of the Coldwater Creek field. Fluid and heat flow and resulting pressure and temperature conditions for the geothermal system were simulated using a dual-porosity numerical model that employed the TOUGH2 code. The model was calibrated against pressure data from the period 1957 to early 1991, and was used to forecast future production rates and reservoir pressures for three field-management scenarios.

While geothermal systems are found in a variety of geologic and tectonic environments and have many different characteristics, they all share a number of common traits. These include: 1) heat source, 2) fluids, 3) permeable flow paths, and 4) impermeable boundaries (BSC 2004 [DIRS 169218], Section 11.2.4). Another important feature present in many vapor-dominated geothermal systems is a heat pipe: a counter-current

flow of liquid and heat between a boiling zone and condensation zone. In a boiling repository environment, heat-pipes would produce localized zones of mineral dissolution and precipitation (BSC 2004 [DIRS 169218], Sections 11.2.4.5, 11.2.10, 11.2.11, and 11.2.12). For the base-case thermal load, maximum temperatures near the drifts are predicted to reach or exceed boiling conditions for up to approximately 1,000 years (Sections 6.2.1.1, 6.2.1.2, 6.2.1.5, and 6.3.1.1). The conditions near the drifts in this case are similar to conditions in a boiling geothermal system.

The foregoing discussion explains how the same physical processes are represented in published corroborating information from site-specific drift-scale testing, and geothermal analogues. Therefore, this criterion is met.

2. *Does the corroboration rely on scale-dependent processes, properties, or initial/boundary conditions, and if so are these treated appropriately in the corroboration?*

   As discussed in Section 7.1.2, the processes represented in modeling of the DST (Birkholzer and Tsang 2000 [DIRS 154608]; Mukhopadhyay and Tsang 2003 [DIRS 160790]) and in the mountain-scale TH model (2-D and 3-D), are either not scale dependent (thermal conduction, phase change) or their scale dependence is described by scale-dependent property values (convective transport). The fracture (bulk) permeability is the only heat- or mass-transport parameter that exhibits important scale dependence (see Sections 4.1 and 6.1.6). Whereas different values for certain thermal and hydrologic properties have been used in these drift-scale and mountain-scale studies, appropriate scale-dependent fracture permeability values are used in the mountain-scale TH model, and the sensitivity of model predictions to other properties has been evaluated. Specifically, sensitivity of DST models to an alternative hydrologic property set has been addressed (BSC 2005 [DIRS 172232], Section 7.4.3), and sensitivity to updated values for host rock matrix porosity and bulk thermal conductivity has been evaluated (Appendix V of this report).

   In addition, as discussed in Section 7.1.2, the boundary and initial conditions for the mountain-scale TH model were developed for the UZ flow model and are the result of calibration against borehole temperature measurements for ambient conditions (BSC 2004 [DIRS 169861], Sections 6.3 and 7.7). Boundary and initial conditions for the TH models of the DST are also consistent with the UZ flow model. Note that the DST represents a point location, whereas the mountain-scale model represents a region of the repository block, and the boundary conditions are selected appropriately from the UZ flow model domain. Both the drift-scale and mountain-scale models are initialized consistent with imposed boundary conditions, using scale-dependent properties as discussed above.

   It is important to recognize certain limitations associated with using geothermal systems to corroborate the mountain-scale TH model. Geothermal systems typically have temperatures greater than 100°C near the heat source and total pressure that increases with depth. In the example of The Geysers geothermal system, the temperature of the near-isothermal primary steam reservoir is around 240°C, while wells in the deeper

Coldwater Creek reservoir in the northwest Geysers have encountered temperatures as high as 342°C (Moore and Gunderson 1995 [DIRS 172947]). As discussed in Sections 6.2.1 and 6.3.1, the repository at Yucca Mountain is predicted to have a spatially limited and short-lived (up to approximately 1,000-year) high-temperature (>100°C) pulse, thus limiting the time when boiling and condensation processes could occur. These differences will result in significantly less water–rock interaction, and thus less modification of rock characteristics by mineral alteration, dissolution, and precipitation, for the repository compared to hotter and longer-lived geothermal systems such as The Geysers. Moore and Gunderson (1995 [DIRS 172947]) and Moore et al. (2000 [DIRS 156318]) describe the complex evolution of the Geysers magmatic-hydrothermal system and its transition from a liquid-dominated to vapor-dominated system as deduced from age dating, fluid inclusion study, measurement of stable isotopic compositions of rock samples, and characterization of the alteration mineralogy of the system.

The extensive use of reservoir modeling in the development and exploitation of geothermal fields provides another useful means of corroborating mountain-scale TH models. The justification for mountain-scale TH models, and the validity of the results, depends on the successful modeling of fluid and heat flow in large geothermal systems, for which extensive experience has been accumulated as summarized in Section 7.1.3. The numerical models used to simulate reservoir behavior of The Geysers (Williamson 1992 [DIRS 156613]; Antunez et al. 1994 [DIRS 172954]) capture many of the same processes relating to heat and fluid flow as listed above for the DST models. As noted earlier, the calibrated reservoir model of Williamson (1992 [DIRS 156613]) used appropriate input data to represent permeability, and successfully matched the actual production data between 1987 and 1989, and was used to predict a continuing decline in reservoir pressure and field production rates with time. In the Williamson (1992 [DIRS 156613]) model, the dominant elements relating to the water/steam component are the initial mass in place and the amount of steam extraction; thus, the effects of natural recharge and discharge were not included in the model. Adsorption and capillarity effects were also not included in the Williamson (1992 [DIRS 156613]) Geysers reservoir model.

The agreement between field data and models of the natural state of geothermal systems, and their use as prediction tools for response to exploitation, provide confidence that mountain-scale TH models based on similar approaches can be used to model and predict the performance of the repository (BSC 2004 [DIRS 170035]). Finally, the TOUGH2 family of codes used for the mountain-scale TH model has been used over the last few decades to model coupled heat and fluid transport in geological media, primarily geothermal systems.

This discussion has shown how scale-dependent processes, properties, and initial/boundary conditions are treated appropriately for corroboration of the mountain-scale TH model. Therefore, this criterion is met.

3. *Are the similarities and differences between the mountain-scale model or its results, and the corroborating information, identified and explained?*

There are important similarities between the mountain-scale TH model and published corroborating information specific to Yucca Mountain (Birkholzer and Tsang 2000 [DIRS 154608]; Mukhopadhyay and Tsang 2003 [DIRS 160790]), including the same conceptual and geological models, modeling approaches, and simulation software. The main difference is that the mountain-scale TH model represents a larger, three-dimensional UZ domain and longer time scales than the published work, which describes two-dimensional simulations of the DST, a relatively short duration field thermal test.

The important similarities and differences between the mountain-scale TH model and processes in geothermal systems, are summarized in Table 7-1. Comparison between models of geothermal reservoirs and the mountain-scale TH model shows that simulation volume and dimensionality are similar. The Williamson (1992 [DIRS 156613]) model uses a uniform Cartesian grid consisting of 2,880 square cells measuring 609.6 m per side. The size of these grid blocks is much larger than those used for the mountain-scale TH models, but appropriate considering the vast extent of The Geysers geothermal field, which extends over an area of about 150 km^2 (Moore and Gunderson 1995 [DIRS 172947]). A more highly discretized representation of The Geysers geothermal field was developed by Antunez et al. (1994 [DIRS 172954]), which employs large gridblocks for the central and southeast Geysers and a more detailed, well-by-well representation of the northwest Geysers area, the focus of their study.

The temporal scale of the mountain-scale TH model significantly exceeds the temporal scales of history-matching reservoir simulations used to predict geothermal reservoir exploitation behavior (see Section 7.1.3). The Geysers geothermal system has a prolonged history of thermal activity dating back to its inception at about 1.2 Ma (Moore et al. 2000 [DIRS 156318]), but commercial production of the field began in 1960 (Antunez et al. 1994 [DIRS 172954]). The history matching data used to calibrate both the Williamson (1992 [DIRS 156613]) and Antunez et al. (1994 [DIRS 172954]) models covers about 40 years of field measurements, and are used to simulate response for 10 to 20 years of exploitation.

It is noted that the temporal scale for the mountain-scale TH model is similar to natural-state thermal modeling of geothermal systems, such as that conducted for The Geysers (Norton and Hulen 2001 [DIRS 172959]) and the neighboring Clear Lake (Stimac et al. 2001 [DIRS 172958]) magmatic-hydrothermal systems. These systems have been subject to magmatic activity over the past 1 to 2 million years, and can be used to compare the results of long-term thermal simulations with observed present-day thermal gradients. The timing, size, and duration of these magmatic events were used by Norton and Hulen (2001 [DIRS 172959]) and Stimac et al. (2001 [DIRS 172958]) to develop two-dimensional models that simulate conductive and convective heat flow over time frames ranging up to 0.7 to 1 Ma.

Temperature and pressure conditions predicted for the repository at Yucca Mountain are well within the ranges associated with geothermal systems such as The Geysers (Williamson 1992 [DIRS 156613]; Antunez et al. 1994 [DIRS 172954]; Moore and

Gunderson 1995 [DIRS 172947). Although repository conditions will not approach the extreme conditions observed in these systems, the geothermal simulation technologies corroborate the approach used in the mountain-scale TH model. Understanding of geothermal systems requires modeling at various scales (i.e., well-scale, producing zone-scale, and field-scale), and modeling for Yucca Mountain also requires modeling at multiple scales (drift-scale, mountain-scale). From this discussion of similarities and differences associated with comparison of the mountain-scale TH model and geothermal reservoir simulation, this criterion is met.

7.1.5 Discussion of Technical Model Validation Review

An independent technical review for post-development model validation of the mountain-scale TH model has been performed by Dr. Marcelo J. Lippmann, Earth Sciences Division of Lawrence Berkeley National Laboratory, Berkeley, California.

The review criteria for the post-development validation review were presented in Section 2.2.1.4.1 of the TWP (BSC 2005 [DIRS 174842]) and are repeated here:

1. The technical approach and algorithms described in the document capture all physical and chemical processes that are significant to the intended use of the model for screening these FEPs.

2. Modeling assumptions are clearly defined and justified as appropriate for the intended use of the model for screening these FEPs.

3. Uncertainties in model parameters, process representation, and assumptions are sufficiently described, and impacts of these uncertainties discussed, as appropriate for the intended use of the model for screening these FEPs.

4. The overall technical credibility of the approach, including assumptions, parameters, equations, and numerical implementation, is appropriate for the intended use of the model for screening these FEPs.

The post-development validation review based on the review criteria was conducted. Dr. Lippmann's technical comments have been appraised and responded to accordingly, based on the instruction in the TWP (BSC 2005 [DIRS 174842], Section 2.2.1.4.1). Any changes made on this report were provided to the reviewer to his concurrence. The conclusion from Dr. Lippmann's review is summarized and presented below:

> *I have conducted an independent review of the Mountain Scale TH Model as presented in Rev. 03 Draft B of the Mountain-Scale Coupled Processes (TH/THC/THM) Report. My review comments dated July 21, 2005 are attached (Attachment 1).*
>
> *After reviewing the response to my comments (Attachment 2) and meeting with Dr. Tsang, I conclude that the changes made to the document resolve all the issues I had on the TH Model.*

Summarizing, I consider that in the Mountain-scale TH model

1. *An appropriate methodology has been followed. That is, the technical approach is correct as well as the algorithms used to describe the thermal and hydrologic processes in the UZ.*

2. *The modeling assumptions (i.e. equations, boundary conditions and initial conditions) used are reasonable and appropriate considering the complexity of the system;*

3. *The assumptions on which the parameters of the model were chosen are clearly described; and*

4. *The uncertainties related to parameters and process representation, and their impact on model results have been adequately considered and discussed.*

In other words, I conclude that the overall technical approach followed in the Mountain-size model is credible and appropriate for screening the UZ FEP's given in Table 4-3 of the document.

The complete text of Dr. Lippmann's review comments and conclusion is presented in Appendix VIII. The conclusion from Dr. Lippmann's post-development validation review fulfills the requirements in the TWP (BSC 2005 [DIRS 174842], Section 2.2.1.4.1) and confirms adequacy of the mountain-scale TH model in model development, data selection and usage, and range of intended use.

7.1.6 Additional Confidence Building through Publication in a Refereed Professional Journal

Additional confidence in the mountain-scale TH model is provided by publication of the model in a refereed professional journal, as permitted by LP-SIII.10Q-BSC, Section 5.3.2(d). Haukwa et al. (2003 [DIRS 165165]) published the two-dimensional simulations which are part of the mountain-scale TH model (Section 6.2), with one difference related to the ventilation efficiency. Whereas a value of 86.3% (portion of waste heat removed during preclosure ventilation for 50 years; see Section 4.1.4) is used for ventilation efficiency in this report, the published version uses a value of 70%, supplemented by sensitivity analysis using zero percent. This difference is not significant to confidence building for several reasons. The value of 70% is within the acceptable range defined in *Ventilation Analysis and Model Report* (BSC 2004 [DIRS 169862], Section 7.2). The difference of approximately 16% between this and the current value (Section 4.1.4) represents a short-lived transient thermal signal that dissipates with time and distance, such that when far-field thermal-hydrologic effects are expressed (e.g., peak temperature at the PTn or CHn unit boundaries) the effect on predicted temperature is attenuated. Consequently, the results of the published work are nearly identical to the two-dimensional part of the mountain-scale TH model (Section 6.2).

7.1.7 Summary and Evaluation of Validation Criteria

In summary, the mountain-scale TH model is validated using confidence-building information derived both during model development and from post-development activities. Information used for confidence-building during model development includes discussion of input data, how calibration was used, initial conditions and boundary conditions, numerical convergence, the range of conditions simulated, and uncertainties (Section 7.1.1). Post-development validation activities consist of corroboration by results from validation of the drift-scale model (Section 7.1.2), corroboration using other information (i.e., publication of field-test simulations and geothermal analogues) from refereed technical publications (Section 7.1.3), technical review for the post-development validation (Section 7.1.5), and confidence building by publication of the model in a refereed professional journal (Section 7.1.6). These activities provide confidence that the mountain-scale TH model is adequate for its intended use, to support screening evaluation of FEPs (BSC 2005 [DIRS 174191], Sections 6.9.9 and 6.9.16), and to serve as the thermal-hydrologic basis of the mountain-scale THC and THM models (Sections 7.2 and 7.3).

7.2 VALIDATION OF THE MOUNTAIN-SCALE THC MODEL

The intended use of the mountain-scale THC model is to support evaluation of FEPs related to effects of coupled THC processes on mountain-scale UZ flow. The mountain-scale THC model supports the treatment of FEPs related to the TSPA component model "UZ Flow" (BSC 2005 [DIRS 174191], Sections 6.9.7 and 6.9.13). For such a model, the applicable planning procedure (LP-2.29Q-BSC, Attachment 3, Table 1) requires Level II validation. Implementation of Level II validation for the mountain-scale THC model is specified in Section 2.2.1.1 of the TWP (BSC 2005 [DIRS 174842]).

Validation of the mountain-scale THC model is achieved through confidence-building activities during model development (Section 7.2.1), by corroboration with the validation of the drift-scale THC model, as presented in *Drift-Scale THC Seepage Model* (BSC 2005 [DIRS 172862]; see Section 7.2.2 below), by corroboration with relevant information from refereed technical publications (Section 7.2.3), and by technical review by reviewers independent of the development, checking, and review of the model documentation (Section 7.2.4).

The mountain-scale THC model addresses coupled THC processes that are affected by variations in geology (structure and lithology), infiltration rate, and temperature at a mountain or repository scale. These are processes that affect the percolation flux to the potential repository horizon (relevant to seepage), and flow below the potential repository (relevant to radionuclide transport in the UZ). Small-scale and localized processes, such as mineral precipitation in the boiling zone, can only be captured in finely gridded drift-scale models. Thus, the mountain-scale THC model is focused on larger-scale changes in chemistry and flow that are not localized to very small regions adjacent to the drift. The mountain-scale THC model is based on the mountain-scale TH model and the conceptual models and data for THC processes documented in *Drift Scale THC Seepage Model* (BSC 2005 [DIRS 172862]). Many of the uncertainties in the conceptual models, and data used for input and model validation are discussed in the latter report. However, the drift-scale THC models are focused primarily on processes that affect seepage (and the chemistry of potential seepage) into drifts which are in devitrified tuff. The effect of THC processes on flow in the volcanic glass-rich units (i.e., Paintbrush hydrogeologic

unit (PTn), the basal vitrophyre of the Topopah Spring tuff, and in the vitric and zeolitic zones in the Calico Hills unit below the potential repository), cannot be directly validated by the Drift Scale Test.

7.2.1 Summary of Confidence Building during Model Development

The mountain-scale THC model has been developed in accordance with the requirements of Section 5.3.2(b) of LP-SIII.10Q-BSC, as specified in the TWP (BSC 2005 [DIRS 174842], Section 2.2.1.2). Confidence building during model development was implemented for the mountain-scale THC model in accordance with the following steps:

1. *Selection of input parameters and/or input data, and a discussion of how the selection process builds confidence in the model [LP-SIII.10Q-BSC, Section 5.3.2(b)(1)].*

   The inputs to the mountain-scale THC model have all been obtained from controlled sources, and model documentation includes discussion about selection of key input parameters (Section 4.1.1, Table 4.1-1). Model assumptions that affect input data are described in Section 5. Detailed discussion of related model concepts is provided in Section 6.4.1. In summary, input data to the mountain-scale THC model have been developed from appropriate sources, and are based on site-specific information where appropriate. Calibrated, mountain-scale fracture permeability data are used as discussed in Section 7.1.1. Thermodynamic and kinetic data are based on parameterization documented for the drift-scale model (BSC 2005 [DIRS 172862], Sections 4.1 and 6.4.8). Model parameters developed from the input data are applied in a modeling framework consistent with the scale of test observations, and the scale of use in the mountain-scale model. Thus, this requirement is satisfied.

2. *Description of calibration activities, and/or initial boundary condition runs, and/or run convergences, simulation conditions set up to span the range of intended use and avoid inconsistent outputs, and a discussion of how the activity or activities build confidence in the model. Inclusion of a discussion of impacts of any non-convergence runs [(LP-SIII.10Q-BSC, Section 5.3.2(b)(2)].*

   Detailed discussion of initial and boundary conditions for the mountain-scale THC model is provided in Sections 6.4.2.3 and 6.4.2.4. Section 6.4.3 provides detailed discussion of various model results (i.e., those of convergence runs), including discussion of the range of conditions studied and how this range is appropriate considering the intended use of the model. Discussion about nonconvergence runs is not relevant for this report. In summary, the far-field thermal, hydrologic, and chemical boundary conditions, as well as the initial conditions (thermal, hydrologic, and chemical) have been developed from appropriate sources representing ambient conditions at Yucca Mountain. These boundary conditions remain unchanged over the heating period because the model boundaries are far away from the waste emplacement drifts. Other boundary conditions such as the heat source imposed in the drifts are based on design inputs. Thus, this requirement can also be considered satisfied.

3. *Discussion of the impacts of uncertainties to the model results including how the model results represent the range of possible outcomes consistent with important uncertainties [(LP-SIII.10Q-BSC, Section 5.3.2(b)(3) and LP-2.29Q-BSC, Attachment 3, Level 1 (d) and (f)].*

   Discussion of model uncertainties and sensitivity analyses are provided in Section 6.4.3. Thus, this requirement can also be considered satisfied. Alteration in the vitric and zeolitic units well below the repository level is dominated by the thermodynamic instability of the primary aluminosilicate minerals and volcanic glass as well as the strong increase in their reaction rates at elevated temperatures. Whereas some components, such as nitrate, sulfate and chloride, are controlled predominantly by the initial water chemistry and are important for seepage water chemistry and the final brine compositions, they have little effect on the extent of mineral–water reactions which give rise to permeability changes under below-boiling conditions. Therefore, the use of a single initial water chemistry in the mountain-scale THC simulations is not likely to result in significant uncertainty with respect to thermal alteration in the Tpt basal vitrophyre or the CHn units.

7.2.2 Corroboration Using Results from Validation of the Drift-Scale THC Model

Methods and criteria for confidence-building after model development are described in the TWP (BSC 2005 [DIRS 174842], Section 2.2.1). For validating the mountain-scale THC model, the TWP designates use of Method 1 (LP-SIII.10Q-BSC, Section 5.3.2(c) item 1, as specified for use of "other relevant information"): corroboration of the mountain-scale THC model using results obtained from validation of the drift-scale THC model (THC seepage model; BSC 2005 [DIRS 172862]).

The drift-scale model was validated against observations from the Drift Scale Test. The validated drift-scale THC model builds confidence in the mountain-scale THC model because: 1) rock thermal and chemical properties are based on qualified data, and identical values can be used in the mountain-scale THC model for each stratigraphic unit; 2) rock hydrologic properties are qualified data based on field measurements and calibrated at an appropriate scale for mountain-scale modeling (Section 7.1.1); 3) constitutive relationships (e.g., rate laws, capillary characteristic equations, relative permeability, fracture-matrix mass-transfer coupling) are consistent with the drift-scale THC model; and 4) the same conceptual model applies to both drift-scale and mountain-scale THC models.

The following discussion of corroboration with the drift-scale THC model is organized in three parts. First the validation of the drift-scale THC model is reviewed, then up-scaling issues are identified and explained, and then consistency in the model results between the mountain-scale and drift-scale THC models is demonstrated. This discussion is followed by evaluation of the explicit criteria identified in the TWP (BSC 2005 [DIRS 174842], Section 2.2.1.4.2).

Review of Validation for the Drift-Scale THC Model – The following discussion summarizes comparison of drift-scale THC model (Drift Scale Test THC submodel) results with measured data from the Drift Scale Test (BSC 2004 [DIRS 169900], Section 6.3.4; BSC 2005 [DIRS 172862], Section 7.1). The DST THC submodel is directly comparable to the drift-scale

THC model for repository predictions (THC seepage model) (BSC 2005 [DIRS 172862], Section 7.1.15). Data from the DST used for comparison consist of analyses of water and gas samples from borehole intervals between packers and observations of mineral precipitation in boreholes. Intervals were selected for comparison based upon the availability of a long, continuous sample record and the absence of interfering factors such as the sampling interval being too long to compare with a particular gridblock or pair of gridblocks, or boreholes being near either end of the DST and affected by three-dimensional transport (see below). The locations of the hydrology boreholes, sampling intervals, and temperature sensors are shown in Figure 7.1-4 of *Drift-Scale THC Seepage Model* (BSC 2004 [DIRS 172862]).

Comparisons of the DST THC model predictions and the DST measurements provide confidence that the model adequately represents the important processes that will affect the repository. The comparisons indicate that the model results are generally consistent with measured data. The drift-scale and mountain-scale THC models represent overall trends and effects of THC processes, and not detailed conditions at specific locations or times, which is consistent with the intended uses of these models. The following points elaborate on this statement, and were originally documented in reference to the drift-scale THC model. The discussion below establishes that the same validation strategy applies to the mountain-scale THC model:

- The DST THC model is a continuum model, using average hydrologic, thermal, and mineralogical properties for individual hydrostratigraphic units at Yucca Mountain, rather than specifically for the DST test location. The mountain-scale THC model uses these same properties, which are considered most representative of the overall repository host rock.

- Continuum models do not simulate individual fractures, which may intersect boreholes near sampling points. The changing fracture aperture and frequency result in different flow rates and temperatures, thus affecting the chemistry of the gas and water samples in that interval. Both the drift-scale THC seepage model and the mountain-scale THC model are continuum models.

- Water and gas samples from the DST were acquired from long borehole intervals (approximately 8 to 10 meters), which traverse regions of rock in which large gradients in temperature and gas-phase composition were observed. Waters resided in the boreholes for varying lengths of time, affecting the degree of interaction with the rock and engineered materials. In contrast, the drift-scale and mountain-scale THC models represent compositions in particular grid blocks (which vary in size relative to the borehole intervals), and represent the fractures or matrix at discrete points in time. Model-data comparisons have been documented and the associated uncertainties quantified (BSC 2005 [DIRS 172862], Section 7.1). The results are applicable to the mountain-scale model, which represents far-field effects involving much smaller gradients in temperature and composition.

- The DST THC model is a two-dimensional slice taken approximately at mid-length of the DST, which does not simulate flow in the third dimension. Similarly, the drift-scale and mountain-scale THC models represent perpendicular cross sections through one or more

emplacement drifts. Three-dimensional THC models at appropriate grid resolution would be computationally infeasible, and more importantly, would not significantly improve matches to geochemical data because three-dimensional models would rely on the same parameterization (e.g., uniform properties within layered units).

- The DST THC model does not explicitly represent all deviations from planned operation of the DST. The impact on confidence-building for the mountain-scale THC model is addressed in documentation of the drift-scale model (BSC 2005 [DIRS 172862], Section 7.1).

- Gas and water samples from the DST were affected by condensation of water vapor during sampling. The impact on confidence-building for the mountain-scale THC model is also addressed in documentation of the drift-scale model (BSC 2005 [DIRS 172862], Section 7.1).

Given these considerations, the strategy for model-validation comparisons between data from the DST and the DST THC model requires that any two of the following three criteria are satisfied (with exceptions readily explained in terms of simple physical and chemical processes; see BSC 2005 [DIRS 172862], Sections 7.1.10 and 7.1.11):

- Observed concentrations for gaseous and aqueous species match predicted concentrations within an order of magnitude (e.g., one pH unit). This range is reasonable because chemical potential is proportional to the logarithm of concentration.

- The simulated variation of gas-phase CO_2 concentration over time shows the same trend as field observations.

- Observations of mineral precipitation agree qualitatively with predictions of locations where mineral precipitation is most likely to occur.

These criteria are met for the drift-scale THC model (BSC 2005 [DIRS 172862], Section 7.1) and as explained above the same validation strategy is consistent with the modeling framework and intended use of the mountain-scale THC model. Thus, the results from validation of the drift-scale model provide confidence that the mountain-scale model is adequate for its intended use.

Up-scaling from Drift Scale to Mountain Scale – The TH components (e.g., gas and liquid phase flow processes, representation of hydrologic properties, and TH initial and boundary conditions) of the mountain-scale THC model are derived directly from the mountain-scale TH model. The validation of these TH processes and their scale-dependency have been discussed in Section 7.1 and a separate discussion is not warranted here. Note that chemical boundary conditions (composition, temperature, fluxes) are not scale dependent.

Chemical processes are dependent on the spatial scale, or resolution of the model, in several ways. First, the finite volume of a grid block and the numerical representation of variability within grid blocks result in averaging, although continuous gradients of chemical composition, temperature, and hydrological variables (e.g., pressure and liquid saturation) exist. This

numerical averaging can potentially lead to block-size dependent differences in calculated dynamic mineral–liquid interaction. Both equilibrium and kinetic reactions are affected, with kinetic reactions potentially exhibiting more complex behavior. However, the primary purpose of the mountain-scale THC model is to predict chemical changes in the far-field. Gradients of chemical composition, temperature, and hydrological variables in the far-field are small compared to those in the near-field, and the sensitivity to block size is decreased for such conditions. Experience with THC modeling using different grids at different scales, and comparison of far-field predicted results from drift-scale vs. mountain-scale models (see below), have not shown scale dependency that leads to different precipitated minerals or unexpected changes in aqueous or gaseous species compositions.

To summarize this discussion, THC processes in the far-field host rock are unlikely to show spatial scale dependency not captured by the mountain-scale THC model. Scale-dependent THC changes in hydrologic properties are small in the far-field, and therefore not important, except locally where thin strata of glass are present in the basal vitrophyre and near the top of the CHn hydrological unit. Because glass alteration in these strata is related primarily to temperature (through dependence of reaction rate on temperature), which is conduction-dominated (not scale-dependent), the grid resolution in the mountain-scale THC model is adequate to capture the local temperature gradients. The far-field flux of liquid water in the unsaturated zone is gravity dominated, generally downward, spatially uniform, and constant with time; therefore, this flux does not exhibit significant scale dependence that could affect results from the mountain-scale THC model.

Uncertainties in the Mountain-Scale THC Model – Limitations in the use of the mountain-scale THC model and uncertainties in the model inputs, and conceptualizations are summarized in Table 7-2.

- Uncertainties in 3-D TH processes at a mountain scale and their effect on THC processes (i.e., gas convection, focused flow)
- Uncertainties in thermodynamic data (i.e., relative stabilities of feldspars, clays, and zeolites) that relate specifically to vitric and zeolitic horizons
- Uncertainties in kinetic data (i.e. aluminosilicate rate laws and parameters and rates of nucleation) also related specifically to vitric and zeolitic horizons
- Uncertainties in geochemical conceptual models (e.g., mineral solid solutions, precipitating mineral assemblages, reactive surface area estimation)
- Uncertainties in the effective mineral–water reactive surface areas in heterogeneous unsaturated fractured rock
- Uncertainties in fracture and lithophysal hydrologic parameters (i.e., fracture and lithophysal porosity and unsaturated hydrologic properties)
- Uncertainties in the distribution of water and gas chemistry in the UZ and in infiltrating water.

Table 7-2. Summary of Uncertainty Issues Related to the Prediction of Mountain-Scale THC Processes

Category	Uncertainty issue	Treatment of uncertainty issue	Affected goals
Conceptual uncertainties	Effect of 3-D TH processes on mountain-scale geochemistry	Not treated directly Treated indirectly by evaluation of 2-D TH processes on geochemistry	Limits range of possible water compositions and amounts of mineral alteration owing to focused gas and liquid flow
	Impact of heating SZ on gas chemistry in UZ	Not treated	CO_2 degassing of SZ water could affect post-thermal water chemistry
	Surface temperature assumed constant instead of variable	Not treated	Variable surface temperature could result in more near surface focussing of heat and vapor, and enhanced percolation flux around these areas
	Changes in infiltrating water chemistry associated with climate changes	Assessed indirectly through drift-scale-THC simulations using alternate water compositions	Results in more uncertainty in range in potential chemical compositions during post-thermal period
	Uncertainty in flow below potential repository and conceptual models for perched water	Not treated	Reaction rates in CHn zeolitic and vitric units are related to fluid fluxes as well as heat and therefore the different conceptual models for perched water may lead to a larger range in uncertainty for mineral alteration and effects on flow and transport
	Uncertainty in spatial distribution of net infiltration	Treated indirectly in drift-scale THC models through evaluation of different infiltration rates Larger-scale effects of different spatial distributions on flow focusing and THC processes not treated	Limits range of possible water compositions and distribution of mineral precipitation and dissolution
Data uncertainties	Uncertainties in mineralogy in repository unit	Treated indirectly by evaluation of mineralogy from two different geologic columns in drift-scale THC models Little data from Calico Hills unit under the potential repository footprint to constrain mineralogical abundances and variability	Limits prediction of potential effects on flow and transport in the Calico Hills unit where glass, zeolite, and clay abundances are highly variable
	Thermodynamic and kinetic data specifically for zeolites, clays and glass	Treated through sensitivity studies on long-term behavior of ambient system water and gas chemistry and mineralogy assuming a fixed infiltration rate Many uncertainties unknown.	Adds uncertainty to ranges of predicted water compositions, mineral assemblages, and changes in hydrological properties

Table 7-2. Summary of Uncertainty Issues Related to the Prediction of Mountain-Scale THC Processes (Continued)

Category	Uncertainty issue	Treatment of uncertainty issue	Affected goals
Parameter uncertainties	Uncertainties in fault parameters	Not treated	Faults may amplify THC processes because of their role as potential conduits for vapor and liquid flow and as a capillary barrier and therefore the range of potential effects have more uncertainty
	Large scale heterogeneity	Large-scale heterogeneity in mineralogical properties treated in part through variation in zeolitic or vitric attributes for layers and their changes in thickness	Heterogeneity in mineralogical properties could amplify local effects on hydrological properties
	Uncertainty propagation	Treated preliminarily through alternate mineral reaction rates	Limits assessment of THC effects on flow, transport and geochemistry in the UZ and of uncertainty for TSPA

Comparison of Mountain-Scale and Drift-Scale THC Model Results – The drift-scale THC model (BSC 2005 [DIRS 172862]) is considered validated because its predictions have been directly compared with measured THC data from the Drift Scale Test. In the following, results from the mountain-scale THC model are compared against those from the validated drift-scale THC model (BSC 2005 [DIRS 172862]). Note that the comparison can only confirm similar (or average) trends in THC results in the drift-scale and mountain-scale THC models, mainly because of the difference in spatial scale of the two models and difference in (spatial) locations of the extracted results. Note also that the TH components of the two models have already been compared in Section 7.1.2 and have been accepted as validated. In this section, therefore, only the results pertinent to chemical changes are discussed. Results for the mountain-scale THC simulations shown in this subsection are obtained from DTN: LB0310MTSCLTHC.001, extracted at Nevada coordinates W-E: 170,600.500 m and N-S: 235,380.386 m (see Figure 6.1-1 for a repository footprint and coordinates). The drift-scale THC model results can be found in DTN: LB0307DSTTHCR2.001 [DIRS 166054].

In the following discussion, similarities between the mountain-scale THC model and the drift-scale THC model results are identified by comparing the temporal evolution of pH and CO_2 partial pressures at the bottom of the PTn stratigraphic unit. In addition, vertical profiles of pH, partial pressure of CO_2, and volume fractions of calcite as predicted by the two models are compared. The temporal evolution and vertical profiles of pH, partial pressure of CO_2, and volume fractions of calcite depend on temperature. Accordingly, the temperatures predicted by the two models are compared first. Such temperature plots will help understand the subsequent THC comparisons more clearly.

A comparison of temperature from the mountain-scale and drift-scale THC models as a function of time is shown in Figure 7.2.2-1. Temperatures shown in Figure 7.2.2-1 are at the bottom of the PTn stratigraphic unit, located approximately at 243 m and 216 m above the drift in the mountain-scale and drift-scale THC models, respectively. The difference in the bottom of the PTn unit is because of their model coordination utilized by the mountain-scale and drift-scale models, for which temporal changes in parameters were recorded during numerical simulations. Since the location of the extracted temperatures from the drift-scale model is closer to the source of heat than that of the mountain-scale model, the former predicts an approximately 12°C higher peak temperature at the bottom of the PTn than the latter. Predicted temperatures along a vertical line from the two models are shown in Figure 7.2.2-2. The temperature comparisons are shown at 10 and 2,000 years. At 10 years, the predicted temperatures from the two models are almost identical, indicating identical initial conditions. At 2,000 years, the temperature predicted by the drift-scale THC model at any vertical location is somewhat larger than that predicted by the mountain-scale THC model. These facts need to be weighed while comparing the THC results from the two models.

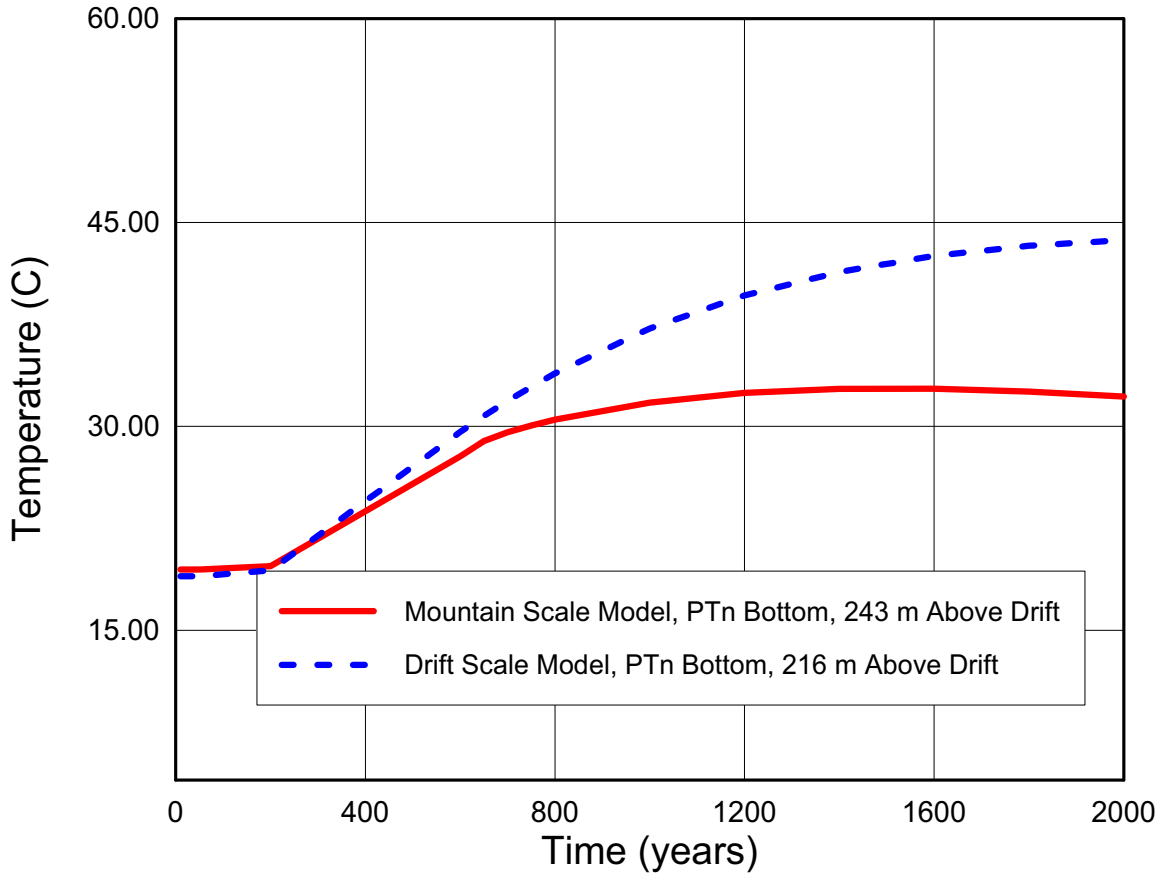

Source: DTN: LB0307DSTTHCR2.001 [DIRS 166054] (for the drift-scale THC results) and DTN: LB0310MTSCLTHC.001 (for the mountain-scale THC results).

NOTE: See Appendix IV (Section IV.3.1) for details of the post-processing of the mountain-scale model results.

Figure 7.2.2-1. Comparison of Temperature at the Bottom of the PTn Stratigraphic Unit as a Function of Time between the Validated Drift-Scale THC Model and the Mountain-Scale THC Model

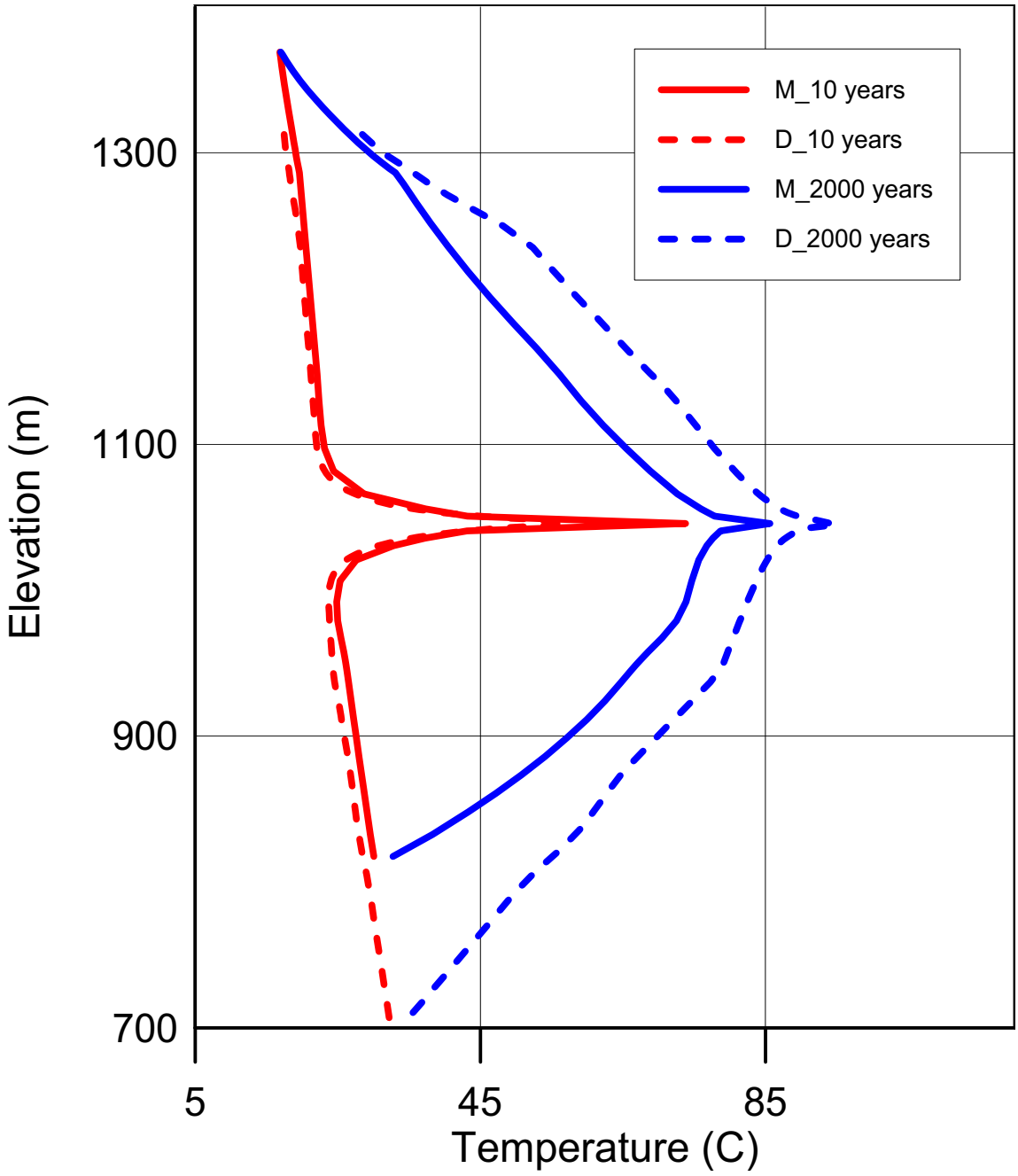

Source: DTN: LB0307DSTTHCR2.001 [DIRS 166054] (for the drift-scale THC results) and DTN: LB0310MTSCLTHC.001 (for the mountain-scale THC results).

NOTE: See Appendix IV (Section IV.3.2) for details of the post-processing of the mountain-scale model results.

Figure 7.2.2-2. Comparison of Temperatures between the Mountain-Scale THC Model and the Validated Drift-Scale THC Model as a Function of Elevation at Various Times (10 and 2,000 Years)

A comparison of simulated pH values from the mountain-scale and drift-scale THC models as a function of time is shown in Figure 7.2.2-3. The pH values shown in Figure 7.2.2-3 are at the bottom of the PTn stratigraphic unit, located approximately at 243 m and 216 m above the drift in the mountain-scale and drift-scale THC models, respectively (location is identical to where the

temperatures are extracted in Figure 7.2.2-1). Both the mountain-scale and the drift-scale THC model predict a similar pattern of change in pH values with time at the bottom of the PTn stratigraphic unit. The small differences in respective pH values at a given time are because of the difference in location of the bottom of the PTn stratigraphic unit in the two models (243 m in the mountain-scale THC model and 216 m in the drift-scale THC model), which also results in a somewhat higher temperature for the drift-scale THC model. It can be concluded that the pH values predicted by the mountain-scale THC model are (at least qualitatively) consistent with those predicted by the validated drift-scale THC model.

CO_2 partial pressures at the bottom of the PTn stratigraphic unit from the two models are compared in Figure 7.2.2-4. Figure 7.2.2-4 yet again confirms that the results from the mountain-scale THC model are consistent with those from the drift-scale THC model, as far as patterns in change of CO_2 partial pressures with time are concerned, notwithstanding the differences (which happen because of differences in location and temperature) in exact numeric values between the two. This further validates the mountain-scale THC model.

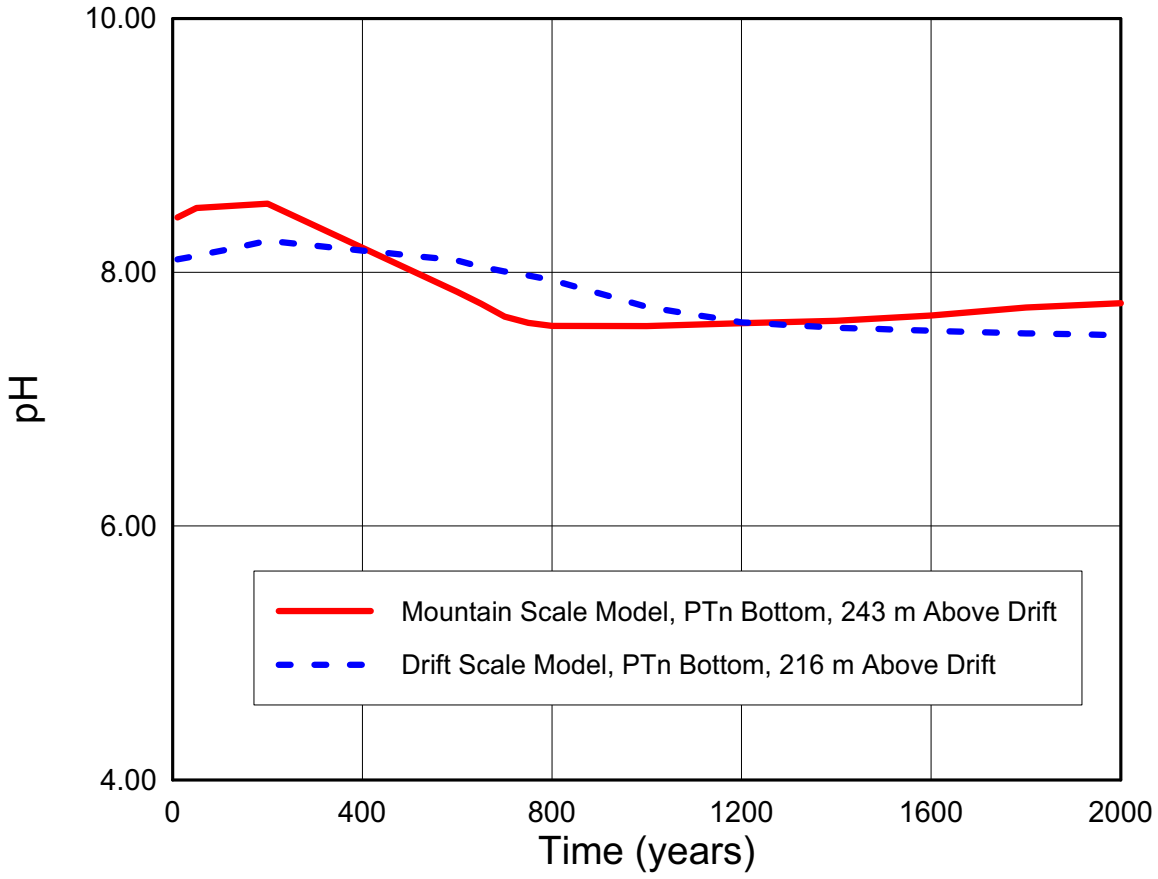

Source: DTN: LB0307DSTTHCR2.001 [DIRS 166054] (for the drift-scale THC results) and DTN: LB0310MTSCLTHC.001 (for the mountain-scale THC results).

Figure 7.2.2-3. Comparison of Fracture Water pH at the Bottom of the PTn Stratigraphic Unit as a Function of Time between the Validated Drift-Scale THC Model and the Mountain-Scale THC Model

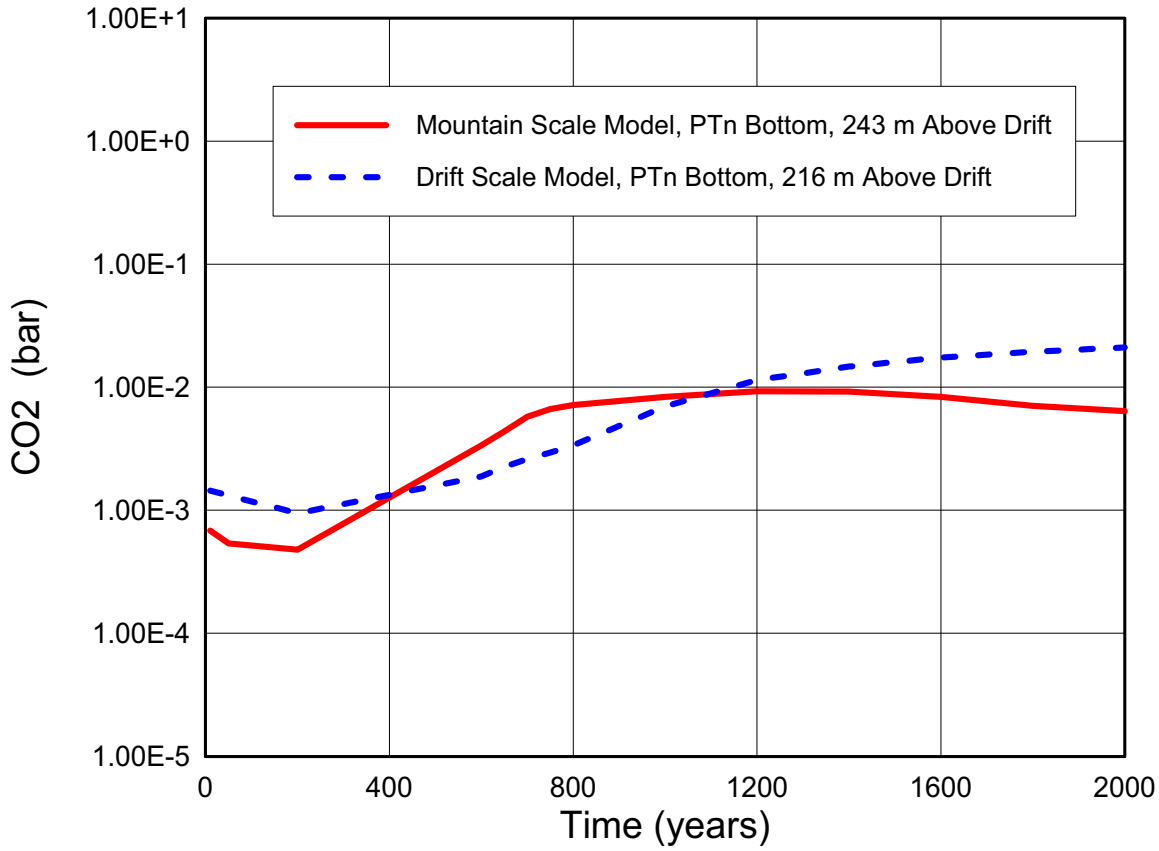

Source: DTN: LB0307DSTTHCR2.001 [DIRS 166054] (for the drift-scale THC results) and DTN: LB0310MTSCLTHC.001 (for the mountain-scale THC results).

Figure 7.2.2-4. Comparison of Fracture CO_2 Partial Pressures at the Bottom of the PTn Stratigraphic Unit as a Function of Time between the Validated Drift-Scale THC Model and the Mountain-Scale THC Model

The similarities between the mountain-scale and drift-scale models and their results are further illustrated in Figures 7.2.2-5, 7.2.2-6, and 7.2.2-7. In these figures, pH, CO_2 partial pressures, and volume fractions of calcite, respectively, are compared between the mountain-scale and drift-scale models as a function of elevation from the groundwater table. The comparison between the two models is shown at various times (10 and 2,000 years). Note that the simulated pH (Figure 7.2.2-5), CO_2 partial pressures (Figure 7.2.2-6), and volume fractions of calcite (Figure 7.2.2-7) from the mountain-scale THC model are similar to those from the validated drift-scale THC model (differences in numerical values at certain times and locations exist). The differences in simulated pH, CO_2 partial pressures, and volume fractions of calcite between the two models are primarily because of the difference in boundary conditions specified for the two models at the locations for which these results were extracted.

This is particularly true for partial pressures of CO_2 (Figure 7.2.2-6) which are much greater in the CHn unit below the repository, for the mountain-scale vs. the drift-scale THC models at 2,000 yrs (Figure 7.2.2-6; also evident in Figure 6.4-16). The difference is caused by differences in the lateral extent of the model domain for the two models. The drift-scale and mountain-scale THC models have the same stratigraphic units (including vitric CHn units), the

same thermodynamic data, the same intrinsic kinetic constants, and the same (or very similar) specific surface area parameter values. The zone of elevated gas-phase CO_2 in Figure 7.2.2-6 (elevation from approximately 860 to 980 m, with allowance for gas-phase dispersion up and down) is located within the group of vitric rock units below the repository. (Note the abundance of the phase "hydglassfe3" for the lowermost TSw units, and CHn units, shown in Table I-1.) In the vitric rock below the repository, heating accelerates dissolution of the glass and clinoptilolite, and precipitation of silicate phases (Figure 6.4-18 through 6.4-24). CO_2 is produced in this zone by exsolution from pore water and from dissolution of calcite. The accumulation of CO_2 over time (a few thousand years) followed by dispersal and incorporation in the liquid and solid phases, is shown in Figure 6.4-16. Compared with the drift-scale THC model, a much greater quantity of CO_2 resides in this vitric interval at 2,000 years. The primary cause of the higher CO_2 concentrations this vitric interval is an order-of-magnitude greater production of feldspars owing to approximately an order-of-magnitude greater surface area for the glass in some of the units. In the drift-scale THC model, all feldspar and glass surface areas were decreased by an order-of-magnitude, whereas in the recalculated surface areas in the mountain-scale model, most were left at their original value reflecting a later reevaluation of the data. (Note that, as mentioned in Section 6.4.3.3.3, the modeled reactions forming feldspars from glass and clinoptilolite dissolution are likely to be thermodynamically or kinetically unfavorable in vitric and zeolitic units such as in the Calico Hills formation. In this respect, the increased CO_2 partial pressure in these units is unlikely.)

The depth profiles for pH and calcite dissolution/precipitation (Figures 7.2.2-5 and 7.2.2-7) are very similar except at the repository horizon (elevation approximately 1,050 m) where the mountain-scale grid is more coarse (drifts represented by single 5-by-5-m grid blocks) and the two models are not directly comparable. Also, the lower pH for the mountain-scale profile in the vitric interval below the repository (Figure 7.2.2-5) is associated with the greater CO_2 concentration there (Figure 7.2.2-6). The increased calcite accumulation above the repository in the drift-scale THC model at 2,000 years (Figure 7.2.2-7, elevation approximately 1,250 m) corresponds with the bifurcation of the temperature profiles in Figure 7.2.2-2. This may result when warmer temperatures in the drift-scale model at this horizon lower the CO_2 solubility and promote calcite precipitation from downward percolating waters, accompanied by slightly elevated pH (Figure 7.2.2-5).

Despite the differences described in the foregoing discussion, the results from the mountain-scale THC model are corroborated by the similar results from the drift-scale THC model. Validation of the drift-scale THC model (BSC 2005 [DIRS 172862], Section 7) therefore provides confidence in the mountain-scale THC model.

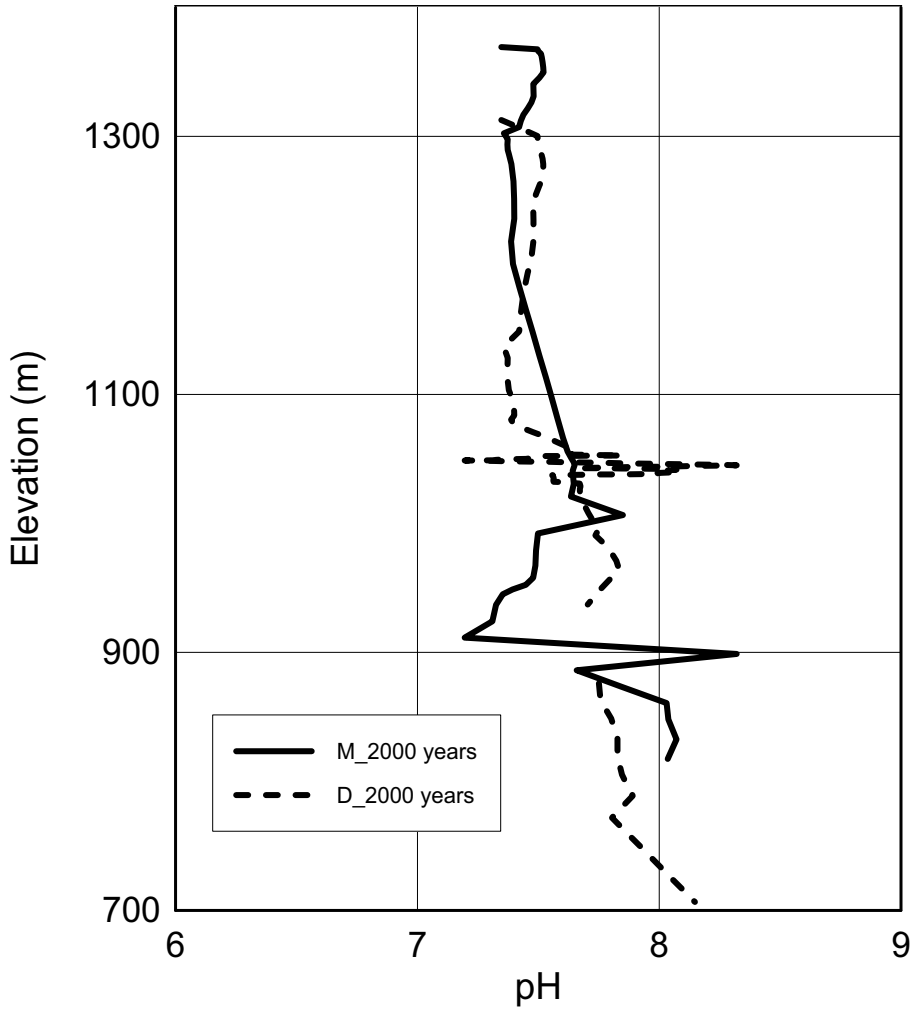

Source: DTN: LB0307DSTTHCR2.001 [DIRS 166054] (for the drift-scale THC results) and DTN: LB0310MTSCLTHC.001 (for the mountain-scale THC results).

NOTE: Early-time (10 years) curves have been omitted because they are not relevant. Drift-scale data is blanked out from the figure because, for the elevations shown, the drift scale model is represented by a single continuum (no fractures) and therefore there are no explicit data for the fracture grid blocks.

Figure 7.2.2-5. Comparison of Simulated Fracture Water pH between the Mountain-Scale THC Model and the Validated Drift-Scale THC Model as a Function of Elevation at Various Times (10 and 2,000 Years)

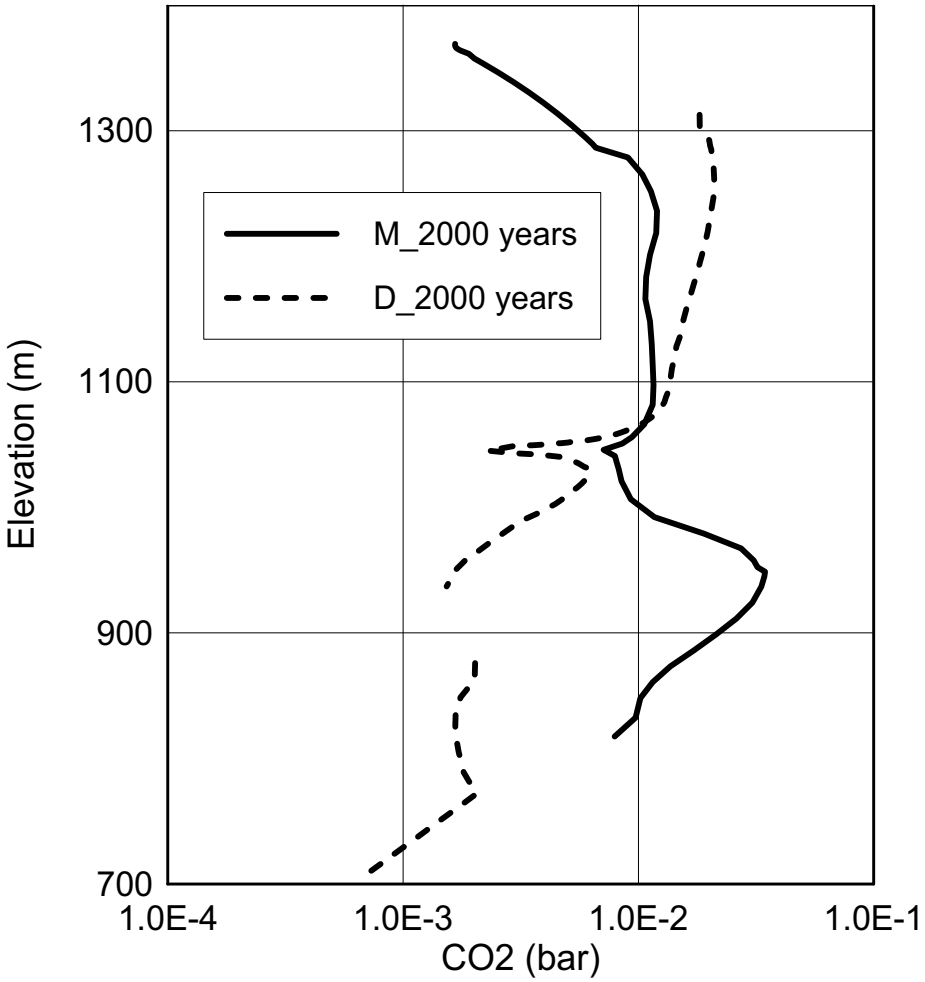

Source: DTN: LB0307DSTTHCR2.001 [DIRS 166054] (for the drift-scale THC results) and DTN: LB0310MTSCLTHC.001 (for the mountain-scale THC results).

NOTE: Early-time (10 years) curves have been omitted because they are not relevant. Drift-scale data is blanked out from the figure because, for the elevations shown, the drift scale model is represented by a single continuum (no fractures) and therefore there are no explicit data for the fracture grid blocks.

Figure 7.2.2-6. Comparison of Simulated Fracture CO_2 Partial Pressures Between the Mountain-Scale THC Model and the Validated Drift-Scale THC Model as a Function of Elevation at Various Times (10 and 2,000 Years)

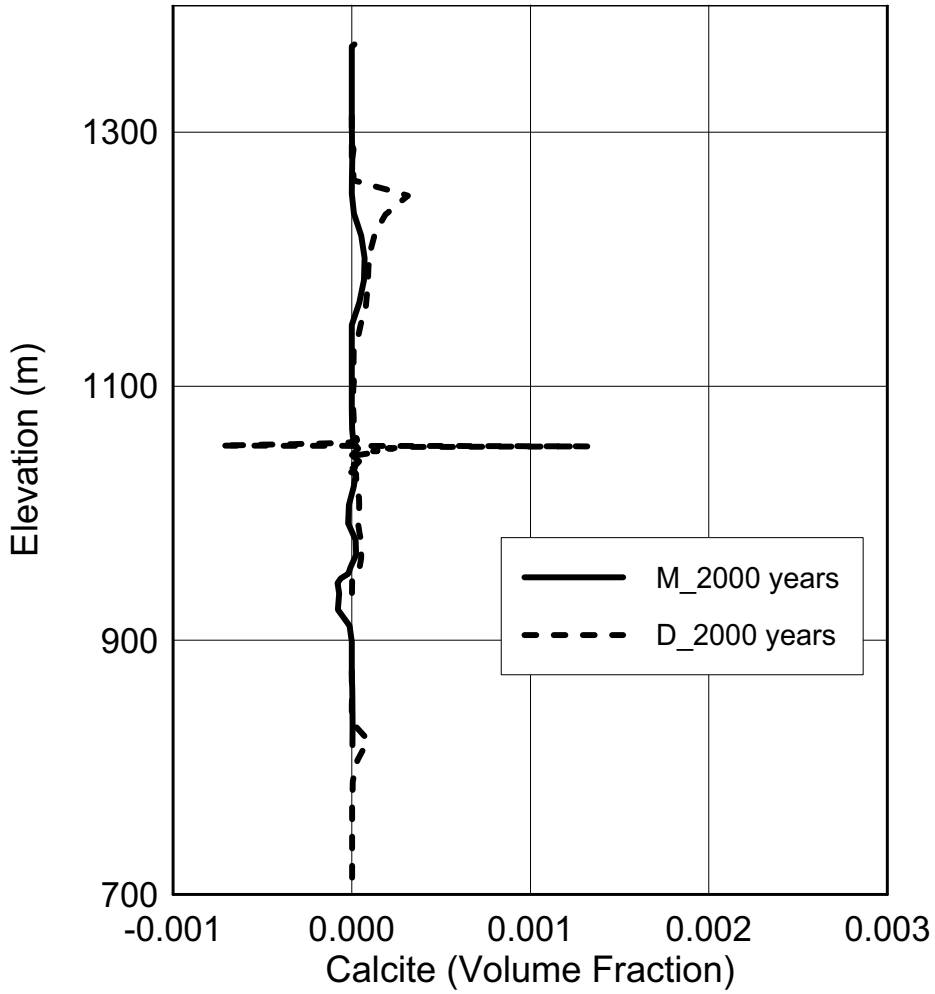

Source: DTN: LB0307DSTTHCR2.001 [DIRS 166054] (for the drift-scale THC results) and DTN: LB0310MTSCLTHC.001 (for the mountain-scale THC results).

NOTE: Early-time (10 years) curves have been omitted because they are not relevant. Drift-scale data is blanked out from the figure because, for the elevations shown, the drift scale model is represented by a single continuum (no fractures) and therefore there are no explicit data for the fracture grid blocks.

Figure 7.2.2-7. Comparison of Simulated Volume Fractions of Fracture Calcite between the Mountain-Scale THC Model and the Validated Drift-Scale THC Model as a Function of Elevation at Various Times (10 and 2,000 Years)

Evaluation of Validation Criteria – The foregoing discussion addresses explicit criteria listed in Section 2.2.1.4.2 of the TWP (BSC 2005 [DIRS 174842]), as explained for each of the criteria:

a. *Does the mountain-scale model represent the same physical and chemical processes as were validated in the drift-scale model?*

   The mountain-scale THC model uses the same conceptualization and mathematical treatment of THC coupled-processes as the drift-scale THC model, including the same thermodynamic and kinetic data. The net effects on porosity and permeability in far-field units (the basal vitrophyre of the TSw, the vitric tuffs in the Calico Hills and the PTn, and the zeolitized and often glass-rich tuffs of the Calico Hills, Prow Pass, and Bullfrog units) are considered to be small in both the mountain-scale and drift-scale models (Section 6.4.3.3.4 and Appendix III; see also BSC 2005 [DIRS 172862], Sections 6.4.4 and 6.5.5.3). Thus, this criterion is satisfied.

b. *Are the scale-dependent processes, properties, and initial/boundary conditions identified and treated appropriately in the corroboration?*

   The initial and boundary conditions used in the mountain-scale THC model (thermal, hydrologic, and chemical) are independent of scale. The thermal and hydrological properties used in the mountain-scale THC models are identical to those used in the mountain-scale TH model; use of these properties including scale dependence of fracture permeability is discussed in Section 7.1.2. Spatial scaling with regard to representation of reactive chemical transport in the mountain-scale THC model does not significantly affect the THC predictions for the far-field host rock, as discussed above. Thus, this criterion is satisfied.

c. *Are the similarities and differences between the mountain-scale and drift-scale model results identified?*

   Similarities and differences between the drift-scale and mountain-scale THC models are discussed in Section 6.4, and in addition the potential effects of spatial up-scaling are discussed above. In accordance with that discussion, this criterion has been satisfied.

d. *Are the scale-dependent numerical issues identified and evaluated with respect to the corroboration?*

   Scale-dependent numerical issues for representing thermal and hydrologic processes at the mountain scale are identified and evaluated in Section 7.2. As explained above, experience with THC modeling using different grids at different scales, and comparison of far-field predicted results from drift-scale vs. mountain-scale models, have not shown scale dependency that leads to different precipitated minerals or unexpected changes in aqueous or gaseous species compositions.

7.2.3 Corroboration with Information from Refereed Technical Literature

Several papers have been published in refereed literature that use TOUGHREACT and are applied to similar coupled THC systems and/or build confidence in specific aspects of the mountain-scale THC model. Note that corroboration of the TH aspects of the THC model (TOUGHREACT implements the same TH processes and numerical approach as TOUGH2) is discussed in Sections 7.1.3 and 7.1.4. Corroboration of the mountain-scale THC model using information from refereed technical literature is specified by the TWP (BSC 2005 [DIRS 174842], Section 2.2.1.4.2), which gives explicit criteria for corroboration. This section describes several published papers and their relation to validation of the mountain-scale THC model, followed by evaluation of the explicit criteria for selected published information.

- "Simulation of Water-Rock Interaction in the Yellowstone Geothermal System using TOUGHREACT." TOUGH Symposium 2003, Proceedings (Dobson et al. 2003 [DIRS 168273]).

  Rationale for corroboration: This paper describes a modeling study of the alteration of volcanic glass-rich rhyolitic tuffs and lavas having a similar composition to those encountered in the Calico Hills units below the repository. TOUGHREACT was used in this analysis for boiling conditions similar to those in the predicted boiling zone at Yucca Mountain. Alteration of glass to zeolites and permeability changes as a result of fracture sealing by silica phases has occurred in these rocks, similar to the processes postulated for alteration at Yucca Mountain. The time-scale of such alteration is on the scale of thousands of years, similar to that of the lifetime of the repository. Much of the same thermodynamic and kinetic data for mineral–water reactions used in the mountain-scale THC model were used in the published analysis.

- "Thermal-Hydrodynamic-Chemical (THC) Modeling Based on Geothermal Field Data." *Geothermics* (Kiryukhin et al. 2004 [DIRS 170653]).

  Rationale for corroboration: This paper describes the application of THC models using TOUGHREACT to some large-scale geothermal reservoirs, where changes to flow as a result of mineral precipitation/dissolution have taken place.

- "Fluid Flow and Reactive Transport Around Potential Nuclear Waste Emplacement Tunnels at Yucca Mountain, Nevada." *Journal of Contaminant Hydrology* (Spycher et al. 2003 [DIRS 162121]).

  Rationale for corroboration: This paper discusses the model developed in *Drift-Scale THC Seepage Model* (BSC 2005 [DIRS 172862]) and the results of mineral precipitation on flow. The conceptual model for THC processes and the geochemical inputs in the mountain-scale THC model are similar to those used in the THC seepage model.

- "A Reactive-Transport Model for Calcite Precipitation and Evaluation of Infiltration Fluxes in Unsaturated Fractured Rock." *Journal of Contaminant Hydrology* (Xu et al. 2003 [DIRS 162124]).

Rationale for corroboration: Abundances of calcite in fractures formed over several million years via percolating water in a geothermal gradient throughout the unsaturated zone at Yucca Mountain were modeled using TOUGHREACT. Modeling showed similar patterns of calcite distribution with depth and in fractures and matrix, compared to measured abundances. The conceptual models used for flow, and input geochemical data, were similar to those in the mountain-scale THC model.

- "Parameterization and Upscaling in Modeling Flow and Transport in the Unsaturated Zone of Yucca Mountain." *Conceptual Models of Flow and Transport in the Fractured Vadose Zone* (Bodvarsson et al. 2001 [DIRS 160133]).

  Rationale for corroboration: Modeling predictions of chloride and strontium concentrations in pore waters at the mountain-scale, using TOUGH2 (LBNL 2003 [DIRS 161491]), are compared to measured values from the ECRB Cross-Drift and from surface-based boreholes. Good agreement between modeled and measured concentrations validate the conceptual models and earlier versions of the numerical models for flow and transport that are the basis for the mountain-scale THC model.

- "Experimental and Numerical Simulation of Dissolution and Precipitation: Implications for Fracture Sealing at Yucca Mountain, Nevada." *Journal of Contaminant Hydrology* (Dobson et al. 2003 [DIRS 165949]).

  Rationale for corroboration: Effects on flow resulting from fracture sealing were validated by comparison of TOUGHREACT simulations to experiments performed on a tuff sample from the Tptpmn unit. These comparisons validate the approach used in the mountain-scale THC model to assess changes in percolation fluxes in the UZ.

Evaluation of Validation Criteria – From the peer reviewed publications in technical literature cited above as corroborating evidence, the publication by Spycher et al. (2003 [DIRS 162121]) is selected for more specific evaluation of the validation criteria (i.e., for validating the mountain-scale THC model). The THC model in the publication by Spycher et al. (2003 [DIRS 162121]) is the closest to the mountain-scale THC model in peer-reviewed technical literature; it is therefore selected for evaluating the validation criteria as discussed below.

1. *Does the corroboration information represent the same physical and chemical processes as the mountain-scale model?*

   The same underlying physical and chemical processes as those in the mountain-scale THC model have been investigated, undergone technical review, and been published in the refereed technical literature (Spycher et al. 2003 [DIRS 162121]), although this particular publication is concerned mainly with processes at smaller temporal and spatial scales (i.e., at the drift scale). Therefore, though the spatial and temporal scales are different, this publication in peer reviewed technical literature corroborates the physical and chemical processes in the mountain-scale THC model.

2. *Does the corroboration rely on scale-dependent processes, properties, or initial/boundary conditions, and if so are these treated appropriately in the corroboration?*

   As discussed earlier (see Section 7.2.2), the initial and boundary conditions used in the mountain-scale THC model (thermal, hydrologic, and chemical) are independent of scale. Thus, as far as these issues are concerned, even though the corroborating THC model (Spycher et al. 2003 [DIRS 162121]) is at a different spatial and temporal scale than the mountain-scale THC model, it is acceptable to use this publication for validating the mountain-scale THC model.

   Conceptually, the THC model in Spycher et al. (2003 [DIRS 162121]) is the same as the drift-scale THC model (BSC 2005 [DIRS 172862]). The issues of up-scaling of THC processes from drift-scale to mountain-scale have been elaborated in Section 7.2.2. The same up-scaling issues are pertinent between the mountain-scale THC model and the THC model in Spycher et al. (2003 [DIRS 162121]). As has been established in Section 7.2.2, the issue of scale is not significant for THC processes in the far-field. Thus, despite the difference in scale between the mountain-scale THC model and the THC model in Spycher et al. (2003 [DIRS 162121]), the latter is a valid corroborating model for the former.

3 *Are the similarities and differences between the mountain-scale model or its results, and the corroborating information, identified and explained?*

   As discussed above, the THC model in Spycher et al. (2003 [DIRS 162121]) is essentially the drift-scale THC model (BSC 2005 [DIRS 172862]). The similarities and differences between the drift-scale THC model (BSC 2005 [DIRS 172862]) and the mountain-scale THC model have been discussed in Section 6.4. The same discussion is applicable between the mountain-scale THC model and the THC model in the corroboration (Spycher et al. 2003 [DIRS 162121]). In addition, the issue of up-scaling has been discussed in Section 7.2.2, which is also applicable between the mountain-scale THC model and the THC model in the corroboration (Spycher et al. 2003 [DIRS 162121]).

7.2.4 Discussion of Independent Technical Model Validation Review

An independent technical review for post-development model validation of the mountain-scale THC model has been performed by Dr. Carl I. Steefel, Earth Sciences Division of Lawrence Berkeley National Laboratory, Berkeley, California.

The review criteria for the post-development validation review were presented in Section 2.2.1.4.2 of the TWP (BSC 2005 [DIRS 174842]) and are repeated here:

- The technical approach and algorithms described in the document capture all physical and chemical processes that are significant to the intended use of the model for screening these FEPs.

- Modeling assumptions are clearly defined and justified as appropriate for the intended use of the model for screening these FEPs.

- Uncertainties in model parameters, process representation, and assumptions are sufficiently described, and impacts of these uncertainties discussed, as appropriate for the intended use of the model for screening these FEPs.

- The overall technical credibility of the approach, including assumptions, parameters, equations, and numerical implementation, is appropriate for the intended use of the model for screening these FEPs.

The post-development validation review based on the review criteria was conducted. Dr. Steefel's technical comments have been appraised and responded to accordingly, based on the instructions in the TWP (BSC 2005 [DIRS 174842], Section 2.2.1.4.2). Any changes made on this report were provided to the reviewer for his concurrence. The conclusion from Dr. Steefel's review is summarized and presented below:

> I find that overall the mountain scale modeling of THC processes to be an impressive piece of work that extends the ground-breaking modeling carried out on the Drift Scale Test (DST) published earlier by the Berkeley group. The DST provides perhaps the most comprehensive validation of a THC model to date and has certainly advanced the state of the science well beyond what has been documented elsewhere in the literature.
>
> In terms of the use of the mountain-scale THC model's use in screening of the relevant FEPs, I find that for the higher temperature processes dominating the thermal period in the vicinity of the Drift Scale Test (i.e., within the repository horizons), the technical approach and algorithms described in the document capture all physical and chemical processes that are significant to the intended use of the model for screening these FEPs. However, the same cannot yet be said with regard to processes in more distal units, especially those lying below the repository horizons. For example, no significant validation is provided for the THC modeling of reactions in the Calico Hills formation at lower temperatures and in rock containing abundant zeolites. In addition, the modeling cannot be said to have captured all of the relevant chemical processes, since formation of zeolites of variable composition (which are expected to have greater thermodynamic stability than pure end member phases) and cation exchange (which will affect the chemistry of water reaching the saturated zone) have not been included. These comments are made in the attached Review Comments and are largely acknowledged by the authors of the AMR. However, I do agree with the responses to my comments that it is likely that the modeling over-estimates reaction rates in these lower horizons and thus probably over-estimates changes in permeability and solution pH. The changes in these physical and chemical parameters, therefore, are most likely even less than predicted by the modeling. The likely smaller range in pH values, for example, makes the presently measured K_d values more rather than less representative of the actual conditions that will

> occur in the mountain below the repository horizons. Therefore, the impact of the high uncertainties and neglect of some chemical processes in the lower horizons is expected to be minimal.
>
> Modeling assumptions are clearly defined as appropriate for the intended use of the model for screening these FEPs. My own belief, however, is that a neglect of variable composition solid solutions and cation exchange cannot be fully justified, although the modeling results presented without these processes are very likely overly conservative. Uncertainties in model parameters, process representation, and assumptions are described in detail, and the impacts of these uncertainties are discussed, as appropriate for the intended use of the model for screening these FEPs. In particular, uncertainties associated with some of the processes highlighted in my technical review are now discussed extensively. The authors have provided additional material to justify the conclusion that where modeling of THC processes is highly uncertain, the results are most likely overly conservative.
>
> The overall technical credibility of the approach, including assumptions, parameters, equations, and numerical implementation, is appropriate for the intended use of the model for screening these FEPs. The neglect of some chemical processes most likely had the effect of making the modeling overly conservative and therefore should not be considered to invalidate the screening of the FEPs.

The complete text of Dr. Steefel's review comments and conclusion is presented in Appendix VIII. The conclusion from Dr. Steefel's post-development validation review fulfills the requirements in the TWP (BSC 2005 [DIRS 174842], Section 2.2.1.4.2) and confirms adequacy of the mountain-scale THC model in model development, data selection and usage, and range of intended use.

7.2.5 Summary and Evaluation of Validation Criteria

In summary, the mountain-scale THC model is validated using confidence-building information derived both during model development and from post-development activities. Information used for confidence-building during model development includes discussion of input data, how calibration was used, initial conditions and boundary conditions, numerical convergence, the range of conditions simulated, and uncertainties (Section 7.2.1). Post-development validation activities consist of corroboration by results from validation of the drift-scale model (Section 7.2.2), corroboration using other information (i.e., publication of field-test simulations and geothermal analogues) from refereed technical publications (Section 7.2.3), and technical review independent of model development for the post-development validation (Section 7.2.4). These activities provide confidence that the mountain-scale THC model is adequate for its intended use, to support screening evaluation of FEPs (BSC 2005 [DIRS 174191], Sections 6.9.7 and 6.9.13).

Effect of Anorthite Reaction Rate on Mineral Alteration and Chemistry – The effect of the modification of the anorthite rate constant was evaluated for the Drift-Scale Test THC model and an earlier version of the mountain-scale THC model in *FY 01 Supplemental Science and Performance Analyses, Volume 1: Scientific Bases and Analyses* (BSC 2001 [DIRS 155950], Section 3.3.6.3). It was found that at the full reaction rate of anorthite there were significant increases in pH and decreases in pCO_2 that were not consistent with measured values at the DST. However, there were little differences in calculated mineral abundances, and some species such as Na, K, and Ca actually fit the measured data more closely using the larger surface area. Since the gas-phase CO_2 measurements were considered to be more suited to validating the DST THC model, the reduced anorthite surface area was used in future studies. The following paragraphs discuss the findings from the Supplemental Science and Performance Analyses mountain-scale THC model (BSC 2001 [DIRS 155950], Section 3.3.6.3) and the DST THC model (CRWMS M&O 2001 [DIRS 154426]).

Supplemental Science and Performance Analyses Mountain-Scale THC Model – To assess uncertainties associated with mineral reaction rates (which were shown to have a strong effect on water and gas chemistry in the drift-scale THC simulations; BSC 2005 [DIRS 172862]), two simulations were performed that used alternative values for the reaction rate of anorthite. The lower rate (by three orders of magnitude) resulted in a smaller deviation in the chemical evolution of the initial water under ambient temperatures (corroborating evidence for effective reaction rates), with the model infiltration rate and initial and boundary gas-phase CO_2 concentrations. This simulation will be referred to as "Extended Case 1" and that with the high rate for anorthite as "Extended Case 2." Some additional parameters were modified that have a less substantive effect on the simulation results, such as the initial precipitation rate of new secondary phases. Some of the more important indicators for the effect of THC processes on hydrological properties and mineralogy are shown in Figure 3.3.6-3 (BSC 2001 [DIRS 155950]) after about 1,400 years of heating (Extended Case 1) and in Figure 3.3.6-4 (BSC 2001 [DIRS 155950]) after 5,000 years (Extended Case 2). The main difference in the results for the two cases was in the gas-phase CO_2 concentrations and pH. The differences were not great enough to markedly change the mineral abundances and distributions.

DST THC Model – Figures 19a and b of *Drift-Scale Coupled Processes (DST and THC Seepage) Models* (CRWMS M&O 2001 [DIRS 154426]) show the evolution of pH in the sampled waters compared to the modeled base-case and extended systems. In general, both geochemical systems capture the trend in pH changes of fracture waters in this region. However, the base-case system captures the drop in pH more closely than the extended system. The system without calcite also shows a reasonable match to the measured pH values compared to the other simulations. The early trend to lower pH is related to the addition of condensate to this area and to increases in CO_2 in the gas phase (due to boiling closer to the heaters and diffusive and advective gas transport outwards). Later increases in pH are related to boiling of the water in this area, leading to a reduction in CO_2 concentrations as the temperature reaches boiling and the zone finally dries out. The simulation using the full anorthite rate shows the highest pH and poorest agreement with the measured values. The model results for interval 60-3 showing complete dryout at approximately 18 months are consistent with the observation that water was absent from this interval shortly after the last sample was collected at 16 months of heating.

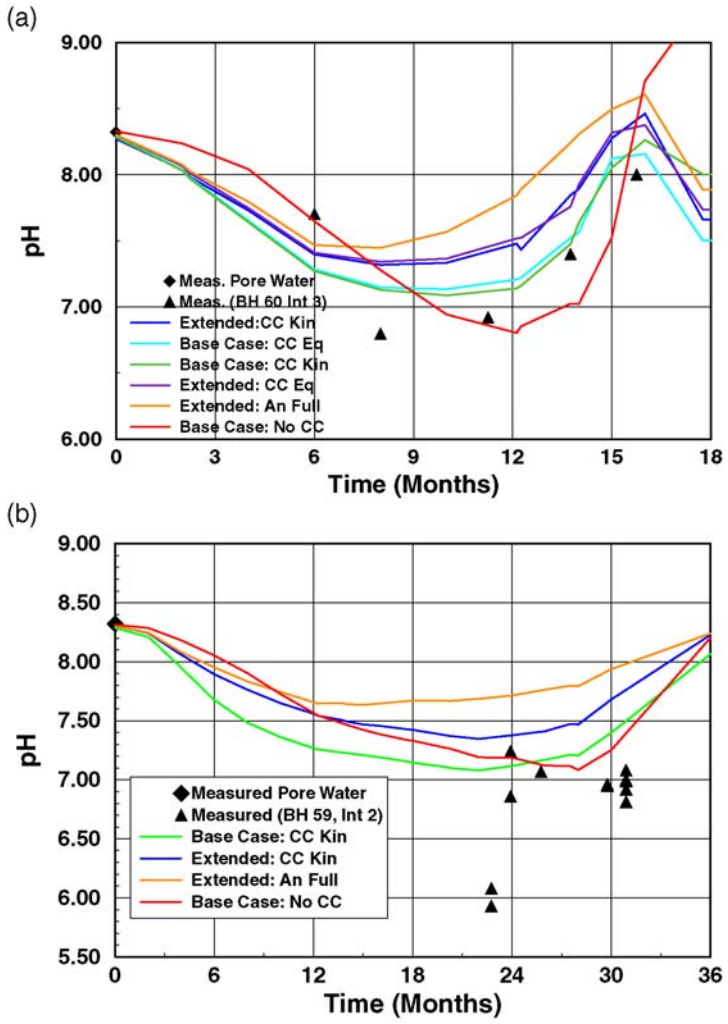

Source: DTNs: LB0011DSTTHCR1.002 (simulated), LL990702804244.100 [DIRS 144922] (measured), LL001200231031.009 [DIRS 153616] (measured), MO0101SEPFDDST.000 [DIRS 153711] (measured), MO0005PORWATER.000 [DIRS 150930] (measured).

NOTE: The ambient pore-water pH is approximately 8.3. "CC Kin" stands for the calcite reacting under kinetic constraints, "CC Eq" stands for the calcite reacting assuming local equilibrium, "No CC" stands for the no calcite present in the system, and "An Full" stands for the full anorthite reaction rate.

Figure 7.2.5-1. Changes in pH in Water Samples Collected from Borehole Intervals 60-3 (a) and 59-2 (b), Compared to Modeled Fracture Water pH at Nearby Model Grid Nodes

Measured sodium concentrations (Figure 7.2.5-2) are also much lower than in the initial pore water and close to the model predictions. However, the extent of dilution in interval 60-3 is only from 3 to 6 times, whereas for Cl it was from 6 to about 20 times (CRWMS M&O 2001 [DIRS 154426], Figure 20a). This difference indicates some contribution of water-rock interaction to the Na concentrations, which is shown in the extended-case model results as a shift to higher Na concentrations from the base-case results. The origin of the sodium in the DST waters could be alkali feldspar and/or reaction or exchange with clays. In the model simulations, the main source of Na is from alkali feldspar dissolution. The sharp rise to higher concentrations at later times is due to rapid dryout.

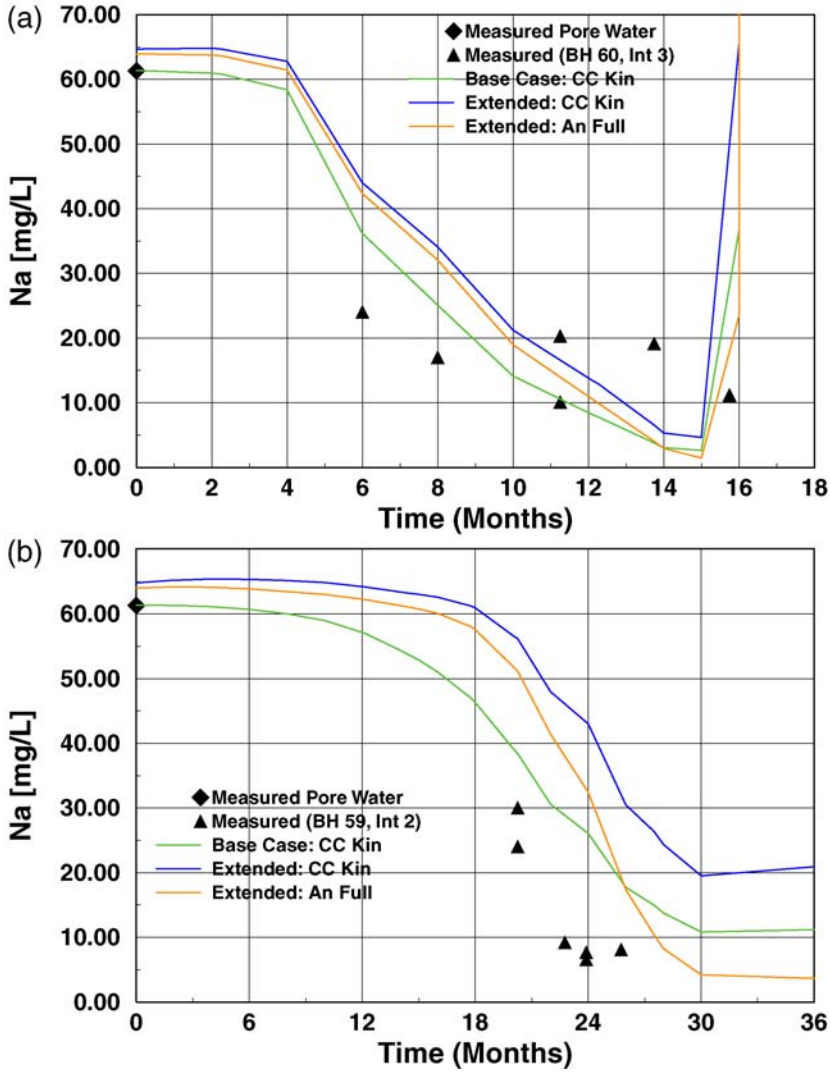

Source: DTNs: LB0011DSTTHCR1.002 (simulated), LL990702804244.100 [DIRS 144922] (measured), LL001200231031.009 [DIRS 153616] (measured), MO0005PORWATER.000 [DIRS 150930] (measured).

NOTE: "CC Kin" stands for the calcite reacting under kinetic constraints, and "An Full" stands for the full anorthite reaction rate.

Figure 7.2.5-2. Changes in Na (mg/L) in Water Samples Collected from Borehole Intervals 60-3 (a) and 59-2 (b), Compared to Modeled Fracture Water Na at Nearby Model Grid Nodes

Calcium is more sensitive to water-rock interaction than some other species because of the fast reaction rate of calcite and its common occurrence in fractures. Other potential sources of Ca in the rock include Ca-rich zeolites, such as stellerite (which is abundant in the fractures), as well as Ca from plagioclase feldspar. Waters collected from intervals 60-3 and 59-2 show a large drop from the pore-water concentration (about 100 mg/L) to below 10 mg/L with a consistent decrease over time in 60-3 (Figure 7.2.5-3). The continued drop in Ca in 60-3 and the very low concentrations in 59-2 may be caused by calcite precipitation, because of its reverse solubility

with increasing temperature. The model results shown in Figure 7.2.5-3 also show a similar drop, albeit not to as low concentrations.

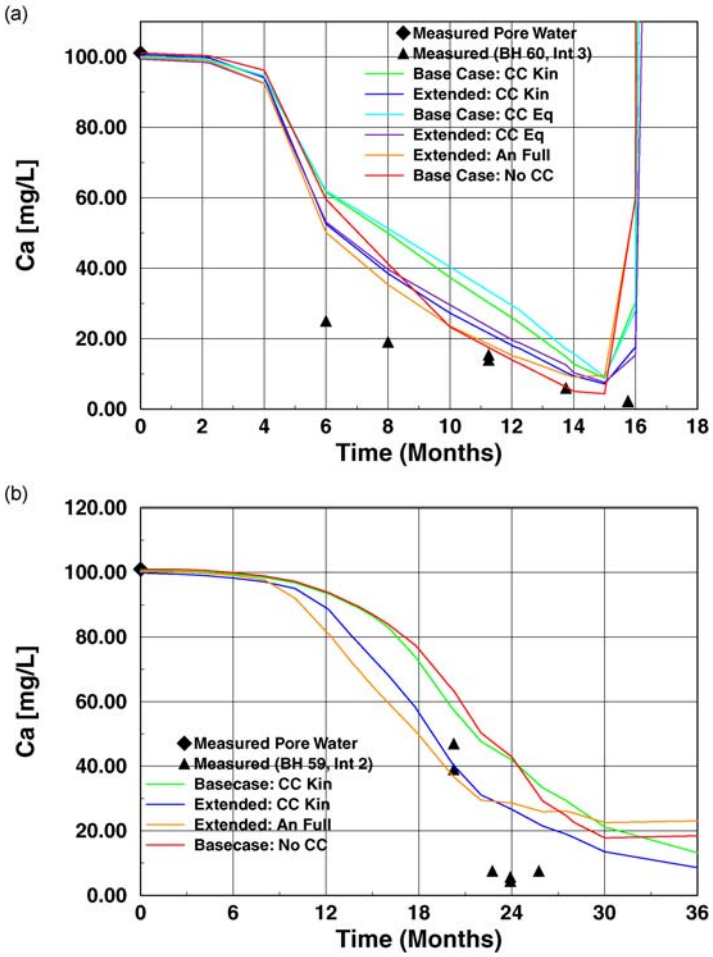

Source: DTN: LB0011DSTTHCR1.002 (simulated), LL990702804244.100 [DIRS 144922] (measured), LL001200231031.009 [DIRS 153616] (measured), MO0005PORWATER.000 [DIRS 150930] (measured).

NOTE: "CC Kin" stands for the calcite reacting under kinetic constraints, "CC Eq" stands for the calcite reacting assuming local equilibrium, "No CC" stands for the no calcite present in the system, and "An Full" stands for the full anorthite reaction rate.

Figure 7.2.5-3. Changes in Ca (mg/L) in Water Samples Collected from Borehole Intervals 60-3 (a) and 59-2 (b), Compared to Modeled Ca in Fracture Water at Nearby Model Grid Nodes

7.3 VALIDATION OF THE MOUNTAIN-SCALE THM MODEL

The intended use of the mountain-scale coupled THM model is to support screening of FEPs related to the TSPA component models "UZ Flow" (BSC 2005 [DIRS 174191], Section 6.9.12) and "SZ Flow" (BSC 2005 [DIRS 174190], Sections 6.2.36 and 6.2.37). For such a model, the applicable planning procedure (LP-2.29Q-BSC, Attachment 3, Table 1) requires Level I validation. Implementation of Level 1 validation for the mountain-scale THM model is specified in Section 2.2.1.1 of the TWP (BSC 2005 [DIRS 174842]).

Validation of the mountain-scale THM model is achieved through confidence-building activities during model development (Section 7.3.1), by corroboration with the validation of the drift-scale THM model, as presented in *Drift-Scale THM Model* (BSC 2004 [DIRS 169864]; see Section 7.3.2 below), by corroboration with relevant information from refereed technical publications (Section 7.3.3), and by technical review by reviewers independent of the development, checking, and review of the model documentation (Section 7.3.4), supplemented by corroboration with an alternative mathematical model (Section 7.3.5). These measures provide confidence that the mountain-scale THM model is adequate for its intended use in FEP screening.

7.3.1 Summary of Confidence Building during Model Development

This section summarizes the achieved confidence building during model development as defined in Section 2.2.1.2 of the TWP (BSC 2005 [DIRS 174842]). In the following discussion each requirement is stated and explanation is provided for how the requirement is met, with pointers to relevant details:

1. *Selection of input parameters and/or input data, and a discussion of how the selection process builds confidence in the model [LP-SIII.10Q-BSC, Section 5.3.2(b)(1)].*

   The direct inputs to the mountain-scale THM model have all been obtained from controlled sources (see Section 4.1 and Table 4.1-1). Section 4.1 gives the basis for selection of values for key parameters. More in-depth justification is given in Section 6.1 and Sections 6.5.6 through 6.5.9. Section 6.1 discusses selection TH parameters that are common for the TH and THM mountain-scale models. Sections 6.5.6 through 6.5.9 describe parameters that are specific to the mountain-scale THM model, including mechanical properties. Thus, this requirement has been satisfied.

2. *Description of initial and boundary conditions runs, and/or run convergences, and a discussion of how the activity or activities build confidence in the model. If appropriate, include a discussion of impacts of any non-convergence runs [(LP-SIII.10Q-BSC, Section 5.3.2(b)(2)].*

   Detailed discussion of initial and boundary condition runs for the mountain-scale THM model is provided in Section 6.5.6. Discussion of nonconvergence runs is not relevant for this model. Thus, this requirement has also been satisfied.

3. *Discussion of the impacts of uncertainties to the model results [LP-SIII.10Q-BSC, Section 5.3.2(b)(3) and LP-2.29Q-BSC, Attachment 3, Level 1 (d) and (f)].*

   Discussion of model uncertainties and their impacts on model results is provided in Section 6.5.15. A summary discussion on model limitations and their impact is given in Section 8.5. Accordingly, this requirement has been satisfied.

7.3.2 Corroboration Using Results from Validation of the Drift-Scale THM Model

Methods and criteria for confidence-building after model development are described in the TWP (BSC 2005 [DIRS 174842], Section 2.2.1). For validating the mountain-scale THM model, the TWP designates use of Method 1 (LP-SIII.10Q-BSC, Section 5.3.2(c) item 1, as specified for use of "other relevant information"): corroboration of the mountain-scale THM model using results obtained from validation of the drift-scale THM model (BSC 2005 [DIRS 169864], Section 7).

Corroboration of the mountain-scale THM model with results from validation of the drift-scale THM model is appropriate because the drift-scale model represents the same physical processes and uses the same underlying conceptual model. Coupled THM processes at the mountain-scale are identical to those at the drift scale but may be different in extent and magnitude as a result of scale-dependent properties. The following discussion of corroboration with the drift-scale THM model is organized in three parts. First the validation of the drift-scale THM model is reviewed. Then up-scaling issues are identified and explained. Finally, consistency in the model results between the mountain-scale and drift-scale THM models is evaluated. This discussion is followed by evaluation of the explicit criteria identified in the TWP (BSC 2005 [DIRS 174842], Section 2.2.1.4.3).

Review of Validation of the Drift-Scale THM Model – The model developed in *Drift Scale THM Model* (BSC 2004 [DIRS 169864]) was first tested by a coupled THM simulation of the DST and a coupled HM simulation of the Yucca Mountain niche experiments (BSC 2004 [DIRS 169864], Sections 7.4 and 7.5). This approach tested the underlying conceptual model for representing the fractured host rock and demonstrated that the drift-scale THM model appropriately captures relevant THM processes. The validation of the drift-scale THM model against the DST was conducted in the following steps, producing results which are relevant to the mountain-scale model:

1. Check that the simulated temperature field was in reasonable agreement with the observed temperature field to ensure that the THM model is properly implemented in terms of thermal behavior. Thermal properties of the host rock are not scale dependent, so this aspect of the validation is directly applicable to the mountain-scale model.

2. Check that simulated rock-mass displacements captured the general trends and average magnitudes of observed displacements (validation of TM processes). The region of influence of the DST extended for tens of meters so the observed displacements are representative of in situ thermal expansivity. The spatial scale of these observations is sufficient to evaluate the potential for large scale TM processes, such as mechanical coupling between adjacent drifts, and thermomechanical edge effects near the boundary of the repository layout. This aspect of the validation is therefore applicable to the mountain-scale model.

3. Check that the simulated changes in air permeability captured the general trends and magnitudes observed in the field (validation of THM processes). Although fracture permeability is scale dependent, such that THM processes may also be scale dependent, the use of drift-scale derived THM coupling relationships does not affect

the intended use of the mountain-scale model. The host rock fracture permeability is orders of magnitude greater than needed to conduct the in situ percolation flux, so downward, free drainage of liquid flux in fractures is assured for all scales. Thermal stress decreases with distance, and proportional changes to fracture permeability do not affect the host rock drainage capacity. Use of drift-scale derived THM coupling relationships at the mountain-scale probably tends to overestimate the proportional effect on fracture permeability at the larger scale, because larger discontinuities are generally much more permeable (see up-scaling discussion below), whereas their deformability changes only moderately with scale, they may tend to be slightly more compliant. This is acceptable for the intended use of the mountain-scale THM model to support FEP evaluation.

Additional confidence in the drift-scale THM model was demonstrated by corroboration with results from an alternative conceptual model, and through publication in refereed professional journals (BSC 2004 [DIRS 169864], Sections 7.6 and 7.7). Multiple lines of evidence were provided from geothermal analogues and from other heater tests (BSC 2004 [DIRS 169864], Section 7.8). These results provide additional confidence in the application of the results from validation of the drift-scale THM model, to corroboration of the mountain-scale model.

Upscaling from Drift Scale to Mountain Scale – In order to use the validation results developed for the drift-scale THM model for validation of the mountain-scale model, potential scale dependency of properties or parameters needs to be considered. The scale dependency related to THM processes is discussed in this section in terms of validation of the mountain-scale model related to TM, HM and THM processes.

Validation for TM processes at the drift scale is applicable to the mountain-scale model because thermal, mechanical, and TM properties are not significantly different at the mountain scale. For example, mechanical displacement along one of the boreholes (BSC 2004 [DIRS 169864], Figure 7.4.2-3) was well captured at both the one-meter scale and the 15-meter scale by a model that does not incorporate a scaling law. Because rock-mass thermal expansion measured at the DST is directly proportional to the thermal expansion coefficient, whereas it is rather insensitive to rock-mass deformation modulus, the DST analysis shows that the thermal expansion coefficient is scale independent. Since the thermal expansion coefficient is not scale dependent, it also indicates that the deformation modulus is not scale dependent for scales >1 m, because both quantities depend on fracture network geometry and fracture deformability. Moreover, at the DST a good agreement was achieved between predicted and measured permeability changes. Such good agreement requires correct prediction of both the thermal stress and the stress-permeability relationship, and thus provides evidence for an accurate representation of the rock-mass deformation modulus. The lack of scale dependency in thermal-mechanical properties from 1 to 15 meters supports use of the drift-scale derived TM and mechanical properties in the mountain-scale model. Lack of scale dependence in thermal-mechanical properties is attributed to non-scale dependent thermal properties, coupled with relatively dense fracturing resulting in homogeneous rock mass mechanical response.

Lack of scale dependence for observed mechanical response at scales larger than about 1 meter is supported by in situ measured values of deformation modulus reported in the literature as well

as by in situ measurements at Yucca Mountain. Typically, the in situ deformation modulus in various types of fractured rocks exhibits a variability and mean values that typically decrease with sample size (da Cunha 1993 [DIRS 168515], Section 3; da Cunha 1993 [DIRS 168514], Figure 10). However, mean values of deformation modulus typically become more constant for measurement scales above one cubic meter. He (1993 [DIRS 168516]) reviewed 53 references with 258 deformation modulus entries for various rock types (igneous, metamorphic, and sedimentary), for which he calculated a mean value of 16.43 GPa. This value is close to the mean value adopted for the repository units in this study both at the drift scale and mountain scale. In situ measurements of modulus of elasticity at Yucca Mountain include:

1) Field rock-mass moduli from borehole jack testing in the SHT block ranged from 3 to 23 GPa (CRWMS M&O 1999 [DIRS 129261], Section 9.6).

2) Plate loading tests conducted at the DST suggested a rock-mass modulus ranging from 11.5 to 29.7 GPa (CRWMS M&O 1998 [DIRS 108306], Table 6-7).

3) Previous in situ experiments in welded tuff in the G-tunnel indicated modulus values from 14.7 GPa to 17.6 GPa, about half of the intact-rock values (CRWMS M&O 1999 [DIRS 129261], pp. 9-19).

These tests have a radius of influence of up to several meters and may therefore represent the rock-mass deformation modulus at the scale of tens of cubic meters.

The validation for HM processes on the drift scale can be extended to that of the mountain scale by considering the potential scale dependence of coupled HM properties (in this case the stress-versus-permeability relationship). Hydraulic properties have been shown to depend on the measurement scale (BSC 2004 [DIRS 170038], Section 6.1.1.1). At Yucca Mountain, mountain-scale calibrated fracture permeability is generally one to two orders of magnitude larger than drift-scale calibrated fracture permeability (BSC 2004 [DIRS 169857], Sections 6.3.2 and 6.3.3). At the same time, as discussed above, there is a lack of scale dependency between that of drift scale and mountain scale in mechanical properties. In other words, the initial rock-mass permeability is higher at the mountain scale, whereas the rock mass deformability is about the same at both scales. In effect, the higher permeability and similar deformability at the mountain scale suggests that permeability changes due to thermal-mechanical effects are smaller at the mountain scale than at the drift scale. This is in agreement with observations from other fractured rock sites, which indicate that permeable, highly conductive fracture zones are generally less sensitive to stress than zones of more competent rock (Rutqvist and Stephansson 2003 [DIRS 162583]). Despite the field evidence for permeability being less sensitive to stress changes at the mountain-scale, a reasonable choice (given the intended uses of the mountain-scale model) was made for the up-scaling of the stress-versus-permeability according to up-scaling method 2 in Section 6.5.9. This up-scaling method implies that permeability in the mountain-scale simulation is equally sensitive to stress changes as in the drift scale. Consequently, a given change in the stress field would result in the same relative change in permeability (permeability correction factor) in the mountain-scale and drift-scale models. Therefore, the calculated permeability changes in the mountain-scale simulation can be quantitatively compared to that of the drift-scale simulation as a consistency check (discussed further below).

The issue of up-scaling THM properties and their impact on the performance assessment of nuclear waste repositories is also part of the international cooperative project DECOVALEX (Liu et al. 2003 [DIRS 166017], Min et al. 2004 [DIRS 172883]). In the recent DECOVALEX III project, the TOUGH2-FLAC3D simulator was applied in a benchmark test to the up-scaling of THM properties at Sellafield, UK. The rock at Sellafield consists largely of welded tuff, a type of rock similar to the repository units at Yucca Mountain. The TOUGH2-FLAC3D code was applied in the DECOVALEX project using the same conceptual model for hydrologic-mechanical (HM) coupling as applied in this report (Boyle 2000 [DIRS 163533]; Liu et al. 2003 [DIRS 166017]); Rutqvist et al. 2003 [DIRS 170400]). Also as part of the DEVOVALEX project, Min et al. (2004 [DIRS 172883]) conducted up-scaling of stress dependent permeability of the Sellafield fractured welded tuff rock using a discrete fracture model. The up-scaled continuum properties were derived using a conceptual model for stress-versus-permeability coupling similar to that used in this report. This included the same type of exponential stress-versus-permeability relationship. Min et al. (2004 [DIRS 172883]) also investigated the development of fracture shear slip and its effect on rock mass permeability. The study by Min et al. (2004 [DIRS 172883]) showed that the complex HM behavior of a fracture rock mass can be represented by an average continuum expression that includes a stress-versus-permeability relationship and criteria for investigating the potential for shear slip. This is also the approach taken for the mountain-scale THM model presented in this report. Thus, the peer-review publication by Min et al. (2004 [DIRS 172883]) supports the conceptual model of stress-versus-permeability coupling applied to the mountain-scale THM model

Comparison of Mountain-Scale and Drift-Scale THM Model Results – Because the THM properties are equivalent at the two scales, the mountain-scale THM model results can be directly compared to the drift-scale THM model results to demonstrate consistency. Some difference in the calculated thermal stress magnitude is expected because of differences in lateral mechanical confinement at the two model scales and differences in grid size near repository drifts. In the drift-scale THM model, symmetry conditions result in zero displacement restrictions for normal displacements at lateral boundaries located halfway between two neighboring drifts (BSC 2004 [DIRS 169864], Figure 6.3-1). As discussed in the drift-scale THM model report (BSC 2004 [DIRS 169864], Section 6.5.3), the use of the lateral fixed boundaries in the drift-scale model provides a bounding case for estimating the impact of THM processes because it leads to the highest possible thermal stress. In the mountain-scale model, on the other hand, the left lateral boundary is placed far away and is a constant stress boundary. Therefore, lower thermal stress is expected in the mountain-scale THM model compared to that of the drift-scale THM model.

The criteria for a comparison between drift-scale and mountain-scale THM results should be consistent with the validation criteria developed for coupled THM processes in the drift-scale THM model report. For the drift-scale THM model it was required that the predicted changes in permeability at the field experiments are in the correct direction and correct within an order of magnitude; that is, log (k/k_i) simulated and measured differ by less than 1 (BSC 2004 [DIRS 169864], Section 7.1.4). The quantitative criterion of simulation results within one order of magnitude was judged reasonable considering the natural variability of permeability at Yucca Mountain, and considering the variability of permeability used in the seepage models for development of drift seepage probabilities. For the mountain-scale THM model the criteria

should be related to the intended use to support screening arguments of FEPs related to effects of THM on permeability, porosity, and mountain-scale flow. The analysis conducted in Section 6.5 of this report shows that there is no significant impact of THM on the flow pattern even for an imposed reasonable conservative change in permeability of three orders of magnitude near the ground surface. This implies that an error in predicted effects of THM by one order of magnitude will not have any significant impact on the flow pattern. Therefore, the criterion that the predicted changes in permeability are in the correct direction and correct within an order of magnitude is met also at the mountain scale. For validation of the drift-scale THM model, an additional validation criterion was developed related to TM changes in the rock mass. In effect it was required that thermal stresses should be predicted within 50%, which in turn would assure that error in the predicted permeability as a result of elastic changes in fracture aperture would be within approximately an order of magnitude (BSC 2004 [DIRS 169864], Section 7.1.4). A criterion that the thermal stresses should be within 50% could also be applied when comparing mountain-scale and drift-scale THM model results. However, caution must be taken due to the fact that the thermal stresses are expected to be lower in the mountain-scale model than in the drift-scale model as a result of differences in lateral mechanical confinement.

The evaluation criteria for comparison of drift-scale and mountain-scale THM results would apply for areas away from the immediate surroundings of the drift, but close to the level of the repository, that are relevant for predicting the effect of THM processes on the mountain scale permeability and percolation flux. A comparison of results within a few meters of the drift wall may not be possible since the smallest grid size near the drifts is five meters in the mountain scale model. Furthermore, a comparison of changes close to the ground surface is not possible because the THM changes in this area cannot be well captured in a drift-scale model. Therefore, comparisons of the mountain-scale and drift-scale model results are focused on the mid-pillar region and regions a few hundred meters above and below the repository.

Based on the criteria discussed above, consistency between the mountain-scale and drift-scale THM models is demonstrated by the following specific comparisons of simulation results:

- The temperature evolution and calculated peak temperature are consistent (Section 6.5.10). Both models predict a maximum temperature of about 130 to 140°C at about 70 to 100 years at the emplacement drift (Figure 6.5.10-1b; BSC 2004 [DIRS 169864], Figure 6.5.2-1b). Both models predict a maximum temperature of 89°C at the mid-pillar (between two repository drifts) occurring at 800 to 900 years (Figure 6.5.10-1b; BSC 2004 [DIRS 169864], Figure 6.5.2-1b). For analysis of THM processes the calculated temperature is important for prediction of TM-induced stresses that in turn affect the evolution of permeability. The mountain-scale thermal stresses are determined by the overall temperature increases at the mountain scale, which is here represented by the mid-pillar temperature. There is a linear dependence between temperature change and thermal stress. Thus, the close agreement in the temperature evolution between the drift-scale and mountain-scale results (differences within a few percent) shows that the mountain-scale THM model is properly implemented in terms of thermal behavior.

- The thermal-stress evolution is consistent (Section 6.5.11). Both models consistently predict a substantial increase in horizontal stress, with peak stress occurring at about 500 to 1,000 years (comparing Figure 6.5.11-1 and BSC 2004 [DIRS 169864], Figure 6.5.3-1). The magnitude of maximum stress at the mid-pillar in the mountain-scale THM model is about 11 MPa, whereas the drift-scale THM model predicts a maximum stress of about 15 MPa at the corresponding location (BSC 2004 [DIRS 169864], Figure 6.7.1-1). Considering that the initial horizontal stress is about 5 MPa at the repository level, the thermally induced stress is about 15 – 5 = 10 MPa in the drift-scale THM model, whereas it is 11 – 5 = 6 MPa in the mountain-scale THM model. The higher thermal stress (10 MPa compared with 6 MPa) in the drift-scale THM model is explained by the differences in lateral confinement discussed above. The differences in thermal stress between the drift-scale THM model and mountain-scale THM model is less than 50% even considering the difference in the lateral boundary conditions. As will be discussed in Section 7.3.3, such differences in thermal stress between the drift-scale and mountain-scale models are confirmed by similar TM analyses conducted in *Drift Degradation Analysis* (BSC 2004 [DIRS 166107], Section 6.2).

- The evolution of stress-induced permeability changes is consistent (Section 6.5.12). Both models consistently predict greatest reduction in vertical permeability at about 1,000 years. Both models predict a vertical permeability reduction by a factor of about 0.6 around an emplacement drift located in the Tptpll unit (comparing Figure 6.5.12-1 and BSC 2004 [DIRS 169864], Figure 6.6.1-2). Thus, there is no significant difference in predicted permeability changes between the drift scale and mountain scale and the difference is clearly within one order of magnitude as required by the evaluation criterion.

- The vertical percolation flux pattern as well as flux magnitudes are consistent (Section 6.5.13). Both models consistently predict the formation of a dryout zone around the drifts, which diverts liquid flow laterally. Both models predict that this dryout zone lasts for more than 1,000 years. The magnitude of vertical flux is consistent throughout the models. Because of different mesh sizes near the drifts (mountain-scale element size at drift is 5 m, whereas drift-scale element size at the drift wall is 0.25 m), the flux pattern around the drift appears to be wider in the mountain-scale model (comparing between Figures 6.5.13-1, 6.5.13-2 and BSC 2004 [DIRS 169864], Figures 6.6.2-1 and 6.6.2-2). However, both drift-scale and mountain-scale models consistently show vertical drainage in the mid-pillar region throughout the 10,000-year simulation time.

Evaluation of Validation Criteria – The evaluation applies the foregoing discussion to the explicit criteria listed in Section 2.2.1.4.3 of the TWP (BSC 2005 [DIRS 174842]):

1. *Does the mountain-scale model represent the same physical and chemical processes as were validated in the drift-scale model?*

   As explained above, the drift-scale and mountain-scale THM models represent the same physical processes and use the same underlying conceptual model. Coupled THM processes at the mountain-scale are essentially the same as those at the drift

scale but may be different in extent and magnitude as a result of scale-dependent properties. Accordingly, this criterion is met.

2. *Are the scale-dependent processes, properties, and initial/boundary conditions identified and treated appropriately in the corroboration?*

   The thermal, hydrologic, and coupled TM and HM processes represented in the mountain-scale THM model are essentially the same as for the drift-scale model. Scale-dependent hydrologic properties are used, specifically the calibrated three-dimensional mountain-scale hydrologic property set is used (Section 4.1.2). Rock mass deformability and THM coupling relationships (e.g., stress–permeability relationship) in the mountain-scale model are the same as in the drift-scale model, which is appropriate for the reasons given above. Boundary conditions are the same (thermal, hydrologic) except for the far-field mechanical boundaries, which are more compliant in the mountain-scale model as discussed above. Thus, the scale-dependent processes, properties, and conditions are identified and treated appropriately, so this criterion is met.

3. *Are the similarities and differences between the mountain-scale and drift-scale model results identified?*

   The previous discussion of comparison between the mountain-scale and drift-scale THM model results addresses the significant similarities and differences. Comparison has determined that the temperature and thermal stress evolution is consistent between the models, the evolution of THM coupling is consistent, and the vertical flux distribution is consistent. Differences between the models are attributed to the different far-field mechanical boundary conditions, and to grid size effects in the near-field close to the drift openings. In addition, the approach for validation of the drift-scale THM model (BSC 2004 [DIRS 169864], Section 7) has been reviewed for consistency with the mountain-scale model. Similarities and differences are identified and evaluated, consistent with confidence building for validation of the mountain-scale THM model. Thus, this criterion is satisfied.

4. *Are the scale-dependent numerical issues identified and evaluated with respect to the corroboration?*

   Scale-dependent numerical issues for representing thermal and hydrologic processes at the mountain scale are identified and evaluated in Section 7.2. Grid-resolution effects on representation of stress concentration and thermal stress changes around the drift openings have been identified, and are consistent with the intended use of the mountain-scale THM model to evaluate far-field changes. Far-field gradients of rock mass stress and strain are small compared to rock mass response near the openings, and are adequately represented by the coarser grid used in the mountain-scale model. Scale-dependent numerical issues have been identified and evaluated. Thus, this criterion is met.

7.3.3 Corroboration with Information from Refereed Technical Literature

Corroboration of the mountain-scale THM model using information from refereed technical literature is specified by the TWP (BSC 2005 [DIRS 174842], Section 2.2.1.4.3), which gives explicit criteria for corroboration. Note that corroboration of the TH aspects of the THM model, including the TOUGH2 code (LBNL 2003 [DIRS 161491]), is discussed in Sections 7.1.3 and 7.1.4. This section describes several published papers and their relation to validation of the mountain-scale THM model, followed by evaluation of the explicit criteria for selected published information.

Corroboration of results by information published in refereed technical literature includes presentation of the TOUGH2-FLAC3D simulator in *International Journal of Rock Mechanics & Mining Sciences* (Rutqvist et al. 2002 [DIRS 162048]). This paper presents the fundamental theories and underlying conceptual models for the TOUGH2 code (LBNL 2003 [DIRS 161491]), the FLAC3D code (LBNL 2002 [DIRS 154783]), and the coupling functions between the two codes. In addition, there are numerous other refereed publications related to each of the codes TOUGH2 and FLAC3D.

The FLAC3D code (LBNL 2002 [DIRS 154783]) has been commercially available for seven years and has over 500 licensees in 42 countries. Examples of recent refereed publications which apply FLAC3D include studies by Carranza-Torres and Fairhurst (1999 [DIRS 172880]), Hakami (2001 [DIRS 172881]), Hart (2003 [DIRS 172882]), and Souley et al. (2001 [DIRS 172884]). These references present applications that include the same physical processes as represented in the mountain-scale THM model, e.g., mechanical, thermal-mechanical, and in some cases hydromechanical processes in fractured rocks. The publication by Hakami (2001 [DIRS 172881]) provides an application of the FLAC3D code with an equivalent scale to that of the mountain-scale THM model.

Refereed publication of application of the TOUGH2-FLAC3D simulator includes publication of the drift-scale THM analysis for the repository at Yucca Mountain (Rutqvist and Tsang 2003 [DIRS 162584]). The TOUGH2-FLAC3D code has also been applied to problems related to HM processes in the geological sequestration of greenhouse gases (Rutqvist and Tsang 2002 [DIRS 162587]). In addition, the study by Min et al. (2004 [DIRS 172883]), discussed in Section 7.3.1, provides support for the conceptual model for the stress-versus-permeability coupling applied in this study. In the publication by Rutqvist and Tsang (2002 [DIRS 162587]), the TOUGH-FLAC code is applied to a scale similar to that of the mountain-scale model, i.e., a kilometer scale model. The scale dependency of the stress-versus-permeability relationship is identified and explained in the recent publication by Min et al. (2004 [DIRS 172883]).

Evaluation of Validation Criteria – The evaluation applies the foregoing discussion to the explicit criteria listed in Section 2.2.1.4.3 of the TWP (BSC 2005 [DIRS 174842]):

1. *Does the corroboration information represent the same physical and chemical processes as the mountain-scale model?*

   The same underlying physical processes, conceptual model and prediction as those of the mountain-scale THM model have been investigated and undergone technical review in

the refereed technical literature (e.g. Rutqvist et al. 2002 [DIRS 162048]; Rutqvist and Tsang 2003 [DIRS 162584]), although these papers are concerned mainly with processes at smaller spatial scales, as discussed below. The basic formulations of physical processes implemented in these sources and the mountain-scale THM model, are represented by the governing and constitutive equations for TH processes (discussed in Section 7.1.4), the equations for the mechanical processes (e.g. Carranza-Torres and Fairhurst (1999 [DIRS 172880]) and Hakami (2001 [DIRS 172881] discussed above), and equations governing the coupling between TH and mechanical processes (described in detail by Rutqvist et al. (2002 [DIRS 162048]). Thus, this criterion is met.

2. *Does the corroboration rely on scale-dependent processes, properties, or initial/boundary conditions, and if so are these treated appropriately in the corroboration?*

   The thermal, hydrologic, and coupled TM and HM processes represented in the mountain-scale THM model are essentially the same as for the cited sources. Scale-dependent hydrologic properties are used; specifically, the calibrated three-dimensional mountain-scale hydrologic property set is used (Section 4.1.2). Rock mass deformability and THM coupling relationships (e.g., stress-permeability relationship) in the mountain-scale THM model are based on the same conceptual and mathematical model as in the cited sources. There is a slight difference in parameterization of the stress-permeability relationship for the mountain-scale THM model and that of Rutqvist and Tsang (2003 [DIRS 162584]). This is partly a result of the considered scale dependency on the hydraulic properties as well as a result of an updated calibration of the stress-versus-permeability relationship, conducted since the publication by Rutqvist and Tsang (2003 [DIRS 162584]). However, the resulting residual permeability for a single fracture compressed at high stress are in both cases about one order of magnitude less than the original permeability. Consequently, a direct comparison of the evolution of permeability changes can be made. Boundary/initial conditions are generally scale-independent. The scale dependency of the stress-versus-permeability relationship is identified and explained both in Section 7.3.2 above and in the recent publication by Min et al. (2004 [DIRS 172883]). Thus, the scale-dependent processes, properties, and conditions are identified and treated appropriately, so this criterion is met.

3 *Are the similarities and differences between the mountain-scale model or its results, and the corroborating information, identified and explained?*

   There are important similarities between the mountain-scale THM model and the published corroborating information specific to Yucca Mountain literature (Rutqvist et al. 2002 [DIRS 162048]; Rutqvist and Tsang 2003 [DIRS 162584]), including the same conceptual and geological models, modeling approaches, and simulation software. A direct comparison of the mountain-scale THM model results can be made with drift-scale THM model results published by Rutqvist et al. (2002 [DIRS 162048]) and Rutqvist and Tsang (2003 [DIRS 162584]). With the exception of applied ventilation efficiency, the input data for the simulations published in these sources are almost identical to those

used in the mountain-scale THM model. In the cited sources a ventilation efficiency of 70% was applied, thus lower than the 86.3% applied in the mountain-scale THM model. Considering the difference in ventilation efficiency, the temperature evolution agrees well between the mountain-scale THM model and that of the cited sources (compare drift wall temperature in Figure 6.5.10-1 with that in Figure 5 of Rutqvist and Tsang 2003 [DIRS 162584]). As expected, a difference is achieved for the peak temperature at the drift wall (about 160°C for 70% ventilation efficiency in cited sources and about 143°C for 86.3% ventilation efficiency in the mountain-scale THM model). The evolution of stress-induced permeability changes is consistent. Both the cited sources and the mountain-scale THM model consistently predict greatest reduction in vertical permeability at about 1,000 years. Both analyses predict a vertical permeability reduction by a factor of about 0.6 around an emplacement drift located in the Tptpll unit (comparing Figure 6.5.12-1 and Rutqvist and Tsang 2003 [DIRS 162584], Figure 6). Thus, there is no significant difference in predicted permeability changes between the cited sources and mountain-scale THM model. Furthermore, both the cited sources and the mountain-scale THM model predict that the effect of THM coupling on the flow field is small (note similarities in vertical flow pattern of TH and THM results in Figure 6.5.13-5 and in Figure 8 of Rutqvist and Tsang 2003 [DIRS 162584]). Because both qualitative and quantitative comparisons have been conducted for sources representing the same physical processes and consistency in simulated effects of THM on permeability and fluid flow has been demonstrated, this criterion is met.

7.3.4 Discussion of Independent Technical Model Validation Review

An independent technical review for post-development model validation of the mountain-scale THM model has been performed by Dr. Tin Chan of Atomic Energy of Canada Limited, Ontario, Canada.

The review criteria for the post-development validation review were presented in Section 2.2.1.4.3 of the TWP (BSC 2005 [DIRS 174842]) and are repeated here:

- The technical approach and algorithms described in the document capture all physical and chemical processes that are significant to the intended use of the model for screening these FEPs.

- Modeling assumptions are clearly defined and justified as appropriate for the intended use of the model for screening these FEPs.

- Uncertainties in model parameters, process representation, and assumptions are sufficiently described, and impacts of these uncertainties discussed, as appropriate for the intended use of the model for screening these FEPs.

- The overall technical credibility of the approach, including assumptions, parameters, equations, and numerical implementation, is appropriate for the intended use of the model for screening these FEPs.

The post-development validation review based on the review criteria was conducted. Dr. Chan's technical comments have been appraised and responded to accordingly, based on the instructions in the TWP (BSC 2005 [DIRS 174842], Section 2.2.1.4.3). Any changes made on this report were provided to the reviewer for his concurrence. The conclusion from Dr. Tin Chan's review is summarized and presented below:

> *I have conducted an independent technical review of the mountain-scale THM model for post-development validation for the intended use of the model for FEP screening. I have reviewed the mountain-scale THM model considering your stated criteria. Based on the current state of knowledge, I can concur that, consistent with the low importance of the "UZ Flow" component to the mean annual dose:*
>
> 1. *The technical approach and algorithms described in the document capture all physical and chemical processes that are significant to the intended use of the model for screening these FEPs.*
>
> 2. *Modeling assumptions are clearly defined and justified as appropriate for the intended use of the model for screening these FEPs.*
>
> 3. *Uncertainties in model parameters, process representation, and assumptions are sufficiently described, and impacts of these uncertainties discussed, as appropriate for the intended use of the model for screening these FEPs.*
>
> 4. *The overall technical credibility of the approach, including assumptions, parameters, equations, and numerical implementation, is appropriate for the intended use of the model for screening these FEPs.*

The complete text of Dr. Chan's review comments and conclusion is presented in Appendix VIII. Since the response made directly on Sections 6.5 and 7.3, some additional text in Appendix VIII.3 was added to point out the changes. The conclusion from Dr. Chan's post-development validation review fulfills the requirements in the TWP (BSC 2005 [DIRS 174842], Section 2.2.1.4.3) and confirms adequacy of the mountain-scale THM model in model development, data selection and usage, and range of intended use.

7.3.5 Supplementary Validation by Corroboration with Alternative Mathematical Models

Additional confidence-building is provided in this section, by corroboration with an alternative THM model. Although not specified in the TWP (BSC 2005 [DIRS 174842]), this method for validation is permitted under the implementing procedure (LP-SIII.10Q-BSC, Section 5.3.2(c)(2)). This section presents quantitative and qualitative comparisons to similar mountain-scale THM simulations for the Yucca Mountain site. Firstly, qualitative comparisons are made to two-dimensional mountain-scale TM (continuum and distinct element) analyses reported by Mack et al. (1989 [DIRS 100677]). Secondly, quantitative comparisons are made to mountain-scale and drift-scale TM analyses reported in *Drift Degradation Analysis* (BSC 2004 [DIRS 166107]). The discussion includes criteria for concluding that the comparisons support validation of the mountain-scale THM model.

Mack et al. (1989 [DIRS 100677]) conducted mountain-scale TM analyses of rock mass modifications resulting from a high-level waste repository at Yucca Mountain. They applied both boundary element (continuum) and distinct element numerical models to calculate TM induced stress changes and to estimate the impact on the mountain-scale permeability distribution. The geometry of their two-dimensional analysis is similar to the one conducted in this report, with a repository located in the unsaturated zone at about 300 m depth. Although Mack et al. (1989 [DIRS 100677]) used a slightly different heat load and material properties than those used in Section 6.5 of this report, a qualitative comparison can be made. Both analyses predict a zone of decreasing permeability near the repository and zones of increasing permeability at a distance above and below the repository (compare Figures 6.5.12-1 and 6.5.12-2 in this report with Figures 3-21 and 3-22 in Mack et al. 1989 [DIRS 100677]). These permeability changes are caused by elastic opening and closure of pre-existing vertical fractures due to the impact of thermal stress. In addition, Mack et al. (1989 [DIRS 100677]) investigated the potential for slip along pre-existing fractures. Similar to the results in Section 6.5.14 of this report, the authors found that slip along pre-existing fractures would be most likely in vertical fractures near the ground surface (Mack et al. 1989 [DIRS 100677], Figure 3-29 and 3-30). Mack et al. (1989 [DIRS 100677], Section 4) also found that the joint deformation behavior observed in the distinct element analysis was consistent with joint behavior inferred from the boundary element (continuum) analysis. Thus, there is a good qualitative agreement between the results of the two analyses by Mack et al. (1989 [DIRS 100677]) and the analysis conducted in Section 6.5 of this report. Because the same types of responses (fracture opening and closure, fracture slip) were identified in the same parts of the model domain, these comparisons provide additional confidence in the mountain-scale THM model predictions.

In *Drift Degradation Analysis* (BSC 2004 [DIRS 166107], Section 6.2), the thermal stress distribution calculated in a three-dimensional mountain-scale analysis was compared to the thermal stress distribution calculated in a two-dimensional drift-scale analysis. The temperature evolution calculated in those two analyses is very similar to the temperature evolution calculated in this report (compare Figure 6.5.10-1 with BSC 2004 [DIRS 166107], Figure 6-26). Because of the similarity in the calculated temperature field, the calculated thermal stress can be readily compared to demonstrate consistency in TM model results. Both drift-scale and mountain-scale analyses in *Drift Degradation Analysis* (BSC 2004 [DIRS 166107], Figures 6-27 to 6-29) consistently predict a substantial increase in horizontal stress, with a peak stress occurring at about 1,000 years. At the mid-pillar region the horizontal stress at 1,000 years is about 8 MPa for the mountain-scale analysis (FLAC3D results in BSC 2004 [DIRS 166107], Figure 6-29) and about 11 MPa for the drift-scale analysis (NUFT-FLAC results in BSC 2004 [DIRS 166107], Figure 6-29). Considering the initial stress of 3 MPa (see stress at the mid-pillar region in BSC 2004 [DIRS 166107], Figure 6-27), the thermally induced stresses are 8 – 3 = 5 MPa in the mountain-scale analysis and 11 – 3 = 8 MPa in the drift-scale analysis. The thermally induced stresses calculated in *Drift Degradation Analysis* (5 and 8 MPa, respectively) should be compared to 6 MPa and 10 MPa calculated by the mountain-scale and drift-scale models related to this report. The thermal stresses are slightly lower in *Drift Degradation Analysis* because of a slightly lower thermal expansion coefficient (the difference in thermal expansion to the drift degradation analysis is discussed in BSC 2004 [DIRS 169864], Section 6.4.3). To summarize, the magnitudes of thermal stress changes, and the differences in magnitude of horizontal stresses between the mountain-scale and drift-scale analyses, as presented in *Drift Degradation Analysis*,

are in agreement (within approximately 1 MPa or less) with results presented in Section 6.5 of this report. Thus, the four sets of calculations, two at the drift-scale and two at the mountain-scale, are consistent regarding thermally induced stresses at the repository level, providing additional confidence in the validation of the mountain-scale THM model.

7.3.6 Summary and Evaluation of Validation Criteria

In summary, the mountain-scale THM model is validated using confidence-building information derived both during model development, and from post-development activities. Information used for confidence-building during model development includes discussion of input data, how calibration was used, initial conditions and boundary conditions, numerical convergence, the range of conditions simulated, and uncertainties (Section 7.3.1). Post-development validation activities consist of corroboration by results from validation of the drift-scale model (Section 7.3.2), corroboration using other information (i.e., publication of field-test simulations and geothermal analogues) from refereed technical publications (Section 7.3.3), independent technical review for the post-development validation (Section 7.3.4), and supplementary confidence building through comparison with alternative mathematical models (Section 7.3.5). These activities provide confidence that the mountain-scale THM model is adequate for its intended use, to support screening evaluation of FEPs (BSC 2005 [DIRS 174191], Section 6.9.12).

INTENTIONALLY LEFT BLANK

8. CONCLUSIONS

This report documents a portion of the scientific basis for postclosure safety, as specified in Section 2.1.1 of the TWP (BSC 2005 [DIRS 174842]). The report addresses the development, results, and validation of the mountain-scale coupled TH, THC, and THM process models in accordance with the requirements of Section 5.2 of LP-SIII.10Q-BSC, *Models*. These models and modeling analyses include the following:

- Mountain-scale two-dimensional TH model results and analyses
- Mountain-scale three-dimensional TH model results and analyses
- Mountain-scale THC two-dimensional model
- Mountain-scale THM two-dimensional model
- Model validation activities and results.

The mountain-scale TH/THC/THM process models are developed to assess mountain-scale hydrologic/chemical/mechanical changes and to predict UZ flow behavior in response to heat release by radioactive decay from the nuclear waste repository at the Yucca Mountain site. These TH/THC/THM coupled-processes models numerically simulate the impact of repository heating on the natural hydrogeological system, including a representation of heat-driven processes occurring at the repository drifts as well as in the far field. The mountain-scale TH model provides predictions for thermally affected liquid saturation, gas- and liquid-phase fluxes, and water and rock temperature. In particular, the TH model calculates the changes in water flux driven by evaporation/condensation and capillary processes, and drainage occurring between drifts. The mountain-scale THC coupled-processes model evaluates TH effects on water and gas chemistry, mineral dissolution/precipitation, and the resulting impact on UZ hydrologic properties and flow and transport processes. The THM component addresses issues concerning changes in permeability caused by mechanical and thermal disturbances in stratigraphic units above and below the repository host rock. The model products (output data simulation input files, and output data summaries), and their associated data tracking numbers from these coupled-processes models, are presented in Table 8-1.

Also listed in Table 8-1 are data developed in Appendices V through VII to examine the sensitivity of the models to changes in the thermal properties input data, discussed in Section 4.1.3. These data compare the impact of using the updated thermal properties in DTN: LB0402THRMLPRP.001 [DIRS 168481] in place of those in the input DTN: LB0210THRMLPRP.001 [DIRS 160799].

Table 8-1. Model Products and Developed Data

DTN	Remarks
Output of TH/THC/THM Models	
LB0310MTSCLTH2.001 Mountain Scale 2D TH Predictions: Simulations	Data for Mountain Scale 2-D TH Simulations: Input/output files, mesh, and data for post-processing.
LB0310MTSCLTH3.001 Mountain Scale 3D TH Predictions: Simulations	Data for Mountain Scale 3-D TH Simulations: Input/output files, mesh, and data for post-processing.
LB0310MTSCLTHC.001 Mountain Scale THC Predictions: Simulations	Mountain Scale THC Simulations: Input/output files for TOUGHREACT simulations.
LB0310MTSCLTHC.002 Mountain Scale THC Predictions: Data Summaries	Mountain Scale THC Predictions: Data Summaries. Extracted information from output results in LB0310MTSCLTHC.001.
LB0310MTSCLTHM.001 Mountain Scale THM Predictions: Simulations	Mountain Scale THM Simulations: Input/output files.
LB0310MTSCLTHM.002 Mountain Scale THM Predictions: Summary Plots	Mountain Scale THM Predictions: Summary plots Tecplot data extracted from LB0310MTSCLTHM.001
Developed Data from Sensitivity Analyses	
LB0404MTSCLTH3.001. Mountain Scale 3D TH Predictions: Simulations.	Data for Mountain Scale 3-D TH Simulations: Input/output files, mesh, and data for post-processing: Sensitivity to revised matrix porosity and thermal properties, Appendix V.
LB0404MTSCLTHC.001. Mountain Scale THC Predictions: Simulations.	Mountain Scale THC Simulations: Input/output files for TOUGHREACT simulations: Sensitivity to revised matrix porosity and thermal properties, Appendix VI.
LB0404MTSCLTHM.001. Mountain Scale THM Predictions: Simulations.	Mountain Scale THM Simulations: Input/output files: Sensitivity to revised matrix porosity and thermal properties, Appendix VII.
LB0404MTSCLTHM.002. Mountain Scale THM Predictions: Summary Plots.	Mountain Scale THM Predictions: Summary plots Tecplot data extracted from DTN: LB0404MTSCLTHM.001: Sensitivity to revised matrix porosity and thermal properties, Appendix VII.

8.1 TH MODEL

In this report, the mountain-scale TH model consists of one two-dimensional and one three-dimensional submodel. Both TH submodels use the dual-permeability modeling approach and the same hydrogeological conceptual model developed in *UZ Flow Models and Submodels* (BSC 2004 [DIRS 169861]). Specifically, the three-dimensional TH model employs the three-dimensional ambient TH model results as its initial and boundary conditions. The three-dimensional TH model grid, though using relatively coarse grid spacing, incorporates every repository drift explicitly by taking into account orientations, lengths, elevations, and spacing of the repository drifts, such that adjacent drifts are represented one-to-one by adjacent gridblocks 81 m wide. In comparison, the two-dimensional model employs refined lateral and

vertical grids with an explicit drift representation along the north–south cross section. In the two-dimensional model, drifts and the space between them are represented by four gridblocks.

The mountain-scale TH model estimates the mountain-scale TH responses to the repository thermal load in the Yucca Mountain UZ system under present and future climates, as well as the effect of ventilation. The models predict TH conditions in the fractured tuffs soon after emplacement of the waste. Sections 6.2 and 6.3 present the simulation results of the two-dimensional and three-dimensional models, respectively, in terms of spatial and temporal distributions and variations of simulated temperature, liquid saturation, and fracture-matrix percolation fluxes. In general, thermal loading at the repository results in significant changes in the temperature conditions and moisture distribution, both at the repository and at the zones directly above and below the repository, which have a large impact on fluid flow near repository drifts at early times, but insignificant impact on unsaturated zone flow fields. These results are summarized as follows:

The two-dimensional model predicts consistently higher temperatures at and near the repository under the same infiltration and thermal-loading conditions (particularly for the first couple of hundreds of years) as those used by the three-dimensional model. This is due to increased grid resolution near drifts in two-dimensional grids and because two-dimensional models do not account for heat transfer or thermal energy loss into the third dimension. These large gridblocks used in the three-dimensional models average out peak temperature values, leading to lower predictions of temperatures.

Higher-temperature regions around the repository drifts enlarge with time. The TH models predict that these reach their maximum extent at about 2,000 years after waste emplacement. During the heating period, the temperatures at the middle pillar regions between two drifts rise in some places to above 80°C, but never reach the boiling point. At 2,000 years, temperatures at the bottom of the PTn reach their highest values of 40 to 50°C. At the same time, peak temperatures at the top of CHn are elevated to 70°C. After 5,000 years, the repository and surrounding rock are significantly cooled down, and the TH effect diminishes.

The three-dimensional TH model predicts that repository heating has, in general, only a limited impact on far-field flow fields with ventilation. However, the TH model predicts much stronger TH effects along highly permeable columns of faults that intersect repository blocks, because of the stronger vapor flow and condensation.

The TH model predicts that repository heating has only a small impact on flow through the pillar regions between two drifts. This is because boiling does not occur in these pillar areas, and moisture conditions there are not much changed from ambient status. Simulated vertical fluxes near the center of the pillar regions show no thermal effects. In fact, flow through the pillar regions is more affected by surface infiltration or climate changes than by repository heating.

8.2 THC MODEL

The purpose of the mountain-scale THC model is to evaluate the coupled THC processes that are influenced by variations in geology (structure and lithology), infiltration rate, and temperature at the mountain-scale or repository-scale. A partial two-dimensional cross section of the repository

was selected from the three-dimensional mountain-scale TH model and used for a series of TH and THC calculations having increasing complexity in terms of processes and chemical components.

The results of the simulations, presented in Section 6.4, indicate that mineral precipitation/dissolution does not significantly affect the hydrologic properties and percolation flux, compared to the effects caused by TH processes alone. Glass-rich layers in the CHn show alteration to zeolites, with clinoptilolite breaking down to form stellerite at elevated temperatures. Changes in water chemistry, mineralogy, and hydrologic properties in the ambient temperature regions are minimal over the 7,000 years of the simulation. In areas where temperature is substantially different from ambient, particularly above the drifts, there is substantial change in the overall water and gas chemistry. For example, CO_2 concentrations in the gas phase differ from ambient by about one to two orders of magnitude, with the difference decreasing over time after the peak thermal period. The range in water pH of about 7 to 9 is strongly linked to changes in gas-phase CO_2 concentrations, relative to the ambient system away from the repository. Differences are smaller in the high-temperature repository center (and the pH is higher) compared to the edges (which have somewhat elevated values and pH values down to approximately 7).

Results from the mountain-scale THC model (presented in Section 6.4) have been submitted to the Technical Data Management System (TDMS) as output under DTNs listed in Section 9.4.

8.3 THM MODEL

The mountain-scale THM model developed in Section 6.5 of this model report is capable of assessing the magnitude and distribution of changes in hydrologic properties and of analyzing the impact of such changes on the mountain-scale vertical percolation flux through the repository horizon. Results from the mountain-scale THM model presented in Sections 6.5.10 to 6.5.14 have been submitted to the TDMS as output under DTNs listed in Section 9.4. The results show that maximum THM-induced changes in hydrologic properties occur at around 1,000 years after emplacement, when average temperature in the mountain peaks. Near the repository level, thermal-elastic stresses tend to tighten vertical fractures to smaller apertures, leading to reduced permeability and increased capillarity. Near the ground surface, compressive stresses are relieved into tension (Section 6.5.11, Figure 6.5.11-1). In this zone, fractures open elastically, and fracturing or shear-slip along preexisting fractures is possible.

Using estimates of input THM properties that would result in upper-bound changes in permeability and percolation rates, changes in permeability by elastic closure or opening of preexisting fractures are within a factor of 0.3 to 5, whereas calculated changes in capillary pressure range between a factor of 0.7 to 1.2. A three-order-of-magnitude increase in permeability and one-order-of-magnitude reduction in capillary pressure were imposed for the zone of possible fracturing and shear slip near the ground surface. Despite these upper-bound estimates of potential changes in hydrologic properties, the main conclusion from the results of Sections 6.5.10 to 6.5.14 is that THM-induced changes in mountain-scale hydrologic properties have no significant impact on the vertical percolation flux through the repository horizon. These results are sufficient for bounding the possible impact of the THM processes on permeability and percolation flux at the mountain scale.

8.4 MODEL VALIDATION

Model validation efforts have been documented in this report for the mountain-scale TH/THC/THM models, according to the requirements in the TWP (BSC 2005 [DIRS 174842], Section 2.2.2.4). The TH model is supported mainly through validation of the drift-scale TH model, which uses essentially the same conceptual and mathematical models. Also, the validation is further corroborated by publication in a refereed technical journal.

The mountain-scale THC model is validated by confidence building with DST experimental data and validation was corroborated through publications in peer-reviewed journals. The following methods are used to evaluate mountain-scale THC effects on flow and geochemistry: the estimation of thermodynamic and kinetic parameters, testing and model validation using large-scale thermal test and laboratory experiments, and predictive process modeling.

The model validation effort for the mountain-scale THM model makes use of the validation results of the drift-scale THM model (BSC 2004 [DIRS 169864]). The validity of the drift-scale THM model gives confidence in the mountain-scale THM model, because the same rock hydrologic, thermal, and mechanical properties are used, and the same THM conceptual and process models apply to both drift-scale and mountain-scale THM models.

8.5 LIMITATIONS

The TH/THC/THM coupled processes models are limited by their mathematical formulations and associated assumptions (Section 5). The models developed in this report are intended for use in mountain-scale screening of FEPs related to unsaturated zone flow, fluid chemistry and rock chemistry, and other temperature induced processes in the unsaturated zone and its interface to the saturated zone during the 10,000 year compliance period. The models provide evaluation of effects of heat on mountain-scale processes during the 50-year preclosure period as well as postclosure period The modeling approaches adopted in this report adequately evaluate the potential significance of FEPs to performance assessment.

The models provide predictions using infiltration rates and hydrologic properties for the mean present-day and future (monsoon and glacial transition) climates. Upper- and lower-bound infiltration cases were not explicitly modeled using the mountain-scale coupled processes models. The effects of these cases would lead to wetter and cooler conditions for the upper-bound infiltration case, and hotter and drier conditions for the lower-bound infiltration case. However, because high and low infiltrations are explicitly included in the mean spatially varying infiltrations, upper- and lower-bound uncertainty in infiltration is implicitly included in the mountain-scale coupled processes models.

Another important limitation with the mountain-scale TH, models is the use of the large-scale volume average modeling approach in numerical model grids. The models use average properties and boundary conditions and, therefore, provide average response and not fine scale temporal variations or spatial heterogeneity. Behavior within repository drifts is not explicitly modeled. Consequently, the mountain-scale TH, model is not appropriate for investigating in-drift or small-scale near-field TH processes (for example within and near drifts), and therefore comparison with drift-scale models is limited. However, the grid resolution used in the

mountain-scale TH/THC/THM models is adequate for modeling large-scale processes represented in these models.

Because the mountain-scale THC model does not intersect faults, it does not model processes occurring within faults. However, the repository edges in the THC model produce processes similar to those occurring within faults (increased vapor refluxing and condensation) and do not result in THC effects on flow towards the repository. Similarly, the THM model does not include faults, and therefore shear/slip processes along faults are not modeled. The THM model without faults maximizes thermal effects and provides bounding predictions of THM effects. Faults are included in the mountain-scale TH models. Results from TH models show that large temperature effects are not predicted within faults because thermal load is not directly applied to the fault zones. However, the three-dimensional TH model predicts stronger vapor flow and condensation flow along highly permeable faults. Like in the ambient unsaturated flow models, faults divert flow away from the repository and do not lead to increased percolation flux above the repository horizon. Therefore, mountain scale TH/THC/THM models adequately account for effects of faults on mountain-scale processes.

8.6 SATISFACTION OF ACCEPTANCE CRITERIA

The acceptance criteria specified in Section 3.2.1 of the TWP (BSC 2005 [DIRS 174842]) are listed in Section 4.2 of this report. The criteria were obtained from Section 2.2.1.3.6.3 of the YMRP (NRC 2003 [DIRS 163274]). The following discussion addresses how each of these acceptance criterion (AC) were satisfied.

- AC 1: *System Description and Model Integration Are Adequate*: The TH/THC/THM system is described in Section 6. This description is based on data from field and laboratory investigations and the UZ flow model (BSC 2004 [DIRS 169861]), and is consistent with standard conceptual models of the UZ at Yucca Mountain. In addition, spatial variability of model parameters is adequately represented by the two-dimensional and three-dimensional model grids, with different types of fracture-matrix properties for each model layer to represent spatial variability across the entire UZ domain (Table 6.1-1). The model calibration and validation activities for the ambient TH model (BSC 2004 [DIRS 169861]) show that this representation is adequate for modeling coupled processes on the mountain scale.

The following is an itemized account describing how the nine *Acceptance Criterion 1* items are addressed in this report.

(1) The total system performance assessment adequately incorporates, or bounds, important design features, physical phenomena, and couplings, and uses consistent and appropriate assumptions throughout the flow paths in the unsaturated zone abstraction process. Couplings include thermal-hydrologic-mechanical-chemical effects, as appropriate.

This report presents analyses of coupled thermal-hydrologic (TH), thermal-hydrologic-chemical (THC), and thermal-hydrologic-mechanical (THM) processes at the mountain scale. Sections 6.1 through 6.3 discuss TH effects. Section 6.4 discusses THC effects and Section 6.5 discusses the THM effects. The model demonstrates that these effects, as they

relate to flow and transport in the unsaturated zone at the mountain scale, need not be abstracted further for use in downstream analyses.

(2) The aspects of geology, hydrology, geochemistry, physical phenomena, and couplings that may affect flow paths in the unsaturated zone are adequately considered. Conditions and assumptions in the abstraction of flow paths in the unsaturated zone are readily identified and consistent with the body of data presented in the description.

This report presents analyses of TH, THC, and THM processes at the mountain scale in the unsaturated zone based upon site-specific geology, hydrology, geochemistry, physical phenomena, and coupling of these processes at the mountain scale. Sections 6.1 through 6.3 discuss TH effects. Section 6.4 discusses THC effects and Section 6.5 discusses the THM effects. The TH models were formulated using the dual-continuum approach to handling fracture-matrix interaction. The report justifies this modeling approach in Section 6.1.2 as consistent with the site-specific parameters.

(3) The abstraction of flow paths in the unsaturated zone uses assumptions, technical bases, data, and models that are appropriate and consistent with other related U.S. Department of Energy abstractions. For example, the assumptions used for flow paths in the unsaturated zone are consistent with the abstractions of quantity and chemistry of water contacting waste packages and waste forms, climate and infiltration, and flow paths in the saturated zone (Sections 2.2.1.3.3, 2.2.1.3.5, and 2.2.1.3.8 of NRC 2003 [DIRS 163274]). The descriptions and technical bases are transparent and traceable to site and design data.

This report uses models that are consistent with other models developed to support predictions of Yucca Mountain repository performance. Examples include the consistency for the TH, THC, and THM models, and comparisons with the DST model. The models are constructed using current design inputs as discussed in Section 4.1.

(4) The bases and justification for modeling assumptions and approximations of radionuclide transport in the unsaturated zone are consistent with those used in model abstractions for flow paths in the unsaturated zone and thermal-hydrologic-mechanical-chemical effects.

The scope of this model does not address radionuclide transport.

(5) Sufficient data and technical bases to assess the degree to which features, events, and processes have been included in this abstraction are provided.

Results of this report are used for exclusion of certain features, events, and processes identified in DTN: MO0407SEPFEPLA.000 [DIRS 170760]. No FEPs are included in TSPA-LA through this report. The basis for exclusion of certain FEPS from TSPA-LA through this report is provided in *Features, Events, and Processes in UZ Flow and Transport* (BSC 2005 [DIRS 174191]).

(6) Adequate spatial and temporal variability of model parameters and boundary conditions are employed in process-level models to estimate flow paths in the unsaturated zone, percolation flux, and seepage flux.

Mountain-scale temporal and spatial variability of model parameters is captured in the inputs to the model, as described in Section 4.1. Percolation, which results from infiltration, is discussed in Sections 6.2 and 6.3. Drift seepage was not explicitly addressed due to the scale of the model.

(7) Average parameter estimates used in process-level models are representative of the temporal and spatial discretizations considered in the model.

Model input parameters were adjusted, as appropriate, to match the gridding and scale of the model. The grids for each of the TH, THC, and THM models were created to capture the phenomena of interest. This gridding and parameter development is discussed in Section 6.1.

(8) Reduction in unsaturated zone transport distances, after a climate-induced water table rise, is considered.

The scope of this model did not consider fluctuations in the water table elevation. This was not included because the purpose of the model was to investigate the relative importance of the TH, THC, and the THM coupled processes on long-term repository performance.

(9) Guidance in NUREG–1297 [Altman et al. 1988 [DIRS 103597] and NUREG–1298 [Altman et al. 1988 [DIRS 103750], or other acceptable approaches for peer review and data qualification, is followed.

There were no peer reviews performed in the development of the mountain scale coupled processes models. As discussed in Section 4.1.4, ventilation efficiency data were qualified for intended use within the document using the criteria found in LP-SIII.10Q-BSC. These criteria represent a subset of the qualifying methods and attributes presented in NUREG 1298 (Altman et al. 1988 [DIRS 103750]), which are meant to provide the level of confidence in the data commensurate with their intended use.

- AC 2: *Data Are Sufficient for Model Justification*: Data from field and laboratory testing as well as three-dimensional model calibration (BSC 2004 [DIRS 169861]) have been synthesized and used in the TH/THC/THM models. The model validation shows that these data are sufficient to justify the model for its intended use.

The following is an itemized account describing how the eight *Acceptance Criterion 2* items are addressed in the report.

(1) Hydrologic and thermal-hydrologic-mechanical-chemical values used in the license application are adequately justified. Adequate descriptions of how the data were used, interpreted, and appropriately synthesized into the parameters are provided.

Hydrologic and thermal-hydrologic-mechanical-chemical data are listed in Section 4.1. These data were derived from several sources listed in Table 4.1 and are technically justified for use in this report.

(2) The data on the geology, hydrology, and geochemistry of the unsaturated zone, are collected using acceptable techniques.

Data relating to geology, hydrology, and geochemistry of the unsaturated zone were based in large part on field studies at Yucca Mountain. The data collection techniques were done in accordance with approved YMP procedures.

(3) Estimates of deep-percolation flux rates constitute an upper bound, or are based on a technically defensible unsaturated zone flow model that reasonably represents the physical system. The flow model is calibrated, using site-specific hydrologic, geologic, and geochemical data. Deep-percolation flux is estimated, using the appropriate spatial and temporal variability of model parameters, and boundary conditions that consider climate-induced change in soil depths and vegetation.

Net infiltration rates, which are the source of percolation fluxes, used as input to this model were developed from site-specific studies of infiltration rates at Yucca Mountain. Estimates of infiltration, both temporally and spatially, include present-day (modern), monsoon, and glacial transition mean infiltration rates as discussed in Section 6.1.4. These estimates were calibrated against field data and the DST model.

(4) Appropriate thermal-hydrologic tests are designed and conducted, so that critical thermal-hydrologic processes can be observed, and values for relevant parameters estimated.

The Drift Scale Test was conducted to provide data to support development of models and parameter estimation that predict TH, THC and THM processes (BSC 2004 [DIRS 169900], Section 6.3). As discussed in Section 6, the mountain-scale model is consistent with the drift-scale THM model, the drift-scale coupled processes (DST and TH seepage) model, and the drift-scale coupled processes (DST and THC seepage) model, all of which were validated against the Drift Scale Test.

(5) Sensitivity or uncertainty analyses are performed to assess data sufficiency, and verify the possible need for additional data.

The scope of this model was to evaluate the nominal conditions that prevail at Yucca Mountain during the repository regulatory period to assess the relative importance of various TH, THC, and THM features events and processes (FEPs screening). Sensitivity studies were not needed as this model did not pass on data to downstream models that feed the total system performance assessment.

(6) Accepted and well-documented procedures are used to construct and calibrate numerical models.

Accepted and well-documented procedures contained in the quality assurance program (Section 2) governed the development of this model. The model has been constructed and documented according to LP-SIII.10Q-BSC. Test and validation methods (Section 7) comply with LP-SIII.10Q-BSC and applicable guidance.

(7) Reasonably complete process-level conceptual and mathematical models are used in the analyses. In particular: (i) mathematical models are provided that are consistent with conceptual models and site characteristics; and (ii) the robustness of results from different mathematical models is compared.

The mathematical models are derived in accordance with conceptual models to capture the relevant processes. The mathematical models are validated in accordance with the requirements of LP-SIII.10Q-BSC. A two-dimensional model is developed and compared with a three-dimensional model and demonstrates the adequacy and robustness of the models for simulating relevant mountain-scale processes. Sections 6.2 and 6.3 address two-dimensional and three-dimensional models for thermal-hydrologic processes.

(8) Any expert elicitation conducted is in accordance with NUREG–1563 (Kotra et al. 1996 [DIRS 100909]), or other acceptable approaches.

Expert elicitation conducted in accordance with NUREG–1563 (Kotra et al. 1996 [DIRS 100909]) was not used to support models used in this report.

- AC3: *Data Uncertainty Is Characterized and Propagated Through the Model Abstraction*: Quantitative propagation of effects of data uncertainty was not conducted during the development of this model. This is because the primary purpose of the model was to assess the relative importance or potential contribution of TH, THC, and THM effects on repository performance at the mountain scale. Generally, only nominal (mean) parameter values were used in the analyses. An abstraction of the results of this model was not developed and no outputs were passed to downstream models for use in the TSPA. Hydrologic and thermal properties used in the TH/THC/THM models have been calibrated (BSC 2004 [DIRS 169861]) using different infiltration maps and field measured temperature data, thus capturing the uncertainty in model parameters.

- AC4: *Model Uncertainty Is Characterized and Propagated Through the Model Abstraction*: A rigorous analysis and propagation of model uncertainty was not associated with the development of this model. The primary purpose of the model was to assess the relative importance or potential contribution of various phenomena associated with TH, THC, and THM effects to impact repository performance at the mountain scale. Generally, only nominal parameter values were used in these analyses. An abstraction of the results of this model was not developed and no data were passed to downstream models for use in the TSPA. Model uncertainty is considered using two-dimensional and three-dimensional TH models, to evaluate the relative sensitivity of output variables to these different modeling approaches.

- AC 5: *Model Abstraction Output Is Supported by Objective Comparisons*. An abstraction of the results of this model was not developed and no data were passed to downstream models for use in the TSPA.

9. INPUTS AND REFERENCES

The following is a list of the references cited in this document. Column 2 represents the unique six digit numerical identifier (the Document Input Reference System [DIRS] number), which is placed in the text following the reference callout (e.g., BSC 2005 [DIRS 172232]). The purpose of these numbers is to assist the reader in locating a specific reference. Within the reference list, multiple sources by the same author (e.g., BSC 2002) are sorted alphabetically by title.

9.1 DOCUMENTS CITED

Altman, W.D.; Donnelly, J.P.; and Kennedy, J.E. 1988. *Peer Review for High-Level Nuclear Waste Repositories: Generic Technical Position.* NUREG-1297. Washington, D.C.: U.S. Nuclear Regulatory Commission. TIC: 200651. 103597

Altman, W.D.; Donnelly, J.P.; and Kennedy, J.E. 1988. *Qualification of Existing Data for High-Level Nuclear Waste Repositories: Generic Technical Position.* NUREG-1298. Washington, D.C.: U.S. Nuclear Regulatory Commission. TIC: 200652. 103750

Antunez, E.U.; Bodvarsson, G.S.; and Walters, M.A. 1994. "Numerical simulation study of the northwest Geysers geothermal field, A case study of the Coldwater Creek Steamfield." *Geothermics, 23,* (2), 127-141. Oxford, United Kingdom: Elsevier. TIC: 257006. 172954

Barton, C.A.; Zoback, M.D.; and Moos, D. 1995. "Fluid Flow Along Potentially Active Faults in Crystalline Rock." *Geology, 23,* (8), 683-686. Boulder, Colorado: Geological Society of America. TIC: 241579. 153826

Bear, J. 1972. *Dynamics of Fluids in Porous Media.* Environmental Science Series. Biswas, A.K., ed. New York, New York: Elsevier. TIC: 217356. 156269

Birkholzer, J.T. and Tsang, Y.W. 2000. "Modeling the Thermal-Hydrologic Processes in a Large-Scale Underground Heater Test in Partially Saturated Fractured Tuff." *Water Resources Research, 36,* (6), 1431-1447. Washington, D.C.: American Geophysical Union. TIC: 248278. 154608

Bish, D.L. and Aronson, J.L. 1993. "Paleogeothermal and Paleohydrologic Conditions in Silicic Tuff from Yucca Mountain, Nevada." *Clays and Clay Minerals, 41,* (2), 148-161. Long Island City, New York: Pergamon Press. TIC: 224613. 100006

Bish, D.L.; Vaniman, D.T.; Chipera, S.J.; and Carey, J.W. 2003. "The Distribution of Zeolites and their Effects on the Performance of a Nuclear Waste Repository at Yucca Mountain, Nevada, U.S.A." *American Mineralogist, 88,* ([11-12, Part 2]), 1889–1902. Washington, D.C.: Mineralogical Society of America. TIC: 255986. 169638

Blum, A.E. and Stillings, L.L. 1995. "Feldspar Dissolution Kinetics." Chapter 7 of *Chemical Weathering Rates of Silicate Minerals.* White, A.F. and Brantley, S.L., eds. Reviews in Mineralogy Volume 31. Washington, D.C.: Mineralogical Society of America. TIC: 222496. 126590

Bodvarsson, G.S. and Witherspoon, P.A. 1989. "Geothermal Reservoir Engineering Part 1." *Geothermal Science and Technology, 2,* (1), 1-68. New York, New York: Gordon and Breach Science Publishers. TIC: 250976. 156337

Bodvarsson, G.S.; Bjornsson, S.; Gunnarsson, A.; Gunnlaugsson, E.; Sigurdsson, O.; Stefansson, V.; and Steingrimsson, B. 1988. "A Summary of Modeling Studies of the Nesjavellir Geothermal Field, Iceland." *Proceedings, Thirteenth Workshop, Geothermal Reservoir Engineering, January 19-21, 1988, Stanford, California.* Workshop Report SGP-TR-113. Pages 83-91. Stanford, California: Stanford University. TIC: 246824. 138603

Bodvarsson, G.S.; Gislason, G.; Gunnlaugsson, E.; Sigurdsson, O.; Stefansson, V.; and Steingrimsson, B. 1993. "Accuracy of Reservoir Predictions for the Nesjavellir Geothermal Field, Iceland." *Proceedings, Eighteenth Workshop, Geothermal Reservoir Engineering, Stanford, California, January 26-28, 1993.* Ramey, H.J., Jr.; Horne, R.N.; Kruger, P.; Miller, F.G.; Brigham, W.E.; and Cook, J.W., eds. Workshop Report SGP-TR-145. Pages 273-278. Stanford, California: Stanford University. TIC: 246821. 138618

Bodvarsson, G.S.; Liu, H.H.; Ahlers, C.F.; Wu, Y-S.; and Sonnenthal, S. 2001. "Parameterization and Upscaling in Modeling Flow and Transport in the Unsaturated Zone of Yucca Mountain." Chapter 11 of *Conceptual Models of Flow and Transport in the Fractured Vadose Zone.* Washington, D.C.: National Academy Press. TIC: 252777. 160133

Bodvarsson, G.S.; Pruess, K.; and Lippmann, M. J. 1986. "Modeling of Geothermal Systems." *Journal of Petroleum Technology,* 1007-1021. Richardson, Texas: Society of Petroleum Engineers. TIC: 246733. 136386

Bodvarsson, G.S.; Pruess, K.; Haukwa, C.; and Ojiambo, S.B. 1990. "Evaluation of Reservoir Model Predictions for Olkaria East Geothermal Field, Kenya." *Geothermics, 19,* (5), 399-414. New York, New York: Pergamon Press. TIC: 246739. 136384

Bodvarsson, G.S.; Pruess, K.; Stefansson, V.; and Eliasson, E.T. 1984. "The Krafla Geothermal Field, Iceland, 2. The Natural State of the System." *Water Resources Research, 20,* (11), 1531-1544. Washington, D.C.: American Geophysical Union. TIC: 246734. 137136

Bodvarsson, G.S.; Pruess, K.; Stefansson, V.; and Eliasson, E.T. 1984. "The Krafla Geothermal Field, Iceland: 3. The Generating Capacity of the Field." *Water Resources Research, 20,* (11), 1545-1559. Washington, D.C.: American Geophysical Union. TIC: 246737. 137139

Bodvarsson, G.S.; Pruess, K.; Stefansson, V.; Bjornsson, S.; and Ojiambo, S.B. 1987. "East Olkaria Geothermal Field, Kenya, 1. History Match with Production and Pressure Decline Data." *Journal of Geophysical Research, 92,* (B1), 521-539. Washington, D.C.: American Geophysical Union. TIC: 236629. 136391

Bodvarsson, G.S.; Pruess, K.; Stefansson, V.; Bjornsson, S.; and Ojiambo, S.B. 1987. "East Olkaria Geothermal Field, Kenya, 2. Predictions of Well Performance and Reservoir Depletion." *Journal of Geophysical Research, 92,* (B1), 541-554. Washington, D.C.: American Geophysical Union. TIC: 246738. 136393

Boyle, W. 2000. "New BMT2 Revision." E-mail from W. Boyle to R. Datta, December 7, 2000, with attachment. ACC: MOL.20010125.0434. 163533

BSC (Bechtel SAIC Company) 2001. *Coupled Thermal-Hydrologic-Mechanical Effects on Permeability Analysis and Models Report.* ANL-NBS-HS-000037 REV 00. Las Vegas, Nevada: Bechtel SAIC Company. ACC: MOL.20010822.0092. 155957

BSC 2001. *FY 01 Supplemental Science and Performance Analyses, Volume 1: Scientific Bases and Analyses*. TDR-MGR-MD-000007 REV 00 ICN 01. Las Vegas, Nevada: Bechtel SAIC Company. ACC: MOL.20010801.0404; MOL.20010712.0062; MOL.20010815.0001. 155950

BSC 2002. *Repository Design, Repository/PA IED Subsurface Facilities Plan Sht. 1 of 5, Sht. 2 of 5, Sht. 3 of 5, Sht. 4 of 5, and Sht. 5 of 5.* DWG-MGR-MD-000003 REV A. Las Vegas, Nevada: Bechtel SAIC Company. ACC: MOL.20020601.0194. 159527

BSC 2002. *Users Manual (UM) for TOUGHREACT V3.0.* 10396-UM-3.0-00. Las Vegas, Nevada: Bechtel SAIC Company. ACC: MOL.20030411.0090. 164454

BSC 2002. *Ventilation Model.* ANL-EBS-MD-000030 REV 01 ICN 01. Las Vegas, Nevada: Bechtel SAIC Company. ACC: MOL.20021106.0055. 160975

BSC 2003. *Subsurface Geotechnical Parameters Report.* 800-K0C-WIS0-00400-000-00A. Las Vegas, Nevada: Bechtel SAIC Company. ACC: ENG.20040108.0001. 166660

BSC 2003. *Underground Layout Configuration.* 800-P0C-MGR0-00100-000-00E. Las Vegas, Nevada: Bechtel SAIC Company. ACC: ENG.20031002.0007. 165572

BSC 2004. *Analysis of Hydrologic Properties Data.* ANL-NBS-HS-000042 REV 00. Las Vegas, Nevada: Bechtel SAIC Company. ACC: DOC.20041005.0004. 170038

BSC 2004. *Calibrated Properties Model.* MDL-NBS-HS-000003 REV 02. Las Vegas, Nevada: Bechtel SAIC Company. ACC: DOC.20041006.0004. 169857

BSC 2004. *Conceptual Model and Numerical Approaches for UZ Flow and Transport.* MDL-NBS-HS-000005 REV 01. Las Vegas, Nevada: Bechtel SAIC Company. ACC: DOC.20040922.0006. 170035

BSC 2004. *D&E / PA/C IED Emplacement Drift Configuration and Environment.* 800-IED-MGR0-00201-000-00B. Las Vegas, Nevada: Bechtel SAIC Company. ACC: ENG.20040326.0001. 168489

BSC 2004. *D&E/RIT IED Subsurface Facilities [Sheet 1 of 4].* 800-IED-WIS0-00101-000-00B. Las Vegas, Nevada: Bechtel SAIC Company. ACC: ENG.20041130.0002. 172801

BSC 2004. *Development of Numerical Grids for UZ Flow and Transport Modeling.* ANL-NBS-HS-000015 REV 02. Las Vegas, Nevada: Bechtel SAIC Company. ACC: DOC.20040901.0001. 169855

BSC 2004. *Drift Degradation Analysis.* ANL-EBS-MD-000027 REV 03. Las Vegas, Nevada: Bechtel SAIC Company. ACC: DOC.20040915.0010. 166107

BSC 2004. *Drift Scale THM Model.* MDL-NBS-HS-000017 REV 01. Las Vegas, Nevada: Bechtel SAIC Company. ACC: DOC.20041012.0001. 169864

BSC 2004. *In-Situ Field Testing of Processes.* ANL-NBS-HS-000005 REV 03. Las Vegas, Nevada: Bechtel SAIC Company. ACC: MOL.20040802.0245. 170004

BSC 2004. *Natural Analogue Synthesis Report.* TDR-NBS-GS-000027 REV 01. Las Vegas, Nevada: Bechtel SAIC Company. ACC: DOC.20040524.0008. 169218

BSC 2004. *Radionuclide Transport Models Under Ambient Conditions.* MDL-NBS-HS-000008, Rev. 02. Las Vegas, Nevada: Bechtel SAIC Company. ACC: DOC.20041101.0002. 164500

BSC 2004. *Seepage Model for PA Including Drift Collapse.* MDL-NBS-HS-000002 REV 03. Las Vegas, Nevada: Bechtel SAIC Company. ACC: DOC.20040922.0008. 167652

BSC 2004. *Simulation of Net Infiltration for Present-Day and Potential Future Climates.* MDL-NBS-HS-000023 REV 00. Las Vegas, Nevada: Bechtel SAIC Company. ACC: MOL.20040823.0228. 170007

BSC 2004. *Thermal Testing Measurements Report.* TDR-MGR-HS-000002 REV 00. Las Vegas, Nevada: Bechtel SAIC Company. ACC: DOC. 20040928.0005. 169900

BSC 2004. *UZ Flow Models and Submodels.* MDL-NBS-HS-000006 REV 02. Las Vegas, Nevada: Bechtel SAIC Company. ACC: MOL.20040804.0253. 169861

BSC 2004. *Ventilation Model and Analysis Report.* ANL-EBS-MD-000030 REV 04. Las Vegas, Nevada: Bechtel SAIC Company. ACC: MOL.20040714.0482. 169862

BSC 2005. *Drift-Scale Coupled Process (DST and TH Seepage) Models.* MDL-NBS-HS-000015 REV 02. Las Vegas, NV: Bechtel SAIC Company. ACC: DOC.20050114.0004. 172232

BSC 2005. *Drift-Scale THC Seepage Model*. MDL-NBS-HS-000001 REV 04. Las Vegas, Nevada: Bechtel SAIC Company, LLC. ACC: DOC.20050218.0001. 172862

BSC 2005. *Features, Events, and Processes in SZ Flow and Transport.* ANL-NBS-MD-000002 REV 04. Las Vegas, Nevada: Bechtel SAIC Company. ACC: DOC.20050822.0012. 174190

BSC 2005. *Features, Events, and Processes in UZ Flow and Transport.* ANL-NBS-MD-000001 REV 03. Las Vegas, Nevada: Bechtel SAIC Company. ACC: DOC.20050809.0002. 174191

BSC 2005. *IED Waste Package Decay Heat Generation [Sheet 1 of 1]*. 800-IED-WIS0-00701-000-00A. Las Vegas, Nevada: Bechtel SAIC Company. ACC: ENG.20050406.0006. 173705

BSC 2005. *Multiscale Thermohydrologic Model.* ANL-EBS-MD-000049 REV 03. Las Vegas, Nevada: Bechtel SAIC Company. ACC: DOC.20050711.0001. 173944

BSC 2005. *Q-List.* 000-30R-MGR0-00500-000-002. Las Vegas, Nevada: Bechtel SAIC Company. ACC: ENG.20050805.0006. 174269

BSC 2005. *Subsurface Facility Description Document.* 800-3YD-SS00-00100-000-002. Las Vegas, Nevada: Bechtel SAIC Company. ACC: ENG.20050714.0015. 174514

BSC 2005. *Technical Work Plan for: Near-Field Environment and Transport: Coupled Processes (Mountain-Scale TH/THC/THM, Drift-Scale THC Seepage, and Post-Processing Analysis for THC Seepage) Report Integration.* TWP-MGR-PA-000017 REV 01 ICN 03. Las Vegas, Nevada: Bechtel SAIC Company. ACC: DOC.20050711.0002. 174842

Bullivant, D.P. and O'Sullivan, M.J. 1998. "Inverse Modelling of the Wairakei Geothermal Field." *Proceedings of the TOUGH Workshop '98, Berkeley, California, May 4-6, 1998.* Preuss, K., ed. LBNL-41995. Pages 53-58. Berkeley, California: Lawrence Berkeley National Laboratory. TIC: 247159. 144410

Buscheck, T.A.; Nitao, J.J.; and Saterlie, S.F. 1994. "Evaluation of Thermo-Hydrological Performance in Support of the Thermal Loading Systems Study." *High Level Radioactive Waste Management, Proceedings of the Fifth Annual International Conference, Las Vegas, Nevada, May 22-26, 1994. 2,* 592-610. La Grange Park, Illinois: American Nuclear Society. TIC: 210984. 105157

Canori, G.F. and Leitner, M.M. 2003. *Project Requirements Document.* TER-MGR-MD-000001 REV 02. Las Vegas, Nevada: Bechtel SAIC Company. ACC: DOC.20031222.0006. 166275

Carey, J.W.; Chipera, S.J.; Vaniman, D.T.; and Bish, D.L. 1998. *Three-Dimensional Mineralogic Model of Yucca Mountain, Nevada: Rev 2.0.* Deliverable SP32BSM4. Los Alamos, New Mexico: Los Alamos National Laboratory, Earth and Environmental Sciences Division. ACC: MOL.20000110.0159. 109051

Carey, J.W.; Chipera, S.J.; Vaniman, D.T.; Bish, D.L.; Viswanathan, H.S.; and Carter-Krogh, K. 1997. *Three-Dimensional Mineralogic Model of Yucca Mountain, Nevada, Rev. 1.* Deliverable SP344BM4. Draft R1. Los Alamos, New Mexico: Los Alamos National Laboratory. ACC: MOL.19971117.0110. 101323

Carranza-Torres C., and Fairhurst, C. 1999. "The Elasto-plastic Response of Underground Excavatations in Rock Masses That Satisfy the Hoek-Brown Failure Criterion." *International Journal of Rock Mechanics and Mining Science & Geomechanics Abstracts, 36*, 777-809. Oxford, England: Pergamon. TIC: 256964. 172880

CRWMS (Civilian Radioactive Waste Management System) M&O (Management and Operating Contractor) 1997. *Yucca Mountain Site Geotechnical Report.* B00000000-01717-5705-00043 REV 01. Two volumes. Las Vegas, Nevada: CRWMS M&O. ACC: MOL.19971017.0736; MOL.19971017.0737. 103564

CRWMS M&O 1998. *Drift Scale Test Progress Report No. 1.* BAB000000-01717-5700-00004 REV 01. Las Vegas, Nevada: CRWMS M&O. ACC: MOL.19990209.0240. 108306

CRWMS M&O 1998. *Geology of the Exploratory Studies Facility Topopah Spring Loop.* BAB000000-01717-0200-00002 REV 01. Las Vegas, Nevada: CRWMS M&O. ACC: MOL.19980415.0283. 102679

CRWMS M&O 1999. *Single Heater Test Final Report.* BAB000000-01717-5700-00005 REV 00 ICN 1. Las Vegas, Nevada: CRWMS M&O. ACC: MOL.20000103.0634. 129261

CRWMS M&O 2000. *Mountain-Scale Coupled Processes (TH) Models.* MDL-NBS-HS-000007 REV 00. Las Vegas, Nevada: CRWMS M&O. ACC: MOL.19990721.0528. 144454

CRWMS M&O 2000. *Unsaturated Zone Flow and Transport Model Process Model Report.* TDR-NBS-HS-000002 REV 00 ICN 02. Las Vegas, Nevada: CRWMS M&O. ACC: MOL.20000831.0280. 151940

CRWMS M&O 2001. *Drift-Scale Coupled Processes (DST and THC Seepage) Models*. MDL-NBS-HS-000001 REV 01. Las Vegas, Nevada: CRWMS M&O. ACC: MOL.20010314.0003. 154426

da Cunha, A.P. 1993. "Research on Scale Effects in the Determination of Rock Mass Mechanical Properties – The Portuguese Experience." *Scale Effects in Rock Masses 93, Proceedings of the Second International Workshop on Scale Effects in Rock Masses, Lisbon, Portugal, 25 June 1993.* da Cunha, A.P., ed. Pages 285-291. Brookfield, Vermont: A.A. Balkema. TIC: 255893. 168515

da Cunha, A.P. 1993. "Scale Effects in Rock Engineering – An Overview of the Loen Workshop and Other Recent Papers Concerning Scale Effects." *Scale Effects in Rock Masses 93, Proceedings of the Second International Workshop on Scale Effects in Rock Masses, Lisbon, Portugal, 25 June 1993*. da Cunha, A.P., ed. Pages 3-14. Brookfield, Vermont: A.A. Balkema. TIC: 255893. 168514

Dobson, P.F.; Kneafsey, T.J.; Sonnenthal, E.L.; Spycher, N.; and Apps, J.A. 2003. "Experimental and Numerical Simulation of Dissolution and Precipitation: Implications for Fracture Sealing at Yucca Mountain, Nevada." *Journal of Contaminant Hydrology, 62-63,* 459-476. New York, New York: Elsevier. TIC: 254205. 165949

Dobson, P.F.; Salah, S.; Spycher, N.; and Sonnenthal, E. 2003. "Simulation of Water-Rock Interaction in the Yellowstone Geothermal System Using TOUGHREACT." *TOUGH Symposium 2003, Proceedings, Revision 2.0, Berkeley, California, May 12-14, 2003.* Berkeley, California: Lawrence Berkeley National Laboratory. TIC: 255880. 168273

Doughty, C. 1999. "Investigation of Conceptual and Numerical Approaches for Evaluating Moisture, Gas, Chemical, and Heat Transport in Fractured Unsaturated Rock." *Journal of Contaminant Hydrology, 38,* (1-3), 69-106. New York, New York: Elsevier. TIC: 244160. 135997

Driscoll, F.G. 1986. *Groundwater and Wells.* 2nd Edition. St. Paul, Minnesota: Johnson Filtration Systems. TIC: 217555. 116801

Finsterle, S. 1999. *ITOUGH2 User's Guide.* LBNL-40040. Berkeley, California: Lawrence Berkeley National Laboratory. TIC: 243018. 104367

Garg, S.K. and Pritchett, J.W. 1990. "Cold Water Injection Into Single- and Two-Phase Geothermal Reservoir." *Water Resources Research, 26,* (2), 331-338. Washington, D.C.: American Geophysical Union. TIC: 247136. 137148

Hakami H. 2001. "Rock Characterization Facility (RCF) Shaft Sinking - Numerical Computations using FLAC." *International Journal of Rock Mechanics and Mining Science & Geomechanics Abstracts, 38*, 59-65. Oxford, England: Pergamon. TIC: 256965. 172881

Hanano, M. 1992. "Reservoir Engineering Studies of the Matsukawa Geothermal Field, Japan." *Geothermal Resources Council Transactions, 16,* 643-650. Davis, California: Geothermal Resources Council. TIC: 247116. 137307

Hart, R. 2003. "Enhancing Rock Stress Understanding Through Numerical Analysis" *International Journal of Rock Mechanics and Mining Science & Geomechanics Abstracts, 40*, 1089-1097. Oxford, England: Pergamon. TIC: 256966. 172882

Haukwa, C.B.; Wu, Y-S.; and Bodvarsson, G.S. 2003. "Modeling Thermal–Hydrological Response of the Unsaturated Zone at Yucca Mountain, Nevada, to Thermal Load at a Potential Repository." *Journal of Contaminant Hydrology, 62-63,* 529-552. New York, New York: Elsevier. TIC: 254205. 165165

He, J. 1993. "A Case Review of the Deformation Modulus of Rock Mass: Scale Effect." *Scale Effects in Rock Masses 93, Proceedings of the Second International Workshop on Scale Effects in Rock Masses, Lisbon, Portugal, 25 June 1993*. da Cunha, A.P., ed. Pages 87-91. TIC: 255893. 168516

Hunt, T.M.; Allis, R.G.; Blakeley, M.R.; and O'Sullivan, M. J. 1990. "Testing Reservoir Simulation Models for the Broadlands Geothermal Field Using Precision Gravity Data." *1990 International Symposium on Geothermal Energy, Transactions, Geothermal Resources Council, 1990 Annual Meeting, 20-24 August, 1990, Kailua-Kona, Hawaii.* Volume 14, Part II. Pages 1287-1294. Davis, California: Geothermal Resources Council. TIC: 246942. 137322

Ingebritsen, S.E. and Sorey, M.L. 1988. "Vapor-Dominated Zones Within Hydrothermal Systems: Evolution and Natural State." *Journal of Geophysical Research, 93,* (B11), 13635-13655. Washington, D.C.: American Geophysical Union. TIC: 247149. 137537

Itasca Consulting Group 1997. *FLAC ^{3D}, Fast Lagrangian Analysis of Continua in 3 Dimensions.* Version 2.0 Five volumes. Minneapolis, Minnesota: Itasca Consulting Group. TIC: 251273. 156788

Jaeger, J.C. and Cook, N.G.W. 1979. *Fundamentals of Rock Mechanics.* 3rd Edition. New York, New York: Chapman and Hall. TIC: 218325. 106219

Kiryukhin, A.; Xu, T.; Pruess, K.; Apps, J.; and Slovtsov, I. 2004. "Thermal-Hydrodynamic-Chemical (THC) Modeling Based on Geothermal Field Data." *Geothermics, 33,* 349-381. New York, New York: Pergamon. TIC: 256270. 170653

Knauss, K.G.; Dibley, M.J.; Leif, R.N.; Mew, D.A.; and Aines, R.D. 1998. "Aqueous Oxidation of Trichloroethene (TCE): A Kinetic and Thermodynamic Analysis." *Physical, Chemical, and Thermal Technologies, Remediation of Chlorinated and Recalcitrant Compounds, Proceedings of the First International Conference on Remediation of Chlorinated and Recalcitrant Compounds, Monterey, California, May 18-21, 1998.* Wickramanayake, G.B. and Hinchee, R.E., eds. Columbus, Ohio: Battelle Press. TIC: 248020. 145003

Kotra, J.P.; Lee, M.P.; Eisenberg, N.A.; and DeWispelare, A.R. 1996. *Branch Technical Position on the Use of Expert Elicitation in the High-Level Radioactive Waste Program.* NUREG-1563. Washington, D.C.: U.S. Nuclear Regulatory Commission. TIC: 226832. 100909

Lam, S.T.; Hunsbedt, A.; Kruger, P.; and Pruess, K. 1988. "Analysis of the Stanford Geothermal Reservoir Model Experiments Using the LBL Reservoir Simulator." *Geothermics, 17,* (4), 595-605. Oxford, United Kingdom: Elsevier. TIC: 247098. 137338

Leverett, M.C. 1941. "Capillary Behavior in Porous Solids." *AIME Transactions, Petroleum Development and Technology, Tulsa Meeting, October 1940, 142.* 152-169. New York, New York: American Institute of Mining and Metallurgical Engineers. TIC: 240680. 100588

Lichtner, P.C.; Keating, G.; and Carey, B. 1999. *A Natural Analogue for Thermal-Hydrological-Chemical Coupled Processes at the Proposed Nuclear Waste Repository at Yucca Mountain, Nevada.* LA-13610-MS. Los Alamos, New Mexico: Los Alamos National Laboratory. TIC: 246032. 121006

Liu, H.H. and Bodvarsson, G.S. 2001. "Constitutive Relations for Unsaturated Flow in a Fracture Network." *Journal of Hydrology, 252,* (1-4), 116-125. New York, New York: Elsevier. TIC: 253269. 160110

Liu, H.H.; Doughty, C.; and Bodvarsson, G.S. 1998. "An Active Fracture Model for Unsaturated Flow and Transport in Fractured Rocks." *Water Resources Research, 34,* (10), 2633-2646. Washington, D.C.: American Geophysical Union. TIC: 243012. 105729

Liu, H-H.; Rutqvist, J.; Zhou, Q.; and Bodvarsson, G.S. 2003. "Upscaling of Normal Stress-Permeability Relationships for Fracture Networks Obeying Fractional Levy Motion." *GeoProc 2003, International Conference on Coupled T-H-M-C Processes in Geo-Systems: Fundamentals, Modelling, Experiments & Applications, Stockholm, Sweden, October 13-15, 2003.* Stephansson, O.; Hudson, J.A.; and Jing, L., eds. *Part 1,* 251-256. Stockholm, Sweden: Royal Institute of Technology. TIC: 255195. 166017

Mack, M.G.; Brandshaug T.; and Brady B.H. 1989. *Rock Mass Modification Around a Nuclear Waste Repository in Welded Tuff.* NUREG/CR-5390. Washington, D.C.: U.S. Nuclear Regulatory Commission. TIC: 229166. 100677

Matyskiela, W. 1997. "Silica Redistribution and Hydrologic Changes in Heated Fractured Tuff." *Geology, 25,* (12), 1115-1118. Boulder, Colorado: Geological Society of America. TIC: 236809. 100058

Menzies, A.J.; Granados, E.E.; Sanyal, S.K.; Merida-I, L.; and Caicedo-A, A. 1991. "Numerical Modeling of the Initial State and Matching of Well Test Data from the Zunil Geothermal Field, Guatemala." *Proceedings, Sixteenth Workshop, Geothermal Reservoir Engineering, January 23-25, 1991, Stanford, California.* Workshop Report SGP-TR-134. Pages 193-201. Stanford, California: Stanford University. TIC: 246832. 137923

Min, K-B.; Rutqvist, J.; Tsang, Chin-Fu; and Jing, Lanru. 2004. "Stress-dependent Permeability of Fractured Rock: A Numerical Study." *International Journal of Rock Mechanics and Mining Science & Geomechanics Abstracts, 41*, 1191-1210. Oxford, England: Pergamon. TIC: 256967. 172883

Molloy, M.W. 1981. "Geothermal Reservoir Engineering Code Comparison Project." *Proceedings, Special Panel on Geothermal Model Intercomparison Study, at the Sixth Workshop on Geothermal Reservoir Engineering, December 16-18, 1980.* Workshop Report SGP-TR-42. Pages 1-26. Stanford, California: Stanford University. TIC: 250930. 156407

Montazer, P. and Wilson, W.E. 1984. *Conceptual Hydrologic Model of Flow in the Unsaturated Zone, Yucca Mountain, Nevada.* Water-Resources Investigations Report 84-4345. Lakewood, Colorado: U.S. Geological Survey. ACC: NNA.19890327.0051. 100161

Moore, J.N. and Gunderson, R.P. 1995. "Fluid Inclusion and Isotopic Systematics of an Evolving Magmatic-Hydrothermal System." *Geochimica et Cosmochimica Acta, 59,* (19), 3887-3907. New York, New York: Elsevier Science. TIC: 257005. 172947

Moore, J.N.; Adams, M.C.; and Anderson, A.J. 2000. "The Fluid Inclusion and Mineralogic Record of the Transition from Liquid- to Vapor-Dominated Conditions in the Geysers Geothermal System, California." *Economic Geology, 95,* ([8]), 1719-1737. Lancaster, Pennsylvania: Economic Geology Publishing. TIC: 250941. 156318

Mukhopadhyay, S. and Tsang, Y.W. 2003. "Uncertainties in Coupled Thermal-Hydrological Processes Associated with the Drift Scale Test at Yucca Mountain, Nevada." *Journal of Contaminant Hydrology, 62-63,* 595-612. New York, New York: Elsevier. TIC: 254205. 160790

Murray, L.E.; Rohrs, D.T.; Rossknecht, T.G.; Aryawijaya, R.; and Pudyastuti, K. 1995. "Resource Evaluation and Development Strategy, Awibengkok Field." *Proceedings of the World Geothermal Congress 1995, Florence, Italy, May 18-31, 1995.* Barbier, E.; Frye, G.; Iglesias, E.; and Pálmason, G.; eds. *5,* 1525-1529. Auckland, New Zealand: International Geothermal Association. TIC: 251065. 156612

Nitao, J.J. 1988. *Numerical Modeling of the Thermal and Hydrological Environment Around a Nuclear Waste Package Using the Equivalent Continuum Approximation: Horizontal Emplacement.* UCID-21444. Livermore, California: Lawrence Livermore National Laboratory. ACC: NNA.19890317.0021. 109911

Norton, D.L. and Hulen, J.B. 2001. "Preliminary Numerical Analysis of the Magma-Hydrothermal History of the Geysers Geothermal System, California USA." *Geothermics, 30,* 211-234. New York, New York: Pergamon. TIC: 257009. 172959

NRC (U.S. Nuclear Regulatory Commission) 2003. *Yucca Mountain Review Plan, Final Report.* NUREG-1804, Rev. 2. Washington, D.C.: U.S. Nuclear Regulatory Commission, Office of Nuclear Material Safety and Safeguards. TIC: 254568. 163274

O'Sullivan, M.J.; Barnett, B.G.; and Razali, M.Y. 1990. "Numerical Simulation of the Kamojang Geothermal Field, Indonesia." *1990 International Symposium on Geothermal Energy, Transactions, Geothermal Resources Council, 1990 Annual Meeting, 20-24 August, 1990, Kailua-Kona, Hawaii.* Volume 14, Part II. Pages 1317-1324. Davis, California: Geothermal Resources Council. TIC: 246942. 137409

O'Sullivan, M.J.; Bullivant, D.P.; Follows, S.E.; and Mannington, W.I. 1998. "Modelling of the Wairakei - Tauhara Geothermal System." *Proceedings of the TOUGH Workshop '98, Berkeley, California, May 4-6, 1998.* Pruess, K., ed. LBNL-41995. Pages 1-6. Berkeley, California: Lawrence Berkeley National Laboratory. TIC: 247159. 154567

O'Sullivan, M.J.; Pruess, K.; and Lippmann, M.J. 2001. "State of the Art of Geothermal Reservoir Simulation." *Geothermics, 30,* (4), 395-429. New York, New York: Elsevier. TIC: 250945. 156353

Pruess, K. 1987. *TOUGH User's Guide.* NUREG/CR-4645. Washington, D.C.: U.S. Nuclear Regulatory Commission. TIC: 217275. 100684

Pruess, K. 1991. *TOUGH2—A General-Purpose Numerical Simulator for Multiphase Fluid and Heat Flow.* LBL-29400. Berkeley, California: Lawrence Berkeley Laboratory. ACC: NNA.19940202.0088. 100413

Pruess, K. and Narasimhan, T.N. 1985. "A Practical Method for Modeling Fluid and Heat Flow in Fractured Porous Media." *Society of Petroleum Engineers Journal, 25,* (1), 14-26. Dallas, Texas: Society of Petroleum Engineers. TIC: 221917. 101707

Pruess, K. and Tsang, Y. 1994. *Thermal Modeling for a Potential High-Level Nuclear Waste Repository at Yucca Mountain, Nevada.* LBL-35381. Berkeley, California: Lawrence Berkeley National Laboratory. ACC: NNA.19940427.0248. 117451

Pruess, K. and Wang, J.S.Y. 1984. "TOUGH - A Numerical Model for Nonisothermal Unsaturated Flow to Study Waste Canister Heating Effects." *Scientific Basis for Nuclear Waste Management VII, Symposium held November 14-17, 1983, Boston, Massachusetts.* McVay, G.L., ed. *26,* 1031-1038. New York, New York: Elsevier. TIC: 204393. 140912

Pruess, K.; Oldenburg, C.; and Moridis, G. 1999. *TOUGH2 User's Guide, Version 2.0.* LBNL-43134. Berkeley, California: Lawrence Berkeley National Laboratory. TIC: 253038. 160778

Pruess, K.; Wang, J.S.Y.; and Tsang, Y.W. 1990. "On Thermohydrologic Conditions Near High-Level Nuclear Wastes Emplaced in Partially Saturated Fractured Tuff, 1. Simulation Studies with Explicit Consideration of Fracture Effects." *Water Resources Research, 26,* (6), 1235-1248. Washington, D.C.: American Geophysical Union. TIC: 221923. 100818

Pruess, K.; Wang, J.S.Y.; and Tsang, Y.W. 1990. "On Thermohydrologic Conditions Near High-Level Nuclear Wastes Emplaced in Partially Saturated Fractured Tuff, 2. Effective Continuum Approximation." *Water Resources Research, 26,* (6), 1249-1261. Washington, D.C.: American Geophysical Union. TIC: 224854. 100819

Rutqvist, J. and Stephansson, O. 2003. "The Role of Hydromechanical Coupling in Fractured Rock Engineering." *Hydrogeology Journal, 11,* (1), 7-40. New York, New York: Springer-Verlag. TIC: 254245. 162583

Rutqvist, J. and Tsang, C-F. 2002. "A Study of Caprock Hydromechanical Changes Associated with CO_2-Injection into a Brine Formation." *Environmental Geology, 42,* (2-3), 296-305. New York, New York: Springer-Verlag. TIC: 254244. 162587

Rutqvist, J. and Tsang, C-F. 2003. "Analysis of Thermal-Hydrologic-Mechanical Behavior Near an Emplacement Drift at Yucca Mountain." *Journal of Contaminant Hydrology, 62-63,* 637-652. New York, New York: Elsevier. TIC: 254205. 162584

Rutqvist, J.; Tsang, C.-F.; and Tsang, Y. 2003. "Analysis of Stress- and Moisture-Induced Changes in Fractured Rock Permeability at the Yucca Mountain Drift Scale Test." *2003 GeoProc, International Conference on Coupled T-H-M-C Processes in Geo-Systems: Fundamentals, Modelling, Experiments & Applications, Stockhom, Sweden, 13-15 October 2003.* Stehpansson, O.; Hudson, J.A.; and Jing, L., eds. Pages 147-152. Stockholm, Sweden: Royal Institute of Technology. TIC: 256087. 170400

Rutqvist, J.; Wu, Y.-S.; Tsang, C.-F.; and Bodvarsson, G. 2002. "A Modeling Approach for Analysis of Coupled Multiphase Fluid Flow, Heat Transfer, and Deformation in Fractured Porous Rock." *International Journal of Rock Mechanics and Mining Sciences, 39,* (4), 429-442. New York, New York: Pergamon. TIC: 253953. 162048

Sass, J.H.; Lachenbruch, A.H.; Dudley, W.W., Jr.; Priest, S.S.; and Munroe, R.J. 1988. *Temperature, Thermal Conductivity, and Heat Flow Near Yucca Mountain, Nevada: Some Tectonic and Hydrologic Implications.* Open-File Report 87-649. Denver, Colorado: U.S. Geological Survey. TIC: 203195. 100644

Simmons, A.M. and Bodvarsson, G.S. 1997. *Building Confidence in Thermohydrologic Models of Yucca Mountain Using Geothermal Analogues.* Milestone SPLE1M4. Berkeley, California: Lawrence Berkeley National Laboratory. ACC: MOL.19970710.0328. 126511

Sobolik, S.R.; Finley, R.E.; and Ballard, S. 1998. "Post-Test Comparison of Thermal-Mechanical Measurements vs. Analyses for the In-Situ Single Heater Test, Yucca Mountain, Nevada." *International Journal of Rock Mechanics and Mining Sciences, 35,* (4-5), 649. New York, New York: Pergamon. TIC: 253944. 162049

Sobolik, S.R.; Finley, R.E.; and Ballard, S. 1999. "Thermal-Mechanical Measurements in the Drift Scale Test, Yucca Mountain, Nevada." *Rock Mechanics for Industry, Proceedings of the 37th U.S. Rock Mechanics Symposium, Vail, Colorado, USA, 6-9 June, 1999.* Amadei, B.; Kranz, R.L.; Scott, G.A.; and Smeallie, P.H.; eds. *2,* 735-742. Brookfield, Vermont: A.A. Balkema. TIC: 245246. 163202

Souley, M.; Homand, F.; Pepa, S.; and Hoxha, D. 2001. "Damage-induced permeability changes in granite: A case example at the URL in Canada." *International Journal of Rock Mechanics and Mining Science & Geomechanics Abstracts, 38*, 297-310. Oxford, England: Pergamon. TIC: 256968. 172884

Spycher, N.F.; Sonnenthal, E.L.; and Apps, J.A. 2003. "Fluid Flow and Reactive Transport Around Potential Nuclear Waste Emplacement Tunnels at Yucca Mountain, Nevada." *Journal of Contaminant Hydrology, 62-63,* 653-673. New York, New York: Elsevier. TIC: 254205. 162121

Steingrimsson, B.; Bodvarsson, G.S.; Gunnlaugsson, E.; Gislason, G.; and Sigurdsson, O. 2000. "Modeling Studies of the Nesjavellir Geothermal Field, Iceland." *Proceedings of the World Geothermal Congress 2000, Kyushu - Tohoku, Japan, May 28 - June 10, 2000.* Iglesias, E.; Blackwell, D.; Hunt, T.; Lund, J.; and Tamanyu, S.; eds. Pages 2899-2904. Auckland, New Zealand: International Geothermal Association. TIC: 251140. 156686

Stimac, J.A.; Goff, F.; and Wohletz, K. 2001. "Thermal Modeling of the Clear Lake Magmatic-Hydrothermal System, California, USA." *Geothermics, 30,* 349-390. New York, New York: Pergamon. TIC: 257008. 172958

Strobel, C.J. 1993. "Bulalo Field, Philippines: Reservoir Modeling for Prediction of Limits to Sustainable Generation." *Proceedings, Eighteenth Workshop, Geothermal Reservoir Engineering, Stanford, California, January 26-28, 1993.* Ramey, H.J., Jr.; Horne, R.N.; Kruger, P.; Miller, F.G.; Brigham, W.E.; and Cook, J.W., eds. Workshop Report SGP-TR-145. Pages 5-10. Stanford, California: Stanford University. TIC: 246821. 156614

Tsang, Y.W. and Birkholzer, J.T. 1999. "Predictions and Observations of the Thermal-Hydrological Conditions in the Single Heater Test." *Journal of Contaminant Hydrology, 38,* (1-3), 385-425. New York, New York: Elsevier. TIC: 244160. 137577

Tsang, Y.W. and Pruess, K. 1987. "A Study of Thermally Induced Convection near a High-Level Nuclear Waste Repository in Partially Saturated Fractured Tuff." *Water Resources Research, 23,* (10), 1958-1966. Washington, D.C.: American Geophysical Union. TIC: 240715. 100688

van Genuchten, M.T. 1980. "A Closed-Form Equation for Predicting the Hydraulic Conductivity of Unsaturated Soils." *Soil Science Society of America Journal, 44,* (5), 892-898. Madison, Wisconsin: Soil Science Society of America. TIC: 217327. 100610

Wang, J.S. 2003. "Scientific Notebooks Referenced in Model Report N0120/U0110, Drift-Scale Coupled Processes (DST and THC Seepage) Models MDL-NBS-HS-000001 REV 02." Interoffice correspondence from J.S. Wang (BSC) to File, June 6, 2003, with attachments. ACC: MOL.20030611.0079. 161665

Wang, J.S. 2003. "Scientific Notebooks Referenced in Model Report U0105 Mountain-Scale Coupled Processes (TH/THC/THM), MDL-NBS-HS-000007 REV 01." Interoffice correspondence from J.S. Wang (BSC) to File, December 4, 2003, with attachments. ACC: MOL.20031208.0371. 165927

White, F.M. 1986. *Fluid Mechanics.* 2nd Edition. New York, New York: McGraw-Hill. TIC: 243415. 111015

White, S.P.; Kissling, W.M.; and McGuinness, M.J. 1997. "Models of the Kawareu Geothermal Reservoir." *Geothermal Resources Council Transactions, 21,* 33-39. Davis, California: Geothermal Resources Council. TIC: 250949. 156340

Williamson, K.H. 1992. "Development of a Reservoir Model for the Geysers Geothermal Field." *Monograph on the Geysers Geothermal Field.* Stone, C., ed. Special Report No. 17. Pages 179-187. Davis, California: Geothermal Resources Council. TIC: 251066. 156613

Witherspoon, P.A.; Wang, J.S.Y; Iwai, K.; and Gale, J.E. 1980. "Validity of Cubic Law for Fluid Flow in a Deformable Rock Fracture." *Water Resources Research, 16,* (6), 1016-1024. Washington, D.C.: American Geophysical Union. TIC: 220088. 123506

Wu, Y-S. and Pruess, K. 2000. "Numerical Simulation of Non-Isothermal Multiphase Tracer Transport in Heterogeneous Fractured Porous Media." *Advances in Water Resources, 23,* (7), 699-723. New York, New York: Elsevier. TIC: 249626. 153972

Wu, Y.S.; Haukwa, C.; and Bodvarsson, G.S. 1999. "A Site-Scale Model for Fluid and Heat Flow in the Unsaturated Zone of Yucca Mountain, Nevada." *Journal of Contaminant Hydrology, 38,* (1-3), 185-215. New York, New York: Elsevier. TIC: 244160. 117161

Wu, Y.S.; Ritcey, A.C.; and Bodvarsson, G.S. 1999. "A Modeling Study of Perched Water Phenomena in the Unsaturated Zone at Yucca Mountain." *Journal of Contaminant Hydrology, 38,* (1-3), 157-184. New York, New York: Elsevier. TIC: 244160. 117167

Wu, Y-S.; Pan, L.; Zhang, W.; and Bodvarsson, G.S. 2002. "Characterization of Flow and Transport Processes within the Unsaturated Zone of Yucca Mountain, Nevada, Under Current and Future Climates." *Journal of Contaminant Hydrology, 54,* (3-4), 215-247. New York, New York: Elsevier. TIC: 253316. 160195

Xu, T.; Sonnenthal, E.; and Bodvarsson, G. 2003. "A Reaction-Transport Model for Calcite Precipitation and Evaluation of Infiltration Fluxes in Unsaturated Fractured Rock." *Journal of Contaminant Hydrology, 64,* (1-2), 113-127. New York, New York: Elsevier. TIC: 254008. 162124

9.2 CODES, STANDARDS, REGULATIONS, AND PROCEDURES

10 CFR 63. 2005 Energy: Disposal of High-Level Radioactive Wastes in a Geologic Repository at Yucca Mountain, Nevada. ACC: MOL.20050405.0118. 173273

AP-2.22Q, Rev. 1, ICN 1. *Classification Analyses and Maintenance of the Q-List*. Washington, D.C.: U.S. Department of Energy, Office of Civilian Radioactive Waste Management. ACC: DOC.20040714.0002.

LP-2.29Q-BSC, Rev 0, ICN 1. *Planning for Science Activities*. Washington, D.C.: U.S. Department of Energy, Office of Civilian Radioactive Waste Management. ACC: DOC.20050718.0002.

LP-SI.11Q-BSC, Rev. 0, ICN 1. *Software Management*. Washington, D.C.: U.S. Department of Energy, Office of Civilian Radioactive Waste Management. ACC: DOC.20041005.0008.

LP-SIII.10Q-BSC, Rev. 0, ICN 1. *Models*. Washington, D.C.: U.S. Department of Energy, Office of Civilian Radioactive Waste Management. ACC: DOC.20050623.0001.

LP-SV.1Q-BSC, Rev. 0, ICN 0. *Control of the Electronic Management of Information*. Washington D.C.: U.S. Department of Energy, Office of Civilian Radioactive Waste Management. ACC: DOC.20050531.0002.

YMP-LBNL-QIP-SV.0, Rev. 2, Mod. 1. *Management of YMP-LBNL Electronic Data*. Berkeley, California: Lawrence Berkeley National Laboratory. ACC: MOL.20020717.0319.

9.3 SOURCE DATA, LISTED BY DATA TRACKING NUMBER

GS000308311221.005. Net Infiltration Modeling Results for 3 Climate Scenarios for FY99. Submittal date: 03/01/2000.	147613
GS950208312232.003. Data, Including Water Potential, Pressure and Temperature, Collected from Boreholes USW NRG-6 and USW NRG-7A from Instrumentation through March 31, 1995. Submittal date: 02/13/1995.	105572
GS951108312232.008. Data, Including Water Potential, Pressure and Temperature, Collected from Boreholes UE-25 UZ#4 & UZ#5 from Instrumentation through September 30, 1995, and from USW NRG-6 & NRG-7A from April 1 through September 30, 1995. Submittal date: 11/21/1995.	106756
GS960308312232.001. Deep Unsaturated Zone Surface-Based Borehole Instrumentation Program Data from Boreholes USW NRG-7A, USW NRG-6, UE-25 UZ#4, UE-25 UZ#5, USW UZ-7A, and USW SD-12 for the Time Period 10/01/95 through 3/31/96. Submittal date: 04/04/1996.	105573
LA9908JC831321.001. Mineralogic Model "MM3.0" Version 3.0. Submittal date: 08/16/1999.	113495
LA9912SL831151.001. Fracture Mineralogy of Drill Core ESF-HD-TEMP-2. Submittal date: 01/05/2000.	146447
LA9912SL831151.002. Percent Coverage by Fracture-Coating Minerals in Core ESF-HD-TEMP-2. Submittal date: 01/05/2000.	146449
LB0205REVUZPRP.001. Fracture Properties for UZ Model Layers Developed from Field Data. Submittal date: 05/14/2002.	159525
LB0208UZDSCPMI.002. Drift-Scale Calibrated Property Sets: Mean Infiltration Data Summary. Submittal date: 08/26/2002.	161243
LB0210THRMLPRP.001. Thermal Properties of UZ Model Layers: Data Summary. Submittal date: 10/25/2002.	160799
LB03013DSSCP3I.001. 3-D Site Scale Calibrated Properties: Data Summaries. Submittal date: 01/27/2003.	162379

LB0303DSCPTHSM.001. Drift-Scale Coupled Process Model for Thermohydrologic Seepage: Simulation Files. Submittal date: 03/20/2003. 163688

LB0303THERMESH.001. Thermal Model Mesh. Submittal date: 03/28/2003. 165168

LB0303THERMSIM.001. UZ Thermal Modeling: Simulations. Submittal date: 03/28/2003. 165167

LB030432DGRIDS.001. Three 2-D Cross-Section Grids. Submittal date: 04/29/2003. 163937

LB0306DRSCLTHM.001. Drift Scale THM Model Predictions: Simulations. Submittal date: 06/26/2003. 169733

LB0307DSTTHCR2.001. Drift-Scale Coupled Processes (DST Seepage) Model: Simulations. Submittal date: 07/24/2003. 166054

LB0307KNTDBRTM.001. Kinetic Database for Reactive Transport Modeling. Submittal date: 07/22/2003. 164433

LB0307THMDBRTM.001. Thermodynamic Database for Reactive Transport Modeling. Submittal date: 07/22/2003. 164434

LB0402THRMLPRP.001. Thermal Properties of UZ Model Layers: Data Summary. Submittal date: 02/20/2004. 168481

LL001200231031.009. Aqueous Chemistry of Water Sampled from Boreholes of the Drift Scale Test (DST). Submittal date: 12/04/2000. 153616

LL990702804244.100. Borehole and Pore Water Data. Submittal date: 07/13/1999. 144922

MO0005PORWATER.000. Perm-Sample Pore Water Data. Submittal date: 05/04/2000. 150930

MO0012MWDGFM02.002. Geologic Framework Model (GFM2000). Submittal date: 12/18/2000. 153777

MO0101SEPFDDST.000. Field Measured Data of Water Samples from the Drift Scale Test. Submittal date: 01/03/2001. 153711

MO0302SPATHDYN.000. Thermodynamic Data Input Files - Data0.YMP.R2. Submittal date: 02/05/2003. 161756

MO0307MWDAC8MV.000. Analytical-La-Coarse-800M Ventilation. Submittal date: 07/15/2003. 165395

MO0407SEPFEPLA.000. LA FEP List. Submittal date: 07/20/2004. 170760

SNL02030193001.026. Mechanical Properties Data (Ultrasonic Velocities, Elastic Moduli and Fracture Strength) for Borehole USW SD-9. Submittal date: 02/22/1996. 108436

9.4 OUTPUT AND DEVELOPED DATA, LISTED BY DATA TRACKING NUMBER

LB0310MTSCLTHM.001. Mountain Scale THM Predictions: Simulations. Submittal date: 10/21/2003.

LB0310MTSCLTHM.002. Mountain Scale THM Predictions: Summary Plots. Submittal date: 10/21/2003.

LB0310MTSCLTH2.001. Mountain Scale 2D TH Predictions: Simulations. Submittal date: 10/21/2003.

LB0310MTSCLTH3.001. Mountain Scale 3D TH Predictions: Simulations. Submittal date: 10/21/2003.

LB0310MTSCLTHC.001. Mountain Scale THC Predictions: Simulations. Submittal date: 10/21/2003.

LB0310MTSCLTHC.002. Mountain Scale THC Predictions: Data Summaries. Submittal date: 10/21/2003.

LB0404MTSCLTH3.001. Mountain Scale 3D TH Predictions: Simulations. Submittal date: 04/14/2004 (Developed data).

LB0404MTSCLTHC.001. Mountain Scale THC Predictions: Simulations. Submittal date: 04/14/2004 (Developed data).

LB0404MTSCLTHM.001. Mountain Scale THM Predictions: Simulations. Submittal date: 04/14/2004 (Developed data).

LB0404MTSCLTHM.002. Mountain Scale THM Predictions: Summary Plots. Submittal date: 04/21/2004 (Developed data).

9.5 SOFTWARE CODES

LBNL 2002. *Software Routine*: 2kgrid8.for. V1.0. DEC-Alpha, PC. 10503-1.0-00. 154787

LBNL 2000. *Software Routine*: 2KGRIDV1.F. V1.0. SUN Ultra Sparc, SUN OS 5.5.1. 10244-1.0-00. 147553

LBNL 2000. *Software Routine*: 2kgridv1a.for. V1.0. PC, DOS Emulation. 10382-1.0-00. 153067

LBNL 2002. *Software Routine*: Delb.dat. V1.0. PC, Windows 98. STN: 10507-1.0-00. 154791

LBNL 1999. *Software Code*: EXT. V1.0. Sun Ultra Sparc, Sun OS 5.5.1. 10047-1.0-00. 147562

LBNL 1999. *Software Code*: EXT. V1.1. Sun, UNIX. 10005-1.1-00. 160768

LBNL 2002. *Software Code*: FLAC3D. V2.0. PC, Windows 98. STN: 10502-2.0-00. 154783

LBNL 2000. *Software Routine*: gen-incon-v0.f. V1.0. DEC Alpha w/OSF1 V4.0. 10220-1.0-00. 147023

LBNL 2000. *Software Routine*: get_a_layer_v0.f. V1.0. DEC Alpha w/OSF1 V4.0. 10221-1.0-00. 147025

LBNL 2000. *Software Routine*: get_temp_v0.f. V1.0. DEC Alpha w/OSF1 V4.0. 10222-1.0-00. 147027

LBNL 2002. *Software Routine*: Gpzones.dat. V1.0. PC, Windows 98. STN: 10509-1.0-00. 154792

LBNL 2003. *Software Code*: GridReader. V1.0. PC,WINDOWS NT 4.0. 10994-1.0-00. 167237

LBNL 2000. *Software Routine*: hsource_v0.f. V1.0. DEC Alpha w/OSF1 V4.0. 10225-1.0-00. 147031

LBNL 2002. *Software Code*: infil2grid. V1.7. DEC-Alpha, PC. 10077-1.7-00. 154793

LBNL 2002. *Software Code*: Tin. V1.1. PC, Windows 98. 10899-1.1-00. 162038

LBNL 2000. *Software Routine*: toptemp_v0.f. V1.0. DEC Alpha w/OSF1 V4.0. 10224-1.0-00. 147030

LBNL 2003. *Software Code*: TOUGH2. V1.6. PC/MS-DOS Windows 98, Sun UltraSparc/Sun OS 5.5.1, DEC-Alpha OSF1 V4.0. 10007-1.6-01. 161491

LBNL 2002. *Software Code*: TOUGHREACT. V3.0. DEC ALPHA/OSF1 V5.1, DEC ALPHA/OSF1 V5.0, Sun UltraSparc/Sun OS 5.5.1, PC/Linux Redhat 7.2. 10396-3.0-00. 161256

LBNL 2002. *Software Code*: WINGRIDDER. V2.0. PC. 10024-2.0-00. 154785

INTENTIONALLY LEFT BLANK

APPENDIX I

INITIAL MINERAL VOLUME FRACTIONS

The source of the initial mineral volume fraction data in Table I-1 is DTN: LB0310MTSCLTHC.001. After downloading the specified DTN, go to the folder "THC_with_86percent_ventilation_simulations/THC_86present_5." Then locate the file "chemical.inp." Inside file "chemical.inp" search and find the keywords "INITIAL MINERAL ZONES." The entries directly below those keywords contain the data in Table I-1.

The first entry declares the total number of rock blocks (76 in this instance). The second entry (=1) describes the initial mineral volume fractions for the first rock block (which is "tcwM1" in this instance). A set of entries is to be found for each rock block. The lines immediately after this (until the next rock block is reached) describe the initial mineral volume fractions and the initial mineral reactive surface areas.

The following example illustrates how the data can be examined. Take the rock block "tcwM1" (this exercise can be repeated for any other rock block).

1. The first entry simply identifies the mineral names ("mineral"), their initial volume fractions ("vol.frac"), and the rock type ("tcwM1").

2. The next entry describes the initial volume fraction (=0.00000) for "hematite". On the third column, there is a flag (=0). Whenever this flag is 0, it is accepted that the mineral is an equilibrium one and no other information is expected for this mineral (other than the initial volume fraction given in second column).

3. The next row identifies the mineral calcite (first column), the initial mineral volume fraction (=0.00358), and the equilibrium/kinetic flag (=0, indicating equilibrium).

4. All the equilibrium minerals are listed first (flag in the third column = 0).

5. Next, all the kinetic minerals are listed (flag in the third column = 1). In this example, the first kinetic mineral is microcline-b with an initial mineral volume fraction of 0.36911.

6. If the flag is 1, and if the reader is interested in only the initial mineral volume fractions, the line immediately following it is to be ignored. The reader can move to the next mineral (in this case, albite-low with an initial mineral volume fraction of 0.27557).

7. The rest of the initial mineral volume fractions can be read from this file and these initial mineral volume fractions are reported in Appendix I-1.

The initial mineral volume fractions are calculated based on methods described in Wang (2003 [DIRS 161665], pp. 35-70). Note that 76 rock blocks are identified in file 'chemical.inp' under "INITIAL MINERAL ZONES," whereas only 74 rock blocks are identified in Table I-1. This is because the "chemical.inp" file has to identify the top and bottom boundaries as two distinct rock blocks (for numerical modeling purposes). For these two boundary rock blocks, all initial mineral volume fractions are specified as zero (check file "chemical.inp) and these are not mentioned in Table I-1, as the boundaries are not real rock blocks.

Calculation of the Rock Matrix Mineralogical Abundances:

1. These data are taken from DTN: LA9908JC831321.001 [DIRS 113495].

2. Download DTN: LA9908JC831321.001 [DIRS 113495] from the ATDT and obtain the file "MM3.0-results.dat.z". Uncompress this file. This may take some time.

3. The location that was chosen for obtaining the mineralogical data has the Nevada Easting and Northing Coordinates of (170597.0, 233202.1). Search for these coordinates in the file and obtain the mineral weight percentages.

4. These were stored in an intermediate file, "ECRB_THalcove_min.xls." This file has the following columns: The name of the UZ model layer; the lithology; the easting, northing, and elevation; the sequence and the layer number (from the mineralogical model); and the weight percentages of the minerals.

5. The UZ model layer name and the weight percentages for each mineral in each model layer are copied over to a different file (say "tptpll_col_min_mtn_rev01-3.xls."

6. These weight percentages were then converted into volume (cm^3) by multiplying each number by the ratio of molar volume (cm^3/mol) and molecular weight (g/mol).

7. Volumes of all minerals in a particular layer are then added up to obtain a total volume for each layer.

8. Volume fraction for each mineral in any layer is then obtained by normalizing the volume of that mineral against the total volume of minerals in that layer.

9. The next phase is recalculation of the solid solution phases to their end-member composition:

    i. Feldspar is subdivided into K-feldspar, albite, and anorthite following the composition in Knauss et al. (1998 [DIRS 145003]).
    ii. Smectite ratios are calculated assuming an ideal solid solution (35% Ca-smectite, 15% Na-smectite, 15% K-smectite, and 35% Mg-smectite). Following Carey et al. (1998 [DIRS 109051], p. 18), these were further modified to account for illite (10% of the smectite volume fraction).
    iii. For nonwelded units, the entire zeolite volume fraction is assigned to clinoptilolite. For welded units, the entire zeolite volume fraction is assigned to stellerite. Zero volume fractions are assigned to mordenite and heulandite..

10. Two minerals are then added as initial mineral phases. They are beta-cristobalite (1%) which is a proxy for opal commonly present in fractures, and fluorite (0.01%). Because of these new additions, the volume fractions were renormalized to come up with the new (and final) volume fractions for each mineral. Several potential mineral and salt phases are included with zero volume fractions, such as amorphous silica, kaolinite, gypsum, and others as listed.

Table I-1. Initial Mineral Volume Fraction

Rock	Zone	microcline-b	albite-low	anorthite	smect-ca-cal	smect-na-cal	smect-mg-cal	illite	tridymite	cristoba-a	quartz	hydglassfe3	hematite	calcite	stell/10-r02	heul/10-r02	mord/10-r02	clpt/10-r02	kaolinite
tcwM1	1	0.369110	0.272570	0.009170	0.001980	0.000850	0.001980	0.001480	0.102850	0.212940	0.009420	0.001390	0.000000	0.003580	0.000000	0.000000	0.000000	0.002780	0.000000
tcwF1	2	0.369110	0.272570	0.009170	0.001980	0.000850	0.001980	0.001480	0.102850	0.212940	0.009420	0.001390	0.000000	0.003580	0.000000	0.000000	0.000000	0.002780	0.000000
tcwM2	3	0.369110	0.272570	0.009170	0.001980	0.000850	0.001980	0.001480	0.102850	0.212940	0.009420	0.001390	0.000000	0.003580	0.000000	0.000000	0.000000	0.002780	0.000000
tcwF2	4	0.369110	0.272570	0.009170	0.001980	0.000850	0.001980	0.001480	0.102850	0.212940	0.009420	0.001390	0.000000	0.003580	0.000000	0.000000	0.000000	0.002780	0.000000
tcwM3	5	0.162390	0.119920	0.004030	0.044030	0.018870	0.044030	0.032840	0.000000	0.125770	0.007440	0.430460	0.000000	0.000320	0.000000	0.000000	0.000000	0.000000	0.000000
tcwF3	6	0.162390	0.119920	0.004030	0.044030	0.018870	0.044030	0.032840	0.000000	0.125770	0.007440	0.430460	0.000000	0.000320	0.000000	0.000000	0.000000	0.000000	0.000000
ptnM1	7	0.051490	0.038020	0.001280	0.024410	0.010460	0.024410	0.018210	0.000150	0.014600	0.007020	0.788880	0.000000	0.010860	0.000000	0.000000	0.000000	0.000280	0.000000
ptnF1	8	0.051490	0.038020	0.001280	0.024410	0.010460	0.024410	0.018210	0.000150	0.014600	0.007020	0.788880	0.000000	0.010860	0.000000	0.000000	0.000000	0.000280	0.000000
ptnM2	9	0.051480	0.038020	0.001280	0.024410	0.010460	0.024410	0.018210	0.000150	0.014600	0.007020	0.788760	0.000150	0.010860	0.000000	0.000000	0.000000	0.000280	0.000000
ptnF2	10	0.051480	0.038020	0.001280	0.024410	0.010460	0.024410	0.018210	0.000150	0.014600	0.007020	0.788760	0.000150	0.010860	0.000000	0.000000	0.000000	0.000280	0.000000
ptnM3	11	0.051490	0.038020	0.001280	0.024410	0.010460	0.024410	0.018210	0.000150	0.014600	0.007020	0.788880	0.000000	0.010860	0.000000	0.000000	0.000000	0.000280	0.000000
ptnF3	12	0.051490	0.038020	0.001280	0.024410	0.010460	0.024410	0.018210	0.000150	0.014600	0.007020	0.788880	0.000000	0.010860	0.000000	0.000000	0.000000	0.000280	0.000000
ptnM4	13	0.051490	0.038020	0.001280	0.024410	0.010460	0.024410	0.018210	0.000150	0.014600	0.007020	0.788880	0.000000	0.010860	0.000000	0.000000	0.000000	0.000280	0.000000
ptnF4	14	0.051490	0.038020	0.001280	0.024410	0.010460	0.024410	0.018210	0.000150	0.014600	0.007020	0.788880	0.000000	0.010860	0.000000	0.000000	0.000000	0.000280	0.000000
ptnM5	15	0.051360	0.037930	0.001280	0.024350	0.010440	0.024350	0.018170	0.000150	0.014600	0.007020	0.786940	0.002390	0.010830	0.000000	0.000000	0.000000	0.000280	0.000000
ptnF5	16	0.051360	0.037930	0.001280	0.024350	0.010440	0.024350	0.018170	0.000150	0.014600	0.007020	0.786940	0.002390	0.010830	0.000000	0.000000	0.000000	0.000280	0.000000
ptnM6	17	0.051370	0.037940	0.001280	0.024360	0.010440	0.024360	0.018170	0.000150	0.014570	0.007010	0.787070	0.002280	0.010840	0.000000	0.000000	0.000000	0.000280	0.000000
ptnF6	18	0.051370	0.037940	0.001280	0.024360	0.010440	0.024360	0.018170	0.000150	0.014570	0.007010	0.787070	0.002280	0.010840	0.000000	0.000000	0.000000	0.000280	0.000000
tswM1	19	0.103620	0.076520	0.002570	0.002130	0.000910	0.002130	0.001590	0.001120	0.019990	0.001180	0.756300	0.004850	0.016930	0.000000	0.000000	0.000000	0.000150	0.000000
tswF1	20	0.103620	0.076520	0.002570	0.002130	0.000910	0.002130	0.001590	0.001120	0.019990	0.001180	0.756300	0.004850	0.016930	0.000000	0.000000	0.000000	0.000150	0.000000
tswM2	21	0.383120	0.282910	0.009520	0.003430	0.001470	0.003430	0.002560	0.159420	0.133130	0.004730	0.000700	0.004390	0.001100	0.000100	0.000000	0.000010	0.000000	0.000000
tswF2	22	0.231790	0.171160	0.005760	0.017670	0.007570	0.017670	0.013180	0.096450	0.080540	0.002860	0.000420	0.002650	0.020460	0.321810	0.000000	0.000010	0.000000	0.000000
tswM3	23	0.363060	0.268100	0.009020	0.007770	0.003330	0.007770	0.005800	0.056300	0.237670	0.026950	0.000000	0.003530	0.000670	0.000000	0.000000	0.000000	0.000040	0.000000
tswF3	24	0.219650	0.162200	0.005460	0.020290	0.008700	0.020290	0.015140	0.034060	0.143790	0.016300	0.000000	0.002140	0.020200	0.321750	0.000000	0.000000	0.000030	0.000000
tswM4	25	0.322650	0.238260	0.008020	0.005170	0.002210	0.005170	0.003850	0.023100	0.355880	0.025260	0.000000	0.000360	0.000070	0.000000	0.000000	0.000000	0.000010	0.000000
tswF4	26	0.195200	0.144150	0.004850	0.018720	0.008020	0.018720	0.013960	0.013970	0.215300	0.015290	0.000000	0.000220	0.019840	0.321750	0.000000	0.000000	0.000000	0.000000
tswM5	27	0.349680	0.258220	0.008690	0.006860	0.002940	0.006860	0.005120	0.023210	0.185890	0.140460	0.000000	0.001620	0.000380	0.000000	0.000000	0.000000	0.000080	0.000000
tswF5	28	0.211550	0.156220	0.005260	0.019740	0.008460	0.019740	0.014730	0.014040	0.112470	0.084980	0.000000	0.000980	0.020030	0.321750	0.000000	0.000000	0.000050	0.000000
tswM6	29	0.362680	0.267820	0.009010	0.003270	0.001400	0.003270	0.002440	0.001950	0.166510	0.168450	0.000000	0.001940	0.000070	0.000000	0.000000	0.000000	0.001180	0.000000
tswF6	30	0.219420	0.162030	0.005450	0.017570	0.007530	0.017570	0.013110	0.001180	0.100740	0.101910	0.000000	0.001180	0.019840	0.321750	0.000000	0.000000	0.000710	0.000000
tswM7	31	0.363220	0.268220	0.009020	0.003280	0.001400	0.003280	0.002440	0.001950	0.166760	0.168700	0.000000	0.000490	0.000070	0.000000	0.000000	0.000000	0.001180	0.000000
tswF7	32	0.219750	0.162270	0.005460	0.017580	0.007530	0.017580	0.013110	0.001180	0.100890	0.102060	0.000000	0.000290	0.019840	0.321750	0.000000	0.000000	0.000710	0.000000
tswM8	33	0.110300	0.081450	0.002740	0.042790	0.018340	0.042790	0.031920	0.000000	0.099810	0.007900	0.495220	0.000000	0.000390	0.000000	0.000000	0.000000	0.056360	0.000000
tswF8	34	0.110300	0.081450	0.002740	0.042790	0.018340	0.042790	0.031920	0.000000	0.099810	0.007900	0.495220	0.000000	0.000390	0.000000	0.000000	0.000000	0.056360	0.000000
tswMv	35	0.061050	0.045080	0.001520	0.027390	0.011740	0.027390	0.020440	0.000000	0.062160	0.014810	0.694270	0.000000	0.000050	0.000000	0.000000	0.000000	0.024110	0.000000
tswFv	36	0.061050	0.045080	0.001520	0.027390	0.011740	0.027390	0.020440	0.000000	0.062160	0.014810	0.694270	0.000000	0.000050	0.000000	0.000000	0.000000	0.024110	0.000000
tswMz	37	0.078290	0.057810	0.001950	0.007470	0.003200	0.007470	0.005570	0.005860	0.069200	0.038310	0.505920	0.000000	0.000240	0.000000	0.000000	0.000000	0.208820	0.000000
tswFz	38	0.078290	0.057810	0.001950	0.007470	0.003200	0.007470	0.005570	0.005860	0.069200	0.038310	0.505920	0.000000	0.000240	0.000000	0.000000	0.000000	0.208820	0.000000
ch1Mv	39	0.098360	0.072630	0.002440	0.006910	0.002960	0.006910	0.005150	0.000790	0.057040	0.048240	0.609210	0.000000	0.000000	0.000000	0.000000	0.000000	0.079460	0.000000
ch1Fv	40	0.098360	0.072630	0.002440	0.006910	0.002960	0.006910	0.005150	0.000790	0.057040	0.048240	0.609210	0.000000	0.000000	0.000000	0.000000	0.000000	0.079460	0.000000
ch1Mz	41	0.078290	0.057810	0.001950	0.007470	0.003200	0.007470	0.005570	0.005860	0.069200	0.038310	0.505920	0.000000	0.000240	0.000000	0.000000	0.000000	0.208820	0.000000
ch1Fz	42	0.078290	0.057810	0.001950	0.007470	0.003200	0.007470	0.005570	0.005860	0.069200	0.038310	0.505920	0.000000	0.000240	0.000000	0.000000	0.000000	0.208820	0.000000
ch2Mv	43	0.098360	0.072630	0.002440	0.006910	0.002960	0.006910	0.005150	0.000790	0.057040	0.048240	0.609210	0.000000	0.000000	0.000000	0.000000	0.000000	0.079460	0.000000
ch2Fv	44	0.098360	0.072630	0.002440	0.006910	0.002960	0.006910	0.005150	0.000790	0.057040	0.048240	0.609210	0.000000	0.000000	0.000000	0.000000	0.000000	0.079460	0.000000
ch2Mz	45	0.078290	0.057810	0.001950	0.007470	0.003200	0.007470	0.005570	0.005860	0.069200	0.038310	0.505920	0.000000	0.000240	0.000000	0.000000	0.000000	0.208820	0.000000
ch2Fz	46	0.078290	0.057810	0.001950	0.007470	0.003200	0.007470	0.005570	0.005860	0.069200	0.038310	0.505920	0.000000	0.000240	0.000000	0.000000	0.000000	0.208820	0.000000

Table I-1. Initial Mineral Volume Fraction (Continued)

Rock	Zone	sio2(amor)	opal_proxy	fluorite	sepiolite	nano3	kno3	halite	sylvite	mgso4	k2so4	na2so4	gypsum
tcwM1	1	0.000000	0.009900	0.000000	0.000000	0.000000	0.000000	0.000000	0.000000	0.000000	0.000000	0.000000	0.000000
tcwF1	2	0.000000	0.009900	0.000000	0.000000	0.000000	0.000000	0.000000	0.000000	0.000000	0.000000	0.000000	0.000000
tcwM2	3	0.000000	0.009900	0.000000	0.000000	0.000000	0.000000	0.000000	0.000000	0.000000	0.000000	0.000000	0.000000
tcwF2	4	0.000000	0.009900	0.000000	0.000000	0.000000	0.000000	0.000000	0.000000	0.000000	0.000000	0.000000	0.000000
tcwM3	5	0.000000	0.009900	0.000000	0.000000	0.000000	0.000000	0.000000	0.000000	0.000000	0.000000	0.000000	0.000000
tcwF3	6	0.000000	0.009900	0.000000	0.000000	0.000000	0.000000	0.000000	0.000000	0.000000	0.000000	0.000000	0.000000
ptnM1	7	0.000000	0.009900	0.000000	0.000000	0.000000	0.000000	0.000000	0.000000	0.000000	0.000000	0.000000	0.000000
ptnF1	8	0.000000	0.009900	0.000000	0.000000	0.000000	0.000000	0.000000	0.000000	0.000000	0.000000	0.000000	0.000000
ptnM2	9	0.000000	0.009900	0.000000	0.000000	0.000000	0.000000	0.000000	0.000000	0.000000	0.000000	0.000000	0.000000
ptnF2	10	0.000000	0.009900	0.000000	0.000000	0.000000	0.000000	0.000000	0.000000	0.000000	0.000000	0.000000	0.000000
ptnM3	11	0.000000	0.009900	0.000000	0.000000	0.000000	0.000000	0.000000	0.000000	0.000000	0.000000	0.000000	0.000000
ptnF3	12	0.000000	0.009900	0.000000	0.000000	0.000000	0.000000	0.000000	0.000000	0.000000	0.000000	0.000000	0.000000
ptnM4	13	0.000000	0.009900	0.000000	0.000000	0.000000	0.000000	0.000000	0.000000	0.000000	0.000000	0.000000	0.000000
ptnF4	14	0.000000	0.009900	0.000000	0.000000	0.000000	0.000000	0.000000	0.000000	0.000000	0.000000	0.000000	0.000000
ptnM5	15	0.000000	0.009900	0.000000	0.000000	0.000000	0.000000	0.000000	0.000000	0.000000	0.000000	0.000000	0.000000
ptnF5	16	0.000000	0.009900	0.000000	0.000000	0.000000	0.000000	0.000000	0.000000	0.000000	0.000000	0.000000	0.000000
ptnM6	17	0.000000	0.009900	0.000000	0.000000	0.000000	0.000000	0.000000	0.000000	0.000000	0.000000	0.000000	0.000000
ptnF6	18	0.000000	0.009900	0.000000	0.000000	0.000000	0.000000	0.000000	0.000000	0.000000	0.000000	0.000000	0.000000
tswM1	19	0.000000	0.009900	0.000100	0.000000	0.000000	0.000000	0.000000	0.000000	0.000000	0.000000	0.000000	0.000000
tswF1	20	0.000000	0.009900	0.000100	0.000000	0.000000	0.000000	0.000000	0.000000	0.000000	0.000000	0.000000	0.000000
tswM2	21	0.000000	0.009900	0.000100	0.000000	0.000000	0.000000	0.000000	0.000000	0.000000	0.000000	0.000000	0.000000
tswF2	22	0.000000	0.009900	0.000100	0.000000	0.000000	0.000000	0.000000	0.000000	0.000000	0.000000	0.000000	0.000000
tswM3	23	0.000000	0.009900	0.000100	0.000000	0.000000	0.000000	0.000000	0.000000	0.000000	0.000000	0.000000	0.000000
tswF3	24	0.000000	0.009900	0.000100	0.000000	0.000000	0.000000	0.000000	0.000000	0.000000	0.000000	0.000000	0.000000
tswM4	25	0.000000	0.009900	0.000100	0.000000	0.000000	0.000000	0.000000	0.000000	0.000000	0.000000	0.000000	0.000000
tswF4	26	0.000000	0.009900	0.000100	0.000000	0.000000	0.000000	0.000000	0.000000	0.000000	0.000000	0.000000	0.000000
tswM5	27	0.000000	0.009900	0.000100	0.000000	0.000000	0.000000	0.000000	0.000000	0.000000	0.000000	0.000000	0.000000
tswF5	28	0.000000	0.009900	0.000100	0.000000	0.000000	0.000000	0.000000	0.000000	0.000000	0.000000	0.000000	0.000000
tswM6	29	0.000000	0.009900	0.000100	0.000000	0.000000	0.000000	0.000000	0.000000	0.000000	0.000000	0.000000	0.000000
tswF6	30	0.000000	0.009900	0.000100	0.000000	0.000000	0.000000	0.000000	0.000000	0.000000	0.000000	0.000000	0.000000
tswM7	31	0.000000	0.009900	0.000100	0.000000	0.000000	0.000000	0.000000	0.000000	0.000000	0.000000	0.000000	0.000000
tswF7	32	0.000000	0.009900	0.000100	0.000000	0.000000	0.000000	0.000000	0.000000	0.000000	0.000000	0.000000	0.000000
tswM8	33	0.000000	0.009900	0.000100	0.000000	0.000000	0.000000	0.000000	0.000000	0.000000	0.000000	0.000000	0.000000
tswF8	34	0.000000	0.009900	0.000100	0.000000	0.000000	0.000000	0.000000	0.000000	0.000000	0.000000	0.000000	0.000000
tswMv	35	0.000000	0.009900	0.000100	0.000000	0.000000	0.000000	0.000000	0.000000	0.000000	0.000000	0.000000	0.000000
tswFv	36	0.000000	0.009900	0.000100	0.000000	0.000000	0.000000	0.000000	0.000000	0.000000	0.000000	0.000000	0.000000
tswMz	37	0.000000	0.009900	0.000000	0.000000	0.000000	0.000000	0.000000	0.000000	0.000000	0.000000	0.000000	0.000000
tswFz	38	0.000000	0.009900	0.000000	0.000000	0.000000	0.000000	0.000000	0.000000	0.000000	0.000000	0.000000	0.000000
ch1Mv	39	0.000000	0.009900	0.000000	0.000000	0.000000	0.000000	0.000000	0.000000	0.000000	0.000000	0.000000	0.000000
ch1Fv	40	0.000000	0.009900	0.000000	0.000000	0.000000	0.000000	0.000000	0.000000	0.000000	0.000000	0.000000	0.000000
ch1Mz	41	0.000000	0.009900	0.000000	0.000000	0.000000	0.000000	0.000000	0.000000	0.000000	0.000000	0.000000	0.000000
ch1Fz	42	0.000000	0.009900	0.000000	0.000000	0.000000	0.000000	0.000000	0.000000	0.000000	0.000000	0.000000	0.000000
ch2Mv	43	0.000000	0.009900	0.000000	0.000000	0.000000	0.000000	0.000000	0.000000	0.000000	0.000000	0.000000	0.000000
ch2Fv	44	0.000000	0.009900	0.000000	0.000000	0.000000	0.000000	0.000000	0.000000	0.000000	0.000000	0.000000	0.000000
ch2Mz	45	0.000000	0.009900	0.000000	0.000000	0.000000	0.000000	0.000000	0.000000	0.000000	0.000000	0.000000	0.000000
ch2Fz	46	0.000000	0.009900	0.000000	0.000000	0.000000	0.000000	0.000000	0.000000	0.000000	0.000000	0.000000	0.000000

Table I-1. Initial Mineral Volume Fraction (Continued)

Rock	Zone	microcline-b	albite-low	anorthite	smect-ca-cal	smect-na-cal	smect-mg-cal	illite	tridymite	cristoba-a	quartz	hydglassfe3	hematite	calcite	stell/10-r02	heul/10-r02	mord/10-r02	clpt/10-r02	kaolinite
ch3Mv	47	0.047080	0.034770	0.001170	0.002160	0.000930	0.002160	0.001610	0.000010	0.046630	0.027470	0.737750	0.000000	0.000000	0.000000	0.000000	0.000000	0.088370	0.000000
ch3Fv	48	0.047080	0.034770	0.001170	0.002160	0.000930	0.002160	0.001610	0.000010	0.046630	0.027470	0.737750	0.000000	0.000000	0.000000	0.000000	0.000000	0.088370	0.000000
ch3Mz	49	0.078290	0.057810	0.001950	0.007470	0.003200	0.007470	0.005570	0.005860	0.069200	0.038310	0.505920	0.000000	0.000240	0.000000	0.000000	0.000000	0.208820	0.000000
ch3Fz	50	0.078290	0.057810	0.001950	0.007470	0.003200	0.007470	0.005570	0.005860	0.069200	0.038310	0.505920	0.000000	0.000240	0.000000	0.000000	0.000000	0.208820	0.000000
ch4Mv	51	0.047080	0.034770	0.001170	0.002160	0.000930	0.002160	0.001610	0.000010	0.046630	0.027470	0.737750	0.000000	0.000000	0.000000	0.000000	0.000000	0.088370	0.000000
ch4Fv	52	0.047080	0.034770	0.001170	0.002160	0.000930	0.002160	0.001610	0.000010	0.046630	0.027470	0.737750	0.000000	0.000000	0.000000	0.000000	0.000000	0.088370	0.000000
ch4Mz	53	0.048200	0.035590	0.001200	0.000580	0.000250	0.000580	0.000430	0.000000	0.037260	0.028780	0.733100	0.000000	0.000030	0.000000	0.000000	0.000000	0.104090	0.000000
ch4Fz	54	0.048200	0.035590	0.001200	0.000580	0.000250	0.000580	0.000430	0.000000	0.037260	0.028780	0.733100	0.000000	0.000030	0.000000	0.000000	0.000000	0.104090	0.000000
ch5Mv	55	0.045510	0.033610	0.001130	0.000460	0.000200	0.000460	0.000350	0.000000	0.021710	0.027070	0.775560	0.000000	0.000040	0.000000	0.000000	0.000000	0.084000	0.000000
ch5Fv	56	0.045510	0.033610	0.001130	0.000460	0.000200	0.000460	0.000350	0.000000	0.021710	0.027070	0.775560	0.000000	0.000040	0.000000	0.000000	0.000000	0.084000	0.000000
ch5Mz	57	0.099310	0.073340	0.002470	0.006200	0.002660	0.006200	0.004630	0.000000	0.058610	0.097350	0.329530	0.000000	0.001500	0.000000	0.000000	0.000000	0.308290	0.000000
ch5Fz	58	0.099310	0.073340	0.002470	0.006200	0.002660	0.006200	0.004630	0.000000	0.058610	0.097350	0.329530	0.000000	0.001500	0.000000	0.000000	0.000000	0.308290	0.000000
ch6Mv	59	0.045510	0.033610	0.001130	0.000460	0.000200	0.000460	0.000350	0.000000	0.021710	0.027070	0.775560	0.000000	0.000040	0.000000	0.000000	0.000000	0.084000	0.000000
ch6Fv	60	0.045510	0.033610	0.001130	0.000460	0.000200	0.000460	0.000350	0.000000	0.021710	0.027070	0.775560	0.000000	0.000040	0.000000	0.000000	0.000000	0.084000	0.000000
ch6Mz	61	0.099310	0.073340	0.002470	0.006200	0.002660	0.006200	0.004630	0.000000	0.058610	0.097350	0.329530	0.000000	0.001500	0.000000	0.000000	0.000000	0.308290	0.000000
ch6Fz	62	0.099310	0.073340	0.002470	0.006200	0.002660	0.006200	0.004630	0.000000	0.058610	0.097350	0.329530	0.000000	0.001500	0.000000	0.000000	0.000000	0.308290	0.000000
pp4Mz	63	0.082830	0.061160	0.002060	0.008290	0.003550	0.008290	0.006190	0.000030	0.066910	0.015120	0.491750	0.000000	0.001630	0.000000	0.000000	0.000000	0.242290	0.000000
pp4Fz	64	0.082830	0.061160	0.002060	0.008290	0.003550	0.008290	0.006190	0.000030	0.066910	0.015120	0.491750	0.000000	0.001630	0.000000	0.000000	0.000000	0.242290	0.000000
pp3Md	65	0.368430	0.272070	0.009150	0.003320	0.001420	0.003320	0.002480	0.005900	0.070750	0.248290	0.000030	0.004740	0.000000	0.000000	0.000000	0.000000	0.000170	0.000000
pp3Fd	66	0.368430	0.272070	0.009150	0.003320	0.001420	0.003320	0.002480	0.005900	0.070750	0.248290	0.000030	0.004740	0.000000	0.000000	0.000000	0.000000	0.000170	0.000000
pp2Md	67	0.368430	0.272070	0.009150	0.003320	0.001420	0.003320	0.002480	0.005900	0.070750	0.248290	0.000030	0.004740	0.000000	0.000000	0.000000	0.000000	0.000170	0.000000
pp2Fd	68	0.368430	0.272070	0.009150	0.003320	0.001420	0.003320	0.002480	0.005900	0.070750	0.248290	0.000030	0.004740	0.000000	0.000000	0.000000	0.000000	0.000170	0.000000
pp1Mz	69	0.094980	0.070140	0.002360	0.006390	0.002740	0.006390	0.004770	0.000010	0.120050	0.026060	0.000540	0.004180	0.000000	0.000000	0.000000	0.000000	0.651500	0.000000
pp1Fz	70	0.094980	0.070140	0.002360	0.006390	0.002740	0.006390	0.004770	0.000010	0.120050	0.026060	0.000540	0.004180	0.000000	0.000000	0.000000	0.000000	0.651500	0.000000
bF3Md	71	0.345350	0.255020	0.008580	0.001720	0.000740	0.001720	0.001280	0.008470	0.112270	0.249720	0.000000	0.004980	0.000240	0.000000	0.000000	0.000000	0.000000	0.000000
bF3Fd	72	0.345350	0.255020	0.008580	0.001720	0.000740	0.001720	0.001280	0.008470	0.112270	0.249720	0.000000	0.004980	0.000240	0.000000	0.000000	0.000000	0.000000	0.000000
bF2Mz	73	0.187310	0.138320	0.004650	0.011680	0.005010	0.011680	0.008710	0.000000	0.010240	0.188170	0.000000	0.004610	0.000910	0.000000	0.000000	0.000000	0.418790	0.000000
bF2Fz	74	0.187310	0.138320	0.004650	0.011680	0.005010	0.011680	0.008710	0.000000	0.010240	0.188170	0.000000	0.004610	0.000910	0.000000	0.000000	0.000000	0.418790	0.000000

Table I-1. Initial Mineral Volume Fraction (Continued)

Rock	Zone	sio2(amor)	opal_proxy	fluorite	sepiolite	nano3	kno3	halite	sylvite	mgso4	k2so4	na2so4	gypsum
ch3Mv	47	0.000000	0.009900	0.000000	0.000000	0.000000	0.000000	0.000000	0.000000	0.000000	0.000000	0.000000	0.000000
ch3Fv	48	0.000000	0.009900	0.000000	0.000000	0.000000	0.000000	0.000000	0.000000	0.000000	0.000000	0.000000	0.000000
ch3Mz	49	0.000000	0.009900	0.000000	0.000000	0.000000	0.000000	0.000000	0.000000	0.000000	0.000000	0.000000	0.000000
ch3Fz	50	0.000000	0.009900	0.000000	0.000000	0.000000	0.000000	0.000000	0.000000	0.000000	0.000000	0.000000	0.000000
ch4Mv	51	0.000000	0.009900	0.000000	0.000000	0.000000	0.000000	0.000000	0.000000	0.000000	0.000000	0.000000	0.000000
ch4Fv	52	0.000000	0.009900	0.000000	0.000000	0.000000	0.000000	0.000000	0.000000	0.000000	0.000000	0.000000	0.000000
ch4Mz	53	0.000000	0.009900	0.000000	0.000000	0.000000	0.000000	0.000000	0.000000	0.000000	0.000000	0.000000	0.000000
ch4Fz	54	0.000000	0.009900	0.000000	0.000000	0.000000	0.000000	0.000000	0.000000	0.000000	0.000000	0.000000	0.000000
ch5Mv	55	0.000000	0.009900	0.000000	0.000000	0.000000	0.000000	0.000000	0.000000	0.000000	0.000000	0.000000	0.000000
ch5Fv	56	0.000000	0.009900	0.000000	0.000000	0.000000	0.000000	0.000000	0.000000	0.000000	0.000000	0.000000	0.000000
ch5Mz	57	0.000000	0.009900	0.000000	0.000000	0.000000	0.000000	0.000000	0.000000	0.000000	0.000000	0.000000	0.000000
ch5Fz	58	0.000000	0.009900	0.000000	0.000000	0.000000	0.000000	0.000000	0.000000	0.000000	0.000000	0.000000	0.000000
ch6Mv	59	0.000000	0.009900	0.000000	0.000000	0.000000	0.000000	0.000000	0.000000	0.000000	0.000000	0.000000	0.000000
ch6Fv	60	0.000000	0.009900	0.000000	0.000000	0.000000	0.000000	0.000000	0.000000	0.000000	0.000000	0.000000	0.000000
ch6Mz	61	0.000000	0.009900	0.000000	0.000000	0.000000	0.000000	0.000000	0.000000	0.000000	0.000000	0.000000	0.000000
ch6Fz	62	0.000000	0.009900	0.000000	0.000000	0.000000	0.000000	0.000000	0.000000	0.000000	0.000000	0.000000	0.000000
pp4Mz	63	0.000000	0.009900	0.000000	0.000000	0.000000	0.000000	0.000000	0.000000	0.000000	0.000000	0.000000	0.000000
pp4Fz	64	0.000000	0.009900	0.000000	0.000000	0.000000	0.000000	0.000000	0.000000	0.000000	0.000000	0.000000	0.000000
pp3Md	65	0.000000	0.009900	0.000000	0.000000	0.000000	0.000000	0.000000	0.000000	0.000000	0.000000	0.000000	0.000000
pp3Fd	66	0.000000	0.009900	0.000000	0.000000	0.000000	0.000000	0.000000	0.000000	0.000000	0.000000	0.000000	0.000000
pp2Md	67	0.000000	0.009900	0.000000	0.000000	0.000000	0.000000	0.000000	0.000000	0.000000	0.000000	0.000000	0.000000
pp2Fd	68	0.000000	0.009900	0.000000	0.000000	0.000000	0.000000	0.000000	0.000000	0.000000	0.000000	0.000000	0.000000
pp1Mz	69	0.000000	0.009900	0.000000	0.000000	0.000000	0.000000	0.000000	0.000000	0.000000	0.000000	0.000000	0.000000
pp1Fz	70	0.000000	0.009900	0.000000	0.000000	0.000000	0.000000	0.000000	0.000000	0.000000	0.000000	0.000000	0.000000
bF3Md	71	0.000000	0.009900	0.000000	0.000000	0.000000	0.000000	0.000000	0.000000	0.000000	0.000000	0.000000	0.000000
bF3Fd	72	0.000000	0.009900	0.000000	0.000000	0.000000	0.000000	0.000000	0.000000	0.000000	0.000000	0.000000	0.000000
bF2Mz	73	0.000000	0.009900	0.000000	0.000000	0.000000	0.000000	0.000000	0.000000	0.000000	0.000000	0.000000	0.000000
bF2Fz	74	0.000000	0.009900	0.000000	0.000000	0.000000	0.000000	0.000000	0.000000	0.000000	0.000000	0.000000	0.000000

Output DTN: LB0310MTSCLTHC.001.

APPENDIX II

INITIAL MINERAL REACTIVE SURFACE AREAS (cm^2/g FOR MATRIX, m^2/m^3 FOR FRACTURES)

The source of the initial mineral reactive surface area data in Table II-1 is DTN: LB0310MTSCLTHC.001. After downloading the specified DTN, go to the folder "THC_with_86percent_ventilation_simulations/THC_86present_5." Then locate the file "chemical.inp." Inside file "chemical.inp" search and find the keywords "INITIAL MINERAL ZONES." The entries directly below those keywords contain the data in Table II-1.

The first entry declares the total number of rock blocks (76 in this instance). The second entry (=1) describes the initial mineral volume fractions for the first rock block (which is "tcwM1" in this instance). A set of entries is to be found for each rock block. The lines immediately after this (until the next rock block is reached) describe the initial mineral volume fractions and the initial mineral reactive surface areas.

The following example illustrates how the data can be examined. Take the rock block "tcwM1" (this exercise can be repeated for any other rock block).

1. The first entry simply identifies the mineral names ("mineral"), their initial volume fractions ("vol.frac"), and the rock type ("tcwM1").

2. Next check the integer on the next line (the third entry). If it is zero, the mineral is an equilibrium mineral and no reactive surface area is needed. The minerals are so organized that the reactive minerals (with flag=0) appear first.

3. Whenever the flag is 1, the mineral is a kinetic one. For these minerals, an additional line is provided with the reactive surface areas (the second entry on this line).

4. For example, for the rock block "tcwM1," the first mineral identified is hematite. For this mineral, the flag is "0" indicating that it is an equilibrium mineral. Thus, only the initial mineral volume fraction (=0.00000) is provided and no data are provided for initial mineral reactive surface area.

5. The next minerals are calcite and gypsum. Both are identified as equilibrium minerals (flag=0) and hence only the initial volume fractions (=0.00358 and 0.00000, respectively) are provided and no data for reactive surface areas for these minerals are given.

6. The next mineral (after gypsum) is microcline-b, which is identified as a kinetic mineral (flag=1). The first line for this mineral gives the initial mineral volume fraction (=0.36911, second entry). Since the flag is 1, this mineral has an additional line of data. *The second entry on this additional line is the initial mineral reactive surface area*. Thus, for the rock block "tcwM1,", the initial mineral reactive surface area is 1398.9 cm^2/gm for microcline-b.

7. Similarly, the initial mineral reactive surface area for albite-low in "tcwM1" is 1398.9.

8. This exercise can be repeated for all the minerals and all the rock blocks. These are then reported as the initial mineral reactive surface areas in Table II-1.

The initial mineral volume fractions are calculated based on methods described in Wang (2003 [DIRS 161665], pp. 35-70). Note that the initial mineral reactive surface areas are given in cm^2/g for matrix and in m^2/m^3 for fractures. Note also that 76 rock blocks are identified in file 'chemical.inp' under "INITIAL MINERAL ZONES," whereas only 74 rock blocks are identified in Table II-1. This is because the "chemical.inp" file has to identify the top and bottom boundaries as two distinct rock blocks (for numerical modeling purposes). For these two boundary rock blocks, all initial mineral reactive surface areas are specified as zero (check file "chemical.inp) and these are not mentioned in Table II-1, as the boundaries are not real rock blocks.

Calculation of the Reactive Surface Areas for Rock Matrix Minerals:

The reactive surface areas for the matrix units are derived using a truncated sphere model. A detailed description of this model is given on page 37 of the scientific notebook YMP-LBNL-YWT-ELS-1 (Wang 2003 [DIRS 161665]). The calculation of reactive surface area for a particular matrix unit, say tcwM1, using the model, is as follows:

1. For matrix unit tcwM1, the matrix porosity is 0.2410 (DTN: LB0208UZDSCMI.002 [DIRS 161243]).

2. Begin with $L_f = 0.0005$ mm, and $L_x = L_z = 0.0005$ mm. Then set the grain volume using

$$V_g = -\frac{8\pi}{3}L_f^3 + \pi L_z\left[L_f^2 - \frac{L_z^2}{12}\right] + 2\pi L_x\left[L_f^2 - \frac{L_x}{12}\right]$$

3. Next, the porosity is set as

$$\phi = 1 - \frac{V_g}{L_x^2 L_z}$$

4. An iterative solution is then initiated by changing L_x and L_z (always keeping these two variables identical) till the calculated porosity matches the measured porosity. At the end of the iteration, the dimensions of the grain are given by L_x and L_z. For the tcwM1 unit with porosity 0.2410, $L_x = L_z = 0.00086$ mm (with $L_f = 0.0005$ mm).

5. The open surface area is then calculated from

$$A_s = \frac{4\pi L_f\left[\frac{L_z}{2} + L_x - 2L_f\right] * (0.1)^2}{(0.001) * (2.65) * V_g}$$

The multiplication factor in the numerator (0.1) is needed to convert mm to cm. The multiplication factor in the denominator (0.001) is needed to convert mm^3 to cm^3. The factor 2.65 is the grain density in gm/cm^3. Thus, the surface area is obtained in cm^2/gm. For tcwM1, the open surface area thus calculated is 1.4170×10^4 cm^2/gm.

6. The next step is to modify this open surface area to account for mineral alteration, see page 38 (step b) of YMP-LBNL-YWT-ELS-1 (Wang 2003 [DIRS 161665]) for justification. The mineral alteration factor for tcwM1 is 0.0128 (sum of initial mineral volume fractions of Ca-smectite, Na-smectite, K-smectite, Mg-smectite, illite, hematite, calcite, stellerite, heulandite, mordenite, and clinoptilolite).

7. For the primary framework minerals: feldspar (K-feldspar, albite, and anorthite), tridymite, alpha-cristobalite, quartz, and glass, the reactive surface area is

$$A_R = A_s(1 - a_{alt}),$$

where a_{alt} is the mineral alteration factor. Thus, the reactive surface area for these minerals in tcwM1 unit is 13989 cm^2/gm.

8. For the minerals hematite, calcite, stellerite, heulandite, mordenite, and clinoptilolite, the reactive surface area is equal to the unaltered surface area. Thus, for these minerals in tcwM1, the reactive surface area is 14170 cm^2/gm.

9. For the minerals in the smectite group, the reactive surface area is calculated using the square plates model for clay particles, see page 38 of YMP-LBNL-YWT-ELS-1 (Wang 2003 [DIRS 161665]) for justification of this choice. First calculate an area ratio (the ratio of A_s and the surface area in cm^2/gm of a sphere with L_f as the radius). For tcwM1, this ratio is

$$A_{ratio} = \frac{A_s}{\dfrac{4\pi L_f^2 (0.01)}{\dfrac{4}{3}\pi L_f^3 (0.001)(2.65)}} = 6.2585 \times 10^{-1}$$

10. For these minerals, the grain volume (in cm^3) is (L_x = 0.005 mm, L_z = 0.001 mm)

$$V_g = L_x^2 L_z (0.001) = 2.5 \times 10^{-11}$$

11. The surface area (in cm^2) of these clay particles is then calculated as

$$A = (2L_z^2 + 4L_x L_z)(0.01) = 2.2 \times 10^{-7}$$

12. The surface area is then recalculated in cm^2/gm following

$$A_s = \frac{A}{V_g \rho_g} = \frac{2.2 \times 10^{-7}}{(2.5 \times 10^{-11})(2.5)} = 3.52 \times 10^3$$

13. The available reactive surface area (in cm^2/gm) for the smectic materials is then calculated as

$$A_S = A_{ratio}\, A_s - \frac{1}{6} A_{ratio}\, A_s = 1836$$

NOTE: An error was made in calculating the open surface area (step 11 above) of smectite clay particles. As a result, the reactive surface areas for smectite mineral endmembers were reported incorrectly in Table II-1. However, since the values appeared unreasonably high because of this error, the calculated reactive surface areas were reduced by a factor of 10 (see step below). Because of this adjustment, and the fact that smectite is a minor phase in the rocks, the impact on model input and results is minimal.

14. Per Page 39 (step d) of YMP-LBNL-YWT-ELS-1 (Wang 2003 [DIRS 161665]), the calculated reactive surface areas are reduced by a factor of 10. Thus, the following are the reactive surface area input to the models (as listed in Table II-1):

    Feldspar (K-feldspar, albite, and anorthite), tridymite, cristobalite, quartz, and glass: 13989/10 = 1398.9 cm^2/gm (step 7 above)

    Hematite, calcite, stellerite, heulandite, mordenite, and clinoptilolite: 14170/10 = 1417 cm^2/gm (step 8 above)

    smectite = 1668.9 cm^2/gm (step 13 above).

Calculation of the Reactive Surface Areas for the Fracture Minerals:

1. Get fracture porosity (ϕ) and fracture-matrix interface area (A_F) data for various UZ layers from DTN: LB0205REVUZPRP.001 [DIRS 159525].

2. See page 40 of YMP-LBNL-YWT-ELS-1 (Wang 2003 [DIRS 161665]) for procedures regarding calculation of reactive surface areas in the fractures. The reactive surface area for the fractures are calculated as

$$A_S = \frac{\pi}{2}\left(\frac{A_F}{\phi}\right)$$

3. The same reactive surface area is assigned for all minerals in a particular UZ model layer. For example, tcwF3, the porosity (ϕ) is 1.3×10^{-2} and the fracture-matrix interface area (A_F) is 3.77 m^2/m^3. Thus, the reactive surface area (m^2/m^3) of all minerals in tcwF1 is

$$A_S = \frac{\pi}{2}\left(\frac{3.77}{1.3\times10^{-2}}\right) = 455.5$$

4. **NOTE**: The fracture reactive surface area of tcwF3 was assigned to tcwF1 and tcwF2 (as reactive surface area of tcwF3 is about the average of reactive surface areas of tcwF1 and tcwF2). Note that fracture reactive surface area for K-feldspar in tcwF1 was inaccurately assigned a value of 1237.2 m^2/m3. However, these units are not

always present in the UZ model domain and temperatures within these units remain at near ambient conditions in THC simulations. Therefore, processes occurring within these units do not affect THC conditions in the mountain and do not affect the conclusions from this model report.

This calculation is then repeated for all other model layers.

INTENTIONALLY LEFT BLANK

Table II-1. Initial Mineral Reactive Surface Area

Rock	Zone	microcline-b	albite-low	anorthite	smect-ca-cal	smect-na-cal	smect-mg-cal	illite	tridymite	cristoba-a	quartz	hydglassfe3	hematite	calcite	stell/10-r02	heul/10-r02	mord/10-r02	clpt/10-r02	kaolinite
tcwM1	1	1398.9	1398.9	1398.9	1668.9	1668.9	1668.9	1668.9	1398.9	1398.9	1398.9	1398.9	1417.0	1417.0	1417.0	1417.0	1417.0	1417.0	1668.9
tcwF1	2	1237.2	455.5	455.5	455.5	455.5	455.5	455.5	455.5	455.5	455.5	455.5	455.5	455.5	455.5	455.5	455.5	455.5	455.5
tcwM2	3	801.5	801.5	801.5	956.2	956.2	956.2	956.2	801.5	801.5	801.5	801.5	811.8	811.8	811.8	811.8	811.8	811.8	956.2
tcwF2	4	455.5	455.5	455.5	455.5	455.5	455.5	455.5	455.5	455.5	455.5	455.5	455.5	455.5	455.5	455.5	455.5	455.5	455.5
tcwM3	5	1095.5	1095.5	1095.5	1502.9	1502.9	1502.9	1502.9	1095.5	1095.5	1095.5	1095.5	1276.0	1276.0	1276.0	1276.0	1276.0	1276.0	1502.9
tcwF3	6	455.5	455.5	455.5	455.5	455.5	455.5	455.5	455.5	455.5	455.5	455.5	455.5	455.5	455.5	455.5	455.5	455.5	455.5
ptnM1	7	174.2	174.2	174.2	2253.3	2253.3	2253.3	2253.3	174.2	174.2	174.2	174.2	191.3	191.3	191.3	191.3	191.3	191.3	2253.3
ptnF1	8	170.7	170.7	170.7	170.7	170.7	170.7	170.7	170.7	170.7	170.7	170.7	170.7	170.7	170.7	170.7	170.7	170.7	170.7
ptnM2	9	188.1	188.1	188.1	2433.5	2433.5	2433.5	2433.5	188.1	188.1	188.1	188.1	206.6	206.6	206.6	206.6	206.6	206.6	2433.5
ptnF2	10	221.5	221.5	221.5	221.5	221.5	221.5	221.5	221.5	221.5	221.5	221.5	221.5	221.5	221.5	221.5	221.5	221.5	221.5
ptnM3	11	126.6	126.6	126.6	1637.3	1637.3	1637.3	1637.3	126.6	126.6	126.6	126.6	139.0	139.0	139.0	139.0	139.0	139.0	1637.3
ptnF3	12	1309.0	1309.0	1309.0	1309.0	1309.0	1309.0	1309.0	1309.0	1309.0	1309.0	1309.0	1309.0	1309.0	1309.0	1309.0	1309.0	1309.0	1309.0
ptnM4	13	182.9	182.9	182.9	2366.3	2366.3	2366.3	2366.3	182.9	182.9	182.9	182.9	200.9	200.9	200.9	200.9	200.9	200.9	2366.3
ptnF4	14	53.4	53.4	53.4	53.4	53.4	53.4	53.4	53.4	53.4	53.4	53.4	53.4	53.4	53.4	53.4	53.4	53.4	53.4
ptnM5	15	205.6	205.6	205.6	2666.7	2666.7	2666.7	2666.7	205.6	205.6	205.6	205.6	226.4	226.4	226.4	226.4	226.4	226.4	2666.7
ptnF5	16	311.3	311.3	311.3	311.3	311.3	311.3	311.3	311.3	311.3	311.3	311.3	311.3	311.3	311.3	311.3	311.3	311.3	311.3
ptnM6	17	205.7	205.7	205.7	2666.7	2666.7	2666.7	2666.7	205.7	205.7	205.7	205.7	226.4	226.4	226.4	226.4	226.4	226.4	2666.7
ptnF6	18	1803.9	1803.9	1803.9	1803.9	1803.9	1803.9	1803.9	1803.9	1803.9	1803.9	1803.9	1803.9	1803.9	1803.9	1803.9	1803.9	1803.9	1803.9
tswM1	19	58.2	58.2	58.2	705.6	705.6	705.6	705.6	58.2	58.2	58.2	58.2	59.9	59.9	59.9	59.9	59.9	59.9	705.6
tswF1	20	1212.7	1212.7	1212.7	1212.7	1212.7	1212.7	1212.7	1212.7	1212.7	1212.7	1212.7	1212.7	1212.7	1212.7	1212.7	1212.7	1212.7	1212.7
tswM2	21	1100.0	1100.0	1100.0	1317.4	1317.4	1317.4	1317.4	1100.0	1100.0	1100.0	1100.0	1118.6	1118.6	1118.6	1118.6	1118.6	1118.6	1317.4
tswF2	22	607.5	607.5	607.5	607.5	607.5	607.5	607.5	607.5	607.5	607.5	607.5	607.5	607.5	607.5	607.5	607.5	607.5	607.5
tswM3	23	1080.1	1080.1	1080.1	1310.4	1310.4	1310.4	1310.4	1080.1	1080.1	1080.1	1080.1	1112.6	1112.6	1112.6	1112.6	1112.6	1112.6	1310.4
tswF3	24	1202.5	1202.5	1202.5	1202.5	1202.5	1202.5	1202.5	1202.5	1202.5	1202.5	1202.5	1202.5	1202.5	1202.5	1202.5	1202.5	1202.5	1202.5
tswM4	25	911.0	911.0	911.0	1091.6	1091.6	1091.6	1091.6	911.0	911.0	911.0	911.0	926.8	926.8	926.8	926.8	926.8	926.8	1091.6
tswF4	26	2502.2	2502.2	2502.2	2502.2	2502.2	2502.2	2502.2	2502.2	2502.2	2502.2	2502.2	2502.2	2502.2	2502.2	2502.2	2502.2	2502.2	2502.2
tswM5	27	990.5	990.5	990.5	1195.3	1195.3	1195.3	1195.3	990.5	990.5	990.5	990.5	1014.9	1014.9	1014.9	1014.9	1014.9	1014.9	1195.3
tswF5	28	1583.9	1583.9	1583.9	1583.9	1583.9	1583.9	1583.9	1583.9	1583.9	1583.9	1583.9	1583.9	1583.9	1583.9	1583.9	1583.9	1583.9	1583.9
tswM6	29	877.5	877.5	877.5	1047.9	1047.9	1047.9	1047.9	877.5	877.5	877.5	877.5	889.7	889.7	889.7	889.7	889.7	889.7	1047.9
tswF6	30	1487.4	1487.4	1487.4	1487.4	1487.4	1487.4	1487.4	1487.4	1487.4	1487.4	1487.4	1487.4	1487.4	1487.4	1487.4	1487.4	1487.4	1487.4
tswM7	31	878.8	878.8	878.8	1047.9	1047.9	1047.9	1047.9	878.8	878.8	878.8	878.8	889.7	889.7	889.7	889.7	889.7	889.7	1047.9
tswF7	32	1487.4	1487.4	1487.4	1487.4	1487.4	1487.4	1487.4	1487.4	1487.4	1487.4	1487.4	1487.4	1487.4	1487.4	1487.4	1487.4	1487.4	1487.4
tswM8	33	408.8	408.8	408.8	597.8	597.8	597.8	597.8	408.8	408.8	408.8	408.8	507.6	507.6	507.6	507.6	507.6	507.6	597.8
tswF8	34	1904.9	1904.9	1904.9	1904.9	1904.9	1904.9	1904.9	1904.9	1904.9	1904.9	1904.9	1904.9	1904.9	1904.9	1904.9	1904.9	1904.9	1904.9
tswMv	35	1223.2	1223.2	1223.2	1622.8	1622.8	1622.8	1622.8	1223.2	1223.2	1223.2	1223.2	1377.8	1377.8	1377.8	1377.8	1377.8	1377.8	1622.8
tswFv	36	1077.6	1077.6	1077.6	1077.6	1077.6	1077.6	1077.6	1077.6	1077.6	1077.6	1077.6	1077.6	1077.6	1077.6	1077.6	1077.6	1077.6	1077.6
tswMz	37	1171.3	1171.3	1171.3	1803.5	1803.5	1803.5	1803.5	1171.3	1171.3	1171.3	1171.3	1531.3	1531.3	1531.3	1531.3	1531.3	1531.3	1803.5
tswFz	38	1077.6	1077.6	1077.6	1077.6	1077.6	1077.6	1077.6	1077.6	1077.6	1077.6	1077.6	1077.6	1077.6	1077.6	1077.6	1077.6	1077.6	1077.6
ch1Mv	39	154.2	154.2	154.2	2023.4	2023.4	2023.4	2023.4	154.2	154.2	154.2	154.2	171.8	171.8	171.8	171.8	171.8	171.8	2023.4
ch1Fv	40	772.5	772.5	772.5	772.5	772.5	772.5	772.5	772.5	772.5	772.5	772.5	772.5	772.5	772.5	772.5	772.5	772.5	772.5
ch1Mz	41	1196.0	1196.0	1196.0	1841.5	1841.5	1841.5	1841.5	1196.0	1196.0	1196.0	1196.0	1563.6	1563.6	1563.6	1563.6	1563.6	1563.6	1841.5
ch1Fz	42	1079.9	1079.9	1079.9	1079.9	1079.9	1079.9	1079.9	1079.9	1079.9	1079.9	1079.9	1079.9	1079.9	1079.9	1079.9	1079.9	1079.9	1079.9
ch2Mv	43	158.8	158.8	158.8	2083.8	2083.8	2083.8	2083.8	158.8	158.8	158.8	158.8	176.9	176.9	176.9	176.9	176.9	176.9	2083.8
ch2Fv	44	877.2	877.2	877.2	877.2	877.2	877.2	877.2	877.2	877.2	877.2	877.2	877.2	877.2	877.2	877.2	877.2	877.2	877.2
ch2Mz	45	1290.7	1290.7	1290.7	1987.4	1987.4	1987.4	1987.4	1290.7	1290.7	1290.7	1290.7	1687.4	1687.4	1687.4	1687.4	1687.4	1687.4	1987.4
ch2Fz	46	1825.5	1825.5	1825.5	1825.5	1825.5	1825.5	1825.5	1825.5	1825.5	1825.5	1825.5	1825.5	1825.5	1825.5	1825.5	1825.5	1825.5	1825.5

Table II-1. Initial Mineral Reactive Surface Area (Continued)

Rock	Zone	sio2(amor)	opal_proxy	fluorite	sepiolite	nano3	kno3	halite	sylvite	mgso4	k2so4	na2so4	gypsum
tcwM1	1	1668.9	1417.0	1417.0	1668.9	1000.0	1000.0	1000.0	1000.0	1000.0	1000.0	1000.0	1000.0
tcwF1	2	455.5	455.5	455.5	455.5	455.5	455.5	455.5	455.5	455.5	455.5	455.5	455.5
tcwM2	3	956.2	811.8	811.8	956.2	1000.0	1000.0	1000.0	1000.0	1000.0	1000.0	1000.0	1000.0
tcwF2	4	455.5	455.5	455.5	455.5	455.5	455.5	455.5	455.5	455.5	455.5	455.5	455.5
tcwM3	5	1502.9	1276.0	1276.0	1502.9	1000.0	1000.0	1000.0	1000.0	1000.0	1000.0	1000.0	1000.0
tcwF3	6	455.5	455.5	455.5	455.5	455.5	455.5	455.5	455.5	455.5	455.5	455.5	455.5
ptnM1	7	2253.3	191.3	191.3	2253.3	1000.0	1000.0	1000.0	1000.0	1000.0	1000.0	1000.0	1000.0
ptnF1	8	170.7	170.7	170.7	170.7	170.7	170.7	170.7	170.7	170.7	170.7	170.7	170.7
ptnM2	9	2433.5	206.6	206.6	2433.5	1000.0	1000.0	1000.0	1000.0	1000.0	1000.0	1000.0	1000.0
ptnF2	10	221.5	221.5	221.5	221.5	221.5	221.5	221.5	221.5	221.5	221.5	221.5	221.5
ptnM3	11	1637.3	139.0	139.0	1637.3	1000.0	1000.0	1000.0	1000.0	1000.0	1000.0	1000.0	1000.0
ptnF3	12	1309.0	1309.0	1309.0	1309.0	1309.0	1309.0	1309.0	1309.0	1309.0	1309.0	1309.0	1309.0
ptnM4	13	2366.3	200.9	200.9	2366.3	1000.0	1000.0	1000.0	1000.0	1000.0	1000.0	1000.0	1000.0
ptnF4	14	53.4	53.4	53.4	53.4	53.4	53.4	53.4	53.4	53.4	53.4	53.4	53.4
ptnM5	15	2666.7	226.4	226.4	2666.7	1000.0	1000.0	1000.0	1000.0	1000.0	1000.0	1000.0	1000.0
ptnF5	16	311.3	311.3	311.3	311.3	311.3	311.3	311.3	311.3	311.3	311.3	311.3	311.3
ptnM6	17	2666.7	226.4	226.4	2666.7	1000.0	1000.0	1000.0	1000.0	1000.0	1000.0	1000.0	1000.0
ptnF6	18	1803.9	1803.9	1803.9	1803.9	1803.9	1803.9	1803.9	1803.9	1803.9	1803.9	1803.9	1803.9
tswM1	19	705.6	59.9	59.9	705.6	1000.0	1000.0	1000.0	1000.0	1000.0	1000.0	1000.0	1000.0
tswF1	20	1212.7	1212.7	1212.7	1212.7	1212.7	1212.7	1212.7	1212.7	1212.7	1212.7	1212.7	1212.7
tswM2	21	1317.4	1118.6	1118.6	1317.4	1000.0	1000.0	1000.0	1000.0	1000.0	1000.0	1000.0	1000.0
tswF2	22	607.5	607.5	607.5	607.5	607.5	607.5	607.5	607.5	607.5	607.5	607.5	607.5
tswM3	23	1310.4	1112.6	1112.6	1310.4	1000.0	1000.0	1000.0	1000.0	1000.0	1000.0	1000.0	1000.0
tswF3	24	1202.5	1202.5	1202.5	1202.5	1202.5	1202.5	1202.5	1202.5	1202.5	1202.5	1202.5	1202.5
tswM4	25	1091.6	926.8	926.8	1091.6	1000.0	1000.0	1000.0	1000.0	1000.0	1000.0	1000.0	1000.0
tswF4	26	2502.2	2502.2	2502.2	2502.2	2502.2	2502.2	2502.2	2502.2	2502.2	2502.2	2502.2	2502.2
tswM5	27	1195.3	1014.9	1014.9	1195.3	1000.0	1000.0	1000.0	1000.0	1000.0	1000.0	1000.0	1000.0
tswF5	28	1583.9	1583.9	1583.9	1583.9	1583.9	1583.9	1583.9	1583.9	1583.9	1583.9	1583.9	1583.9
tswM6	29	1047.9	889.7	889.7	1047.9	1000.0	1000.0	1000.0	1000.0	1000.0	1000.0	1000.0	1000.0
tswF6	30	1487.4	1487.4	1487.4	1487.4	1487.4	1487.4	1487.4	1487.4	1487.4	1487.4	1487.4	1487.4
tswM7	31	1047.9	889.7	889.7	1047.9	1000.0	1000.0	1000.0	1000.0	1000.0	1000.0	1000.0	1000.0
tswF7	32	1487.4	1487.4	1487.4	1487.4	1487.4	1487.4	1487.4	1487.4	1487.4	1487.4	1487.4	1487.4
tswM8	33	597.8	507.6	507.6	597.8	1000.0	1000.0	1000.0	1000.0	1000.0	1000.0	1000.0	1000.0
tswF8	34	1904.9	1904.9	1904.9	1904.9	1904.9	1904.9	1904.9	1904.9	1904.9	1904.9	1904.9	1904.9
tswMv	35	1622.8	1377.8	1377.8	1622.8	1000.0	1000.0	1000.0	1000.0	1000.0	1000.0	1000.0	1000.0
tswFv	36	1077.6	1077.6	1077.6	1077.6	1077.6	1077.6	1077.6	1077.6	1077.6	1077.6	1077.6	1077.6
tswMz	37	1803.5	1531.3	1531.3	1803.5	1000.0	1000.0	1000.0	1000.0	1000.0	1000.0	1000.0	1000.0
tswFz	38	1077.6	1077.6	1077.6	1077.6	1077.6	1077.6	1077.6	1077.6	1077.6	1077.6	1077.6	1077.6
ch1Mv	39	2023.4	171.8	171.8	2023.4	1000.0	1000.0	1000.0	1000.0	1000.0	1000.0	1000.0	1000.0
ch1Fv	40	772.5	772.5	772.5	772.5	772.5	772.5	772.5	772.5	772.5	772.5	772.5	772.5
ch1Mz	41	1841.5	1563.6	1563.6	1841.5	1000.0	1000.0	1000.0	1000.0	1000.0	1000.0	1000.0	1000.0
ch1Fz	42	1079.9	1079.9	1079.9	1079.9	1079.9	1079.9	1079.9	1079.9	1079.9	1079.9	1079.9	1079.9
ch2Mv	43	2083.8	176.9	176.9	2083.8	1000.0	1000.0	1000.0	1000.0	1000.0	1000.0	1000.0	1000.0
ch2Fv	44	877.2	877.2	877.2	877.2	877.2	877.2	877.2	877.2	877.2	877.2	877.2	877.2
ch2Mz	45	1987.4	1687.4	1687.4	1987.4	1000.0	1000.0	1000.0	1000.0	1000.0	1000.0	1000.0	1000.0
ch2Fz	46	1825.5	1825.5	1825.5	1825.5	1825.5	1825.5	1825.5	1825.5	1825.5	1825.5	1825.5	1825.5

Table II-1. Initial Mineral Reactive Surface Area (Continued)

Rock	Zone	microcline-b	albite-low	anorthite	smect-ca-cal	smect-na-cal	smect-mg-cal	illite	tridymite	cristoba-a	quartz	hydglassfe3	hematite	calcite	stell/10-r02	heul/10-r02	mord/10-r02	clpt/10-r02	kaolinite
ch3Mv	47	159.9	159.9	159.9	2083.8	2083.8	2083.8	2083.8	159.9	159.9	159.9	159.9	176.9	176.9	176.9	176.9	176.9	176.9	2083.8
ch3Fv	48	877.2	877.2	877.2	877.2	877.2	877.2	877.2	877.2	877.2	877.2	877.2	877.2	877.2	877.2	877.2	877.2	877.2	877.2
ch3Mz	49	1290.7	1290.7	1290.7	1987.4	1987.4	1987.4	1987.4	1290.7	1290.7	1290.7	1290.7	1687.4	1687.4	1687.4	1687.4	1687.4	1687.4	1987.4
ch3Fz	50	1825.5	1825.5	1825.5	1825.5	1825.5	1825.5	1825.5	1825.5	1825.5	1825.5	1825.5	1825.5	1825.5	1825.5	1825.5	1825.5	1825.5	1825.5
ch4Mv	51	159.9	159.9	159.9	2083.8	2083.8	2083.8	2083.8	159.9	159.9	159.9	159.9	176.9	176.9	176.9	176.9	176.9	176.9	2083.8
ch4Fv	52	877.2	877.2	877.2	877.2	877.2	877.2	877.2	877.2	877.2	877.2	877.2	877.2	877.2	877.2	877.2	877.2	877.2	877.2
ch4Mz	53	1506.8	1506.8	1506.8	1987.4	1987.4	1987.4	1987.4	1506.8	1506.8	1506.8	1506.8	1687.4	1687.4	1687.4	1687.4	1687.4	1687.4	1987.4
ch4Fz	54	1825.5	1825.5	1825.5	1825.5	1825.5	1825.5	1825.5	1825.5	1825.5	1825.5	1825.5	1825.5	1825.5	1825.5	1825.5	1825.5	1825.5	1825.5
ch5Mv	55	161.6	161.6	161.6	2083.8	2083.8	2083.8	2083.8	161.6	161.6	161.6	161.6	176.9	176.9	176.9	176.9	176.9	176.9	2083.8
ch5Fv	56	877.2	877.2	877.2	877.2	877.2	877.2	877.2	877.2	877.2	877.2	877.2	877.2	877.2	877.2	877.2	877.2	877.2	877.2
ch5Mz	57	1125.9	1125.9	1125.9	1987.4	1987.4	1987.4	1987.4	1125.9	1125.9	1125.9	1125.9	1687.4	1687.4	1687.4	1687.4	1687.4	1687.4	1987.4
ch5Fz	58	1825.5	1825.5	1825.5	1825.5	1825.5	1825.5	1825.5	1825.5	1825.5	1825.5	1825.5	1825.5	1825.5	1825.5	1825.5	1825.5	1825.5	1825.5
ch6Mv	59	157.0	157.0	157.0	2023.4	2023.4	2023.4	2023.4	157.0	157.0	157.0	157.0	171.8	171.8	171.8	171.8	171.8	171.8	2023.4
ch6Fv	60	877.2	877.2	877.2	877.2	877.2	877.2	877.2	877.2	877.2	877.2	877.2	877.2	877.2	877.2	877.2	877.2	877.2	877.2
ch6Mz	61	1012.4	1012.4	1012.4	1787.1	1787.1	1787.1	1787.1	1012.4	1012.4	1012.4	1012.4	1517.3	1517.3	1517.3	1517.3	1517.3	1517.3	1787.1
ch6Fz	62	1079.9	1079.9	1079.9	1079.9	1079.9	1079.9	1079.9	1079.9	1079.9	1079.9	1079.9	1079.9	1079.9	1079.9	1079.9	1079.9	1079.9	1079.9
pp4Mz	63	1224.4	1224.4	1224.4	1983.4	1983.4	1983.4	1983.4	1224.4	1224.4	1224.4	1224.4	1684.0	1684.0	1684.0	1684.0	1684.0	1684.0	1983.4
pp4Fz	64	1825.5	1825.5	1825.5	1825.5	1825.5	1825.5	1825.5	1825.5	1825.5	1825.5	1825.5	1825.5	1825.5	1825.5	1825.5	1825.5	1825.5	1825.5
pp3Md	65	1647.7	1647.7	1647.7	1971.4	1971.4	1971.4	1971.4	1647.7	1647.7	1647.7	1647.7	1673.9	1673.9	1673.9	1673.9	1673.9	1673.9	1971.4
pp3Fd	66	987.8	987.8	987.8	987.8	987.8	987.8	987.8	987.8	987.8	987.8	987.8	987.8	987.8	987.8	987.8	987.8	987.8	987.8
pp2Md	67	1328.6	1328.6	1328.6	1589.6	1589.6	1589.6	1589.6	1328.6	1328.6	1328.6	1328.6	1349.7	1349.7	1349.7	1349.7	1349.7	1349.7	1589.6
pp2Fd	68	987.8	987.8	987.8	987.8	987.8	987.8	987.8	987.8	987.8	987.8	987.8	987.8	987.8	987.8	987.8	987.8	987.8	987.8
pp1Mz	69	508.8	508.8	508.8	1888.9	1888.9	1888.9	1888.9	508.8	508.8	508.8	508.8	1603.8	1603.8	1603.8	1603.8	1603.8	1603.8	1888.9
pp1Fz	70	1825.5	1825.5	1825.5	1825.5	1825.5	1825.5	1825.5	1825.5	1825.5	1825.5	1825.5	1825.5	1825.5	1825.5	1825.5	1825.5	1825.5	1825.5
bF3Md	71	1173.7	1173.7	1173.7	1397.5	1397.5	1397.5	1397.5	1173.7	1173.7	1173.7	1173.7	1186.5	1186.5	1186.5	1186.5	1186.5	1186.5	1397.5
bF3Fd	72	987.8	987.8	987.8	987.8	987.8	987.8	987.8	987.8	987.8	987.8	987.8	987.8	987.8	987.8	987.8	987.8	987.8	987.8
bF2Mz	73	744.1	744.1	744.1	1641.2	1641.2	1641.2	1641.2	744.1	744.1	744.1	744.1	1393.5	1393.5	1393.5	1393.5	1393.5	1393.5	1641.2
bF2Fz	74	1825.5	1825.5	1825.5	1825.5	1825.5	1825.5	1825.5	1825.5	1825.5	1825.5	1825.5	1825.5	1825.5	1825.5	1825.5	1825.5	1825.5	1825.5

Table II-1. Initial Mineral Reactive Surface Area (Continued)

Rock	Zone	sio2(amor)	opal_proxy	fluorite	sepiolite	nano3	kno3	halite	sylvite	mgso4	k2so4	na2so4	gypsum
ch3Mv	47	2083.8	176.9	176.9	2083.8	1000.0	1000.0	1000.0	1000.0	1000.0	1000.0	1000.0	1000.0
ch3Fv	48	877.2	877.2	877.2	877.2	877.2	877.2	877.2	877.2	877.2	877.2	877.2	877.2
ch3Mz	49	1987.4	1687.4	1687.4	1987.4	1000.0	1000.0	1000.0	1000.0	1000.0	1000.0	1000.0	1000.0
ch3Fz	50	1825.5	1825.5	1825.5	1825.5	1825.5	1825.5	1825.5	1825.5	1825.5	1825.5	1825.5	1825.5
ch4Mv	51	2083.8	176.9	176.9	2083.8	1000.0	1000.0	1000.0	1000.0	1000.0	1000.0	1000.0	1000.0
ch4Fv	52	877.2	877.2	877.2	877.2	877.2	877.2	877.2	877.2	877.2	877.2	877.2	877.2
ch4Mz	53	1987.4	1687.4	1687.4	1987.4	1000.0	1000.0	1000.0	1000.0	1000.0	1000.0	1000.0	1000.0
ch4Fz	54	1825.5	1825.5	1825.5	1825.5	1825.5	1825.5	1825.5	1825.5	1825.5	1825.5	1825.5	1825.5
ch5Mv	55	2083.8	176.9	176.9	2083.8	1000.0	1000.0	1000.0	1000.0	1000.0	1000.0	1000.0	1000.0
ch5Fv	56	877.2	877.2	877.2	877.2	877.2	877.2	877.2	877.2	877.2	877.2	877.2	877.2
ch5Mz	57	1987.4	1687.4	1687.4	1987.4	1000.0	1000.0	1000.0	1000.0	1000.0	1000.0	1000.0	1000.0
ch5Fz	58	1825.5	1825.5	1825.5	1825.5	1825.5	1825.5	1825.5	1825.5	1825.5	1825.5	1825.5	1825.5
ch6Mv	59	2023.4	171.8	171.8	2023.4	1000.0	1000.0	1000.0	1000.0	1000.0	1000.0	1000.0	1000.0
ch6Fv	60	877.2	877.2	877.2	877.2	877.2	877.2	877.2	877.2	877.2	877.2	877.2	877.2
ch6Mz	61	1787.1	1517.3	1517.3	1787.1	1000.0	1000.0	1000.0	1000.0	1000.0	1000.0	1000.0	1000.0
ch6Fz	62	1079.9	1079.9	1079.9	1079.9	1079.9	1079.9	1079.9	1079.9	1079.9	1079.9	1079.9	1079.9
pp4Mz	63	1983.4	1684.0	1684.0	1983.4	1000.0	1000.0	1000.0	1000.0	1000.0	1000.0	1000.0	1000.0
pp4Fz	64	1825.5	1825.5	1825.5	1825.5	1825.5	1825.5	1825.5	1825.5	1825.5	1825.5	1825.5	1825.5
pp3Md	65	1971.4	1673.9	1673.9	1971.4	1000.0	1000.0	1000.0	1000.0	1000.0	1000.0	1000.0	1000.0
pp3Fd	66	987.8	987.8	987.8	987.8	987.8	987.8	987.8	987.8	987.8	987.8	987.8	987.8
pp2Md	67	1589.6	1349.7	1349.7	1589.6	1000.0	1000.0	1000.0	1000.0	1000.0	1000.0	1000.0	1000.0
pp2Fd	68	987.8	987.8	987.8	987.8	987.8	987.8	987.8	987.8	987.8	987.8	987.8	987.8
pp1Mz	69	1888.9	1603.8	1603.8	1888.9	1000.0	1000.0	1000.0	1000.0	1000.0	1000.0	1000.0	1000.0
pp1Fz	70	1825.5	1825.5	1825.5	1825.5	1825.5	1825.5	1825.5	1825.5	1825.5	1825.5	1825.5	1825.5
bF3Md	71	1397.5	1186.5	1186.5	1397.5	1000.0	1000.0	1000.0	1000.0	1000.0	1000.0	1000.0	1000.0
bF3Fd	72	987.8	987.8	987.8	987.8	987.8	987.8	987.8	987.8	987.8	987.8	987.8	987.8
bF2Mz	73	1641.2	1393.5	1393.5	1641.2	1000.0	1000.0	1000.0	1000.0	1000.0	1000.0	1000.0	1000.0
bF2Fz	74	1825.5	1825.5	1825.5	1825.5	1825.5	1825.5	1825.5	1825.5	1825.5	1825.5	1825.5	1825.5

Output DTN: LB0310MTSCLTHC.001.

APPENDIX III

PERMEABILITY MODEL PARAMETERS

The source of the permeability model parameters given in Table III-1 is DTN: LB0310MTSCLTHC.001. After downloading the specified DTN, go to the folder "THC_with_86percent_ventilation_simulations/THC_86present_5." Then locate the file "chemical.inp". Inside file "chemical.inp," search and find the keywords "Permeability Zones." The entries directly below those keywords contain the data in Table III-1.

The first entry declares the total number of rock blocks (76 in this instance). The second entry (=1) describes the initial mineral volume fractions for the first rock block (which is "tcwM1" in this instance). A set of entries is to be found for each rock block. The lines immediately after this (until the next block is reached) describe the model permeability parameters.

The following example illustrates how the data can be examined. Take the rock block "tcwM1" (this exercise can be repeated for any other rock block).

1. The first entry simply identifies the permeability model ("perm law"), the parameters ("a-par" and "b-par") for the applicable permeability model, and the rock type ("tcwM1").

2. Next check the integer on the next line (the first entry). This identifies which permeability law is applicable for that rock block. For 'tcwM1,' the permeability law is '1.' *This is given in the third column in Table III-1.*

3. The second entry on this line provides the 'a-par.' For 'tcwM1,' this is 0.0000E+00. For 'tcwF1', this parameter is 0.1538E-01. *These 'a-par' parameters are tabulated against each rock block in the fourth column of Table III-1.*

4. The third entry on this line provides the 'b-par.' For 'tcwM1,' this is 0.0000E+00. For 'tcwF1', this parameter is 0.1087E-01. *These 'b-par' parameters are tabulated against each rock block in the fifth column of Table III-1.*

5. This exercise can be repeated for all the minerals and all the rock blocks. These are then reported as the permeability model parameters in Table III-1.

The permeability models (law 1 and law 4) are defined in the TOUGHREACT V3.0 User's Manual (Sonnenthal et al. 2002 [DIRS 164454], Section 10.3.5).

Note that 76 rock blocks are identified in file 'chemical.inp' under "Permeability Zones," whereas only 74 rock blocks are identified in Table III-1. This is because the "chemical.inp" file has to identify the top and bottom boundaries as two distinct rock blocks (for numerical modeling purposes). For these two boundary rock blocks, all permeability model parameters are specified as zero (check file "chemical.inp) and these are not mentioned in Table III-1, as the boundaries are not real rock blocks.

How to Get the Permeability Model Parameters:

1. The permeability model parameters for all matrix blocks are assigned values of 0.0 because no value is required for the direct coupling of permeability and porosity (the input file identifies the permeability of the matrix to follow law '1' which does not require any additional input parameters; thus they are set to zero).

2. The source of the permeability model parameters for fracture blocks is LB0205REVUZPRP.001 [DIRS 159525].

3. The first model parameter (aperture) is calculated by taking ratio of the porosity (-) and the interface area (m^2/m^3) . Thus for tcwF1, the first model parameter is

$$2.4 \times 10^{-2} \Big/ 1.56 = 1.585 \times 10^{-2} \text{m}.$$

4. The second permeability model parameter (spacing fracture spacing) is simply the reciprocal of the fracture frequency. Thus, for tcwF1 with a fracture frequency of 0.92, the spacing is 1/0.92 = 1.0870 m.

5. This calculation is then repeated to obtain the permeability model parameters for the other layers.

Table III-1. Permeability Model Parameters

Rock	Zone	Law	A-Par	B-Par
tcwM1	1	1	0.00E+00	0.00E+00
tcwF1	2	4	1.54E-02	1.09E+00
tcwM2	3	1	0.00E+00	0.00E+00
tcwF2	4	4	1.27E-03	5.24E-01
tcwM3	5	1	0.00E+00	0.00E+00
tcwF3	6	4	3.45E-03	3.58E-01
ptnM1	7	1	0.00E+00	0.00E+00
ptnF1	8	4	9.20E-03	1.49E+00
ptnM2	9	1	0.00E+00	0.00E+00
ptnF2	10	4	7.09E-03	2.17E+00
ptnM3	11	1	0.00E+00	0.00E+00
ptnF3	12	4	1.20E-03	1.75E+00
ptnM4	13	1	0.00E+00	0.00E+00
ptnF4	14	4	2.94E-02	2.17E+00
ptnM5	15	1	0.00E+00	0.00E+00
ptnF5	16	4	5.05E-03	1.92E+00
ptnM6	17	1	0.00E+00	0.00E+00
ptnF6	18	4	8.71E-04	1.03E+00
tswM1	19	1	0.00E+00	0.00E+00
tswF1	20	4	1.30E-03	4.61E-01
tswM2	21	1	0.00E+00	0.00E+00
tswF2	22	4	2.59E-03	8.93E-01

Table III-1. Permeability Model Parameters (Continued)

Rock	Zone	Law	A-Par	B-Par
tswM3	23	1	0.00E+00	0.00E+00
tswF3	24	4	1.31E-03	1.23E+00
tswM4	25	1	0.00E+00	0.00E+00
tswF4	26	4	6.28E-04	2.32E-01
tswM5	27	1	0.00E+00	0.00E+00
tswF5	28	4	9.92E-04	3.17E-01
tswM6	29	1	0.00E+00	0.00E+00
tswF6	30	4	1.06E-03	2.49E-01
tswM7	31	1	0.00E+00	0.00E+00
tswF7	32	4	1.06E-03	2.49E-01
tswM8	33	1	0.00E+00	0.00E+00
tswF8	34	4	8.25E-04	2.29E-01
tswMv	35	1	0.00E+00	0.00E+00
tswFv	36	4	1.46E-03	1.04E+00
tswMz	37	1	0.00E+00	0.00E+00
tswFz	38	4	1.46E-03	1.04E+00
ch1Mv	39	1	0.00E+00	0.00E+00
ch1Fv	40	4	2.03E-03	1.00E+01
ch1Mz	41	1	0.00E+00	0.00E+00
ch1Fz	42	4	1.45E-03	2.50E+01
ch2Mv	43	1	0.00E+00	0.00E+00
ch2Fv	44	4	1.79E-03	7.14E+00
ch2Mz	45	1	0.00E+00	0.00E+00
ch2Fz	46	4	8.60E-04	7.14E+00
ch3Mv	47	1	0.00E+00	0.00E+00
ch3Fv	48	4	1.79E-03	7.14E+00
ch3Mz	49	1	0.00E+00	0.00E+00
ch3Fz	50	4	8.60E-04	7.14E+00
ch4Mv	51	1	0.00E+00	0.00E+00
ch4Fv	52	4	1.79E-03	7.14E+00
ch4Mz	53	1	0.00E+00	0.00E+00
ch4Fz	54	4	8.60E-04	7.14E+00
ch5Mv	55	1	0.00E+00	0.00E+00
ch5Fv	56	4	1.79E-03	7.14E+00
ch5Mz	57	1	0.00E+00	0.00E+00
ch5Fz	58	4	8.60E-04	7.14E+00
ch6Mv	59	1	0.00E+00	0.00E+00
ch6Fv	60	4	1.79E-03	7.14E+00
ch6Mz	61	1	0.00E+00	0.00E+00
ch6Fz	62	4	1.45E-03	2.50E+01
pp4Mz	63	1	0.00E+00	0.00E+00

Table III-1. Permeability Model Parameters (Continued)

Rock	Zone	Law	A-Par	B-Par
pp4Fz	64	4	8.60E-04	7.14E+00
pp3Md	65	1	0.00E+00	0.00E+00
pp3Fd	66	4	1.59E-03	5.00E+00
pp2Md	67	1	0.00E+00	0.00E+00
pp2Fd	68	4	1.59E-03	5.00E+00
pp1Mz	69	1	0.00E+00	0.00E+00
pp1Fz	70	4	8.60E-04	7.14E+00
bF3Md	71	1	0.00E+00	0.00E+00
bF3Fd	72	4	1.59E-03	5.00E+00
bF2Mz	73	1	0.00E+00	0.00E+00
bF2Fz	74	4	8.60E-04	7.14E+00

Output DTN: LB0310MTSCLTHC.001.

APPENDIX IV

PREPARATIONS AND CALCULATIONS FOR POST-PROCESSING TH/THC/THM MODEL RESULTS

This appendix presents the details and examples for preparing plotting files of postprocessing TH/THC/THM model simulation output results in this report.

IV.1 POSTPROCESSING OF TWO-DIMENSIONAL TH MODEL RESULTS OF SECTION 6.2

The 'grep' operation is carried out on a Unix platform (DEC Alpha Computer System with operating system OSF V4.0 or OSF V5.1). The Microsoft Excel operations and plotting with Tecplot8 were carried out on PC with Microsoft Windows98 operating system.

IV.1.1 Preparing Contour Plots

Contour plots have been developed for three variables, namely temperature (T), matrix liquid saturation, and fracture liquid saturation. To develop contour plots for any one of these variables, follow the procedures given below. As an example, the procedure for the case where 86.3 percent of heat was removed by ventilation is described in the following.

i. There are a number of output files in that directory, as follows:

1. th_2dt.out_1: for output between 0 and 600 years.
2. th_600y_2000y_vent_0.863.out: for output between 600 and 1,500 years.
3. th_600y.out: use this output file if you want a contour plot at 2,000 years.
4. th_2000y.out_1: output between 2,000 and 5,742 (approximately) years is recorded in this file.
5. th_2000y.out_2: provides output to the end of the simulation.

ii. First, decide the time (say, 100 years or 0.31557e10 seconds) at which the contour plot is to be placed. Then, select the output file from the list given in (iii) above. Using a text editor, separate the output (only the primary variables' portion) at that selected time from the rest of the output. Save this data in a file called (for example) out.0100y.

iii. Next, for temperature and matrix liquid saturation, grep the matrix elements out of that file. This can be accomplished by executing the command:

```
>> grep –v 'F' out.0100y > sim_0100y
```

In other words, this Unix command will remove the fracture elements (all starting with 'F') and direct the resulting output to sim_0100y (notice now sim_0100y has output information only for the matrix elements at 100 years).

iv. Similarly, for fracture liquid saturation, execute the following command:

```
>> grep –v 'M' out.0100y > sif_0100y
```

File sif_0100y will now contain output at 100 years for the fracture elements only.

v. Now, two TOUGH2 mesh files are required to go with these sim_0100y and sif_0100y files. To obtain these mesh files, do the following:

>> grep –v 'F' MESH > mesh_ns_th.mat

>> grep –v 'M' MESH > mesh_ns_th.fra

The commands are self-explanatory. The first command extracts the matrix elements out of MESH and directs them to mesh_ns_th.mat, which now contains only the matrix elements. Similarly, mesh_ns_th.fra contains only the fracture elements.

vi. To generate contour plots for temperature and matrix liquid saturation, open the two files sim_0100y and mesh_ns_th.mat in Microsoft Excel (with the fixed width option). First, copy the "y" and 'z" coordinates from mesh_ns_th.mat into the first two columns of a new sheet. Next, copy temperature (Column 4) and liquid saturation (Column 6) from sim_0100y on to Columns 3 and 4 of the new sheet. Save this file with the name sim_0100y and with the option "Text (Tab delimited)" in Microsoft Excel (do not save in Excel format).

vii. To generate contour plots for fracture liquid saturation, open the two files sif_0100y and mesh_ns_th.fra in Microsoft Excel (with the fixed width option). First, copy the "y" and 'z" coordinates from mesh_ns_th.fra into the first two columns of a new sheet. Next, copy liquid saturation (Column 6) from sif_0100y on to Column 3 of the new sheet. Save this file with the name sif_0100y and with the option "Text (Tab delimited)" in Microsoft Excel (do not save in Excel format).

Now, open Tecplot 8.0 for plotting. Load data file "sim_0100y" or "sif_0100y" and choose the "2D" plot option in Tecplot. Next, select "Triangulate" under "Data" in Tecplot. Select ZONE 001 and finish triangulation. Plotting from here on is straightforward.

IV.1.2 Preparing Line Plots along North-South Axis

Line plots of temperature (or matrix liquid saturation or fracture liquid saturation) versus location (at various times) along the north-south axis of the two-dimensional model grid have been developed for the following scenarios:

1. Just above the repository
2. Just below the repository
3. At the bottom of the PTn stratigraphic unit
4. At the bottom of the TSw stratigraphic unit.

Development of plots for the case where 86.3 percent of the heat is removed by ventilation is described here as an example. Also, only the process at the bottom of the Tsw will be described. Plots for the other cases can be obtained similarly.

1. At the bottom of the Tsw stratigraphic unit:

i. Locate the file "MESH", which contains the numerical grid used for 2-D TH simulations.

ii. First those elements from "MESH" that lie at the bottom of the Tsw unit must be extracted. To do this, first a file is "MESH.ELE" is created (using a text editor) with only

the 'ELEME' section of file 'MESH' (i.e., by removing the element connections in the 'CONNE' section of file 'MESH'). Next, the following Unix commands were executed:

>> grep 'tswFv' MESH.ELE > layer_tswFv_ele

>> grep 'tswFz' MESH.ELE > layer_tswFz_ele

>> cat layer_tswFv_ele >> layer_tswFz_ele

>> grep 'tswMv' MESH.ELE > layer_tswMv_ele

>> grep 'tswMz' MESH.ELE > layer_tswMz_ele

>> cat layer_tswMv_ele >> layer_tswMz_ele

The first grep command produces a file with only the fracture elements; the second one produces a file with only the matrix elements.

iii. There are five output files from the 2-D TH simulations (they are listed under Item iii of Subsection a of Section A). As an example, select th_2dt.out_1. From this file, using a text editor, extract the output at 100 years (=0.31557e+08 seconds). Save this output in file out.0100y.

iv. Execute the following commands:

>> fgrep –f layer_tswFz_ele out.0100y > prm_tswFz_0100y

>> fgrep –f layer_tswMz_ele out.0100y > prm_tswMz_0100y

The first command extracts the primary variables out of the output file out.0100y for the elements listed in file "layer_tswFz_ele" into the output file prm_tswFz_0100y. This file now has primary variables for all fracture elements just below the repository at 100 years. The second command similarly produces primary variables for all matrix elements at the bottom of the Tsw at 100 years.

v. For temperature and matrix liquid saturation, open file prm_tswMz_0100y in Microsoft Excel. Open also the file layer_tswMz_ele. Both these files should be opened as text files with the fixed width option.

vi. On the first column of a new worksheet, copy the 6th column ("y" coordinates) from "layer_tswMz_ele." Then copy columns 3,4, and 6 (pressure, temperature, and liquid saturation, respectively) from file "prm_tswMz_0100y into Columns 2 through 4 of the new worksheet.

vii. Save the new worksheet as prm_tswMz_0100y.txt with the "Text (Tab Delimited)" option of Microsoft Excel.

viii. For fracture saturation, repeat the above steps, but with files "prm_tswFz_0100y" and "layer_tswFz_ele." Save the file at the end of step vii as "prm_tswFz_0100y.txt" with the "Text (Tab delimited)" option of Microsoft Excel.

ix. For plotting, open either file "prm_tswMz_0100y" or file "prm_tswFz_0100y" and plot Column 1 ("y" coordinates, locations along the north-south axis of the repository) against Column 4 (for temperature) or Column 5 (for matrix liquid saturation) of

"prm_tswMz_0100y.txt) or Column 5 (for fracture liquid saturation) of "prm_tswFz_0100y."

x. Plots at other times can be obtained similarly by using an appropriate output file and following Steps ii through ix.

IV.1.3 Preparing Line Plots along Selected Columns in the Numerical Grid

Line plots of temperature (or matrix liquid saturation or fracture liquid saturation) versus depth (at various times) along selected columns of the two-dimensional model grid have been developed for the following scenarios

1. Column a62 (location approximately 231972 m along Nevada North-South coordinate)
2. Column b62 (location approximately 234102 m along Nevada North-South coordinate)
3. Column c38 (location approximately 235721 m along Nevada North-South coordinate).

Below, procedures are described for developing these plots for Column b62; the procedures are similar for the other columns. Development of plots for the case where 86.3 percent of the heat is removed by ventilation is described here. Plots for the no ventilation case can be developed similarly.

Line plot development for Column b62 is as follows:

i. Locate the file "MESH", which contains the numerical grid used for 2D TH simulations. In the numerical grid, the elements along Column b62 have names ending with 'b62.' For fractures, these element names begin with 'F' and, for matrix, they begin with 'M.'

ii. First, those elements from "MESH" must be extracted. To do this, first a file is "MESH.ELE" is created (using a text editor) with only the 'ELEME' section of file 'MESH' (i.e., by removing the element connections in the 'CONNE' section of file 'MESH'). Next, the following Unix commands are executed:

>> grep 'F*b62' MESH.ELE > column_b62_ele_F

>> grep 'M*b62' MESH.ELE > column_b62_ele_M

The first grep command produces a file with only the fracture elements along Column 'b62'; the second one produce a file with only the matrix elements of the same column.

iii. There are five output files from the 2-D TH simulations (they are listed under Item iii of Subsection 'a' of Section A). As an example, select th_2dt.out_1. From this file, using a text editor, extract the output at 100 years (=0.31557e+08 seconds). Save this output in file out.0100y.

iv. Execute the following commands:

>> fgrep –f column_b62_ele_F out.0100y > prm_CFb62_0100y

>> fgrep –f column_b62_ele_M out.0100y > prm_CMb62_0100y

The first command extracts the primary variables out of the output file out.0100y for the elements listed in file "column_b62_ele_F" into the output file prm_CFb62_0100y. This file now has primary variables for all fracture elements just above the repository at 100 years. The second command similarly produces primary variables for all matrix elements just above the repository at 100 years.

v. For temperature and matrix liquid saturation, open file prm_CMb62_0100y in Microsoft Excel. Open also the file column_b62_ele_M. Both these files should be opened as text files with the fixed width option.

vi. On the first column of a new worksheet, copy the 7th column ("z" coordinates) from "column_b62_ele_M." Then copy Columns 3, 4, and 6 (pressure, temperature, and liquid saturation, respectively) from file "prm_CMb62_0100y into Columns 2 through 4 of the new worksheet.

vii. Save the new worksheet as prm_CMb62_0100y.txt with the "Text (Tab Delimited)" option of Microsoft Excel.

viii. For fracture saturation, repeat steps (iv) through (vii) but with files "prm_CFb62_0100y" and "column_b62_ele_F." Save the file at the end of step (vii) as "prm_CFb62_0100y.txt" with the "Text (Tab delimited)" option of Microsoft Excel.

ix. For plotting, open either file "prm_CMb62_0100y" or file "prm_CFb62_0100y" and plot Column 1 ("z" coordinates, depth along column 'a62' of the numerical grid) against Column 3 (for temperature) or Column 4 (matrix liquid saturation) of "prm_CMb62_0100y.txt) or Column 4 (fracture liquid saturation) of "prm_CFb62_0100y."

x. Plots at other times can be obtained similarly by using an appropriate output file and following steps (ii) through (ix).

IV.1.4 Time History Plots

For plotting temperature as a function of time, the following postprocessing steps are needed. For illustration purposes, Column 'b58' of the numerical grid is selected as a representative column. Column b58 is located at 234017 m along the Nevada North-South coordinate.

There are 10 elements along Column 'b58' for which temperature versus time data were obtained from TOUGH2 simulations. These elements are (refer to the TOUGH2 input files):

1. M001Bb58 located at z=1428.8 m
2. M0007b58 located at z=1321.1 m
3. M009Bb58 located at z=1283.1 m
4. M0010b58 located at z=1279.6 m
5. M0011b58 located at z=1271.2 m
6. RP14Db58 located at z=64.6 m (a repository element)
7. M014Eb58 located at z=64.6 m (next to a repository element)

8. M0017b58 located at z=952.1 m
9. M0019b58 located at z=929.2 m
10. M0025b58 located at z=832.0 m

Describe postprocessing of data for each of these elements when 86.3% of the heat is removed by ventilation. Postprocessing of the no-ventilation case data can be done similarly.

i. There are altogether four files containing the temperature versus time data for all the elements specified in the TOUGH2 input file. These are:

1. GASOBS.DAT_th_2dt.out_1: Data through first 600 years.
2. GASOBS.DAT_th_600y.out: Data between 600 and 2000 years.
3. GASOBS.DAT_th_2000y.out_1: Data between 2000 years and 5742 years (app.).
4. GASOBS.DAT_th_2000y.out_2: Data beyond 5742 years.

ii. Element ‘M001Bb58’

For temperature versus time evolution data in element ‘M001B58’, first execute the following commands:

>> grep ‘M001Bb58’ GASOBS.DAT_th_2dt.out_1 > out.1

>> grep ‘M001Bb58’ GASOBS.DAT_th_600y.out > out.2

>> grep ‘M001Bb58’ GASOBS.DAT_th_2000y.out_1 > out.3

>> grep ‘M001Bb58’ GASOBS.DAT_th_2000y.out_2 > out.4

>> mv out.1 si_heat_M001Bb58.sen

>> cat out.2 >> si_heat_M001Bb58.sen

>> cat out.3 >> si_heat_M001Bb58.sen

>> cat out.4 >> si_heat_M001Bb58.sen

File si_heat_M001Bb58.sen now contains temperature versus time data for element ‘M001Bb58’ from start to end of simulation.

iii. Element ‘M0007b58’

For temperature versus time evolution data in element ‘M001B58’, first execute the following commands:

>> grep ‘M0007b58’ GASOBS.DAT_th_2dt.out_1 > out.1

>> grep ‘M0007b58’ GASOBS.DAT_th_600y.out > out.2

>> grep ‘M0007b58’ GASOBS.DAT_th_2000y.out_1 > out.3

>> grep ‘M0007b58’ GASOBS.DAT_th_2000y.out_2 > out.4

>> mv out.1 si_heat_M0007b58.sen

>> cat out.2 >> si_heat_M0007b58.sen

>> cat out.3 >> si_heat_M0007b58.sen

>> cat out.4 >> si_heat_M0007b58.sen

File si_heat_M0007b58.sen now contains temperature versus time data for element ‘M0007b58’ from start to end of simulation.

iv. Element ‘M009Bb58’

For temperature versus time evolution data in element ‘M001B58’, first execute the following commands:

>> grep ‘M009Bb58’ GASOBS.DAT_th_2dt.out_1 > out.1

>> grep ‘M009Bb58’ GASOBS.DAT_th_600y.out > out.2

>> grep ‘M009Bb58’ GASOBS.DAT_th_2000y.out_1 > out.3

>> grep ‘M009Bb58’ GASOBS.DAT_th_2000y.out_2 > out.4

>> mv out.1 si_heat_M009Bb58.sen

>> cat out.2 >> si_heat_M009Bb58.sen

>> cat out.3 >> si_heat_M009Bb58.sen

>> cat out.4 >> si_heat_M009Bb58.sen

File si_heat_M009Bb58.sen now contains temperature versus time data for element ‘M009Bb58’ from start to end of simulation.

v. Element ‘M0010b58’

For temperature versus time evolution data in element ‘M001B58’, first execute the following commands:

>> grep ‘M0010b58’ GASOBS.DAT_th_2dt.out_1 > out.1

>> grep ‘M0010b58’ GASOBS.DAT_th_600y.out > out.2

>> grep ‘M0010b58’ GASOBS.DAT_th_2000y.out_1 > out.3

>> grep ‘M0010b58’ GASOBS.DAT_th_2000y.out_2 > out.4

>> mv out.1 si_heat_M0010b58.sen

>> cat out.2 >> si_heat_M0010b58.sen

>> cat out.3 >> si_heat_M0010b58.sen

>> cat out.4 >> si_heat_M0010b58.sen

File si_heat_M0010b58.sen now contains temperature versus time data for element 'M0010b58' from start to end of simulation.

vi. Element 'M0011b58'

For temperature versus time evolution data in element 'M001B58', first execute the following commands:

>> grep 'M0011b58' GASOBS.DAT_th_2dt.out_1 > out.1

>> grep 'M0011b58' GASOBS.DAT_th_600y.out > out.2

>> grep 'M0011b58' GASOBS.DAT_th_2000y.out_1 > out.3

>> grep 'M0011b58' GASOBS.DAT_th_2000y.out_2 > out.4

>> mv out.1 si_heat_M0011b58.sen

>> cat out.2 >> si_heat_M0011b58.sen

>> cat out.3 >> si_heat_M0011b58.sen

>> cat out.4 >> si_heat_M0011b58.sen

File si_heat_M0011b58.sen now contains temperature versus time data for element 'M0011b58' from start to end of simulation.

vii. Element 'RP14Db58'

For temperature versus time evolution data in element 'M001B58', first execute the following commands:

>> grep 'RP14Db58' GASOBS.DAT_th_2dt.out_1 > out.1

>> grep 'RP14Db58' GASOBS.DAT_th_600y.out > out.2

>> grep 'RP14Db58' GASOBS.DAT_th_2000y.out_1 > out.3

>> grep 'RP14Db58' GASOBS.DAT_th_2000y.out_2 > out.4

>> mv out.1 si_heat_RP14Db58.sen

>> cat out.2 >> si_heat_RP14Db58.sen

>> cat out.3 >> si_heat_RP14Db58.sen

>> cat out.4 >> si_heat_RP14Db58.sen

File si_heat_RP14Db58.sen now contains temperature versus time data for element 'RP14Db58' from start to end of simulation.

viii. Element 'M014Eb58'

For temperature versus time evolution data in element 'M001B58', first execute the following commands:

>> grep 'M014Eb58' GASOBS.DAT_th_2dt.out_1 > out.1

>> grep 'M014Eb58' GASOBS.DAT_th_600y.out > out.2

>> grep 'M014Eb58' GASOBS.DAT_th_2000y.out_1 > out.3

>> grep 'M014Eb58' GASOBS.DAT_th_2000y.out_2 > out.4

>> mv out.1 si_heat_M014Eb58.sen

>> cat out.2 >> si_heat_M014Eb58.sen

>> cat out.3 >> si_heat_M014Eb58.sen

>> cat out.4 >> si_heat_M014Eb58.sen

File si_heat_M014Eb58.sen now contains temperature versus time data for element 'M014Eb58' from start to end of simulation.

ix. Element 'M0017b58'

For temperature versus time evolution data in element 'M001B58', first execute the following commands:

>> grep 'M0017b58' GASOBS.DAT_th_2dt.out_1 > out.1

>> grep 'M0017b58' GASOBS.DAT_th_600y.out > out.2

>> grep 'M0017b58' GASOBS.DAT_th_2000y.out_1 > out.3

>> grep 'M0017b58' GASOBS.DAT_th_2000y.out_2 > out.4

>> mv out.1 si_heat_M0017b58.sen

>> cat out.2 >> si_heat_M0017b58.sen

>> cat out.3 >> si_heat_M0017b58.sen

>> cat out.4 >> si_heat_M0017b58.sen

File si_heat_M0017b58.sen now contains temperature versus time data for element 'M0017b58' from start to end of simulation.

x. Element 'M0019b58'

For temperature versus time evolution data in element ‘M001B58’, first execute the following commands:

>> grep ‘M0019b58’ GASOBS.DAT_th_2dt.out_1 > out.1

>> grep ‘M0019b58’ GASOBS.DAT_th_600y.out > out.2

>> grep ‘M0019b58’ GASOBS.DAT_th_2000y.out_1 > out.3

>> grep ‘M0019b58’ GASOBS.DAT_th_2000y.out_2 > out.4

>> mv out.1 si_heat_M0019b58.sen

>> cat out.2 >> si_heat_M0019b58.sen

>> cat out.3 >> si_heat_M0019b58.sen

>> cat out.4 >> si_heat_M0019b58.sen

File si_heat_M0019b58.sen now contains temperature versus time data for element ‘M0019b58’ from start to end of simulation.

xi. Element ‘M0025b58’

For temperature versus time evolution data in element ‘M001B58’, first execute the following commands:

>> grep ‘M0025b58’ GASOBS.DAT_th_2dt.out_1 > out.1

>> grep ‘M0025b58’ GASOBS.DAT_th_600y.out > out.2

>> grep ‘M0025b58’ GASOBS.DAT_th_2000y.out_1 > out.3

>> grep ‘M0025b58’ GASOBS.DAT_th_2000y.out_2 > out.4

>> mv out.1 si_heat_M0025b58.sen

>> cat out.2 >> si_heat_M0025b58.sen

>> cat out.3 >> si_heat_M0025b58.sen

>> cat out.4 >> si_heat_M0025b58.sen

File si_heat_M0025b58.sen now contains temperature versus time data for element ‘M0025b58’ from start to end of simulation.

xii. Now open any one of these files in Microsoft Excel with the fixed width open.

xiii. Copy the second through the last column on to a new worksheet. The first column of this new sheet is ‘Time’ (in days) and the third column is Temperature (in ^{o}C).

xiv. Save this new worksheet with the same name but as a text file (with the Tab Delimited option in Microsoft Excel).

xv. Open this file in Tecplot 8.0 and using the data alteration option in Tecplot (go to Data/Alter/Specify Equation) convert Time (in days) to Time (in years) by specifying V6=V1/365.24, and then plot V6 (as x-axis) and V4 (temperature as y-axis).

xvi. Repeat the process for the other files representing the 10 elements.

IV.2 POSTPROCESSING OF 3-D TH MODEL RESULTS OF SECTION 6.3

The data extraction operations can be carried out on any Unix platform where the "grep" and "fgrep" are available. The Microsoft Excel operations and plotting with Tecplot9 were carried out on PC with the Microsoft Windows 2000 operating system.

IV.2.1 Extraction of Temperature and Saturation at PTn Bottom, Repository Horizon, and CHn Top

(1) Copy output data for a certain time from the original output file of the 3D TH model. For example, 500y_v.out represents ventilation model output results for time at 500 years.
(2) Grep data for different layers by:
fgrep –f ch1top_th.cel 500y_v.out>chn_500y_v.dat
fgrep –f ptn_bot_th.cel 500y_v.out>ptn_500y_v.dat
fgrep –f repo_th.cel 500y_v.out>repo_500y_v.dat
fgrep –f 3DTH_NSCross.cel 500y_v.out>ns_500y_v.dat

where

ch1top_th.cel contains the list of gridblocks located at the top of CHn unit.
ptn_bot_th.cel contains the list of gridblocks located at the bottom of PTn unit.
repo_th.cel contains the list of gridblocks located at the repository horizon.
3DTH_NSCross.cel contains the list of gridblocks located at the N-S cross section.

(3) Use a text editor to edit the output file from above fgrep command. Delete columns and rows that are not needed.
(4) Use "grep" command to separate output results for fracture and matrix continuum.
(5) Use MS Excel or text editor to combine coordinates for each gridblock. The final file will contain three columns: x, y, and variable (can be temperature, saturation, or other parameters).

The following four files provide coordinates of all cells at different layers:

REPO_TH: x and y coordinates for gridblocks at the repository horizon.
PTN:xy: x and y coordinates for gridblocks at the bottom of PTn unit.
CHN.xy: x and y coordinates for gridblocks at the top of CHn unit.
3D_TH_NSCross.xy: x and y coordinates for gridblocks at the N-S cross section.

(6) Use "Tecplot" to plot the 2-D results on a 2-D contour map.

IV.2.2 Extraction of Vertical Flux at PTn Bottom, Repository Horizon, and CHn Top

The same procedure is used as described in *UZ Flow Models and Submodels* (BSC 2004 [DIRS 169861], Appendix C, Section C2).

IV.2.3 Extraction of Temperature and Saturation with Time, or Profiles for Different Columns

These results were obtained by "greping" the gridblock name or a column "identification" from observation output files.

For example:

(1) Temperature or saturation change with time for the gridblock "DP12h47" was obtained by:

grep 'DP12h47' GASOBS.DAT_TH_V16.OUT_1>tem.dat
grep 'F0' tem.dat> DP12h47_t_F.dat (for temperature or saturation in fracture)
grep 'M0' tem.dat> DP12h47_t_M.dat (for temperature or saturation in matrix)

Then a text editor was used to remove unnecessary information from the above output file.

(2) Temperature, saturation, or vertical flux in the column "h47".
All gridblocks in this column have a name with the last three characters of "h47".
Therefore, data was abstracted for this column by:

grep 'h47' TH_V16.out_1>h47.dat.

h47.dat contains data for multiple years and using a text editor to get the data required.

IV.3 POSTPROCESSING OF THC MODEL RESULTS OF SECTION 6.4

IV3.1 Extraction of Temperature and Liquid Saturation Breakthrough Information from TOUGH2REACT Output Files

Data extraction was carried out on a Unix platform where the "grep" and "fgrep" commands are available. Microsoft Excel operations and plotting with Tecplot were carried out on a PC with the Microsoft Windows 2000 operating system.

(1) Output file

GASOBS.DAT

(2) Operation

Step 1: Apply the following UNIX commends to grep the temperature and gas saturation:

grep AAE38 GASOBS.DAT >AAE38
grep AAZ92 GASOBS.DAT >AAZ92
grep AAc90 GASOBS.DAT >AAc90
grep ABJ61 GASOBS.DAT >ABJ61

where AAE38 AAZ92 AAc90 ABJ61 are block names representing the position of where the temperature and saturation need to be extracted. These names are also used as the filename storing the information.

Step 2: Copy the second column (time), the fourth column (gas saturation) and the fifth column (temperature), from Files AAE38, AAZ92, AAc90 and ABJ61, respectively. Paste the time column and the saturation column, the time column and the temperature column onto two different intermediate files, respectively, for later plotting. Note that the gas saturation is converted into liquid saturation as follows:

$S_L=1-S_G$

where S_L and S_G are liquid and gas saturation, respectively.

The conversion is performed in a worksheet using command:

Column C=1–Column B

where Column B stores gas saturation and Column C gives the liquid saturation.

(3) Extracted information (files):

The extracted temperature and liquid saturation are stored in the following two files:

Temp_T.dat (temperature)
Sat_T.dat (saturation)

IV.3.2. Extraction of Temperature and Saturation Spatial Distribution Information from the TOUGH2REACT Output File

(1) Output file:

flow.out

(2) Operation:

Step 1: Create files FRACTURE and MATRIX, storing the fracture and matrix blocknames, respectively. Open MESH file, copy digital column19 (should be F or M indicating fracture or matrix), paste it twice immediately after this column then. Tsing UNIX commands:

grep FFF MESH>FRACTURE
grep MMM MESH>MATRIX

Open FRACTURE and MATRIX, delete the connection rows and columns other than the block names, retrieve the coordinates of each block, and save them in files, Temp_pres.plt and file, Saturation_pres_F.plt and Saturation_pres_M.plt, respectively, as the first two columns.

Step 2: Applying the following UNIX commands to extract the fracture liquid saturation and matrix liquid saturation, respectively:

fgrep –f FRACTURE flow.out>flow_F.out
fgrep –f MATRIX flow.out>flow_M.out

Step 3: Delete the rows of iteration information and keep the rows of output information of each block. Copy the fourth column and paste it together with the coordinates into Temp_pres.plt. Note that the temperature of fracture blocks and the relevant matrix blocks are almost the same. Copy the sixth column (liquid saturation) from flow_F.out and flow_M.out, and paste them onto Saturation_pres_F.plt and Saturation_pres_M.plt, respectively. Add captions into the file, following the Tecplot format for the later plotting.

Step 4: Apply this operation also to the monsoon mean and glacial mean infiltration scenarios.

(3) Extracted information (files)

The extracted information are saved in the following files:

Temp_pres.plt (temperature, present mean, 0–600 years)
Saturation_pres_F.plt (fracture saturation, present mean, 0–600 years)
Saturation_pres_M.plt (matrix saturation, present mean, 0–600 years)

Temp_mon.plt (temperature, monsoon mean, 600–2,000 years)
Saturation_mon_F.plt (fracture saturation, monsoon mean, 600–2,000 years)
Saturation_mon_M.plt (matrix saturation, monsoon mean, 600–2,000 years)

Temp_gla.plt (temperature, glacial mean, 2,000–100,000 years)
Saturation_gla_F.plt (fracture saturation, glacial mean, 2,000–100,000 years)
Saturation_gla_M.plt (matrix saturation, glacial mean, 2,000–100,000 years)

IV.3.3 Extraction of Percolation Flux through the Repository Horizon from TOUGH2REACT Output

(1) Output file

flow.out

(2) Operation

Step 1: Create files containing information of:

a) Fracture block names of the repository horizon:
   Repo_Fblocks.dat

b) Matrix block names of the repository horizon:
   Repo_Mblocks.dat
c) A downward vertical fracture connection of the repository horizon:
   Repo_Fcon.dat (note: no space between two blocknames of each connection)
d) A downward vertical matrix connection of the repository horizon:
   Repo_Mcon.dat (note: no space between two blocknames of each connection)

These files were manually created by just copy and paste operation from the MESH file.

Step 2: Using UNIX command to create files containing information of gridblock coordinates, connection areas:

Fgrep –f Repo_Fblocks.dat MESH>aa

Edit AA to get the coordinates of each block (pick up column 51–80)

Apply the same operation for matrix blocks

Save the coordinates in:

Repo_Fcor.dat
Repo_Mcor.dat

Step 3: Using UNIX command to create files containing information of connection areas:

fgrep –f Repo_Fcon.dat Mesh>aa

edit aa to obtain connection area (picking up column 51–60) and save them in:

Repo_Tarea.dat
Repo_Marea.dat

Note that the connection areas of fractures and matrix are set the same.

Step 4: Extract percolation flux

Open flow.out, delete rows regarding the blocks and keep only the rows of connections. Save the modified file as flux.out. Delete the space between the two block names in flux.out. Apply the following UNIX commands:

fgrep –f Repo_Fcon.dat flux.out>repo_Fflux.dat (fracture flux in kg/s)
fgrep –f Repo_Mcon.dat flux.out>repo_Mflux.dat (matrix flux in kg/s)

Step 5: Combine the fracture flux and matrix flux and convert the unit from kg/s to mm/year

Perform the following conversion in a worksheet:

Flux (mm/year)= (fracture flux (kg/s)+matrix flux (kg/s))*86400*365

Step 6: Repeat the above operation for each simulation scenario and each time step of interestd.

(3) Extracted information (files)

The extracted information is stored in the following files:

XEPO~4.DAT (percolation flux through the repository horizon calculated with the harmonic scheme for permeability weighting and without vapor diffusion)

FLUX.DAT (percolation flux through the repository horizon calculated using TH and THC simulation with upstream scheme for permeability weighting with consideration of vapor diffusion)

All above-mentioned files are submitted in the following DTNs:

LB0310MTSCLTH2.001, LB0310MTSCLTH3.001, and LB0310MTSCLTHC.001

IV.4 POSTPROCESSING OF THM MODEL RESULTS OF SECTION 6.5

The postprocessing of results from the mountain-scale THM model are described by the flow schemes given below. Yellow boxes contain input files for postprocessing, and blue boxes are outputs in the form of graphical presentations in Section 6.5 of this report. Orange boxes represent data manipulations with standard functions in TECPLOT V8.0, and they are described in detail. Filenames marked with extension *.out and Gasobs.dat in yellow boxes denotes output files from TOUGH2 V1.6 (LBNL 2003 [DIRS 161491]). Files marked *.sav in yellow boxes denote FLAC3D V2.0 (LBNL 2001 [DIRS 154783]) save files. Filenames marked with extension *.tec are TECPLOT formatted text files, which can be imported to TECPLOT V8.0 for graphical presentation. All these files have been submitted to the TDMS. Postprocessing of data with code Ext V1.0 (LBNL 1999 [DIRS 147562]) was carried out on a Sun-Sparc workstation with operating system SunOs V5.5.1. Plotting by Tecplot V8.0 was performed on a PC with a Microsoft Windows 98 Operating System.

Figure IV-1. Flow Scheme 1 for Postprocessing of Results from Mountain-Scale THM Model

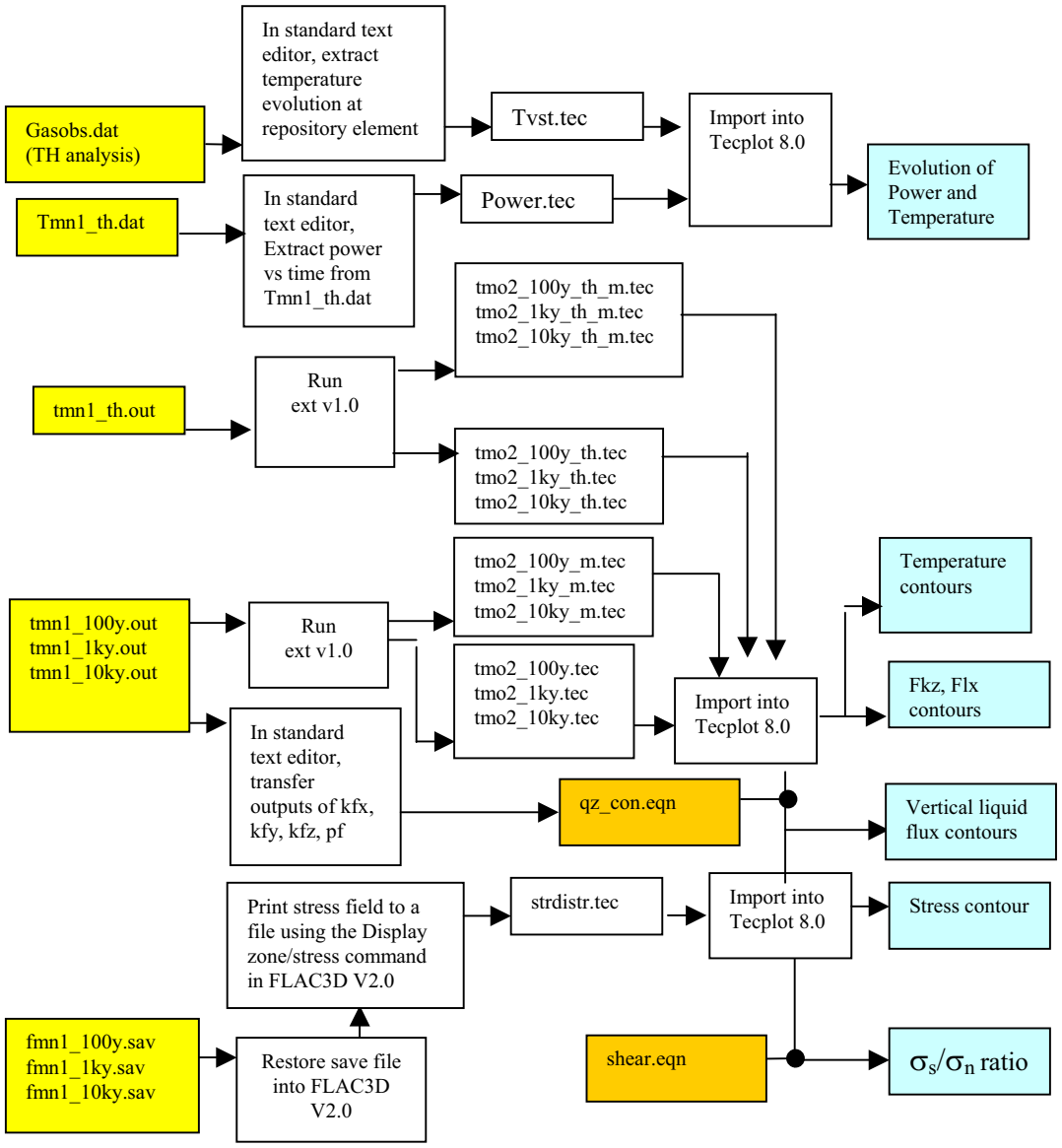

Figure IV-1. Flow Scheme 2 for Postprocessing of Results from Mountain-Scale THM Model

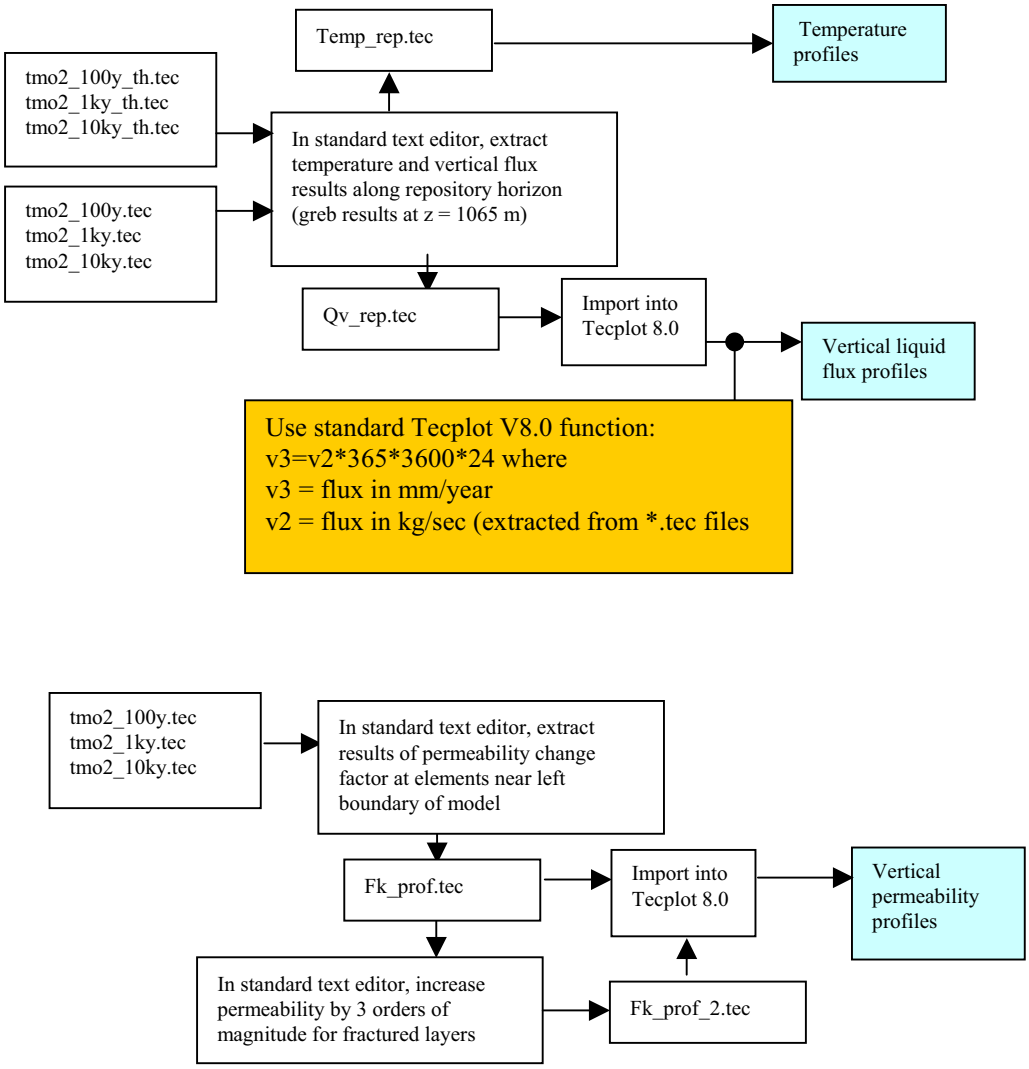

Figure IV-3. Data Manipulations with Standard Functions

Explanation to box qz_con.eqn :

qz_con.eqn contains standard Tecplot V8.0 functions:

v4=v3*365*24*3600
v5=v4[1]+v4[2]

where
v3 is vertical flux in kg/sec (imported from *.tec files for both fracture and matrix in separate TECPLOT zones [1] and [2])
v4 is vertical flux in mm/year
v4[1] is vertical flux in mm/year for TECPLOT zone [1] which is fracture vertical flux
v4[2] is vertical flux in mm/year for TECPLOT zone [2] which is matrix vertical flux
v5 is the total vertical flux in mm/year (including matrix and fracture)

Explanation to box shear.eqn on page 232:

In shear.eqn the following standard TECPLOT V8.0 functions are used:

v10=abs(v9)/(max(-v4,0.1))
v11=abs(v9)/(max(-v6,0.1))

where

v4 is stress in x-direction (imported from strdistr.tec file)
v6 is stress in z-direction (imported from strdistr.tec file)
v9 is xz-shear stress (imported from strdistr.tec file)
v10 is sigxz/sigx (with sigx limited to compression)
v11 is sigxz/sigz (with sigz limited to compression)

v10 and v11 is plotted as shear over normal stress ratio for vertical and horizontal fractures, respectively.

INTENTIONALLY LEFT BLANK

APPENDIX V

SENSITIVITY TO REVISED MATRIX POROSITY AND THERMAL PROPERTIES FOR THE THREE-DIMENSIONAL TH MODEL

This attachment provides a description of additional simulation runs that were conducted using revised thermal property data for the various stratigraphic layers in the UZ at Yucca Mountain. Some of the DTNs providing input parameters in Section 4 were changed after the simulation runs in Section 6.3 had been completed for REV 01 of this report. The simulation results in this attachment (DTN: LB0404MTSCLTH3.001) are to demonstrate that the impact of these parameter changes on the mountain scale TH response is insignificant, so that all the conclusions summarized in Section 8.1 still hold when using the revised properties. The following is a comparative analysis of simulations with the new property set that are in Section 6.3.

V.1 INPUT DATA

The revised thermal properties used here are given in DTN: LB0402THRMLPRP.001 [DIRS 168481]. As noted in Section 4.1.3, the original thermal properties were provided in DTN: LB0210THRMLPRP.001 [DIRS 160799]. The simulation runs in this attachment use the following properties from these DTNs: matrix porosity, matrix rock grain density, matrix specific heat capacity, bulk dry thermal conductivity, and bulk wet thermal conductivity. The revisions to the properties affected only the matrix porosity, the rock grain density, and the dry and wet heat conductivities; minor changes in heat capacity stem from rounding-off differences. Only the non-repository units were affected by these changes. The properties of the repository units remain essentially unchanged.

V.2 SIMULATION WITH REVISED PROPERTY SET FOR THE THREE-DIMENSIONAL TH MODEL

The simulation presented in this appendix uses the same grid as the three-dimensional TH Model grid, which consists of 980 mesh columns of both fracture and matrix continua, 86,440 gridblocks, 343,520 connections in a dual-permeability grid, and an average of 45 computational grid layers. The boundary and initial conditions are identical to that in Section 6.3. Here, only one infiltration scenario, the present-day mean infiltration, is considered. Other modeling conditions, such as rock hydrogeological properties, are also identical to that in Section 6.3.

V.3 SIMULATION RESULTS COMPARED TO THOSE PRESENTED IN SECTION 6.3

Temperature

Figures V-1 and V-2 show the predicted temperatures by the new simulation at the repository horizon at 100 and 1,000 years after emplacement. These temperature distribution contours indicate how TH conditions along these layers are impacted by the repository thermal load at different times.

At earlier times (100 years), the simulation result (Figure V-1) shows very limited spatial thermal disturbance from repository heating. As repository heating continues, the thermal impact on far-field thermal conditions appears more evident. Figure 2 displays the increase in temperature at the repository horizon at 1000 years. A careful comparison of Figures V-1 and V-2 to their counterparts using different matrix porosity and thermal properties (Figures 6.3.1a and 6.3.1-3a), show that the results for the two simulations are almost identical, except a little lower temperature for several repository gridblocks at 1,000 years.

The vertical spatial variations in temperature along the NS cross section of the three-dimensional model at 1,000 years are shown in Figure V-3. At this time, the heated zones around the repository start to cool down, and the predicted maximum temperatures are 95°C at repository rock, which is below the ambient boiling point. Figure V-3 shows almost identical temperature influence zone of the repository as those in Section 6.3 (Figure 6.3.1-3d), Figure V-3 displays a little smaller region of the hottest spots.

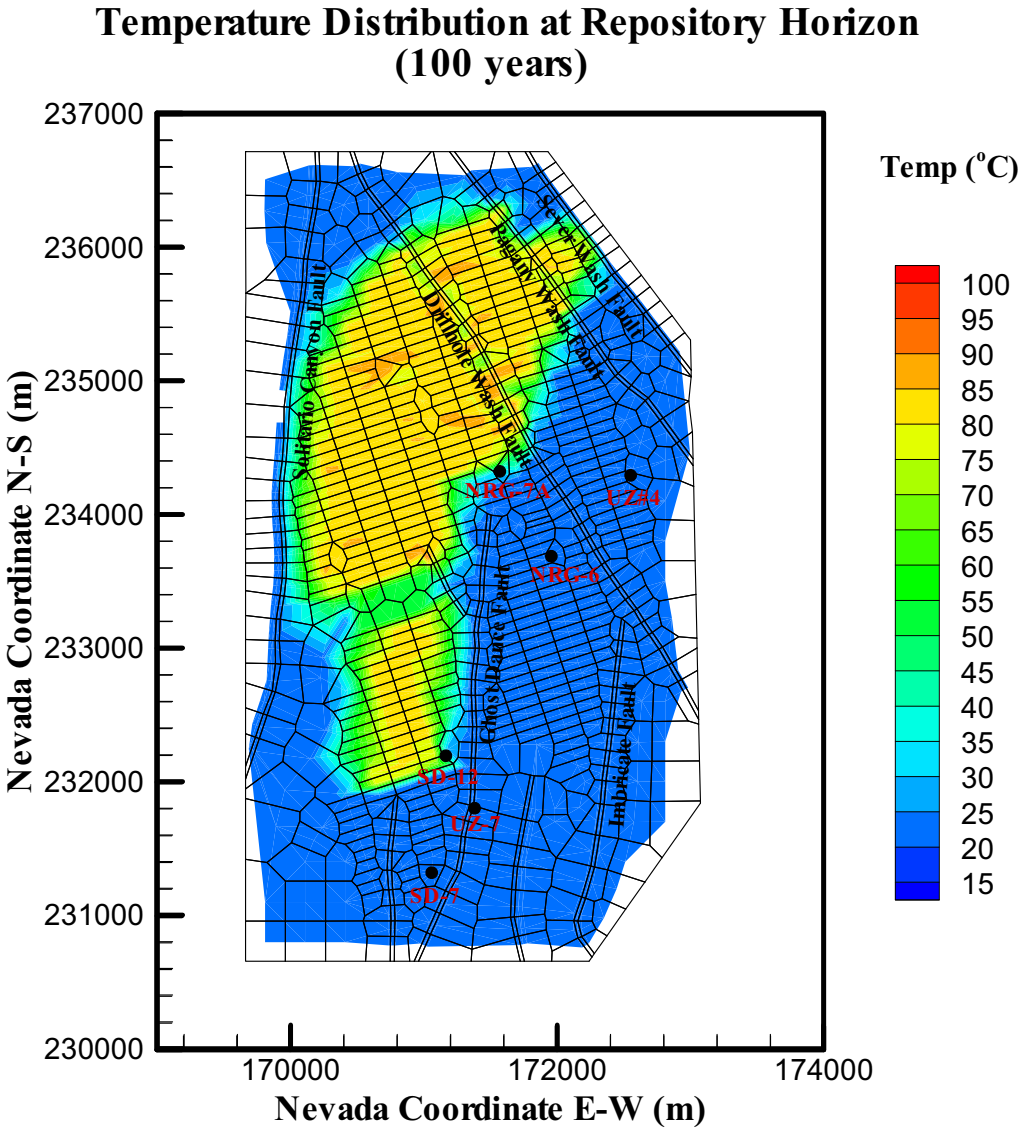

DTN: LB0404MTSCLTH3.001.

NOTE: Base-case model with ventilation, using new estimates of thermal properties.

Figure V-1. Model-Predicted Rock Temperature Distribution at the Repository Horizon at Time of 100 Years after Nuclear Waste Emplacement

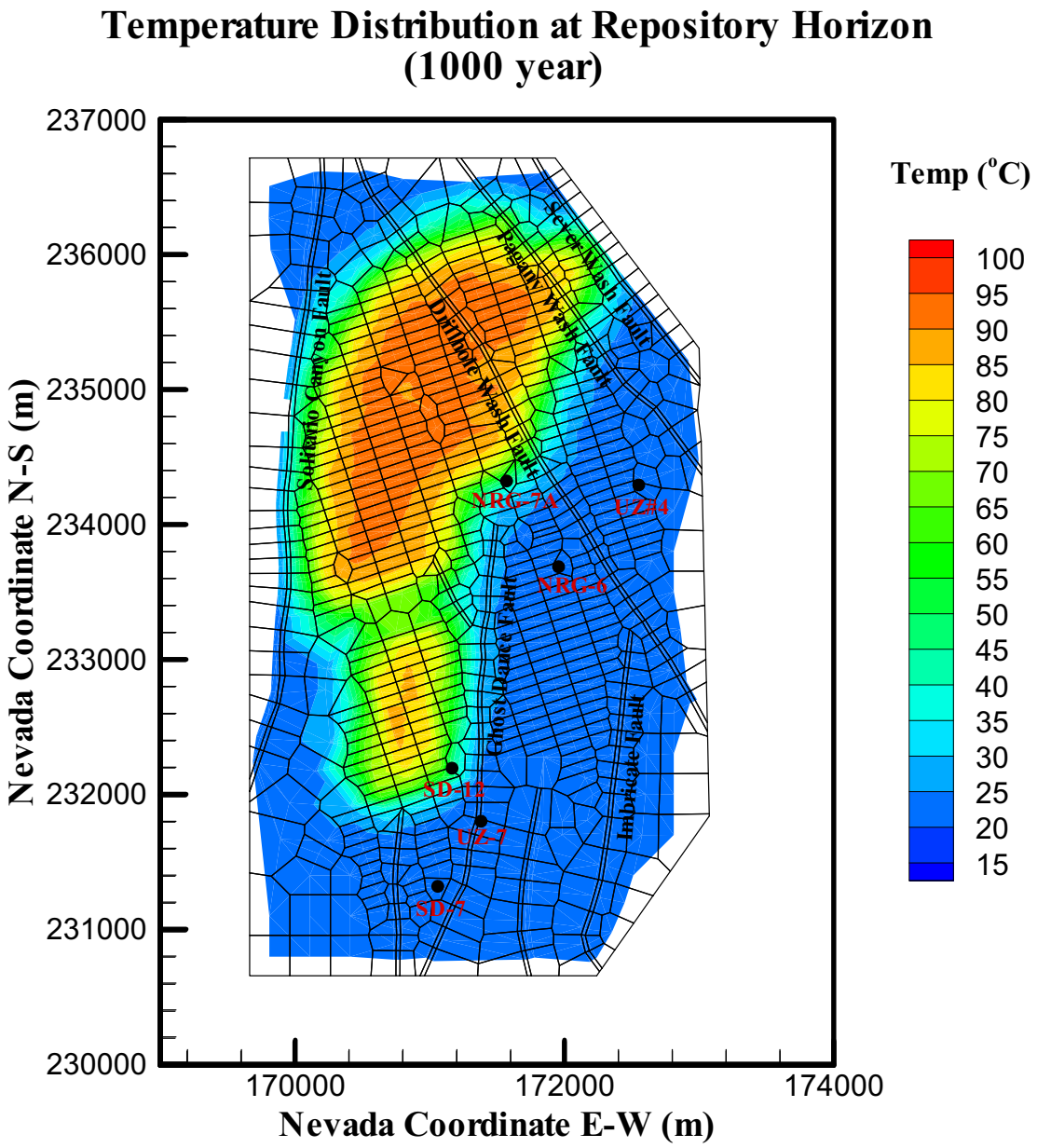

DTN: LB0404MTSCLTH3.001.

NOTE: Base-case model with ventilation, using new estimates of thermal properties.

Figure V-2. Model-Predicted Rock Temperature Distribution at the Repository Horizon at Time of 1000 Years after Nuclear Waste Emplacement

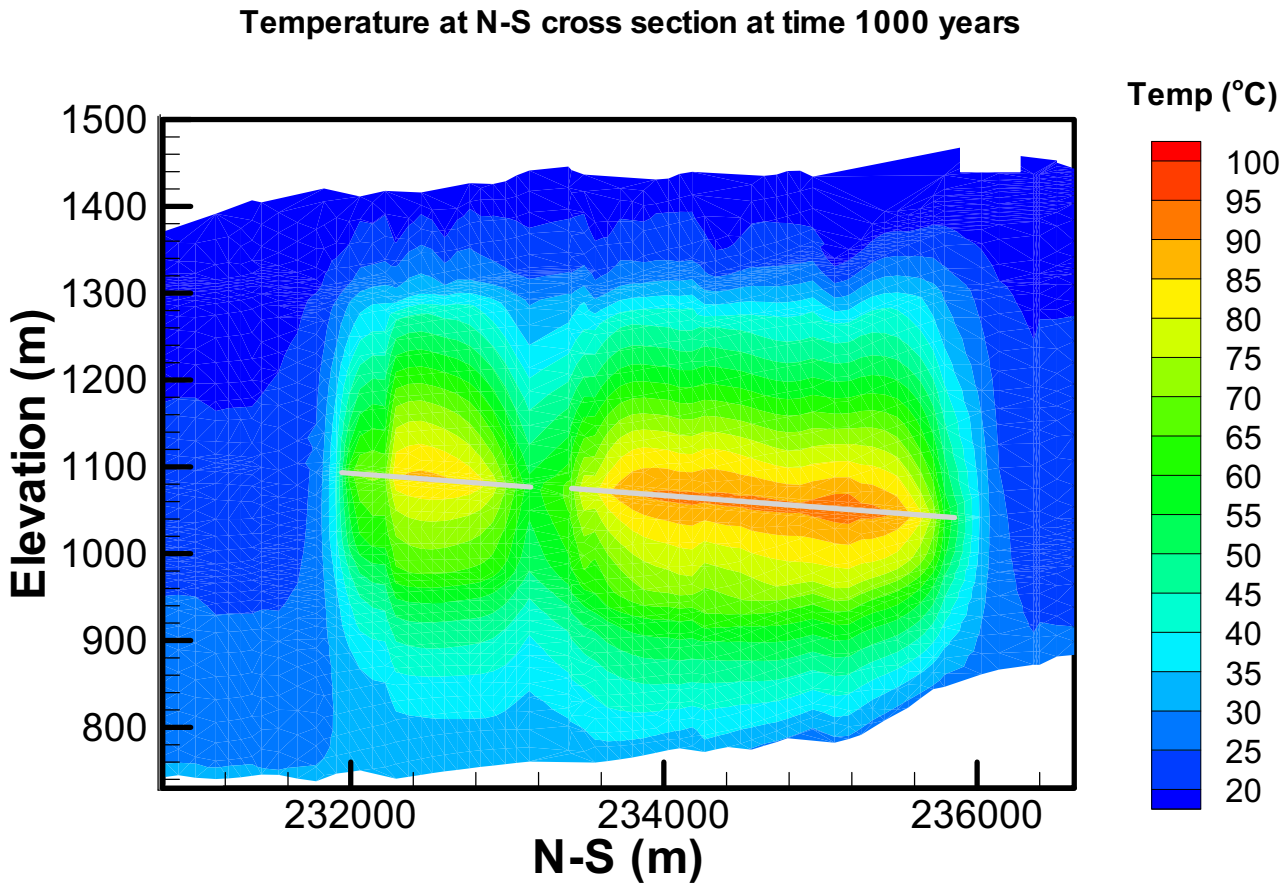

DTN: LB0404MTSCLTH3.001.

NOTE: Base-case model with ventilation, using new estimates of thermal properties.

Figure V-3. Model-Predicted Temperature Distribution at the N-S Cross Section at 1,000 Years after Nuclear Waste Emplacement

Figure V-4 displays two one-dimensional vertical profiles of simulated temperatures in observation columns A (the center of the southern or small repository block) and F (the center of the northern, main repository block) at different times (10, 100, 500, 600, 800, 1,000, 1,500, and 2,000 years. The vertical temperature distributions at Observation Column A and Column F in Figure 4 indicate a sharp temperature peak (or jump) to boiling conditions, which develops at the repository horizon at column F, i.e., the center of the northern or main repository block during a period of 100 to 500 years in this particular location. In the southern repository, the peak temperature is lower than the local boiling point during the entire thermal-load period. These results do not display any significant difference from those in Section 6.3 (see Figure 6.3.1-6).

Figure V-5 displays variations of simulated temperatures with time at three elevations along column F, repository level, lower portion of PTn, and upper CHn for the first 2, 000 years after waste emplacement. The results also appear identical to their corresponding results from Section 6.3 (Figure 6.3.1-7).

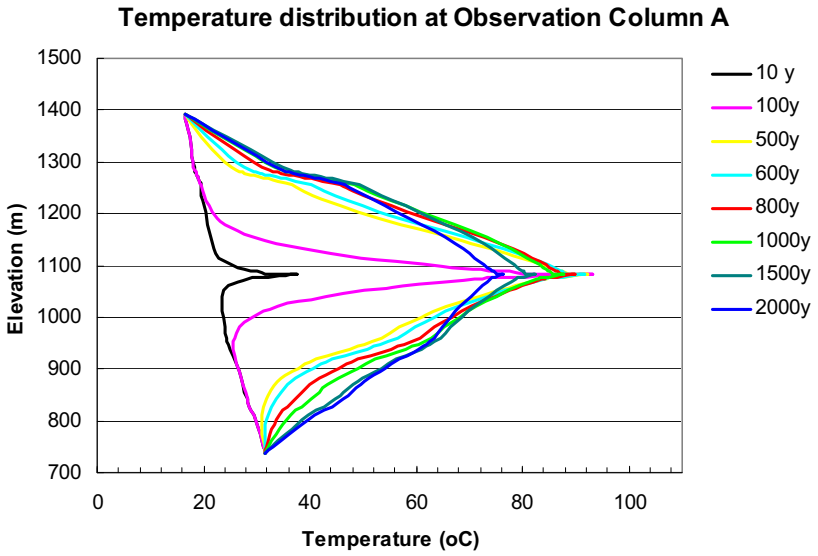

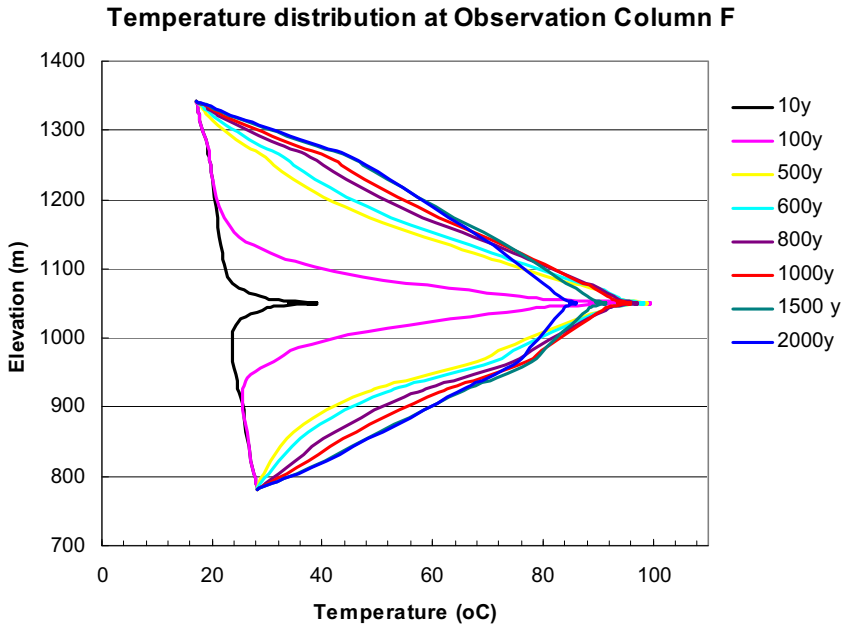

DTN: LB0404MTSCLTH3.001.

NOTE: Base-case model with ventilation, using new estimates of thermal properties.

Figure V-4. Model-Predicted Temperature Profiles at Different Times Along Observation Columns A (Southern Repository Block Center) and F (Northern, Main Repository Block Center)

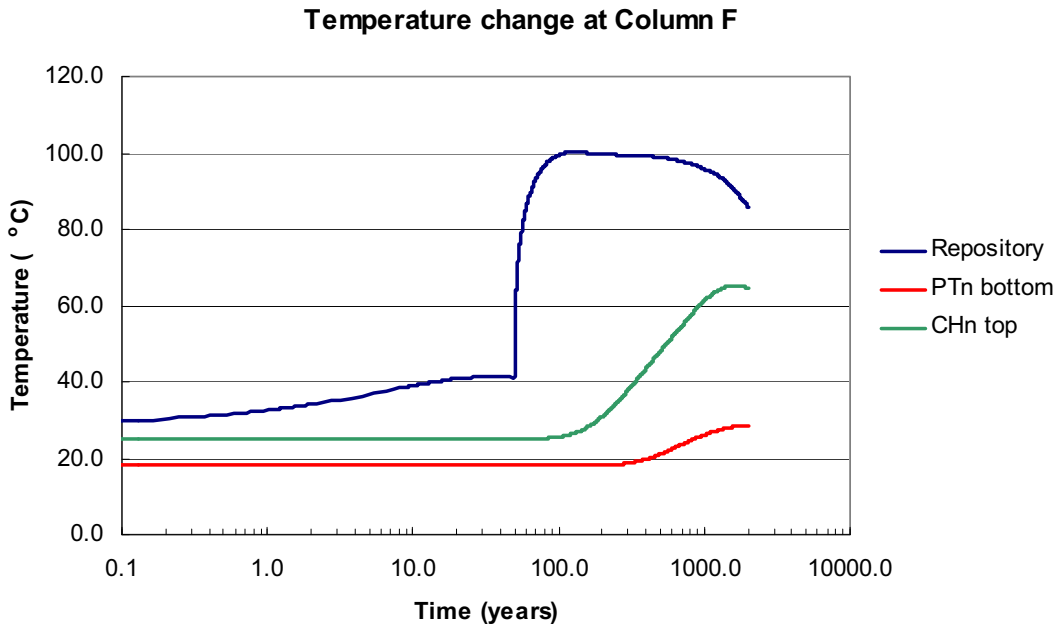

DTN: LB0404MTSCLTH3.001.

NOTE: Ptn bottom is situated at an elevation of 1,307.5 m; CHn top is situated at an elevation of 961 m; Observation Column F is located in the Northern or Main Repository Block Center. Figure shows base-case model with ventilation, using new estimates of thermal properties.

Figure V-5. Model-Predicted Temperature Changes with Times at Repository Horizon, Bottom PTn, and Top CHn Along the Observation Column F

Liquid Saturation

Figure V-6 shows the plot of matrix liquid saturation at the repository horizon at times of 1,000 years. The contour plots of the matrix liquid saturation 1,000 years after initial thermal load along the N-S cross section is shown in Figures V-7. Comparing these two figures to their corresponding results from simulations using different matrix porosity thermal properties (see Figure 6.3.1-9 and Figure 6.3.1-12), shows no significant difference between the results of the two simulations.

Similar sensitivity to changes in matrix porosity and thermal properties is expected between three-dimensional and two-dimensional TH models. This appendix demonstrates that the differences in thermal properties have little impact on the conclusions drawn from simulation results presented in Sections 6.2 and 6.3 of this report.

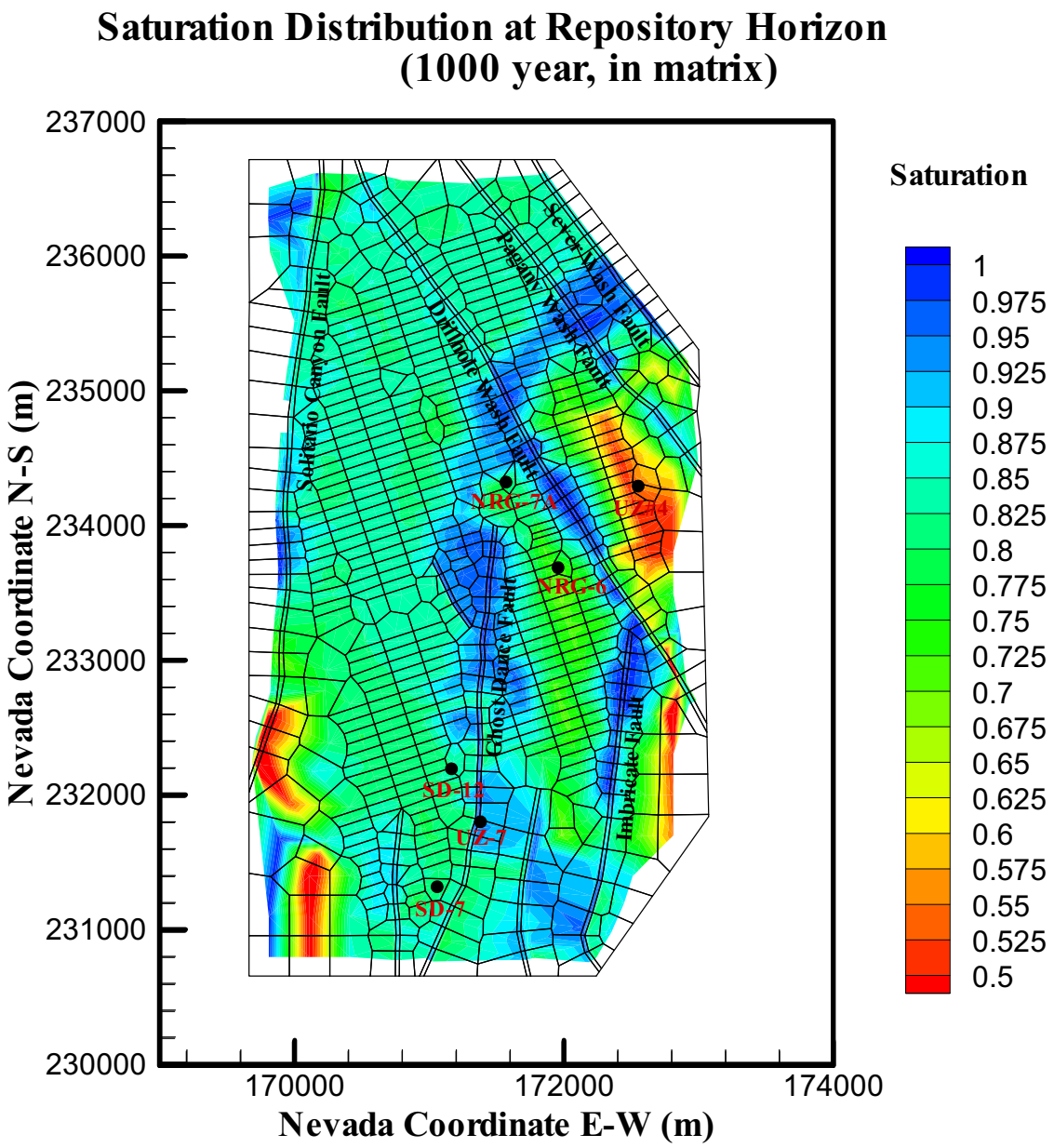

DTN: LB0404MTSCLTH3.001.

NOTE: Base-case model with ventilation, using new estimates of thermal properties.

Figure V-6. Model-Predicted Matrix Liquid Saturation Distribution at Repository Horizon at 1,000 Years After Nuclear Waste Emplacement

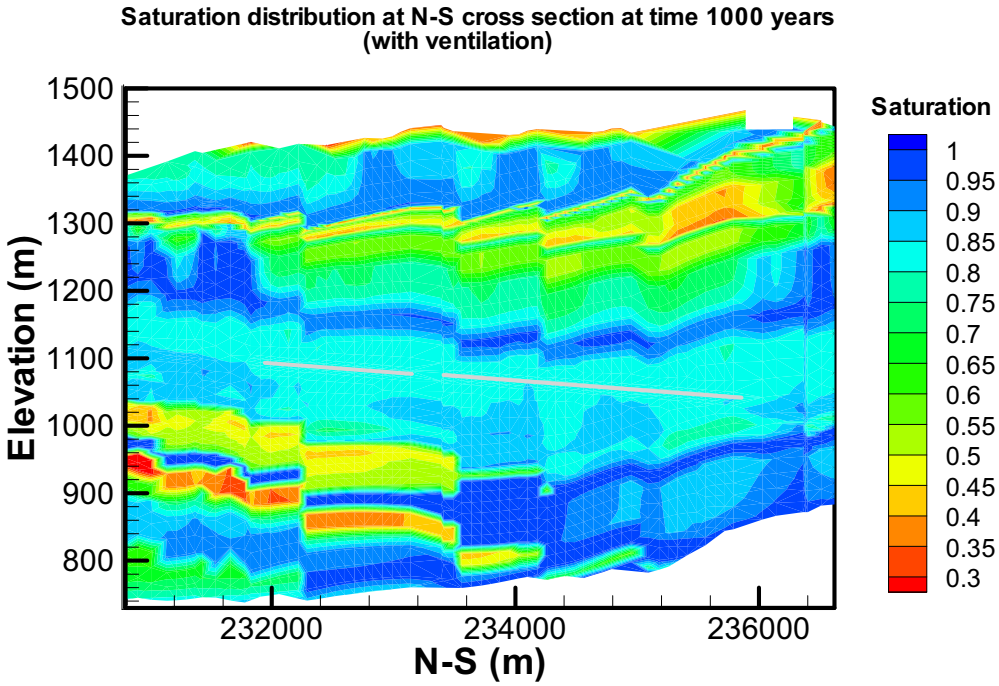

DTN: LB0404MTSCLTH3.001.

NOTE: Base-case model with ventilation, using new estimates of thermal properties.

Figure V-7. Model-Predicted Matrix Liquid Saturation Distribution at the N-S Cross section at 1,000 Years After Nuclear Waste Emplacement

APPENDIX VI

SENSITIVITY TO REVISED MATRIX POROSITY AND THERMAL PROPERTIES FOR THE MOUNTAIN SCALE THC MODEL

This appendix provides a description of additional simulation runs that were conducted using revised thermal properties for hydrogeological model layers in the UZ at Yucca Mountain. DTNs providing input parameters for thermal properties in Section 4 were modified after the simulation runs in Section 6.4 had been completed for REV 01 of this report. The simulation results in this appendix (DTN: LB0404MTSCLTHC.001) document the impact of these parameter changes on mountain scale THC responses to thermal loading. The results of these simulations are presented in Section VI.2 below.

Conclusions summarized in Section 8.2 still hold when using the revised properties.

VI.1 INPUT DATA

The revised thermal properties used here are given in DTN: LB0402THRMLPRP.001 [DIRS 168481]. As noted in Section 4.1.3, the original thermal properties were provided in DTN: LB0210THRMLPRP.001 [DIRS 160799]. The simulation runs in this appendix use the following properties from these DTNs: matrix porosity, matrix rock grain density, matrix specific heat capacity, bulk dry thermal conductivity, and bulk wet thermal conductivity. The revisions to the properties affected only the matrix porosity, the rock grain density, the dry and wet heat conductivities, with minor changes in heat capacity owing to rounding-off differences. Only the non-repository units were significantly affected by these changes, with very minor differences in the properties of the repository units.

VI.2 SIMULATION RESULTS FOR REVISED THERMAL PROPERTIES COMPARED TO THOSE PRESENTED IN SECTION 6.4

The revised thermal properties and matrix porosity are seen to have negligible effects on temperatures, gas compositions, and water chemistry as evidenced by the contour plots shown in Figure VI-1 as compared to Figures 6.4-16 and 6.4-17. Calcite precipitation is very similar to that seen in Figure 6.4-18, illustrating the limited impact of changes to repository units and those above. Clinoptilolite dissolution after 2000 years is similar to that seen in Figure 6.4-24, except in the region below the repository where the extent of dissolution is less owing to modifications to the porosity. However, the general trends in mineral reactions are similar to that seen previously. Only very small differences in the temperature contours can be seen after 2,000 years around the repository drifts.

In conclusion, this appendix demonstrates that the differences in thermal properties in the nonrepository layers do not change the main conclusions drawn from simulation results for the mountain-scale THC model presented in Section 6.4 of this report.

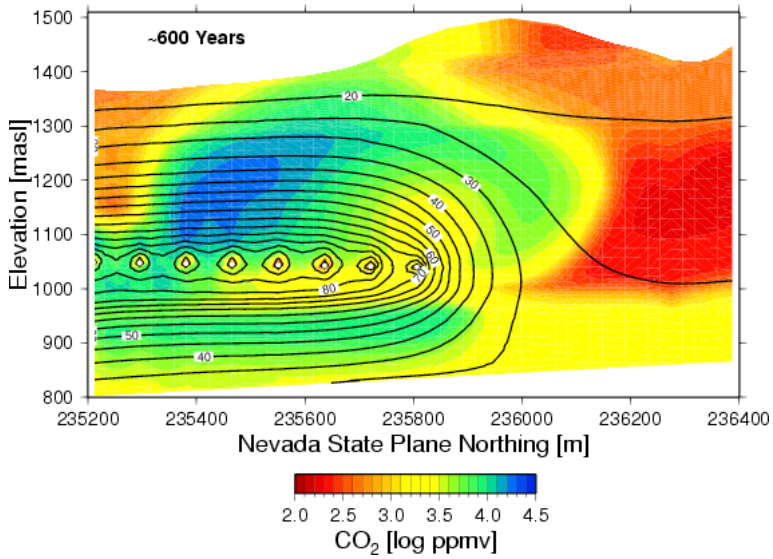

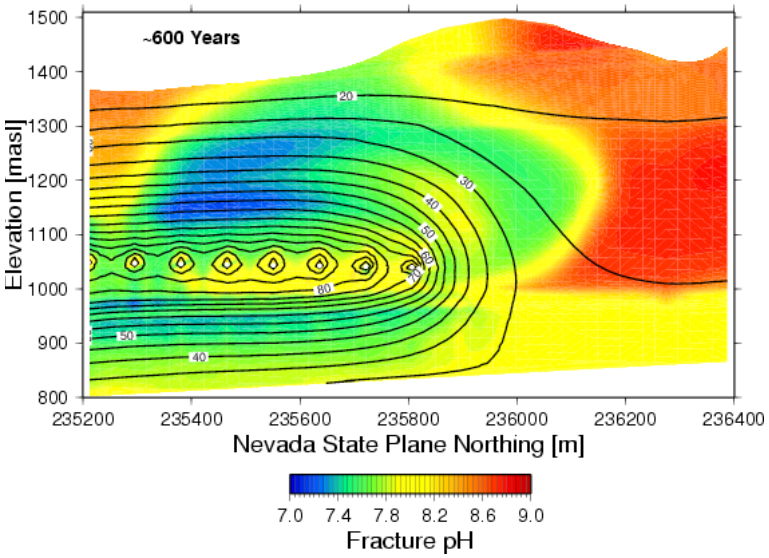

DTN: LB0404MTSCLTHC.001.

NOTE: Temperature contours are overlain.

Figure VI-1. Gas Phase CO2 Concentration and pH in Fracture Water after 600 Years

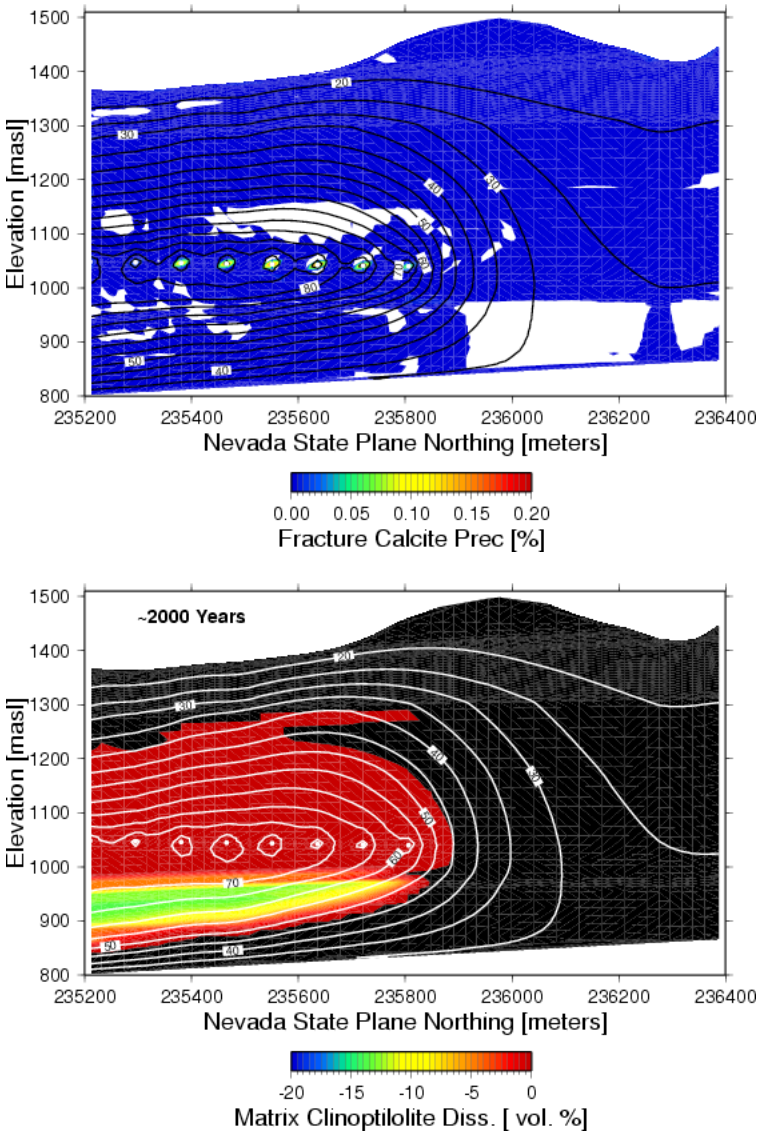

DTN: LB0404MTSCLTHC.001.

NOTE: Temperature contours are overlain.

Figure VI-2. Calcite Precipitation in Fractures after 1,000 Years and Clinoptilolite Dissolution in the Rock Matrix after 2,000 Years

INTENTIONALLY LEFT BLANK

APPENDIX VII

SENSITIVITY TO REVISED MATRIX POROSITY AND THERMAL PROPERTIES FOR THE MOUNTAIN SCALE THM MODEL

This appendix provides a description of additional simulation runs that were conducted using revised thermal property data for the various stratigraphic layers in the UZ at Yucca Mountain. Some of the DTNs providing input parameters in Section 4 were changed after the simulation runs in Section 6.5 had been completed for REV 01 of this report. The simulation results in this appendix (DTN: LB0404MTSCLTHM.001) are to demonstrate that the impact of these parameter changes on the mountain scale THM response is insignificant, so that all the conclusions summarized in Section 8.3 still hold when using the revised properties. The following, is a comparative analysis of simulations with the new property set that are in Section 6.5.

VII.1 INPUT DATA

The revised thermal properties used here are given in DTN: LB0402THRMLPRP.001 [DIRS 168481]. As noted in Section 4.1.3, the original thermal properties were provided in DTN: LB0210THRMLPRP.001 [DIRS 160799]. The simulation runs in this appendix use the following properties from these DTNs: matrix porosity, matrix rock grain density, matrix specific heat capacity, bulk dry thermal conductivity, and bulk wet thermal conductivity. The revisions to the properties affected only the matrix porosity, the rock grain density, and the dry and wet heat conductivities; minor changes in heat capacity stem from rounding-off differences. Only the non-repository units were affected by these changes. The properties of the repository units remain essentially unchanged.

VII.2 SIMULATION RESULTS FOR REVISED THERMAL PROPERTIES COMPARED TO THOSE PRESENTED IN SECTION 6.5

Figure VII-1 presents vertical profiles of temperatures and vertical permeability correction factors along a vertical section located at the left most boundary of the model, representing the interior of the repository. The vertical permeability is selected for comparison since it is most relevant for the gravity driven water percolation flux. In Figure VII-1, the simulation results of temperature and vertical permeability for original and revised thermal properties are almost identical.

Figure VII-2 displays vertical flux through the repository horizon at 1,000 years. The 1,000 year case was selected for this comparison since at this time the thermal-mechanical effects on permeability is the strongest. In Figure VII-2, there is no visible difference in the vertical flux for the two simulation cases.

In conclusion, this appendix demonstrates that the differences in thermal properties in the non-repository layers have no impact on the conclusions drawn from simulation results for the mountain-scale THM model presented in Section 6.5 of this report.

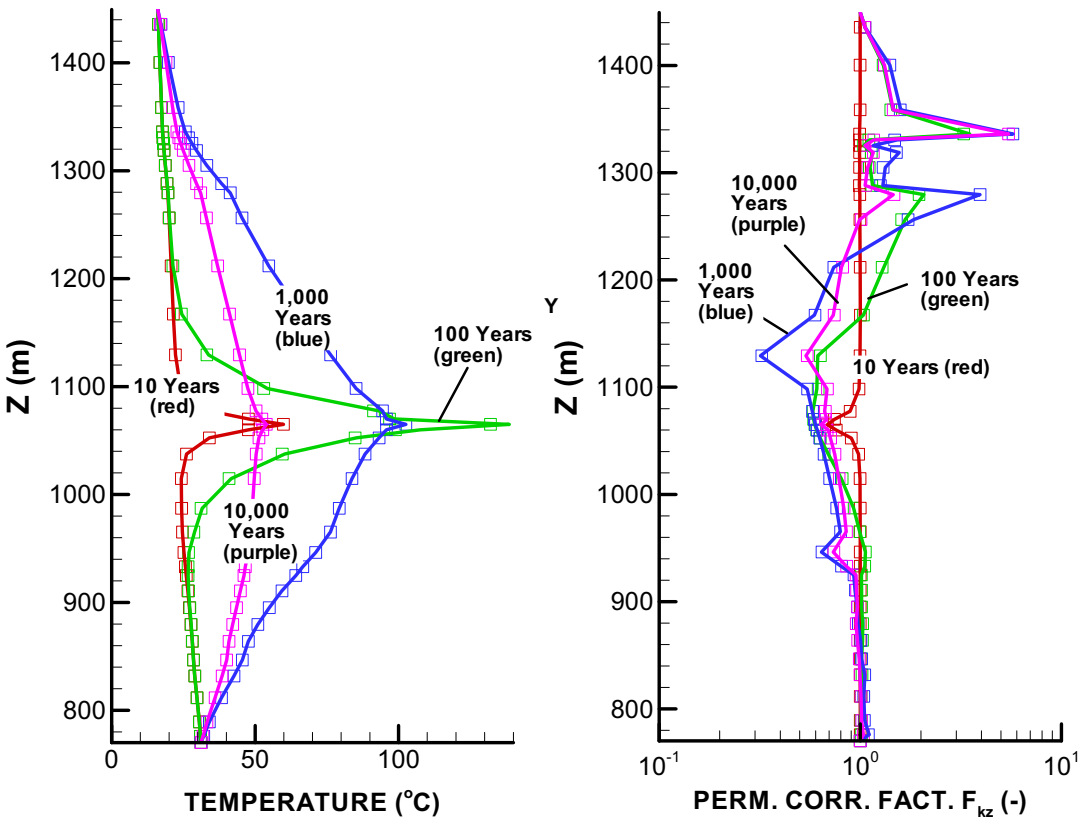

DTNs: LB0404MTSCLTHM.002 and LB0310MTSCLTHM.002.

NOTE: Revised thermal properties are represented by symbols; original thermal properties are represented by lines.

Figure VII-1. Vertical Profiles of Simulated (a) Temperature and (b) Vertical Permeability Correction Factor ($F_{kz} = k_z/k_i$) Using Revised and Original Thermal Properties

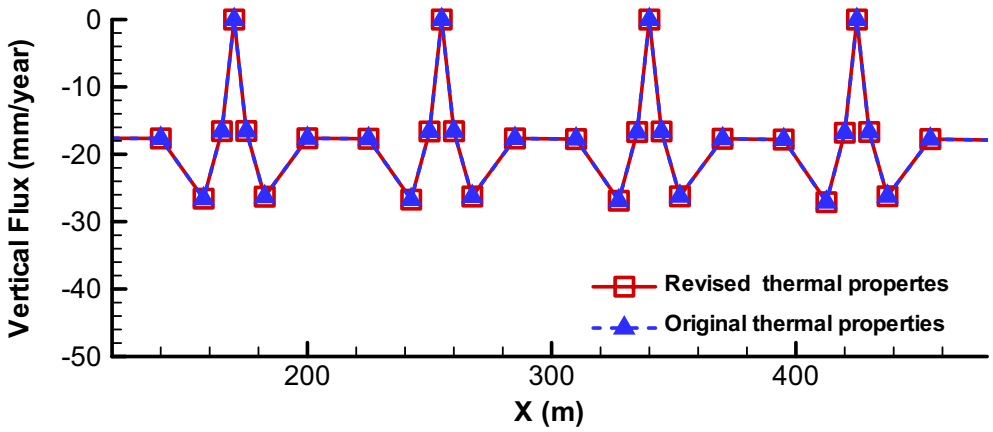

DTNs: LB0404MTSCLTHM.002 and LB0310MTSCLTHM.002.

NOTE: Revised thermal properties are represented by solid red lines; original thermal properties are represented by dashed blue lines.

Figure VII-2. Simulated Vertical Percolation Flux (Q_z) at 1,000 years Across the Repository Horizon Near Four Emplacement Drifts Using Revised and Original Thermal Properties

INTENTIONALLY LEFT BLANK

APPENDIX VIII

TECHNICAL REVIEWS FOR POST-DEVELOPMENT VALIDATION OF THE MOUNTAIN SCALE TH/THC/THM MODEL

This appendix provides complete lists of the independent post-development model validation reviews for the mountain scale TH, THC, and THM models (Sections 7.1.5, 7.2.4, and 7.3.4). The reviews were conducted following the review criteria of the post-development validation review as presented in Section 2.2.1.4 of the TWP (BSC 2005 [DIRS 174842]).

The independent post-development model validation have been performed by Dr. Marcelo J. Lippmann, Earth Sciences Division of Lawrence Berkeley National Laboratory; Dr. Carl I. Steefel, Earth Sciences Division of Lawrence Berkeley National Laboratory; and Dr. Tin Chan, Atomic Energy of Canada Limited. Each reviewer has at least 20 years research experience and is considered a leading expert in the relevant subject field. The comments/responses have been reproduced in this appendix.

Note that, since the response made directly on Sections 6.5 and 7.3 for Dr. Chan's comments, some additional text in Appendix VIII.3 was added to point out the changes. His concurrence on the response was made verbally, and an additional memo was not created since his conclusion in the memo already concurred the adequacy of the mountain-scale THM model (Section 7.3.4).

Dr. Lippmann received his Ph.D. from University of California, Berkeley, at the field of Engineering Sciences. He has 30 years of research experience in Engineering Sciences and related fields including but not limited to geohydrology, geothermal reservoir engineering, heat and mass transfer in geologic systems, geologic sequestration of carbon dioxide, and underground storage of natural gas. Currently, he is the editor-in-chief of *Geothermics* journal.

Dr. Steefel received his Ph.D. from Yale University in the field of Geochemistry, and has over 18 years of experience in developing models for multicomponent reactive transport in porous media and applying them to topics in reactive contaminant transport and water-rock interaction. He has also worked extensively in applying reactive transport modeling to natural systems, including hydrothermal, contaminant, and chemical weathering environments.

Dr. Chan received his Ph.D. from Yale University in the field of Theoretical Physics specializing in the theory of liquid metals. He has 30 years of research and development experience in analytical and finite-element modeling of coupled processes (i.e., rock mechanical, thermal, hydrogeological, and contaminant transport) associated with deep geological disposal of nuclear wastes, working with LBNL (Lawrence Berkeley National Laboratory, University of California, 1977-81) and AECL (Atomic Energy of Canada Limited, 1975-77 and 1982-present). Currently he is Senior Scientist of the Engineered Barrier and Analysis Branch, AECL, responsible for mathematical modeling of coupled thermo-hydro-mechanical and transport processes in the subsurface.

VIII.1 INDEPENDENT POST-DEVELOPMENT VALIDATION REVIEW FOR THE MOUNTAIN SCALE TH MODEL

August 4, 2005

MEMORANDUM

To: Ernest Harding/YM/RWDOE
Cc: Yvonne Tsang//YM/RWDOE
From: Marcelo J. Lippmann – Independent Reviewer

Re: Independent Model Validation Review of Mountain-Scale Coupled Processes – TH Model

I have conducted an independent review of the Mountain Scale TH Model as presented in Rev. 03 Draft B of the Mountain-Scale Coupled Processes (TH/THC/THM) Report. My review comments dated July 21, 2005 are attached (Attachment 1).

After reviewing the response to my comments (Attachment 2) and meeting with Dr. Tsang, I conclude that the changes made to the document resolve all the issues I had on the TH Model.

Summarizing, I consider that in the Mountain-scale TH model

1. An appropriate methodology has been followed. That is, the technical approach is correct as well as the algorithms used to describe the thermal and hydrologic processes in the UZ.
2. The modeling assumptions (i.e. equations, boundary conditions and initial conditions) used are reasonable and appropriate considering the complexity of the system;
3. The assumptions on which the parameters of the model were chosen are clearly described; and
4. The uncertainties related to parameters and process representation, and their impact on model results have been adequately considered and discussed.

In other words, I conclude that the overall technical approach followed in the Mountain-size model is credible and appropriate for screening the UZ FEP's given in Table 4-3 of the document.

Let me know if you require additional input on this matter.

The following information is a record of the comments and the responses from the reviewer and the responders. Based on the information, the conclusion in the previous memo (i.e., the adequacy of the mountain-scale TH model) was made.

ATTACHMENT 1

COMMENTS BY MARCELO LIPPMANN

INDEPENDENT REVIEWER FOR THE MOUNTAIN-SCALE TH MODEL

JULY 21, 2005

General Comments

No significant changes are needed.
No gaps in the arguments used have been found.
The processes relevant to modeling TH behavior have been identified and incorporated into the model.
The assumptions used in developing the TH model (Section 5.1) are justified and adequate.

SPECIFIC COMMENTS

1. Was the model stable (i.e. under steady-state conditions) from the thermal and hydrological point of view at zero modeling time?

2. At time zero, did the computed geothermal heat flow values agree with those measured in the field?

3. How were the infiltration scenarios/climate changed used in the model (i.e. present, monsoon and glacial transition) and their times selected? I could not find that mentioned in the document. These scenarios are specified on pages 6-11, 6-42, and in Table 6.1-2

4. Line 1604. The term “thermal seepage” should be defined. It is not clear to me what it means.

5. Line 1616. Should this line read: “any effects related to the two-dimensional nature of the model have been found to be of only short term in duration.” ?

6. Line 1635. Should it read; " …, the base-case TH model (i.e. Base Case Thermal Loading) uses only …"

7. For consistency, the legends on the vertical axis of Figures 6.2-1b. 6.2-2b and 6.3-3b, 6.2-4b and 6.2-5b should be the same as those of Figure 6.2-1a (and others)

8. Move Figure 6.2-6b to page 6-32, after it is mentioned in the text.

9. Line 1792. The underestimation in temperature increase should be specified or discussed. Saying "somewhat underestimated" is very vague and might be criticized.

10. Line 1798. Should this line read: "above the repository drift in the repository horizon. …" ?

11. Line 1860. There is mention of Column "b62." The column should be identified in Figures 6.1-1 and/or 6.1-2 (on pages 6-5 and 6-6).

12. Line 1862. Should this line read: "table; in this column the repository is at an elevation of xxx m"?

13. Line 1875 (and following pages). There is mention of the "pillar regions," but have not been identified in any of the figures

14. Line 1877. It should read: "below about 925 m elevation (and no …" Throughout the document one should refer to elevations not to "m above/below sea level."

15. Line 1880. Apparently starting with this line there is mention of "fluxes" with units of mm/yr. Should these be velocities or fluxes per unit cross-section?

16. Figure 6.2-9d. The legend on the vertical axes should be "Elevation (m)."

17. Move legend of Figure 6.2-10b to page 6-41.

18. The legend on the horizontal axes of this and other figures showing cross sections should be "Nevada Coordinate N-S (m) instead of "N-S (m)".

19. Lines 2088 and 2089. Also mention that location of Columns A and B are given in Table 6.3-1 (on page 6-43).

20. Figures 6.3.1-6, 6.3.1-13, 6.3.1-17 and 6.3.1-18. The elevation of the repository should be indicated.

21. Line 2232. Also mention that location of Observation Columns F and C are given in Table 6.3-1 (on page 6-43).

Attachment 2

Response to comments by Marcelo Lippmann, independent reviewer for the Mountain Scale TH Model

JULY 29, 2005

The response will be tied to the numbering system used by the reviewer:

1. Yes, the model is run to steady state under ambient conditions, before applying the heat load of the potential repository.

2. The ambient mountain scale TH model is calibrated against hydrological, geochemical, and temperature data. The measured temperature profiles in several boreholes are reproduced by the mountain TH model, at time zero, prior to application of repository heat.

3. Selection of the infiltration scenario/climate change (i.e. present, monsoon and glacial transition) are based on two other Analysis and Modeling Reports. They are referenced on pages 6-11, and in Table 6.1-2 by the DIR (direct input reference) number, and the DTN (data tracking number).

4. Clarification on "thermal seepage" is made (line 1612 in revised document).

5. Revised as suggested (line 1626 in revised document).

6. Revised as suggested (line 1646 in revised document).

7. Since the range on the vertical axis in the Figures 6.2-1b. 6.2-2b, 6.3-3b, 6.2-4b, and 6.2-5b is identical to that of their respective Figure #.#-a counterpart (e.g. 6.2.1-a, 6.2-2a etc.), even though the legend in one is Z(m), and the other is Elevation (m), it should be obvious to the readers that they are same. For consistency in format, they could all have the same legend. However, since these figures are traceable to a DTN (data tracking number) relating to computer output, it is preferable not to modify the figures in this report.

8. Figures 6.2-6a, b, and c on page 6-31 and 6-32 are kept before the text discussion, rather than the reviewer's suggestion of putting the text first and pulling the Figure 6.2-6a to page 6-32 to follow after. Both arrangements have advantages and disadvantages.

9. The text has been modified, with the phrase "less than 5^{o}C" in parenthesis inserted (line 1804 in revised document).

10. Revised to read " at the repository horizon directly above the repository drift" (line 1810 in revised document)

11. The location of column b62 at Nevada Coordinate N-S 234100 m is specified in the text so readers can interpret the results accordingly.

12. Revised as suggested with the repository horizon at 1063.5 m inserted (line 1875 in revised document).

13. “Pillar” is the region between two-drifts, as the usage in mining literature. Definition is added in text (line 1889 in revised document)

14. Revised as suggested (line 1891 in revised document). The term meters above sea level can be traced to the Project’s geological framework model, a basis for most of the mountain-scale modeling. On this project, traceability often take precedence over editorial elegance.

15. The common project usage expresses flux per unit cross-section in mm/year, but refer to it simply as flux. To address this comment, “per unit cross-section” is added in parenthesis at this first mention (line 1894 in revised document).

16. See response to common 14 for reference to meters above sea level.

17. Production staff will ensure that the figure caption appears on the same page as the figure.

18. Add “Nevada Coordinate” to those figures whose horizontal axis legend is simply “N-S (m)” (e.g. 6.3-1-1d, 6.3.1-3d, 6.3.1-5d etc.)

19. Reference to Table 6.3-1 for coordinates of Column A through F added (line 2105 in revised document).

20. The elevation of repository horizon in Column A (1083 m) and Column F (1050 m) is added to text together with the response to 19 (line 2106 in revised document).

21. Add “The coordinates of Observation Columns F and C are also given in Table 6.3-1” to line 2232, as in response to comment 19.

VIII.2 INDEPENDENT POST-DEVELOPMENT VALIDATION REVIEW FOR THE MOUNTAIN SCALE THC MODEL

August 10, 2005

Dr. Ernest Hardin
BSC

Dear Ernie:

I have read the entire Mountain Scale Coupled Processes (TH/THC/THM) Models AMR, in addition to the relevant FEP screening arguments that cite the Mountain-Scale THC Model. Specifically, this technical review addresses the use of the mountain-scale THC model for screening: a) UZ FEPs 2.2.08.03.0B and 2.2.10.06.0A (Table 4-3) pertaining to TSPA components "UZ Flow" and "UZ Radionuclide Transport"; and b) use of the mountain-scale THC model for information on geochemical conditions at the water table for screening SZ FEP 2.2.10.08.0A and 2.2.10.13.0A (Table 4-3) pertaining to TSPA component "SZ Flow and Radionuclide Transport."

I find that overall the mountain scale modeling of THC processes to be an impressive piece of work that extends the ground-breaking modeling carried out on the Drift Scale Test (DST) published earlier by the Berkeley group. The DST provides perhaps the most comprehensive validation of a THC model to date and has certainly advanced the state of the science well beyond what has been documented elsewhere in the literature.

In terms of the use of the mountain-scale THC model's use in screening of the relevant FEPs, I find that for the higher temperature processes dominating the thermal period in the vicinity of the Drift Scale Test (i.e., within the repository horizons), the technical approach and algorithms described in the document capture all physical and chemical processes that are significant to the intended use of the model for screening these FEPs. However, the same cannot yet be said with regard to processes in more distal units, especially those lying below the repository horizons. For example, no significant validation is provided for the THC modeling of reactions in the Calico Hills formation at lower temperatures and in rock containing abundant zeolites. In addition, the modeling cannot be said to have captured all of the relevant chemical processes, since formation of zeolites of variable composition (which are expected to have greater thermodynamic stability than pure end member phases) and cation exchange (which will affect the chemistry of water reaching the saturated zone) have not been included. These comments are made in the attached Review Comments and are largely acknowledged by the authors of the AMR. However, I do agree with the responses to my comments that it is likely that the modeling over-estimates reaction rates in these lower horizons and thus probably over-estimates changes in permeability and solution pH. The changes in these physical and chemical parameters, therefore, are most likely even less than predicted by the modeling. The likely smaller range in pH values, for example, makes the presently measured K_d values more rather than less representative of the actual conditions that will occur in the mountain below the repository horizons. Therefore, the impact of the high uncertainties and neglect of some chemical processes in the lower horizons is expected to be minimal.

Modeling assumptions are clearly defined as appropriate for the intended use of the model for screening these FEPs. My own belief, however, is that a neglect of variable composition solid solutions and cation exchange cannot be fully justified, although the modeling results presented without these processes are very likely overly conservative. Uncertainties in model parameters, process representation, and assumptions are described in detail, and the impacts of these uncertainties are discussed, as appropriate for the intended use of the model for screening these FEPs. In particular, uncertainties associated with some of the processes highlighted in my technical review are now discussed extensively. The authors have provided additional material to justify the conclusion that where modeling of THC processes is highly uncertain, the results are most likely overly conservative.

The overall technical credibility of the approach, including assumptions, parameters, equations, and numerical implementation, is appropriate for the intended use of the model for screening these FEPs. The neglect of some chemical processes most likely had the effect of making the modeling overly conservative and therefore should not be considered to invalidate the screening of the FEPs.

Sincerely,

Carl I. Steefel
Staff Scientist
Earth Sciences Division

The following information is a record of the comments and the responses from the reviewer and the responders. Based on the information, the conclusion in the previous memo (i.e., the adequacy of the mountain-scale THC model) was made.

Comments on MSTHMC Model
Carl Steefel
Lawrence Berkeley National Laboratory

General Comments:

Comment by C. Steefel: My biggest problem with the validation of the Mountain Scale model is that it is based strictly on the Drift Scale Test validation. This test, which was quite high temperature, will have tested mostly higher temperature thermodynamic and kinetics. While the lower temperature kinetic rate constants may have been in the database, the results of the DST will be largely insensitive to these. In contrast, reactions occurring in the PTn or the Calico Hills are largely low temperature and therefore the minerals that form (thermodynamically and kinetically) cannot be considered to have been validated based on the high T Drift Scale test. One might argue that the parameters from the DST will tend to overestimate the amount of reaction and that therefore the results are conservative, but this is a tricky path to go down. In addition, it may be that some phases formed at lower temperature (e.g., clays) may have a larger effect on the permeability than would a feldspar, for example. In any case, formation of feldspars (which to my knowledge is unknown at temperatures close to 25^{o}C, and even below 100^{o}C) will result in a lower pH and therefore higher CO_2 than would a more easily formed clay or zeolite phase.

Response by N. Spycher: It is recognized that the Drift Scale Test validation mostly applies to higher temperatures higher than those away from the repository units, such as in the PTn or the CHn. Simulations of ambient conditions (low temperatures), however, were carried out with the drift-scale THC Seepage model, and used to provide confidence in model results for repository units under ambient conditions (i.e., model results yielding trends reasonably similar to those observed in the actual system at the proposed repository location). Nevertheless, it is agreed that the model was not strictly validated for units away from the repository such as vitric and zeolitic units of the CHn and PTn. As a result, predicted reaction trends in such units have a high uncertainty. Additions were made to the text to more strongly reflect this, including statements about the low likelihood of feldspar precipitation at low temperatures and low likelihood of clinoptilolite alteration to phases other than those observed in these units. The mineralogy of the zeolitic units (primarily clinoptilolite), by itself, represents an analogue to natural thermal alteration that has occurred at Yucca Mountain for millions of years, and provides a strong argument that significant alteration on top of what has already occurred is not expected as a result of waste emplacement. Statements were added to the text to this effect, including the fact that modeled reactions rates were likely overestimated

Comment by C. Steefel: This is the critical problem in my view. The minimum required is a more careful discussion of these kinetic and thermodynamic effects and why or why not the results will not be affected by this. At this stage, this discussion is absent. The general talk of "upscaling", without being specific as to what parameters and/or processes are involved, doesn't help here. The preferred path would be to conduct at least some additional work to demonstrate

that the Mountain Scale model captures the broad features of the ambient chemistry. Some of this may be built in to the Mountain Scale model as calibration, but this is not discussed at all. Can the Mountain Scale model capture the vertical gradients in the cation ratios, with Ca gradually being replaced by Na at depth? I doubt it, since ion exchange is not in the model (it should be once the Mountain Scale system is addressed). One possibility would be to conduct a more careful modeling of the uranium series disequilibria (which provides information on silicate dissolution rates) along with the ambient major element chemistry to establish that the Mountain Scale model can accurately predict pore fluid chemistry (which will affect the chemistry of reactive gases like CO_2 as well) and mineralogy. This may be part of the reason for the high CO_2 below the repository, since the precipitation of feldspar will tend to increase the CO_2.

Response by N. Spycher: See the statement above. Currently, the model does not always capture the broad features of the ambient chemistry away from repository units, in part because ion exchange and zeolite solid solutions were not implemented in the model. Also, it appears the clinoptilolite stability may have been underestimated. Statements were added in the text to this effect. The result is inconsequential, however, because the strongest argument against significant alteration of the CHn (from waste emplacement) is not the model results (which over-predicts alteration), but the observed natural thermal alteration history of the mountain.

Comment by C. Steefel: The use of pure end members, especially anorthite, in the model is unrealistic as discussed below. When anorthite is added, it remains always far from equilibrium because of its huge solubility, while a solid solution feldspar may stabilize at more reasonable water chemistries. The anorthite is made to match only by slowing it down by 3 orders of magnitude. Feldspar dissolves as a single phase, not as a mechanical mixture of anorthite and albite. The neglect of solid solutions in the clays (smectite) and zeolite may be problematic as well.

Response by E. Sonnenthal: The added discussion and figures regarding anorthite rate effects address the comment.

Additional Response by N. Spycher: It is noted further below, and was added to the text, that reducing the reaction rate for anorthite essentially suppressed the reaction of this mineral, which is consistent with the fact that calcic plagioclase would be expected to have weathered completely during the natural thermal alteration of the mountain.

Comment by C. Steefel: Also neglected is the effect of cation exchange. Without this, it would be difficult to capture the change in Ca/Na ratio that occurs downhole, although there has been some discussion about whether this is a steady-state or transient effect.

Response by N. Spycher: This is recognized, as discussed in above comments.

Comment by C. Steefel: In summary, I think some additional work is needed to validate the Mountain Scale model based on ambient chemistry. At a minimum, this should capture the broad trends in major element chemistry, especially cation ratios. Uranium series disequilibria might be included as an additional constraint on primary mineral dissolution.

Detailed Comments:

Section 6.2: It is not clear how a two dimensional model for TH processes is justified based on what is presented here. Some mention is made of the 2D effects lasting only a short while, but I see nothing on the 3D effects. For example, in the drift scale test, boiling occurs at times that are on the order of 1,000 years different from what is obtained in the 3D modeling. Presumably there is some correction in the heat load that might account for the conduction of heat in the 3rd dimension that is not considered in the 2D model.

Response by E. Sonnenthal: Temperatures in the 2D and 3D models are a little different because the 2D models are cross-sections perpendicular to the drifts and into the repository center.

Section 6.3 (line 2016): Here it is stated that the 3D model is consistent with the 2D model, particularly in terms of the time for the cessation of boiling (about 2,000 years). This does not seem to agree with the multi-scale model (Livermore model), but also does not make a great deal of sense unless the 2D model is run with some accounting for the thermal load that adjusts for the loss of heat in the third dimension.

Response by E. Sonnenthal: Temperatures in the 2D and 3D models are a little different because the 2D models are cross-sections perpendicular to the drifts and into the repository center.

Section 6.4.2.4 (line 2406): Anorthite is used an an end member composition of feldspar. Most importantly, the thermodynamics of the Yucca Mountain feldspar (17-20% AN) cannot be described with a mechanical mixture of 80% albite and 20% anorthite. In the mechanical mixture, the anorthite has an extremely high solubility and also very high rates of reaction. It will dissolve rapidly, leaving the albite component much less reactive. However, the solid solution will not have this high solubility, first because of the entropy of mixing even in the case of an ideal solid solution, which lowers the Gibbs free energy relative to a mechanical mixture of the two end members, and second because as Na^+ increases in solution, it can stabilize the feldspar much more readily than one can ever saturate the pore fluid with respect to anorthite. This effect occurs even without considering non-ideal effects. In any case, it is hardly surprising that the anorthite rate should not apply, considering there is no anorthite present in the mountain (line 2412). There should be a single rate constant and a single saturation state (log Q/Keq, or reaction affinity) for the feldspar dissolution reaction.

Response by E. Sonnenthal: The added text on uncertainties in Section 7.2.2 addresses this comment.

Response by N. Spycher: Note that using a plagioclase solid solution in the model (instead of two separate endmembers) was considered, although this capabability for plagioclase (i.e., non-ideal solution) is not currently implemented in the code. The lowering of the anorthite effective reaction rate by 3 orders of magnitude essentially results in the suppression of this mineral, which is consistent with the fact that one would expect calcic plagioclase to have already weathered completely during the natural thermal alteration of the mountain, which lasted millions of years.

Similar considerations apply to the other end member compositions, although the effect is most extreme with anorthite because of the significantly higher solubility of this phase.

Response by E. Sonnenthal: Added more discussion on mineral evolution uncertainties to Section 6.4.3.3.3.

Response by N. Spycher: Also see answer to above comment.

There should either be a table or a list in the text showing the salt minerals that are allowed to precipitate, and the order in which they do so.

Response by E. Sonnenthal: Added detailed discussion and list of salt phases to Section 6.4.2.4.

Table 6.4.2: Why are there no aluminum pore water analyses? There is always the possibility of colloid formation, but this generally happens in strongly supersaturated solutions. In any case, this effect can be evaluated by comparing various filtration fractions (0.45 μm, 0.1 μm, and smaller). These could be extremely useful in establishing the solubility of secondary phases allowed to precipitate. They are also important in controlling the saturation state of the system with respect to feldspar.

Response by E. Sonnenthal: The added discussion in Section 6.4.2.4 addresses this comment.

Response by N. Spycher: Aluminum was analyzed in the water used in the simulations but was below detection limits. This is not surprising, given the fact that truly dissolved (i.e., non-colloidal) aluminum concentrations in subsurface natural waters are typically in the micro- to nano-molal range, or even lower. In our case, it was observed that the pore water compositions at YM typically plot near the illite/K-spar equilibrium boundary. We observed that by computing Al concentrations assuming equilibrium with illite, the calculated Al concentration also yielded close equilibrium with K-feldspar, thus providing confidence in our approach.

Section 6.4.3.1.1 and 6.4.3.1.2: How do these results differ from the 2D mountain scale TH results already presented? It would seem wiser to summarize the salient differences, rather than go through all the description again here (and then leave it to the reader to figure out where there actually is a difference).

Response by E. Sonnenthal: The added short statements in the introduction part of Section 6.4.3 as to the reasons for discussing detailed TH results address this comment.

Response by N. Spycher: TH results are presented so that the THC processes that are directly affected by TH processes can be directly compared. There are no systematic differences between the TH model discussed in Section 6.4.3 compared to those described in previous sections; however, because the cross-section is much more limited, there are boundary condition effects that lead to different local behavior in flow and temperature.

Section 6.4.3.3.3 (line 2869): Is there any evidence from anywhere that albite or potassium feldspar can form as a result of the alteration of volcanic glass at near-ambient temperatures? I don't know of any descriptions of this.

Response by E. Sonnenthal: The added paragraph and references to Section 6.4.3.3.3 address this comment.

Response by N. Spycher: The modeled reactions forming feldspars and stellerite from glass and clinoptilolite dissolution are likely to be thermodynamically or kinetically unfavorable in vitric and zeolitic units such as the Calico Hills formation. In this respect, it is likely that the modeled mineral transformations in these units reflect overestimated reaction rates, and unrealistic end products yielding greater volume changes than reasonably expected from observations of the natural thermal alteration at Yucca Mountain. This could be caused by an underestimated thermodynamic stability of clinoptilolite, as suggested by simulation results presented by Dobson et al. (2003 [DIRS 168273]). Also, model improvements including zeolite solid solutions and cation exchange reactions would likely result in better agreement between the model results and observed thermal alteration mineralogy.

Section 7, Confidence Building 1: It is stated that validation using the Drift Scale Test is sufficient for the mountain scale model. However, the results in the DST will be largely be controlled by relatively high temperature processes, especially geochemical. In contrast, the Mountain Scale model depends much more on lower temperature reactions, especially in such units as the Calico Hills and the PTn. This is an issue especially with regard to the kinetics, which shows up in the Mountain Scale model perhaps as an overestimation of the rate of precipitation of minerals like albite and potassium feldspar (which generally do not form at all at near-ambient temperatures).

Response by E. Sonnenthal: The added statement at the beginning of Section 7 addresses this comment.

Section 7.1.3: It is stated that the most recent version of the multiscale model is not published in the peer-reviewed literature. My impression was that this was described in detail in the recent Journal of Contaminant Hydrology volume edited by G. Bodvarsson. Again, my memory tells me that boiling stopped in many of the multiscale model runs at 800-1,000 years, in contrast to the 2,000 years cited here.

Response by N. Spycher: The THC seepage model represents one case of the thermal history for a point at the center of the repository, and compares fairly well with results of the MSTH model for the hottest regions within the repository boundary (when TH-only effects are considered, boiling ends ~ 1400 years). Note that the "boiling period" is assumed to end when the temperature drops below 96°C at the drift wall, however, rewetting of the drift wall is modeled to occur at lower temperature (thus later, ~ 2000 years) in the THC seepage model when mineral precipitation is taken into account, because of reduced fluxes above the drift crown (high evaporation below boiling temperatures, yielding longer dryout).

Section 7.2.1 (line 4506): Same comment here. The DST would have validated mostly higher temperature reactions. This is an issue mainly for mineral-water reactions, which have a strong dependence of reaction rates on the temperature. In the Mountain Scale model where lower temperature reactions dominate, it is very difficult to see how the DST results would validate these. While one might argue that the overall extent of reaction might be over- rather than under-estimated by using kinetic parameters validated in DST, it could be that there will be preferential formation of some phases with higher molar volumes than would be the case close to chemical equilibrium (e.g., clays as opposed to feldspars).

Response by E. Sonnenthal: The added uncertainty text in Section 7.2.2 addresses this comment.

Response by N. Spycher: It is agreed that the DST validates mostly higher temperature reactions.

Section 7.2.2 (line 4644): I don't see how it can be stated in advance, or at least based on any work by Manteufel, that chemical processes will not modify the thermal hydrologic regime. This is a function of the extent of reaction-induced permeability change under a specific set of conditions at Yucca Mountain. This has been studied in the Drift Scale Test and the comments of Manteufel are not relevant here.

Response by E. Sonnenthal: Removed reference to Manteufel.

(Line 4661): The lack of effect of the grid size is presumably due to the high rates of reaction used, such that the grid Damkohler number is always large enough that close to equilibrium results will be obtained. Otherwise, there should be a grid size effect. This is often the case with transition state theory (TST) type rate laws, although these rate laws for precipitation have not been demonstrated to apply in natural environments.

Response by E. Sonnenthal: Conduction dominated effects are already discussed in the upscaling text (last paragraph).

Response by N. Spycher: It is agreed that high Damkohler numbers pervade.

Section 7.2.2 (line 4761): There seems to be a substantial difference between the Mountain Scale and Drift Scale model results in the CO_2 distribution. This could be due to lateral transport, as mentioned in the text, but also possibly to the effect of reactions occurring here, especially the precipitation of feldspars. Dissolution of feldspars consumes CO_2, while precipitation will form it. To the extent that feldspars do not precipitate, then that CO_2 source will not be available.

Response by E. Sonnenthal: Roughly an order of magnitude more feldspar is produced, which results in the production of hydrogen ion, thus lowering the pH. This results from a higher surface area used for the glass in the mountain-scale model.

Response by N. Spycher: As mentioned above and added in Section 6.4.3.3.3, the modeled reactions forming feldspars from glass and clinoptilolite dissolution are likely to be thermodynamically or kinetically unfavorable in vitric and zeolitic units such as in the Calico Hills formation. In this respect, increased CO_2 partial pressure in these units is unlikely.

Section 7.2.3: None of the refereed literature, with the possible exception of "Fluid Flow and Reactive Transport Around Potential Nuclear Waste Emplacement Tunnels at Yucca Mountain, Nevada." by N. Spycher (Journal of Contaminant Hydrology, 2003) addresses the issue of lower temperature reactions. In the sections that follow, there is no comparison made between the temperatures at the Mountain Scale and the temperatures discussed in Spycher's report. Specifically, validation based on ambient or nearly ambient conditions is needed. It may be in Spycher's report, but the only point discussed is "upscaling". See line 4396.

Response by E. Sonnenthal: Added uncertainty section and several new caveats in text.

Response by N. Spycher: Xu et al. focusses on lower temperature. Aslo, see answers in the general comments section.

VIII.3 INDEPENDENT POST-DEVELOPMENT VALIDATION REVIEW FOR THE MOUNTAIN SCALE THM MODEL

Tin Chan
416 592 5296; 905-887-9731
chant@aecl.ca ; tinchan@rogers.com

Memo

To: Ernest Hardin, BSC

From: Tin Chan

CC: Yvonne Tsang, LBNL

Date: 07/27/05

Re: **Review of Mountain-Scale THM Model**

I have reviewed the Mountain-Scale THM Model as presented in Rev 03 Draft B of the Mountain-Scale Coupled Processes (TH/THC/THM) Report (MDL-NBS-HS-000007 REV 03 DRAFT B). Specifically, I have perused Sections 5.3, 6.5, 7.3, 8.3, and Appendix VII, as well as pertinent information elsewhere in the report, e.g., Sections 4.1, 6.1, 8.4 and 8.5. I have also read several papers by Rutqvist et al and other authors on validation of the Drift-Scale Model against in situ measurements in the DST in the context of the International DECOVALEX project as published in the Proceedings of the Geoproc 2003 International Symposium. In my professional judgement the Mountain-Scale THM Model represents the leading edge of the current state of science of coupled THM modelling.

I have conducted an independent technical review of the mountain-scale THM model for post-development validation for the intended use of the model for FEP screening. I have reviewed the mountain-scale THM model considering your stated criteria. Based on the current state of knowledge, I can concur that, consistent with the low importance of the “UZ Flow” component to the mean annual dose:

1. The technical approach and algorithms described in the document capture all physical and chemical processes that are significant to the intended use of the model for screening these FEPs.

2. Modeling assumptions are clearly defined and justified as appropriate for the intended use of the model for screening these FEPs.

3. Uncertainties in model parameters, process representation, and assumptions are sufficiently described, and impacts of these uncertainties discussed, as appropriate for the intended use of the model for screening these FEPs.

4. The overall technical credibility of the approach, including assumptions, parameters, equations, and numerical implementation, is appropriate for the intended use of the model for screening these FEPs.

In the course of the review I have prepared a list of detailed questions and technical comments on the THM sections of Mountain-Scale Model report and have communicated the list to the authors both verbally and by email. Hopefully, clarification of these points would further enhance the documentation. I understand that the authors are making revisions to the report to address these questions and suggestions. I will further communicate with you once I have reviewed the revised document and authors' responses..

Thank you for the opportunity to review this state-of-the art report. Attached is the list of questions and comments that I have sent to the authors. Should you have any questions, please do not hesitate to call me.

The following information is a record of the comments and the responses from the reviewer and the responders. Based on the information, the conclusion on the previous memo (i.e., the adequacy of the mountain-scale THM model) was made.

QUESTIONS AND COMMENTS ON THM SECTIONS OF THE MOUNTAIN-SCALE COUPLED PROCESSES MODELS REPORT

Part 1: On Section 6.5

Note: #nnnn refers to the line number(s) in the review copy of the pdf file of the report. Questions and comments are arranged roughly in the order they occur in the report but the author can make changes anywhere in the report as appropriate. I am required by DOE to review the changes after they have been made; so if you are using MS WORD be sure to turn on the highlight Tool. Ernie Hardin (BSC)'s schedule is that I need to complete the review and summarize it in a memo to him and Yvonne by this Friday.

1) #2990-2991 Thermal stress is directly proportional to the product of temperature change, thermal expansion coefficient and rock mass deformation modulus. Where is the justification that the Mountain-scale THM model predicts maximum possible thermal stress? Consider:

   i. Fixed-temperature boundary condition at the bottom of the model may lead to a slightly low temperature. *Response by J. Rutqvist:* No change made. The effect of fixed-temperature is small and considered insignificant for the mountain-scale THM model results.
   ii. Although theoretically the in situ thermal expansion coefficient is expected to be < or = the lab measurement, Fig. 4 of the Geoproc paper by Millard and Rutqvist appears to indicate that the displacement (directly proportional to the product of delta T and thermal expansion coefficient) simulated by the LBNL Drift-scale THM model lies close to the low end of the measured range. *Response by J. Rutqvist:* No change made. The mountain-scale THM model used the qualified sources of the thermal expansion coefficient available in the YMP. As discussed in Section 6.5.9, the intact thermal expansion coefficient was valid to simulated behaviors of the DST.
   iii. I don't have all the DST and other in situ tests reports at YMP. Are there measurements of drift excavation induced displacements or drift wall convergence to allow in situ rock mass deformation modulus to be backed out? Are thermally induced stress changes measured in the DST or the SHT? *Response by J. Rutqvist:* No change made. The mentioned factors were considered and measured in the DST and the SHT.

   Theoretically thermally induced displacement is not sensitive to rock mass deformation modulus. For example, Alain Millard's CEA elasto-brittle model uses a higher Young's modulus and got almost identical displacements to the LBNL model (Fig. 7 of the Geoproc paper by Millard and Rutqvist).

2) #3002 Does FLAC3D compute "changes in hydrologic properties"? *Response by J. Rutqvist:* It was replaced with "stress and displacement".

3) Section 6.5.2 Is the thermoelastic equivalent of Biot's hydroelastic coupling included in the TOUGH2-FLAC3D simulations? If not, what would be the impact

of neglecting thermal stress "squeezing" out water and vapour from fractures close to the repository, creating increasing downward fluxes towards the water table? *Response by J. Rutqvist:* No change made. As discussed in Section 6.5.1, this is a partially coupled THM analysis. The effect of "squeezing" was ignored since it is sufficient to calculate changes in the mean permeability value for the bounding case of relatively large THM-induced changes in permeability.

4) #3004 Replace "thermal expansion" with "thermal stress". *Response by J. Rutqvist:* Replaced as suggested.

5) #3016-3017 Give some idea of how low the fluid pressures are to justify neglecting them. (e.g., PFLAC <0.1 MPa – atmospheric pressure – cf. thermal stress of up to 10 MPa and in situ stress 5-8.3 MPa at repository level?). *Response by J. Rutqvist:* A discussion was added for the justification.

6) #3052 Is stress change due to excavation of the drifts simulated in the mountain-scale model? Clarify. *Response by J. Rutqvist:* The effect of excavation was not considered in the mountain-scale THM model. A clarification was added in Section 6.5.6.

7) #3102 Perhaps should read "maximum closure of mechanical aperture". *Response by J. Rutqvist:* A note (i.e., frequently denoted maximum closure in rock mechanics literature) added.

8) #3105 Should be σ'_n and σ'_{ni} as in Eq. 6.5.5-8? *Response by J. Rutqvist:* No change made. σ'_n is the correct term.

9) #3158 Can't find "Assumption 1" in Section 5.3. The assumptions are not numbered there. *Response by J. Rutqvist:* "Assumption 1" removed.

10) #3161 "Mechanically fixed" should read "zero-normal displacement. "Fixed" may be interpreted as fixing both displacement components. *Response by J. Rutqvist:* Corrected as suggested.

11) #3173 See comment re #3158 above. *Response by J. Rutqvist:* "Assumption 1" removed.

12) #3174 Why use "saturated bulk rock density" in UZ? *Response by J. Rutqvist:* No change made. As shown in Figure 6.2-7a, the matrix saturation is about 90%. An engineering judgement was made to simplify the model. No justification required.

13) #3205 The equivalent continuum for a rock mass with 3 orthogonal sets of fractures will have orthotropic mechanical properties (worked out by Goodman, Amadei, etc.; also quoted in Kibok Min's thesis). If isotropic properties are assumed, state this as an approximation (perhaps with some justification?). *Response by J. Rutqvist:* No change made. The mechanical properties were developed without the consideration of anisotropy, and justified in their qualification. No action required.

14) Section 6.5.8 Were any of the rock mass deformation modulus values back-calculated from in situ measurements or all lab measurements adjusted by something like RMI or RQD? Please state explicitly. *Response by J. Rutqvist:* A statement was added referring Drift Scale THM Model and in situ measurements.

15) #3252-3260 See previous comments on #2990-2991, Point 2. *Response by J. Rutqvist:* No change made. The mountain-scale THM model used the qualified sources of the thermal expansion coefficient available in the YMP. As discussed in Section 6.5.9, the intact thermal expansion coefficient was valid to simulated behaviors of the DST.

16) #3303 and corresponding row in Table 6.5.9-1 "ratio k/kd" should read, "ratio (k/kd)1/3". *Response by J. Rutqvist:* Corrected as suggested.

17) #3331-3332 Can't see location of mid-pillar in that figure. *Response by J. Rutqvist:* The text was modified with a clearer decryption.

18) #3410 After "an increase in capillary pressure", should add (not illustrated). *Response by J. Rutqvist:* Added as suggested.

19) #3568-3571 There seems to be a jump between the two sentences. Perhaps elaborate a little. Why not use a simple Coulomb friction model. Are measured values of Coulomb friction angle available? *Response by J. Rutqvist:* A sentence was added to clarify.

20) Figure 6.5.14-1 Unit of stress in the legend in all 3 frames (MPa) should read (Pa). *Response by J. Rutqvist:* Corrected.

21) #3654-3670 Perhaps also discuss the uncertainties related to possibly underestimating the thermal stress in view of the comments on #2990-2991 above? *Response by J. Rutqvist:* No change made. The possible underestimation on the thermal stress in view of the comments on #2990-2991 was considered insignificant as discussed previously.

Part 2: On Section 7.3

22) #5052-5053 It appears to me that only TM displacements were measured and compared to Drift-scale THM simulations. Thermally induced displacements are not sensitive to in situ rock mass deformation modulus if this is the intended meaning of "in situ deformability" The displacements are representative of in situ thermal expansion coefficient. *Response by J. Rutqvist:* Changed to "in situ thermal expansivity"

23) #5066-5070 If larger discontinuities are more compliant, then applying the drift-scale derived stress-permeability relationship to mountain-scale fractures will tend to underestimate the change of fracture permeability because you are assuming the larger discontinuities to be as stiff as the smaller drift-scale fractures. *Response by J. Rutqvist:* The sentence corrected to ", whereas their deformability changes only moderately with scale,"

24) #5074 Perhaps the refereed articles can also be cited here. *Response by J. Rutqvist:* No change made. The comment rejected.

25) #5086 Perhaps insert "by a THM model that does not incorporate a scaling law" after the word, "scale". *Response by J. Rutqvist:* The words added as suggested.

26) #5086-5088 Again thermally induced displacements are directly proportional to thermal expansion coefficient but not sensitive to rock mass deformation modulus (Young's modulus). Perhaps you can argue that since thermal expansion coefficient is not scale dependent, it is also likely that deformation modulus is not scale dependent for scales >1m because both quantities depend on fracture network geometry and fracture deformability. *Response by J. Rutqvist:* A discussion added.

27) However, your best evidence may be the good agreement of your predicted permeability changes with the DST air-permeability measurements. To achieve that agreement you would likely need to predict the thermal stress and the stress-permeability relationship correctly. It is possible, but highly unlikely, that the agreement is due to a fortuitous cancellation of errors in stress and the stress-permeability relationship. *Response by J. Rutqvist:* A discussion added.

28) #5092-5101 Good. I read the Geoproc paper by Datta et al. Near the bottom of the LHS column on p.142 they mentioned in situ plate-bearing tests. Can the results of these tests be quoted to further support the deformation modulus used in your Mountain-scale Model? *Response by J. Rutqvist:* Citations for the in situ measurements at YMP added.

29) #5109-5114 These two sentences require some clarification. See previous comment on #5066-5070. Also, your exponential stress-fracture aperture relationship indicates that when a fracture is wide open (more permeable), it is more sensitive to stress changes (Fig. 6.5.5-2). *Response by J. Rutqvist:* Text added for the clarification.

30) #5147-5149 Perhaps add, "and grid size" or something to that effect before the period. *Response by J. Rutqvist:* The words added as suggested.

31) #5170 Perhaps add, "near ground surface" or something to that effect before the period. *Response by J. Rutqvist:* The words added as suggested.

32) #5232-5241 Should also say whether flux magnitudes predicted by the Drift-scale Model and the Mountain-scale Model are comparable. *Response by J. Rutqvist:* The "flux magnitudes" added.